UNIVERSITY OF SOUTHAMPTON

FACULTY OF ENVIRONMENTAL AND LIFE SCIENCES

Geography and Environmental Science

The Morphological Evolution and the Sustainability of Deltas in the 21st Century

By

Sarah Jane Spinney

Thesis for the degree of Doctor of Philosophy

April 2019

UNIVERSITY OF SOUTHAMPTON

ABSTRACT

FACULTY OF SOCIAL, HUMAN AND MATHEMATICAL SCIENCES

Geography

Thesis for the degree of Doctor of Philosophy

THE MORPHOLOGICAL EVOLUTION AND THE SUSTAINABILITY OF DELTAS IN THE 21ST CENTURY

Sarah Jane Spinney

Utilising the cellular automata model CAESAR-Lisflood, a novel set of metrics is developed to explore the nature of multidecadal morphological change in delta catchment systems under a range of climatic and environmental change scenarios. Whilst this study has a specific focus on the Mahanadi Delta in India, these scenarios are designed in such a way so as to encapsulate stressors that are common to a broad range of deltaic environments; including increased exposure to meteorological extremes, sediment starvation and eustatic sea-level rise.

Compared to terrestrial systems, there have been relatively few studies that focus on the successful simulation of long-term emergent phenomena in coastal catchments, especially in the specific context of deltas. To address this gap, this research aims to enhance our understanding of how emergent processes influence the multidecadal evolution of deltaic environments, and how we can use this information to understand how the system may respond to increasing conditions of climatic stress.

This study also seeks to explore how changes in the emergent morphological system may impact certain factors that influence the habitability of the Mahanadi Delta. Through the development of a novel vulnerability index, this study explores: (1) the impacts of an extreme flood event; (2) potential changes in habitat cover; (3) the effectiveness of the model to explore engineering strategies, with a focus on re-naturalising the delta.

Table of Contents

Table of Contents i
Table of Tables v
Table of Figures vii
Academic Thesis: Declaration of Authorship xvii
Acknowledgements xix
Definitions and Abbreviations xxi
Chapter 1 Introduction 1

1.1 Context 1
1.2 Aims and objectives 3

Chapter 2 Modern Controls on Delta Morphology 9

2.1 Morphological Processes in Deltaic Environments 9
2.2 Anthropogenic Controls 19

2.2.1 Sediment Starvation 19
2.2.2 Groundwater and hydrocarbon extraction 23

2.3 Climatic Controls 25

2.3.1 Eustatic sea-level rise 25
2.3.2 Meteorological extremes 27

Chapter 3 Modelling Deltas 33

3.1 Key Challenges in Studying the Morphological Evolution of Deltas in the 21st Century 33

3.1.1 Temporal complexity – Magnitude versus frequency 34
3.1.2 Spatial complexity – Understanding and quantifying emergence 40
3.1.3 Uncertainty in morphological models 43
3.1.4 Quantifying vulnerability 46

3.2 Numerical Modelling Approaches 49
3.3 CAESAR-Lisflood 65

3.3.1 Introduction 65
3.3.2 Morphological and Hydrological Processes 67

3.3.3 Habitat cover 75

Chapter 4 The Mahanadi Delta, India 79

4.1 Introduction 79
4.2 Morphological setting and catchment selection 84
4.3 System stressors 91
4.4 Impacts to ecosystem services 97

Chapter 5 Model setup and applied metric development 101

5.1 Introduction 101
5.2 Scenario Design 103
5.2.1 Individual scenarios 103
5.2.2 Synergistic scenarios 121
5.3 Model Setup – Morphological modelling in CAESAR-Lisflood 127
5.3.1 Data requirements 127
5.3.2 Setup of baseline scenario and model validation 133
5.3.3 Outputs and results of validation 138
5.3.4 Utilising morphological outputs for habitability analysis 156
5.3.4.1 Flood hazard following an extreme cyclone event 157
5.3.4.2 Changes in habitat cover 157
5.3.4.3 Engineering strategies 157

Chapter 6 Morphological Modelling 160

6.1 Presentation of Results 160
6.1.1 Devi Catchment 162
6.1.1.1 Sediment loss and elevation change 162
6.1.1.2 Morphological Response Units (MRUs) 174
6.1.1.3 Fractal dimension 190
6.1.1.4 Distribution of island sizes 192
6.1.1.5 Nearest-edge distance 197
6.1.2 Mahanadi Catchment 200
6.1.2.1 Sediment loss and elevation change 200

6.1.2.2 Morphological Response Units (MRUs) 206
6.1.2.3 Fractal dimension 210
6.1.2.4 Distribution of island sizes 212
6.1.2.5 Nearest-edge distance 214
6.2 Discussion of Results 217

Chapter 7 Linking Morphology and Habitability 243

7.1 Introduction 243
7.2 Flood hazard following a severe cyclone event 245
7.3 Changes in habitat cover 257
7.4 Engineering strategies 271

Chapter 8 Conclusions 279

8.1 Introduction 279
8.2 Objective 1: The influence of emergent processes 279
8.3 Objective 2: Linking morphology and habitability 283
8.4 Objective 3: To provide outputs that are useful to stakeholders 285
8.5 Recommendations for further research 287

Appendix 289

A. Parameter setup – baseline scenario (TST) 289
B. Setup of remaining synergistic scenarios 300

1WWW (Wet monsoon, Wet post-monsoon, Wet dry season, moderate temperature increase) 300
2DDD (Dry monsoon, Dry post-monsoon, Dry dry season, moderate temperature increase) 300
3WDD (Wet monsoon, Dry post-monsoon, Dry dry season, moderate temperature increase) 300
4DWD (Drier, more variable monsoon, Wet post-monsoon, Dry dry season, variable sediment supply, moderate temperature increase) 301
5DWA (Drier, more variable monsoon, Wet post-monsoon, Accelerated drought in dry season, moderate temperature increase, variable sediment supply) 301

6WDDH (Wet monsoon, Dry post-monsoon, Dry dry season, High sea-level rise, high temperature increase)..... 302
7DWDH (Drier, more variable monsoon, Wet post-monsoon, Dry dry season, High sea-level rise, high temperature increase, variable sediment supply)..... 302
8DWAH (Drier, more variable monsoon, Wet post-monsoon, Accelerated drought in dry season, High sea-level rise, high temperature increase, variable sediment supply) 302
9DWDC (Drier, more variable monsoon, Wet post-monsoon, Dry dry season, increase severe Cyclone frequency, moderate temperature increase, variable sediment supply) 303
10DWDF (Drier, more variable monsoon, Wet post-monsoon, Dry dry season, Failure of monsoon rains from 2065, moderate temperature increase, variable sediment supply) 303

C. Morphological modelling results..... 304
D. Outputs utilised to explore potential changes in habitat cover ... 339

List of References..... 345
Supplementary materials 365

Table of Tables

Table 2.1 Syvitski *et al.* (2009:684) present environmental data from 33 deltas.....18
Table 3.1 Summary of the benefits and limitations associated with a selected group of twelve models used in morphodynamic applications.....59
Table 4.1 Environmental data for the Mahanadi Delta from Syvitski *et al.* (2009:4). 96
Table 5.1 Calculated long-term average annual water discharge and sediment loads for the years 2045 and 2075 under each meteorological scenario. 115
Table 5.2 Individual scenarios designed to explore a variety of pathways for each of the four drivers of morphological change, as listed in chapter 2. 119
Table 5.3 List of synergistic scenarios to be explored.....123
Table 5.4 Format of text file for the input of hydrological and sediment data. 131
Table 5.5 Parameter setup in C-L for model calibration and scenario TST.....137
Table 5.6 Identification of morphological response units (MRUs). 141
Table 6.1 Net sediment change, Devi catchment 170
Table 6.2 Box-counting dimension (D), Devi catchment 191
Table 6.3 Total number and size of islands, Devi catchment 196
Table 6.4 Net sediment change, Mahanadi catchment.....205
Table 6.5 Box-counting dimension (D), Mahanadi catchment.....211
Table 6.6 Total number and size of islands, Mahanadi catchment.....213
Table 7.1 Scoring utilised to define categorical measures of vulnerability to habitat cover change.. 265

Table of Figures

Figure 2.1 Ternary framework for the classification of delta morphologies based on Galloway (1975) 11
Figure 2.2 The four categories of ecosystem services, as defined by the Millennium Ecosystem Assessment (2005) 13
Figure 2.3 Examples of ecosystem services provided by mangrove forest (Source: coastvserosion.wikispaces.com) 15
Figure 2.4 Example of a short (A) and long (B) feedback mechanism between supporting ecosystem services and morphological processes. 16
Figure 2.5 Left Image: Historical location of distributary channels in the Indus delta (colour, year): blue, 1847; green, 1861; red, 1897; black, 1922. Right Image: Modern irrigation channel system with main water distribution stations. (Source: Syvitski *et al.,* 2009: 683). 21
Figure 2.6 Methods of delta restoration that mimic natural processes (Source: Giosan *et al*., 2014). 23
Figure 3.1 Social-ecological transformations can be illustrated in two ways: (a) a regime change between several stable states after passing through a threshold, or (b) as a tipping point. (Image source: Olsson and Folke, 2008). 37
Figure 3.2 The Oxfam 'Doughnut'. (Image source: kateraworth.com). 38
Figure 3.3 (A): 2001 LANDSAT Advanced spaceborne thermal emission and reflectance radiometer (ASTER) image of the Mississippi delta and (B): overhead photo of experimental delta created with cohesive sediment mixture; both images from Edmonds *et al.* (2009: 759). 40
Figure 3.4 Types of uncertainty associated with morphological modelling, as defined by Van Asselt (2000) 45
Figure 3.5 Connections between modules in the MDM also showing the time steps over which they operate. Habitat change takes place annually as salinity, biomass, and relative elevation cross pre-established thresholds. Source: Martin *et al.* (2002:359). 56
Figure 3.6 Conceptual diagram showing the structure of CAESAR and CAESAR-Lisflood, based on Van De Wiel *et al.* (2007) 67
Figure 4.1 Location of the Mahanadi Delta showing major distributary channels, key settlements and elevati 83
Figure 4.2 Figure by Mahilik *et al.* (1996) showing the four major stages in the morphological evolution of the Mahanadi Delta over the late Holocene. 86
Figure 4.4 Outlines of the watersheds for the Devi River (yellow) and the Mahanadi River (red) 90
Figure 4.5 Coastal erosion at Satabhaya following Cyclone Hudhud in November 2014 95
Figure 5.1 Conceptual diagram showing the two sediment starvation scenarios to be included in the model 105

Table of Figures

Figure 5.2 Diagram showing sea-level rise scenarios for Puri provided by the Met Office for (A) RCP4.5 and (B) RCP8.5. Image and data courtesy of Matt Palmer (2016)..... 107
Figure 5.3 Individual meteorological scenarios to be tested in the model. Baseline scenarios are noted..... 109
Figure 5.4 Schematic diagram to show the method of calculation for water and sediment inflow data for each meteorological scenario representing shifts to long-term climate factors (thus excluding tropical cyclone frequency) 114
Figure 5.5 Severe cyclone frequency scenarios to be tested in the model. A reoccurrence interval of 50 years represents the baseline value as determined from the 1999 Odisha cyclone event..... 118
Figure 5.6 (A): Identifying and (B): removing false blockages from the channel in RasterEdit using interpolation method 128
Figure 5.7 Prepared DEMs in RasterEdit showing the location of the inflow points for the Mahanadi catchment (top) and Devi catchment (bottom). Sediment and water inflow points are shared and shown in red. Tidal inflow areas are shown in orange. 129
Figure 5.8 Binary images showing the distributary channel network in the Mahanadi (top image) and Devi (bottom image) catchments. 130
Figure 5.9 LANDSAT images of the Devi River catchment from the years 1973 and 2003. 135
Figure 5.10 LANDSAT images of the Mahanadi River catchment, from the years 1973 and 2003.. 136
Figure 5.11 Matlab script for calculating the fractal box-counting dimension (D). CHAN refers to the prepared binary image of the skeletonised channel network. D is the correlation coefficient on the calculated line of best fit. 143
Figure 5.12 Matlab script for identifying island areas, where CHAN refers to the prepared binary image of the skeletonised channel network. Island size is then calculated from the number of pixels within each island boundary.. 144
Figure 5.13 Matlab script for calculating NED distribution, where CHAN refers to the prepared binary image of the skeletonised channel network. D refers to the NED value for any given point. 144
Figure 5.14 Elevation change in the Devi catchment at year 30 of scenario TST. 147
Figure 5.15 Net sediment volume change in the Devi catchment at year 30 of scenario TST. The x-axis corresponds to distance from the catchment apex (left) to the catchment outflow (right). 148
Figure 5.16 Elevation change in the Mahanadi catchment at year 30 of scenario TST 149

Figure 5.17 Net sediment volume change in the Mahanadi catchment at year 30 of scenario TST. The x-axis corresponds to distance from the catchment apex (left) to the catchment outflow (right).....151
Figure 5.18 Box-counting dimension, D, for the delta networks analysed by Edmonds *et al.* (2011). They found all delta networks to be fractal and characterized by a D ≈ 1.3.....152
Figure 5.19 (A) Island size distribution for the Devi catchment at 0 and 30 years of scenario TST and (B) Island size distribution for the Mahanadi catchment at 0 and 30 years of scenario TST.....153
Figure 5.20 (A) Distribution of normalised NED values in the Devi and Mahanadi catchments at 0 years and 30 years under scenario TST. (B) Distribution of normalised NED values found by Edmonds *et al.* (2011). 155
Figure 5.21 (A) Spatial distribution of normalised NED values in the Devi at 0 years under scenario TST (B) in the Devi at 30 years under scenario TST (C) in the Mahanadi at 0 years under scenario TST (D) in the Mahanadi at 30 years under scenario TST. The x axis represents distance along the main channel from the catchment apex (left) to mouth (right).....156
Figure 6.1 (A) Net sediment loss and (B) Elevation change at 30 years under scenario TST, Devi catchment. The x-axis in figure A corresponds to distance from the catchment apex (left) to the catchment outflow (right).....163
Figure 6.2 (A) Net sediment loss and (B) Elevation change at 50 years under scenario TST, Devi catchment. The x-axis in figure A corresponds to distance from the catchment apex (left) to the catchment outflow (right).....164
Figure 6.3 Elevation change between 30 and 50 years under scenario TST, Devi catchment.....165
Figure 6.4 Net sediment loss at 30 years for scenarios TST, 1WWW, 2DDD, 3WDD, 6WDDH, 5DWA and 8DWAH; Devi catchment. Blue indicates net sediment loss and green indicates net sediment gain. The x-axis in figure A corresponds to distance from the catchment apex (left) to the catchment outflow (right).....166
Figure 6.5 Net sediment loss at 30 years for scenarios TST, 4DWD, 7DWDH, 9DWDC and 10DWDF; Devi catchment. Scenario TST (baseline) is shown for reference. Blue indicates net sediment loss and green indicates net sediment gain. The x-axis in figure A corresponds to distance from the catchment apex (left) to the catchment outflow (right).....167
Figure 6.6 Net sediment loss at 50 years for scenarios TST, 1WWW, 2DDD, 3WDD, 6WDDH, 5DWA and 8DWAH; Devi catchment. Blue indicates net sediment loss and green indicates net sediment gain. The x-axis in figure A corresponds to distance from the catchment apex (left) to the catchment outflow (right).....168

Table of Figures

Figure 6.7 Net sediment loss at 50 years for scenarios TST, 4DWD, 7DWDH, 9DWDC and 10DWDF; Devi catchment. Net sediment loss at 60 years is also shown for scenario 10DWDF. Scenario TST (baseline) is shown for reference. Blue indicates net sediment loss and green indicates net sediment gain. The x-axis in figure A corresponds to distance from the catchment apex (left) to the catchment outflow (right). 169
Figure 6.8 Floodplain morphological responses units (MRUs) for scenarios TST, 1WWW and 2DDD; Devi catchment..... 176
Figure 6.9 Floodplain morphological responses units (MRUs) for scenarios 3WDD and 6WDDH Scenario 6 shows a high sea-level variation of scenario 3.... 177
Figure 6.10 Floodplain morphological responses units (MRUs) for scenarios 5DWA and 8DWAH; Devi catchment. Scenario 8 shows a high sea-level variation of scenario 5..... 178
Figure 6.11 Floodplain morphological responses units (MRUs) for scenarios 4DWD, 7DWDH and 9DWDC; Devi catchment. Scenarios 7 and 9 show variations of scenario 4. 179
Figure 6.12 Floodplain morphological responses units (MRUs) for scenario 10DWDF; Devi catchment. 180
Figure 6.13 Example of levee formation under scenario TST; Devi catchment. 181
Figure 6.14 Channel morphological responses units (MRUs) for scenarios TST and 1WWW; Devi catchment. 184
Figure 6.15 Channel morphological responses units (MRUs) for scenarios 2DDD and 4DWD; Devi catchment. 185
Figure 6.16 Channel morphological responses units (MRUs) for scenarios 3WDD and 6WDDH; Devi catchment. Scenario 6 shows a high sea-level variation of scenario 3..... 186
Figure 6.17 Channel morphological responses units (MRUs) for scenarios 5DWA and 8DWAH; Devi catchment. Scenario 8 shows a high sea-level variation of scenario 5..... 187
Figure 6.18 Channel morphological responses units (MRUs) for scenarios 7DWDH and 9DWDC; Devi catchment..... 188
Figure 6.19 Channel morphological responses units (MRUs) for scenario 10DWDF. .. 189
Figure 6.20 Island size distribution for scenarios TST, 1WWW, 2DDD, 3WDD, 6WDDH, 5DWA and 8DWAH; Devi catchment. Scenarios 6 and 8 show variations of scenarios 3 and 5, respectively. 194
Figure 6.21 Island size distribution for scenarios TST, 4DWD, 7DWDH, 9DWDC and 10DWDF; Devi catchment. Scenarios 7, 9 and 10 all show variations of scenario 4. Scenario TST (baseline) is shown for reference). 195
Figure 6.22 Normalised nearest-edge distance (NED) at 30 years, Devi catchment.... 198

Figure 6.23 Normalised nearest-edge distance (NED) at 50 years, Devi catchment. NED at 60 years is also shown for scenario 10DWDF. 199
Figure 6.24 (A) Net sediment loss and (B) Elevation change at 30 years under scenario TST, Mahanadi catchment. 201
Figure 6.25 (A) Net sediment loss and (B) Elevation change at 50 years under scenario TST, Mahanadi catchment. 202
Figure 6.26 Elevation change between 30 and 50 years under scenario TST, Mahanadi catchment 203
Figure 6.27 Net sediment loss for scenarios TST and 4DWD; Mahanadi catchment. Blue indicates net sediment loss and green indicates net sediment gain..204
Figure 6.28 Floodplain morphological responses units (MRUs) for scenarios TST and 4DWD; Mahanadi catchment. 207
Figure 6.29 Levee formation under scenarios TST; Mahanadi catchment.....208
Figure 6.30 Channel morphological responses units (MRUs) for scenarios TST and 4DWD; Mahanadi catchment 209
Figure 6.31 DEMs at 50 years for scenarios TST and 4DWD; Mahanadi catchment. ...210
Figure 6.32 Island size distribution for scenarios TST and 4DWD; Mahanadi catchment. 213
Figure 6.33 Normalised nearest-edge distance (NED) at 30 years, Mahanadi catchment.214
Figure 6.34 Normalised nearest-edge distance (NED) at 50 years, Mahanadi catchment.215
Figure 6.35 Net sediment change across all scenarios; Devi catchment. Two distinctive morphological pathways emerge from the results, referred to as group A (shown in shades of blue) and group B scenarios (shown in shades of red). 220
Figure 6.36 Net sediment change under scenarios TST and 4DWD; Devi and Mahanadi catchments. The dotted lines represent the morphological response of the Mahanadi catchment. 232
Figure 6.37 A new channel system develops between 30 and 50 years under scenario TST, thereby connecting two bifurcations of the main Mahanadi channel (highlighted in red).....234
Figure 7.1Water depth following the extended flood simulation run utilising the (A) baseline (0 year) DEM and (B) the 4DWD 50 year DEM; Devi catchment.247
Figure 7.2 Water depth following the extended flood simulation run utilising the (A) baseline (0 year) DEM and (B) the 4DWD 50 year DEM; Mahanadi catchment.....248
Figure 7.3 Floodplain inundation depth at the end of the one year extended simulation period (utilising the 4DWD 50 year DEM); Devi catchment. The inset graph shows the frequency distribution of flood depth values.....249
Figure 7.4 Floodplain inundation depth at the end of the one year extended simulation period (utilising the 4DWD 50 year DEM); Mahanadi catchment. The inset graph shows the frequency distribution of flood depth values.....250

Table of Figures

Figure 7.5 (A) Floodplain inundation depth at the end of the one year extended simulation period (utilising the 4DWD 50 year DEM) and (B) Elevation change between 30 and 50 years under scenario 4DWD, highlighting areas of levee erosion and levee development; Devi catchment 252
Figure 7.6 Categorical measure of vulnerability to an extreme flooding event, scenario 4DWD; Devi catchment. Large settlements at high or moderate risk are shown for reference. 255
Figure 7.7 Categorical measure of vulnerability to an extreme flooding event, scenario 4DWD; Mahanadi catchment. Large settlements at high or moderate risk are shown for reference. 256
Figure 7.8 Dominant habitat classifications in the Devi catchment; extracted utilising land-use data from Wetlands International (2014a). Agricultural land covers approximately 79% of the catchment area. 263
Figure 7.9 Dominant habitat classifications in the Mahanadi catchment; extracted utilising land-use data from Wetlands International (2014a). Agricultural land covers approximately 67% of the catchment area; whilst forests and plantations cover 20%. 264
Figure 7.10 categorical measures of vulnerability to habitat cover change under scenario 4DWD; Devi catchment. The scores correlate to those described in table 7.1. 269
Figure 7.11 Categorical measures of vulnerability to habitat cover change under scenario 4DWD; Mahanadi catchment. The scores correlate to those described in table 7.1 270
Figure 7.12 Creation of an artificial levee breach in the RasterEdit software by taking the baseline 0 year DEM for the Devi catchment (A) and modifying the elevation of cells to remove the levee structure (B). Modified cells are highlighted with white dots. 272
Figure 7.13 Creation of an artificial subdelta in the RasterEdit software by taking the baseline 0 year DEM for the Devi catchment (A) and modifying the elevation of cells to create a new distributary network (B). Modified cells are highlighted with white dots. 272
Figure 7.14 (A) Localised elevation change for a chosen section of the Devi catchment at 30 years under scenario 4DWD, where no modifications have been made to the initial baseline DEM (B) Localised elevation change for the same section after the simulated levee break has been applied. The location of the break (as shown in figure 7.12) is outlined by the red box. 273
Figure 7.15 (A) Localised elevation change for a chosen section of the Devi catchment at 30 years under scenario 4DWD, where no modifications have been made to the initial baseline DEM (B) Localised elevation change for the same

section after the simulated subdelta has been created. The location of the subdelta (as shown in figure 7.13) is outlined by the red box.....274
Figure 7.16 (A) Localised elevation change at the mouth of the Devi catchment at 30 years under scenario 4DWD, where no modifications have been made to the initial baseline DEM; and (B) Localised elevation change for the same section after the simulated subdelta has been created. The colour scale has been modified to highlight changes in the structure of the mouth bar. 276
Figure C.1 **(A)** Net sediment loss and (B) Elevation change at 30 years under scenario 1WWW, Devi catchment. The x-axis in figure A corresponds to distance from the catchment apex (left) to the catchment outflow (right).....304
Figure C.2 (A) Net sediment loss and (B) Elevation change at 50 years under scenario 1WWW, Devi catchment. The x-axis in figure A corresponds to distance from the catchment apex (left) to the catchment outflow (right).....305
Figure C.3 Elevation change between 30 and 50 years under scenario 1WWW, Devi catchment.....306
Figure C.4 (A) Net sediment loss and (B) Elevation change at 30 years under scenario 2DDD, Devi catchment. The x-axis in figure A corresponds to distance from the catchment apex (left) to the catchment outflow (right).....307
Figure C.5 (A) Net sediment loss and (B) Elevation change at 50 years under scenario 2DDD, Devi catchment. The x-axis in figure A corresponds to distance from the catchment apex (left) to the catchment outflow (right).....308
Figure C.6 Elevation change between 30 and 50 years under scenario 2DDD, Devi catchment.....309
Figure C.7 (A) Net sediment loss and (B) Elevation change at 30 years under scenario 3WDD, Devi catchment. The x-axis in figure A corresponds to distance from the catchment apex (left) to the catchment outflow (right).....310
Figure C.8 (A) Net sediment loss and (B) Elevation change at 50 years under scenario 3WDD, Devi catchment. The x-axis in figure A corresponds to distance from the catchment apex (left) to the catchment outflow (right).....311
Figure C.9 Elevation change between 30 and 50 years under scenario 3WDD, Devi catchment.....312
Figure C.10 (A) Net sediment loss and (B) Elevation change at 30 years under scenario 4DWD, Devi catchment. The x-axis in figure A corresponds to distance from the catchment apex (left) to the catchment outflow (right).....313
Figure C.11 (A) Net sediment loss and (B) Elevation change at 50 years under scenario 4DWD, Devi catchment. The x-axis in figure A corresponds to distance from the catchment apex (left) to the catchment outflow (right).....314
Figure C.12 Elevation change between 30 and 50 years under scenario 4DWD, Devi catchment.....315

Figure C.13 (A) Net sediment loss and (B) Elevation change at 30 years under scenario 5DWA, Devi catchment. The x-axis in figure A corresponds to distance from the catchment apex (left) to the catchment outflow (right). 316
Figure C.14 (A) Net sediment loss and (B) Elevation change at 50 years under scenario 5DWA, Devi catchment. The x-axis in figure A corresponds to distance from the catchment apex (left) to the catchment outflow (right). 317
Figure C.15 Elevation change between 30 and 50 years under scenario 5DWA, Devi catchment. 318
Figure C.16 (A) Net sediment loss and (B) Elevation change at 30 years under scenario 6WDDH, Devi catchment. The x-axis in figure A corresponds to distance from the catchment apex (left) to the catchment outflow (right). 319
Figure C.17 (A) Net sediment loss and (B) Elevation change at 50 years under scenario 6WDDH, Devi catchment. The x-axis in figure A corresponds to distance from the catchment apex (left) to the catchment outflow (right). 320
Figure C.18 Elevation change between 30 and 50 years under scenario 6WDDH, Devi catchment. 321
Figure C.19 (A) Net sediment loss and (B) Elevation change at 30 years under scenario 7DWDH, Devi catchment. The x-axis in figure A corresponds to distance from the catchment apex (left) to the catchment outflow (right). 322
Figure C.20 (A) Net sediment loss and (B) Elevation change at 50 years under scenario 7DWDH, Devi catchment. The x-axis in figure A corresponds to distance from the catchment apex (left) to the catchment outflow (right). 323
Figure C.21 Elevation change between 30 and 50 years under scenario 7DWDH, Devi catchment. 324
Figure C.22 (A) Net sediment loss and (B) Elevation change at 30 years under scenario 8DWAH, Devi catchment. The x-axis in figure A corresponds to distance from the catchment apex (left) to the catchment outflow (right). 325
Figure C.23 (A) Net sediment loss and (B) Elevation change at 50 years under scenario 8DWAH, Devi catchment. The x-axis in figure A corresponds to distance from the catchment apex (left) to the catchment outflow (right). 326
Figure C.24 Elevation change between 30 and 50 years under scenario 8DWAH, Devi catchment. 327
Figure C.25 (A) Net sediment loss and (B) Elevation change at 30 years under scenario 9DWDC, Devi catchment. The x-axis in figure A corresponds to distance from the catchment apex (left) to the catchment outflow (right). 328
Figure C.26 (A) Net sediment loss and (B) Elevation change at 50 years under scenario 9DWDC, Devi catchment. The x-axis in figure A corresponds to distance from the catchment apex (left) to the catchment outflow (right). 329

Figure C.27 Elevation change between 30 and 50 years under scenario 9DWDC, Devi catchment.....330
Figure C28 (A) Net sediment loss and (B) Elevation change at 30 years under scenario 10DWDF, Devi catchment. The x-axis in figure A corresponds to distance from the catchment apex (left) to the catchment outflow (right).....331
Figure C.29 (A) Net sediment loss and (B) Elevation change at 50 years under scenario 10DWDF, Devi catchment. The x-axis in figure A corresponds to distance from the cathment apex (left) to the catchment outflow (right).....332
Figure C.30 (A) Net sediment loss and (B) Elevation change at 60 years under scenario 10DWDF, Devi catchment. The x-axis in figure A corresponds to distance from the catchment apex (left) to the catchment outflow (right).....333
Figure C.31 Elevation change between 30 and 50 years under scenario 10DWDF, Devi catchment.....334
Figure C.32 Elevation change between 50 and 60 years under scenario 10DWDF, Devi catchment.....335
Figure C.33 (A) Net sediment loss and (B) Elevation change at 30 years under scenario 4DWD, Mahanadi catchment. The x-axis in figure A corresponds to distance from the catchment apex (left) to the catchment outflow (right). 336
Figure C.34 (A) Net sediment loss and (B) Elevation change at 50 years under scenario 4DWD, Mahanadi catchment. The x-axis in figure A corresponds to distance from the catchment apex (left) to the catchment outflow (right). 337
Figure C.35 (A) Elevation change between 30 and 50 years under scenario 4DWD, Mahanadi catchment 338
Figure D.1 Categorical measure of vulnerability to an extreme flooding event, scenario 4DWD; Devi catchment.....340
Figure D.2 Categorical measure of vulnerability to an extreme flooding event, scenario 4DWD; Mahanadi catchment 340
Figure D.3 Modal hypsometry values under scenario 4DWD; Devi catchment.....341
Figure D.4 Modal hypsometry values under scenario 4DWD; Mahanadi catchment....341
Figure D.5 Net elevation change under scenario 4DWD; Devi catchment.....342
Figure D.6 Net elevation change under scenario 4DWD; Mahanadi catchment 342
Figure D.7 Dominant floodplain morphological response units (MRUs) under scenario 4DWD; Devi catchment.....343
Figure D.8 Dominant floodplain morphological response units (MRUs) under scenario 4DWD; Mahanadi catchment. 343
Figure D.9 Dominant channel morphological response units (MRUs) under scenario 4DWD; Devi catchment t. 344
Figure D.10 Dominant channel morphological response units (MRUs) under scenario 4DWD; Mahanadi catchment. 344

Academic Thesis: Declaration of Authorship

I, Sarah Jane Spinney

declare that this thesis and the work presented in it are my own and has been generated by me as the result of my own original research.

I confirm that:

1. This work was done wholly or mainly while in candidature for a research degree at this University;
2. Where any part of this thesis has previously been submitted for a degree or any other qualification at this University or any other institution, this has been clearly stated;
3. Where I have consulted the published work of others, this is always clearly attributed;
4. Where I have quoted from the work of others, the source is always given. With the exception of such quotations, this thesis is entirely my own work;
5. I have acknowledged all main sources of help;
6. Where the thesis is based on work done by myself jointly with others, I have made clear exactly what was done by others and what I have contributed myself;
7. None of this work has been published before submission

Signed:

Sarah Jane Spinney

Date: 9 April 2019

Acknowledgements

I would like to express my sincere gratitude to my supervisors Professor Stephen Darby and Professor John Dearing. Their guidance and motivation has been invaluable to me throughout the PhD process, particularly during the challenging times. I would also like to thank everyone on the DECCMA project for their support and insightful comments over the years. It has been a privilege to work in such a vibrant multidisciplinary team. I am also particularly grateful to Professor Tom Coulthard, Doctor Eli Lazarus, Professor Daniel Parsons and Doctor Julian Leyland for their advice throughout this research project. Last but certainly not least, I would like to thank my family and friends for supporting me over the years: in particular my partner, Alex; my parents, Jane and John; my sister, Emma; and my dear friend and 'PhD-buddy', Pav. Thanks to all of you for always supporting me through this journey. To my son, Finn (who was born just a couple of weeks after completion of the first draft of this project!), I hope I've made you proud.

This work is carried out under the Deltas, vulnerability and Climate Change: Migration and Adaptation (DECCMA) project (IDRC 107642) under the Collaborative Adaptation Research Initiative in Africa and Asia (CARIAA) programme with financial support from the UK Government's Department for international Development (DFID) and the International Development Research Centre (IDRC), Canada. The views expressed in this work are those of the creators and do not necessarily represent those of DFID and IDRC or its Boards of Governors.

Definitions and Abbreviations

ABM - Agent-based model: A class of computational model in which a system is divided into a collection of autonomous decision-making entities called agents (Bonabeau, 2012).

CA - Cellular automata model: A class of models in which the conditions in each cell are determined by a series of rules that govern how both it and its neighbouring cells will evolve.

C-L - Caesar-Lisflood: A cellular automata model comprising of the CAESAR landscape evolution model (Coulthard, 2000; 2016) and the Lisflood-FP 2d hydrodynamic flow model (Bates *et al*., 2010).

CSES - Complex social-ecological system: A system consisting of a biophysical unit and its associated social actors and institutions (Becker, 2010); linked by a series of non-linear interactions operative over a variety of temporal and spatial scales.

Distribution of island sizes: In this study islands within the catchment system are mapped by tracing the edges of land polygons that are completely surrounded by water of 1 metre depth or greater. As in Edmonds *et al.* (2011), no distinction is made between islands formed by deposition within the channel and those formed by channels that carve into existing land.

DPSIR - Driving forces-pressures-states-impacts-responses: A modelling framework that assumes cause-effect relationships between interacting components of environmental, social and economic systems, and also assumes that an infinite range of future states can be limited to a range of descriptive categories (Rotmans *et al*., 1994).

Fractal box-counting dimension: U measure of channel density. Edmonds *et al*. (2011) state that this value should vary from 1 to 2; where 1 suggests the object is self-similar and 2 suggests a more complex network that is space filling.

GBM - Ganges-Brahmaputra-Meghna: Delta in Bangladesh and India.

GIS- Geographical information system: A computational system utilised to capture, store and analyse geographic data.

IAT - Integrated assessment tool: A suite of interactive modelling frameworks and/or platforms that provides a systematic way to integrate knowledge across disciplines, models and tempo-spatial scales (Uthes *et al*., 2010).

NED Nearest-edge distance: The nearest distance to channelised or unchannelised water from any given point on land (Edmonds *et al.,* 2010).

Chapter 1 **Introduction**

1.1 Context

Situated at the dynamic interface between fluvial and coastal processes, deltas are major socioeconomic and ecological centres that are widely recognised as being highly vulnerable to the impacts of climate change (Olesen *et al.,* 2011). Whilst physical processes such as channel avulsion, bifurcation and subsidence render these complex social-ecological systems as inherently dynamic environments, this dynamism also creates fertile lowland habitats; rich in biodiversity and with abundant ecosystem services, explaining why populations have been attracted to settle in deltaic regions for millennia. Providing anthropogenic influence is minimal, the rate of sea-level rise is steady, and sediment supply is sufficient, deltas generally continue to extend seaward (Sanchez-Arcilla *et al.,* 1998; Wolinsky *et al.,* 2010). However, recent rapid population growth and associated changes in land use practices are accelerating the rate of morphological change in many deltas to an extent that has not previously been evident in the historical record (Seto, 2011).

In a sample of 40 deltas (inclusive of all global megadeltas) by Ericson *et al.* (2006), the average population density was estimated at 500 people per km^2, with the highest density in the Nile (1,920 people per km^2) and the largest population in the Ganges-Brahmaputra-Meghna (GBM) delta (~111 million people at the time of Ericson's publication). Whilst there are localised differences in the specific forms and magnitude of the anthropogenic influence in these deltas, arguably the two major human activities leading to accelerated relative sea-level rise and morphological change in deltaic environments are (1) enhanced subsidence due to groundwater and hydrocarbon extraction (Martin *et al.,* 2013) and (2) reduction of sediment supply due to dam and reservoir construction that reduces the delta's capacity to offset subsidence, resulting in increased erosion and land loss (Yang *et al.,* 2010; Syvitski *et al.,* 2005). These activities, combined with the additional pressures of pollution, salinisation and wetland reclamation, not to mention accelerated eustatic sea-level rise, are resulting in widespread declines in agricultural productivity and increased water stress in these environments (Wichelns, 2010; Stanley and Warne, 1993).

An exponential increase in human activity layered upon what is already a naturally dynamic regime has the clear potential to greatly affect the morphological response of deltas to the physical impacts of anthropogenic climate change, particularly eustatic sea-level rise (Nicholls *et al.*, 2007). Climatic hazards arise from both direct impacts (including increasing rates of eustatic sea-level rise, projected increases in precipitation/monsoon variability and rising surface temperatures) and indirect effects (such as erosion and biodiversity loss). This complex combination of natural and anthropogenic stressors will make it increasingly difficult for the millions of people exposed to these hazards to thrive in deltaic environments into the 21st century (Wong *et al.,* 2013). Furthermore, these hazards can manifest at multiple temporal and spatial scales: coastal inundation, for example, may occur as a slow-onset event due to gradual relative sea-level rise, or as a high magnitude, low frequency storm surge event (Gornitz, 1991).

It is critical that morphological research focuses on developing a clearer understanding of how these synergistic stressors, operating at a variety of temporal and spatial scales, influence the multidecadal evolution of deltaic environments. It is also crucial that the tools developed to simulate morphological change are able to be integrated successfully with other components of the biophysical system that influence the habitability of a delta. Furthermore, tools should be designed to be transferable for application in a broad range of deltaic settings; particularly the densely populated megadeltas of Asia and Africa. Given the unprecedented rate of environmental change that is already affecting the livelihoods of millions, it is vital that such tools are developed quickly in order to develop feasible adaptation strategies that could enable their populations to thrive under conditions of increasing climatic stress.

1.2 Aims and objectives

The overall aim of this study is to develop a management relevant set of tools that explore the nature of multidecadal morphological change in delta catchment systems under a range of climatic and environmental change scenarios. Whilst this study is undertaken at a site-specific level, these scenarios should encapsulate stressors that are common to a broad range of deltaic environments such that this methodological approach can be easily transferred. More specifically, the aims of this research can be split into three distinct objectives:

(1) To enhance our understanding of how emergent processes influence the multidecadal evolution of deltaic environments: Through adopting a complex systems approach it is hoped this investigation will enhance our understanding of how emergent processes influence the multidecadal evolution of deltaic environments. In particular I am interested in how deltaic catchments may respond to increasing conditions of climatic stress. Compared to terrestrial systems, there are relatively few studies that focus on the successful simulation of long-term emergent phenomena in coastal catchments (Dearing *et al.* 2006), and even fewer in deltas. Furthermore, compared to tributary systems, there are far fewer studies that attempt to use quantitative metrics to describe emergent features in distributary channel networks (Edmonds *et al.,* 2011; Fagherazzi *et al.,* 1999). By demonstrating the application of a range of metrics and how they can be utilised to help improve our understanding of the emergent system, this objective can make a significant contribution from a methodological perspective towards filling these knowledge gaps in deltaic regions.

(2) To explore how these changes in the emergent morphological system may influence the habitability of the delta: This objective will explore how the metrics above may be utilised to identify important connections between the emergent morphological system and factors that influence the habitability of the delta. Specifically, three research questions are defined as follows:

(i) How do changes in these slow-onset, emergent processes effect the hazard within the delta to short-term, extreme events, such as a severe tropical cyclone?

(ii) How do these changes influence potential changes in habitat cover? Specifically morphological metrics such as hypsometry and inundation

extent will be used as a proxy for what kind of vegetation will thrive in these conditions.

(iii) How effective is the model as a platform to investigate potential engineering strategies that could enhance the resilience of a particular location? Here the focus is on strategies that involve re-naturalising the channel network.

(3) To provide outputs that are directly useful to stakeholders: It is hoped that the application of the morphological metrics discussed above, combined with the novel way in which these are utilised to explore impacts to the broader social ecological system, provides a unique framework of tools that could be utilised in the Mahanadi region. As is discussed in detail in chapter 4, the Mahanadi Delta provides an ideal case study to explore a broad range of environmental stressors, relating to both climate change and anthropogenic activity, in a biophysically diverse deltaic landscape. Thus whilst transferability to global deltas is crucial to the methodological design of this project, it is equally hoped that the outputs of this research can be used to provide valuable information to stakeholders in the Mahanadi region. The Mahanadi system has regularly been highlighted in recent research as one that is at significant risk from climate change and increased anthropogenic interventions within its distributary network (Syvitski *et al.,* 2009; Jena *et al.,* 2014). Through the production of various hotspot maps and time series data, it is hoped that these outputs could contribute towards the development of climate-resilient adaption strategies.

The structure of this thesis is as follows:

Chapter 2 – Modern controls on delta morphology

This chapter introduces the fundamental geomorphological processes operating in deltaic regions. It reviews the dominant anthropogenic, climatic and biogeomorphological controls influencing the evolution of deltas over the 21st century.

Chapter 3 – Modelling deltas

This chapter discusses some of the challenges faced with regards to modelling deltas, within the broader context of modelling complex social-ecological systems and emergent phenomena. It then goes on to review some of the models available

to study deltaic evolution, based on the current literature. Finally, the reasons for choosing the model utilised in this research project are presented.

Chapter 4 – Study site

This chapter introduces the chosen study site for this project, the Mahanadi Delta in India. It presents the morphological setting of the delta and the dominant stressors affecting the biophysical system.

Chapter 5 – Methodology

This chapter provides a thorough description of the methodology employed in this study, including scenario design, model setup and model validation.

Chapter 6 – Morphological modelling

This chapter presents and discusses the results of morphological modelling.

Chapter 7 – Linking morphology and habitability

This chapter explores the questions presented in research objective 2. The results of additional model runs - exploring (1) morphology and flood hazard; (2) morphology and potential habitat cover change; and (3) re-naturalising the channel network - are presented and discussed.

Chapter 8 – Conclusions

This chapter presents a summary of the key findings of this study, before discussing its successes and limitations.

Chapter 2 Modern Controls on Delta Morphology

2.1 Morphological Processes in Deltaic Environments

Before analysing the impacts of recent climatic change and anthropogenic development on modern deltas, it is important to re-examine the processes that result in their formation and long-term evolution in order to place these changes within a historical context (Tamura *et al*., 2012). Deltas are dynamic, partially subaqueous depositional landforms that occur where river systems carrying significant sediment loads enter the sea or another body of water. Over millennial scales, delta progradation can be seen as "sensitive recorders of the interplay between climate and tectonics" (Jerolmack and Swenson, 2007: 1), fundamentally being controlled by a delicate balance between sediment supply and relative sea-level. The iconic ternary framework developed by Galloway (1975) provides a simple way to classify distinctive delta planforms (figure 2.1); whereby morphology is postulated to be controlled by the changing intensity of, and subsequent balance between, fluvial, wave and tidal processes.

Whilst this framework provides a strong theoretical base, in reality multiple drivers across multiple temporal and spatial scales create a dynamic, complex and diverse morphological landscape. As will be discussed in detail in the next chapter, there are a number of more intricate metrics that can be used to describe delta morphometry, and in particular the emergent morphological features that comprise the distributary channel network. Whilst there is no precise definition as to what components of a deltaic landscape are classified as emergent morphological phenomena, a broader classification across all landscapes focuses attention on morphological features that only become visible at a given scale larger than that of process-form relationships (Schumm and Lichty, 1965). Thus for the purpose of this study, analysing change over multidecadal temporal scales, examples of emergent morphological phenomena in a delta focus on the structure of the channel network; including the fractality of the distributary channels, the distribution of islands, and channel migration.

As a river discharges into the sea its velocity is reduced abruptly resulting in deposition of the river's sediment load. The rate of this sedimentation process is dependent upon an array of fluvial and basin characteristics, including the density

of the water body relative to the river water, the velocity of the river flow, and the extent of frictional retardation at the coast (Huddart and Stott, 2010). Providing adequate sediment supply is maintained to offset eustatic sea-level rise and subsidence (due to tectonic activity and soil compaction), this deposition will continue to extend seaward forming a singular deltaic lobe. Initiation of this process in present-day megadeltas occurred almost simultaneously during the Holocene (Zong *et al.,* 2009), when an abrupt deceleration in the rate of postglacial eustatic sea-level rise ~6ka resulted in the reduction of accommodation space such that deposits began to prograde (Stanley and Warne, 1994). Since this initial deposition, these deltas have followed individual evolutionary pathways depending on their specific geomorphic setting. The rate of progradation in the Mahanadi Delta in eastern India over the Holocene has been approximately 9.1 km per millennia (Somanna *et al.,* 2013). This compares to 7.5 km and 10 km in the Krishna and Cauvery deltas respectively, also both located on the eastern coast of India; 20 km in the Mississippi delta, USA; 3.5 km in the Rhone delta, France; 8.5 km in the Po delta, Italy; and 30 km in the GBM delta, India and Bangladesh (Somanna *et al.,* 2013).

Jerolmack (2009) identifies two fundamental unit processes that dominate the creation of complex distributary networks, thereby determining the surface topography of the deltaic plain: avulsion and mouth-bar deposition. The process of avulsion is also known as delta switching: as the deltaic lobe advances the gradient of the active channel decreases, resulting in the deposition of sediment within the channel and thus raising the elevation of the bed relative to the floodplain. This increases the likelihood of the levees being breached during a flood event, therefore facilitating avulsion to a new channel that provides a more efficient, steeper pathway to the ocean (Slingerland and Smith, 1998). Following this switching event, the abandoned or partially-abandoned channel naturally lowers due to a reduction in fluvial sediment supply and becomes increasingly tidally-dominated (Woodroffe, 2002). In heavily-vegetated deltas, or those comprised of cohesive sediment, avulsion tends to be the dominant mechanism via which the delta undergoes lateral expansion, creating a series of long distributaries across the deltaic plain. However, in highly erodible systems such as the Mississippi delta, bank erosion (often referred to as ‘sweeping’) has been found to be the primary control of channel migration, inhibiting the formation of multiple channels (Hudson and Kesel, 2000). The precise mechanisms controlling

the timing of avulsion is at present poorly understood, in part because the process of avulsion occurs across a variety of temporal and spatial scales. Lobe switching at the apex of the Mississippi occurs ~1ka for example, whereas intradelta lobe switching occurs within the active channel once a century (Edmonds *et al.,* 2009).

The second fundamental process described by Jerolmack (2009) is mouth-bar deposition at the active river mouth and subsequent channel bifurcation, leading to the generation of complex fractal networks whereby the delta exhibits a systematic decrease in channel lengths, widths, and depths with increasing bifurcation order (Edmonds and Slingerland, 2007). These branching distributary networks tend to be found in prograding fluvial-dominated deltas as high wave energy acts to suppress mouth-bar formation (Jerolmack and Swenson, 2007). Mid-channel bar formation, which can occur anywhere upstream of the river mouth, also acts in this way to create complex fractal networks across the existing extent of the delta plain.

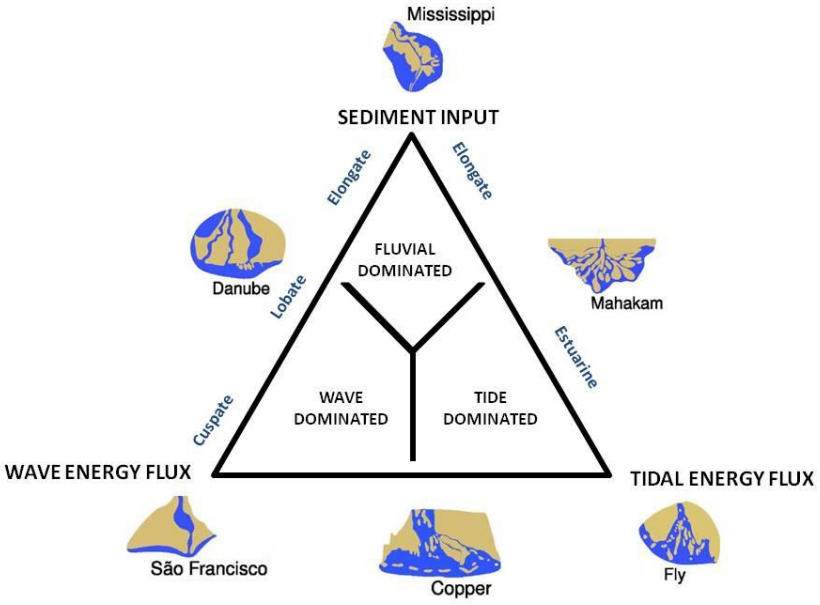

Figure 2.1 Ternary framework for the classification of delta morphologies based on Galloway (1975) and indicating specific delta type sites (Delta image sources: geocaching.com)

Various biotic components are intimately linked with the physical processes that drive deltaic evolution; creating a complex web of biogeomorphological interactions that are fundamental in determining its morphology and the availability of ecosystem services (Pasternack and Brush, 2002). The extent and

complexity of these interactions vary across time and space. The role of biogeomorphological processes is particularly important in the coastal fringes of the delta, where small changes in factors such as salinity and elevation can have large consequences in terms of habitat cover. Morphological metrics can thus help to predict floral and faunal assemblages on deltas. Nearest-edge distance (NED), for example, is defined as the shortest straight line distance from a given point to water. Edmonds *et al.* (2011) describe how deltas with a high average NED might be preferentially colonized with species that need less access to water.

The fertile lowlands of delta plains provide a diverse range of habitats, supporting a rich biodiversity and providing abundant ecosystem services. 'Ecosystem services' is the term used to describe the multitude of benefits humans gain from ecosystems. Maintaining the provision of these services is viewed as synonymous with maintaining ecosystem health. The Millennium Ecosystem Assessment (2005) categorises services into four broad groups (figure 2.2): **provisioning**, describing products obtained directly from ecosystems, such as fuel; **regulating**, describing benefits gained from regulatory ecosystem processes, such as waste decomposition; **cultural**, describing non-material benefits humans gain through interaction with the natural environment; and lastly, **supporting**, describing those services that are necessary for the production of all other ecosystem services. These supporting services include processes such as soil formation, water cycling and primary production (MEA, 2005).

A high proportion of those living in deltaic environments generate their income through rural livelihoods, and are thus highly vulnerable to changes in ecosystem services (ESPA, 2015). It is therefore important to understand how changes in the morphological regime of deltaic CSESs will affect the capacity for certain ecosystem services to be maintained over forthcoming decades. Ligon *et al*. (1995) argue that geomorphological studies directed at ecologically significant morphological processes in hydrological systems may be more valuable to understanding long-term ecosystem health following human disturbance than biological research alone. In their study investigating the downstream geomorphic impact of dams, the authors emphasise how the capacity for ecosystem services to be maintained is intimately linked to morphological processes: reduction in downstream sediment supply, for example, as a consequence of dam installation on the McKenzie river in Oregon, is inhibiting

mouth-bar deposition thus causing the river to become exclusively a single-thread channel. Ligon *et al*. (1995) describe the negative impact this has had on the native salmon population, which as a keystone species has a detrimental effect over ecosystem health as a whole (Willson and Halupka, 1995).

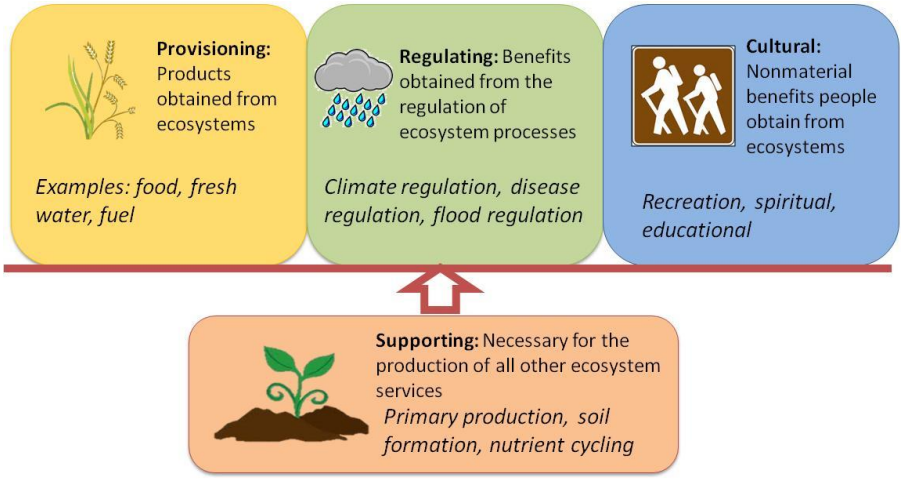

Figure 2.2 The four categories of ecosystem services, as defined by the Millennium Ecosystem Assessment (2005)

Mangrove forests, common across a large number of deltas in tropical regions, provide a perfect example of how important biogeomorphological feedbacks are within the deltaic system. These unique halophyte forests provide a vast range of ecosystem services (figure 2.3): They are biodiversity hotspots, acting as breeding sites for many species of bird and marine wildlife (Alongi, 2002). The forests also provide shelter for many commercially important species, with positive correlations observed between coastal shrimp and fish catches and mangrove area cover (Baren and Hambrey, 1998). Mangroves also act as an efficient buffer against storm surge and floods; limiting coastal erosion rates and reducing death toll and structural damage during extreme storm events (Das, 2009). The distribution of mangroves is intrinsically linked to geomorphological development, and can be viewed as a direct response to microtopographic characteristics related to elevation and the frequency of inundation (Baltzer, 1970 in Woodroffe, 1992).

A number of 'short' and 'long' feedback mechanisms between mangrove vegetation and the morphological environment may be identified: A 'short' mechanism refers to those that occur over limited spatial and temporal scales with few interacting factors (figure 2.4a). A decline in forest area due to a sudden

coastal erosion event such as a storm, for example, instantly renders the region less morphologically resilient to further erosive forces, thus amplifying the rate at which erosion occurs. As a result the immediate habitable land area is reduced and the area behind the remaining forest is subject to increasing erosive forces (Chua, 1992). A 'long' mechanism refers to a more complex network of interactions between the ecological and morphological systems: Although the initial trigger of the change may be the same as in the 'short' feedback loop, the consequences of the change propagate further into the system, and thus operate over longer timescales (figure 2.4b). A decline in forest area due to coastal erosion, for example, will as before result in a positive feedback mechanism through which the erosion rate is amplified and inundation increased. In many tropical deltas, large areas of agricultural land are protected from coastal forces by mangrove forests (Mahata *et al*. 2010). A decline in mangrove area will therefore have detrimental impacts to agricultural yields, resulting in subsequent changes to habitat cover further inland. Alongi (2009) describes further how a reduction in forest density will also impact on the natural feedback relationships that exist among the vegetation, water and sediments within the mangrove ecosystem itself: the presence of trees induces friction to slow the movement of water and sediment, allowing the waterway to silt and elevation to increase. As forest density decreases tidal flow velocity increases, resulting in a reduction of aggradation rates and decreased resilience to erosive forces. Furukawa and Wolanski (1996:3) emphasise the importance of mangrove ecosystems as sediment sinks, arguing that they are "not just opportunistic trees colonising mud banks but actively contribute to the creation of mud banks". The spatial extent to which the forest plays a role in influencing morphological processes can also be thought of in vertical dimensions: the fine roots of mangrove trees act as efficient sediment binders (Woodroffe, 1992), slowing or preventing bank erosion to a depth of several metres (Wolanski *et al.,* 2009); the trunks limit tidal flow velocity and dissipate hydraulic energy; and the canopy density influences the success of other species that inhabit the mangrove ecosystem, through controlling exposure to wind, precipitation and sunlight (Alongi, 2009).

What is clear from the example above is that understanding how these feedback dynamics operate and the spatial scale over which they occur is crucial in order to provide accurate multidecadal morphological projections. At present there is a significant knowledge gap in the modelling of coastal wetlands, in that

many studies completely neglect the role of these interactions (Wolanski *et al*., 2009; Reyes, 2009). How exactly this study aims to integrate morphological processes with habitat cover is presented in further detail in the methodology in chapter 5.

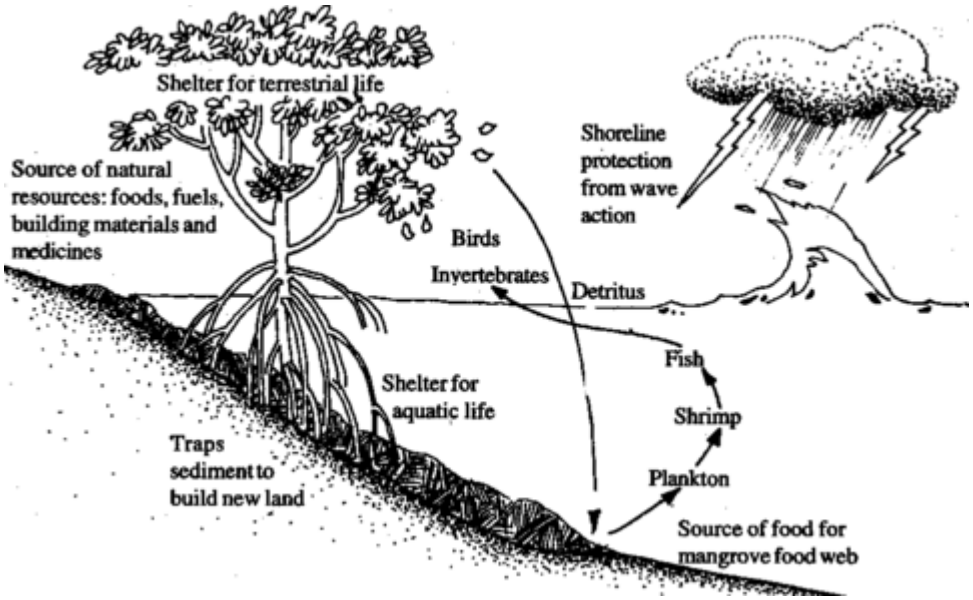

Figure 2.3 Examples of ecosystem services provided by mangrove forest (Source: coastvserosion.wikispaces.com)

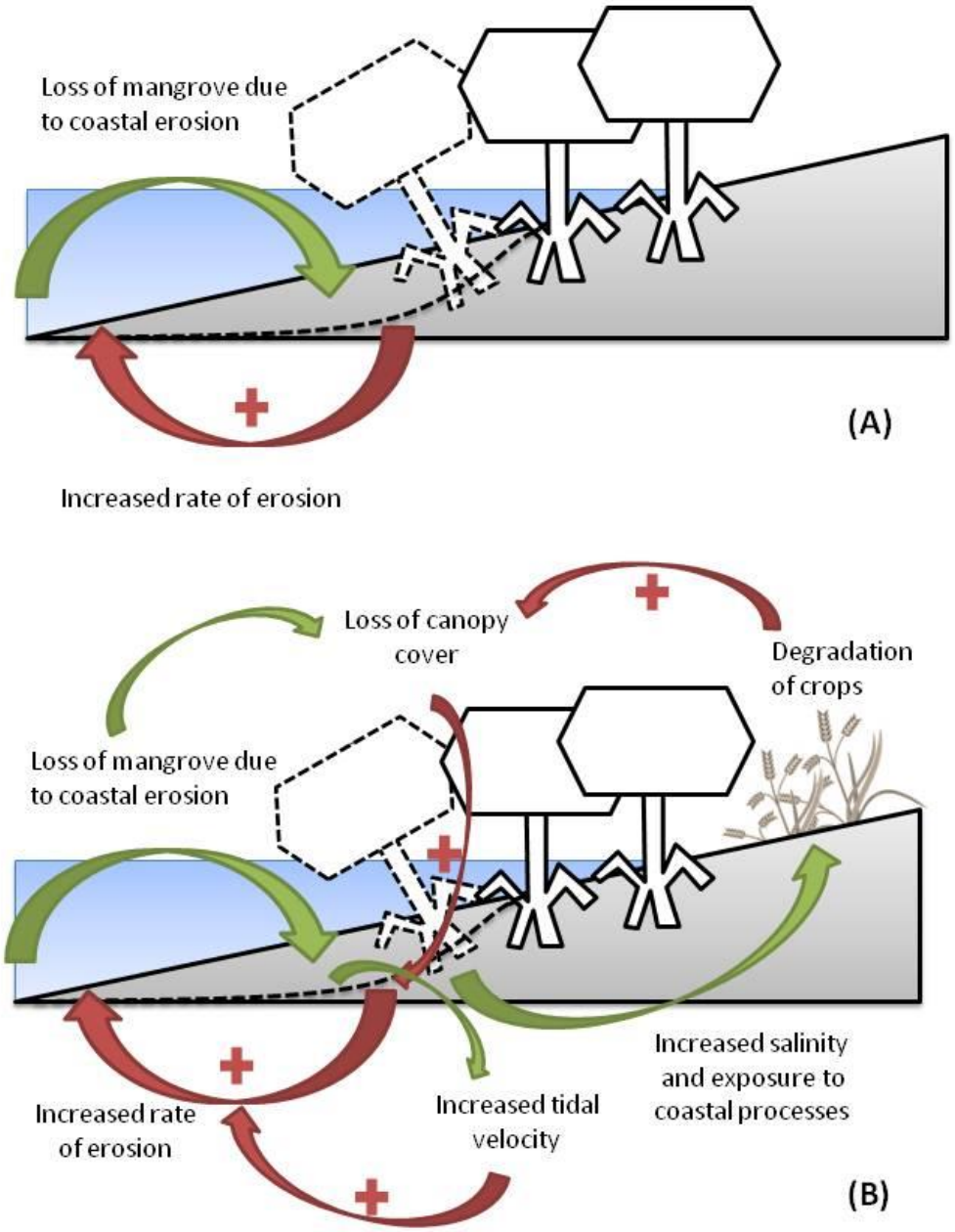

Figure 2.4 Example of a short (A) and long (B) feedback mechanism between supporting ecosystem services and morphological processes. Short mechanisms occur over limited spatial and temporal scales with few interacting factors. Conversely, a long mechanism refers to a more complex web of interactions, whereby the consequences of the change propagate further into the system.

Over the last century, climate change and an exponential increase in anthropogenic activity have acted to modify the delicate balances established between the processes outlined above, resulting in unprecedented rates of morphological change in many deltas worldwide (see table 2.1 for a summary of global data compiled by Syvitski *et al.,* 2009). Thus whilst modern controls on delta morphology remain fundamentally similar to those influencing historical deltas, the way in which we understand these processes must be re-examined in order to assess the impacts of accelerated environmental change. Key research themes have shifted in recent years from understanding the centennial evolution of deltaic environments towards developing a better knowledge of how delta growth dynamics and unit processes are modified at the multi-decadal scale (Woodroffe, 2010; Wolinksy *et al.,* 2010). The methodological approaches by which this is currently being achieved, and the challenges they encompass, are discussed in greater detail in chapter 3. Here, two dominant anthropogenic controls (sediment starvation and accelerated subsidence) and two major climatic pressures (eustatic sea-level rise and meteorological extremes) acting on these environments are discussed within the context of impacts to the deltaic morphological regime, and the subsequent effects this has on ecosystem services.

Table 2.1 Syvitski *et al.* (2009:684) present environmental data from 33 deltas. Nearly all have reduced or eliminated aggradation rates and 13 show a reduction in the number of distributary channels. (For storm surge data LP refers to low potential of event occurrence; MP to moderate potential and SP to significant potential).

Delta	Area < 2 m above sea level (km^2)	Storm-surge area (km^2)	Recent area of river flooding (km^2)	Recent area of *in situ* flooding (km^2)	Sediment reduction (%)	Floodplain or delta flow diversion	Distributary channel reduction (%)	Subsurface water, oil and gas mining	Early-twentieth-century aggradation rate (mm yr^{-1})	Twenty-first-century aggradation rate (mm yr^{-1})	Relative sea-level rise (mm yr^{-1})
Deltas not at risk: aggradation rates unchanged, minimal anthropogenic subsidence											
Amazon, Brazil	1,960	0; LP	0	9,340	0	No	0	0	0.4	0.4	Unknown
Congo, DRC	460	0; LP	0	0	20	No	0	0	0.2	0.2	Unknown
Fly, Papua New Guinea	70	0; MP	140	280	0	No	0	0	5	5	0.5
Orinoco, Venezuela	1,800	0; MP	3,560	3,600	0	No	0	Unknown	1.3	1.3	0.8–3
Mahaka, Borneo	300	0; LP	0	370	0	No	Unknown	0	0.2	0.2	Unknown
Deltas at risk: reduction in aggradation, but rates still exceed relative sea-level rise											
Amur, Russia	1,250	0; LP	0	0	0	No	0	0	2	1.1	1
Danube, Romania	3,670	1,050	2,100	840	63	Yes	0	Minor	3	1	1.2
Han, Korea	70	60	60	0	27	No	0	0	3	2	0.6
Limpopo, Mozambique	150	120	200	0	30	No	0	0	7	5	0.3
Deltas at greater risk: reduction in aggradation where rates no longer exceed relative sea-level rise											
Brahmani, India	640	1,100	3,380	1,580	50	Yes	0	Major	2	1	1.3
Godavari, India	170	660	220	1,100	40	Yes	0	Major	7	2	3
Indus, Pakistan	4,750	3,390	680	1,700	80	Yes	80	Minor	8	1	>1.1
Mahanadi, India	150	1,480	2,060	1,770	74	Yes	40	Moderate	2	0.3	1.3
Parana, Argentina	3,600	0; LP	5,190	2,600	60	No	Unknown	Unknown	2	0.5	02-Mar
Vistula, Poland	1,490	0; LP	200	0	20	Yes	75	Unknown	1.1	0	1.8
Deltas in peril: reduction in aggradation plus accelerated compaction overwhelming rates of global sea-level rise											
Ganges, Bangladesh	6,170	10,500	52,800	42,300	30	Yes	37	Major	3	2	8–18
Irrawaddy, Myanmar	1,100	15,000	7,600	6,100	30	No	20	Moderate	2	1.4	3.4–6
Magdalena, Colombia	790	1,120	750	750	0	Yes	70	Moderate	6	3	5.3–6.6
Mekong, Vietnam	20,900	9,800	36,750	17,100	12	No	0	Moderate	0.5	0.4	6
Mississippi, USA	7,140	13,500	0	11,600	48	Yes	Unknown	Major	2	0.3	5–25
Niger, Nigeria	350	1,700	2,570	3,400	50	No	30	Major	0.6	0.3	7–32
Tigris, Iraq	9,700	1,730	770	960	50	Yes	38	Major	4	2	4–5
Deltas in greater peril: virtually no aggradation and/or very high accelerated compaction											
Chao Phraya, Thailand	1,780	800	4,000	1,600	85	Yes	30	Major	0.2	0	13–150
Colorado, Mexico	700	0; MP	0	0	100	Yes	0	Major	34	0	2–5
Krishna, India	250	840	1,160	740	94	Yes	0	Major	7	0.4	3
Nile, Egypt	9,440	0; LP	0	0	98	Yes	75	Major	1.3	0	4.8
Pearl, China	3,720	1,040	2,600	520	67	Yes	0	Moderate	3	0.5	7.5
Po, Italy	630	0; LP	0	320	50	No	40	Major	3	0	4–60
Rhone, France	1,140	0; LP	920	0	30	No	40	Minor	7	1	2–6
Sao Francisco, Brazil	80	0; LP	0	0	70	Yes	0	Minor	2	0.2	3–10
Tone, Japan	410	220	0	160	30	Yes	N/A	Major	4	0	>10
Yangtze, China	7,080	6,700	3,330	6,670	70	Yes	0	Major	1.1	0	3–28
Yellow, China	3,420	1,430	0	0	90	Yes	80	Major	49	0	8–23

2.2 Anthropogenic Controls

Sediment starvation and accelerated subsidence are arguably the two dominant anthropogenic controls that act to alter the morphological regime in modern deltaic environments. Of course, the former may also occur naturally in principle, but is in this modern era more commonly attributed to anthropogenic interventions.

2.2.1 Sediment Starvation

For several millennia, increasing human development in the catchments upstream of deltas led to increased terrestrial erosion and a corresponding ample sediment discharge that promoted net aggradation in many deltas (Syvitski *et al.,* 2005). However, over recent decades changes in land use practices and widespread channel modification have decreased the sediment load of many rivers, thus triggering erosion in their deltas as the fluvial accretion rate is no longer sufficient to offset sea-level rise and subsidence (Yang *et al.,* 2010; Walling and Webb, 1996). Deltas situated on coastlines subject to high wave energy are particularly sensitive to changes in fluvial sediment supply as they are highly susceptible to coastal erosion (Giosan *et al.,* 2006). In a recent study by Syvitski *et al.* (2009) comparing historical maps (covering the period 1760-1922) and high resolution satellite data, the authors found that of the 33 major world deltas analysed all had reduced or eliminated sediment delivery (table 2.1). The most widespread cause of sediment starvation in modern deltas is due to the construction of dams (Blum and Roberts, 2009). The downstream channel of the Yangtze delta in China, for example, has shifted from an accretion rate of ~90MT.yr^{-1} between 1950-1980, to an erosion rate of ~60MT.yr^{-1} following the closure of the Three Gorges Dam in 2003 (Yang *et al.,* 2010). Ly (1988) presents evidence for rapid increases in localised shoreline retreat of up to 10m.yr^{-1} following the closure of the Akosombo Dam in 1964, located 60 km upstream of the Volta delta in Ghana. However, as described by Anthony and Blivi (1995), the strong littoral current (1.5x10^{6}m^{3}.yr^{-1}) that dominates sediment transport along the Bight of Benin coast has resulted in spatially variable erosion rates. This effect has been exacerbated by the subsequent hard coastal engineering that has been installed to manage it. Some areas of the delta display shoreline advance rates of ~1m.yr^{-1} due to sediment delivery from heavily eroded regions becoming trapped in natural and artificial embayments. Following the closure of the Aswan Dam in 1964, sediment delivery to the Nile delta in Egypt has been almost entirely

eliminated, resulting in net transgression of the shoreline (Frihy, 1988; McManus, 2002). The annual flooding of the Nile that has been the lifeblood of Egyptian agriculture for millennia was immediately stopped following the closure of the dam, due to the reduced delivery of sediment-rich nutrients to the deltaic plain (Vörösmarty *et al.,* 2009). The small quantity of sediment that does flow through the Aswan Dam (estimated at ~2% of the load before its construction) is later trapped by a network of irrigation channels (Stanley and Warne, 1998). Thus, what water does reach the coastline now provides almost no sediment to promote aggradation of the delta, and is also polluted from agricultural practices (Shaban *et al.,* 2010). The Rosetta promontory in the western Nile delta is particularly vulnerable to coastal erosion due to sediment starvation from both fluvial and longshore sources, combined with high exposure to wave action. Indeed, 12.29 km^2 of land was lost at the Rosetta headland between 1973 and 2008, with the highest annual rate of erosion observed in 1978 at 132$m.yr^{-1}$ (Hereher, 2011). However, as is the case along the Bight of Benin, reworking of sediments driven by longshore currents can create significant localised shoreline advance reaching rates of 6.8$m.yr^{-1}$ in the Nile delta despite the elimination of fresh fluvial sediment supply (Frihy, 1998).

Whilst river damming generally causes the net transgression of delta systems, the examples above highlight how sediment delivery to these dynamic environments is a non-linear process that occurs as a hierarchy of pulses operating over a wide range of spatial and temporal scales (Day Jr. *et al.,* 2007). It is therefore crucial that future research takes into account localised variability due to factors such as littoral transportation and seasonal variations in wave energy and sediment delivery, in order to identify both multidecadal evolutionary trends in these environments and areas that are exceptions to those trends.

After river damming, the second most prevalent cause of sediment starvation in deltaic environments is channelization and modifications to the existing distributary network. In many deltas the numbers of active channels has been reduced for navigational purposes, and of those many have become fixed with artificial levees in order to protect local communities from flooding (Syvitski *et al.,* 2007). This prevents the natural sedimentation of the deltaic plain via the lateral channel migration processes described previously, triggering erosion and depriving the floodplain of vital nutrients, often with detrimental effects to ecosystem productivity (Day Jr. *et al.,* 1999). Syvitski *et al.* (2009) show how the

number of mobile distributary channels transporting sediments across the Indus flood plain in Pakistan have been dramatically reduced since the construction of a complex irrigation network during the 1960s (figure 2.5). The authors also note how fixation from levee construction increases within-channel aggradation rates, thereby creating distributaries that are super-elevated relative to their surrounding floodplain. This has been observed on the Po delta in Italy, where channels are becoming super-elevated at rates of 4-10 $cm.yr^{-1}$ (Syvitski, 2008). As a consequence, flood risk can actually be locally increased by the very schemes designed to mitigate against such a hazard.

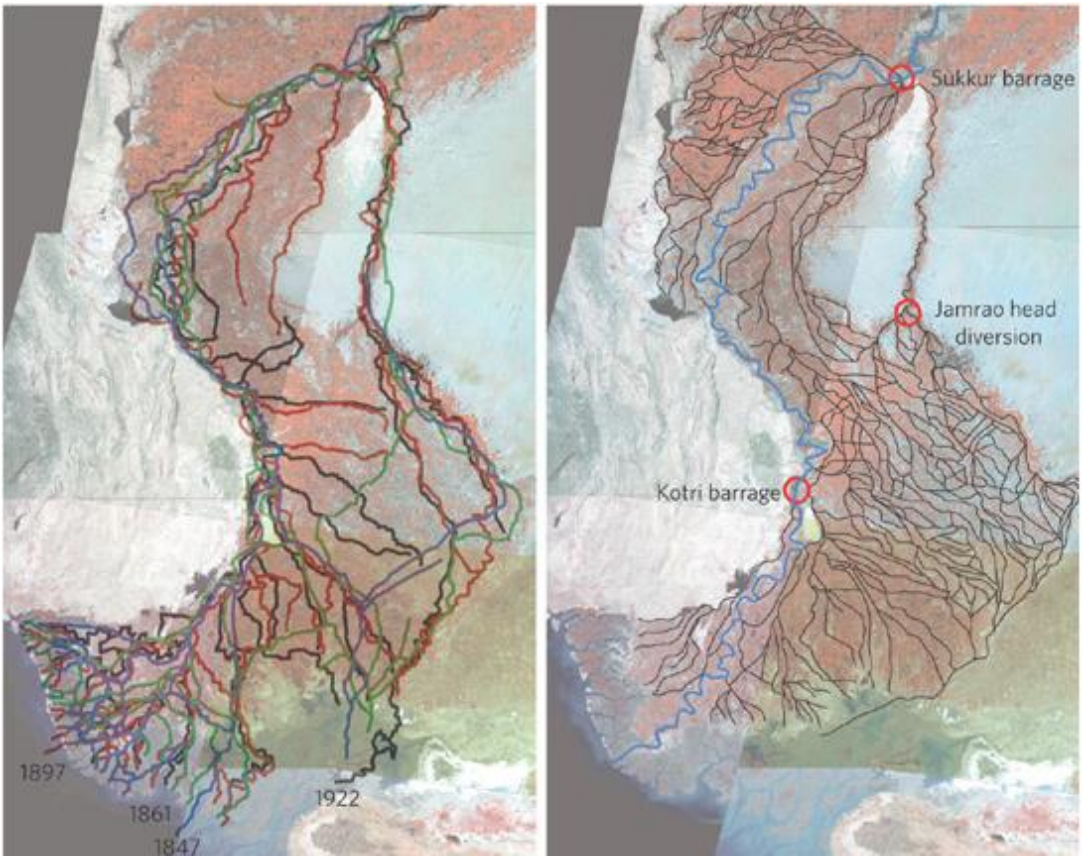

Figure 2.5 Left Image: Historical location of distributary channels in the Indus delta (colour, year): blue, 1847; green, 1861; red, 1897; black, 1922. Right Image: Modern irrigation channel system with main water distribution stations. Only one channel (blue) now carries significant water to the ocean. (Source: Syvitski *et al.*, 2009: 683).

Increasing sediment delivery has become a central concern in delta restoration projects over recent years (Giosan *et al.*, 2013). Often this will require management decisions to be made outside of the delta itself, such as the installation of flushing mechanisms to allow sediment to flow past dams (Kondolf

et al., 2014). Within the delta system most restoration strategies focus on increasing the trapping efficiency of the plain and coast (Kim *et al*., 2009). Giosan *et al*. (2014) suggest four methods of restoration that mimic natural processes, a concept also known as 'de-engineering' (figure 2.6). Such strategies include: channelization, in which new channels are installed to spread sediments across the plain and promote natural wetland accretion; deliberately breaching levees to create crevasse splays; constructing artificial internal subdeltas, resulting in increased sedimentation in lakes and lagoons; and lastly, lobe building in areas naturally protected from high wave energy and tidal action. In coastal regions of the deltaic plain, the installation of hard engineering structures may be the only viable option to trap sediment in the most vulnerable locations. Engineering however is expensive: the Mississippi Plan incorporates numerous strategies to prevent future land loss in the Mississippi delta, including the installation of new defences; channel diversion; channel dredging and marsh restoration. Initiated by the Louisiana Coastal Protection and Restoration Authority, the plan will run for approximately 50 years at an estimated cost of US$500m-$1.5b a year (Giosan *et al*., 2014). This magnitude of funding may not be viable in poorer nations, or indeed where catchments cross socio-political borders. Where managed retreat is a viable option, this may reduce pressure elsewhere both morphologically and financially. In the Mahanadi Delta, Das *et al*. (1997) have suggested restoration of mangrove forest as another potential management strategy to alleviate some negative impacts of climate change. Similarly, Wetlands International (2014c) have also taken an ecologically-based approach to management in the Mahanadi Delta; developing strategies to maximise freshwater availability to the Chilika Lagoon ecosystem.

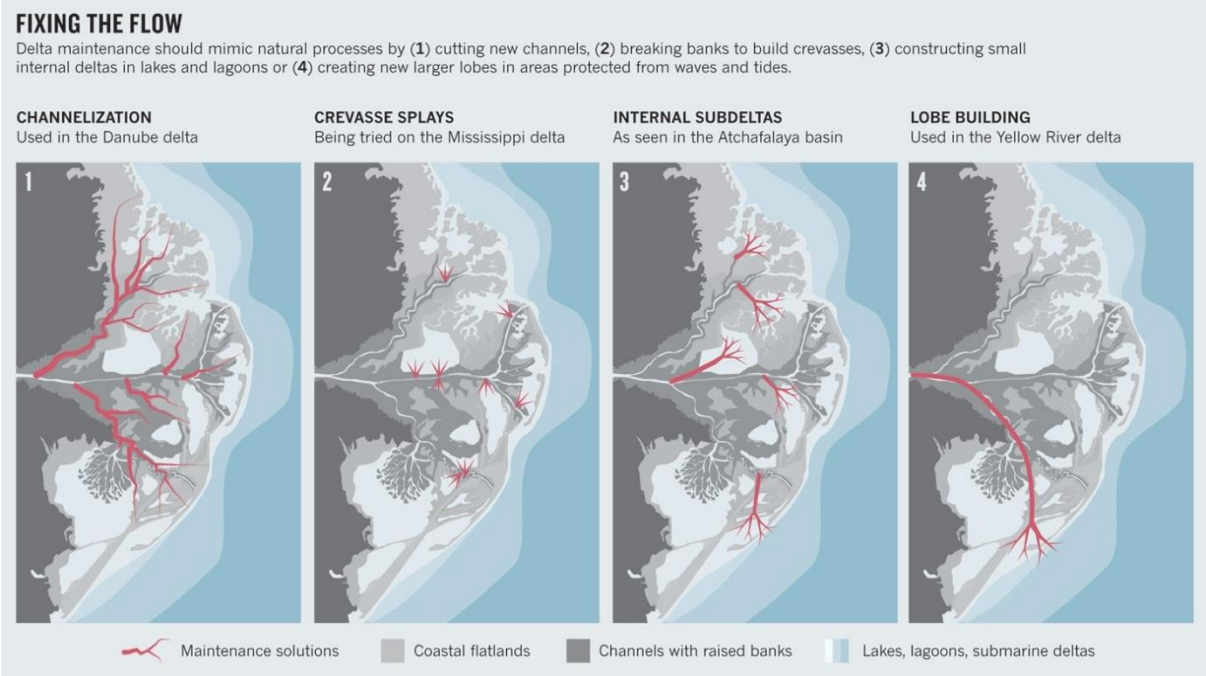

Figure 2.6 Methods of delta restoration that mimic natural processes (Source: Giosan *et al.*, 2014).

2.2.2 Groundwater and hydrocarbon extraction

When new sediment is added to deltaic deposits, this additional weight reduces the water content in the underlying sediment due to reduced between-grain-void space, causing natural subsidence of the delta surface (Morton and Bernier, 2010). The rate at which this occurs varies between deltas: generally the rate does not exceed 3mm.yr^{-1} (Meckel *et al.,* 2007), however in areas predominantly composed of peat and sand deposits, such as the Mississippi delta in the USA, the rate of natural compaction may reach magnitudes of ~5mm.yr^{-1} (Torbjörn *et al.*, 2008). Peat deposits in deltas that are intensively farmed subside particularly rapidly due to the creation of an aerobic environment that favours the rapid microbial oxidation of carbon (Ingebritsen *et al.,* 2000). Natural compaction rates therefore vary laterally across a delta surface dependent upon the location of these fast-compacting deposits, and will also vary vertically as the rate slows with depth of burial (Bahr *et al.,* 2001 in Syvitski, 2008). Anthropogenic compaction, often as a result of hydrocarbon and groundwater extraction, can accelerate the subsidence of delta plains substantially, resulting in amplified relative sea-level rise, inundation and coastal erosion. Mazzotti *et al.* (2009) show

that natural compaction of shallow Holocene deposits in the Fraser delta, Canada, results in subsidence of < 2 $mm.yr^{-1}$, whereas areas of the delta that are affected by artificial loading are subsiding locally at rates of 8 $mm.yr^{-1}$. Over the late 20^{th} century, subsidence rates in the Po Delta in Italy have reached 300 $mm.yr^{-1}$ due to large scale methane extraction (Teatini *et al.,* 2011). In the Chao Phraya delta in Thailand, excessive groundwater extraction triggered subsidence that peaked at ~200 $mm.yr^{-1}$ during the mid-80s (Haq, 1994). This rapid subsidence, combined with sediment starvation and the deforestation of mangroves, resulted in erosion rates of ~1 $km.yr^{-1}$ at the active river mouth during this time period (Saito *et al.,* 2007). In many of the examples cited above, efforts have been made to reduce accelerated subsidence from water and hydrocarbon extraction through stricter regulation. The subsidence rate in the Po delta, for example, has since been reduced to 4 $mm.yr^{-1}$ (Simeoni *et al.,* 2007). Strategies can also be implemented to reduce subsidence in regions suffering with relatively high rates of natural compaction, such as the Mississippi delta: Ingebritsen *et al.* (2000) describe how intentional shallow flooding can be used in certain locations to slow peat oxidation, thus decreasing the rate of subsidence.

2.3 Climatic Controls

Further adding to the stresses of increasing human activity are two major climatic pressures: eustatic sea-level rise and the increased occurrence of meteorological extremes. Climate change does of course have an anthropogenic component, but for the purpose of this study is discussed separately from direct human interventions to deltaic processes.

2.3.1 Eustatic sea-level rise

Accelerated eustatic sea-level rise as a result of recent climatic change is one of the greatest challenges deltaic environments will face over forthcoming decades. According to the Intergovernmental Panel on Climate Change (IPCC) Fifth Assessment Report (Church *et al*., 2013), global mean sea-level rise (GMSLR) occurred at a rate of 3.2 $mm.yr^{-1}$ between 1993 and 2010, mainly due to thermal expansion of the oceans and reduction of terrestrial freshwater stores. It is very likely that the rate of GMSLR by 2100 will exceed the present rate under all representative concentration pathways (RCPs); for RCP8.5, the rise by 2100 is 0.52-0.98 m with a rate during 2081–2100 of 8-16 $mm.yr^{-1}$. Although confidence in these global projections is high, regional changes in sea-level are far more uncertain and could be far greater than the likely limits expressed above as a result of isostatic rebound, ocean circulation patterns, local bathymetry and interannual variability (Zhang and Church, 2012). As has already been discussed, relative sea-level rise in deltas is amplified due to sediment starvation and accelerated subsidence (Mcleod *et al.,* 2010). Over decadal to centennial scales, the impacts of sea-level rise include increased flooding, coastal erosion and saltwater intrusion as a result of slow-onset inundation and the gradual rise of the plane of activity at which waves and tides operate. Over shorter timescales the same impacts occur more episodically, due to an increase in the frequency and magnitude of high sea-level events. The latter will be discussed in section 2.3.2 in relation to intensified storm activity. It is crucial that future research focuses on understanding how this localised response to sea-level rise influences the morphological evolution of deltas over decadal scales, in order to increase confidence in regional projections (Lata and Nunn, 2012).

The fertile plains and wetlands that comprise the agricultural heartlands of many deltas are highly vulnerable to sea-level rise, being threatened by a combination of land loss and salinisation. Approximately 78% of the land in the

Mekong delta in Vietnam is used for rice production, with approximately 20,900 km^2 of this land situated <2 m above mean sea-level (Syvtiski *et al*., 2009). Sea-level rise is increasing the area flooded during the wet season and prolonging the time crops are inundated, often resulting in the crop being drowned or harvested late. During the dry season, saline intrusion further reduces the rice yield, putting increasing pressure on food security (Xenarios *et al.,* 2013). Traditionally in the dry season, farmers have taken advantage of these high salinity levels to breed shrimp during the time when rice stocks are low. However, higher salinity levels all year round as a result of sea-level rise mean an increasing number of farmers in the Mekong, and in many other similar deltas in South-East Asia, have abandoned rice production altogether and have adopted shrimp farming.

Whilst at the individual-scale this strategy is a sustainable way to mitigate against some of the impacts of climate change, on industrial scales shrimp farming is contributing to deltaic transgression (Szuster, 2003) and thus is arguably unsustainable: Groundwater extraction in order to fill aquaculture ponds during the dry season is accelerating local subsidence, raising relative sea-levels and increasing water stress. Reduction in freshwater supplies, combined with the addition of brackish water that is channelled in to help shrimp stocks thrive, further intensifies saline conditions. As a result, Falk (2000) finds that after 10 years many of these intensively farmed areas are no longer agriculturally productive. Furthermore, large scale aquaculture can have detrimental impacts on mangrove ecosystems. Traditional rice-shrimp farming, whereby crops were rotated between the wet and dry seasons, had little impact on mangrove forests (Stonich *et al*., 1997). These valuable ecosystems provide breeding sites for many species of birds and marine wildlife; buffer against coastal erosion and storm surge; and are accumulation sites for nutrients (Alongi, 2002). However the scale of modern shrimp farming has resulted in the widespread deforestation of mangroves, leading to increased coastal erosion (Saito *et al.,* 2007). In the Sunderbans, located on the abandoned tributaries of the western Ganges-Brahmaputra-Meghna (GBM) delta, saline intrusion is also threatening mangrove ecosystems by providing the perfect conditions for *Botryoshaeria ribis*, a fungus that kills Sundari trees (*Heritiera fomes)* (Allison 1998). These examples highlight the intimate and complex links between sea-level and ecosystem services in deltaic environments that are critical in order to produce accurate projections of delta morphology under conditions of increasing climate stress.

2.3.2 Meteorological extremes

The combined effects of sediment starvation, subsidence and eustatic sea-level rise influence the ability of a delta to cope with the morphological impacts of meteorological extremes. For the purpose of this discussion, 'meteorological extremes' refer to significant changes in the magnitude and/or frequency of weather events (e.g. drought; tropical cyclones) or significant shifts in long-term climate patterns (e.g. monsoon precipitation intensity) that are likely attributed to anthropogenic climate change. Global average combined land and ocean surface temperatures increased by 0.85˚C between 1880 and 2012, and by 0.72˚C over the period 1951-2012 (Hartmann *et al.*, 2013). This rise in global average temperatures raises the baseline upon which localised meteorological events are superimposed, leading to intensification of the hydrological cycle and the more frequent occurrence of extreme hot outliers (Hansen *et al.,* 2012). In a recent study by Martin *et al.* (2013), households in the GBM delta in Bangladesh identified an increase in extreme summer temperatures as one of the predominant climate stresses that would cause them to migrate due to concerns over food security and water stress. Faisal and Parveen (2004) predict that in Bangladesh rice production will by 2050 drop by 8 percent and wheat production by 32 percent, due to rising air temperatures. These conditions also create the perfect environment for many invasive species to thrive, due to physiological advantages that enable them to cope better than native species under conditions of increased climate stress (see Sorte *et al.* (2010) for a more detailed discussion). For example, the leaf roller caterpillar (*Cnaphalocrocis medinalis*), has become one of the predominant pests devastating rice yields in Bangladesh since the 1980s due to rising temperatures and the decline of the native *Mythimna separata* (Haq *et al.,* 2010).

Over forthcoming decades, more frequent oscillations between drought episodes and flood-rich periods are predicted to occur, and the intensity of individual rainfall events is projected to increase (Olesen *et al.,* 2011). The Mahanadi Delta in India has suffered 5 major floods in the last decade, primarily due to an increase in extreme precipitation events in the central basin during the monsoon season (May-November) (Jena *et al.,* 2014). The socioeconomic impacts of such flood events are largely detrimental, resulting in significant loss of life and property. However, the morphologic response to such precipitation events can in some instances be positive in terms of delta aggradation, as despite localised erosion intense rainfall also stimulates pulses of fluvial sediment

delivery to the delta plain (Hensel *et al.,* 1999). Panda *et al.* (2013) also highlight the impacts of increased rainfall intensity in the Mahanadi Delta, with coastal sectors found to be the most susceptible to flooding and the Eastern Ghats most vulnerable to hydrological drought. The authors also identify linkages between precipitation, streamflow and large-scale climate indices including the El Niño-Southern Oscillation (ENSO), the Indian Ocean Dipole (IOD) and the South-West Monsoon.

As increasing hydroclimatological variability makes it more challenging to accurately predict morphological change in these complex systems, understanding the effect of slow-varying components of the climate system associated with large-scale air-sea interactions could significantly help improve long-range streamflow forecasting (Piechota *et al.,* 1998). Numerous studies have found that streamflow prediction models that incorporate ENSO consistently produce reliable seasonal projections, owing to the fact that its associated mechanisms of air-sea heat transfer, and thus the subsequent precipitation response, are predictable many months ahead (Chiew and McMahon, 2009; Gutiérrez and Dracup, 2001). In deltas affected by monsoon rainfall, understanding the impacts of climate change on this regime is of crucial importance to producing reliable morphological projections, as it is during this time that peak discharge and sedimentation occurs (Michels *et al.,* 1998; Allison, 1998; Jena *et al.,* 2014).

Tropical cyclones and their associated storm surges can also have devastating impacts on deltaic environments, causing significant damage to infrastructure via flooding, erosion, salinisation and remobilisation of subaqueous deposits (Dail *et al.*, 2007). On May 2nd 2008 Cyclone Nargis made landfall in Myanmar's Ayeyarwady delta. In most areas 2 metre high waves were superimposed upon a five metre storm surge, resulting in substantial coastal erosion and inundation up to 50 km in land (Fritz *et al.,* 2009). The morphological impacts were further amplified due to extensive deforestation of primary mangrove forests that would normally act as a natural buffer to dissipate coastal energy. It was the first tropical cyclone in Myanmar's history to make landfall in the delta; located near the equator where cyclogenesis is usually inhibited by coriolis forcing (Henderson-Sellers *et al.,* 1998). Fritz *et al.* (2009) argue that as a consequence of this, lack of awareness and preparedness for such a hazard was largely to blame for the catastrophic loss of life in the delta,

reaching 80% of the population in some villages. Despite some active debate in the literature, it is now widely agreed that rising sea-surface temperatures will inevitably intensify storms; however increasing vertical wind shear is likely to generate a negative feedback loop into the system, as the latent heat released to the upper troposphere during cyclogenesis is adverted in a different direction relative to lower levels (Zhao *et al*, 2009). Thus although the overall frequency is not likely to increase the probability of severe tropical cyclones is greater; as is the likelihood of these storms maintaining strength into a greater range of latitudes than at present (Pielke Jr. *et al.,* 2005). As demonstrated in the Ayeyarwady delta, subtle changes to cyclone track locations, regardless of shifts in intensity or frequency, can have both significant morphological impacts and devastating consequences for local communities in areas that are not usually exposed to storms of such magnitude. It is clear from the discussion above that modern controls on delta morphology are diverse, interactive and operative over a variety of temporal and spatial scales. This complexity, combined with the uncertainties shrouding climate change projections and trajectories of societal development, poses significant challenges when attempting to create reliable multidecadal projections of delta evolution. This study aims to develop a methodological framework that can provide stakeholders with a means to organise this complexity; by developing a suite of metrics that can enhance our understanding of how various physical and social components of a delta catchment system interact under increasing conditions of climatic stress. The following chapter presents a detailed discussion of the epistemological setting for developing such a framework as well as the various modelling approaches that could be utilised to achieve this.

Chapter 3 **Modelling Deltas**

3.1 Key Challenges in Studying the Morphological Evolution of Deltas in the 21st Century

The mathematical concepts of complexity theory are increasingly being adopted by researchers in both the environmental and social sciences in order to organise the complex interactions between humans and nature, and to better understand the non-linear and emergent responses to these interactions that can lead to unpredictable system change (Becker, 2010). Thus the epistemological setting for much of the recent research attempting to understand these interactions in present and future deltaic environments utilises methods that view deltas as complex social-ecological systems (CSESs); that is, deltas are viewed as consisting of a biophysical unit and its associated social actors and institutions (Becker, 2010).

Glasser *et al.* (2008) identify five key themes that are central to systems theory: Firstly, components in CSESs are linked by *multiple non-linear interactions*, resulting in numerous combinations of positive and negative feedback mechanisms. This leads to highly dynamic and often highly unpredictable systematic change (Becker and Jahn, 2006 in Glasser *et al.,* 2008). Secondly, CSESs display *emergent behaviour*, whereby the cumulative effects of small-scale phenomena influence large-scale system properties (Cilliers, 1998), the effects of which may be over or underestimated dependent upon the scale of observation. As critical transitions can occur at any given scale within the system, it is vital to understand their cumulative properties as the effects of crossing multiple thresholds at smaller scales can aggregate to become of greater concern (Lenton, 2013). The third central concept, *resilience*, can be defined as the capability of a system to retain functioning following a perturbation (Folke, 2006). Within the context of this study, the resilience of a delta refers to its ability to cope with the array of anthropogenic and climatic stressors discussed in chapter 2. Conversely, the fourth key concept of *vulnerability* describes the extent to which a system is unable to cope with the undesirable impacts of a perturbation. Within a purely morphological context, vulnerability may refer to the erodibility or cohesiveness of sediment, or the exposure of deposits to a destructive force. The final concept listed by Glasser *et al.*

is *adaptive capacity*; also referred to as 'transformability' (Olsson *et al.* 2006 in Glasser *et al.,* 2008). Complex adaptive systems (CASs) are CSESs that have the capacity to change and learn from experience (Rotmans and Loorbach, 2009; Dammers *et al.,* 2014). Whilst one may consider this capacity to predominantly exist within the human-based network of a CSES, biophysical components also possess this ability: Levin (1998), for example, argues that the process of natural selection provides the mechanism via which an ecosystem becomes increasingly resilient to perturbations by 'learning' from past experience.

In this section, two key issues that arise from the CSES themes listed above are discussed within a methodological context: firstly, issues of temporal complexity centred on the concept of magnitude versus frequency; and secondly, issues of spatial complexity arising from the debate of reductionism versus emergence. The aim of this discussion is to provide deeper insight into the key challenges faced when studying these complex systems, and the solutions suggested to overcome them. The final section provides an overview of the types of uncertainty associated with morphological modelling.

3.1.1 Temporal complexity – Magnitude versus frequency

In order to produce reliable multidecadal projections of delta evolution it is critical to gain a better understanding of how the predominant controls of delta morphology vary and interact over different timescales. At the heart of this lies a debate concerning the relative importance of the magnitude of a given event versus its frequency; in other words, is morphological change in deltaic systems predominantly controlled by gradual stressors, such as eustatic sea-level rise, or by sudden shocks, such as a storm surge? The magnitude of an event is a quantifiable expression of the total energy released (Mayhew, 2009) that can also be linked to the duration of the event (Lytle and Poff, 2004). Whilst it is clear that events of higher magnitude have the potential to cause a greater morphological response, the greater reoccurrence intervals between them may allow sufficient time for the system to recover from the perturbation via negative feedback mechanisms (Turner *et al.,* 1989). Such oscillations are regularly seen over seasonal timescales in deltas fronted by beach systems, as sediment that was eroded during winter storms may be re-worked to form convex profiles during the summer when wave energy is low

(Fox *et al.,* 1978; Fanos, 1995). Unprecedented rates of environmental change through both increased human activity and climatic variability will redefine reoccurrence intervals of the natural processes that control delta morphology, constraining the recovery period and altering complex feedback mechanisms. In order to understand how shifts in the magnitude and timing of events will alter delta regimes over forthcoming decades, potential critical thresholds must be identified.

The discourse of modern environmental change has transferred from one of changes to average conditions towards the concept of tipping points, beyond which large-scale, abrupt and often irreversible shifts in system state pose significant threats to society (Lenton *et al.,* 2008). These changes can occur at a variety of spatial scales, and may not take place immediately following the triggering event (Lenton, 2012). This complexity makes tipping points incredibly challenging to incorporate into numerical models (Alley *et al.,* 2003). Olsson *et al.* (2008) identify tipping points as one of two trajectories a CSES may follow after a perturbation, in which the system fails to recover to a stable state (figure 3.1).

At the forefront of this discourse is the planetary boundaries framework. First developed by Rockström *et al*. (2009a) the framework proposes nine interlinked biophysical boundaries at the planetary scale that society should remain within in order to avoid dangerous environmental change. In 2012, the concept was extended to include a baseline boundary representing the extent to which these biophysical components must be utilised in order to meet critical human needs; a framework that has become known as the 'Oxfam doughnut' (Raworth, 2012) (figure 3.2). Whilst the 'doughnut' has focused on planetary-scale pressures, there is an increasing call in the literature for the identification of these social and ecological boundaries at the regional level (Dearing *et al.,* 2014); such that similar frameworks could be applied to help understand social-ecological tipping points in megadeltas. Renaud *et al.* (2014) propose, for example, that delta CSESs be viewed in one of four hierarchical states: a delta that is assumed to be in natural equilibrium with its environment is referred to as a *Holocene delta CSES*; the authors give the example of the Orinoco delta in Venezuela. If intensive human activity transforms these natural processes the delta is then classified as an *Anthropocene delta CSES;* a given example is the Ebro delta in Spain. A *Holocene modified delta*

CSES is defined as the transition stage between the two states above; here the authors identify the Danube delta in Romania as an example. Lastly, a *collapsed delta CSES* can be defined as one where the biophysical environment has been drastically altered due to human activity, which then leads to alterations in the activities themselves including outmigration. Renaud *et al.* (2014) give the example of the Indus delta in Pakistan, also identified by Syvitski *et al.* (2009), as an area where anthropogenic activity has had significant morphological impact. The further through this transition a delta CSES is the more difficult it would be, the authors argue, to 'tip back' to a more favourable configuration. However, as stressed in an earlier paper by Renaud *et al.* (2013), 'de-engineering' deltas to allow for natural processes to dominate could be employed to reverse the evolutionary trajectory of the system. Non-linear systematic change that leads to the crossing of critical thresholds can be triggered by both a large event and the amalgamation of dangerous aggregate effects (Rockström *et al.*, 2009b). As the dominant geomorphic agent in many deltaic systems, humans have the capacity to trigger tipping points via both temporal pathways: The gradual degradation of agricultural land in the GBM delta due to intensive shrimp farming, has an identifiable tipping point after ~10 years of resource exploitation whereby the land can no longer be utilised for crop production (Falk, 2000). Equally, numerous authors argue that the closure of a large dam triggers a tipping point as the system shifts from net progradation to erosion (see references to Frihy, 1988; Ly, 1988; McManus, 2002 and Yang *et al.,* 2010 in chapter 2).

As many tipping points display hysteretic characteristics, in which the transition is determined not only by the current imposed force but by a lagged response to historical environmental pressures, the identification of early warning signals in the morphological response would be very useful (Ditlevsen and Johnsen 2010; Dearing *et al.*, 2014). Scheffer *et al.* (2009) propose that there are a set of generic "symptoms" – such as increasing variance or skewness within time series data - that appear in a wide range of complex systems as the tipping point is approached. Such information could be recognised in the outputs of morphological models. The successful simulation of emergent phenomena could make significant steps towards this.

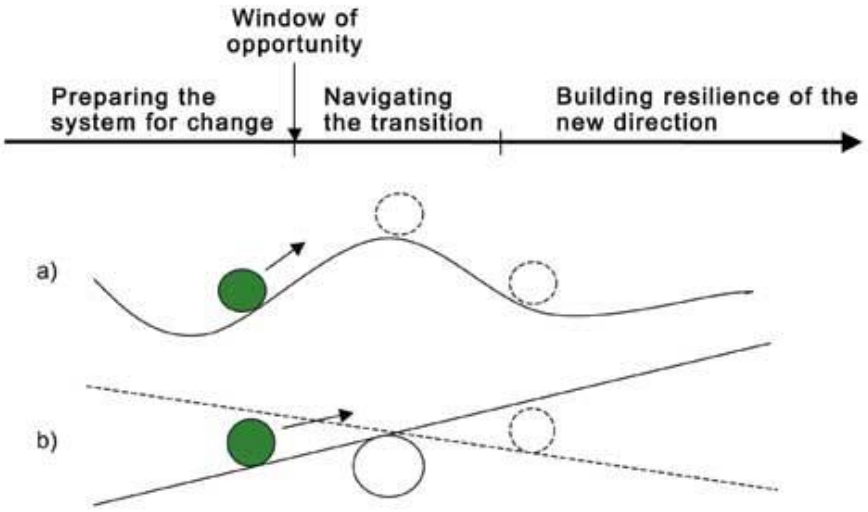

Figure 3.1 Social-ecological transformations can be illustrated in two ways: (a) a regime change between several stable states after passing through a threshold, or (b) as a tipping point. Three phases are identified within these transformations: preparation and navigation, which are linked through a window of opportunity for action, and lastly stabilisation. (Image source: Olsson and Folke, 2008).

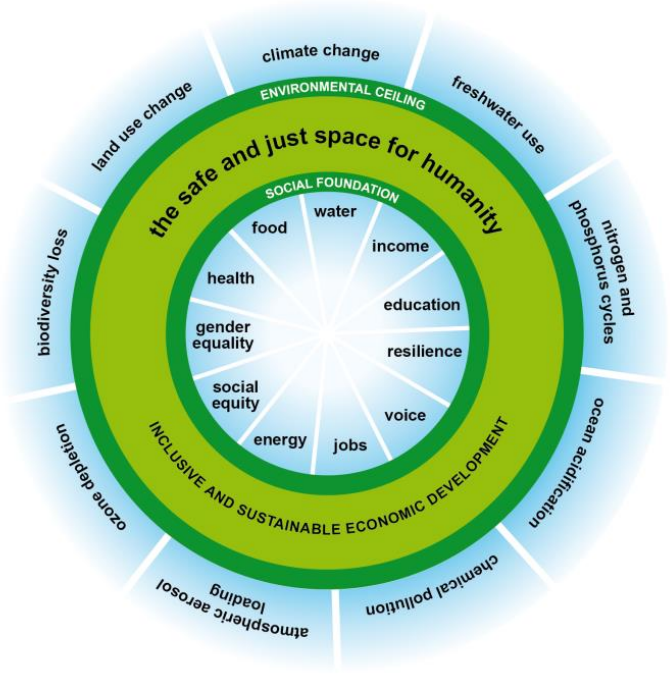

Figure 3.2 The Oxfam 'Doughnut': the environmental ceiling consists of the nine planetary boundaries as defined by Rockstrom *et al* (2009a). The social foundation consists of the eleven social priorities identified preceding Rio+20. Between the social and planetary boundaries lies an environmentally safe and socially just space in which humanity can thrive. (Image source: kateraworth.com).

Modelling morphological change in these dynamic environments that are the cumulative product of feedbacks occurring over long-term, seasonal and short-term timescales is a challenging task. A reliable model must be able to recognise the key non-linear interactions between fast and slow processes that result in the breach of critical morphological thresholds and identify when such a change is likely to occur under a range of social-ecological scenarios. In order to build such a model it is essential to place present-day rates of change within a longer-term context so as to establish critical thresholds that have occurred within the limits of natural morphological variability. There is an abundance of paleoenvironmental studies in the literature that aim to establish baseline variability in deltas in response to a number of stressors, particularly those related to climate change: Soria *et al.* (2005), for example, determine Holocene subsidence rates and paleo sea-level

history of the delta plain at Manila Bay in the Philippines using sediment cores and radiocarbon dating. Using historical data from their study and comparing it with geologically-similar deltas around the globe, the authors find that modern subsidence rates in some areas of the delta are likely to be 97% attributed to human-induced compaction. Paleoenvironmental methods can also provide useful information when data records are limited, as stated by Tamura *et al.* (2012) who used luminescence dating of beach ridges in the Mekong delta, Vietnam, to establish the mobility of shoreline changes over centennial scales. The use of long-term records alone, however, is unlikely to provide empirical evidence of the processes that lead to deltaic evolution at decadal scales, and is also limited in that there is no analogue in the past for the current rate of environmental change (Stanley and Warne, 1993).This is due in part to the relative geological youth of delta systems and the overwhelming influence of anthropogenic activity. Aerial photographs, satellite imagery and direct field measurements can be used to determine rates of more recent volumetric change at interannual to multidecadal scales (Anthony and Blivi, 1999; Woodroffe, 2010). This temporal resolution of observation is coarse enough to identify many emergent features of deltaic evolution and yet still high enough to provide input for mechanistic delta models; something that is critical in order to resolve self-organising channel dynamics and to couple these to ecosystem processes (Paola *et al.,* 2011).

Numerical delta models such as Delft3D (see Edmonds and Slingerland (2010) for a detailed description) can be manipulated to accelerate the timing of morphological changes and test the response of deltas to shifts in event frequency. Such methodologies clearly complement field-based investigation, which cannot logistically permit the real-time study of long-term evolutionary processes or the collection of such detailed data on isolated control variables (Paola *et al.,* 2011). Edmonds *et al.* (2010), for example, use Delft3D to investigate how river-dominated delta networks are likely to respond to the likely changes in flow discharge that are predicted to occur over the next century as a result of environmental change. The authors find that for an increase in discharge of up to 60% over the initial value, a decrease results in distributary abandonment, whereas an increase has no significant effect on network structure. Thus their results suggest that deltas in drought prone regions will be more likely to experience significant rearrangement

of their channel networks. Such an experiment would be incredibly challenging to undertake in the field alone.

Physical experimental models of deltas can also be used to accelerate morphological change and are useful tools for observing the influence of sediment properties such as cohesiveness (Paola *et al.,* 2011). For example, Edmonds *et al.* (2009), used an experimental tank (see figure 3.3) to quantitatively define avulsion cycles, enabling them to produce mathematical rules for predicting the growth of intradelta lobes. Key challenges for the future design of both numerical and physical models include coupling these morphological rules with social-ecological components of the delta system, and furthermore calibrating for non-linear change for which there is no comparable analogue in the past.

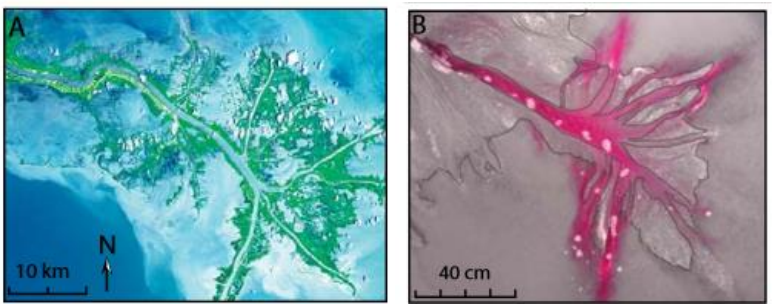

Figure 3.3 (A): 2001 LANDSAT Advanced spaceborne thermal emission and reflectance radiometer (ASTER) image of the Mississippi delta and (B): overhead photo of experimental delta created with cohesive sediment mixture; both images from Edmonds *et al.* (2009: 759).

3.1.2 Spatial complexity – Understanding and quantifying emergence

In parallel to understanding the multiple timescales over which deltaic processes occur, there is the need to recognise the spatial scale at which the factors driving those processes operate. In order to produce reliable multidecadal projections of delta evolution it is important to understand how the magnitude of dominant controls can vary across space to create a complex landscape. For example: as abandoned channels become increasingly tidal-dominated over time, a gradient is formed in the lateral plane whereby the ratio of tidal energy relative to fluvial energy decreases towards the active river mouth (Woodroffe, 2010). This gradient results in diverse morphology across the delta plain. The GBM delta

provides a classic example, whereby the western region of the delta has developed into a complex series of mangrove-lined creeks typical of tidal-dominated deltas, whilst towards the active mouth morphology is increasingly determined by fluvial processes (Woodroffe and Saito, 2011). Morphological models should be designed with these key energy balances as central components in order to be transferable between deltas. However, it is equally important that these models are flexible such that unique controls at particular locations can be included. Snowmelt, for example, will obviously not contribute to the evolution of deltas worldwide; however the discharge of the Brahmaputra River typically increases one month before that of the Ganges in the dry season due to the contribution of snowmelt from the Himalayas, thus influencing significantly bank erosion rates and sedimentation in certain regions of the delta (Allison, 1998).

In addition, the design of models should be such that the appropriate spatial resolution of controls is utilised, in order to identify important trends in shifting environmental regimes that influence morphological change: The Volta delta in Ghana, for example, has become subject to an increasingly sharp rainfall gradient whereby coastal regions can receive annual precipitation totals ten times greater than in the arid northern basin (Ogundtunde *et al.,* 2006). It is therefore important that the spatial scale of precipitation data is such that the model recognises the increasing locality of rainfall events in the Volta basin. However, high resolution projections are not always appropriate as even the most reliable climate models can fail to forecast precipitation accurately at the scale of individual catchments (Pagano and Garen, 2005). Habets *et al.* (2004) describe three types of error that prevent accurate downscaling of precipitation projections from global climate models to the regional level: Firstly, the localisation of events, as an error of a few kilometres can mean precipitation falls in a different watershed; Secondly, the timing of events, as the initial conditions are determined by previous events; and lastly, errors associated with the intensity of precipitation, which is inherently challenging to model at all spatial scales. Thus a balance must be found between a spatial scale that best reflects reality without becoming data intensive or subject to significant downscaling errors. Clearly this is easier said than achieved and is also significantly limited by data availability; a barrier that is inevitable given that many basins cross political boundaries. Differential data quality in itself should be viewed as a form of spatial complexity, as the availability and resolution of data heavily influences our

approach to understanding the dominant controls of delta morphology and may lead to misrepresentation of which areas are vulnerable.

The issues raised above refer primarily to macroscale spatial variability. However, further complexity is added when one begins to consider the spatial variability occurring at the microscale in response to drivers of morphological change. At the heart of this issue lies a debate that has been central to geomorphological study for many decades: reductionism versus emergence. The former approach argues that a CSES can be understood by reducing the system to its fundamental components and attempting to analyse the interactions between them (Werner, 2003). This mechanistic, bottom-up approach has been used to establish detailed laws governing process-form relationships, with such rules often providing input to numerical models (Harrison, 2001). However such an approach does not provide an explanation for emergent characteristics of the system, whereby phenomena only become visible at a given scale larger than that of process-form relationships (Schumm and Lichty, 1965). Emergence occurs as CSESs are insensitive to changes in initial conditions and are thus stable with respect to changes at the microscopic level (Anderson, 1972). Harrison (2001) therefore argues that emergent properties should be viewed as qualitative structures that arise from the organisation of quantitative phenomena in complex systems. He gives the example that although we can measure the changes in kinetic energy associated with gas-liquid-solid transitions, the structures that emerge (condensation, clouds etc.) have properties which are not predictable from the quantitative analysis of the transitions alone (e.g. the ability to transmit light). In a deltaic setting, a similar argument could be given that one cannot extrapolate from the properties of individual sediment grains on a river bed to understand the behaviour of channel avulsions.

Further adding to this complexity is the problem of equifinality, where an end state can be reached by two or more different means. Beven (2007) argues that the models we use to represent CSES are in themselves equifinal, as different mathematical laws may mimic an observed natural process equally well. When seeking to understand the morphological response to a given driver, such as increased surface temperatures for example, one may use an ensemble of climate models all operating at similar spatial resolutions to provide a probabilistic-based

output of which responses are most consistently reproduced. In an integrated assessment tool however, numerous models are likely to be integrated that independently focus on different components of the CSES, and thus will inevitably vary in their spatial resolution. Geographical Information Systems (GIS) can provide a geoscientific framework for coping with this mismatch of data scales, and allows the system to be viewed at an array of different levels of complexity dependent upon the questions being proposed (Woodroffe, 2010).

Emergent morphology across the deltaic landscape can be relatively easy to qualitatively describe but difficult to quantitatively define. As discussed in chapter 2, traditional metrics describing river deltas focus on the external shape of the deposit, based on the relative contributions of rivers, waves, and tides (as shown in the ternary diagram by Galloway, 1975). In these early approaches quantification of the internal structure of the deltaic network was still excluded. This has changed significantly in recent years, with a number of studies attempting to apply metrics to analyse the network properties of different delta classifications, and understanding what this reveals about the processes driving deltaic evolution (Geleynse *et al*., 2012; Passalacqua *et al*., 2013). Tejedor *et al.* (2015), for example, conceptualize a delta channel network as a graph and use its Laplacian—a matrix summarizing the information about the node connections and their strengths—to answer questions about the dynamics of a delta network. Edmonds *et al.* (2011) also explore this issue in detail. As discussed in chapter 5, it is their metrics that are taken forward to analyse changes in the emergent system in this study. These metrics include the distribution of island sizes, the fractal box-counting dimension, and nearest-edge distance distribution.

3.1.3 Uncertainty in morphological models

Van Asselt (2000) identifies two broad sources of uncertainty that arise from the modelling of CSES; the quantification of which presents another methodological obstacle (figure 3.4): Firstly, uncertainty arises due to problems characterising natural variability. Both the ocean and atmosphere exhibit significant interannual variability and chaotic system behaviour that cannot be predicted with great accuracy over long timescales (Déqué *et al*., 2007). This significantly increases the

level of uncertainty in predictions made by atmosphere-ocean general circulation models (AOGCMs); the projections from which are ultimately used as part of the input to CSES models. Similarly, human agency displays significant variability that creates uncertainty in long-term projections. This includes the amplitude of anthropogenic emissions; changes in land-use and land-cover; and the steps we take to mitigate against the impacts of climate change. These largely unpredictable and yet crucial decisions are influenced by a complex array of social and economic factors, including both unconscious and intentional actions, operating at individual, societal and global levels (Leemans *et al.,* 2003). Agent-based models (ABMs) provide a method with which to integrate human choice with the fundamental physical rules governing environmental change applied in morphological models. Although such models obviously cannot reliably predict the infinite number of ways humans could interact with the environment in the future, they do provide a powerful multidisciplinary tool with which to test scenario-based adaptation strategies under a range of environmental stressors and decision pathways (Druckenmiller *et al*., 2004; Balbi *et al*., 2010). Lambin *et al*. (2003) provide an excellent review of the potential to model future land-use change in complex adaptive systems using an agent-based approach. The authors describe how climate-driven land-cover modifications interact with land-use changes; the latter being driven by synergetic combinations of resource scarcity, changing economic opportunities, policy intervention, level of adaptive capacity, and changes in social attitudes; as well as feedbacks from the resultant changes in ecosystem services. ABMs can also provide vital input to integrated assessment tools (IATs). As will be discussed in section 3.2, IATs have become the desired goal of many research projects examining environmental change due to the fact they provide a systematic way to integrate knowledge across disciplines, models and tempo-spatial scales (Uthes *et al*., 2010). Their flexible numerical-conceptual approach also permits the integration of data of variable quality (Scrase and Sheate, 2002), which can make it easier to cope with errors associated with uncertainty due to natural variability.

The second category of uncertainty described by Van Asselt (2000) is 'structural' uncertainty: The formulation of a model creates an initial level of uncertainty associated with how accurately it captures the effects of various forcings. This is the fundamental foundation upon which uncertainty due to natural variability and chaotic behaviour is imprinted. Utilising ensembles of models can

help understand and reduce the uncertainties associated with formulation, either through testing the same model under variable initial conditions; the same model using different formulations; or indeed between similar models (Met Office, 2014). Structural uncertainty also arises from the forcing of a high resolution model, such as a regional climate model (RCM), by a low resolution model, such as an AOGCM. The localisation, timing and intensity of climatic events, and in particular precipitation predictions, can lead to significant downscaling errors that amplify uncertainties of long-term climate projections at the regional level (Habets *et al.,* 2004). This presents a significant challenge in modelling deltaic environments, which are highly sensitive to shifts in local hydroclimatic conditions, such as the frequency of storm events (Pisaric *et al.,* 2011). Validation of models with empirical observations can help identify such sources of uncertainty and quantify their magnitude. However, Nicholas (2005) warns that when doing so one must ensure that validation criteria reflect the appropriate scale of the modelling objectives: validation of process representation, for example, will not necessarily ensure a model is capable of reliably simulating long-term system dynamics; thus validation of both high and low level system behaviours would be preferable.

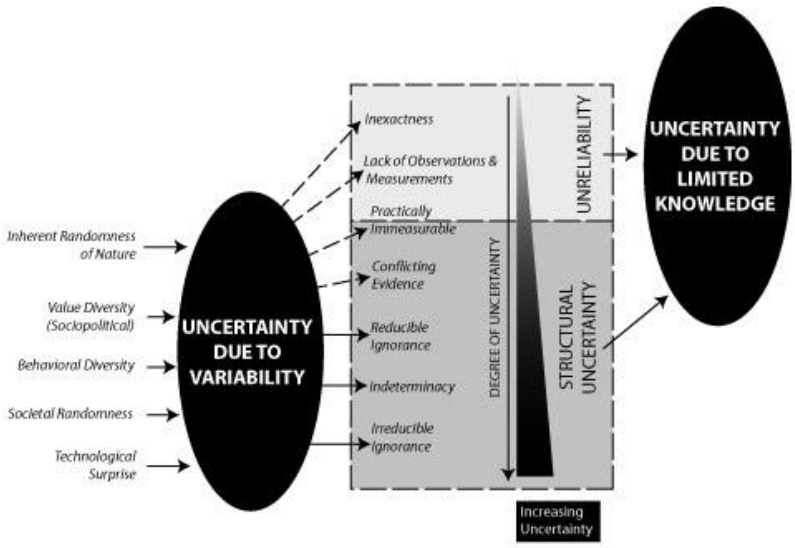

Figure 3.4 Types of uncertainty associated with morphological modelling, as defined by Van Asselt (2000) (Image source: www.joewheaton.org)

3.1.4 Quantifying vulnerability

As discussed in section 1.2, a major aim of this research is to develop a framework of morphological metrics that are directly usable by stakeholders. Providing a categorical measure of vulnerability for a given area over a given time period, under various environmental change and management scenarios, will provide an efficient and policy-relevant means of representing how the nature of physical change across the delta system may impact the habitability of certain regions. Given that the concept of vulnerability encompasses a variety of factors dependent upon the context to which it is applied, it is crucial to explicitly define how vulnerability will be quantified in this study. Vulnerability is widely defined as the potential to be harmed, measured by comparing susceptibility with resilience (SEPA, 2011). The IPCC (2007) define vulnerability to climate change as a function of physical exposure, sensitivity and adaptive capacity.

Whilst this study aims to provide a measure of the severity of exposure to biophysical change (through quantification of event timing, magnitude, persistence and potential reversibility), it cannot give a true, complete measure of vulnerability as many of the factors influencing sensitivity and adaptive capacity are inferred and not explicitly modelled. Rather, the output should be recognised as a quantification of potential vulnerability to biophysical change. This can be therefore be viewed as a GIS-based suitability analysis; whereby the capacity of the system to meet the needs of a stakeholder is assessed (Malczewski, 2004). In this study, the system is the biophysical component of the delta CSES; 'needs' refers to biophysical processes that directly influence factors determining basic habitability, such as elevation above sea-level and habitat cover; and stakeholders would be populations occupying the deltaic region upon which the idealised system is based, as well as populations in the feeder catchment. The vulnerability of an area will increase as the rate and magnitude of biophysical change increases in such a way as to reduce the capacity for basic habitable needs to be met. It is important to stress that the focus of this research remains on investigating the nature of morphological change in deltas under various scenarios, with a particular interest in identifying potential critical system thresholds and early warning signals. It is not meant to be a substitute to a more detailed, more accurate risk assessment for a specific site. Rather, providing a measure of vulnerability in this way provides a policy-relevant

output from the theories formulated from morphological investigation, and furthermore allows the consequences of different management strategies to be more easily compared.

3.2 Numerical Modelling Approaches

There are a number of different methodological approaches that can be implemented in order to collect morphological data from a delta, and the decision as to what is most appropriate is largely dependent upon the issues of temporal and spatial complexity that affect the question being proposed. Direct field measurements may be used, for example, to determine the transport mechanisms leading to interannual to decadal volumetric fluxes over a beach ridge (see Frihy *et al*., 1998), whereas this would be an inappropriate method with which to identify centennial shoreline variability. Similarly remote sensing is an excellent tool with which to identify the rate and location of recent land use change across a delta plain (see Weng, 2006); however data may not be available at sufficient spatial resolution to identify drivers of process-form relationships. Once data has been gathered via an appropriate means there is then a further decision to be made with regards to the type of model used to make projections of morphological change. Many numerical modelling suites (such as Delft3D) focus on the biophysical drivers of delta evolution, as do physical water tank models. Segregating these biophysical drivers of morphological change (such as wave propagation, catchment sediment input, density currents etc.) permits detailed analysis of the mathematical rules governing deltaic evolution, allowing one to observe how processes vary and interact over an array of tempo-spatial scales; analysis that goes far beyond what is logistically viable in the field alone.

Whilst such a focused approach is crucial in order to produce reliable morphological projections, clearly there are multiple drivers beyond the biophysical components of the system that will indirectly influence the rate and magnitude of deltaic evolutionary processes. Integrated assessment tools (IATs) provide a systematic way with which to incorporate knowledge across models, reducing several sources of information into a singular analysis that explores the interconnections between biophysical, economic and social system components (Maunder and Punt, 2013; Uthes *et al*., 2010). The development of an IAT has become a favoured aim of many research projects examining environmental change in CSESs as their mixed numerical-conceptual approach permits the integration of multiple disciplines, scales and degrees of certainty (Scrase and Sheate, 2002). Susnik *et al*. (2014) and Nicholls *et al*. (2004) both argue that such a framework is

essential in order to translate morphological projections into policy-relevant, adaptive pathways that allow a range of management responses to be considered. Examples of IATs being developed to inform management decisions in deltaic environments include Climate Induced Changes on Water and Security (CLIWASEC) (see Susnik *et al*., 2014) in the Nile delta; the CALFED Bay Delta Program (see Norgaard *et al*., 2009) based in the California Delta, USA; Deltas Vulnerability and Climate Change: Migration and Adaption (DECCMA) which focuses on the GBM delta, the Volta delta and the Mahanadi Delta (see DECCMA, 2015); and the Mississippi River Hydrodynamic and Delta Management Study (Little Jr. and Biedenharn, 2014).

There are two dominant approaches highlighted in the literature that are frequently adopted to develop IATs: Fuzzy logic is a commonly implemented method that offers an organised way of reasoning with imprecise concepts and data using 'fuzzy sets' (classes with inexact boundaries) (Hanson *et al*., 2007). Most notably fuzzy logic is utilised in the 'driving forces-pressures-states-impacts-responses' (DPSIR) modelling framework that has been adopted by many environmental management institutions including the Environmental Protection Agency and the European Environment Agency (EEA, 2014). The DPSIR framework assumes cause-effect relationships between interacting components of environmental, social and economic systems, and also assumes that an infinite range of future states can be limited to a range of descriptive categories (Rotmans *et al*., 1994). This framework reduces the complexity of interacting system components into a chain of causal links, providing an accessible way to link policy-relevant values with scientific data (Giupponi, 2007; Benini *et al.,* 2011). It is also easily integrated with GIS-based frameworks, as in Feoli *et al*. (2002) who use fuzzy logic to analyse the driving forces behind environmental degradation in northern Ethiopia. Wei *et al*. (2014) demonstrate a modified fuzzy logic method utilising the concept of integrated carrying capacity (ICC) in order to establish potential coastal management pathways in Natong, China. In this methodology, the boundaries of the sets used in the DPSIR framework are defined by the carrying capacity of each system component (e.g. maximum resource use) in order to reveal the loading capacity between human activity and the ecosystem. The most commonly used alternative approach to fuzzy logic is qualitative scenario analysis: whilst the overall framework remains fundamentally similar to that of DPSIR models there is an

explicit emphasis on the role of human behaviour and changes to the social components of CSESs (Sharma and Norton, 2005). A familiar form of scenario analysis within the context of climate change is the 'tolerable windows approach', based on sets of tolerable climate impacts (e.g. a 2˚C rise in global mean surface temperatures) and proposed emission quotas (Bruckner *et al*., 1999). The reverse of this forward-working framework is backcasting: a type of scenario analysis concerned with the attainment of desirable futures (Robinson, 2003) in which a desired end point is defined and the model is run backwards in order to determine the feasibility of the measures required to achieve it (Sharma and Norton, 2005).

Both IATs based on fuzzy logic and those based on qualitative scenario analyses are able to handle differential data types, quality and resolution over multiple disciplines (Reidsma *et al*., 2011). For the purpose of modelling deltaic evolution, it is critical that the tools utilised in this study are able to successfully capture the interplay between abiotic and biotic components of the system, including non-linear dynamics. Nicholls and Goodbred Jr. (2004) suggest a scenario-based IAT in order to model the morphological evolution of the Ganges-Brahmaputra-Megnha delta, whereby sets of scenarios dependent upon human-based decisions are created for each of the identified dominant morphologic drivers (natural subsidence, enhanced subsidence, sediment supply, climate change and flood management). Haasnoot *et al*. (2014) suggest a similar framework in order to explore adaption pathways under a range of flood and drought risk scenarios in the Rhine delta in the Netherlands. A similar methodological framework may therefore also be appropriate for this study; whereby a numerical morphological model that is able to simulate changes over accelerated timescales under various environmental and climatic scenarios is integrated with a model that can demonstrate linkages between morphological change and relevant biotic processes.

Significant improvements in computational power, and in our understanding of interactions in CSESs, have led to a substantial increase in the number of geomorphological studies utilising numerical models to explain and project environmental change in deltas (Wolinsky *et al.,* 2010; Edmonds and Slingerland, 2010). Such models have been used in a broad range of biophysical research; from heavily mechanistic studies analysing sediment transportation in deltaic environments (such as Gelfenbaum *et al.* (2009) and Edmonds *et al.* (2010)), to

ecological studies (such as Feng *et al.* (2015) and Hu *et al.* (2015)). Of course, fieldwork is still an undoubtedly crucial component of understanding how a biophysical system operates, providing observations that can be used to both generate and calibrate the mathematical and conceptual theories that drive morphological processes in numerical models (Hubbard and Glasser, 2005). Paleoenvironmental studies are critical in order to provide trajectories of biophysical change over evolutionary timescales in particular, permitting the identification of baseline or 'pre-human' levels against which present and future change can be contextualised (Dearing, 2007). Numerical and field-based approaches are, therefore, undoubtedly complementary. However, for the purpose of generating geomorphological projections in this study, numerical modelling possesses several distinct logistical advantages over purely field-based methods: Firstly, a model can be manipulated to accelerate the rate of morphological processes, thus permitting the study of long-term deltaic evolution that could not be practically, or indeed cost-efficiently, observed in real-time in the field (Paola *et al.,* 2011). Modelling also allows one to test the geomorphological response of deltas to shifts in event frequency and/or magnitude that are perhaps beyond that observed at present or in the available paleoenvironmental record. As there is no direct analogue in the past for the current pressures causing environmental change in many deltas (Stanley and Warne, 1993), this is a potentially critical way in which tipping points in the deltaic CSES may be identified as these pressures become even more amplified in the future.

Furthermore, numerical modelling allows individual drivers of environmental change to be isolated or manipulated at the user's discretion, in order to collect detailed data on certain elements of the CSES and to test hypotheses concerning individual system components or forcing factors (Paolo *et al.,* 2011). This creates a richer understanding of system dynamics, and also permits scenario-based analysis. The use of abstract CSES in particular can overcome the noise of real-world complexity, allowing simulations to take place within a more controlled setting (Coulthard and Van De Wiel, 2012).

The range of drivers and processes that can be manipulated in numerical models, and the variety of spatio-temporal scales at which they can be explored, is what makes these tools so powerful; yet it also presents methodological obstacles.

As discussed at the beginning of this chapter, one of the key challenges faced in the design of numerical models is the ability to capture emergent phenomena (Dearing, 2007). As described previously, the long-standing debate of 'reductionism versus emergence' is ongoing in morphological modelling, as researchers must find an appropriate balance between a model capturing emergent phenomena in a CSES, whilst maintaining sufficient quantitative accuracy at the process-scale. Bottom-up, reductionist approaches are highly valued for establishing the mathematical laws that provide mechanistic input to many numerical models (Harrison, 2001). However, as our understanding of complexity theory has advanced in recent decades, it has been increasingly recognised that in order to realistically capture the non-linear, dynamic evolution of CSESs, one cannot simply reduce the system to its mechanistic components. This is because morphological change in CSESs is controlled by an accumulation of interactions between processes at multiple scales, whereby preceding conditions constantly determine the nature of present conditions, resulting in complex and often unpredictable behaviour (Nicolis and Nicolis, 2012).

In order to achieve the aims and objectives of this research project, as listed in section 1.2, a numerical model is required that can reliably simulate the natural processes of deltaic evolution, such as channel avulsion, channel bifurcation and subsidence. It must also meet the following specifications: Firstly, the model *must be able to efficiently produce multidecadal projections of morphological change*, taking into account short-term factors such as seasonal flow variability, without becoming too computationally intensive. Secondly, the model *must be able to operate at regional spatial scales (10s – 100s km*). Preferably, the model can be easily integrated with gridded spatial data and GIS software that produces accessible outputs for policy makers. Furthermore, the model *must have the capacity to integrate morphological change with certain biogeomorphological feedback mechanisms* that influence deltaic evolution at the system scale. Lastly, the model *must be able to simulate user-defined scenarios of environmental change*; such as the rate of sea-level rise. Although the focus of this research remains biophysical rather than socioeconomic, the model *must also be able to incorporate some level of human agency* in order to test the viability of potential management strategies.

Whilst there is of course the option to develop a biophysical model especially for this study, this would arguably be an inefficient methodological approach given that there are already a number of existing models that have the potential to be utilised. Table 3.1 provides a brief summary of the benefits and limitations associated with a selected group of twelve models; all of which may possess appropriate formulations to satisfy some of the criteria above. These models were chosen as they represent a broad spectrum of modelling approaches and applications, and have all been applied to recent morphodynamic studies in deltaic environments. Of course the disadvantage to utilising existing models, as opposed to developing a tool specifically for the study, is that trade-offs inevitably have to be made between factors such as spatial resolution, computational efficiency and the number of system components able to be formulated. Of the twelve models shortlisted, two were explored in further detail during methodological development: Delft3D and CAESAR-Lisflood. The results of this preliminary investigatory work are discussed below, before describing the selected model in detail in section 3.3.

System-based models operate under reduced complexity in order to decrease run times, resulting in more efficient simulation of long-term system behaviour. Of those system-based models listed in table 3.1, the Mississippi Delta Model (MDM) (Martin, 2000) displays the greatest potential to meet the desired specifications. In a report by Moffatt and Nichol Engineers (2000) examining the reliability of 32 hydrodynamic models used on the Mississippi delta, USA, the authors found that the MDM possessed a unique ability to simulate prograding deltaic environments that was beyond the scope of its peers. This report included the Barataria-Terrebone Ecological Landscape Spatial Simulation (BTELSS) (Reyes *et al.,* 2000) and the Coastal Ecological Landscape Spatial Simulation (CELSS) (Constanza *et al.*, 1990) models, also listed in table 3.1. This is due to the highly accurate formulation of ecological and soil modules within the MDM, that when integrated with hydrodynamic routines are able to simulate habitat change over multidecadal timescales (Martin *et al.,* 2002). The MDM is a landscape model that typically runs at a gridded spatial resolution of 1 km^2 for ecological modules, and 100 km^2 for hydrodynamic modules (Martin *et al.,* 2000). In order to provide initial conditions, each 1 km^2 cell is categorised as one of six habitat types utilised by the U.S. Fish and Wildlife Service: swamp; fresh marsh; brackish marsh; salt marsh; open water; and upland/agricultural. Within each cell, the above ground and below ground

ecological processes shown in figure 3.5 are simulated. At each time step, the cell exchanges materials with its four nearest neighbours as a function of hydrodynamic conditions, as well as external forcings such as climatic variables. As the MDM was designed to be applied at the regional scale, it cannot be expected to identify precise locations of habitat change (Martin *et al.,* 2000). Rather, the model has proved to be highly accurate at predicting large-scale temporal and spatial patterns of habitat change, and has been found to simulate ecosystem dynamics well at this resolution (Reyes *et al.,* 2009). However, it is questionable as to whether the coarse spatial resolution of the hydrodynamic module, although sufficient to capture overland flooding, would realistically capture the morphological detail of deltaic evolution desired by this study. Furthermore, the model has been developed specifically for use in the Mississippi region, and it may not be logistically viable to alter it for use in other locations.

Of the physics-based morphodynamic models listed in table 3.1, Delft3D has the potential to satisfy all of the designated model specifications. Produced by Deltares, an institute for applied research in coastal regions and river basins, the model is a popular choice amongst the scientific community due to its detailed morphological inputs, flexibility and user-friendly interface (Caldwell and Edmonds, 2010). Crucially for the purpose of this study, the model is capable of handling the interactions between physical factors such as sediment transport, morphology and storm surge with ecosystem services such as water quality and ecological health (Deltares, 2014). Furthermore, the model has been shown to provide reliable predictions in both natural and artificial environments, making it transferable between deltas of varying anthropogenic activity and also suggesting it could be used to successfully test the viability of various engineering strategies. Delft3D could therefore be the perfect tool with which to explore if morphological thresholds exist in deltaic CSESs, and the ways in which morphological processes interact with ecosystem services. Process-based models such as Delft3D are excellent tools for geomorphological analysis due to both the range of components able to be incorporated, and their scalar flexibility. However, the predominant drawback of such tools is that they are often computationally intensive); resulting in lengthy run-times and rendering calibration logistically challenging (French, 2015). Unfortunately this limitation was found to be detrimental to utilising Delft3D for this research during methodological development. The numerical complexity of

solving the shallow water equations that render Delft3D such a powerful hydrodynamic tool restrict its application to short timescales and/or coarse spatial resolutions (Vaz *et al.,* 2009). It became apparent during the development stage of a model for the Mahanadi Delta that the spatial resolution would have to either be made too coarse, or that the timescales observed would need to be reduced. Thus after considerable investigation and trial runs, the decision was made to discontinue the use of Delft3D in this project; despite its numerous benefits, the cost of gaining these was too great a compromise to the initial goals of the research.

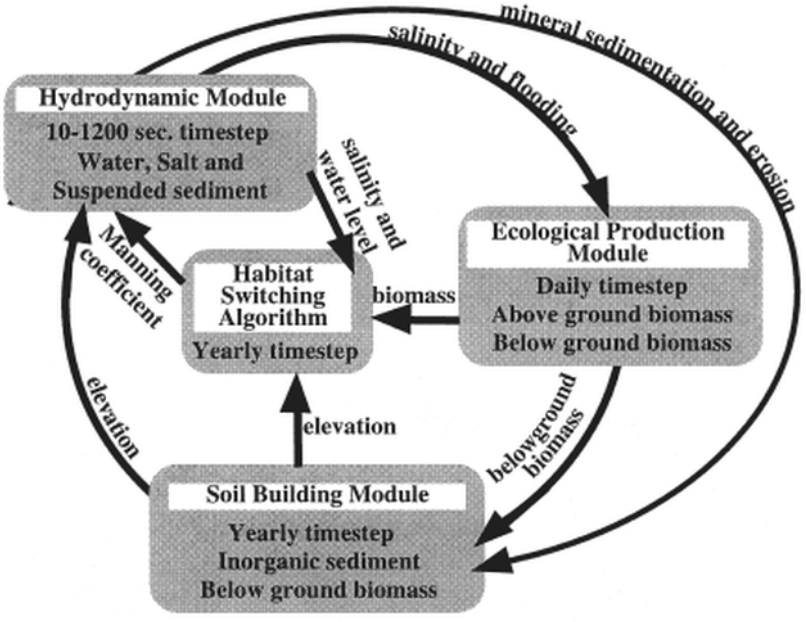

Figure 3.5 Connections between modules in the MDM also showing the time steps over which they operate. Habitat change takes place annually as salinity, biomass, and relative elevation cross pre-established thresholds. Source: Martin *et al*. (2002:359).

Cellular automata (CA) models – such as Coulthard's two-dimensional flow and sediment transport model, CAESAR-Lisflood; and Murray and Paola's CA model for

braided rivers (1994) – provide an alternative route to physics-based models that is less computationally expensive. CA models have become increasingly popular in geomorphological study as they are able to effectively simulate emergent phenomena. Furthermore, such models are well suited to the spatial nature of many geographical processes and also the widespread availability of gridded datasets from remote sensing, allowing these types of models to be easily integrated with geographical information systems (GIS) software (Coulthard, 1999). In CA models, the conditions in each cell are determined by a series of rules that govern how both it and its neighbouring cells will evolve. At each given time-step the conditions of each cell are updated in order to create a new baseline upon which the rules are then reapplied. As each cell is determined by both its own evolutionary pathway, and by continuous interaction with its neighbouring cells, CA models successfully portray how complex networks of interacting processes transform simple mathematical rules into emergent phenomena (Wolfram, 1984). Whilst the relative simplicity of CA models is suited to capturing emergent phenomena in purely physical processes, the integration of ecological and social system components into these models has proved challenging in the past (Coulthard, 1999); although this situation is ever-improving. Because of this, CA models have traditionally been applied to more 'abstract situations' rather than physical landscapes; thus validation of these models has been largely limited to qualitative evaluation, as opposed to quantitative validation using real-world observations (Coulthard *et al.,* 2007). Despite these limitations, the ability of CA models to simulate emergent behaviour makes them a useful tool with which to better understand the drivers that may lead to the crossing of critical thresholds in CSESs, and the temporal scales over which these phenomena may emerge (Dearing *et al*, 2006).

The cellular automata model CAESAR-Lisflood was also explored further in preliminary testing. Although initially Delft3D appeared the most appropriate choice of model, after the realisation that it may not be the most suitable tool for the desired spatial and temporal scales required by this research CAESAR-Lisflood was deemed the most appropriate for this study. Indeed, the only reason it had not been selected initially was due to the fact that it does not permit the investigation of as many ecological processes as Delft3D, and those that are able to be included do not vary across space. However, as will be discussed in section 3.3.3, current

developments to the model combined with the potential for collaborating with other research ongoing in the Mahanadi Delta, has made this much less of a compromise to objective two of this study (as referred to in chapter 1). Most importantly, CAESEAR's reduced complexity relative to Delft3D facilitates the investigation of a much larger range of scenarios over longer timescales, which is critical in order to achieve the successful simulation of emergent phenomena. Being able to study larger areas over longer time periods also arguably increases the value of the outputs produced from this research for optimum use in the Mahanadi region. Preliminary investigations using CAESAR-Lisflood produced promising results (see chapter 5 for a full description of model validation) relative to the trials undertaken in Delft3D, and thus the decision was made to continue utilising CAESAR-Lisflood. In the following section, the representation of morphological processes within CAESAR-Lisflood is introduced. A full description of the model setup specific to this study can be found in the methodology in chapter 5.

Table 3.1 Summary of the benefits and limitations associated with a selected group of twelve models used in morphodynamic applications

Model	Abbreviation and *model type*	Application (Example citation)	Optimum temporal resolution	Grid size	Primary drivers of morphological change	Can morpho-dynamics be simulated in sufficient detail?	Is integration of morphology and some ecological factors possible?	Can management scenarios be included?	Flexibility across global sites	Comments
Aggregated Scale Morphological Interaction between Inlets and Adjacent coast	ASMITA *System-based*	Morphological evolution of estuaries (Stive *et al.,* 1998).	Annual-centennial	>100m^2	Sea-level rise, wave climate, management	Yes	Not integrated at present	Yes	Yes	Potentially useful for large-scale sediment transport study but lacks an ecological module
Barataria–Terrebone Ecological Landscape Spatial Simulation	BTELSS *System-based*	Wetland evolution in the Mississippi Delta (Reyes *et al.,* 2000)	Annual	1km^2-100km^2	Climate, hydrodynamic conditions	Limited	Yes	Limited	Limited	Limited use as site-specific, and coarse representation of morphodynamics

Bay of Bengal Model	BoBM *System-based*	Hydrodynamics in the Bay of Bengal basin, particularly storm surge prediction (Debsarma, 2007)	Short-term events	3.5km^2	climate, storm surge	Yes	Not integrated at present	Limited	Limited	Potentially useful to examine storm surges in numerous deltas in the Bay of Bengal region, but hard to transfer elsewhere. Limited range of morphological drivers
CAESAR-Lisflood	C-L *Cellular automata*	Morphological evolution in river catchments (Coulthard, 1999).	Hourly-millennial	1m^2-2500m^2	climate, land cover	Yes	Limited as environmental controls are spatially uniform (Wang, 2013)	Yes	Yes	A useful geomorphological tool that is ideal for working at multidecadal temporal scales
Coastal Ecological Landscape Spatial Simulation	CELSS *System-based*	Wetland evolution in the Mississippi Delta (Constanza *et al.* 1990)	Annual-decadal	1km^2	climate, hydrodynamic conditions	Limited	Yes	Yes	Limited	Limited as site-specific, and coarse representation of morphodynamics
Coastal Evolution Model	CEM	Evolution of wave-dominated deltas	Short-term events	1m^2-1km^2	wave climate	Yes	Not integrated at present	Limited	Yes	Restricted to wave-dominated deltas, and

	Cellular automata	(Ashton and Murray, 2006)								also limited temporal resolution
Constanza and Ruth (1998) STELLA	STELLA *Cellular automata*	Simulation model of the Louisiana coastal wetlands (Constanza and Ruth, 1998).	Decadal - centennial	$1km^2$	climate, management	Limited	Yes	Yes	Limited	Potentially useful ecological elements but unable to capture deltaic morphodynamics at sufficient resolution.
Delft3D	D3D *Physics-based*	Response of delta channel networks to changes in river discharge (Edmonds *et al.*, 2010)	Short-term events-centennial	$1m^2$ - $>1000m^2$	climate, morphodynamic, management, ecological	Yes	Yes	Yes	Yes	Diverse and widely-used modelling suite, elements of which could be very useful for this study
High Resolution Cellular Model for Coastal Simulation	CEMCOS *Cellular automata*	Estuarine sediment dynamics (Dearing *et al.,* 2005).	Decadal - centennial	$2,500m^2$	wave climate, tidal regime, sea-level rise, management	Yes	Yes	Yes	Limited	Potentially useful model although designed for UK estuaries
Mississippi Delta Model	MDM *System-based*	Integrated hydrodynamic-ecological model for the Mississippi	Annual-centennial	$1km^2$-$100km^2$	climate, hydrodynamic conditions	No	Yes	Limited	Limited	Insufficient representation of morphodynamic processes but excellent ecological module for

		Delta (Martin *et al.,* 2002).								the purposes of this study
MOCDENS3D	MOCDENS3D *Physics-based*	Simulates fresh, brackish and saline groundwater flow in hydrogeological systems (Giambastiani *et al.,* 2007)	Annual-centennial	250m^2	salinisation, subsidence, sea-level rise, climate	Limited	Not integrated at present	Limited	Yes	Potentially useful model to examine accelerated subsidence but limited other uses
Sea Level Affecting Marshes Model	SLAMM *System-based*	Wetland evolution under sea-level rise scenarios (Clough and Park, 2007)	Decadal	5m^2-30m^2	sea-level rise	Limited	Yes	Limited	Yes	A potentially useful model, however at present representation of morphodynamic processes driven by factors other than tides are insufficient

3.3 CAESAR-Lisflood

3.3.1 Introduction

CAESAR is a cellular automata (CA) landscape evolution model, in which topography drives slope and fluvial processes in river catchments or reaches, for periods of hours up to thousands of years (Coulthard *et al.*, 2012). CAESAR-Lisflood, as used in this study, is the most recent development of CAESAR; combining the Lisflood-FP 2d hydrodynamic flow model (Bates *et al.*, 2010) with the CAESAR geomorphological model. Versions of the original CAESAR model had been developed and used successfully over 15 years to simulate erosion and depositional changes in river catchments over a range of temporal and spatial scales. However, a limitation of the model was that the representation of river flow was steady state and did not conserve mass of water nor momentum (Coulthard, 2014). The developer of the model, Thomas Coulthard (2014), goes on to describe how full 2d flow models at the time were too slow to simulate erosion and deposition over timescales greater than 10 years. However reduced complexity 2d flow models, such as Lisflood, were being developed to conserve mass without explicitly simulating secondary or cross channel circulation; primarily for application in predicting inundation areas from flood events. Small time steps of no more than two seconds were required to prevent numerical instability in these reduced complexity models. Coulthard describes how the Lisflood-FP code of Bates *et al*. (2010) made crucial steps by including a simple momentum term that dramatically reduced numerical instability allowing significantly longer time steps to be used. This increase in speed facilitated the inclusion of the 2d flow model within a landscape evolution model such as CAESAR; albeit with significant alterations to the code (over 70%). Both versions of CAESAR would have been suitable for this study; however, CAESAR-Lisflood (hereby referred to as C-L) provides the most up to date tool.

C-L has a number of enhancements compared to its predecessor, including additional parameters for lateral movement of sediment; and a method for speeding up the flow of the model during low discharge or times when the system is in steady state. Furthermore, Lisflood-FP itself has been shown to be especially adept at simulating rapid wetting and drying, making them ideal for dealing with areas prone to flood inundation (Bates *et al.*, 2010), and has already been applied successfully in deltaic environments in the Bay of Bengal (Lewis *et al.*, 2013).

C-L represents river catchments and/or reaches with a regular mesh of grid cells of uniform sizes, and follows a relatively simple structure to determine landscape evolution (figure 3.6). To run the model, each cell contains information on initial conditions such as elevation, grain size distribution, vegetation cover and roughness; as well as two forcing conditions at set inflow points on the grid: sediment discharge and water discharge (Van De Wiel *et al.,* 2007). At every given time step during landscape simulation, these properties are modified according to the interaction between a cell and its neighbours, based on rules that represent various morphological and hydrological processes. This alters the topography of the landscape accordingly, which in turn alters the starting point for the next iteration. Although individually these rules are relatively simple representations of fluvial and hillslope processes, their combined and repeatedly iterated effect is such that complex non-linear behaviour, and both positive and negative feedbacks can emerge (Van De Wiel *et al.,* 2007). A description of these processes is provided below in section 3.3.2. A thorough description of all model parameters and the latest updates to the C-L model can be found in Coulthard (2016).

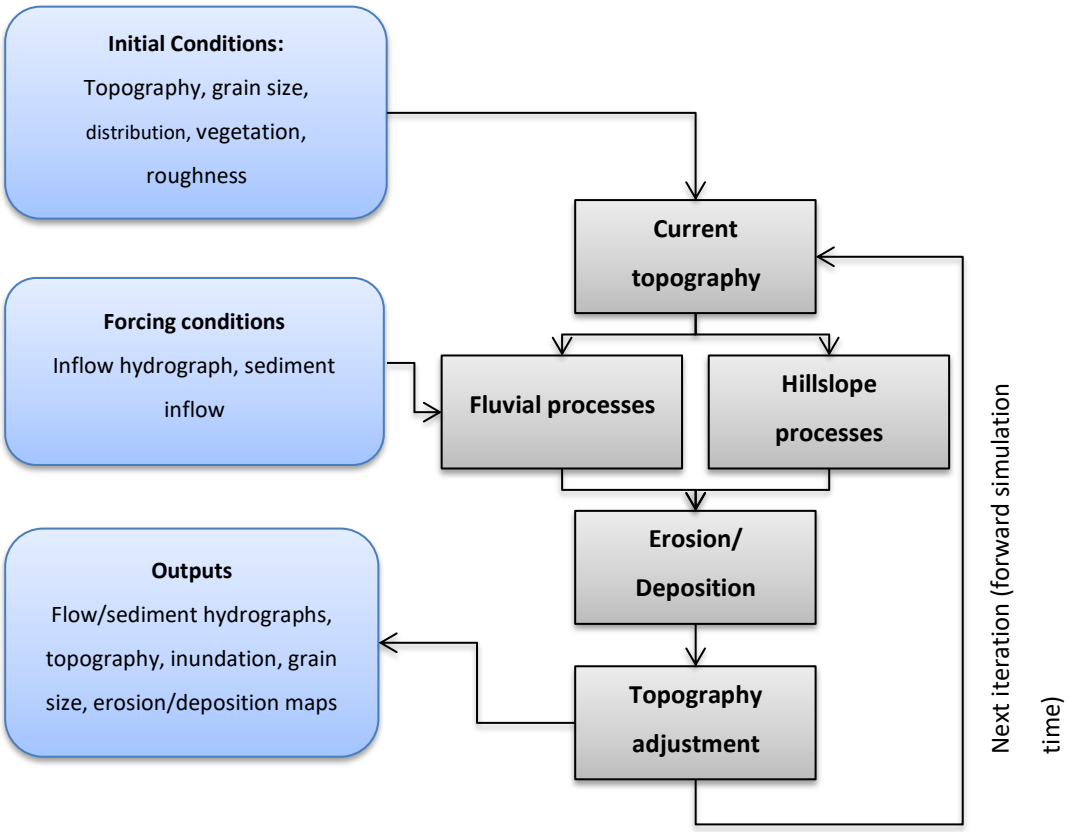

Figure 3.6 Conceptual diagram showing the structure of CAESAR and CAESAR-Lisflood, based on Van De Wiel *et al.* (2007)

3.3.2 Morphological and Hydrological Processes

The C-L model can be operated in two modes: reach mode, as utilised in this study and discussed below; and catchment mode, which is described in Coulthard *et al.* (2002) and Van De Wiel *et al.* (2007). In reach mode, sources of both water and sediment discharge are added at user-defined points on the digital elevation model (DEM). As no standalone manual exists for the most recent update of CAESAR, much of the following descriptions of morphological and hydrological processes in C-L are based on a paper written by the model developers (Coulthard *et al.,* 2013), in which the transition from CAESAR to C-L is discussed in detail; and a paper by Van De Wiel *et al.* (2007), which discusses the processes formulated in CAESAR.

The flow model in the original version of CAESAR utilises a flow-sweeping algorithm, which calculates a uniform, steady state flow approximation of the flow field (Coulthard *et al.*, 2013). Discharge from a cell is distributed to all cells within a 2 – 5 cell range in 8 directions, dependent upon the differences between

the water surface elevation of the contributing cell and the bed elevations of its neighbours. If none of the neighbours are found to be suitable receiving cells, the discharge remains in the initial cell to be distributed in subsequent sweeps during the same scan. Flow and depth velocity are then calculated using Manning's equation (Coulthard *et al.,* 2013). In C-L, the flow sweeping algorithm has been replaced by the Lisflood-FP model (Bates *et al.,* 2010). Lisflood-FP is a one-dimensional model derived from the full shallow water equations, that when applied in both the *x*- and *y*- directions simulates two dimensional flow over a raster grid. The flow between cells (Q) is calculated by Equation 1:

$$Q = \frac{q - g h_{flow} \Delta t \frac{\Delta(h+z)}{\Delta x}}{(1 = g h_{flow} \Delta t n^2 |q| h_{flow}^{10/3}} \Delta x \quad [1]$$

Where q is the flux between cells from the previous iteration (m^2s^{-1}), g is acceleration due to gravity (ms^{-1}), n is Mannings roughness coefficient ($m^{1/3}s^{-1}$), h is depth (m), z is elevation (m), h_{flow} is the maximum depth of flow between cells, Δx is the grid cell width (m) and t is time (s).

Once discharge has been calculated across all four boundaries of a cell, the water depth (h) is updated using Equation 2:

$$\frac{\Delta h^{i,j}}{\Delta t} = \frac{Q_x^{i-1,j} - Q_x^{i,j} + Q_y^{i,j-1} - Q_y^{i,j}}{\Delta x^2} \quad [2]$$

Here, i and j are the cell co-ordinates in the *x*- and *y*- directions, respectively. In the final component of the Lisflood formulation, the time step (Δt) is controlled by the shallow water Courant–Freidrichs–Lewy (or CFL) condition in Equation 3; which requires that the wave does not propagate across more than one cell per time step:

$$\Delta t_{max} = a \frac{\Delta x}{\sqrt{gh}} \quad [3]$$

Where a is a coefficient with a value between 0.3 and 0.7, that enhances the model's robustness in nonlinear systems (Bates *et al.,* 2010). An important difference to note between the sweeping algorithm in CAESAR and the Lisflood-FP flow model in C-L is that the former routes flow from a cell in 8 directions, and the latter only 4. This presents a limitation that must be considered when utilising C-L; in that it does not permit single-thread channels to develop diagonally in coarse resolution DEMs. Coulthard *et al.* (2013) discuss how the use of hexagonal cells would provide a solution to this problem, but that this would hinder the easy interchange of data between models and GIS packages.

C-L can distinguish between up to nine different sediment fractions, both horizontally and vertically. Sediment is transported as either bed load or suspended load dependent upon grain size: Bed load is moved directly between cells; whereas the movement of suspended load is dependent upon fall velocities and the concentration of sediment in suspension within a given cell (Coulthard *et al.,* 2013). Sediment transport is driven by a mixed-size formula (Equation 4) which calculates transport rates, q_i, for each sediment fraction i (Wilcock and Crowe, 2003):

$$q_i = \frac{F_i U_*^3 W_i^*}{(s-1)g} \quad [4]$$

Where F_i is the fractional volume of the sediment in the active layer, U^* is the shear velocity, s is the ratio of sediment to water density, and $W_i^*$is a complex function that relates to the fractional transport rate to the total transport rate. It is important to note that the Wilcock and Crowe formulation was designed primarily for sand/gravel mixtures, and its use has been extrapolated in various versions of CAESAR to include finer non-cohesive sediments. Although untested, Van De Wiel *et al.* (2007) deem this extrapolation a sufficient initial approximation for most investigative studies in fluvial systems. However as this study is investigating change in a predominantly silt-based sediment system, it is something to bear in mind.

Rates of transport are converted into volumes, V_i, by multiplying q_i by the time step of the iteration, $\mathrm{d}t$, as in Equation 5:

$$V_i = q_i \mathrm{d}t \quad [5]$$

C-L uses time steps of variable length for each iteration, such that the maximum rate of entrainment, $q_{\max}$, results in a maximal allowed elevation change, $\Delta Z_{\max}$ (Equation 6).

$$\mathrm{d}t = \frac{\Delta Z_{\max} C_{\mathrm{w}}^2}{q_{max}} \quad [6]$$

with the default $\Delta Z_{\max} = 0.1\ L_{\mathrm{h}}$, where L_{h} is the thickness of the sediment layers. The implementation of variable time steps allows the model to operate at high temporal resolution (sub-second) during periods of high geomorphological activity, and at a coarser resolution (hourly) during quieter periods. However, as the new flow model in C-L has its own control on model time step that wasn't present in earlier versions of CAESAR (Equation 3), sometimes this creates situations where the flow model time step is smaller than the erosion/deposition time step, particularly during low flows (Coulthard *et al.,* 2013). Conversely, situations also arise when during high flows, the erosion/deposition time step is much smaller than that of the flow model. C-L will automatically choose the smaller time step from either component. To overcome slow computational times during these situations, C-L measures the difference between hydrological inputs and drainage basin outputs. If the difference is lower than the threshold defined by the user (e.g. 1 $m^3 s^{-1}$) then the time step will be conditioned by the flow model in Equation 3. Effectively, the time period between two high flow events may be overlooked in the hydrodynamic model, though all sediment transport is simulated, so that the overall model time advances faster; a method that has also been implemented by Lesser *et al.* (2004) and Crosato *et al.* (2012).

Transportation of sediments varies between bed load and suspended load. Bed load is distributed proportional to the local bed slope (Equation 7):

$$V_{i,k} = \frac{S_k}{\sum S} V_i$$

[7]

Where i denotes the sediment fraction, k is the direction of the neighbour, V is volume, S is slope. Only neighbouring cells with lower elevations are considered for bed load transport. The routing of suspended load, however, is based on flow velocity and was updated between CAESAR and C-L (Equation 8):

$$Q_s = Q(S_{tot}/_h)$$

[8]

Where Q_s denotes the suspended sediment moving between cells (m^3s^{-1}), Q is water flow, and S_{tot} is the total suspended sediment depth in a cell. Then as per the flow model in equation 2, changes in sediment flux are totalled (Equation 9).

$$\frac{\Delta S_{tot} i,j}{\Delta \mathrm{t}} = \frac{Qs_x^{i-1,j} - Qs_x^{i,j} + Qs_y^{i,j-1} - Qs_y^{i,j}}{\Delta x^2}$$

[9]

Deposition of sediments also varies between bed load and suspended load. At each iteration all bed load material is deposited in the receiving cells ($V_{i,\mathrm{dep}} = V_i$), where it can be re-entrained in subsequent iterations. Suspended sediment is deposited dependent upon fall velocities, v_i, and suspended sediment concentrations, K_i, for an individual suspended fraction (Equation 10). The remaining volume of suspended sediment is retained for the next iteration.

$$V_{i,dep} = K_i V_i c_w^2 \mathrm{d}t$$

[10]

Selective erosion, transport and deposition of the different sediment fractions results in spatially variable sediment distributions. C-L expresses this variability both horizontally and vertically, thus a method of storing sub-surface sediment data is required (Van De Wiel *et al.,* 2007). Sediment layers in C-L consist of an active layer, which has a variable thickness; multiple buried layers of up to 20 strata of fixed thickness (L_h); a base layer, comprising the lower part of the buried

regolith; and a bedrock layer which cannot be eroded. As erosion takes places sediment is removed from the active layer. If the thickness of the active layer is reduced below 0.25 L_h, then the upper stratum is incorporated in the active layer, creating a new, thicker active layer. Alternatively, if deposition occurs the active layer increases in size. If the thickness of the active layer is increased above 1.5 L_h, then a new stratum is created, leaving a thinner active layer (Van De Wiel *et al.,* 2007).

A major improvement to the latest version of CAESAR, which has also been preserved in C-L, is the implementation of a lateral erosion algorithm. Van De Wiel *et al.* (2007: 288) describe how the algorithm is split into three conceptual sections. The first and most time consuming aspect is to determine the local channel curvature, R_{ca}. Several passes are made over the grid during this calculation. During the first pass, edge cells are identified; these being defined as dry cells ($h = 0$) with at least one wet neighbour ($h > 0$) in one of the four primary (non-diagonal) directions. During the second pass, a filter is applied to determine inside and outside banks. Where an edge cell exists at the centre of the filter, the total number of dry cells is calculated, excluding other edge cells. Simultaneously, the number of wet cells is summed. Only the largest connected series of wet cells in the filter is counted, in order to avoid false identification of inside banks in near-cut off situations. The total number of wet cells is subtracted from the number of dry cells, and this value is assigned to the edge cell at the centre of the filter. This value represents a local expression of R_{ca}, while its sign identifies it as an outside (positive) or inside (negative) bank. This step, Van De Wiel *et al.* (2007) argue, provides only a rough measure of curvature, given that a meander can appear to contain elements of both inside and outside banks. To reduce this roughness a smoothing filter is applied that averages the curvature along the edge cells. The final R_{ca} value is thus a dimensionless approximation of the actual radius of curvature, *R*. Coulthard and Van De Wiel (2006) showed a significant correlation between the R_{ca} and R (r^2=0.9998; n=6) (Equation 11)*:*

$$R = 2.13 \mid R_{ca} \mid^{-1.08} c_w \qquad [11]$$

The second stage of the lateral erosion algorithm is to calculate the lateral erosion rate, ζ, as shown in Equation 12:

$$\zeta = E_{ca} R_{ca} U_{nb} h_{nb}$$

[12]

Where E_{ca} is a bank erosion coefficient, U_{nb} denotes the near-bank flow velocity and h_{nb} is the water depth in the wet cells neighbouring the edge cell.

The final stage of the lateral erosion algorithm is to distribute the eroded sediments across the channel. An added feature in C-L that was not formulated in CAESAR is an 'in channel' lateral erosion function (Equation 13). This allows for the process in which following river bed erosion, the areas adjacent to the incision will lose material to the area that has just been eroded via collapse of lateral movement of sediment, without resulting in unnatural channel narrowing as a result of positive feedback (see Coulthard *et al.* 2013).

$$\Delta z_{i-1,j} = \Delta z_{i,j} L \frac{z_{i-1,j} z_{i,j}}{\Delta x}$$

[13]

Where the amount of material moved from a cell ($\Delta z_{i-1,j}$) adjacent to a cell that erodes is proportional to the amount eroded from the cell ($\Delta z_{1,j}$), a constant (L), and the slope between cells. Coulthard *et al.* (2013) highlight that this formulation is similar to the lateral sediment movement function utilised in Murray and Paola's (1997) braided river model.

Tidal and sea-level data are not required to run C-L, but can easily be incorporated where appropriate as an elevation (m) relative to the level that the DEM is set to for each time step. If this function is selected, C-L fixes the water elevation to that height for those cells, and the flow routing processes alter accordingly (Coulthard, 2016).

3.3.3 Habitat cover

Land cover change, and in particular changes in vegetation cover, is a dynamic and complex process that has a significant influence on erosion rates in river basins and the capacity to maintain ecosystem services (Leh *et al*., 2011; Fernandez *et al*., 2015). Changes in habitat also effect geomorphological processes within river channels themselves: Godoy and Lacerda (2014), for example, found that a large increase in the area of land converted to plantations in the Jaguaribe River basin, Brazil, resulted in an additional 282,322 $t.yr^{-1}$ of sediment reaching the estuary. Other activities increasing sediment load to the estuary include increasing urbanisation, shrimp farming and livestock grazing. The authors found the combined influence of these significant land cover changes had resulted in an increase of 24.15 ha in the area of islands in the channel between 1988 and 2010, and a subsequent increase in the area of mangrove vegetation colonising these depositional landforms. Whilst this has had beneficial impacts in terms of reducing erosion rates, this has also made navigation in the estuary increasingly difficult over recent years, and is also aggravated by the decrease in river flow in recent decades due to a combination of damming and decreases in annual precipitation (Godoy and Lacerda, 2014).

In both CAESAR and recent versions of C-L, the effects of land cover change have been formulated in such a way that they have few explicit interactions with the hydrological model and are represented homogenously across the catchment. Using a linear growth model, vegetation simply exists to allow a protective turf mat to develop over flood deposits over monthly time steps (Coulthard, 2000). Provided the cell remains dry for ten years, full cover will develop. If the layer is eroded, material is removed from the vegetation fraction of the active layer and treated as if washed out of the catchment, as opposed to being re-deposited as sediment would be. The presence of vegetation in C-L has no effect upon the elevation of the cell, but the partial removal allows exposed material underneath to be eroded. As will be explained in detail in chapter 5, in the most recent version of C-L being utilised in this study, the user can also define how quickly vegetation reaches maturity, and to what extent it limits lateral erosion. Furthermore, a spatially variable Manning's roughness coefficient file can be added to the model, in order to allow for different types of land cover. Both of these factors are significant improvements that have been developed since commencing this research project. Despite its relatively simple representation therefore, C-L provides a useful tool to investigate how land cover changes over

multidecadal timescales interact with flow and sediment transport patterns. A new version of C-L is currently being developed in which spatially variable vegetation cover can also be applied to the catchment; adding further detail to the spatially variable roughness coefficients file.

Chapter 4 **The Mahanadi Delta, India**

4.1 Introduction

The Mahanadi Delta is one of several deltas on the eastern coast of India that drain into the Bay of Bengal. Located in the state of Odisha (formally known as Orissa), the delta extends over the entirety of the districts of Puri and Jagatsinghapur. It also includes a large area of the districts of Khorda, Cuttack and Kendrapara; and small areas of the districts of Bhadrak, Jajapur, Nayagarh and Ganjam. For the purpose of this study, the Mahanadi Delta area outlined in figure 4.1 matches the boundary defined by Wetlands International (2014a). The delta is an ecological and socio-economic hotspot, supporting more than one third of the population of Odisha, 68% of who are farmers (Wetlands International, 2014a).

The Mahanadi region was chosen for this study as it provides an ideal setting to explore a broad variety of environmental stressors in a biophysically diverse landscape. The predominant drivers of morphological change in the Mahanadi system (as discussed in section 4.3) are representative of modern pressures experienced in many other world deltas, rendering the results of this research transferable to other locations. Whilst such a site-flexible approach is an important goal of this study, this research will also provide morphological projections that can be used to help develop and test climate-resilient strategies in the Mahanadi Delta itself; a system that has regularly been highlighted in recent research as one at significant risk from climate change and increased anthropogenic interventions within its distributary network (Syvitski *et al.,* 2009; Jena *et al.,* 2014). Furthermore, one of the greatest stressors to those living in the delta is the decreased return period between extreme flood and drought events (Pearce, 2014). The Mahanadi therefore provides a perfect platform to explore the effects of shifts in the magnitude and frequency of stressors, and potential thresholds in the morphological system; elements crucial to developing a clearer understanding of deltaic complex socio-ecological system dynamics more generally.

The Mahanadi was also chosen due to the wide range of active multidisciplinary research taking place in the delta, providing a substantial amount of hydroclimatic data with which to help design and validate the model setup (see chapter 5 for a detailed description of the data utilised). The global non-

governmental organisation (NGO), Wetlands International, have been actively working to promote stakeholder-led integrated water resource management in the Mahanadi Delta region for over a decade. Their primary aims include reducing flood risk and promoting sustainable food and water security, through a combination of wetland restoration, environmental monitoring and community engagement (Wetlands International, 2014b). Wetlands International was one of several NGOs to be involved in the reconnection of the Chilika Lake lagoon system to the sea, which had rapidly degraded over the latter 20th century due to increased siltation. In September 2000, the installation of a new channel through the barrier beach at Satapura restored the natural flows of water and salinity levels, resulting in a sevenfold increase in fish yield and a reduction of freshwater weeds (Kumar, 2014 in Wetlands International, 2014c). Despite the success of this hydrological intervention, Wetlands International recognise that current knowledge as to how the delta will be affected by shifts in climatic regimes is lacking (Wetlands International, 2014b). It is hoped that the biophysical projections provided by this study could be of use to the sustainable planning of important ecosystems in the delta.

The Mahanadi Delta is also one of three study sites examined by the international research project, DECCMA (Deltaic Environments, Vulnerability and Climate Change: Migration and Adaptation) (DECCMA, 2015a); together with the Ganges-Brahmaputra-Meghna in Bangladesh and India, and the Volta in Ghana. DECCMA's research is concerned with understanding and reducing the vulnerabilities of these complex social-ecological systems in the face of growing environmental and climatic stressors. The five year project aims to develop methods to predict how these three deltas may evolve over the next century, and to provide the knowledge and tools to ensure future policy is of maximum benefit to their populations. A particular focus of DECCMA's research is to assess the benefits of planned migration as a potential adaptation strategy in some suitable locations. Migration has notoriously been portrayed as a failure to adapt to the physical effects of climate change; this negative perspective exacerbated by the perpetuating vulnerability it can cause to those left behind and the fact it is viewed as a forced action as opposed to free choice (Martin *et al.,* 2013). However, planned and equitable migration can also increase the resilience of the migrant household relative to other available adaption strategies which may not be adequate to cope with increasing conditions of environmental stress, such as disaster risk reduction,

land use management or polders (DECCMA, 2015a). In order to identify where migration could increase resilience in these deltas over forthcoming decades, DECCMA aims to develop an integrated assessment tool (IAT) that is able to combine economic, social and biophysical knowledge to inform a wide range of stakeholders of the implications of various adaption options. It is therefore hoped that the biophysical projections provided by this study can contribute significantly to the development of DECCMA's IAT, and through being integrated with socio-economic data in this way the impact of this research can be maximised. Specifically, this study can contribute towards the identification of biophysical vulnerability hotspots in the Mahanadi in order to meet the aims of DECCMA Work Package 2 (see DECCMA, 2015b), and as such may feed more directly into the development of climate-resilient policies in the delta. Of course, an additional advantage of choosing the Mahanadi as the study site for this project is the logistical support of a strong and vibrant multidisciplinary team, involving researchers from a broad range of social and physical sciences, many of whom are focusing on the Mahanadi specifically.

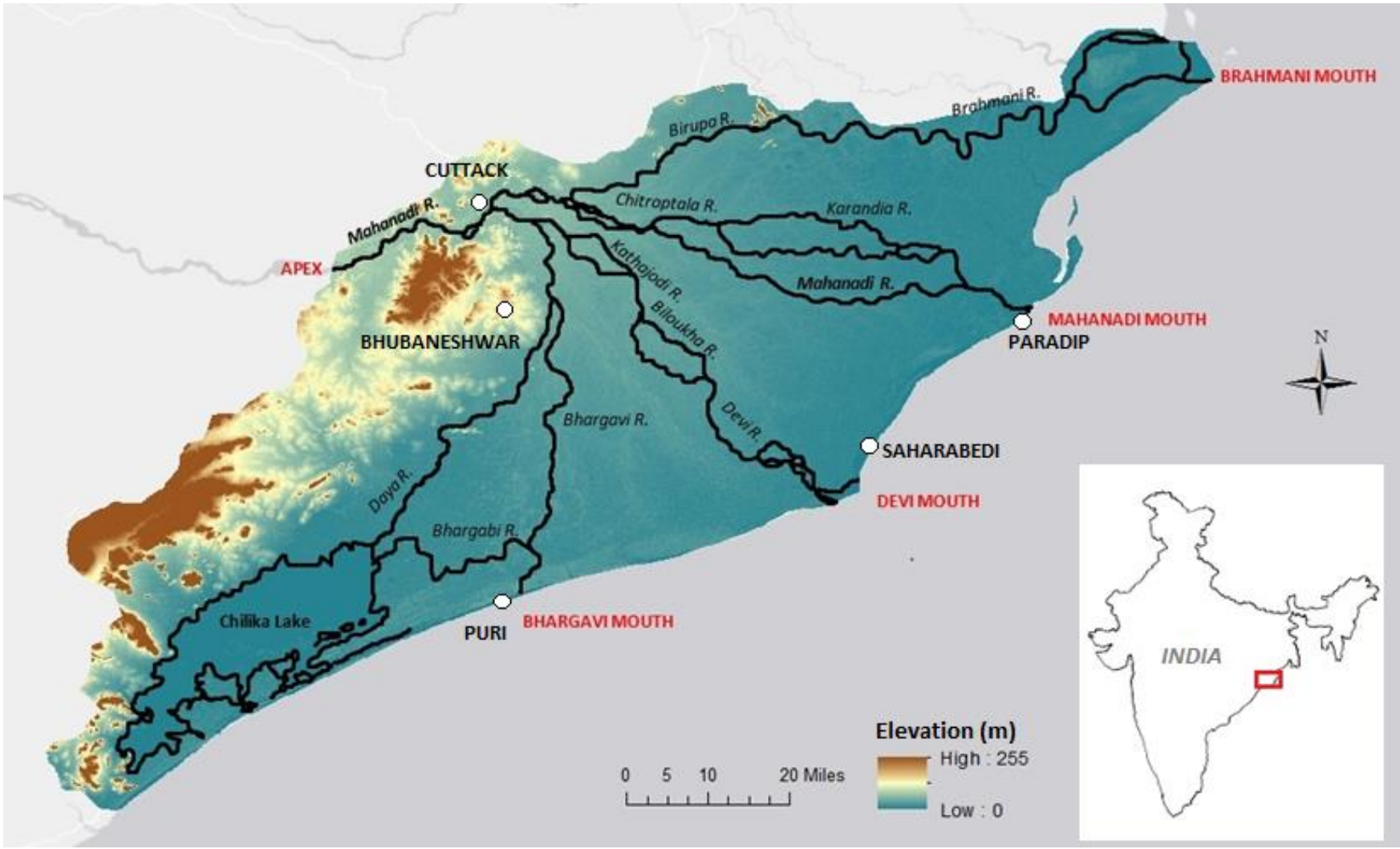

Figure 4.1 Location of the Mahanadi Delta showing major distributary channels, key settlements and elevation

4.2 Morphological setting and catchment selection

The arcuate deltaic plain extends over an area of 14,873 km^2, covering a coastline of 280 km. It is likely that the initial formation of the delta was triggered ~6ka following an abrupt deceleration of global sea-level rise (Mohanti and Swain, 2011). Sambasiva Rao *et al.* (1978) support this, having dated the oldest beach deposits found in the delta at 6000 yrs. B.P. A majority of delta building occurred between 6000 – 800 years ago (Mohanti, 1993), during which time progradation has occurred at a rate of ~9.1 km per millennia (Somanna *et al.,* 2013). Mahalik *et al.* (1996) describe four major stages in the evolution of the delta over the late Holocene (figure 4.2): During the first stage, the main channel of the Mahanadi River branched off to give rise to its earliest distributary system, the Old Kathjodi. The coastline at this time was approximately 40 km further inland than at present. A northward bend evident in the paleochannels of the Old Kathjodi system indicates that a northerly littoral drift was occurring at the coast, as is still present today. During the second stage, two new groups of distributary channels emerged and extended the delta plain laterally to the north and south; the Sukbhadra and the Burdha systems. Ancient beach ridges are evident running parallel to the present day-coast. In the third stage described by Mahilik *et al.* (1996), three further distributary systems – the Prachi, Ratnachira and the Alaka – formed. The Prachi was the largest, flowing south easterly from the main branch of the Mahanadi and giving rise to the Ratnachira channels. The Alaka branched off of the Bhurda River, making the latter system defunct. Many of the paleochannels formed during this stage can be seen clearly in the present-day Mahanadi system; as can a series of ancient beach ridges as the coast continued to advance eastwards. In the final stage, the major rivers that we see today formed causing the above systems to become abandoned. Many of these ancient channels are defunct although some may still flow periodically during floods. The coastline extended further east near to its present position, with a series of spits and bars formed by a strong northerly littoral current.

The densely populated upper regions of the delta consist of extensive plains, levées and palaeochannels. Sixty percent of the land is utilised for agricultural purposes, comprised mostly of single-crop rice fields, and a further 25% is dense

forest (Jena *et al.,* 2014) (see figure 4.3 for land use data). The less heavily populated coastal regions are comprised of a patchwork of tidal-dominated landforms such as creeks, mangroves and swamps; and wave-dominated beaches, spits and bars. The coastline extends between the mangroves of Bhitarkanika National Park in the north and the ecologically-rich wetlands of Chilika Lake in the south. Chilika Lake is the largest brackish water wetland complex in Asia, and was declared as a Ramsar site under the convention on "Wetlands of International Importance" in 1981 (Kumar and Pattnaik, 2010; Nayak *et al.,* 2004). As discussed briefly in section 4.1, water quality in the lake has been dramatically improved in recent years due to the installation of a new channel at Satapura, reconnecting the sea to the lagoon that had previously become choked with fluvial silt.

With the exception of small hills in the south-western fringe of the delta, elevation is extremely low (figure 4.1) with approximately 10% of the total area situated less than 2 metres above mean sea-level (Syvitski *et al*., 2009). Figure 4.1 also shows the location of the major active channels across the delta plain. The northernmost area of the Mahanadi Delta is combined with deltaic deposits from two other major rivers that drain into the Bay of Bengal: the Brahmani and Baitarani. Approximately 32 km east of the delta apex near the city of Cuttack, the main channel of the Mahanadi River bifurcates into 2 major distributaries. The most southerly, the Kathajodi River, bifurcates again after 9 km to form 2 major channels: the most southerly of these, the Kuakhai River, bifurcates approximately 26 km downstream. The southern channel, the Daya River, flows into Chllika Lake. The northern branch of the Kuakhai, the Bhargavi River, also has distributaries that flow into Chilika Lake, and is partially restricted at the mouth by a sand bar. The northern bifurcation of the Kathajodi River reaches the coast near Saharabedi as the River Devi; the most active distributary channel in the delta (Mahalik *et al.,* 1996). Approximately 15 km after its initial bifurcation, the Mahanadi River bifurcates further into two branches: the main channel continues for 85 km, reaching the coast near town of Paradip. The northern branch, the Birupa River, travels across the northern extent of the deltaic plain, merging with distributary channels from the Brahmani River system before reaching the coast near the town of Dhamara.

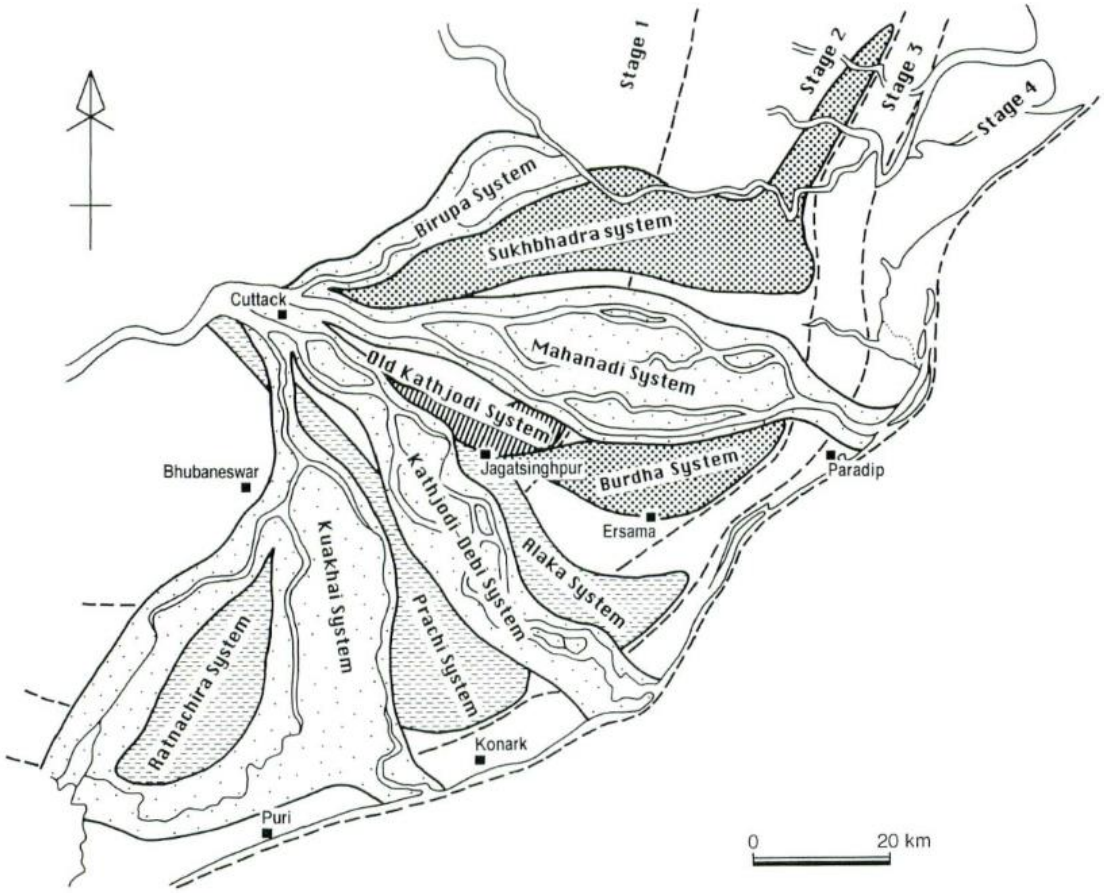

Figure 4.2 Figure by Mahilik *et al.* (1996) showing the four major stages in the morphological evolution of the Mahanadi Delta over the late Holocene.

This study aims to compare the impacts of various environmental stressors between different watersheds that represent a specific morphological region of the delta. This decision reflects a trend that has emerged in the environmental sector in recent years, towards favouring a catchment-based approach to both fluvial and coastal management (Patterson and Billington, 2013). A watershed provides a natural scale to bring together the numerous and multi-faceted social and ecological factors influencing a river system. This approach has also been shown to bring together often conflicting stakeholders, given their shared interest in a particular water source (DEFRA, 2013). The decision to work at the catchment scale was also made in order to test the application of the proposed framework between regions of a delta that are dominated by differing morphological processes, and/or variable rates of physical change. Given the huge diversity of processes and stressors that influence modern deltaic evolution (as discussed in chapter 2), it is hoped that this more focused approach will maximise the transferability of this research to other deltas around the world. Furthermore, the size of a deltaic river catchment (often 10s – 100s km from delta apex to mouth) provides an ideal spatial scale with which to study the multidecadal evolution of the delta environment.

As is discussed further in section 6.2, there are of course some limitations to choosing to work at a catchment level as opposed to considering the entire delta system. The low-lying topography of the delta landscape means that the boundaries of these watersheds are not fixed during times of particularly high flows; as they would be in an upland catchment system. This must be considered when analysing processes occurring at the boundaries of the modelled catchment. Furthermore, some of the metrics presented in the methodology in chapter 5 were designed to be utilised at the delta system level. Whilst they are able to be downscaled to the catchment scale (see section 5.3.3 for a description of how these were adapted) this does of course impact the validation of these tools in this study when comparing it with results from the existing literature. Despite these limitations it is felt that the advantages of operating at the catchment level offset the restrictions that it presents, and it is particularly important from a governance perspective to work towards creating frameworks that are able to be applied at this scale. It also does not mean that a whole delta system cannot be studied utilising this framework, given that an integrated

catchment approach could be adopted in order to study all of the catchments across a deltaic plain.

In this study two contrasting watersheds in the Mahanadi Delta have been selected: that of the Devi River in the south and the Mahanadi River in the north (figure 4.4). As stated above the Devi River is currently the most active distributary in the delta in terms of channel migration. Conversely, the main channel of the Mahanadi River has become increasingly morphologically inactive over recent decades; providing the opportunity to contrast the active fluvial-dominated lobe with one that could potentially become abandoned in the long-term. There is also significant coastal erosion at the coast of the Mahanadi River catchment near Paradip, providing the opportunity to test the application of the model in the regions of the delta where coastal processes dominate. Furthermore, the two other dominant active watershed systems in the Mahanadi Delta – the Birupa in the north and the Kuakhai in the south – both have slightly unusual morphological characteristics that may not be suitable for an exploratory investigation as employed in this study: The Birupa system merges the with the Brahmani-Baitarani delta located outside of the Mahanadi basin; whilst the Kuakhai drains into Chilika Lake and is therefore subjected to a different range of geomorphic processes.

Mean annual rainfall in the region is 1572 mm, over 70% of which is precipitated during the southwest monsoon between June and September (Mohanti and Swain, 2011). Cyclonic storms are common during the post-monsoon (October-November) and pre-monsoon (March-May) periods, with the highest rainfall totals experienced in coastal regions (Mohanti, 2000). The average discharge of the Mahanadi channel is 2,119 $m^3.s^{-1}$, with flooding typically occurring when discharge at the mouth exceeds 17,150 $m^3.s^{-1}$ (Mohanti and Swain, 2011). During the most severe floods this figure may exceed 45,000 $m^3.s^{-1}$. The nearest gauging station to the delta apex is located 110 km upstream of Cuttack at Tikarapara. For this study, daily discharge data for this site from 1972 – 2012 has been obtained from the Central Water Commission (courtesy of Sugata Hazra, Rahul Sharma and the WRIS). At Tikarapara, mean discharge for the period 1972 – 2012 was 1,515 $m^3.s^{-1}$, with a maximum flow of 33,800 $m^3.s^{-1}$ and a minimum flow of 23 $m^3.s^{-1}$. At this location, peak precipitation occurs in July and peak discharge occurs during September.

Sediment deposition is principally monsoon-dominated: An average suspended load of 7.08 MT and a bedload of 2.70 MT are carried to the mouth of the active lobe during the monsoon season (June – September) (Delta Development Plan, 1986 in Mohanti and Swain, 2011). Daily sediment data from 1973 – 2012 has also been obtained from Tikarapara gauging station (courtesy of Rahul Sharma and the WRIS). As discussed in chapter 5, daily concentrations of coarse (> 0.2 mm), medium (0.2 - 0.075 mm) and fine (< 0.075 mm) grains in units of grams per litre were provided and converted into volume using the known discharge of the river and the density of the grains. The relative proportions of each sediment fraction were taken from Ghose *et al.* (2011), who found the load at Tikarapara to consist of 95%, 2.7% and 2.3% of fine, medium and coarse fractions respectively. The suspended load enters the Bay of Bengal as a hypopycnal buoyant plume that may extend up to 15 km from the coast during months of high discharge (Mohanti, 1993).

Wave processes dominate between March and November, with modal wave heights typically reaching 1.5 metres, increasing to 3.3 metres during storm conditions (Natesan *et al.,* 2013). Waves tend to strike at an oblique angle inducing a north-easterly longshore drift, responsible for transporting 1.4×10^6 $m^3 \cdot yr^{-1}$ (2.9 $MT.yr^{-1}$) of sediment along the coast (Mohanti and Swain, 2011). This strong littoral drift has resulted in a dynamic complex of sand shoals, bars and spits along the Mahanadi coastline, features that are highly vulnerable to sudden and severe erosion during cyclonic conditions, where storm surges frequently reach 12 metres (Mohanti, 2000). The coastline is microtidal with a mean range of just 1.29 metres along much of the coast (Mohanti and Swain, 2011), although tidal amplitude can reach 4.5 metres in the active estuary mouth (Selvam, 2003). Subsequently it is only during the dry season, when discharge is low and wave activity is reduced, that tidal processes have a significant influence over deltaic morphology. Tidal processes are particularly dominant in the northern abandoned lobes (Coleman and Huh, 2004). Water salinity in the wetlands of the Mahanadi varies from 2 to 6 parts per thousand (ppt) during the monsoon season, 18 to 30 ppt during the winter season, and 25 to 32 ppt during the summer months (Selvam, 2003).

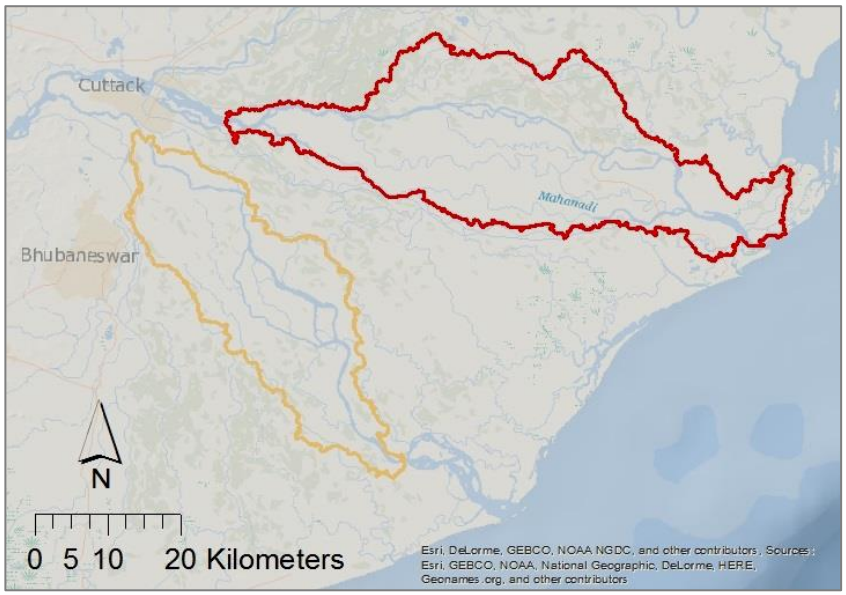

Figure 4.3 Outlines of the watersheds for the Devi River (yellow) and the Mahanadi River (red)

4.3 System stressors

The Mahanadi system provides the ideal setting to explore the broad range of stressors stated in chapter 2. Over recent decades, the delta has been increasingly affected by poor water resource management and increasing hydroclimatic variability. Changes in land-use, extensive channel modification and changes to agricultural practices have all put increasing pressure on the biophysical component of the delta system. This, combined with more regular fluctuations between extreme precipitation events and drought periods, as well as an increase in the magnitude of these meteorological events, has made it ever more difficult for those communities living in the worst affected regions to cope with present rates of biophysical change (Jena *et al.,* 2014).

In their review of 33 world deltas chosen to be representative of a broad range of deltaic environments and modern system stressors, Syvitski *et al.* (2009) categorise the Mahanadi Delta as a system 'at greater risk', whereby a reduction in aggradation rate has occurred so that it no longer exceeds relative sea-level rise (see chapter 3, table 3.1 for environmental data from this study). The authors show that aggradation rates have decreased from 2 $mm.yr^{-1}$ in the early twentieth century, to just 0.3 $mm.yr^{-1}$ in the twenty-first century; a rate insufficient to keep pace with present relative sea-level rise of 1.3 $mm.yr^{-1}$. The dominant driver of this change has been a 74% reduction in sediment reaching the delta plain over the last century (Syvitksi *et al.,* 2009). The construction of the Hirakud dam upstream of the delta across the Mahanadi River has played a significant role in this depletion. As discussed in section 2.2.1, sediment starvation from damming outside of the delta plain is a dominant cause of elevation loss in numerous delta systems worldwide, highlighting the transferability of the Mahanadi's narrative to understanding geomorphological change in other locations. Since its completion in 1957, the Hirakud dam has remained a controversial topic: whilst official discourse in Odisha credits the dam for controlling floods, many other stakeholders share the view that such an intervention has transformed the delta "from being a flood dependent agrarian regime to a flood vulnerable landscape" (D'Souza, 2002:1262). Indeed, many hold the opinion that British colonial rule has compromised the flood vulnerability of the delta over much longer timescales, through the gradual widespread construction of embankments, canals and defences across the Mahanadi basin that have almost eliminated natural morphological evolution in some locations (Chhotray and Few, 2012). Pearce (2014) describes how communities that once benefited from floods distributing

fertile silt across the delta now live behind embankments that actually increase flood risk: Although such structures provide localised protection, wider risk is increased as the plain is deprived of sediment replenishment, and flows are concentrated where they burst through weak points in the flood defences. Furthermore, farmers are becoming increasingly dependent on expensive artificial fertilisers in order to replace the nutrients that are no longer naturally delivered to the agricultural plains (Kumar; in Pearce, 2014). This is becoming an increasing issue not just in the Mahanadi region but in many of the Asian megadeltas, such as the Mekong in Vietnam (Chapman and Darby, 2016).

Land-use changes across the Mahanadi basin have also acted to increase the rate of run-off into the river, and thus the velocity of flows during times of heavy precipitation. This has made it increasingly difficult to manage flows through the Hirakud dam. Before the dam's construction, maximum flood depth occurred 3-4 days after peak rainfall intensity; this has now been reduced to 1-2 days (Jena *et al*., 2014). The opening of the reservoir during times of intense rainfall has resulted in several severe flash floods in the delta, most notably in 2003, 2008, and 2011 (Panda *et al*., 2013). Flooding has occurred more times in the last decade than in any other recorded period, putting pressure on agricultural productivity and freshwater resources, and resulting in high levels of disease related to poor drinking water quality (Pearce, 2014). Many settlements along the banks of the Mahanadi, Bhargavi and Brahmani channels have been severely affected by river bank erosion following large flood events. Although channel migration is a natural deltaic process, increased modifications to network structure and alterations to flow regimes have intensified the rate at which this occurs at certain vulnerable locations. Managing threats from bank erosion is another controversial issue in the state, with many feeling that the government present an apathetic attitude towards helping those affected: "The villagers can do nothing other than waiting for doomsday when the village completes the journey from geography to history" (Pati, 2015:1).

Whilst extensive modifications to the Mahanadi's distributary network have played a significant role in causing the observed increase in the magnitude and frequency of flood events in the delta, an increase in monsoon precipitation intensity and cyclone activity has also contributed to the problem. The Mahanadi is expected to be the worst affected river basin in India in terms of the projected increase in flood intensity attributed to climate change (Jena *et al.,* 2014). Kumar

and Pattnaik (2010) suggest a 15% increase in total monsoon rainfall over the next century at the national scale, with a warmer atmosphere increasing the probability of extreme rainfall events. The authors also describe that downscaled assessments for Odisha confirm this trend, as well as an increase in the variability of flows in the Mahanadi basin. The delta has suffered 5 major floods in the last decade as a result of an increase in extreme precipitation events in the central basin during the monsoon season (Jena *et al.,* 2014). Panda *et al.* (2013) also highlight the impacts of increased rainfall intensity in the central Mahanadi Delta, with coastal sectors found to be the most susceptible to flooding. The authors also identify linkages between precipitation, streamflow and large-scale climate indices including the El Niño-Southern Oscillation (ENSO), the Indian Ocean Dipole (IOD) and the South-West Monsoon. Dry season droughts have also become more severe as a result of recent anthropogenic climate change, with the Eastern Ghats and upper deltaic plains experiencing the driest conditions (Panda, *et al.,* 2013). Between December and March rainfall is extremely low in the delta, rarely exceeding 30 mm per month (Coleman and Huh, 2004). Kumar and Pattnaik (2010) suggest a high likelihood of a further decline in winter rainfall of up to 25% over this century. Average air temperatures during the dry season have also increased by 1.1˚C across the Mahanadi basin during the twentieth century as a likely result of climate change, as well as due to more localised shifts in agricultural practices leading to surface albedo changes and increased methane emissions (Rao, 1993). This combined with widespread groundwater extraction and increasing salinisation is exacerbating the water crisis across much of the delta. Increasing salinisation has caused many coastal farmers in the Mahanadi, as indeed in many other deltaic regions in southern Asia, to abandon agricultural livelihoods altogether and turn instead to aquacultural practices (Johnson, 2014). Whilst at the individual-scale this provides a means of mitigation against some of the impacts of climate change, on industrial scales aquaculture is contributing to deltaic transgression (Szuster, 2003). Groundwater extraction during the dry season in order to fill the aquaculture ponds is accelerating local subsidence, raising relative sea-levels and increasing water stress. This combined with the addition of brackish water further intensifies saline conditions, rendering many areas agriculturally unproductive after around ten years of intensive shrimp farming (Falk, 2000). Since 1975, a third of the Mahanadi Delta's wetlands, including large areas of mangrove forest, have been lost to drainage schemes, industrial plants and aquaculture ponds (Pearce, 2014). The loss of mangrove

ecosystems leads to increased rates of coastal erosion, particularly during cyclonic conditions (Saito *et al.,* 2007).

Several large tropical cyclones have hit the Odisha coast in recent decades, resulting in major flooding, erosion, salinisation and remobilisation of subaqueous deposits. On 29 October 1999, Cyclone 05B, otherwise known as Kalinga, made landfall in the Mahanadi Delta with peak wind speeds exceeding 260 $km.hr^{-1}$; the most powerful storm recorded in the northern Indian Ocean (Panigrahi, 2003). The coastal districts of Kendrapara and Jagatsinghpur were submerged by a 7 metre storm surge that extended 20 km inland (Khatua and Dash, 2013). A total of 9,803 people are known to have died directly as a result of the storm, with millions more affected, many from the delta's coastal regions (Mohanti, 2000). Many communities here struggled to cope as floods deposited vast quantities of sand on homesteads, further limiting the cultivation of crops even after the flood waters receded (Chhotray and Few, 2012). In October 2013 the second strongest recorded storm to make landfall in the delta, Cyclone Phailin, struck the Odisha coast. Due to the successful evacuation of over one million people, the loss of life as a direct result of the storm was minimal compared to Kalinga. Nonetheless the storm resulted in the widespread destruction of wetland and mangrove ecosystems, and the loss of 500,000 hectares of agricultural land to saltwater inundation (Mehta *et al.,* 2013). The greatest devastation from Phailin came not during the storm itself, but rather in the days and months following the event: The lag between heavy downpours in the central Mahanadi basin, and peak flows reaching the deltaic plains, meant many were taken by surprise by the fluvial flooding, thinking the worst of the inundation has passed. As documented by the Indian Express (in Pearce, 2014:1): "just as the people were congratulating themselves for surviving the cyclone, they were hit by a wave of flooding that few had bargained for". As a result of the secondary flooding event, more mangrove trees were washed away, and levees concentrated flows towards unprotected areas, waterlogging agricultural fields and inundating homes. Shukla *et al.* (2003) found that between 1877 and 1990, 309 depressions, 87 storms, and 26 severe storms crossed the Odisha coastline. This equates to approximately 3 depressions per year, 3 storms every four years, and 1 severe storm every five years.

Coastal erosion, due to both gradual and high magnitude events, has displaced thousands of people in the delta over recent decades. One of the worst

affected areas is the village of Satabhaya, located 15 km south of the of Brahmani River mouth in Kendrapara. The shoreline retreated by 6 km between 1981 and 2014; this rate has since enhanced following the breach of a large sand dune during Cyclone Hudhud in October 2014 (figure 4.5) (Kar, 2014). Since the loss of this protective barrier the village has become increasingly vulnerable to coastal erosion and flooding, forcing many to abandon their homes. The decision to relocate hundreds of families living in the Satabhaya region to new homes a few kilometres inland in Bagapatia was made in 2008; however little action was taken until the destruction caused by Cyclone Hudhud prompted a series of protests by villagers (New Indian Express, 2015). The state's first ever resettlement project for people displaced by sea erosion subsequently begun in July 2015; although at present many people do not wish to be rehomed, or have not received sufficient support to do so (Odisha Channel Bureau, 2015).

Figure 4.4 Coastal erosion at Satabhaya following Cyclone Hudhud in November 2014 (Source: Indian Telegraph, 2014).

Table 4.1 Environmental data for the Mahanadi Delta from Syvitski *et al*. (2009:4). Storm surge, river (distributary) and in situ (precipitation) flooding are from MODIS satellite data since 2000. Sediment load reduction, distributary reduction, and level of subsurface mining is across the 20th century. Rates of sea-level rise are time-variable.

Environmental data for the Mahanadi Delta	
Area <2m above sea-level (km^2)	150
Storm surge area (km^2)	1480
Recent area of river flooding (km^2)	2060
Recent area of in situ flooding (km^2)	1770
Sediment reduction (%)	74
Floodplain or delta flow diversion	Yes
Distributary channel reduction (%	40
Subsurface water, oil and gas mining	Moderate
Early twentieth century aggradation rate ($mm.yr^{-1}$)	2

4.4 Impacts to ecosystem services

In the Mahanadi Delta, one of the most significant changes in land cover over recent decades has been a reduction in mangrove forest area. Pattanaik and Prasad (2011) report a loss of 2606 ha of mangrove forest in the delta between 1973 and 2006. Some of this loss is attributable to morphological change, particularly coastal erosion events during storm surges and large floods. However, the rapid growth of the aquaculture industry in the region has also played a significant role in this decline, with Pattanaik and Prasad (2011) reporting an increase in the area utilised of 357 ha. This is reflective of a pattern seen across India: total national aquaculture production of aquatic animals rose from 6.7 million tonnes in 1984 to 42.3 million tonnes in 2003; equivalent to 6.2% of total global aquaculture production (FAO in Pattanaik and Prasad, 2011). Whilst the loss of mangrove forest area may have short-term economic benefits, the impacts of losing this valuable habitat are more detrimental with regards to the long-term sustainability of deltaic ecosystem services (Szutzer, 2003; Ali, 2011). The mangrove forests of the Mahanadi are biodiversity hotspots, providing breeding sites for a huge variety of wildlife and commercially important species (Baran and Hambrey, 1998). The abundance of wildlife also generates substantial income from tourism, particularly in reserves such as the wetlands of Bhitarkanika National Park in the northern delta. Mangroves also act as an efficient buffer against storm surge and floods; limiting coastal erosion rates and reducing death toll and structural damage during these extreme events (Das, 2009). Furthermore, the presence of trees provides friction to slow the movement of water and sediment, allowing the waterway to silt and elevation to increase (Alongi, 2009). A decline in mangrove forest has left an increasing proportion of agricultural land exposed to coastal erosion, inundation and increasing salinisation, with detrimental effects to rice yield (Chua, 1992; Mahata *et al.* 2012).

Water quality is also intrinsically linked to delta morphodynamics. Water quality varies seasonally in the Mahanadi as a result of monsoon rainfall. It also varies spatially across the delta due to numerous anthropogenic and natural factors; including erosion rates, land cover, urbanisation, industrialisation and agricultural activities (Dixit *et al.*, 2013). The Mahanadi River and its tributaries serve as a major source of domestic water supply to urban settlements in the delta. Subsequently untreated domestic waste water and effluents from industrial sources directly affect water quality in the delta, in addition to the input of

pollutants from upstream (Panda *et al.,* 2006). Fertiliser, paper and textile factories are amongst the most common sources of industrial effluent, primarily from the cities of Sambalpur, Cuttack and Paradip (Radhakrishna, 2001). This has resulted in enhanced levels of phosphorus and acidification in the estuarine regions of the delta. Runoff from agricultural sources is another major control of water quality in both urban and rural regions. Bhawan (2014) found high concentrations of nitrate in the districts of Cuttack (179 ppm) and Puri (80 ppm). Bhawan also found that groundwater near irrigation channels in the delta contained high values of fertilizer related chemicals; reaching 280 ppm nitrate, 8.5 ppm phosphate, 133 ppm mg/l potassium, 525 mg/l chloride and 509 ppm sulphate. Wetland salinity levels have increased substantially over recent decades due to a combination of rising sea-levels, increased groundwater extraction and the addition of brackish water to aquaculture farms (Wetlands International, 2014a). Such a change will not have a significant impact upon plant species naturally present in the two marshland habitats. However in a rice-dominated agricultural system such as the Mahanadi, this is likely to have detrimental impacts to productivity (Grattan *et al.,* 2002). Groundwater salinity has also become an increasing threat to drinking water supplies in the coastal regions of the delta (Bhawan, 2014).

.

Chapter 5 **Model setup and applied metric development**

5.1 Introduction

The overall aim of this study is to develop a management relevant set of metrics that explore the nature of multidecadal morphological change in delta catchment systems under a range of climatic and environmental change scenarios. The design of these should encapsulate stressors that are common to a broad range of deltaic environments around the world, as described in chapter 2. Two distinct catchments within the Mahanadi Delta plain have been chosen as study areas: that of the most morphologically-active river, the Devi; and that of the main Mahanadi River channel. Both of these channels are bifurcations of the Mahanadi River system at the apex of the delta, and therefore experience similar inflow and climatological conditions in their upper reaches. It is hoped that by adopting this approach more general rules about how particular regions of a delta plain are impacted by environmental change can be identified and contrasted and that the framework's usefulness to stakeholders in the region will be maximised.

More specifically, the aims of this research can be split into three distinct objectives: The first is **to enhance our understanding of how emergent processes influence the multidecadal evolution of deltaic environments**. A range of metrics will be utilised to identify the nature and rate of morphological change, and areas of the catchment that may be at greatest risk from this change. This information will then be used to better understand how the morphological system may respond to increasing conditions of environmental stress. As was discussed thoroughly in the literature review in chapter 3, the cellular automata model CAESAR-Lisflood (C-L) has been chosen for this research project. Although individually the rules governing morphological change in C-L are relatively simple representations of fluvial and hillslope processes, their combined and repeatedly iterated effect is such that complex non-linear behaviour, and both positive and negative feedbacks can emerge (Van De Wiel *et al.,* 2007).

The second objective of this study is **to explore how these changes in the emergent morphological system may influence the habitability of the delta**. Within this, three questions will be addressed:

(1) *How do changes in these slow-onset, emergent processes effect the impact of short-term, extreme events?* In the Mahanadi Delta, the impacts of a severe tropical cyclone on the morphological system are analysed.

(2) *How do these changes influence potential habitat cover change?* Specifically morphological metrics such as hypsometry and inundation are used as a proxy for what kind of vegetation will thrive in these conditions.

(3) *How effective is the model as a platform to investigate potential engineering strategies that could enhance the resilience of a particular location?* Here the focus is on strategies that involve re-naturalising the channel network.

The final objective of this study is **to deliver a framework that is directly useful to stakeholders in the Mahanadi region**; a system that has regularly been highlighted in recent research as one at significant risk from climate change and increased anthropogenic interventions within its distributary network (Syvitski *et al.,* 2009; Jena *et al.,* 2014). It is hoped the results of this study could be used to contribute towards the development of climate-resilient adaption strategies, in particular via the DECCMA project as discussed in chapter 4.

This chapter firstly introduces the scenario design for the research project. It then goes on to provide a thorough explanation of the setup of the C-L model in each catchment, including the running of a baseline scenario and validation of the model. Next, the outputs of this research are discussed in detail; before the setup of the model parameters for the remaining scenario runs are presented. Finally, additional scenarios and analysis required to address research objectives two and three are also discussed.

5.2 Scenario Design

As described in chapter 2, sediment starvation and accelerated subsidence are arguably the two dominant anthropogenic controls that act to alter the morphological regime in modern deltaic environments. Further adding to this stress are two major climatic pressures: eustatic sea-level rise and the increased occurrence of meteorological extremes. Together, these stressors have acted to modify the natural processes of deltaic evolution, resulting in rapid rates of morphological change in many deltas worldwide (Syvitski *et al.*, 2009). In order to produce reliable multidecadal projections in to the future, one could argue that it is more profitable to include all four of these drivers of change in a model, albeit through simplified inputs, rather than to focus on one driver and risk underestimating the cumulative impacts of these pressures. This perspective has heavily influenced the scenario design discussed below. The scenarios are to be investigated over two multi-decadal time periods: 2015-2045 and 2045-2065. One scenario, exploring extreme shifts in monsoon precipitation, will run until 2075 in line with current projections. The data utilised in the following scenarios is described in the next section.

5.2.1 Individual scenarios

River damming and channel modification are currently the two most prevalent causes of sediment starvation in many deltaic environments, often triggering widespread erosion and depleting the floodplain of vital nutrients (Vörösmarty *et al.*, 2009). For example, such interventions have resulted in a 74% reduction in sediment reaching the Mahanadi Delta plain over the 20th century (Syvtiksi *et al.,* 2009). It is important to distinguish between the effects of anthropogenic interventions upstream of the delta plain as opposed to those located within the delta itself. Damming in the feeder catchment upstream of the delta, for example, would not be explicitly represented within a morphological model of the delta but would lead to significant variations in boundary conditions, particularly sediment delivery. Similarly, whilst levée construction within the delta disconnects the channel from the delta plain and thus depriving it of sediment, the same intervention upstream could act to accelerate sediment flux to the delta surface. In

order to assess the impacts of sediment starvation on deltaic evolution from external sources in this study, a similar methodological framework to that of Neunhuis (2011) is implemented. In Neunhuis' study, the impact of permanent elimination of sediment supply on the long-term evolution of a wave-dominated delta shoreline was compared against a scenario whereby fluvial sediment was periodically eliminated, such as in a monsoon-dominated climate. Under each scenario, a one-contour-line cellular automata model (Ashton and Murray, 2006) was used to explore the mechanisms responsible for triggering morphological change within an abstract delta system; the model was then run again to simulate change in real landscapes in order to validate the findings. Here, two scenarios of sediment delivery to the delta apex will be investigated (figure 5.1): Firstly, *reduced (post-dam) sediment delivery*, to represent the influence of a large structure in the feeder catchment of the delta plain. Under this scenario, which also provides the baseline for this study, fluctuations attributed to natural cycles remain in place, but the amplitude of these fluxes are heavily impacted by anthropogenic activity. El-Moattassem *et al*. (2015) emphasise the importance of incorporating seasonal variations in flow and sedimentation rates, and the lag that occurs between their peaks, in order to reliably model both the downstream morphological influence of a dam, as well as sedimentation rates within its reservoir. In the Mahanadi basin, the southwest monsoon dominates sediment supply, creating a highly seasonal pattern of deposition in its delta (Mohanti and Swain, 2011). Total sediment delivery has been reduced by 74% in the Mahanadi compared to pre-dam totals. For each period investigated, historical data from 1974-2004 was utilised (section 5.3 describes the nature of the historical data used in this study in greater detail). Under the second scenario, *increasingly variable sediment delivery* shall be explored, whereby the amplitude of seasonal fluxes is increased. Sediment delivery becomes increasingly variable (+/- 25%) by the 50th year of simulation.

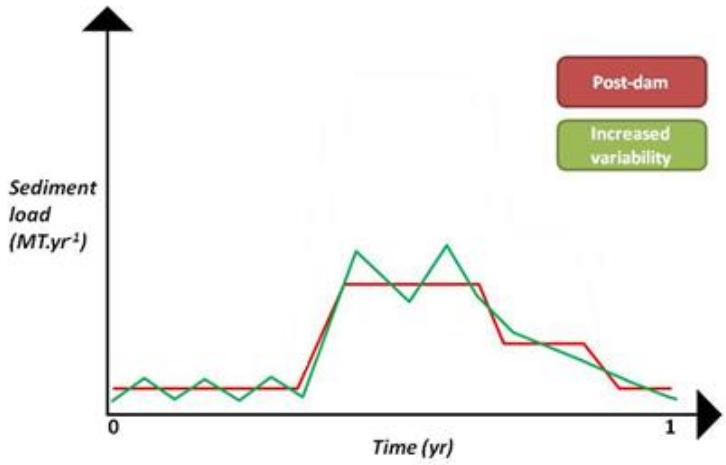

Figure 5.1 Conceptual diagram showing the two sediment starvation scenarios to be included in the model

As described in chapter 2, natural subsidence rates are spatially variable across a delta surface dependent upon sediment type, depth of burial, and vegetation cover (Syvitski, 2008). Activities such as hydrocarbon and groundwater extraction can also act to accelerate the rate of subsidence substantially in affected areas. Ideally this variability would be represented in the Devi and Mahanadi models, in order to more accurately assess the impacts of amplified relative sea-level rise on inundation and erosion rates. However, as it is not at present possible to incorporate subsidence before the post-processing stage of modelling in C-L, it is also not yet possible to produce accurate projections for spatially variable rates. Furthermore, no reliable or high resolution subsidence data is available for the Mahanadi Delta, so it would in any case be difficult to accurately describe where the highest rates may lie at the grid cell scale. A *baseline subsidence rate of 3 mm.yr*^{1} shall therefore be applied throughout this study at the post-processing stage of data analysis. As sediment type, vegetation cover and anthropogenic activity do not vary significantly across the Devi and Mahanadi catchments it is unlikely that the exclusion of spatially variable subsidence will have a significant impact on this study. However if it were to be applied to other deltas with significant levels of hydrocarbon extraction, for example, this would be a more important limitation.

The effects of accelerated eustatic sea-level rise as a result of anthropogenic climate change are further amplified in deltaic environments due to the combined

impacts of sediment starvation and accelerated subsidence. Regional sea-level rise scenarios for the Mahanadi Delta (calculated at Puri) have been provided by the Met Office (figure 5.2). Unlike globally-average scenarios, these account for regional variability due to local bathymetry, isostatic rebound and ocean circulation patterns (Zhang and Church, 2012).These scenarios will be utilised to analyse the morphological response of the delta to slow-onset inundation and the gradual rise of the plain of activity at which waves and tides operate. Short-term fluctuations in sea-level will be analysed in the next section within the context of meteorological extreme events. From the data provided by the Met Office, the scenarios analysed in this study are: High (utilising the highest RCP8.5 scenario whereby *sea-level at Puri rises 0.6 m by 2075*); Moderate (utilising the medium RCP4.5 scenario whereby *sea-level rises by 0.36 m by 2075*); and Low (utilising the lowest RCP4.5 scenario whereby *sea-level rises by 0.22 m by 2075*).

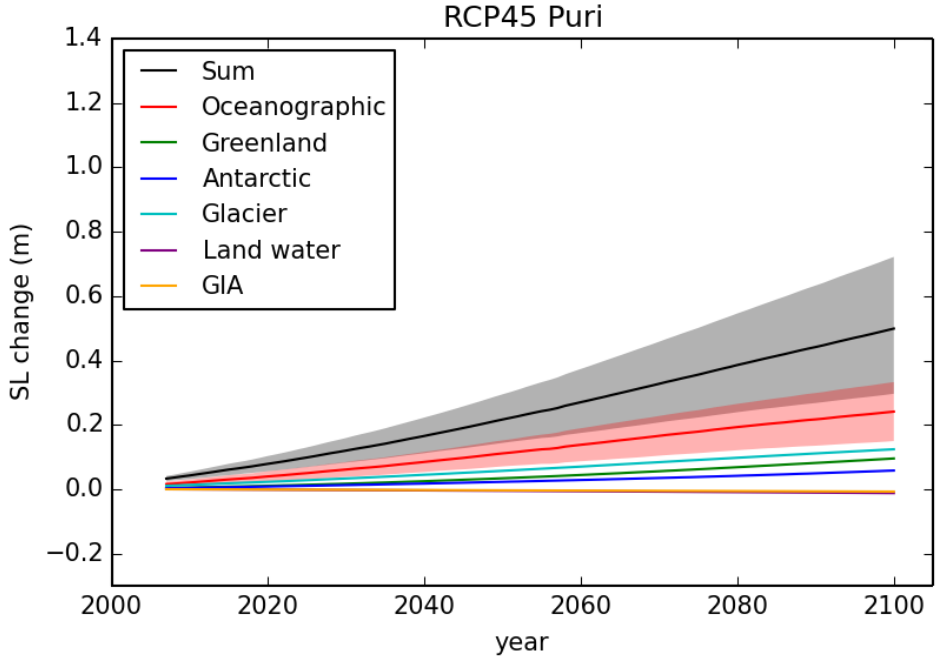

(A)

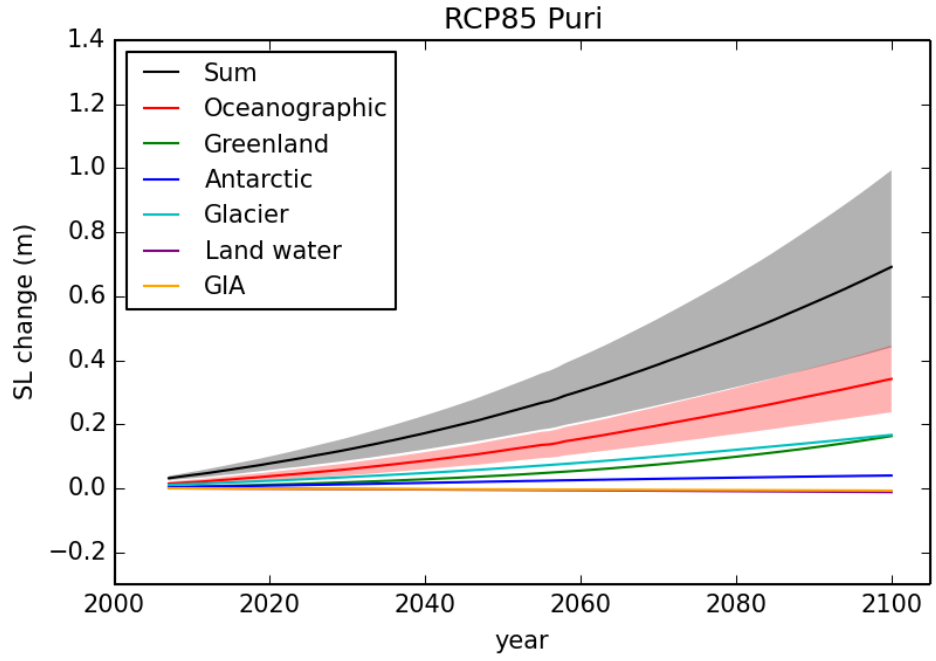

(B)

Figure 5.2 Diagram showing sea-level rise scenarios for Puri provided by the Met Office for (A) RCP4.5 and (B) RCP8.5. Image and data courtesy of Matt Palmer (2016).

Of the four drivers of morphological change highlighted here, meteorological extremes are arguably the most challenging to assign designated scenarios to: Firstly, there is no singular measure that can quantify the true impact of the cumulative effects of all elements of an event. The widely-used Saffir-Simpson hurricane scale, for example, whilst an excellent tool to describe the relative intensity of a storm, cannot be used as a direct proxy for storm surge height (Schott *et al*., 2012). Furthermore, even if two events are meteorologically very similar (in terms of factors such as precipitation intensity, storm surge height and maximum wind speed) the impacts will very likely be dissimilar due to differences in the timing and location of the event, the preceding conditions, and the resilience of the affected delta; not all of which can be quantitatively measured in a model such as C-L. Secondly, an increased occurrence of extreme conditions manifests over different temporal scales; referring to both shifts in the magnitude and/or frequency of short-term events, such as tropical cyclones, as well as to gradual changes to long-term, large-scale climate patterns, such as monsoon precipitation intensity. Thirdly, significant interannual variability means that multidecadal predictions of shifts in localised meteorological extremes carry high levels of uncertainty (Goswami and Mohan, 2001). Despite these obstacles, it is critical that the occurrence of extreme events is able to be simulated in the model, due to their significant influence on erosion rates, sedimentation and ecosystem health.

Figure 5.3 shows the 18 meteorological scenarios that have been designed to explore both shifts in long-term climatic regimes, and short-term weather events in the Mahanadi region. These scenarios would only require minimal modification for application in other Asian mega deltas in which the morphological regime is monsoon-dominated, or for tropical deltas that also experience a wet and dry season. These 18 scenarios are split between 5 categories: *shifts in monsoon precipitation* (June-September); *shifts in post-monsoon precipitation* (October and November); *shifts in dry season precipitation* (December-May); *changes to annual average air temperature*; and finally *changes in severe cyclone frequency* (using the 1999 Odisha Cyclone as a baseline severe event). As will be described fully later in this chapter, all scenarios were created based on historical meteorological data from the Mahanadi Delta.

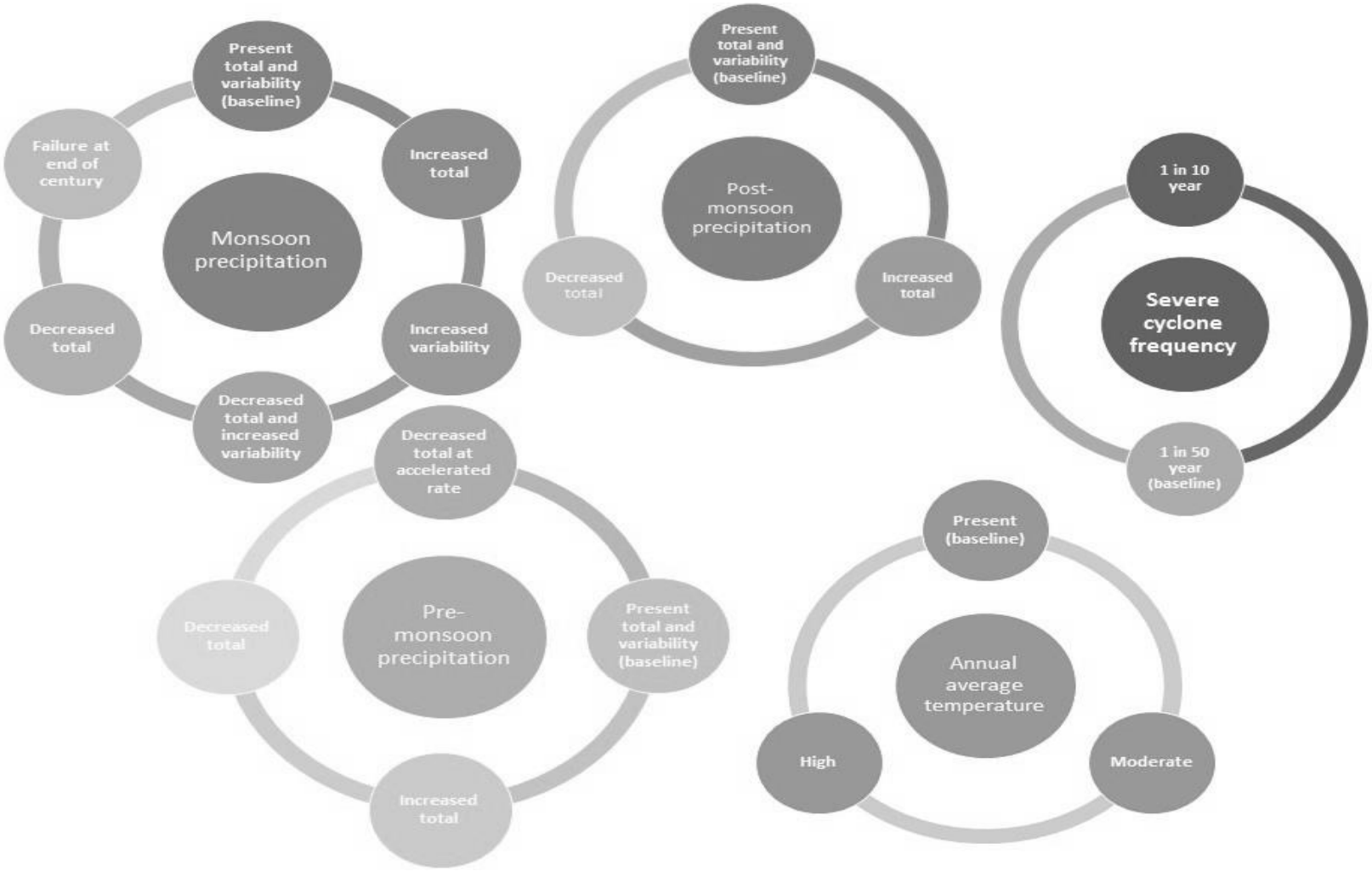

Figure 5.3 Individual meteorological scenarios to be tested in the model. Baseline scenarios are noted.

Monsoon precipitation variability has a significant influence on sedimentation patterns in affected deltas (Goodbred Jr., 2003), and is the focus of the meteorological scenarios tested in this research. In the Mahanadi basin, more than 90% of the sediment discharge to the delta occurs during the monsoon season (June-September) (Chakrapani and Subramanian, 1990). Thus whilst monsoon storms can over short timescales result in significant flooding and erosion, over decadal timescales they are also an invaluable source of sediment, particularly to abandoned tidal regions. Singh *et al.* (2014) stress that both interseasonal and interannual variability in monsoon precipitation can adversely impact water resources, agriculture and human systems for more than 1/6th of the world's population. It is thus vital that future research focuses on improving our understanding of the driving forces behind observed monsoon variability over a range of temporal scales.

The monsoon precipitation scenarios listed in figure 5.3 were created based on a range of projections for the Mahanadi region presented in the current literature: Singh *et al.* (2014) find that from 1951-2011 there has been a statistically significant decrease in peak season precipitation totals that has co-occurred with an increase in daily-scale precipitation variability. Such a trend has produced notable events in India over recent years: The infamous break of July 2002 saw 56% less rainfall in the monsoon core, resulting in substantial agricultural losses (Bhat, 2007). In the monsoon of 2005, short periods of extremely intense rainfall resulted in devastating flooding in Mumbai (Wynn, 2014). There has also been a statistically significant increase in the frequency of dry spells over this period, although the intensity of these droughts has actually decreased. The authors suggest that this pattern could prevail into the 21st century due to the increasing intensification of the hydrological cycle, and an observed pattern of fewer, more intense monsoon depressions. There have also been suggestions that the monsoon onset could be delayed by up to 15 days over this period (Ashfaq *et al.*, 2009). Shifts in monsoon onset have had devastating impacts in the past, such as in July 2004 when the early arrival of monsoon rains resulted in major flooding in northeastern India and Bangladesh. Conversely, Kumar and Pattnaik (2010) propose that a warmer world will result in an increase of up to 15% in total monsoon precipitation. Whilst a warmer atmosphere will hold more moisture and thus theoretically result in an

increase in precipitation totals, several studies (Turner and Annamalai, 2012; Bollasina *et al.*, 2011) have proposed that the large increasing trend of aerosol concentration over south Asia in the late 20th century could be the reason there has not yet been an emergence of increasing monsoon rainfall. Listing another potential scenario, Schewe and Levermann (2012) suggest that a progressively weaker Walker Circulation in the Pacific Ocean would lead to the more frequent subsidence of dry air over much of India, thus resulting in the complete failure of the monsoon rains towards the end of the century. In this study the impacts of monsoon failure during an extension of the simulation period (2065-2075) are investigated.

The remaining precipitation scenarios for other seasons have also been designed based on the range of pathways projected in the current literature. Significantly less geomorphological work is done during the post-monsoon (October-November) and dry season (December-May) periods. In the Mahanadi Delta, just 10% of annual average sediment loads are carried to the delta over these 8 months (Chakrapani and Subramanian, 1990). Nonetheless, it is important to explore shifts in precipitation during these seasons given that they determine the hydrological conditions in the delta at monsoon onset. Furthermore, extreme precipitation and drought events often occur during these months over India, with tropical cyclones and heat waves both common in the weeks preceding and after the summer monsoon. Dash *et al.* (2007) show that over the last century there has been an increase in the frequency of occurrence of severe cyclonic storms in India during November, and subsequently an increase in total precipitation. The authors also find an increase in precipitation totals in the latter months of the dry season. Kumar and Pattnaik (2010a) suggest there could be a 25% decrease in winter precipitation in India over forthcoming decades. Asokan and Dutta (2008) also find that there is likely to be an increased incidence of drought during the dry season, with significant decreases in run off in the Mahanadi basin during April, particularly towards the end of the century. Conversely, Yadav *et al.* (2010b) suggest precipitation will increase during the winter months throughout the 21st century. As with monsoon precipitation, precipitation variability during the drier months has been linked to ENSO variability; a relationship that may strengthen over forthcoming decades (Yadav *et al.,* 2010a).

Whilst it is possible to utilise precipitation as an input in C-L, only river discharge data at designated inflow points is required to run the model. This meant that river flow data would need to be modified to represent shifts in precipitation regimes during scenario design. Although lag times between peak precipitation and peak river flow obviously exist over short temporal scales, a basic correlation analysis showed that over annual timescales precipitation and river flow display a strong positive relationship (r = 0.95). Thus an x% change in precipitation over a given scenario period was also assumed to cause an x% change in river flow values by the end of that simulation period. In order to generate a scenario in which there is a 15% increase in precipitation totals with no change in variability, for example, historical river flow data was multiplied by 1.15 to form the end value, with a linear rate of increase calculated for the years in between.

In addition to river discharge, the other inflow data required to drive C-L is sediment supply. To calculate future projections of average annual suspended sediment load (Q_s) (MT) in the Mahanadi Delta, the BQART equation (Syvitksi and Milliman, 2007) was utilised (Equations 14 and 15):

$$Q_S = \omega B Q^{0.31} A^{0.5} R T \quad [14]$$

$$1.\ B = IL(1 - T_E)E_h \quad [15]$$

where ω is a constant relating to unit conversion (0.0006 for the Mahanadi), Q is the long-term annual discharge (km^3yr^{-1}) using the discharge scenarios calculated as above, A is basin area (141, 600 km^2), R is maximum basin relief (m) and T is long-term average annual basin temperature (˚C). The factor B accounts for geological and anthropogenic factors that were excluded from the original ART model (see Syvitski and Milliman, 2007), where I is the glacial erosion factor $(I \geq 1)$, L is an average basin-wide lithology factor, T_E is the trapping efficiency of lakes and reservoirs such that $1 - T_E \leq 1$, and E_h is a human influenced soil erosion factor (*f(Population density, GNP)).*

When tested on a database of 488 rivers, the BQART model was found to account for 96% of the between-river variation in the long-term (30 years) sediment load (Syvitski and Milliman, 2007). The authors found that geological parameters (basin area, relief, lithology, ice erosion), accounted for 65% of the between-river sediment load. Climatic factors (precipitation and temperature) account for 14% of the variability and anthropogenic factors account for 16%. The glacial factor contributed just 1% of the signal represented. The BQART model is not able to predict the sediment flux following episodic events, such as typhoons and earthquakes. Nonetheless it provides a powerful tool to calculate the influence of long-term shifts in precipitation and temperature on sediment supply, as required by this multidecadal study. Furthermore, shifts in precipitation intensity, for example, can still be incorporated in C-L within the river discharge data input, and thus the influence of short-term events is not excluded. In order to reduce the sensitivity of the delta sediment scenarios to biases in the BQART model that are associated with basin-wide factors, the decision was made to calculate the percentage change of the output as opposed to the actual sediment yield calculated by the model. This also seemed the most appropriate approach given that the predominant aim of this study is to better understand how the Mahanadi system may respond to different scenarios, as opposed to developing robust predictions of actual future change. The percentage change in Q_s was then applied to the present-day measured long-term average to calculate the projected sediment totals for the years 2045, 2065 and 2075. Q_s is calculated assuming the present-day sediment trapping efficiency of upstream dams and reservoirs (74%).

The temperature scenarios listed in figure 5.3 were selected based on current projections for the Mahanadi region. A moderate temperature rise of 1.1˚C reflects the current rate of increase in annual average temperatures observed by Rao (1995) and Dash *et al.* (2007). The high temperature rise scenario reflects an approximate doubling of this rate. Yadav *et al.* (2010b) suggest that a high rise scenario could reach 5˚C in parts of India by the latter 21st century. However, due to the sensitivity of BQART to temperature increase, such a rise in mean temperatures was excluded from this study. Annual average temperatures are investigated as fluctuations at the intraseasonal level have a reduced geomorphological impact over multidecadal timescales.

Figure 5.4 summaries the method of calculation for the water and sediment discharge for input into C-L; whilst table 5.1 shows the specific values for the periods 2015-2045 and 2045-2075 within the time series data for each scenario.

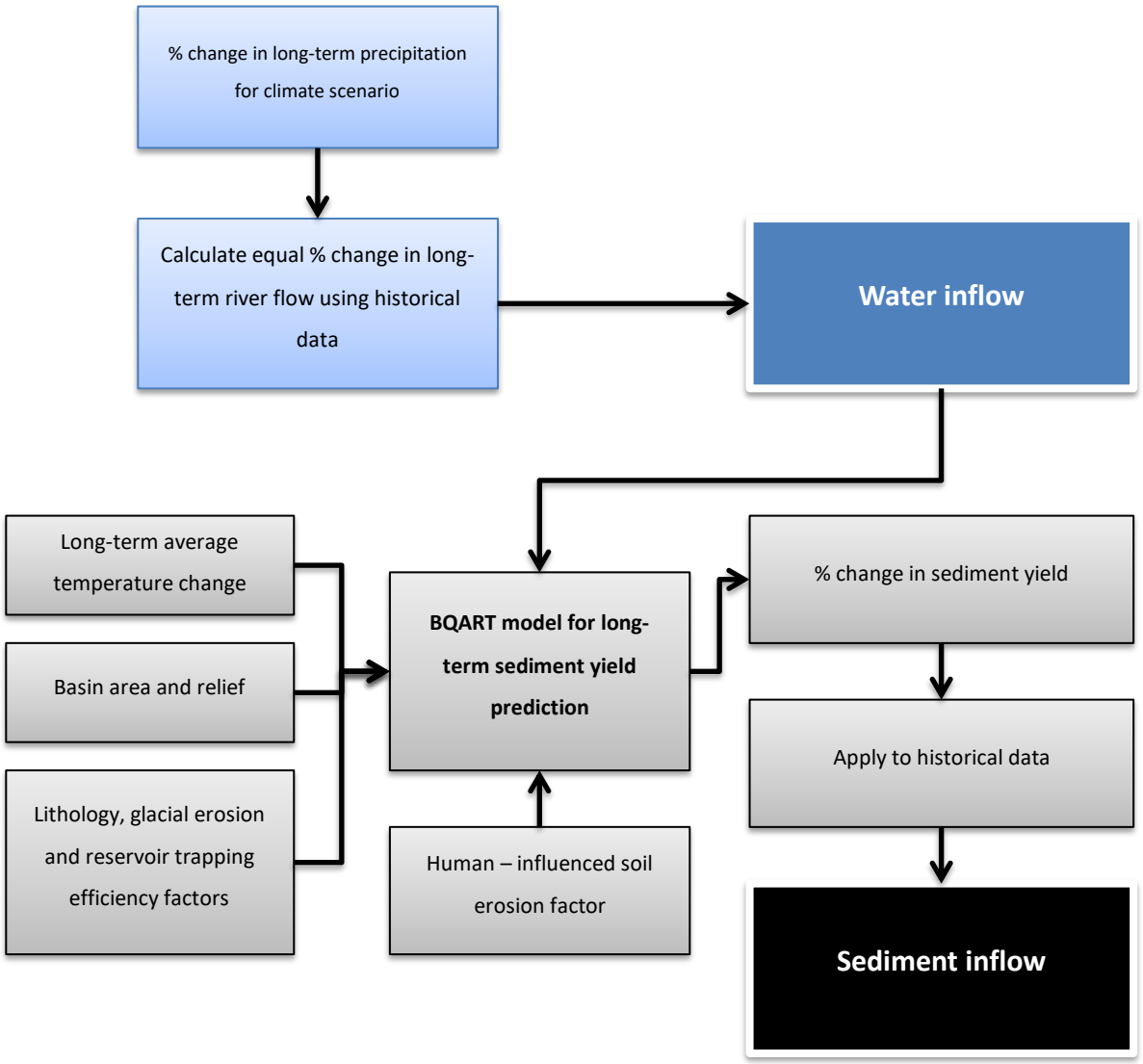

Figure 5.4 Schematic diagram to show the method of calculation for water and sediment inflow data for each meteorological scenario representing shifts to long-term climate factors (thus excluding tropical cyclone frequency)

Table 5.1 Calculated long-term average annual water discharge and sediment loads for the years 2045 and 2075 under each meteorological scenario. Note that for scenarios in which precipitation becomes increasingly variable, this does not affect the final value for 2045 or 2075 as such dynamics are only visible at the interannual scale. Similarly shifts in tropical cyclone frequency are excluded as they are assumed not to influence the long-term annual average.

Time period: 2015-2045					Time period: 2045-2075				
Scenario(s) description	**Q: Mean annual river discharge ($km3.yr^{-1}$)**	**Q_s: Calculated mean suspended sediment ($MT.yr^{-1}$)**	**Q_s as a percentage of baseline Q_s**	**Annual suspended sediment load in Mahanadi basin ($MT.yr^{-1}$)**	**Scenario description**	**Q: Calculated mean river discharge ($km3.yr^{-1}$)**	**Q_s: Calculated mean suspended sediment ($MT.yr^{-1}$)**	**Q_s as a percentage of baseline Q_s**	**Annual suspended sediment load in Mahanadi basin ($MT.yr^{-1}$)**
Jun-Sep precipitation									
Present-day	**48.691**	13.95	100.00%	**12.59**	Continue with values as in 2015-2045				
Wetter/ Wetter and more variable	**54.936**	14.48	103.80%	**13.07**	Further 15% increase	**62.117**	15.05	107.89%	**13.58**
Drier/ Drier and more variable	**38.283**	12.95	92.83%	**11.69**	Further 25% decrease	**30.478**	12.07	86.52%	**10.89**
Failure of the monsoon	**11.929**	9.02	64.66%	**8.14**	Continue with values as in 2015-2045				

Oct-Nov precipitation									
Present-day / More variable	**48.691**	13.95	100.00%	**12.59**	Continue with values as in 2015-2045				
Wetter	**49.02**	13.98	100.22%	**12.62**	Further 15% increase	**49.400**	14.01	100.43%	**12.64**
Drier	**48.143**	13.9	99.64%	**12.54**	Further 25% decrease	**47.732**	13.87	99.43%	**12.52**
Dec-May precipitation									
Present-day / More variable	**48.691**	13.95	100.00%	**12.59**	Continue with values as in 2015-2045				
Wetter	**49.421**	14.02	100.50%	**12.65**	Further 15% increase	**49.303**	14.01	100.43%	**12.64**
Drier	**47.474**	13.84	99.21%	**12.49**	Further 25% decrease	**45.602**	13.67	97.99%	**12.34**
Annual mean temperature									
Present-day	**48.691**	13.95	100.00%	**12.59**	Continue with values as in 2015-2045				
Moderate increase (0.55°C)	**48.691**	14.24	102.08%	**12.85**	Further 0.55°C increase	**48.691**	14.53	104.16%	**13.11**
High increase (1.15°C)	**48.691**	14.55	104.30%	**13.13**	Further 1.15°C increase	**48.691**	15.15	108.60%	**13.67**

Understanding long-term shifts in precipitation such as those discussed above is crucial in order to produce multidecadal projections of sediment flux in deltaic regions. Daily-weekly fluctuations in precipitation may have the biggest human impact, but are largely determined by internal dynamics that would be extremely challenging to adequately represent in a long-term geomorphological model (Turner and Annamalai, 2012). However, representing meteorological scenarios based on hydrological boundary conditions at the delta apex alone will not capture the geomorphological work carried out on the delta plain during short-term events. To compensate for this, the impacts of shifts in severe cyclone frequency shall also be explored. Hydrological and tidal parameters representing those experienced during the 1999 Odisha cyclone, which caused widespread devastation in the Mahanadi Delta, shall be run at two differing reoccurrence intervals: 1 *severe storm every 10 years* and *one every 50 years* (figure 5.5). During a tropical cyclone such as this, it is the storm surge component of the event that tends to have the most significant and long-lasting morphological impact on deltas; resulting in devastating inundation and erosion in some locations, whilst providing a substantial sediment source for others (Turner *et al.,* 2006; Williams, 2012). Such sedimentation is particularly vital in maintaining the elevation of abandoned delta lobes that are otherwise disconnected from major distributary sources of sediment (Dail *et al.,* 2007). In their study in the Mississippi delta, Tweel and Turner (2014) found that hurricane associated deposits make up at least 65% of the inorganic content of topsoil in abandoned delta lobes, and up to 80% in the Chenier Plain. Furthermore, they also found that whilst the most sedimentation from a given event results from the most intense storms, over longer timescales it is actually moderate storms (930-990mb) that contributed the vast majority (78%) of long-term hurricane sedimentation. Storm surges in the Mahanadi region typically reach up to 12 metres during cyclonic conditions (Mohanti and Swain, 2011). The height and period of wind-generated waves are of particular importance in wave-dominated delta regions, and have a significant influence on coastal geomorphological structures. At present the inclusion of waves is not possible in C-L; and thus further study is required to assess the full impacts of long-term shifts in tropical cyclone frequency on coastal delta morphology.

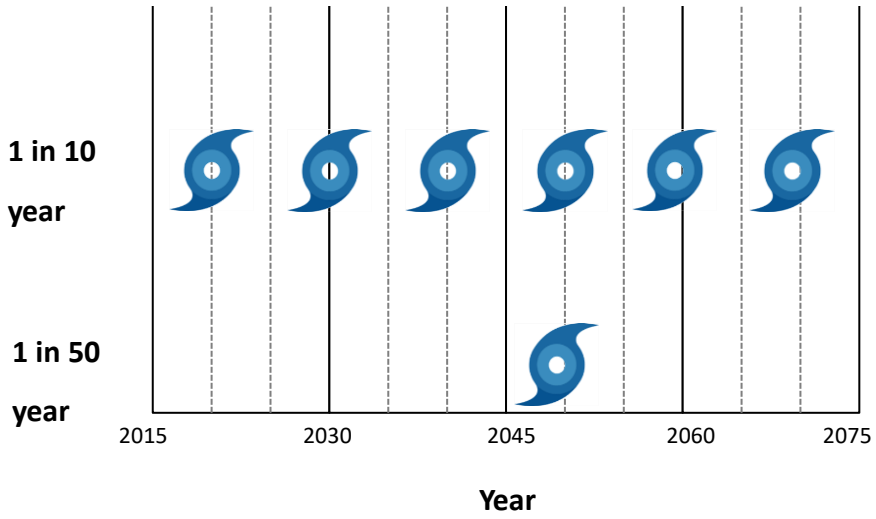

Figure 5.5 Severe cyclone frequency scenarios to be tested in the model. A reoccurrence interval of 50 years represents the baseline value as determined from the 1999 Odisha cyclone event.

Table 5.2 provides a summary of the scenarios discussed above as well as specific values for increases/decreases in parameter totals and variability. The following section describes how various combinations of these stressors have been chosen to form the synergistic scenarios that are to be run in C-L.

Table 5.2 Individual scenarios designed to explore a variety of pathways for each of the four drivers of morphological change, as listed in chapter 2. Various combinations of these stressors are used to form the synergistic scenarios to be run in C-L. 'Present totals/variability' refers to historical data from 1974-2004.

Driver of change	Scenario	Code	Description
Sediment starvation	Baseline: reduced (post-dam)	SS1	Post-dam annual totals, present daily variability
	Increased variability	SS2	Post-dam annual totals, daily sediment becoming increasingly variable (+/- 25% by 2075)
Accelerated subsidence	3 mm.yr-1	AS1	Subsidence rate 3 $mm.yr^{-1}$
Eustatic sea-level rise	High	SL1	Local mean sea-level increases 0.60 m by 2075
	Baseline: Moderate	SL2	Local mean sea-level increases 0.36 m by 2075
	Low	SL3	Local mean sea-level increases 0.22 m by 2075
Meteorological extremes, monsoon precipitation (J,J,A,S)	Baseline	MP1	Present seasonal totals and daily variability
	Increased total	MP2	Seasonal total increases by 15% by 2075, present daily variability
	Increased total and variability	MP3	Seasonal total increases by 15% by 2075, daily variability increases by +30/-15% by 2075
	Decreased total and increased variability	MP4	Seasonal total decreases by 25% by 2075, daily variability increases by +25/-50% by 2075
	Decreased total	MP5	Seasonal total decreases by 25% by 2075, present daily variability
	Failure at end of century	MP6	Dry season totals persist into the summer months from 2065 -2075

Meteorological extremes, post monsoon precipitation (O,N)	Baseline	PM1	Present seasonal totals and daily variability
	Increased total	PM2	Seasonal total increases by 15% by 2075, present daily variability
	Decreased total	PM3	Seasonal total decreases by 25% by 2075, present daily variability
Meteorological extremes, dry season and pre-monsoon precipitation (D,J,F,M,A,M)	Baseline	DS1	Present seasonal totals and daily variability
	Increased total	DS2	Seasonal total increases by 15% by 2075, present daily variability
	Decreased total	DS3	Seasonal total decreases by 25% by 2075, present daily variability
	Decreased total at accelerated rate	DS4	Seasonal total decreases by 50% by 2075
Meteorological extremes, annual average air temperature	Baseline	TI1	Present annual values continue
	Moderate increase	TI2	Increases 1.1°C by 2100
	High increase	TI3	Increases 2.3°C by 2100
Meteorological extremes, severe cyclone frequency	Baseline: 1 in 50 year event	TC1	Severe cyclone based on the 1999 Odisha cyclone occurs once every 50 years
	1 in 10 year event	TC2	Severe cyclone based on the 1999 Odisha cyclone occurs once every 10 years

5.2.2 Synergistic scenarios

The individual scenarios listed above provide a clear structure with which to carry out a preliminary investigation into the impacts of various drivers of morphological change. This could be achieved by analysing the effects of shifts in one driver individually, whilst keeping all others at the chosen baseline value. However, utilising such an approach would not necessarily capture how these various stressors interact over a range of temporal and spatial scales, and thus may lead to inaccurate projections of change and of emergent processes.

Here 11 scenarios were created to represent the synergistic impacts of various stressors following numerous trajectories. These have been designed with a focus on exploring different climatic pathways. In light of the fact that the monsoon is the predominant natural driver of morphological change in the Mahanadi system, this has been explored in the greatest depth in this study. Table 5.3 introduces these synergistic scenarios: Scenario TST (TeST scenario) is a baseline scenario, whereby historical data for each stressor is utilised. The purpose of this is to provide a reference model run with which to compare the morphological changes emerging in subsequent scenarios. Scenarios 1WWW – 8DWAH focus on exploring the interactions of various sea-level, temperature and sediment supply scenarios under numerous possible trajectories of precipitation. As outlined further in Appendix B, the first three letters given in the notation for these scenarios describes the precipitation conditions experienced during each season: whereby 'W' indicates wetter conditions; 'D' indicates drier conditions; and 'A' indicates accelerated drought conditions. For example, scenario 3WDD describes a climatic scenario in which precipitation totals increase during the monsoon season (June to September); decrease during the post-monsoon period (October – November); and decrease during the dry season (December – May). Where applicable, the fourth letter in the scenario notation indicates an additional stressor on the system: 'H', for example, indicates a higher rate of sea-level rise. Scenarios 5DWA, 7DWDH, 9DWDC and 10DWDF all explore variations of the 'most likely meteorological pathway'. This pathway (scenario 4DWD) describes the meteorological scenario that is most frequently suggested to occur in the current literature and thus should be explored in greater detail: *a drier, more variable monsoon; a wetter post-monsoon period; a*

drier dry season; all of which occurs with a more variable sediment supply and under a moderate annual temperature increase. Scenarios 9DWDC and 10DWDF explore the effects of an increase in severe cyclone frequency (as indicated by the notation 'C') and monsoon failure (as indicated by the notation 'F') respectively. All scenarios are run from 2015 – 2065; with the exception of 10DWDF which is run for an extended 10 year period until 2075 in order to capture a more likely timing for monsoon failure (Schewe and Levermann, 2012).

All 11 scenarios are run in the Devi catchment; the most morphologically-active in the Mahanadi Delta. Two of these (TST and 4DWD) are also run in the Mahanadi catchment, in order to compare the morphological impacts of certain environmental stressors in a larger, increasingly tidal dominated catchment.

Table 5.3 List of synergistic scenarios to be explored. Grey shading indicates where a parameter is set to a non-baseline value. The codes listed for each mechanistic scenario are as listed in table 5.2. Scenario 4DWD (highlighted in bold) represents the meteorological scenario that is deemed as the most likely to occur in the Mahanadi Delta. Those scenarios marked with * represent variations upon this scenario. Scenarios in italics represent those run in both the Devi and Mahanadi catchments.

Scenario	**Description**	**Mechanistic scenarios**							
TST	*All drivers at baseline (historical) values*	*MP1*	*PM1*	*DS1*	*TI1*	*TC1*	*SL3*	*SS1*	*AS1*
1WWW	Wetter during all seasons	MP2	PM2	DS2	TI2	TC1	SL2	SS1	AS1
2DDD	Drier during all seasons	MP5	PM3	DS3	TI2	TC1	SL2	SS1	AS1
3WDD	Wetter, more variable monsoon; drier post-monsoon; drier dry season	MP3	PM3	DS3	TI2	TC1	SL2	SS1	AS1
4DWD	***Drier, more variable monsoon; wetter post-monsoon; drier dry season; variable sediment supply***	***MP4***	***PM2***	***DS3***	***TI2***	***TC1***	***SL2***	***SS2***	***AS1***
5DWA	Drier, more variable monsoon; wetter post-monsoon; drier dry season with accelerated decrease in rainfall totals; variable sediment supply*	MP4	PM2	DS4	TI2	TC1	SL2	SS2	AS1
6WDDH	Wetter, more variable monsoon; drier post-monsoon; drier dry season; high temperature increase; high sea-level rise	MP3	PM3	DS3	TI3	TC1	SL1	SS1	AS1
7DWDH	Drier, more variable monsoon; wetter post-monsoon; drier dry season; variable sediment supply' high temperature increase; high sea-level rise*	MP4	PM2	DS3	TI3	TC1	SL1	SS2	AS1

8DWAH	Drier, more variable monsoon; wetter post-monsoon; drier dry season accelerated decrease in rainfall totals; variable sediment supply; high temperature increase; high sea-level rise*	MP4	PM2	DS4	TI3	TC1	SL1	SS2	AS1
9DWDC	As in 4DWD, with 1 in 10 year severe cyclone frequency*	MP4	PM2	DS3	TI2	TC2	SL2	SS2	AS1
10DWDF	As in 4DWD, with monsoon rains failing from 2065*	MP6	PM2	DS3	TI2	TC1	SL2	SS2	AS1

5.3 Model Setup – Morphological modelling in CAESAR-Lisflood

In the following section, the data requirements for this study are presented and a thorough description of the model setup for each catchment is discussed.

5.3.1 Data requirements

In order to run C-L in reach mode for the Mahanadi and Devi catchments, four basic inputs are required by the user: (1) A digital elevation model (DEM) for each catchment; (2) Water discharge at designated inflow points; (3) Sediment discharge at designated inflow points; (4) The relative proportion of different grain sizes in the sediment discharge. In addition to these essential requirements, sea-level and/or tidal data and local Manning's values are also desirable for optimum simulation of morphological processes in the Mahanadi Delta. In-situ evaporation rates are also preferable.

The DEMs for each catchment must first undergo some processing in order to operate efficiently and accurately in C-L. This was done according to the instructions provided by Coulthard (2016). SRTM data (90 metre spatial resolution) was extracted for the Mahanadi study region courtesy of Duncan Hornby (2015). The SRTM DEM was then clipped in ArcMap 10.3 to the boundary of the watersheds for each catchment. Using the hydrological analysis tools in ArcMap, the main channels in the catchment (where flow accumulation > 500 cells) were identified and 'burned' into the DEM by reducing the elevation by 6 metres. This ensures the most efficient flow in C-L, and prevents inaccurate overbank flow in areas where the coarse DEM has not captured the true elevation of the channel. The outlets of the two catchments were then unblocked (cells set to 'no data' value, -9999) using a supplementary program provided in the C-L package, DEMEditor. The final stage of DEM preparation is to ensure that there are no false blockages to the channel system, caused by structures such as bridges. This was achieved utilising another supplementary program, RasterEdit, as shown in figure 5.6.

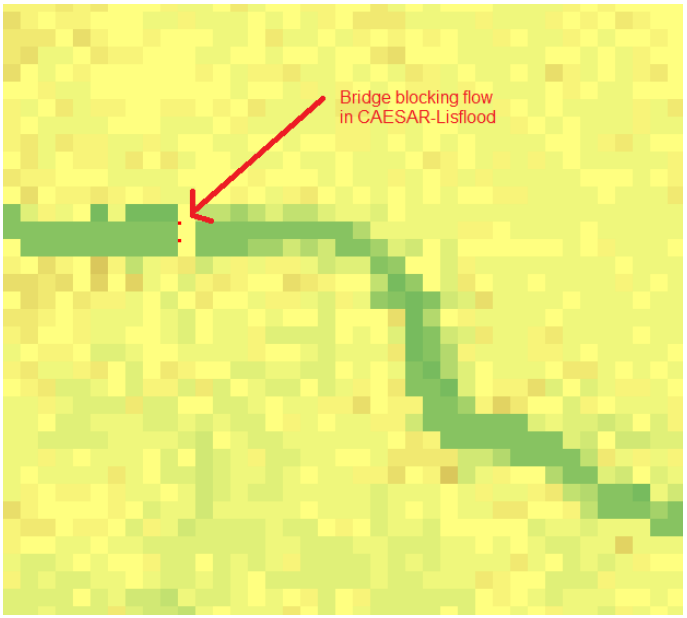

(A)

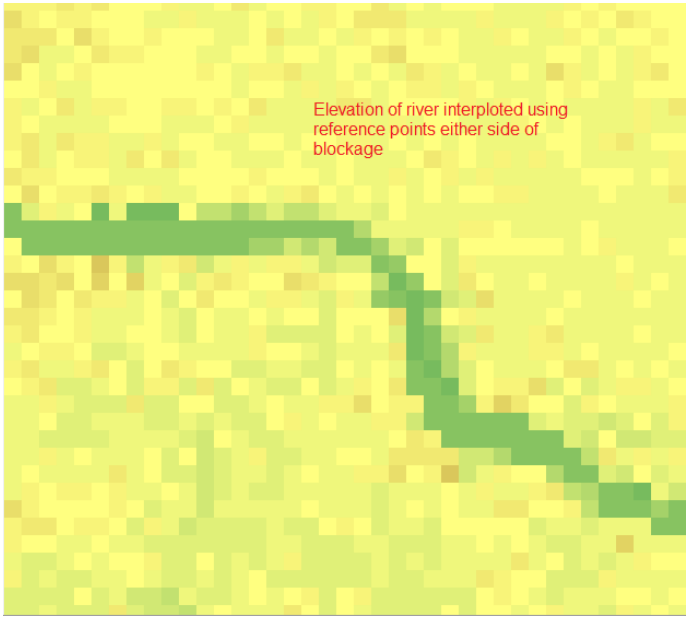

(B)

Figure 5.6 (A): Identifying and (B): removing false blockages from the channel in RasterEdit using interpolation method

RasterEdit was also utilised to identify the coordinates of the sediment and water inflow points and tidal inflow regions for the Mahanadi and Devi catchments (figure 5.7). Two points are used for both water and sediment input to avoid

extreme scouring in the upper catchment. The total values for sediment and water inflow data at each time step is then divided by two in C-L so as to spread out the input. Tidal inflow occurs over a region of the channel defined by the user (x1, x2, y1, y2) as opposed to a specific point (x1, y1). This data does not need to be divided as it refers to the elevation of the water rather than the flow of the tide.

The DEM generated for each catchment was then utilised to create a binary image of the channel network; whereby all channels with a depth greater than 1 metre are assigned a value of 1, and all other pixels a value of 0 (figure 5.8). As is described in section 5.3.3, this is required for post-processing analysis.

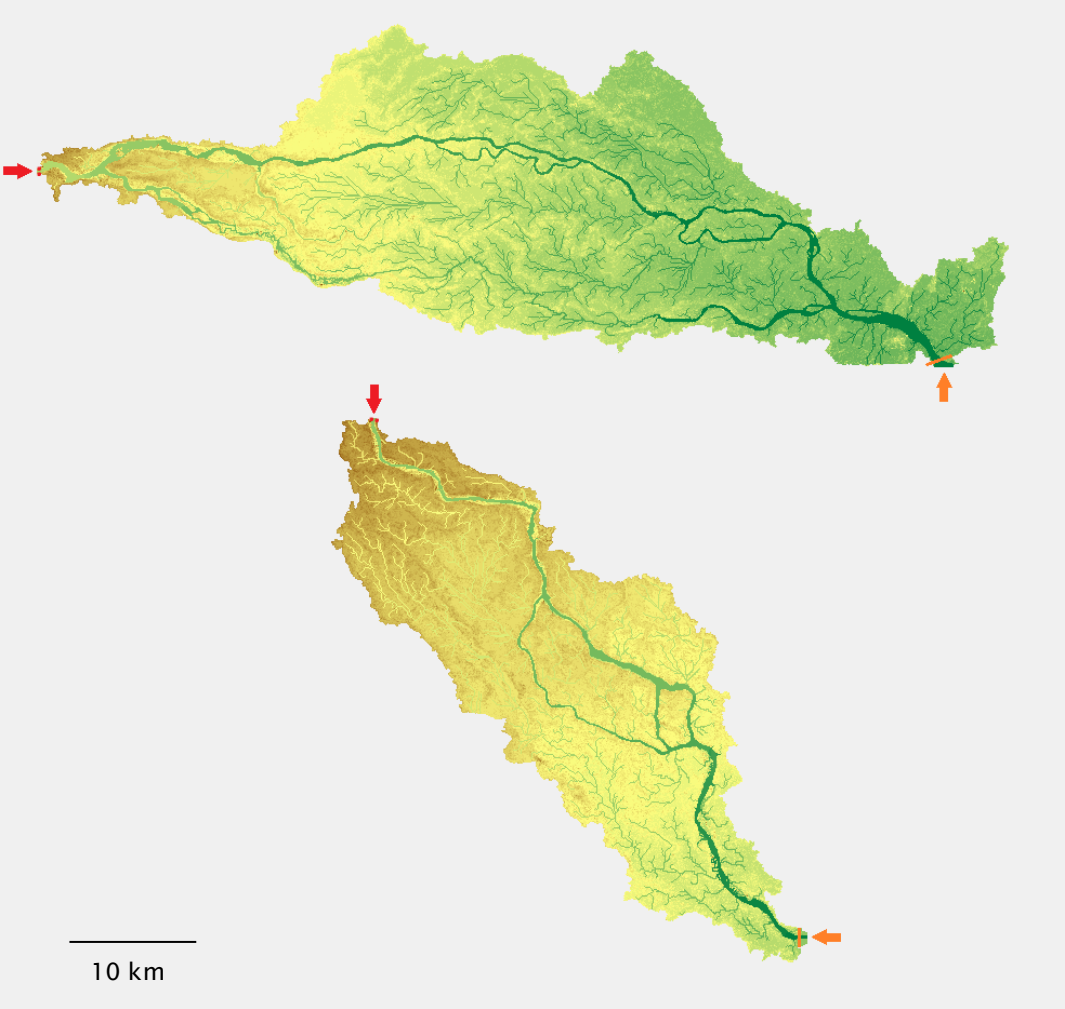

Figure 5.7 Prepared DEMs in RasterEdit showing the location of the inflow points for the Mahanadi catchment (top) and Devi catchment (bottom). Sediment and water inflow points are shared and shown in red. Tidal inflow areas are shown in orange.

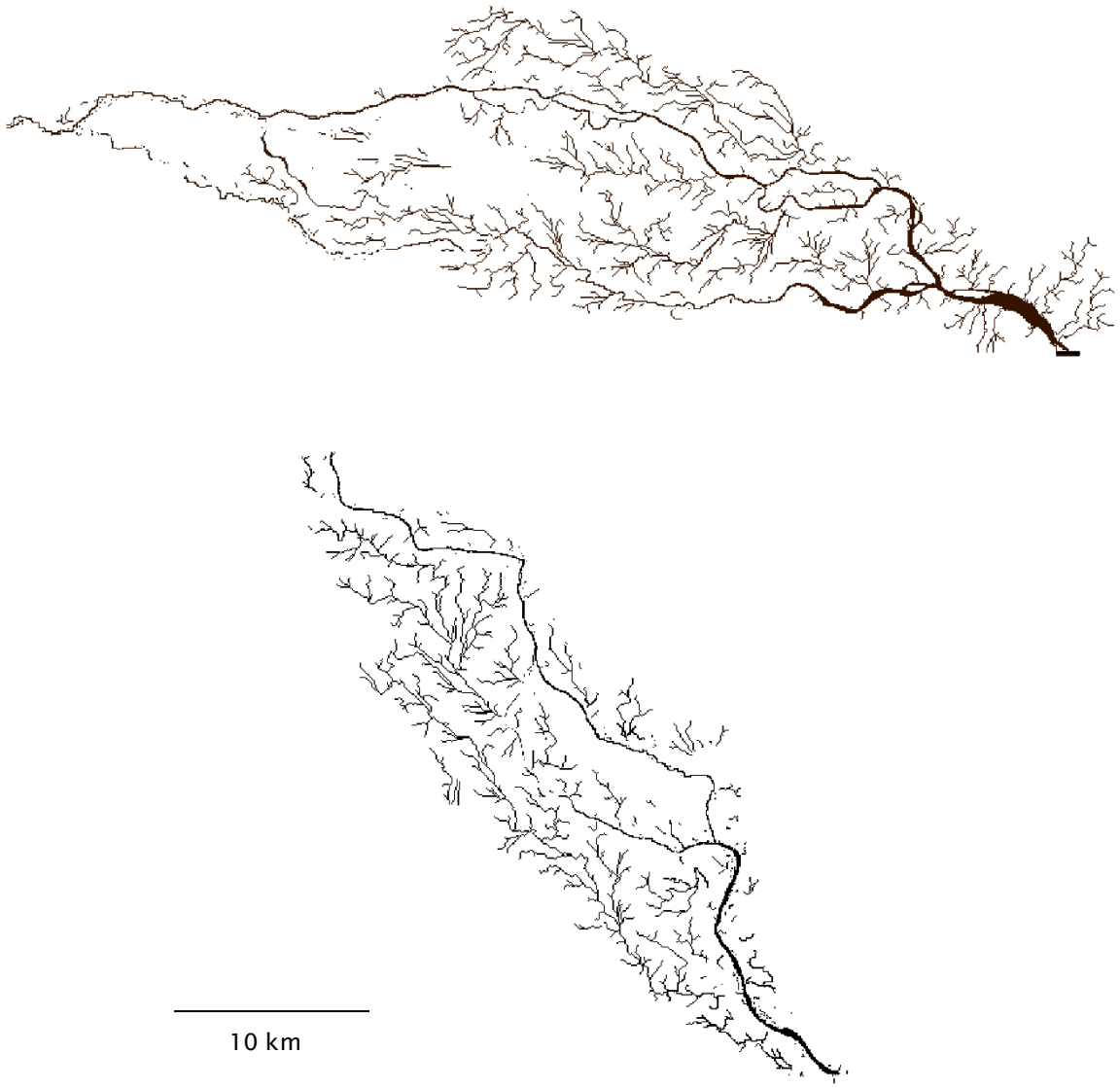

Figure 5.8 Binary images showing the distributary channel network in the Mahanadi (top image) and Devi (bottom image) catchments.

Located just over 100 km upstream, Tikarapara is the nearest gauging station upstream of the Mahanadi Delta apex. Daily water discharge data ($m^3.s^{-1}$) from the Tikarapara station was obtained for the time period 1972 – 2012 from the Central Water Commission for this study (courtesy of Sugata Hazra, Rahul Sharma and the WRIS). Daily sediment data ($g.l^{-1}$) from 1973 – 2012 was also obtained from Tikarapara (courtesy of Rahul Sharma and the WRIS). The 30 year period from

January 1 1974 – December 31 2003 has been utilised as the baseline for this study. This period was chosen as it was the first year in which there was both continuous sediment and water discharge data. In order to be input into C-L, the daily concentrations of coarse (> 0.2 mm), medium (0.2 - 0.075 mm) and fine (< 0.075 mm) grains were converted into volumes using the known discharge of the river and the density of the grains. The relative proportions of each sediment fraction were taken from a study by Ghose *et al.* (2011), who found the load at Tikarapara to consist of 95%, 2.7% and 2.3% of fine, medium and coarse fractions respectively. The historical data of daily water discharge, total sediment discharge, fine sediment discharge, medium sediment discharge and coarse sediment discharge, were then arranged into single columns to be read by the model. The format of hydrological and sediment data input for C-L is shown in table 5.4.

Table 5.4 Format of text file for the input of hydrological and sediment data. Columns 3 and 4 are to be left blank with a value of 0

Column	**1**	**2**	**3**	**4**	**5**	**6**	**7**	**8**	**9**	**10**	**11**	**12**	**13**	**14**
Name	Time	Water discharge	0	0	Total sediment discharge	Grain size 1	Grain size 2	Grain size 3	Grain size 4	Grain size 5	Grain size 6	Grain size 7	Grain size 8	0 Grain size 9
Units	Integer	m^3/sec			m^3	m^3	m^3	m^3	m^3	m^3	m^3	m^3	m^3	m^3

As previously shown in figure 5.2, annual rates of eustatic sea-level rise for the Mahanadi Delta covering the period 2015 - 2100 have been supplied by the Met Office (courtesy of Matt Palmer, 2016). Of the multiple scenarios provided, those analysed in this study are: High (utilising the highest RCP8.5 scenario whereby sea-level at Puri rises 0.6 m by 2075); Moderate (utilising the medium RCP4.5 scenario whereby sea-level rises by 0.36 m by 2075); and Low (utilising the lowest RCP4.5 scenario whereby sea-level rises by 0.22 m by 2075). C-L requires sea-level data to be input as a singular column of water elevation (m) at a given time step. Utilising this gradual annual rise in sea-level alone would provide a rather coarse representation of this stressor, and would not permit the investigation of short-term

extreme sea-level events. Given the morphological importance of tidal processes in the Mahanadi Delta, a month of tidal data was collected for Puri from an online resource (MS, 2016). Annual rates of sea-level rise were then imposed on top of this value, over the period 2015 – 2075. Two high tides and two low tides occur each day at Puri, and thus the time step for input into C-L is 6 hours.

For all scenarios except 9DWDC, severe cyclone frequency is set at a baseline level of 1 in 50 years. For the purposes of this study, a severe cyclone describes a storm where peak wind speeds exceed 250 $km.hr^{-1}$. On 29 October 1999, Cyclone 05B, otherwise known as Kalinga, made landfall in the Mahanadi Delta with peak wind speeds exceeding 260$km.hr^{-1}$; the most powerful storm recorded in the northern Indian Ocean (Panigrahi, 2003). In order to capture the conditions preceding and following landfall of the cyclone, river discharge data from 25th October – 10th November 1999 were obtained from the source described above. These values were then added into the hydrological data files for each scenario at the appropriate reoccurrence intervals. Where frequency was set at 1 in 50 years the storm event occurs from 25th October – 10th November 2049, 50 years after the original event. Where frequency is set at 1 in 10 years, the storm event occurs in 2019, 2029, 2039 and so on. Smaller storms are assumed to be included at a baseline frequency due to the fact that the future scenarios are built on modifying historical data by a set percentage. Tidal data over the same time period was increased by 8 m during the event to represent the height of the storm surge experienced during the 1999 event.

A spatially homogenous Manning's coefficient of 0.03 was selected to represent vegetation cover in the Mahanadi and Devi catchments, using the reference guide suggested in the C-L user manual (Forest Science Labs, 2015). Whilst there is an option to generate a spatially variable Manning's coefficient file for the Mahanadi Delta, the decision was made not to incorporate this level of detail in this study. This is due to the fact that land cover maps for the region do not exist at an appropriate spatial scale for catchment modelling; either being so coarse that the entire catchment is given the same value, or being so fine that this would significantly increase computational times in C-L with minimal differences in model output.

The mean daily evaporation rate at Cuttack, located at the apex of both catchments, is 4.46 mm (Rao *et al.*, 2012). This figure fluctuates seasonally (4.02 mm during October-December, and 5.51 mm March – May); however C-L cannot at present incorporate a dynamic evaporation rate.

5.3.2 Setup of baseline scenario and model validation

The scenario TST, in which all drivers are set at a baseline value, was set up for both catchments. Hydrological and sediment inflows for the 50 year period are created from two cycles of historical data from 1974-2004. Only the first 30 year cycle is utilised to validate model performance. LANDSAT images were obtained for the years 1973 and 2003 in order to see if the rate and pattern of accretion and erosion in the model was significantly different from that observed in the delta. Although this is not a wholly reliable means of model validation, in a delta with limited data availability it is one of the most efficient ways to test if the performance of the model lies within the desired boundaries of accuracy at the catchment scale. It should also be noted that this period was a time of significant environmental stress on the delta due to the rapid expansion of anthropogenic effects. Local data from the literature can also be used where available to validate C-L. However there is a bias towards coastal monitoring that is not as relevant to this study, particularly given that waves cannot be incorporated at present. Changes in the fractal dimension, the distribution of island sizes and nearest-edge distance over the 30 year period were compared with the results of Edmonds *et al.* (2011), who demonstrated the application of these metrics to a broad range of real and theoretical deltas (see section 5.3.3).

Figure 5.9 shows LANDSAT images for the lower and upper Devi catchment in the years 1973 and 2003. Central regions of the catchment undergo relatively little morphological change, with channel position remaining stable and width varying by a maximum of just 0.05 km. The catchment apex and estuarine mouth both display a reduction in the size of deposits within the channel. There has also been an increase in sinuosity at the mouth. The most significant change to channel morphology is observed at the coast, where the width of the mouth has decreased by 1.1 km and the sand spit parallel to the coast has become increasingly elongated. Whilst this region lies outside the boundaries of the Devi catchment

itself, it is nonetheless important to consider due to the proximity to the model domain.

Figure 5.10 shows LANDSAT images of the Mahanadi River catchment, also from the years 1973 and 2003. As in the Devi, the main channel in the central regions of the catchment shows little morphological change in terms of its position and width. This is also true at the catchment apex, although here there has been considerable movements of the deposits within the channel. However, the area in between these regions has undergone significant morphological change, with meanders appearing to shift downstream by up to 1 km and channel width decreasing by up to 100m. There has been a significant decrease in island size in the coastal regions of the floodplain, with many islands decreasing by 100 m in length. Conversely, channel width in this region has increased by up to 150 m. The area of greatest morphological change occurs again at the shoreline, with significant erosion of up to 100 m along the coastal frontage. Unlike the Devi catchment however, the coastline of the Mahanadi catchment does lie within the model domain.

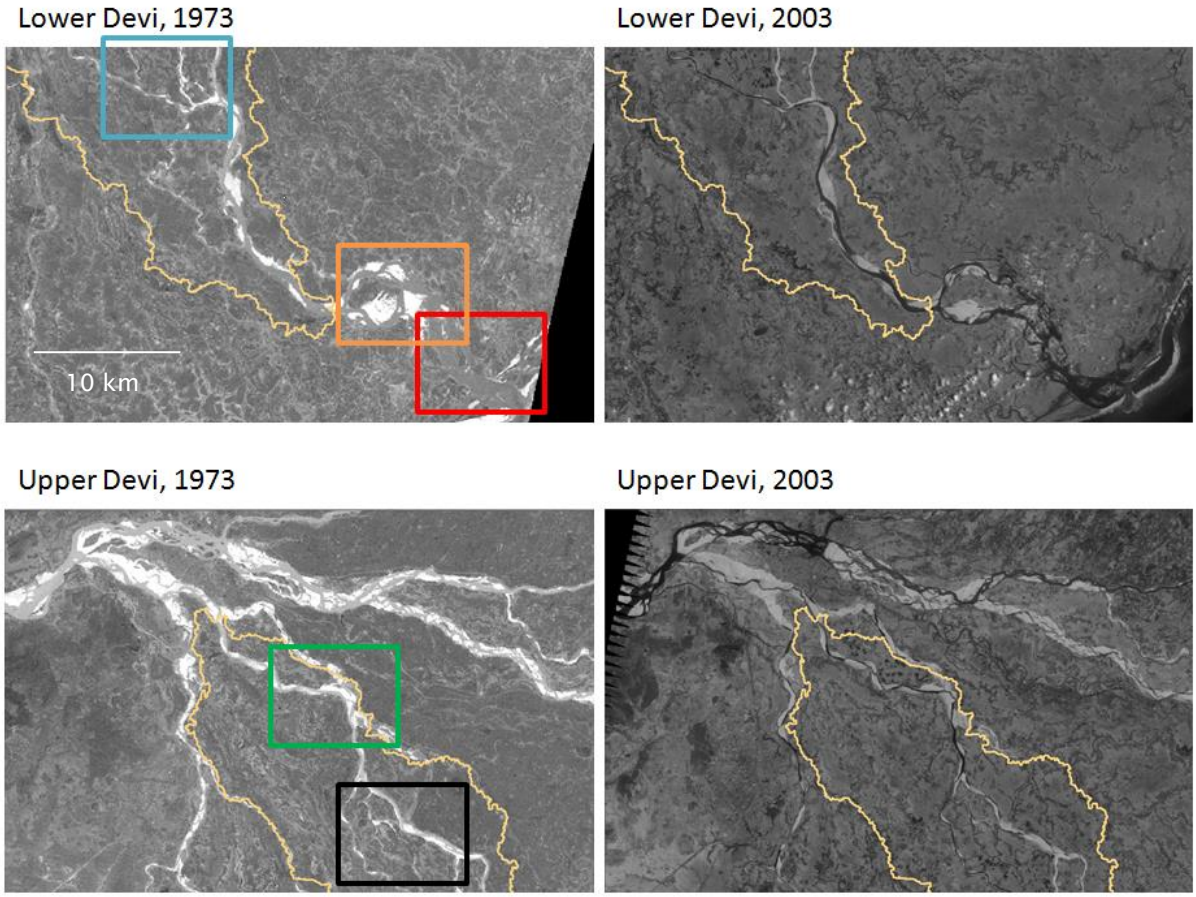

Figure 5.9 LANDSAT images of the Devi River catchment from the years 1973 and 2003. Yellow identifies the border of the catchment. Central regions of the catchment (blue and black outlines) undergo relatively little morphological change, with channel width varying by a maximum of 0.05 km. The apex of the catchment (green outline) and the estuarine mouth (orange outline) both display a reduction in size of sand deposits. There has also been an increase in sinuosity at the mouth. The most significant change has occurred in coastal regions (red outline), where the width of the mouth has decreased from 1.5 km to 0.4 km. Furthermore, the spit parallel to the coast has become increasingly elongated. (Image source: USGS, 2016).

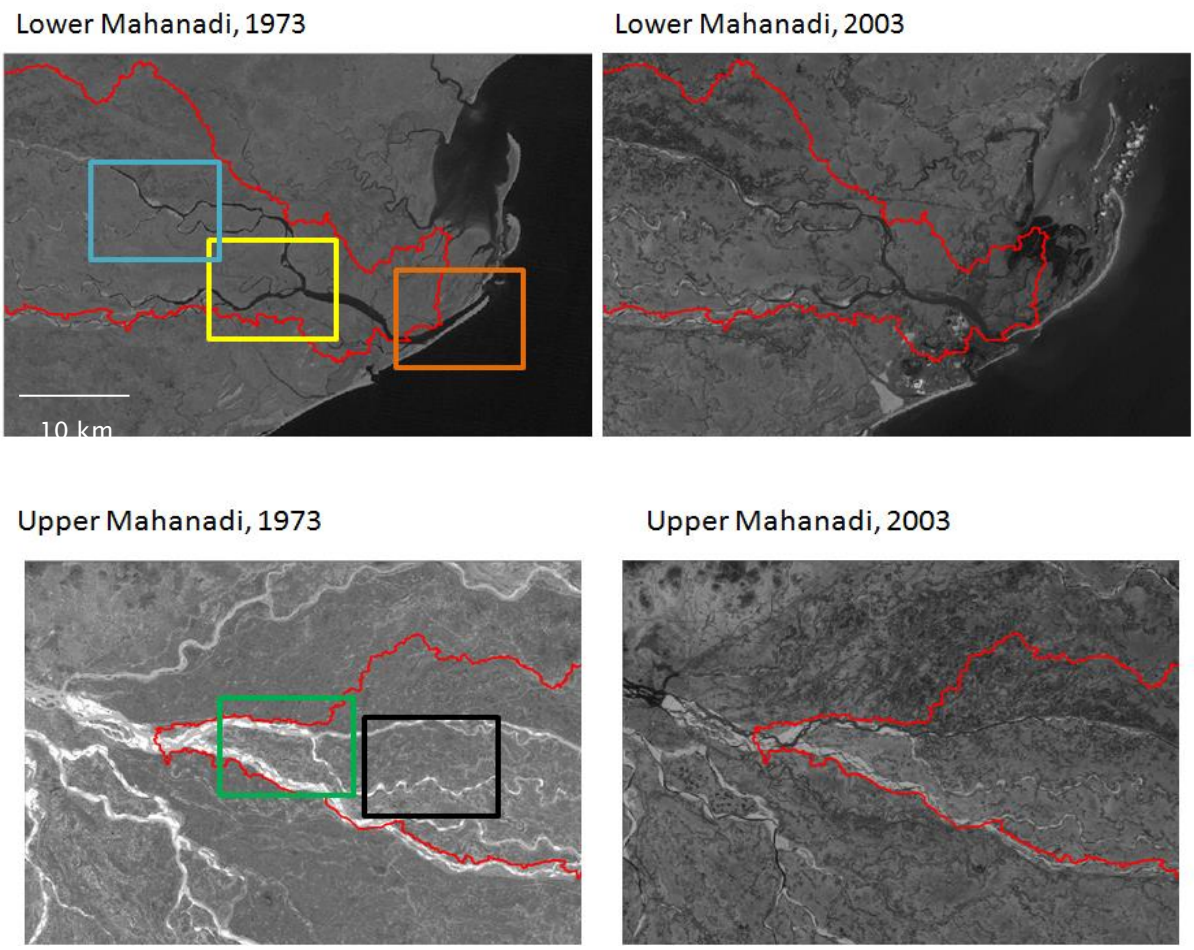

Figure 5.10 LANDSAT images of the Mahanadi River catchment, from the years 1973 and 2003. Red identifies the border of the catchment. The main channel in the central region of the catchment (blue outline) shows little morphological change in terms of its position and width. This is also true at the catchment apex (green outline), however here there has been considerable movements to the deposits within the channel. However, the area in between (black outline) has undergone significant morphological change, with meanders appearing to shift downstream by up to 1 km and channel width decreasing by up to 100m. There has been a significant decrease in island size in the coastal regions of the floodplain (yellow outline) with many islands decreasing by 100 m in length, and the channel width increasing by up to 150 m. As in the Devi the area of greatest morphological change occurs nearer the coast, with significant erosion of up to 100 m along the shoreline frontage. Image source: USGS, 2016.

Table 5.5 shows the setup of each parameter for the TST scenario in C-L; which are described further in Appendix A. Repeated runs of TST have been made to improve the setup of these parameters, to reach the best configuration of the C-L model for the Mahanadi Delta. These parameters will therefore be kept the same for all other scenarios, with the exception of input files for the relevant hydrological, sediment, tidal and DEM data. The setup for all remaining synergistic scenarios is described in Appendix B.

Table 5.5 Parameter setup in C-L for model validation and scenario TST

Parameter	Setup
Mode	Reach and Tidal
DEM file	Devi or Mahanadi as required
Grain Data file	Null
Bedrock data file	Devi or Mahanadi as required
Save file every (minutes)	1440 for daily, 525600 for annual
Generate time series output	Yes
Minimum time step (seconds)	60
Maximum time step (seconds)	3600
Run start time (hours)	0
Maximum run duration (hours)	8760 for a year, as required
Memory limit	1
Run with all grain sizes	No
Grain size 1 (metres); proportion	0.00005; 0.95
Grain size 2 (metres); proportion	0.000075; 0.027
Grain size 3 (metres); proportion	0.0002; 0.023
Grain size 4 (metres); proportion	0.004; 0
Grain size 5 (metres); proportion	0.008; 0
Grain size 6 (metres); proportion	0.016; 0
Grain size 7 (metres); proportion	0.032; 0
Grain size 8 (metres); proportion	0.064; 0
Grain size 9 (metres); proportion	0.128; 0
Suspended sediment fall velocity (metres per second)	0.024
Sediment transport law	Wilcock and Crowe
Maximum velocity to calculate Tau	5
Maximum erode limit	0.02
Active layer thickness	0.1
Proportion of sediment to be re-circulated	None
In channel lateral erosion rate	20
Lateral erosion	On
Lateral erosion rate	0.0001
Number of passes for edge smoothing filter	10
Number of cells to shift lateral erosion downstream	1
Maximum difference allowed in cross channel smoothing edge values	0.0001
Description	Scenario code

Override header	No
Inflow coordinates (x,y)	(42,2) , (40, 2) for Devi; (9, 136) , (9, 138) for Mahanadi
Inflow header file	Scenario as required
Divide inputs by	2
Input data time step (minutes)	1440
M value	n/a
Rainfall data file	n/a
Rainfall data time step (minutes)	n/a
Spatially variable rainfall	n/a
Stage/Tidal input	Scenario as required
Stage/Tidal coordinates (x_{min}, x_{max}, y_{min} y_{max})	(443, 440, 483, 481) for Devi; (830, 847, 316, 318) for Mahanadi
Input data time step (minutes)	360
Grass maturity growth rate	1
Vegetation critical shear	180
Proportion of erosion that can occur when vegetation is grown	0.5
Creep rate	0.0025
Slope failure threshold	45
Soil erosion rate	0
Soil erosion varies according to j_mean	No
SIBERIA sub model	No
Dune model	No
Input/output difference allowed (cumecs)	350
Minimum Q for depth calculation	0.9
Maximum Q for depth calculation	1000
Water depth thresholds over which erosion will happen (m)	0.01
Slope for edge cells	0.002
Evaporation rate (metres per day)	0.0046
Courant number	0.7
hFlow threshold (metres)	0.00001
Frounde number flow limit	0.8
Mannings n	0.03
Spatially variable Mannings n	No
Soil development	n/a

5.3.3 Outputs and results of validation

C-L provides a range of output data including both time series and spatial information. In this study, water depth; elevation change; grain size distribution; and flow velocity are saved at five year intervals. Total sediment and water discharges are saved annually. From this six key results were extracted to identify the nature and rate of morphological change, and areas of the catchment that may

be at greatest risk from this change. Each result is analysed at the end of the first 30 year period, and again at the end of the simulation (50 or 60 years as required).

Firstly, DEMs of difference are produced in ArcGIS 10.3 to analyse areas of the catchment where erosion or accretion has taken place and the extent of this change. In all scenarios a baseline subsidence rate of 3 $mm.yr^{-1}$ is applied to the DEM post-processing. Net sediment change is calculated for a cross section of the catchment. Secondly, channels with a water depth greater than 1 metre are extracted to create a map of the distributary network. This is then converted to a binary image to be utilised in the next stage of analysis. Channel width is also analysed and compared with historical data.

To provide a transferable framework for analysing these results between the different scenarios and catchments, the concept of Fluvial Geomorphic Response Units (FGRUs) proposed by Lindenschmidt and Long (2012) was adapted. In their study, a FGRU describes a river segment of at least 1 km in length based on the relative proportion of four geomorphic properties: sinuosity; slope; fractal dimension; and channel width. This provides a framework for identifying morphological patterns at the segment scale (one to tens of kilometres in length) at which transitions between major channel and floodplain features may be observed (Frissell *et al.,* 1986). The model also provides links between the hydrological regime and riverine habitats (Carr *et al.,* 2016; Thorp *et al.,* 2006, 2008). With the additional benefit of the geomorphic properties being able to be derived solely from GIS data, the FGRU concept is therefore a particularly valuable tool to aid water resource management at the catchment scale.

Many of the properties applied by Lindenschmidt and Long (2012) will not display significant spatial variability in the lower reaches of the delta plain: Both sinuosity and the fractal dimension will have relatively high values; whilst the slope will remain relatively low from the delta apex to the channel mouth. These therefore may not be the most appropriate factors with which to segregate areas of differing morphological response to shifts in the hydrological regime. Thus in this study the FGRUs concept was adapted to develop an approach that better reflects the dominant morphological processes that control the multidecadal evolution of deltaic environments. Instead seven morphological response units (MRUs) were identified. Rather than these being based on the relative proportion of various

geomorphic properties, these are identified by the emergence of distinct landforms based on the analysis of elevation data.

MRUs are split into two categories (table 5.6): Firstly, those that describe the **dominant channel processes** that occur within the channel itself**.** These include: **(1)** Lateral erosion – resulting in widening of the river channel; either on both sides of the channel or the outside of a meander bend. This may eventually lead to channel migration; **(2)** Channel incision – resulting in scouring and deepening of the river channel; **(3)** Mid-channel bar formation – evident from accumulations of sediment within the channel that may be re-arranged or inundated during large floods. This process is an important driver of deltaic evolution as the subsequent channel bifurcation that occurs around the bar leads to the generation of complex fractal networks across the flood plain (Edmonds and Slingerland, 2007). **(4)** Point-bar formation – evident from the deposition of sediment on the inside of meanders. This process is critical to alluvial stratigraphy and meander migration.

The second category of MRUs describe the **dominant floodplain processes** that occur outside of the main channel. These include: **(5)** Levee formation – evident from accretion of sediment adjacent to the channel. Maximum levee height is proportional to maximum flood depth. **(6)** Crevasse splay formation – a fan-shaped deposit which formed when a channel breaches its levees during high flows. Whilst a crevasse splay is active it may form a microdelta on the floodplain; however if sediment supply is reduced or terminated the crevasse splay may become abandoned. **(7)** Floodplain channels – identified as channels that are disconnected from the distributary system except for during high flow events. These channels may become partially or fully abandoned over time.

It should be noted that despite being a dominant process in the evolution of deltaic environments, channel avulsion is not included as a designated MRU in this study. This is because channel switching tends to occur over temporal scales of centuries – millennia (Edmonds *et al.,* 2009), as opposed to the multidecadal scales analysed in this study. However MRUs including lateral erosion, mid-channel bar formation and crevasse splay formation could all represent areas of the catchment avulsion could emerge beyond the extent of the simulation.

Table 5.6 Identification of morphological response units (MRUs). MRUs represent the emergence of distinct landforms that drive deltaic evolution at the multidecadal scale.

	MRU	**Identified by**	**Thematic example** (where red = elevation loss; black = elevation gain; blue = channel)
Channel processes			
1	Lateral erosion	Widening of the river channel	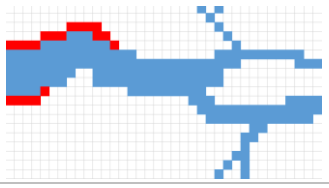
2	Channel incision	Deepening of the river channel	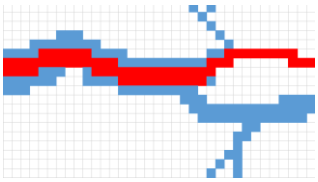
3	Mid-channel bar formation	Deposition of sediment within the river channel	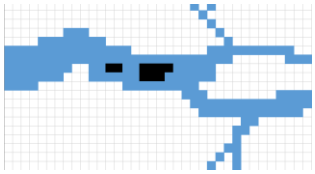
4	Point-bar formation	Deposition of sediment on the inside of a meander bend	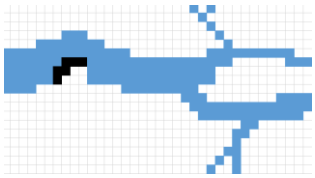
Floodplain processes			
5	Levee formation	Deposition of sediment adjacent to the channel	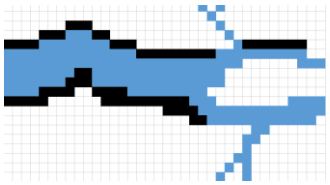
6	Crevasse splay formation	Fan-shaped deposit formed where a levee has been breached	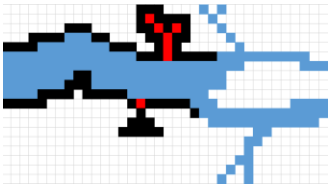
7	Floodplain channels	Channels (≥ 1 metre in depth) that are disconnected from the main distributary system	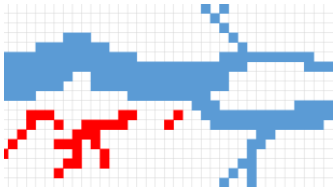

Next, three quantitative metrics are identified that help to describe emergent features in the distributary network; based on those utilised by Edmonds *et al* (2011). Here the authors sought to identify a series of metrics for deltas that had direct analogues with those utilised for tributary networks. Metrics that describe tributary systems tend to focus on the spatial and temporal characteristics of the hydrograph (Rodriguez-Iturbe and Rinaldo, 1997). Edmonds *et al.* however adopted a "sediment-focused" approach; based on the assumption that the primary driver of delta morphodynamics is the need to distribute sediment over the plain and maintain the surface transport slope in the face of progradation and relative sea level rise. All three metrics are analysed using Matlab software.

The first of these metrics is the fractal box-counting dimension (D). This is a common measure in geomorphological pattern analysis and has been utilised in many studies to characterise both river basin patterns and coastlines (Seybold *et al*., 2007; Maritan *et al*., 1996). Edmonds *et al*. (2011) state that this value should vary from 1 to 2; where 1 suggests the object is self-similar and 2 suggests a more complex network that is space filling. Delta networks that are not heavily influenced by mouth bar bifurcation will have a D closer to 1 because that characteristic geometry is not repeated at all scales. This would be found in deltas with a singular active channel, such as the Ebro delta in Spain. Conversely, delta networks will have a D closer to 2 if more channels are created through bifurcation across the system. This will apply to deltas with a high channel density, such as the Lena delta in Russia. Figure 5.11 shows the Matlab script used to calculate D values.

Next the distribution of island sizes across the catchment system was analysed. Islands are mapped by tracing the edges of land polygons that are completely surrounded by water of 1 metre depth or greater, using the Matlab script shown in figure 5.12. As in Edmonds *et al.* (2011), no distinction is made between islands formed by deposition within the channel and those formed by channels that carve into existing land. Older deltas or more avulsive deltas will tend toward a bimodal island size distribution with both large and small islands, and a higher average island size overall. Jerolmack and Swenson (2007) suggest this is because they are dominated by aggradation. In contrast the distribution of island sizes for younger deltas with many bifurcations should be more continuously

distributed (unimodal), and will be dominated by smaller islands. The migration of islands through the system was also tracked.

Finally the nearest-edge distance (NED) distribution for the catchment was calculated. Edmonds *et al.* (2011) define NED as the nearest distance to channelised or unchannelised water from any given point on land. This is the inverse of drainage density for tributary networks (the ratio of total channel length to basin area). They suggest that delta networks organise to maintain a spatially consistent average NED. They propose that this is driven by an internal feedback mechanism, whereby areas with high NED receive less sediment over time, and eventually become topographic depressions. Such depressions should tend to attract channels, thereby reducing the NED. Organic growth could however regulate this feedback mechanism. As discussed in chapter 2, NED can be used to help predict floral and faunal assemblages on the delta plain. Figure 5.13 shows the Matlab script used to calculate NED.

```
>> [n,r] = boxcount_nofig(CHAN);

figure
loglog(r, n, 'r*')
xlabel('r')
ylabel('n')
axis tight

figure; hold on;
loglog(r, n, '.');
% fit in log domain
p = polyfit(log(r), log(n), 1);
% compute fit in linear domain
n_hat = exp(p(1) * log(r) + p(2));
% make log log plot
loglog(r, n_hat);

label = ['log(y) = ' num2str(p(1)) 'log(x) + ' num2str(p(2))];
legend('data', label);
```

Figure 5.11 Matlab script for calculating the fractal box-counting dimension (D). CHAN refers to the prepared binary image of the skeletonised channel network. D is the correlation coefficient on the calculated line of best fit.

```
>> [B,L,N,A] = bwboundaries(CHAN);
figure; imshow(CHAN); hold on;
% Loop through object boundaries
for k = 1:N
    % Boundary k is the parent of a hole if the k-th column
    % of the adjacency matrix A contains a non-zero element
    if (nnz(A(:,k)) > 0)
        boundary = B{k};
        plot(boundary(:,2),...
            boundary(:,1),'r','LineWidth',2);
        % Loop through the children of boundary k
        for l = find(A(:,k))'
            boundary = B{l};
            plot(boundary(:,2),...
                boundary(:,1),'g','LineWidth',2);
        end
    end
end
```

Figure 5.12 Matlab script for identifying island areas, where CHAN refers to the prepared binary image of the skeletonised channel network. Island size is then calculated from the number of pixels within each island boundary.

```
>> [D,IDX] = bwdist(CHAN)
```

Figure 5.13 Matlab script for calculating NED distribution, where CHAN refers to the prepared binary image of the skeletonised channel network. D refers to the NED value for any given point.

Edmonds *et al.* (2011) analyse two further metrics in their study that we choose not to apply in this research project. Firstly, they analyse the synthetic distribution of sediment fluxes. This provides a measure of the spatial distribution of bed load and suspended load sediment fluxes delivered to the shoreline. Secondly, they calculate the nourishment area for the delta. This provides an estimate of the delta area nourished by sediment passing through a given channel cross section; this being analogous to drainage area in tributary systems. Both metrics were omitted from this study as they are not as relevant to morphodynamics operating at the catchment scale.

To validate the setup of the model, scenario TST was run for 30 years in both catchments. As discussed in section 5.3.2, the results were compared against LANDSAT images from 2003 in order to see if the rate and pattern of accretion and erosion in the model was considerably different from that observed in the real delta. As the fractal dimension, the distribution of island sizes and NED have not been applied in the Mahanadi Delta before, these results were extracted at year 0 of the simulation. The changes seen in these metrics after 30 years were then compared with those observed by Edmonds *et al.* (2011).

Channel width varied by a maximum of 0.09 km over the validation period; this is 0.04 km higher than that demonstrated by the LANDSAT imagery in figure 5.9. This figure however is the product of having a grid cell size of 0.09 km^2, and is thus not a likely cause for concern in terms of model performance. Figure 5.14 shows a map of elevation change in the Devi catchment at year 30 of scenario TST. Figure 5.15 shows net sediment volume change over the same period. Erosion has occurred throughout the upper, middle and lower reaches of the catchment via scouring of the main channel. Scouring occurred to a maximum depth of 9 metres. Levees have also been formed throughout the catchment, and are most pronounced in the lower reaches. The small areas demonstrating unusually high rates of accretion (≤ 16 metres) represent areas where the channel has migrated. A large volume of sediment has been distributed over the flood plain in the upper reaches. A bar has also developed at the mouth of the estuary. Whilst this feature does not exist at this location in the real Mahanadi Delta, a large area of deposition is located just outside of the model domain. Overall the catchment gained 0.009 km^3 of sediment: 0.017 km^3 was lost in the upper reach; 0.010 km^3 was lost in the middle reach; and 0.020 km^3 was gained in the lower reach. A more detailed description of these results is presented in the next chapter.

In the Mahanadi catchment channel width decreased by a maximum of 0.09 km in the middle and lower reaches. This is 0.8 km higher than that demonstrated by the LANDSAT imagery in figure 5.10; however as before this is likely as a result of grid cell size. More importantly, this demonstrates that C-L has successfully reproduced the correct locations of channel narrowing in the model domain. Figure 5.16 shows a map of elevation change in the Mahanadi catchment at year 30 of scenario TST. Figure 5.17 shows net sediment volume change over the same period.

As in the Devi, significant erosion has occurred throughout the upper, middle and lower reaches of the catchment via scouring of the main channel. Scouring occurred to a maximum depth of 9 metres. Levees have also been formed throughout the catchment, and are most pronounced in the upper and lower reaches. As expected, the most noteworthy changes have occurred in the upper and coastal regions of the catchment. As C-L does not include waves, it would not be possible for the model to accurately reproduce the formation of a spit at the mouth of the estuary. This limitation must be taken into account during analysis of the other scenario runs. Overall the catchment lost 0.062 km^3 of sediment: 0.032 km^3 was lost in the upper reach; 0.001 km^3 was lost in the middle reach; and 0.031 km^3 was lost in the lower reach. A more detailed description of these results is presented in the next chapter.

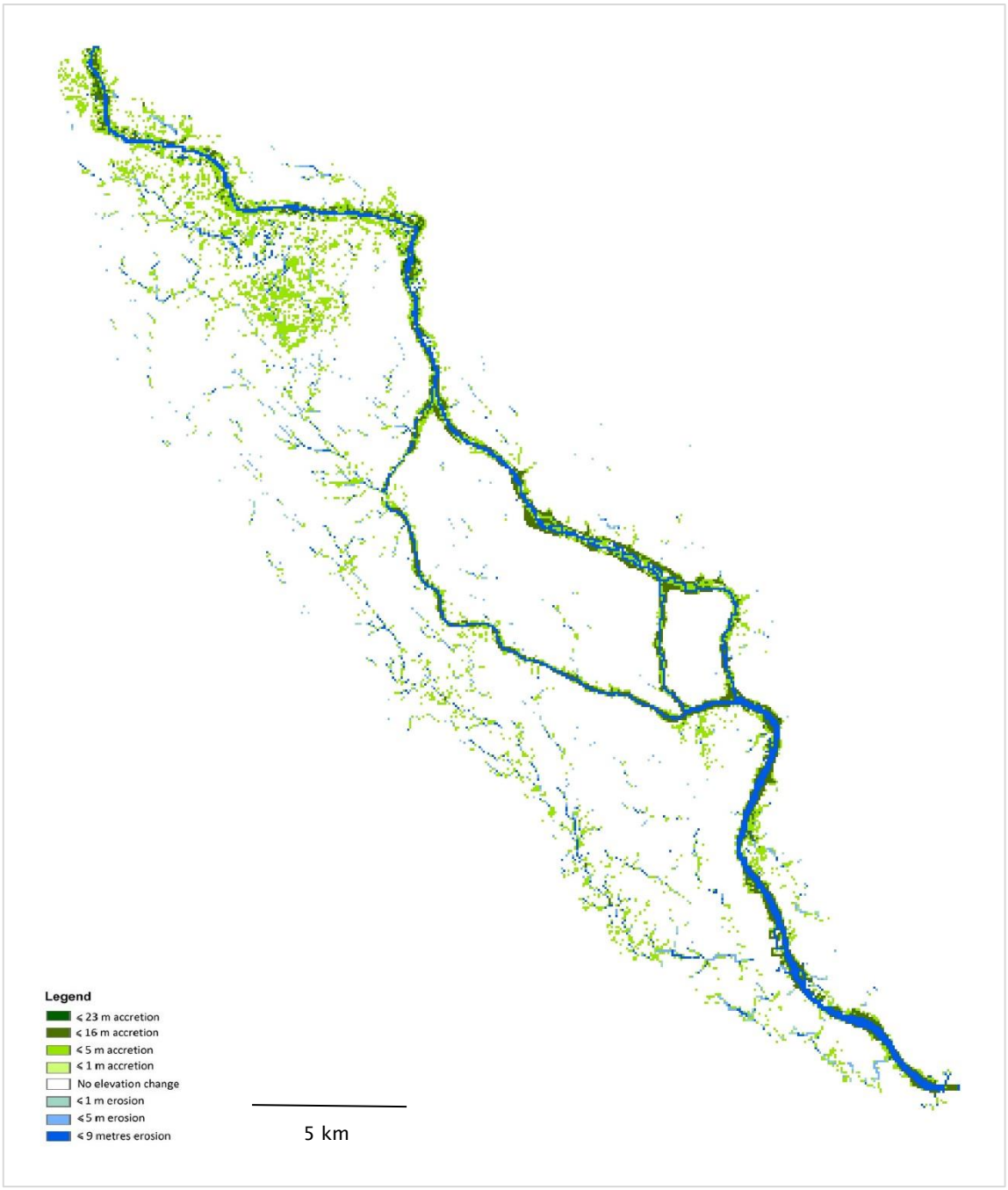

Figure 5.14 Elevation change in the Devi catchment at year 30 of scenario TST.

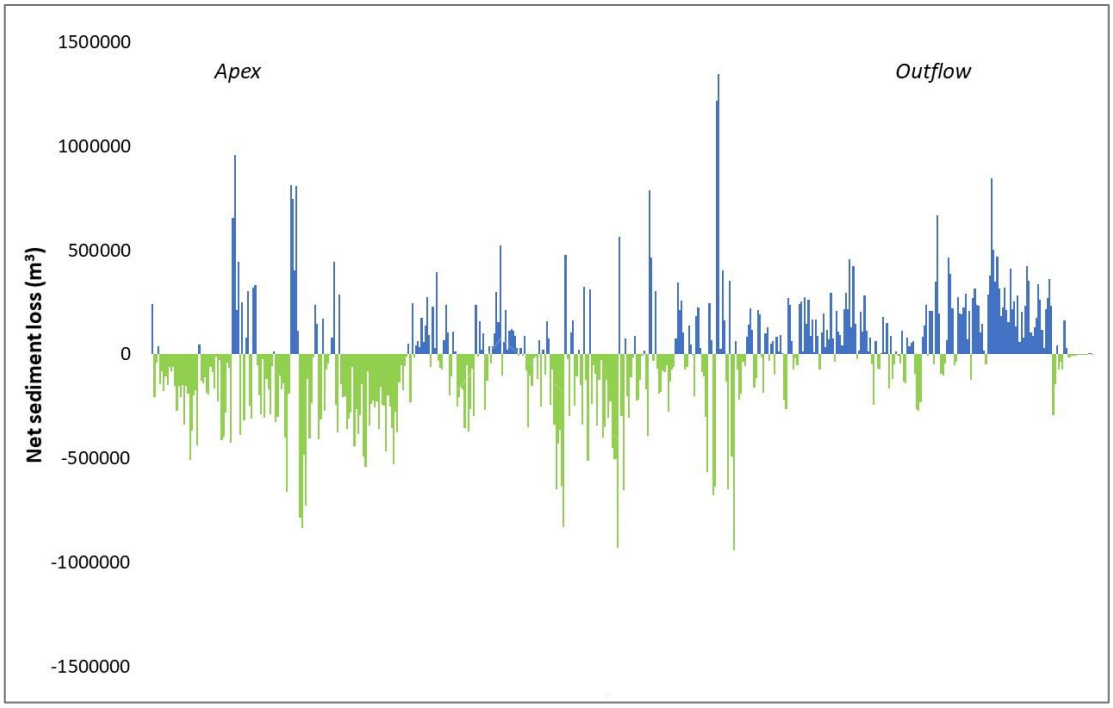

Figure 5.15 Net sediment volume change in the Devi catchment at year 30 of scenario TST. The x-axis corresponds to distance from the catchment apex (left) to the catchment outflow (right).

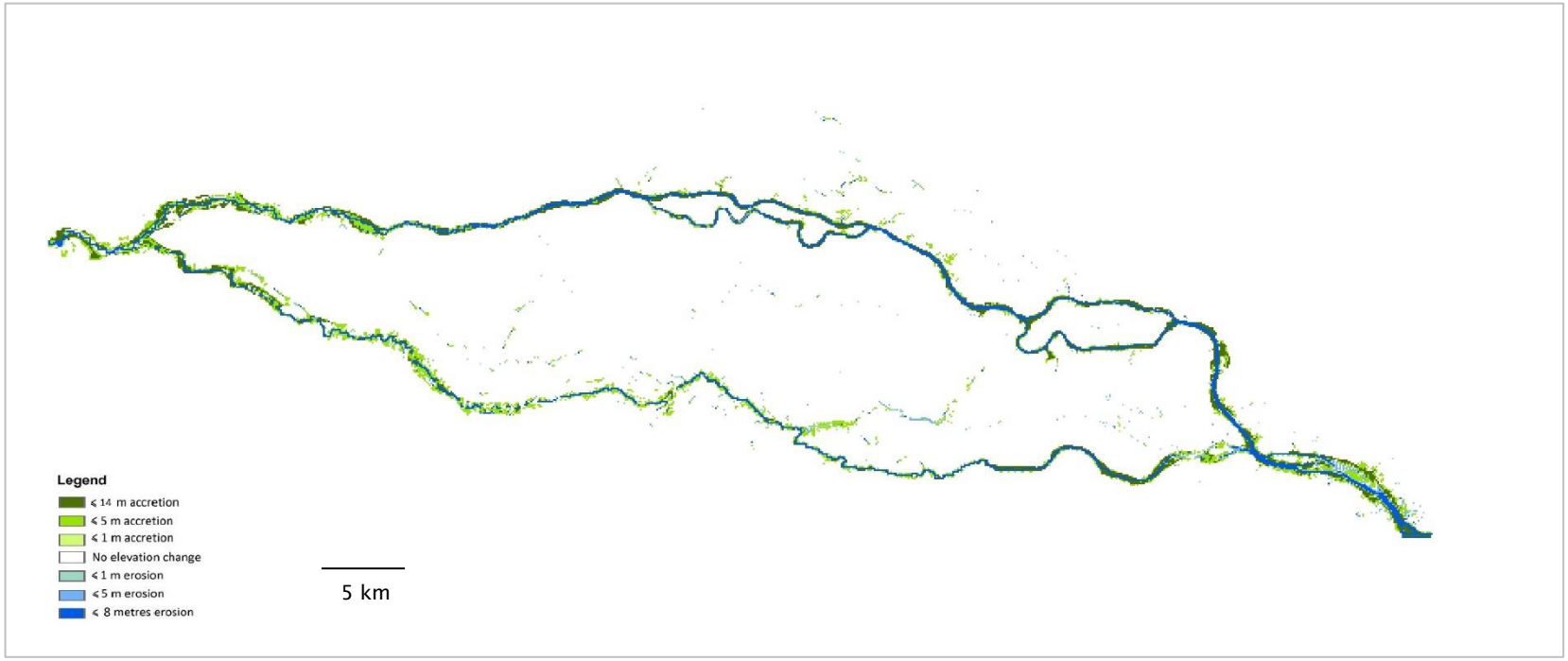

Figure 5.16 Elevation change in the Mahanadi catchment at year 30 of scenario TST

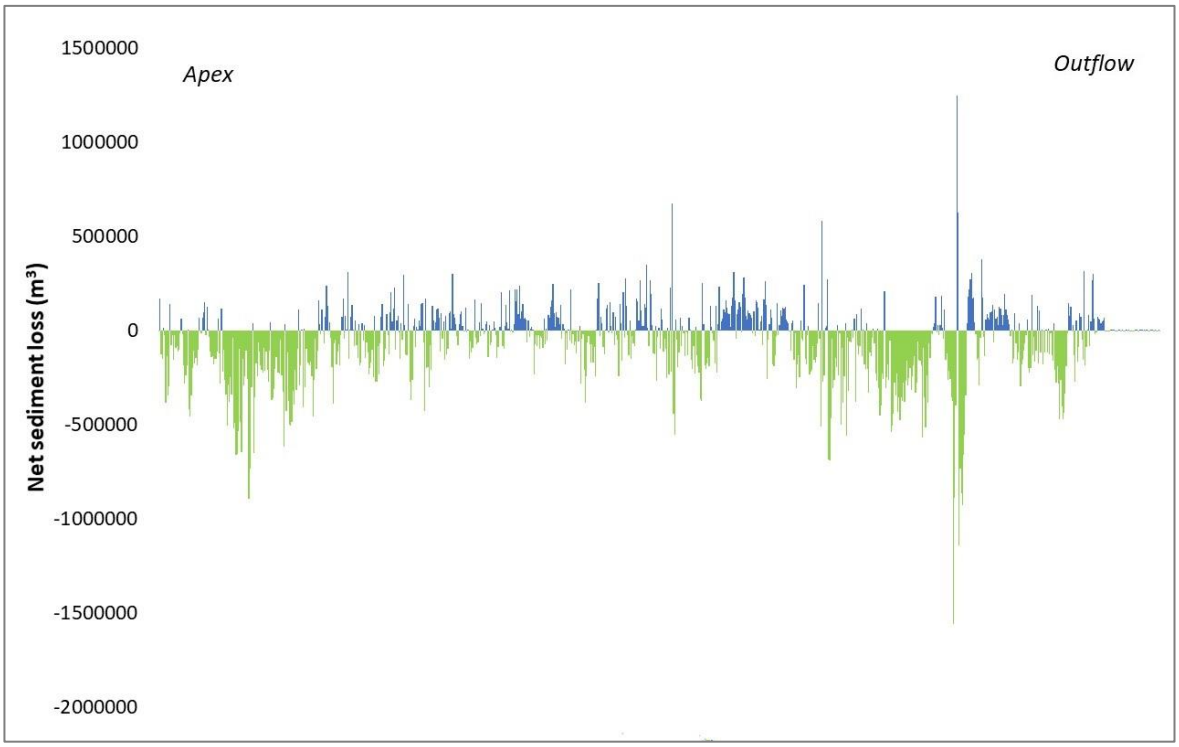

Figure 5.17 Net sediment volume change in the Mahanadi catchment at year 30 of scenario TST. The x-axis corresponds to distance from the catchment apex (left) to the catchment outflow (right).

Channel density increased over the 30 year period in the Devi catchment, demonstrated by the fractal box-counting dimension value (D) increasing from 1.46 to 1.51. However, in the Mahanadi catchment, the D value decreased from 1.48 to 1.44. This reflects the previous analysis which showed a tendency towards increasingly narrower, straighter channels in the middle and lower reaches. These values are slightly higher than those found by Edmonds *et al.* (2011) (figure 5.18), which ranged between 1.24 and 1.30. However the values for the Mahanadi and Devi catchments are not outside the expected range for deltas. This could be reflective of the fact that Edmonds *et al.* applied these metrics to the entire delta plain as opposed to individual watersheds. Conversely it could reflect the dominance of channel bifurcation, particularly in the Devi catchment. Seybold *et al.* (2007) found the Lena delta in Russia to have a D value of 1.8, and their simulated delta to have a D value of 1.85.

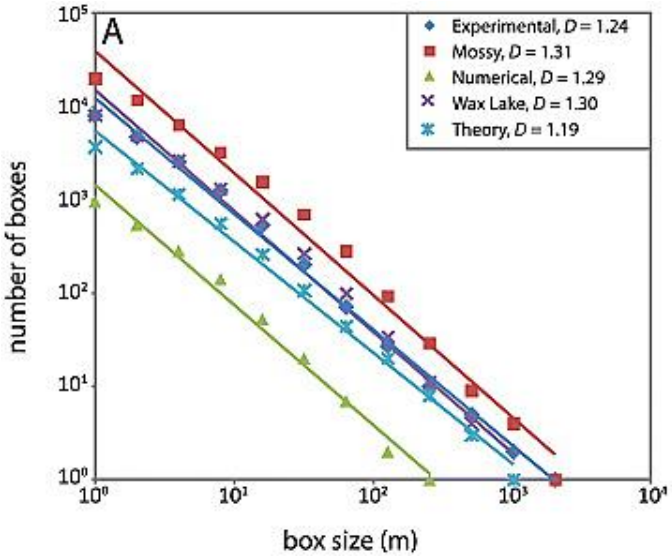

Figure 5.18 Box-counting dimension, D, for the delta networks analysed by Edmonds *et al.* (2011). They found all delta networks to be fractal and characterized by a D ≈ 1.3.

Next the distribution of island sizes across the catchment system were analysed. As shown in figure 5.19a, there is an increase in the number of larger islands In the Devi catchment over the 30 year validation period although there is a clear dominance of smaller islands. The total number of islands increased slightly from 37 to 42. Most new islands were formed in the mid and lower regions of the catchment. Mean island size increased from 1.57 km^2 to 5.67 km^2 (0.011% and 0.038% of total delta area, respectively); however modal island size remained the same at 0.36 km^2 (0.002% total delta area). In the Mahanadi catchment, the total number of islands increased from 20 to 47. As shown in figure 5.19b, the Mahanadi catchment is also dominated by smaller islands over the 30 year validation period. Mean island size decreased from 25.9 km^2 to 12.08 km^2 (0.175% and 0.086% of total delta area, respectively); however modal island size increased from 0.36 km^2 (0.002% total delta area) to 0.54 km^2 (0.004% total delta area) Most islands remained stationary over the 30 year period, but fluctuated in width and length. This is reflective of the patterns observed in LANDSAT images.

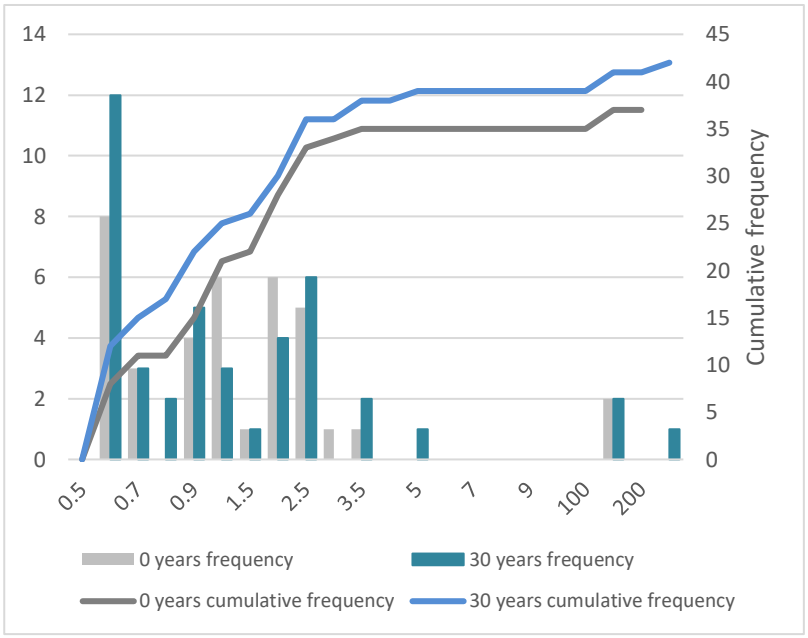

(A)

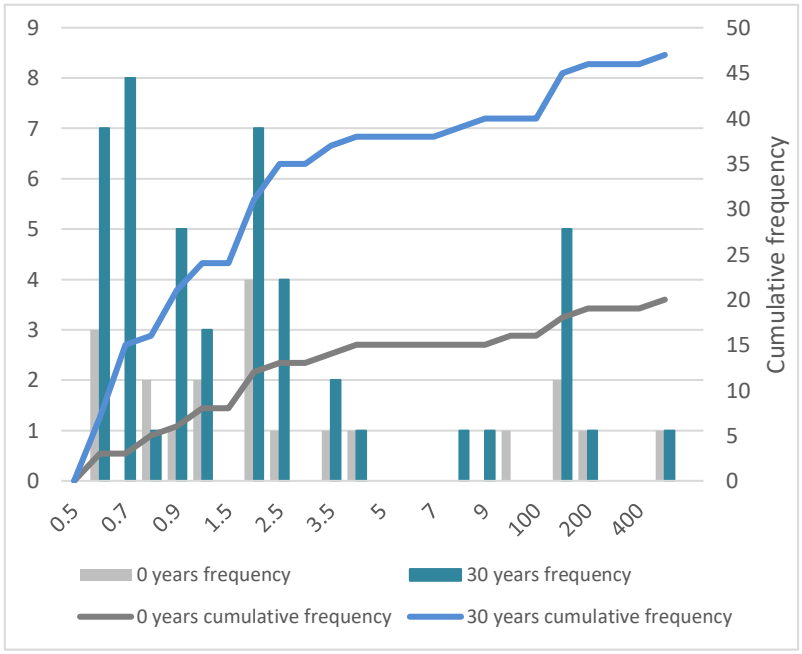

(B)

Figure 5.19 (A) Island size distribution for the Devi catchment at 0 and 30 years of scenario TST and (B) Island size distribution for the Mahanadi catchment at 0 and 30 years of scenario TST

Finally the nearest-edge distance (NED) distribution for both catchments were calculated. As shown in figure 5.20, we find a similar distribution in both the Devi and Mahanadi catchments to that found by Edmonds *et al.* (2011); with the exception of a second peak at a value of ~0.20. This is likely to be related to the fact that the shape of the catchment watershed is different to that of the overall delta plain; and considering this the results are still remarkably similar. Overall there is little change to NED distribution over the 30 year period. As concluded by Edmonds *et al.* (2011) the mean NED for the Devi catchment also remains spatially consistent across the delta plain, with the exception of a small peak in the upper catchment (figure 5.21). This is not the case however in the Mahanadi catchment, where 2 peaks in NED values are observed in the upper and lower regions of the catchment. This is likely caused by the high abundance of floodplain channels across the centre of the catchment.

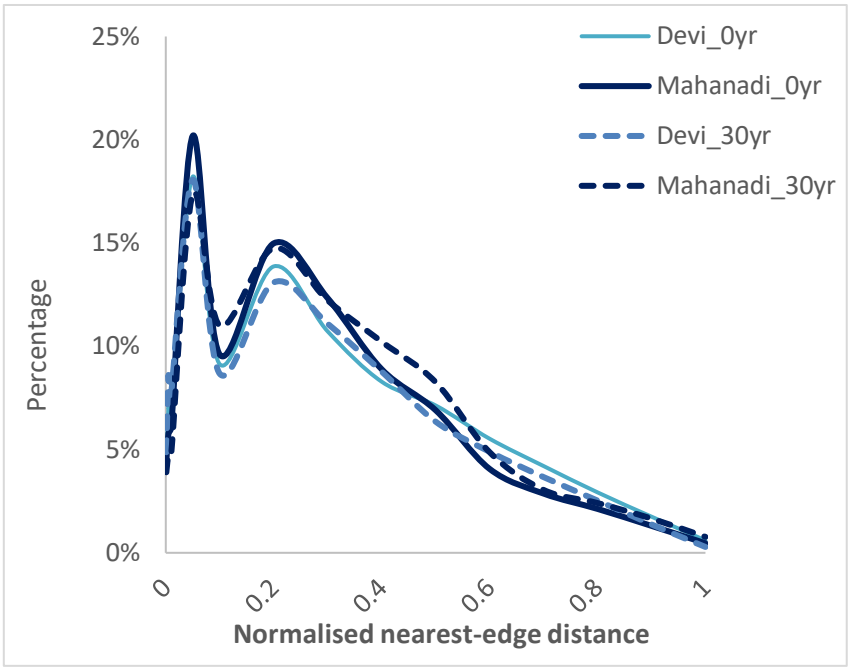

(A)

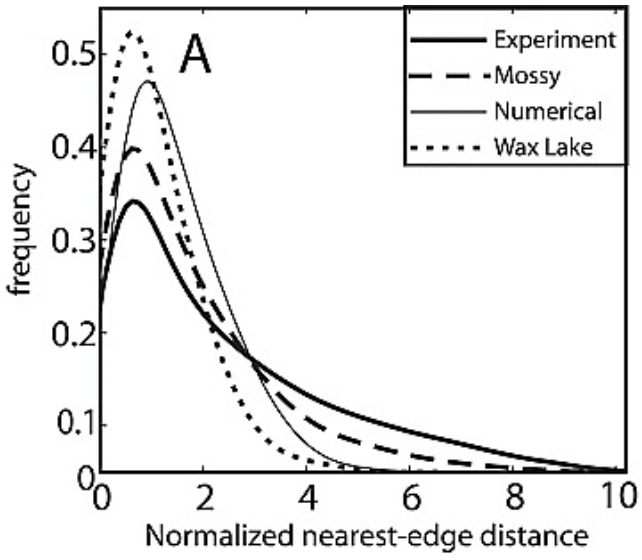

(B)

Figure 5.20 (A) Distribution of normalised NED values in the Devi and Mahanadi catchments at 0 years and 30 years under scenario TST. (B) Distribution of normalised NED values found by Edmonds *et al.* (2011).

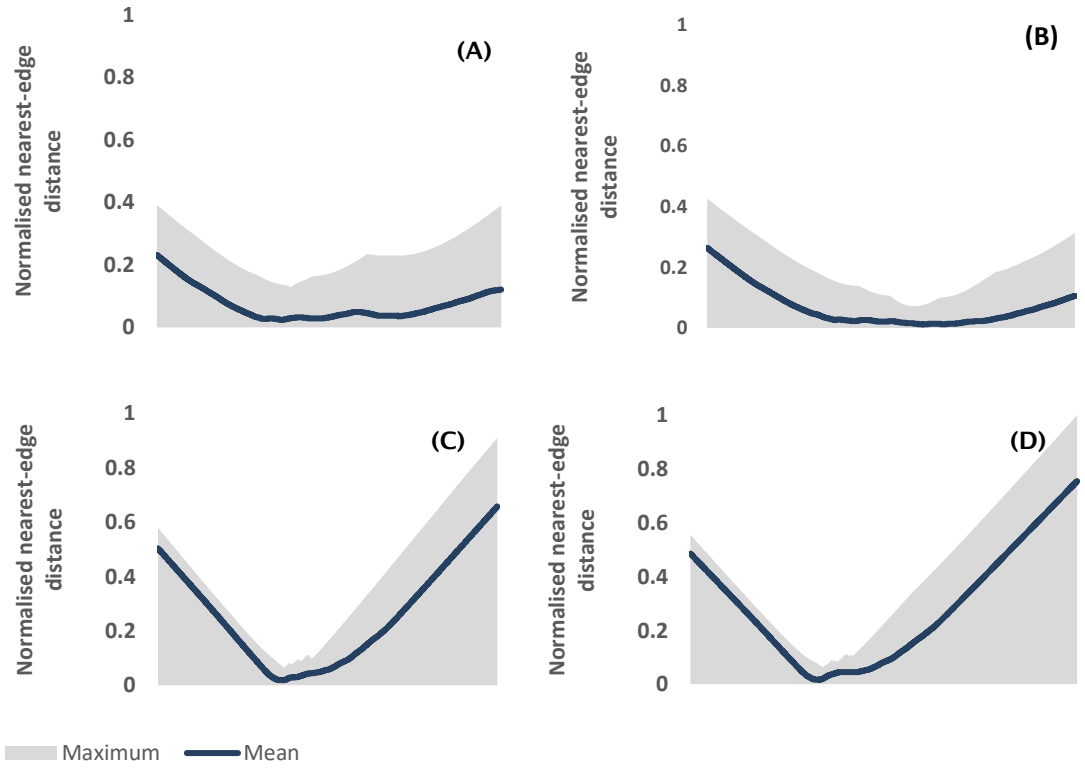

Figure 5.21 (A) Spatial distribution of normalised NED values in the Devi at 0 years under scenario TST (B) in the Devi at 30 years under scenario TST (C) in the Mahanadi at 0 years under scenario TST (D) in the Mahanadi at 30 years under scenario TST. The x axis represents distance along the main channel from the catchment apex (left) to mouth (right).

5.3.4 Utilising morphological outputs for habitability analysis

The second objective of this study is to explore how changes in the emergent morphological system may impact certain factors that influence the habitability of the Mahanadi Delta. Specifically I explore how the analysis of morphological behaviour enables the development of a further series of metrics that assess **(1)** inundation following an extreme flood event; **(2)** potential changes in habitat cover; **(3)** the effectiveness of potential engineering strategies, with a focus on re-naturalising the channel network. This comes together to achieve the third objective of this study: to produce outputs that are directly usable by stakeholders. As discussed in chapter 3, providing a categorical measure of vulnerability for a given area over a given time period, under various environmental change and management scenarios, will provide an efficient and policy-relevant means of representing how the nature of physical change across

the delta system may impact the habitability of certain regions. To achieve this, a number of additional model runs and analyses are required. The scenario design for these runs is described below; whilst the methodology for this component of the study is discussed in detail in chapter 7. The following additional runs will all be undertaken utilising the setup of scenario 4DWD; the scenario describes the 'most likely pathway' for the Mahanadi region based on the current literature.

5.3.4.1 Flood hazard following an extreme cyclone event

This scenario is designed to explore potential inundation extent due to an extreme flood event following 50 years of morphological change under scenario 4DWD. Two additional 1 year runs will be undertaken; firstly using the original DEM for the catchment and secondly using the DEM generated by year 50 of 4DWD. During this year the hydrological and tidal parameters representing those experienced before and during the 1999 Odisha cyclone will be input in to C-L, and water depth outputs shall be extracted at daily intervals. Inundation areas are then compared at years 0 and 50 for each catchment. This process is discussed in greater detail in chapter 7.

5.3.4.2 Changes in habitat cover

Vegetation change is a dynamic and complex process that has a significant influence on erosion rates across the delta plain and within the river channels themselves. As discussed in chapter 3, despite its relatively simple representation of these biophysical interactions, C-L provides a useful tool to infer how land cover changes over multidecadal timescales interact with flow and sediment transport patterns. To explore possible changes in habitat cover under scenario 4DWD, we extract a number of morphological outputs for each catchment. We then use this information to infer the impacts this may have on existing habitat cover (using the land cover map presented in chapter 4). We utilise hypsometry, flood inundation extent, net elevation change, floodplain MRUs and channel MRUs to generate categorical measures of vulnerability to habitat change. This process is discussed in full in chapter 7.

5.3.4.3 Engineering strategies

For all of the scenarios in this study, it is assumed that no active intervention is taken to prevent morphological change between 2015 and

2065(75). An existing flood defence is not explicitly modelled, but equally is not deliberately removed from the DEM, provided the spatial resolution at which it is presented does not intercept channel flow. As well as providing a baseline against which alternative interventions can be compared, these runs also provide insight into a scenario for any locations in which the introduction of new defences or engineering strategies are not financially or logistically viable at present.

Increasing sediment delivery has become a central concern in delta restoration projects (Giosan *et al.,* 2013). Often such strategies require management decisions to be made outside of the delta itself, such as the installation of flushing mechanisms to allow sediment to flow past dams (Kondolf *et al.,* 2014). As C-L will not explicitly model structures outside of the catchment, such modifications would need to be tested through changes to overall sediment delivery. Modifications to hydraulic structures within the system can be modelled through appropriate changes to river flow and sedimentation rates at a given junction in the channel network, as well as to the DEM. Other restoration strategies focus on increasing the trapping efficiency of the delta plain and coastline (Kim *et al.,* 2009). As mentioned previously, Giosan *et al.* (2014) suggest four methods of restoration that mimic natural processes: channelization, in which new channels are installed to spread sediments across the plain and promote natural wetland accretion; deliberately breaching levees to create crevasse splays; constructing artificial internal subdeltas, resulting in increased sedimentation in lakes and lagoons; and lastly, lobe building in areas naturally protected from high wave energy and tidal action. In coastal regions of the deltaic plain, the installation of hard engineering structures, represented by changes to flow and elevation at designated junctions in the channel network, may be the only viable option to trap sediment in the most vulnerable locations.

In this final exploratory investigation, we demonstrate the use of the C-L model to simulate two engineering strategies that could be applied in the Mahanadi region in order to reduce the impacts of detrimental morphological change. These include the deliberate breach of a levee structure, and the installation of an artificial subdelta. Specifically we focus on areas of the catchments that have been defined as vulnerable in previous analysis. The years 2015 – 2045 are re-run in each catchment following the implementation of each engineering strategy. Once again, this process is presented in full in chapter 7.

Chapter 6 **Morphological Modelling**

6.1 Presentation of Results

In this chapter the results of morphological modelling in CAESAR-Lisflood (C-L) are presented for each of the synergistic scenarios. Section 6.1.1 provides an overview of the results for the scenarios run in the Devi catchment, whilst section 6.1.2 compares these results with those scenarios run in the Mahanadi catchment. A full discussion of these results is then presented in section 6.2.

To provide a transferable framework for analysing the results between the different scenarios and catchments, I have adapted two analytical concepts: Firstly the concept of Fluvial Geomorphic Response Units (FGRUs) (Lindenschmidt and Long, 2012). As discussed in the methodology in section 5.3.3, FGRUs provide a framework for identifying morphological patterns at the segment scale (one to tens of kilometres in length) at which transitions between major channel and floodplain features may be observed (Frissell *et al.,* 1986). The model also provides links between the hydrological regime and riverine habitats (Carr *et al.,* 2016; Thorp *et al.,* 2006, 2008). In this study the FGRUs concept was adapted to develop an approach that better reflects the dominant morphological processes that control the multidecadal evolution of deltaic environments. Specifically, seven morphological response units (MRUs) were identified based on the analysis of elevation data. Firstly, those that describe the **dominant channel processes that occur within the main channel itself**. These include: Lateral erosion; Channel incision; Mid-channel bar formation; and point-bar formation. The second category of MRUs describe the **dominant floodplain processes** that occur outside of the main channel. These include: Levee formation; crevasse splay formation; and floodplain channels.

The second analytical concept utilised by this study is based on the approach of Edmonds *et al.* (2011). As described in detail in section 5.3.3, three quantitative metrics are utilised that help to describe emergent features in the distributary network: The first of these metrics is the **fractal box-counting dimension (D).** Edmonds *et al.* (2011) state that this value should vary from 1 to 2; where 1 suggests the object is self-similar and 2 suggests a more complex network that is space filling. Next the **distribution of island sizes** across the catchment system

was analysed. Islands are mapped by tracing the edges of land polygons that are completely surrounded by water of 1 metre depth or greater. As in Edmonds *et al.* (2011), no distinction is made between islands formed by deposition at the river mouth and those formed by channels that carve into existing land. Finally I calculated the **nearest-edge distance (NED) distribution** for the catchment. NED is defined as the nearest distance to channelised or unchannelised water from any given point on land. This is the inverse of drainage density for tributary networks (the ratio of total channel length to basin area).

6.1.1 Devi Catchment

6.1.1.1 Sediment loss and elevation change

Figures 6.1 and 6.2 show net sediment loss and elevation change at 30 years and 50 years, respectively, under scenario TST. Figure 6.3 shows elevation change between 30 and 50 years for scenario TST; enabling a clearer analysis of areas of significant channel widening and levee formation. Under this TST scenario all drivers are run utilising historical values. This therefore provides a baseline run in which there are no significant changes to external forcings, against which other scenarios can subsequently be compared. For clarity of discourse, maps showing elevation change under all other synergistic scenarios in the Devi catchment can be found in the Appendix, although they may be referred to in this chapter. Figures 6.4 - 6.7 do however show net sediment loss for all other scenarios, for ease of comparison.

Table 6.1 shows the total net sediment change in the Devi catchment under each scenario at 30 and 50 years. As described in chapter 5, scenario 10DWDF is run for an extended 10 year period in order to capture the simulated failure of the monsoon rains from the year 2065.

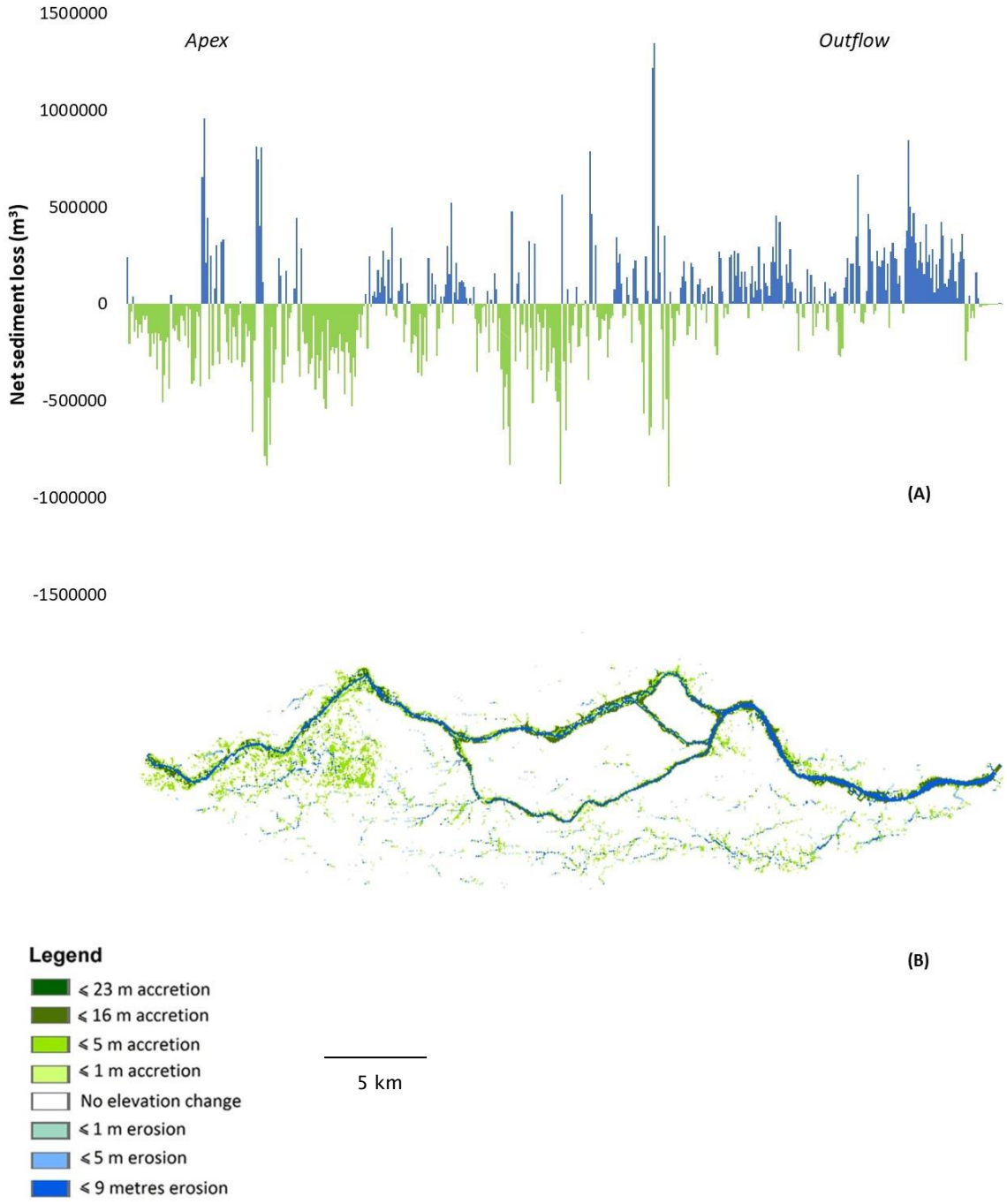

Figure 6.1 (A) Net sediment loss and (B) Elevation change at 30 years under scenario TST, Devi catchment. The x-axis in figure A corresponds to distance from the catchment apex (left) to the catchment outflow (right).

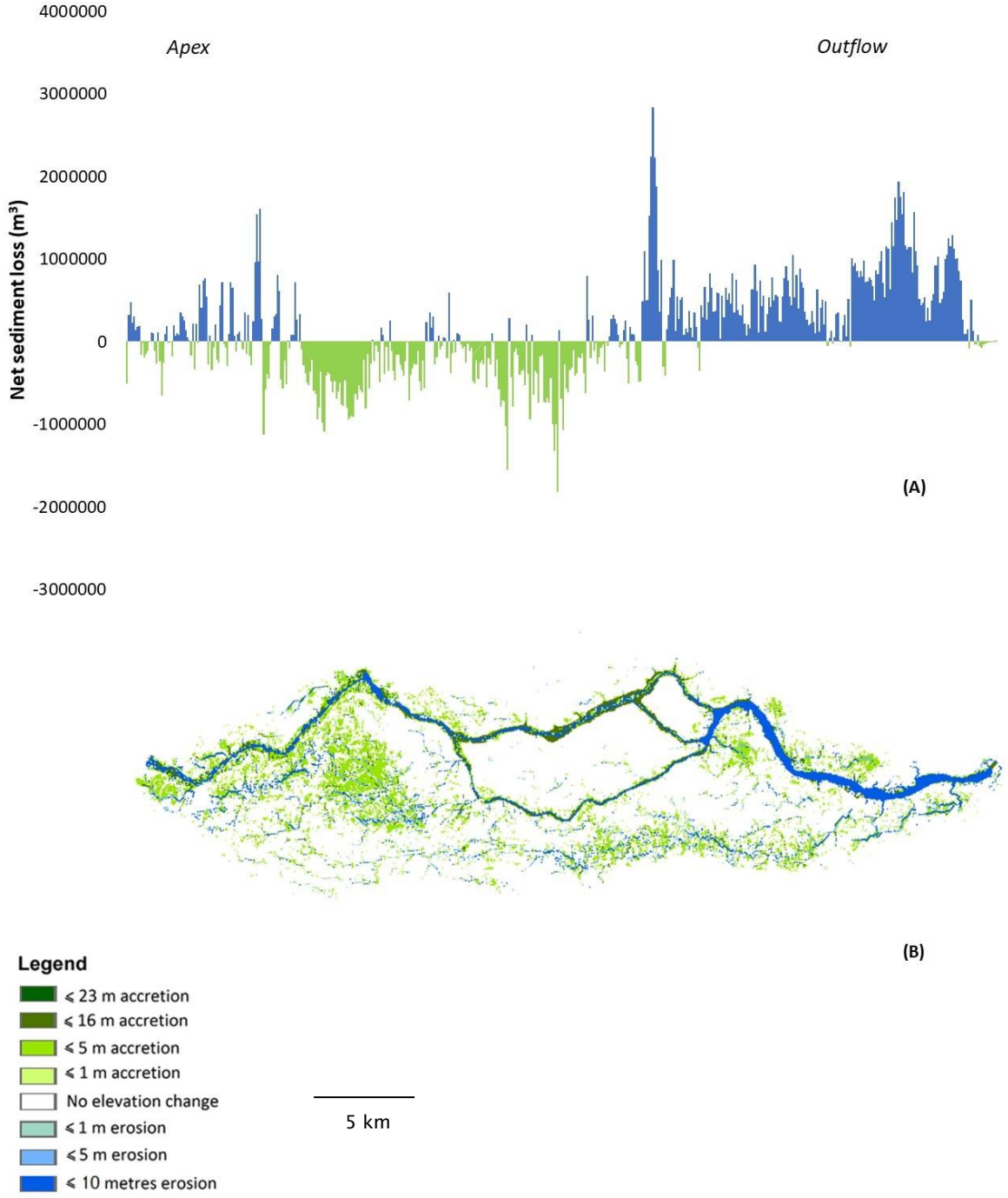

Figure 6.2 (A) Net sediment loss and (B) Elevation change at 50 years under scenario TST, Devi catchment. The x-axis in figure A corresponds to distance from the catchment apex (left) to the catchment outflow (right).

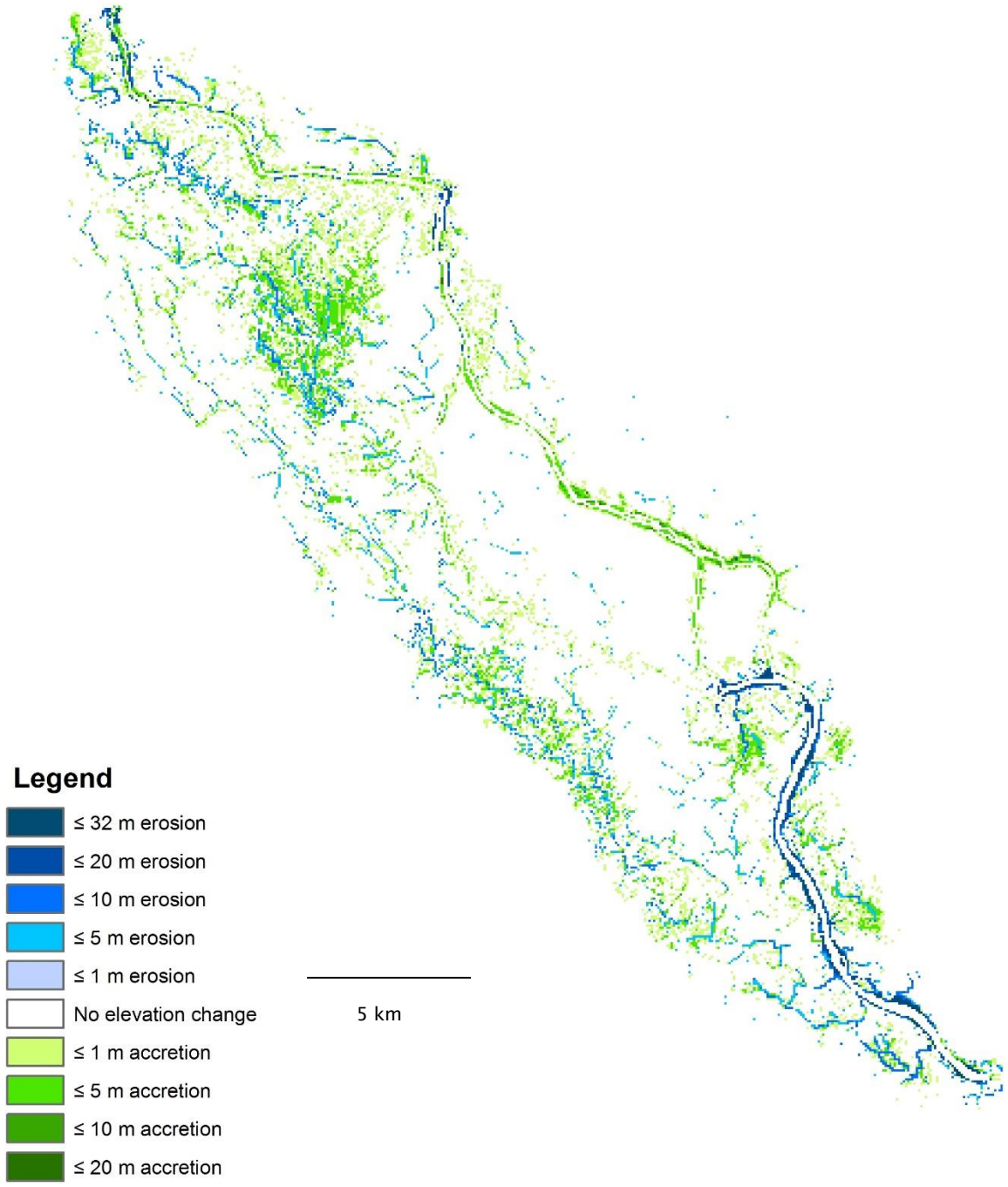

Figure 6.3 Elevation change between 30 and 50 years under scenario TST, Devi catchment.

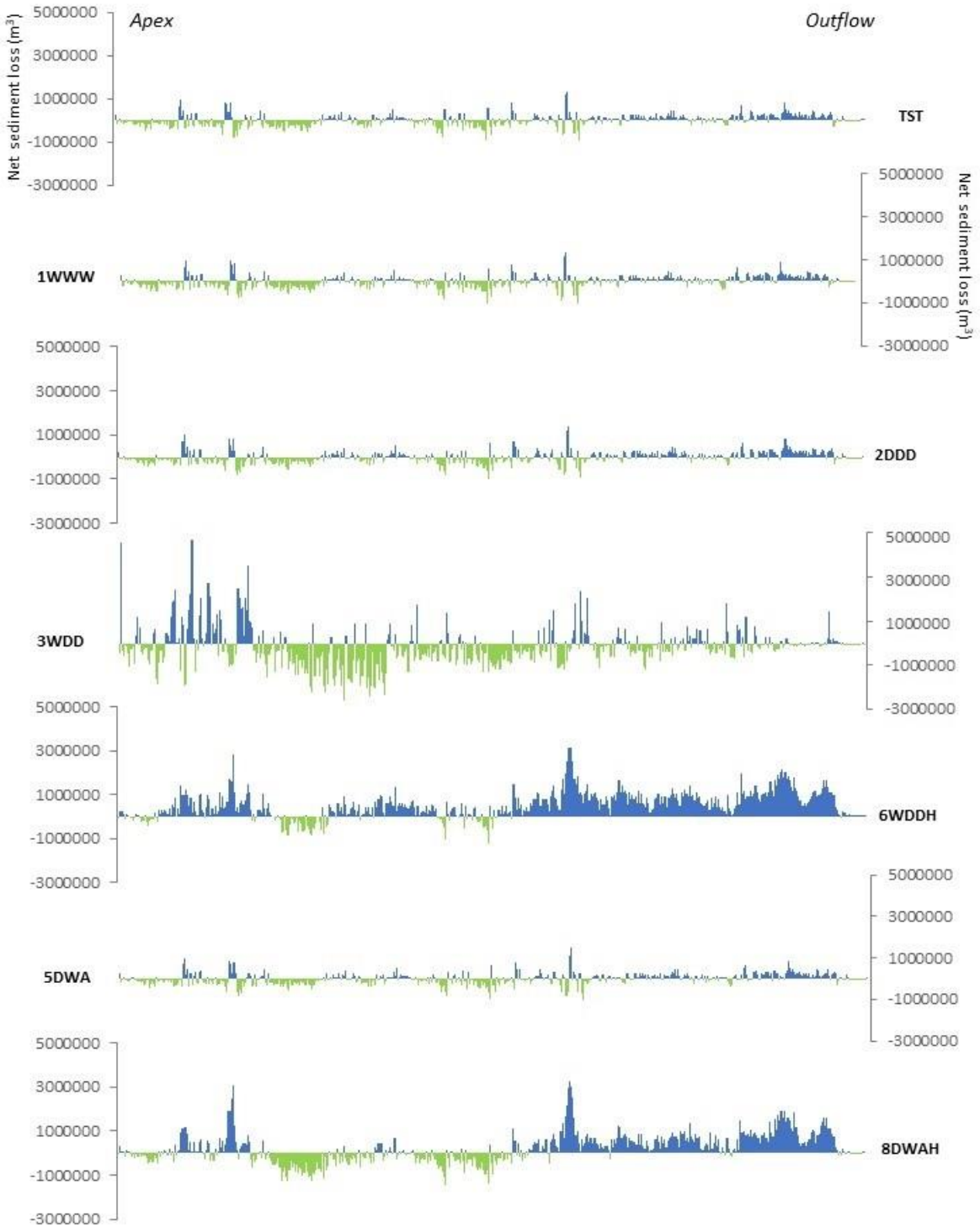

Figure 6.4 Net sediment loss at 30 years for scenarios TST, 1WWW, 2DDD, 3WDD, 6WDDH, 5DWA and 8DWAH; Devi catchment. Blue indicates net sediment loss and green indicates net sediment gain. The x-axis in figure A

corresponds to distance from the catchment apex (left) to the catchment outflow (right).

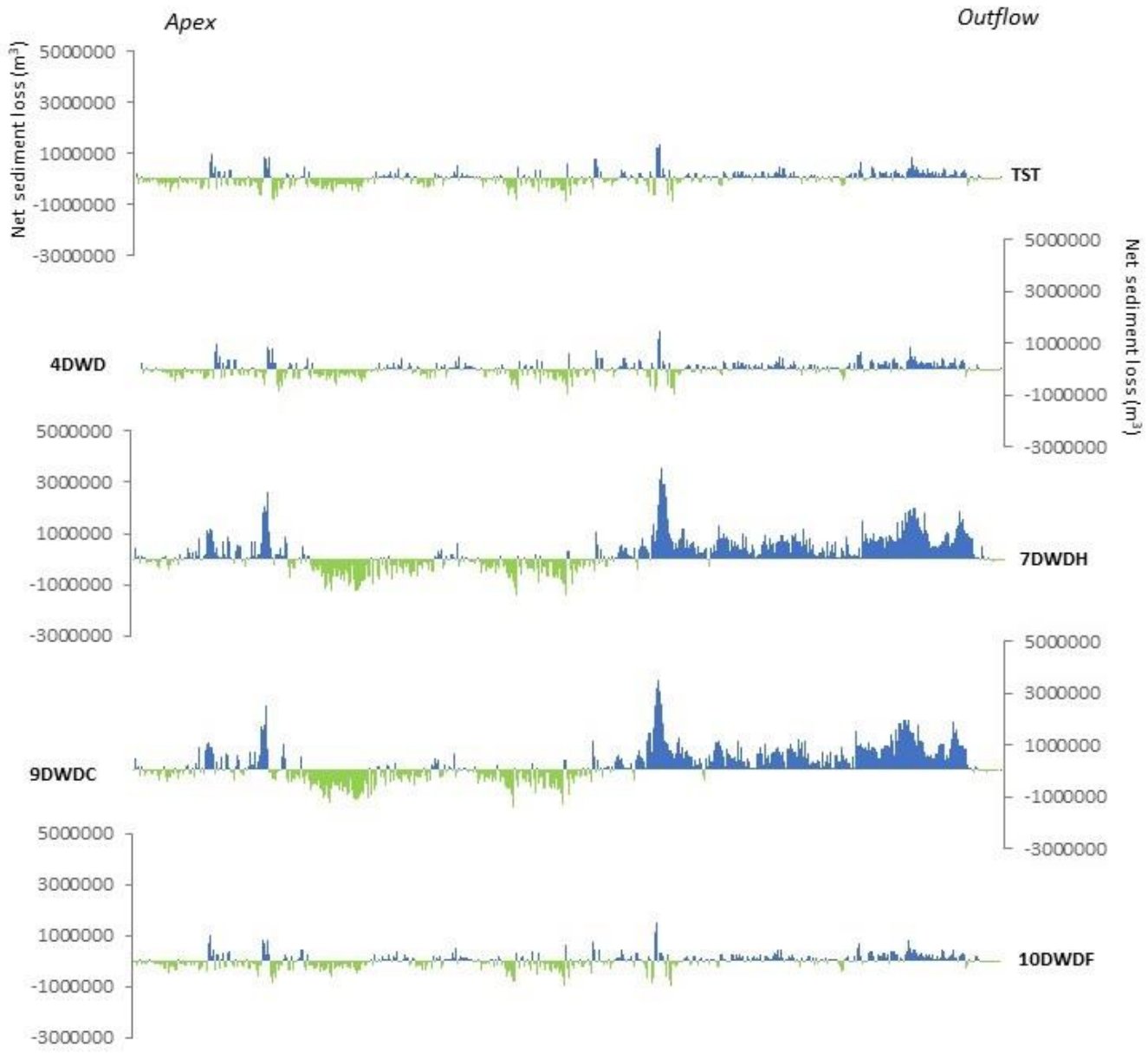

Figure 6.5 Net sediment loss at 30 years for scenarios TST, 4DWD, 7DWDH, 9DWDC and 10DWDF; Devi catchment. Scenario TST (baseline) is shown for reference. Blue indicates net sediment loss and green indicates net sediment gain. The x-axis in figure A corresponds to distance from the catchment apex (left) to the catchment outflow (right).

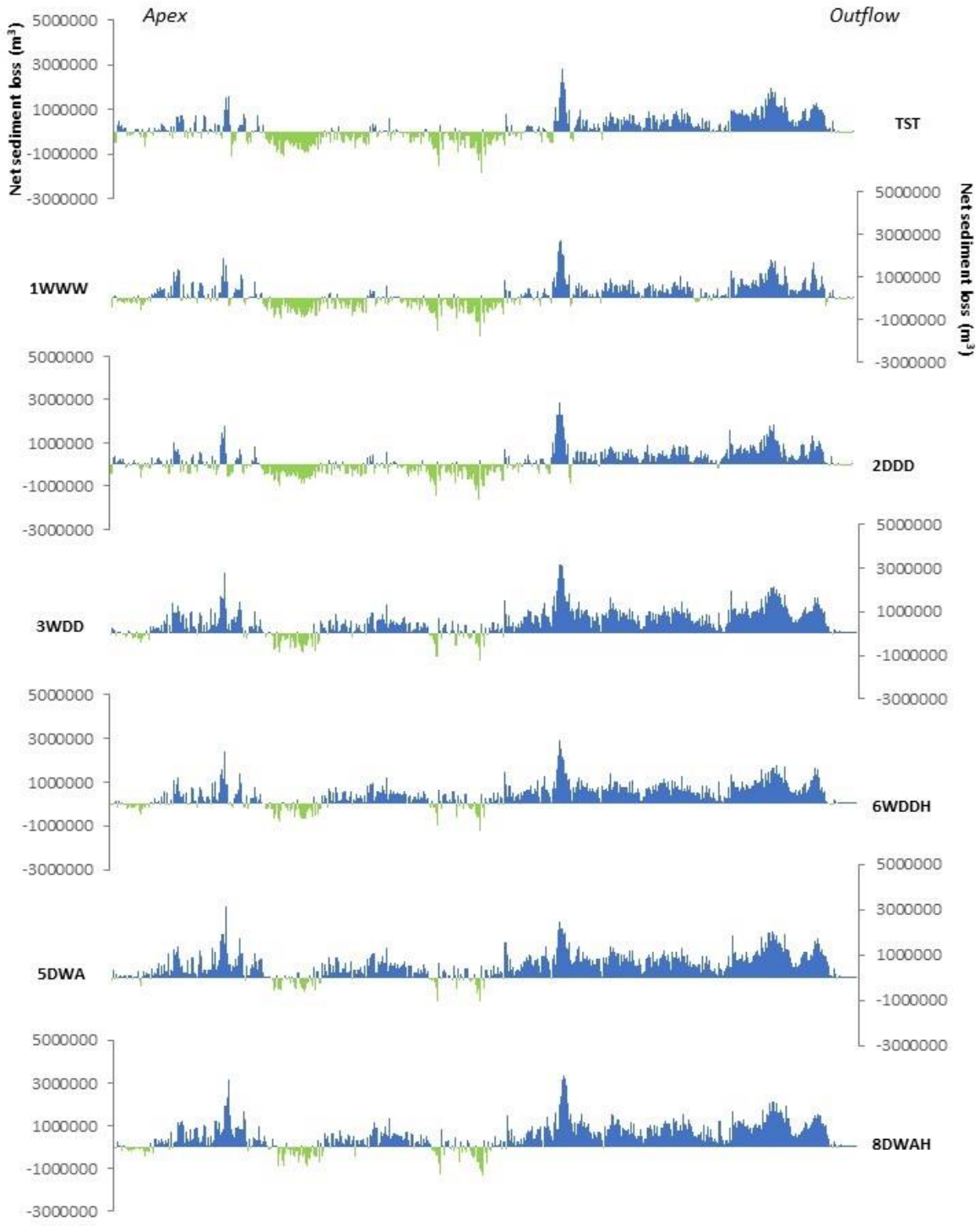

Figure 6.6 Net sediment loss at 50 years for scenarios TST, 1WWW, 2DDD, 3WDD, 6WDDH, 5DWA and 8DWAH; Devi catchment. Blue indicates net sediment loss and green indicates net sediment gain. The x-axis in figure A corresponds to distance from the catchment apex (left) to the catchment outflow (right).

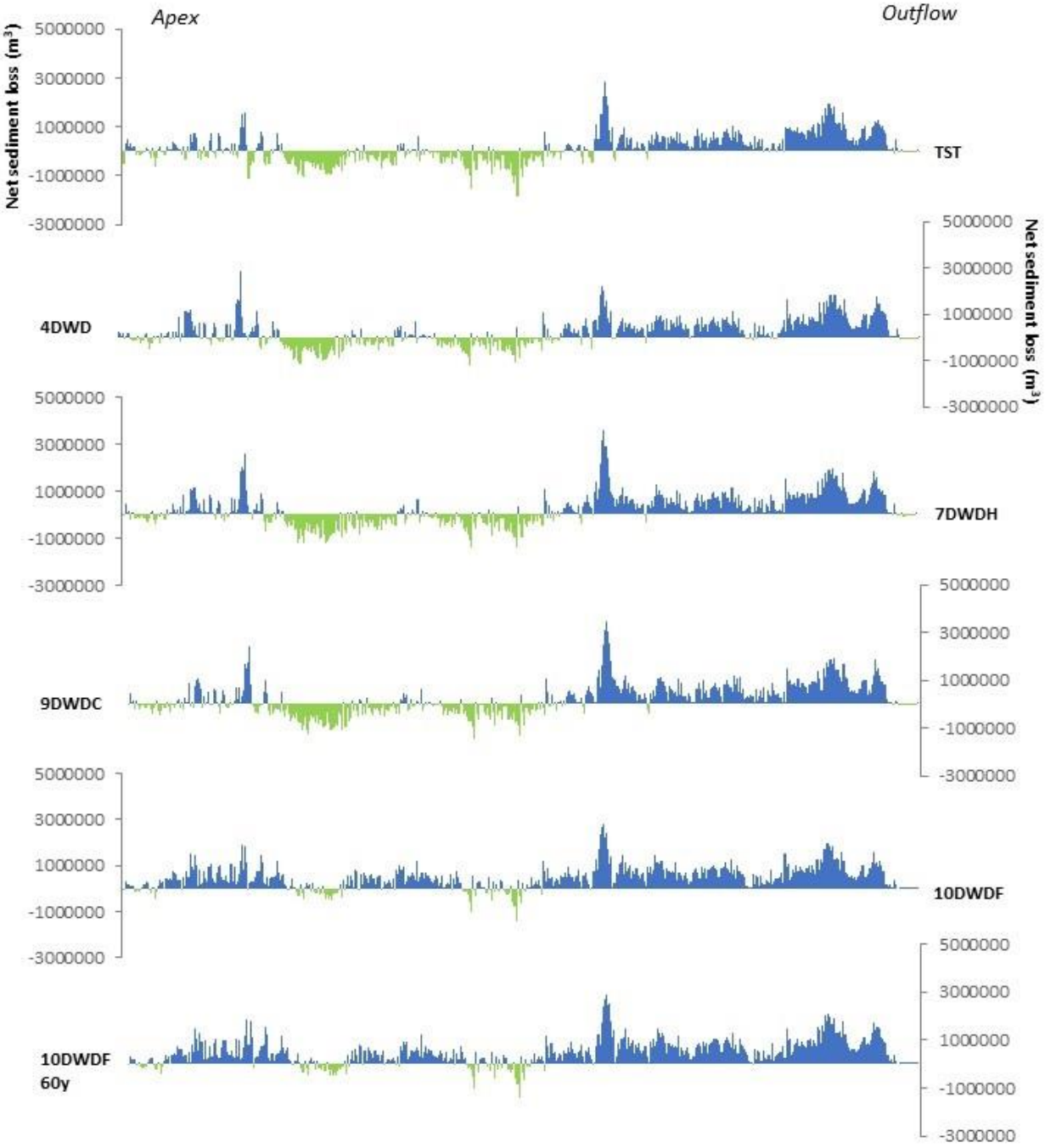

Figure 6.7 Net sediment loss at 50 years for scenarios TST, 4DWD, 7DWDH, 9DWDC and 10DWDF; Devi catchment. Net sediment loss at 60 years is also shown for scenario 10DWDF. Scenario TST (baseline) is shown for reference. Blue indicates net sediment loss and green indicates net sediment gain. The x-axis in figure A corresponds to distance from the catchment apex (left) to the catchment outflow (right).

Table 6.1 Net sediment change, Devi catchment (Blue indicates increase; red indicates decrease)

Scenario	Net sediment change (m^3)		
	30 years	50 years	60 years (10DWDF only)
TST	9.03E+06	-6.60E+07	-
1WWW	1.36E+07	-6.89E+07	-
2DDD	1.14E+07	-6.77E+07	-
3WDD	-1.05E+08	-2.66E+08	-
4DWD	9.86E+06	-6.50E+07	-
5DWA	-1.04E+08	-2.75E+08	-
6WDDH	-1.13E+08	-2.20E+08	-
7DWDH	-1.10E+08	-2.51E+08	-
8DWAH	-1.10E+08	-2.67E+08	-
9DWDC	-1.09E+08	-2.68E+08	-
10DWDF	9.86E+06	-2.43E+08	-2.46E+08

The spatial pattern of elevation change and net sediment loss under scenario TST observed in figures 6.1 – 6.3 demonstrates a remarkably close resemblance with that of scenarios 1WWW, 2DDD, 4DWD and 10DWDF (Figures C.1 C.3; C.4 – C.6; C.10 – C.12 and C.28 – C.31, respectively). This is reflected in figures 6.4 - 6.7. At 30 years into the simulation, areas of net sediment loss and gain are spread relatively evenly across the catchment from apex to mouth; although there is a more pronounced gain in the upper reaches and more pronounced loss in the lower reaches. In contrast to all other scenarios, overall there is a net gain of sediment within the catchment across these five scenarios (table 6.1). The greatest gain is observed under scenario 1WWW (1.36E+07 m^3); the scenario that explores the impact of increased precipitation throughout all seasons. Net sediment gain is equal under scenarios 4DWD and 10DWDF, which is to be expected given that mechanistic drivers for each are set to equal values at this stage in the simulation. Maximum accretion for all of these scenarios is 23 m at 30 years; although this occurs over very few cells where levee development has taken place over areas that were previously channels. Given that levee heights are typically up to 15 m and channel depths typically up to 10 m, this significant difference is not implausible. Maximum erosion at 30 years varies between 9 and 10 m for these scenarios.

By 50 years into the simulation, there is a substantial net loss of sediment across the catchment under these five scenarios (table 6.1). For scenarios TST, 1WWW, 2DDD and 4DWD this loss varies between 6.89E+07 m^3 and 6.50E+07 m^3. Sediment loss under scenario 10DWDF is far greater, at 2.43E+08 m^3. A very distinctive pattern emerges for these scenarios whereby sediment gain is primarily observed in the middle reaches of the catchment (as also shown in figures C.1 C.3; C.4 – C.6; C.10 – C.12 and C.28 – C.31). Sediment accumulates on the floodplain west of the main river channel; and in areas of levee development in the centre of the catchment where the main channel bifurcates before merging again further downstream. Maximum accretion for these scenarios remains at 23 m; although maximum erosion increases to 10 m for 1WWW and 2DDD, and to 11 m for scenario 10DWDF. Sediment loss in the lower reaches of the catchment is high, primarily due to substantial scouring and widening of the main river channel. As shown in figure 6.7, there is very little change in spatial patterns of sediment loss and elevation change at 60 years for scenario 10DWDF. However as shown in figure C.30, there is no further scouring or widening across much of the main river channel. In fact,

levee formation occurs near to the mouth of the catchment in the region where net sediment loss had previously been highest. This results in the higher value of maximum accretion of 26 m observed in figure C.30; compared to 20 m for all other scenarios run to 50 years.

As shown in figures 6.4 – 6.7, net sediment loss for scenarios 3WDD, 5DWA, 6WDDH, 7DWDH, 8DWAH and 9DWDC also follow a very similar spatial pattern. At 30 years into the simulation, net sediment loss is observed throughout the catchment for these scenarios; in contrast to the gain observed for the five scenarios discussed previously (table 6.1). The greatest loss is experienced under scenario 6WDDH at 1.13E+08 m^3. Indeed, a pattern emerges that is very similar to that observed at 50 years for the other scenarios, with substantial loss in the lower reaches of the catchment. The only exception to this is for scenario 5DWA; under which enhanced drought conditions are experienced during the dry season. For this scenario, a similar spatial pattern of change is observed however the total loss is much lower, at 1.04E+08 m^3. Scenarios 6WDDH and 8DWAH explore high sea-level variations of scenarios 3WDD and 5DWA, respectively. It would therefore be expected for these to follow a similar pattern, particularly in the earlier stages of the simulation period. However the same cannot be said for scenarios 7DWDH and 9DWDC, which explore the impacts of higher rates of sea-level rise and increased cyclone frequency on scenario 4DWD, and yet show a very different pattern of change to that observed in 4DWD. Maximum accretion for all of these scenarios is just 16 m at 30 years, compared to 23 m for the five other scenarios discussed previously.

At 50 years into the simulation, scenarios 3WDD, 5DWA, 6WDDH, 7DWDH, 8DWAH and 9DWDC continue to demonstrate remarkably similar patterns of sediment loss and elevation change; with net loss occurring under all scenarios and ranging between 2.20E+08 m^3 and 2.75E+08 m^3 (table 6.1). As shown in figures 6.4-6.7, the spatial distribution of areas of loss and gain remains similar to that of the other five scenarios, with distinctive areas of sediment gain in the middle reaches where the main channel bifurcates; and sediment loss occurring primarily in the lower reaches where these channels merge. The amount of loss however is more pronounced for these scenarios and is instead more similar to that observed under scenario 10DWDF. As shown by the maps in figures C.8, C.14, C.17, C.23 and C.26,

the reason for this is likely the minor but widespread erosion of ephemeral channels across much of the floodplain. Maximum accretion for these scenarios does however reach the value of 23 m, matching those runs discussed previously.

6.1.1.2 Morphological Response Units (MRUs)

The floodplain MRUs identified in figures 6.8 – 6.11 reinforce the patterns observed in the analysis of sediment loss and elevation change. Once again there is a distinctive resemblance in the spatial distribution of features at 30 years for scenarios TST, 1WWW, 2DDD, 4DWD and 10DWDF; and similarly for scenarios 3WDD, 6WDDH, 7DWDH, 8DWA and 9DWDC. In particular, there is more widespread development of floodplain channels in the latter group of scenarios; which would support the hypothesis that the enhanced rates of net sediment loss seen under these scenarios is likely due to the relatively minor but widespread erosion across the floodplain. Floodplain channels become even more extensive by year 50 of the simulation across all scenarios; and at 60 years under scenario 10DWDF. Scenarios where the rate of sea-level rise is higher have a greater extent of active floodplain channels.

Crevasse splay formation occurs in the upper reach of the catchment under all scenarios; although the frequency and distribution of these features varies. Crevasse splays commonly form between 5 and 20 km downstream of the apex. Approximately 55km downstream a large crevasse splay forms under scenarios 3WDD, 5DWA, 6WDDH, 7DWDH, 8DWAH and 9DWDC at 30 years. A splay at the same location is formed in scenarios 2DDD, 4DWD and 10DWDF by 50 years into the simulation. No splay is formed in this location however in scenarios TST or 1WWW.

Widespread levee formation along the main channel is observed in the upper and middle reaches of the catchment across all scenarios. This reflects the areas of substantial accretion seen in previous net sediment analysis. Major levee development in the lower catchment is only observed under scenarios TST, 1WWW, 2DDD, 4DWD and 10DWDF; with only very minor and fragmented areas of levee development seen under all remaining scenarios, with the exception of 3WDD. The image shown in figure 6.13 shows an example area of levee formation for scenario TST that is of typical morphology to the development seen across all other scenarios. At 30 years 78.3% of levees measure between 1 and 5 m in height; increasing to 87.6% at 50 years. The proportion of levees measuring between 10

and 15 m however decreases over this period; from 8.1% to 4.4%. This is not due to the erosion of existing stable levee formations, but rather due to the more extensive development of minor levees (< 5 m) across the delta plain.

Figure 6.8 Floodplain morphological responses units (MRUs) for scenarios TST, 1WWW and 2DDD; Devi catchment.

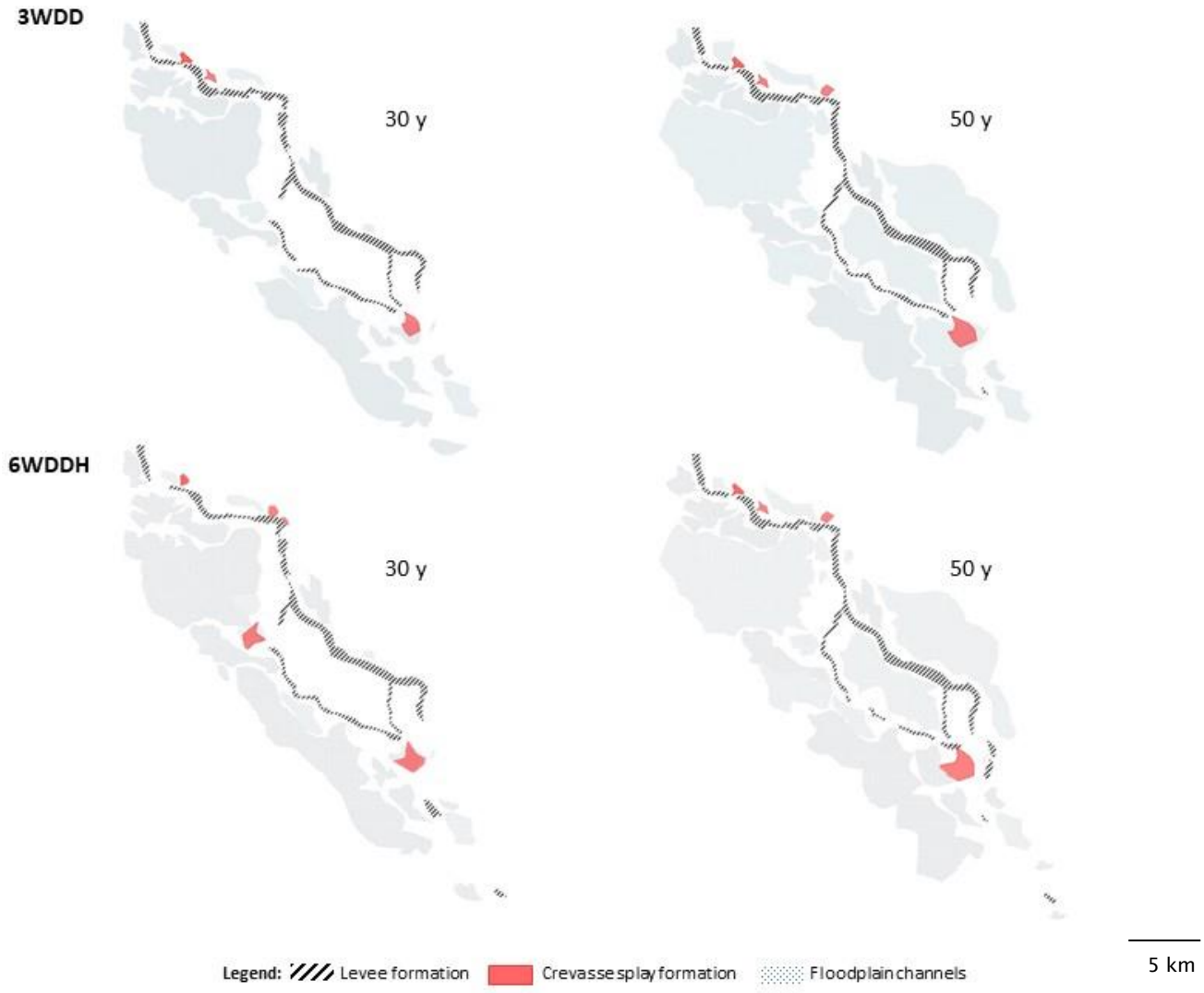

Figure 6.9 Floodplain morphological responses units (MRUs) for scenarios 3WDD and 6WDDH Scenario 6 shows a high sea-level variation of scenario 3.

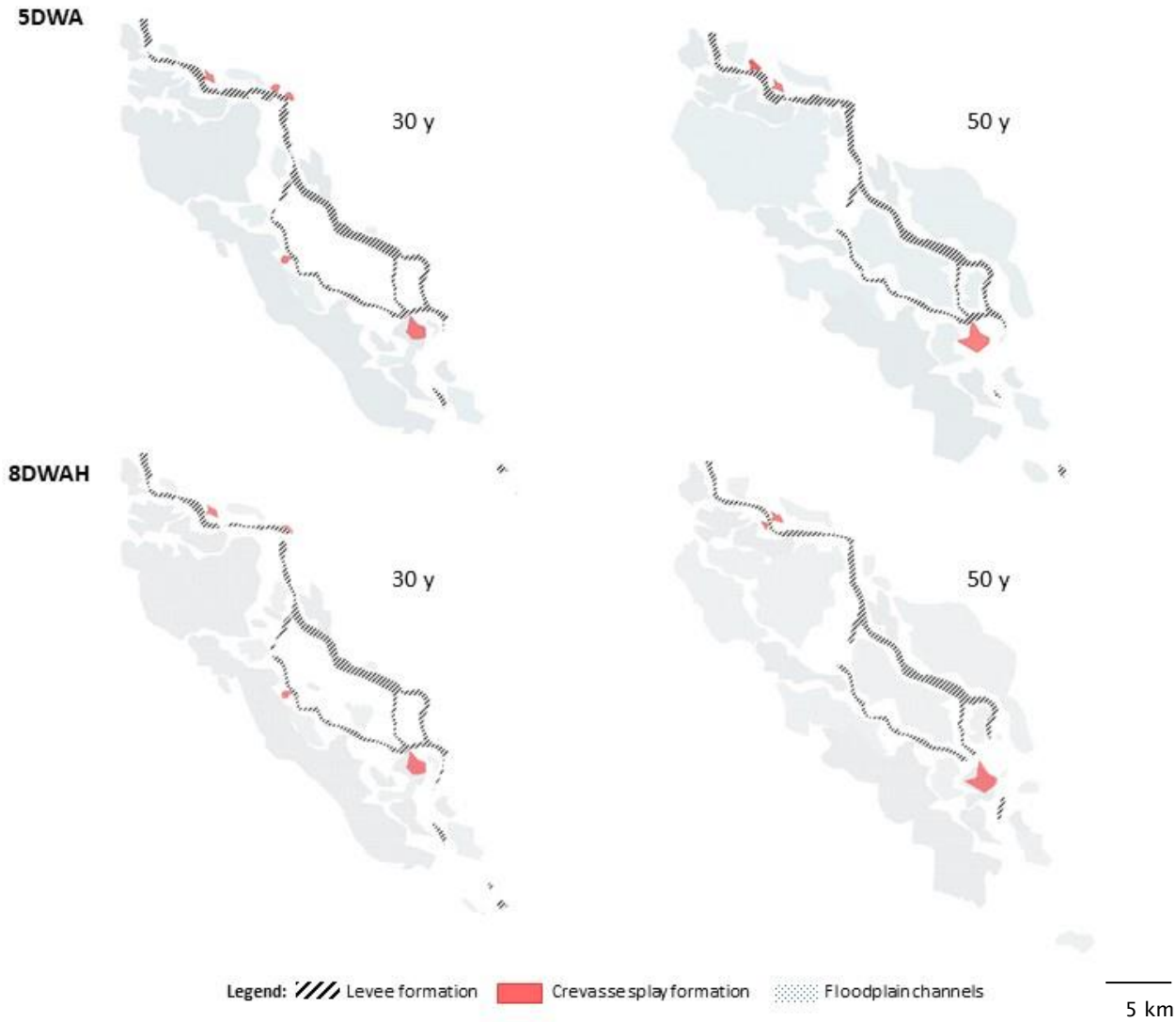

Figure 6.10 Floodplain morphological responses units (MRUs) for scenarios 5DWA and 8DWAH; Devi catchment. Scenario 8 shows a high sea-level variation of scenario 5.

Figure 6.11 Floodplain morphological responses units (MRUs) for scenarios 4DWD, 7DWDH and 9DWDC; Devi catchment. Scenarios 7 and 9 show variations of scenario 4.

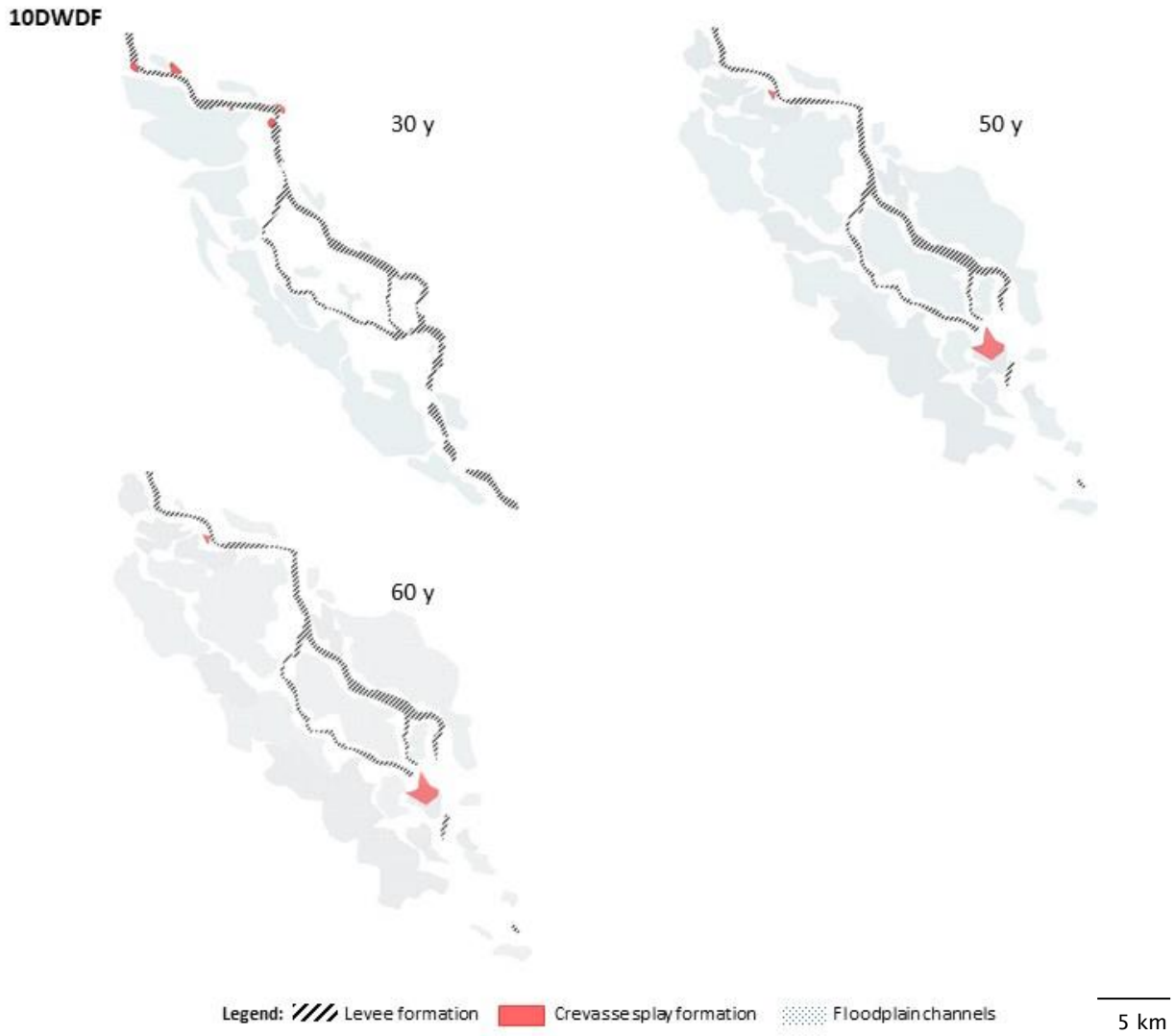

Figure 6.12 Floodplain morphological responses units (MRUs) for scenario 10DWDF; Devi catchment.

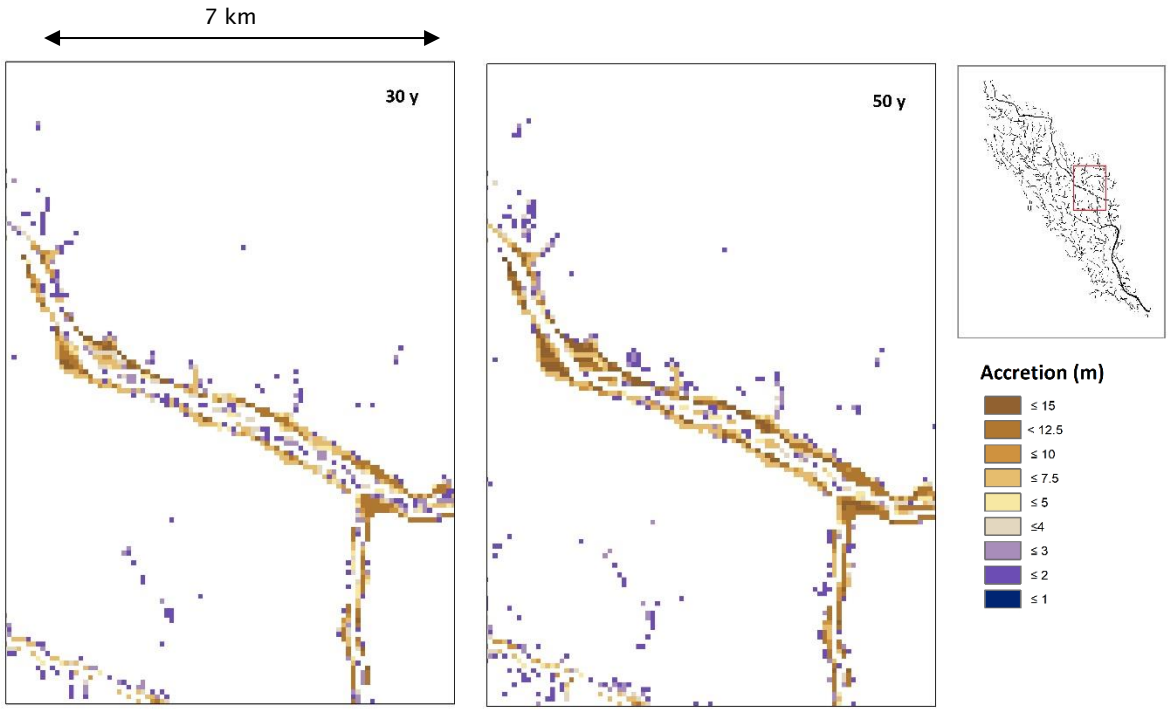

Figure 6.13 Example of levee formation under scenario TST; Devi catchment.

Figures 6.14 – 6.19 show channel MRUs for the Devi catchment; whereby each grid represents an area of 5 x 5 grid cells in the model (where each grid cell measures 90 m^2). As might be expected given prior analysis, by 50 years into the simulation there is a notable spatial resemblance between the identified features under all 11 scenarios. At 30 years however more distinct patterns can be observed between the different model runs. Most notably lateral erosion is far more extensive in all scenarios where the rate of sea-level rise is high, predominantly in the lower catchment. The mean occurrence count of lateral erosion MRUs is 81.33 for those scenarios where sea-level rise is high, compared to just 24.50 for those where it is moderate or low. There is an increase in the area affected by lateral erosion of 20.3% between scenarios 3WDD and 6WDDH; 1500% between scenarios 4DWD and 7DWDH; and 200% between scenarios 5DWA and 8DWAH. By 50 years into the simulation, this difference is no longer evident. A high amount of lateral erosion is also observed at 30 years for scenario 9DWDC; whereby there is a 1420% increase in the affected area compared to scenario 4DWD. Lateral erosion inhibits levee formation for these scenarios as discussed previously. At 30 years into the simulation, scenario 2DDD has the least area effected by lateral erosion (just one grid) whilst 8DWAH is the greatest (87 grids). Until now the analysis of scenarios 1WWW and 2DDD has shown remarkably similar patterns of results, despite the

stark contrast between the mechanistic drivers in the two model runs (1WWW explores increasingly wet climatic conditions whilst 2DDD explores increasingly dry). Here however distinct differences in the morphological response begin to emerge: At 30 years the number of grid cells impacted by lateral erosion is 83.3% less in scenario 2DDD compared to the baseline TST; compared to 66.7% for scenario 1WWW. By 50 years the number reduces to 7.7% for 2DDD, and 5.1% for 1WWW.

Channel incision was evident throughout the main channel for all scenarios at 30 and 50 years; and at 60 years for scenario 10DWDF. Maximum channel incision varies between 9 and 10 m at 30 years; and 10 and 11 m at 50 and 60 years. The rate of incision was therefore much greater in the early stages of the simulation period. As is discussed later in section 6.2, it is likely that this is limited by the bedrock parameter; a layer beyond which erosion and slope processes cannot occur. As a result of this lateral erosion becomes a far more dominant feature in the latter part of the simulation period, particularly in the lower reaches of the delta plain.

The number of mid-channel bar MRUs at 30 years ranged between 22 for scenarios 5DWA and 8DWAH, and 30 for scenario 4DWD; with a mean value of 26.0. At 50 years into the simulation period, this number ranged between 23 for scenario 7DWDH, and 35 for scenario 2DDD; with a mean value of 26.8. Scenarios TST, 4DWD, 7DWDH, 9DWDC and 10DWDF all saw a reduction in mid-channel bar formation between 30 and 50 years. All other scenarios, with the exception of 1WWW, saw an increase. Between 50 and 60 years for scenario 10DWDF however, the number of grids with mid-channel bars increased again to 29; 1 higher than the initial 30 year total. Once again a distinct difference appears between the contrasting scenarios 1WWW and 2DDD: the former sees an increase in mid-channel bar formation of 3.9% and 12.5% at 30 and 50 years, respectively, when compared to baseline run TST. For scenario 2DDD, these values are considerably higher at 15.4% and 45.8%. The rate of sea-level rise appears to play a less significant role than it did over lateral erosion: The mean occurrence count of mid-channel bar MRUs at 30 years is 23.3 for those scenarios where sea-level rise is high, compared to 27.0 for those where it is moderate or low. At 50 years these figures are 26.0% and 27.1, respectively. The spatial distribution of mid-channel bar MRUs remains

fairly consistent across all scenarios, with the most significant development often occurring in the middle reaches at the point of channel bifurcation. However, as will be discussed in section 6.1.1.4, there is substantial variability in the distribution of island sizes across the delta plain as a whole.

The number of point bar MRUs at 30 years ranged between 6 for scenarios 6WDDH and 10DWDF, and 16 for scenarios TST and 3WDD; with a mean value of 10.6. At 50 years into the simulation period, this number ranged between 1 for scenarios 5DWA and 6WDDH, and 13 for scenario 9DWDC; with a mean value of 7.4. Scenarios TST, 1WWW 4DWD, 5DWA, 6WDDH and 8DWAH all saw a reduction in mid-channel bar formation between 30 and 50 years. 2DDD and 7DWDH saw no change, whilst 9DWDC and 10DWDF saw an increase. Between 50 and 60 years for scenario 10DWDF however, the number of grids with mid-channel bars decreased to 4; 2 lower than the initial 30 year total. A stark contrast remains between scenarios 1WWW and 2DDD: the former sees a decrease in point bar formation of 6.3% and 14.3% at 30 and 50 years, respectively, when compared to baseline run TST. For scenario 2DDD, this reduction is considerably higher at 25.0% and 71.4%. The mean occurrence count of mid-channel bar MRUs is 7.3 at 30 years for those scenarios where sea-level rise is high, compared to 11.8 for those where it is moderate or low. At 50 years these figures are 5.3 and 8.1, respectively. An exception to this pattern are scenarios 5DWA and 8DWAH; whereby a higher rate of sea-level rise results in a 700% increase in the number of point bar MRUs by 50 years into the simulation period. The spatial distribution of point bar MRUs is far more variable than that of mid-channel bar MRUs, however there are certain points along the channel where these features emerge under several contrasting scenarios. A large point bar develops between 5 and 10 km upstream of the mouth, for example, at 50 years under scenarios TST, 1WWW, 2DDD, 4DWD, 7DWDH, 8DWA, 9DWDC, 10DWDF.

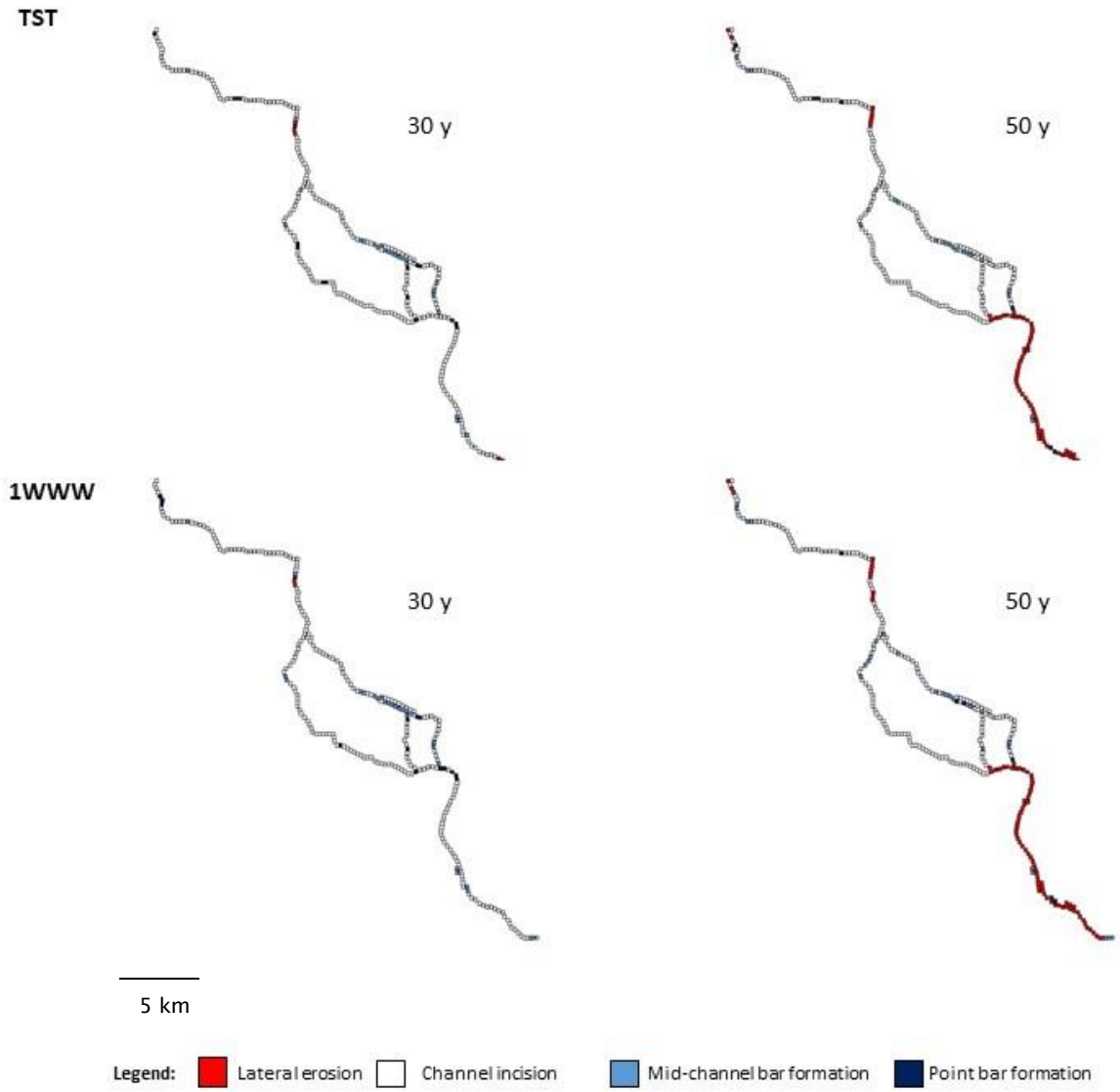

Figure 6.14 Channel morphological responses units (MRUs) for scenarios TST and 1WWW; Devi catchment.

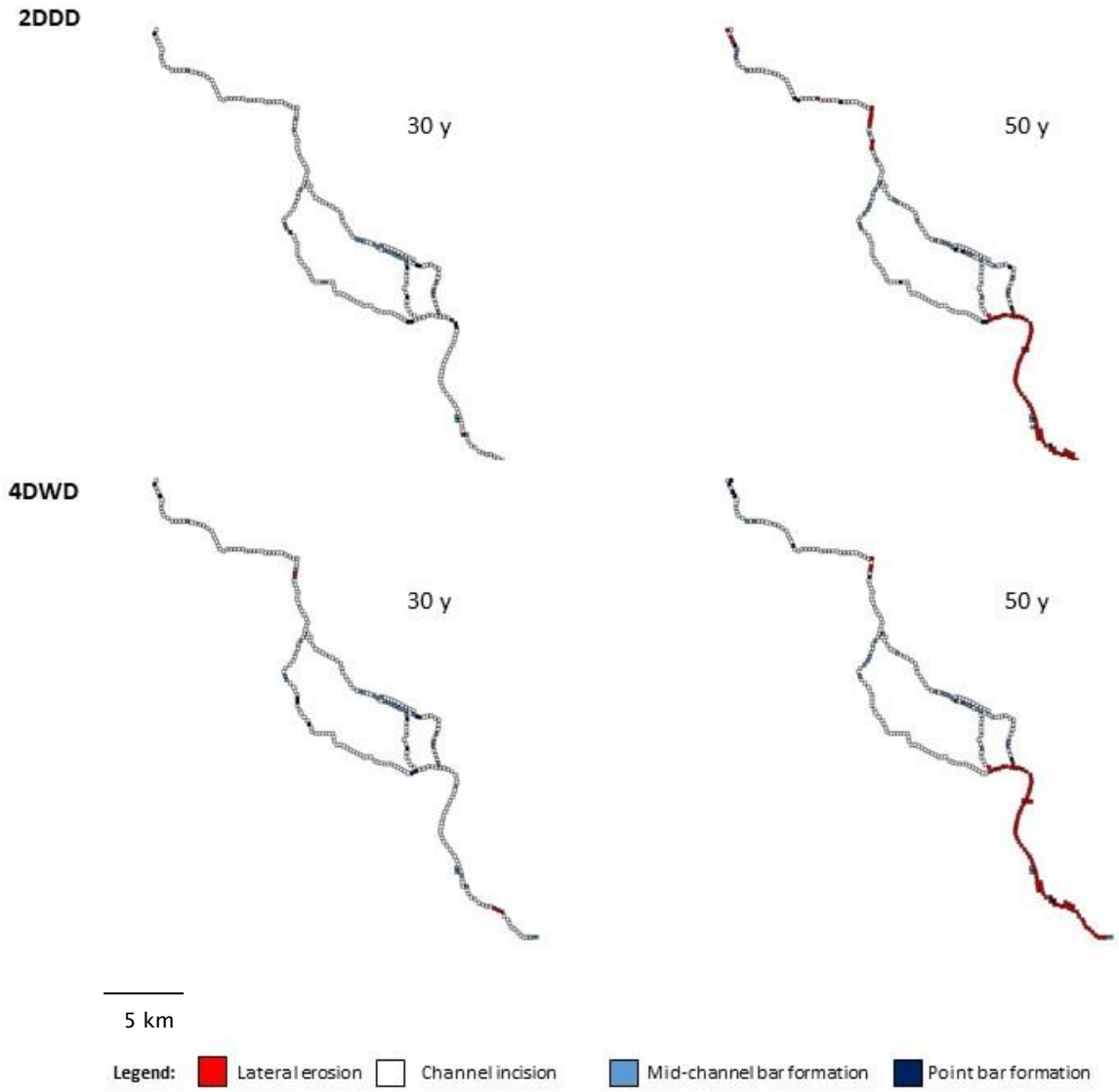

Figure 6.15 Channel morphological responses units (MRUs) for scenarios 2DDD and 4DWD; Devi catchment.

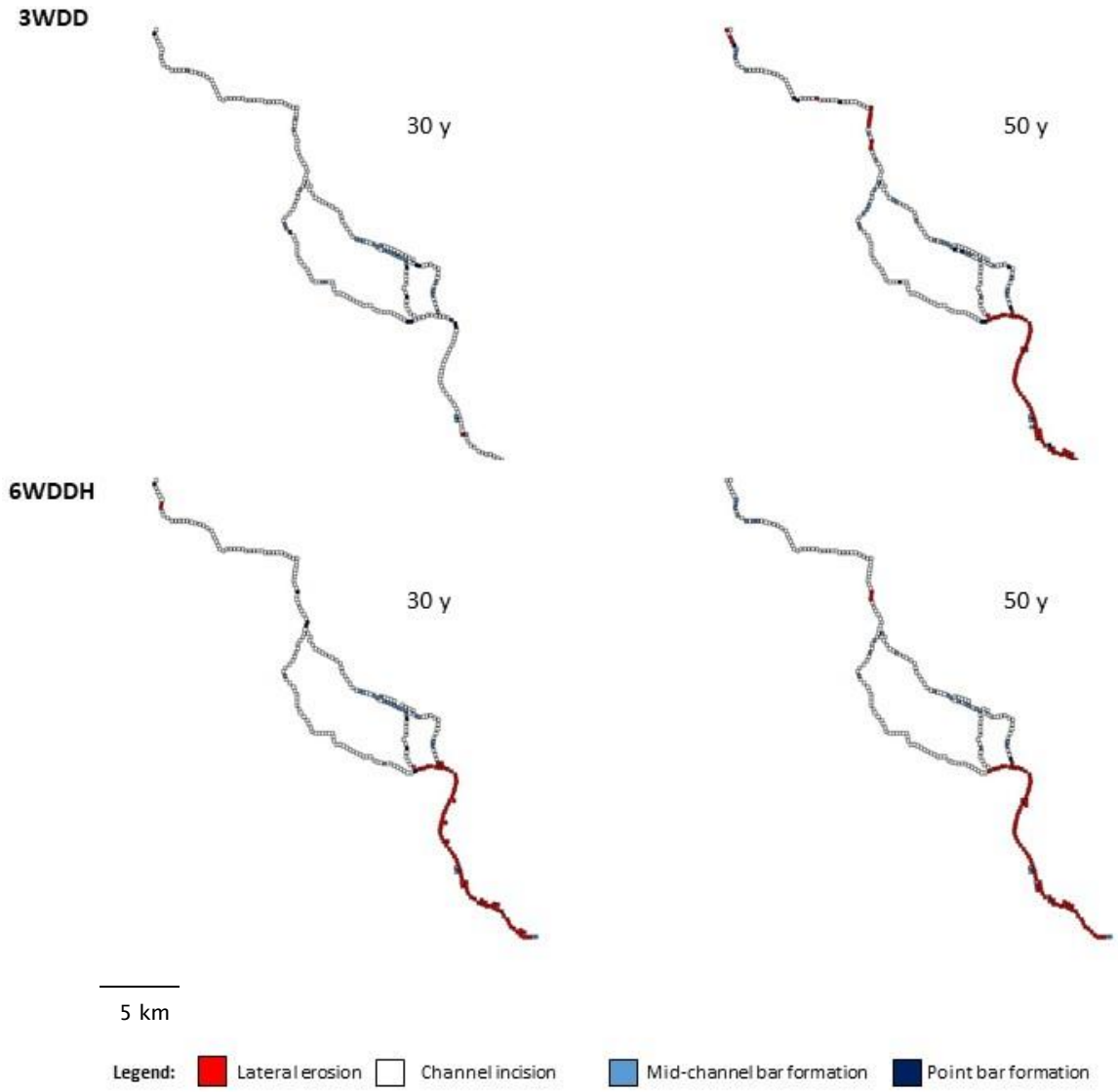

Figure 6.16 Channel morphological responses units (MRUs) for scenarios 3WDD and 6WDDH; Devi catchment. Scenario 6 shows a high sea-level variation of scenario 3.

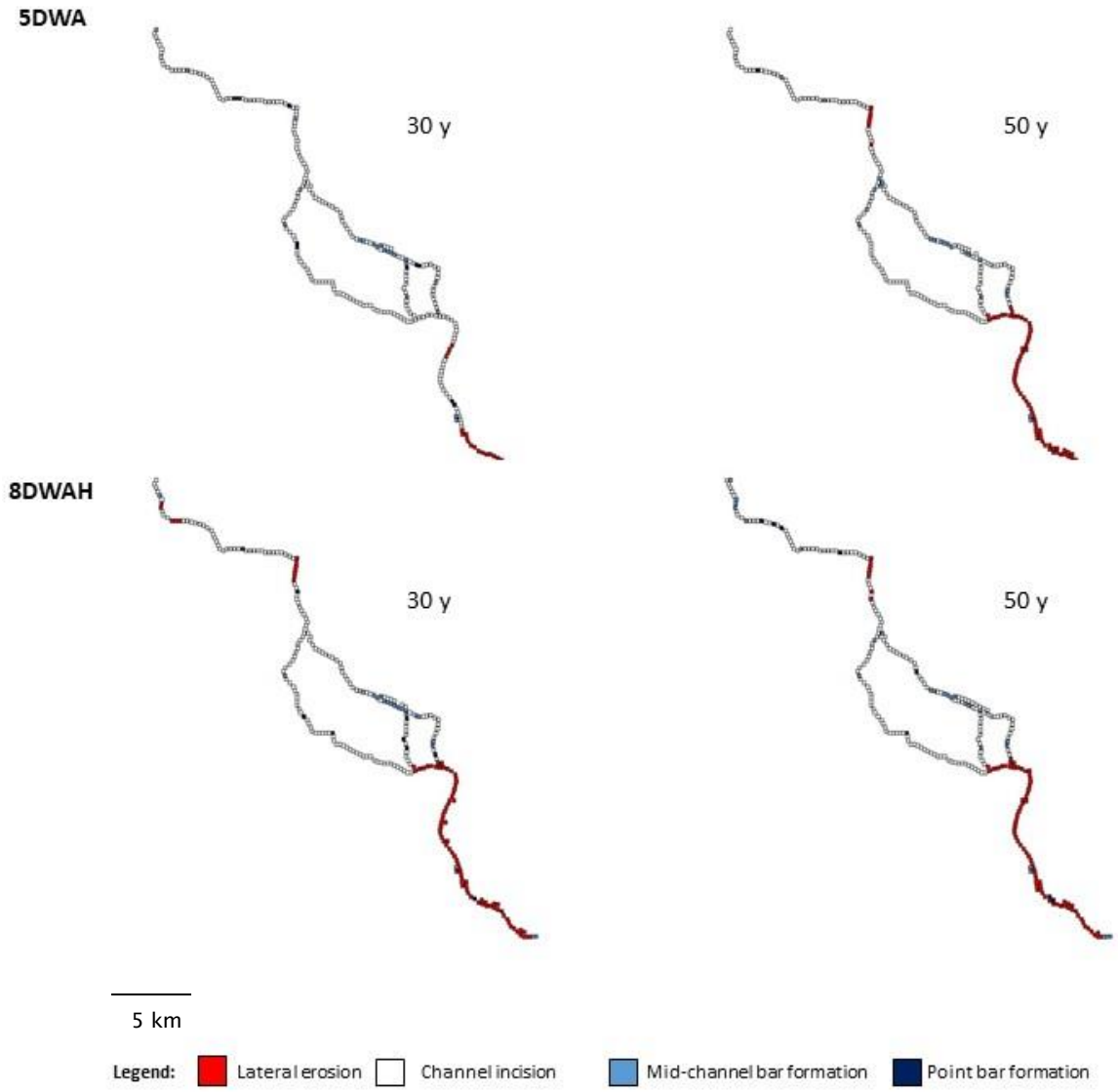

Figure 6.17 Channel morphological responses units (MRUs) for scenarios 5DWA and 8DWAH; Devi catchment. Scenario 8 shows a high sea-level variation of scenario 5.

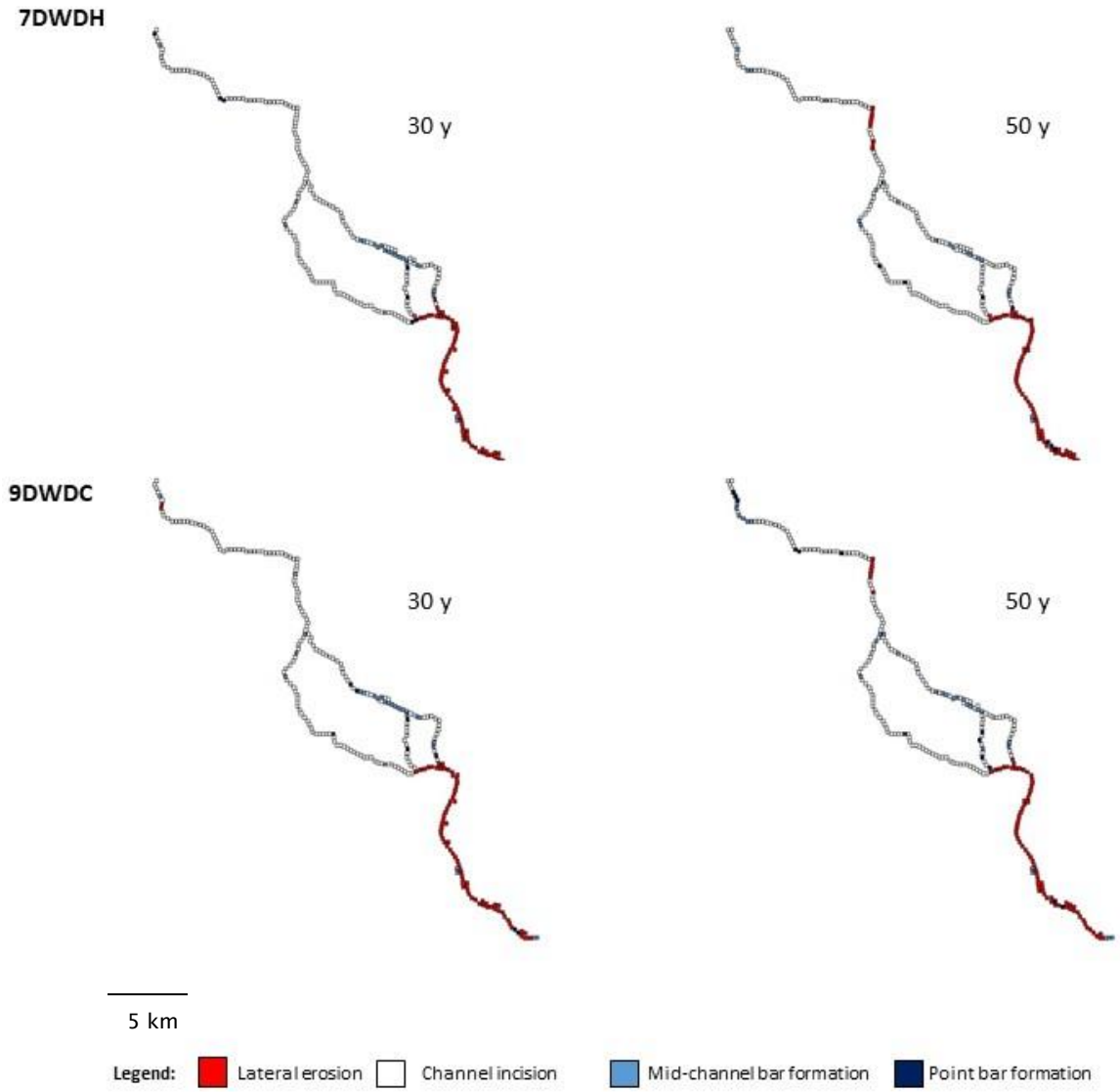

Figure 6.18 Channel morphological responses units (MRUs) for scenarios 7DWDH and 9DWDC; Devi catchment.

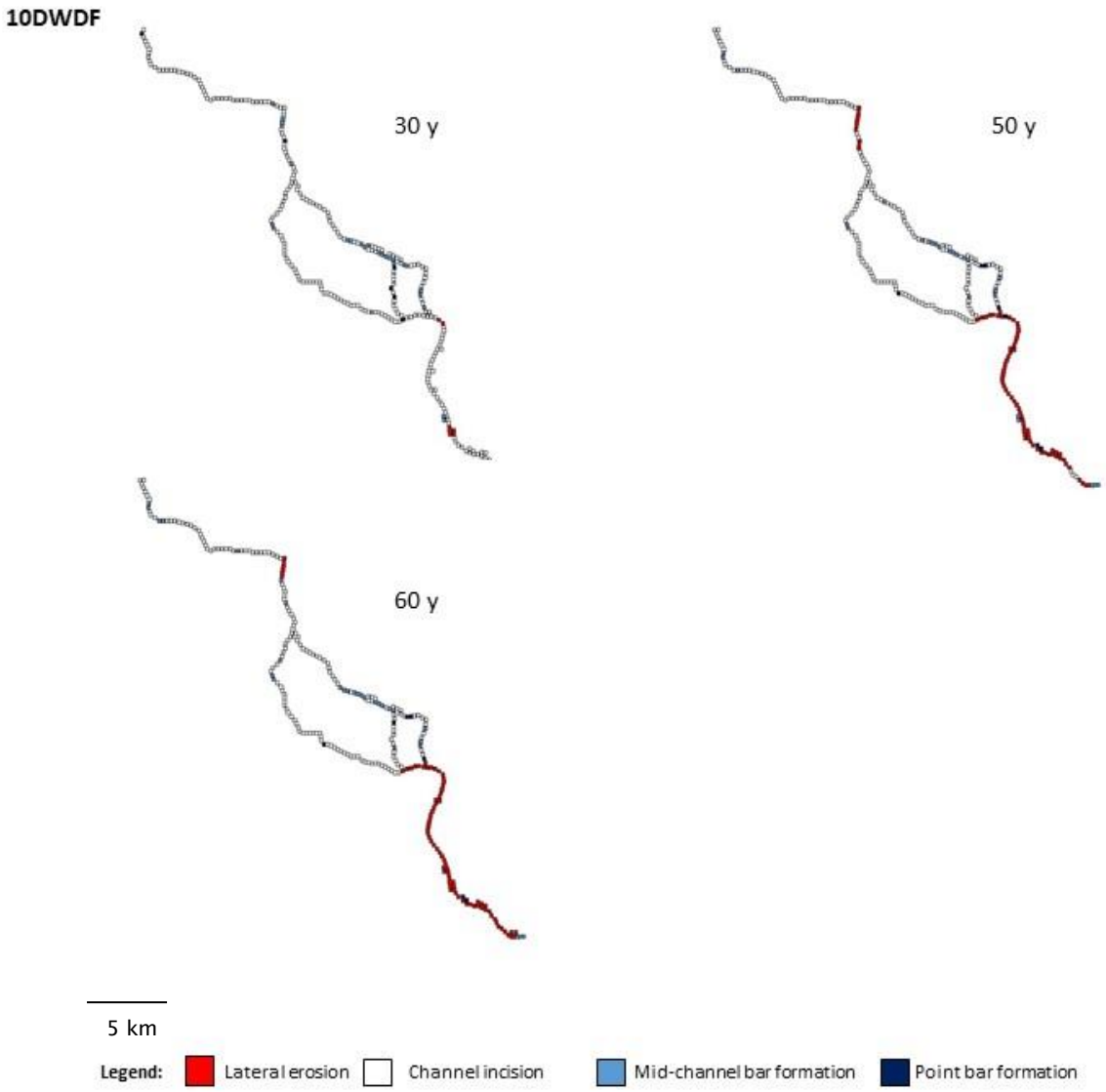

Figure 6.19 Channel morphological responses units (MRUs) for scenario 10DWDF.

6.1.1.3 Fractal dimension

Fractality increased over the initial 30 year simulation period for all scenarios, demonstrated by the fractal box-counting dimension value (D) increasing from 1.46 at 0 years to between 1.50 and 1.55 (table 6.2). Under the TST baseline scenario, D increased by 0.05. At 50 years into the simulation, scenarios TST, 1WWW, 2DDD, 3WDD and 10DWDF continued to increase; whilst scenarios 5DWA, 7DWDH, 8DWAH and 9DWDC showed no change at D = 1.53. Scenarios 4DWD and 6WDDH showed a reduction in channel density with D = 1.53 and 1.52 respectively; although these values still represent an overall increase over the 50 year period compared to the 0 year baseline. As has been apparent in previous analysis, it would seem that the greater variability observed over the initial 30 year period begins to become smoothed as the simulation reaches 50 years: 9 of the eleven scenarios, including the baseline run TST, shared a value of D = 1.53. Overall scenario 1WWW produced the largest increase in channel density (+0.08); suggesting a higher rate of channel bifurcation across the system (Edmonds *et al.,* 2011). As this scenario did not rank highest for the frequency of mid-channel bar MRUs, this might suggest that some of this change is occurring in ephemeral floodplain channels rather than being isolated within the main channel of the Devi itself. This would seem highly possible given the increased frequency of floods that will occur under this scenario. By 60 years for scenario 10DWDF, D reduces from 1.53 to 1.5. It is unclear as to whether this is driven by the failure of the monsoon rains reducing total discharge and thus channel bifurcation potential; or whether this pattern may also be emerging in scenarios 4DWD and 6WDDH.

All values found in this study are slightly higher than those found by Edmonds *et al.* (2011) ($1.24 \leq D \leq 1.30$); but are not outside the expected range for deltas. This could be reflective of the fact that Edmonds *et al.* applied these metrics to the entire delta plain as opposed to individual watersheds. Conversely it could reflect the dominance of channel bifurcation, particularly in the Devi catchment. Seybold *et al.* (2007) found the Lena delta in Russia to have a D value of 1.8, and their simulated delta to have a D value of 1.85.

Table 6.2 Box-counting dimension (D), Devi catchment (Blue indicates increase; red indicates decrease)

Scenario	Box-counting dimension (*D*)			
	0 years	30 years	50 years	60 years (10DWDF only)
TST	1.46	1.51 (+0.05)	1.53 (+0.02)	-
1WWW		1.50 (+0.04)	1.54 (+0.04)	
2DDD		1.50 (+0.04)	1.53 (+0.03)	-
3WDD		1.52 (+0.06)	1.53 (+0.01)	-
4DWD		1.55 (+0.09)	1.53 (-0.02)	-
5DWA		1.53 (+0.07)	1.53	-
6WDDH		1.53 (+0.07)	1.52 (-0.01)	-
7DWDH		1.53 (+0.07)	1.53	-
8DWAH		1.53 (+0.07)	1.53	-
9DWDC		1.53 (+0.07)	1.53	-
10DWDF		1.50 (+0.04)	1.53 (+0.03)	1.5 (-0.03)

6.1.1.4 Distribution of island sizes

Islands are mapped by tracing the edges of land polygons that are completely surrounded by water of 1 metre depth or greater. As in Edmonds *et al.* (2011), no distinction is made between islands formed by deposition within the channel itself, and those formed by channels that carve into existing land. Figure 6.20 shows island size distribution for scenarios TST, 1WWW, 2DDD, 3WDD, 6WDDH, 5DWA and 8DWAH. Figure 6.21 shows island size distribution for run 4DWD alongside three variations of this scenario: 7DWDH, 9DWDC and 10DWDF. These figures show a clear dominance of smaller island sizes across all scenarios, with over half of islands in all model runs measuring ≤1 km^2 at 30 years into the simulation period. At 50 years into the simulation, between 87.8% (2DDD) and 96.5% (9DWDC) of islands measured ≤5 km^2. Large islands measuring ≤100 km^2 only account for between 1.8% (9DWDC) and 7.1% (TST) at 30 years, and between 1.5% (TST) and 7.3% (7DWDH) at 50 years.

This unimodal distribution is similar to that found by Edmonds *et al.* (2011), which would be expected in a morphologically active catchment such as the Devi where bifurcation will be a dominant driver of change. A distinct difference with the study by Edmonds *et al.*, however, is that they defined small islands as those that represent < 3% of total delta area (equivalent to 446 km^2 for the Mahanadi Delta); and large islands as those that represent < 10% (equivalent to 1487.3 km^2). In this study, the largest islands found in the Devi catchment only equal 1.3% of the total delta area. This is primarily due to the fact that by splitting the delta into catchments, large areas of land that may exist between active channels will not be designated as being part of an island area in this study. Nonetheless, a similar unimodal distribution would suggest an emerging pattern that occurs across multiple spatial scales.

Table 6.3 outlines the total number of islands for each scenario as well as the modal, minimum and maximum island size values. All scenarios show an increase in the total number of islands forming within the catchment from the 0 year count of 37. Once again at 30 years into the simulation period there is a distinctive split between two sets of scenarios: For scenarios TST, 1WWW, 2DDD, 4DWD and 10DWDF, the total island count ranges between 42 and 50. For the remaining seven scenarios the total island count is higher, ranging between 55 and 61. By 50 years

into the simulation period, all scenarios with the exception of 5DWA, 6WDDH and 9DWDC show a further increase in island occurrence. The largest number of islands (71) is observed under scenario 3WDD, and the lowest (41) is observed under scenario 6WDDH. This provides an interesting result as, for other scenarios where only the rate of sea-level rise has been increased, this has resulted in a slightly higher number of islands. With the exception of scenario 6WDDH, those scenarios where total monsoon precipitation has remained at a baseline or increased demonstrate a higher island count than for those where it has declined. By 60 years into the simulation period for scenario 10DWDF, the total number of islands decreases to 49.

The modal island size for scenarios TST, 1WWW, 4DWD and 7DWDH remains at 0.36 km^2 by 30 years into the simulation. Minimum island size also decreases for these scenarios, from 0.27 km^2 to 0.18 km^2. For scenarios TST and 4DWD the modal value remains unchanged at 50 years. Modal island size ranges between 0.45 and 0.72 km^2 for all other scenarios at 30 years. By 50 years modal island size increases further for scenarios 1WWW, 2DDD, 6WDDH and 7DWDH. Scenarios 5DWA, 8DWAH, 9DWDC and 10DWDF, conversely, see a decrease. A decrease in minimum island size is also observed for these scenarios at 50 years. At 60 years for scenario 10DWDF however, both modal and minimum island size rise once again to 0.72 km^2 and 0.27 km^2, respectively. Maximum island size increases for all scenarios by 30 years, with values ranging between 151.5 km^2 and 189.6 km^2. This large increase is due to the fact that at the point of measuring islands at 0 years (6 months into the simulation), the large island situated between the bifurcation of the main channel in the mid catchment was not completely filled with water greater than a depth of 1m. At 50 years maximum island size increases further for scenarios 1WWW, 2DDD, 4DWD and 5DWA; ranging between 178.8km^2 and 192.3 km^2. A decrease is observed for all other scenarios, with a notable decrease of 71.6km^2 seen under scenario TST.

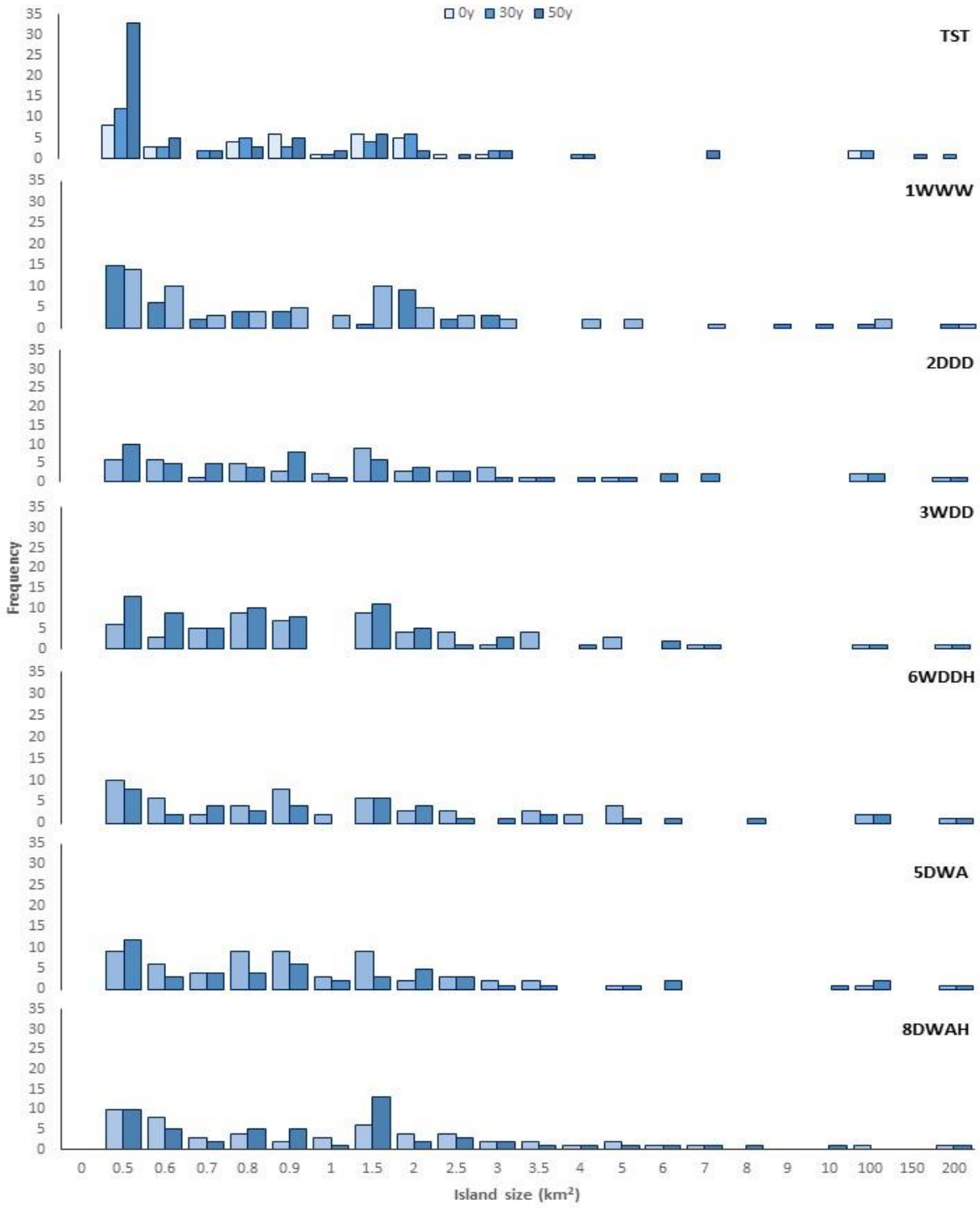

Figure 6.20 Island size distribution for scenarios TST, 1WWW, 2DDD, 3WDD, 6WDDH, 5DWA and 8DWAH; Devi catchment. Scenarios 6 and 8 show variations of scenarios 3 and 5, respectively.

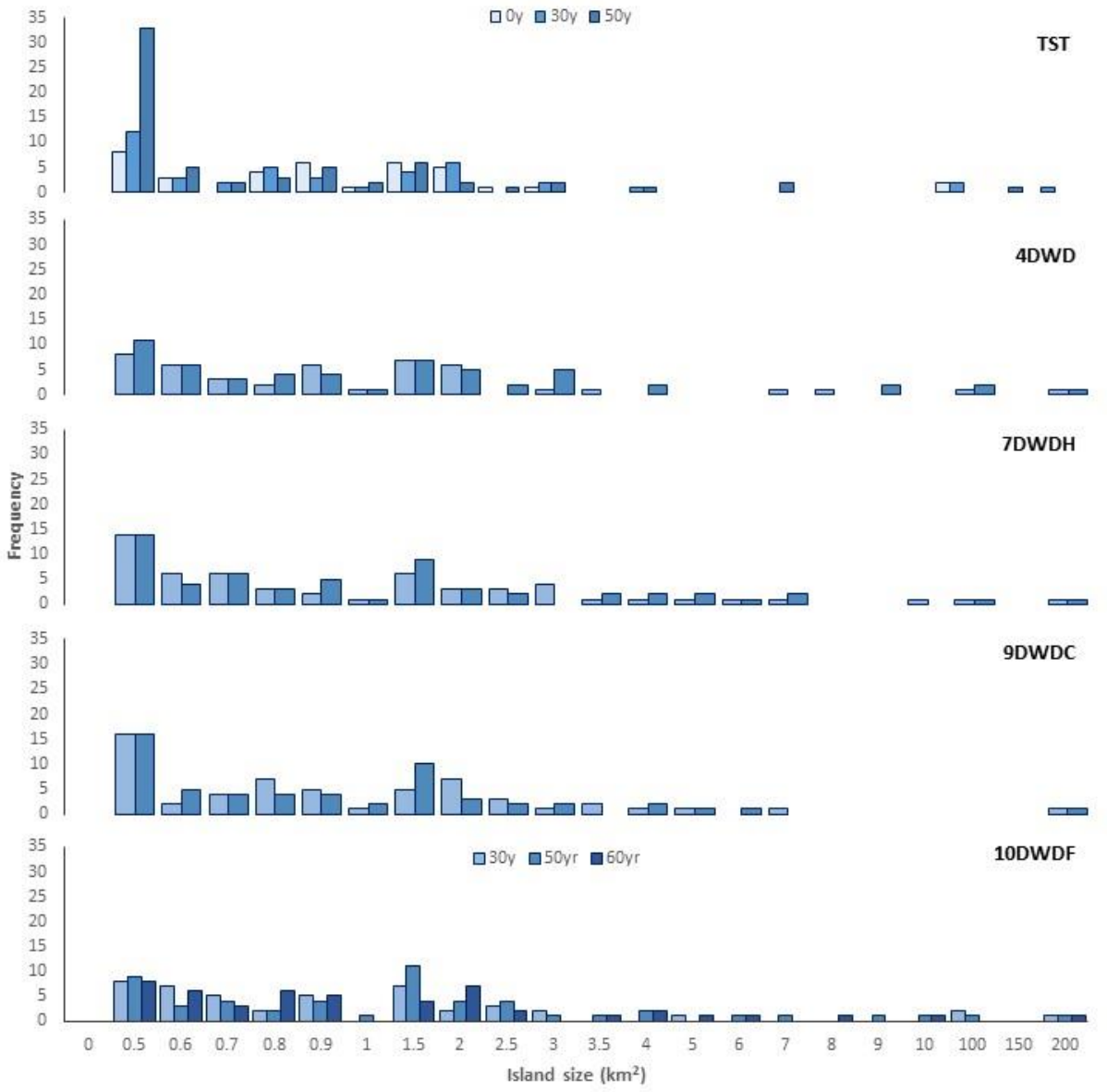

Figure 6.21 Island size distribution for scenarios TST, 4DWD, 7DWDH, 9DWDC and 10DWDF; Devi catchment. Scenarios 7, 9 and 10 all show variations of scenario 4. Scenario TST (baseline) is shown for reference).

Table 6.3 Total number and size of islands, Devi catchment (Blue indicates increase; red indicates decrease)

Scenario	Total number of islands				Modal island size (km²)				Minimum island size (km²)				Maximum island size (km²)			
	0 yr	30 yr	50 yr	60 yr (10 DWDF only)	0 yr	30 yr	50 yr	60 yr (10 DWDF only)	0 yr	30 yr	50 yr	60 yr (10 DWDF only)	0 yr	30 yr	50 yr	60 yr (10 DWDF only)
TST	37	42	65	-	0.36	0.36	0.36	-	0.27	0.18	0.09	-	12.60	175.86	104.31	-
1WWW		50	67	-		0.36	0.54	-		0.18	0.18	-		179.28	184.23	-
2DDD		47	57	-		0.54	0.81	-		0.36	0.18	-		184.50	187.47	-
3WDD		58	71	-		0.72	0.72	-		0.36	0.18	-		176.22	172.89	-
4DWD		45	55	-		0.36	0.36	-		0.18	0.18	-		151.47	178.82	-
5DWA		61	51	-		0.72	0.36	-		0.18	0.09	-		173.88	192.33	-
6WDDH		56	41	-		0.45	0.63	-		0.27	0.27	-		189.63	180.45	-
7DWDH		56	58	-		0.36	0.45	-		0.18	0.27	-		177.75	175.32	-
8DWAH		55	56	-		0.54	0.45	-		0.27	0.18	-		180.27	174.6	-
9DWDC		57	57	-		0.72	0.45	-		0.27	0.18	-		173.07	168.57	-
10DWDF		45	52	49		0.54	0.45	0.72		0.27	0.18	0.27		183.60	176.76	175.05

6.1.1.5 Nearest-edge distance

Figures 6.22 and 6.23 show normalised nearest-edge distance (NED) at 30 years and 50(60) years, respectively. NED is the nearest distance to channelised or unchannelised water from any given point on land. The results show a similar distribution of NED values for all scenarios in the Devi catchment to those found by Edmonds *et al.* (2011); with the exception of a second peak at a value of ~ 0.2. This is likely related to the fact that the present analysis considers only one catchment as opposed to the entire delta plain; and considering this the results are still remarkably similar. This, combined with the fact that the mean NED remains spatially consistent across the length of the catchment, strengthens the conclusion of Edmonds *et al.* that delta networks organise to maintain a spatially consistent average NED via an internal feedback mechanism (as discussed in chapter 5). Overall there is very little change to NED distribution for all scenarios between 30 and 50 years into the simulation period; and indeed to 60 years for scenario 10DWDF. For all scenarios the modal class is $0.01 \leq \text{NED} \; 0.05$; representing between 16.8% (1WWW) and 19.0% (10DWDF) of values at 30 years, and 15.4% (TST) and 18.0% (9DWDC) of values at 50 years.

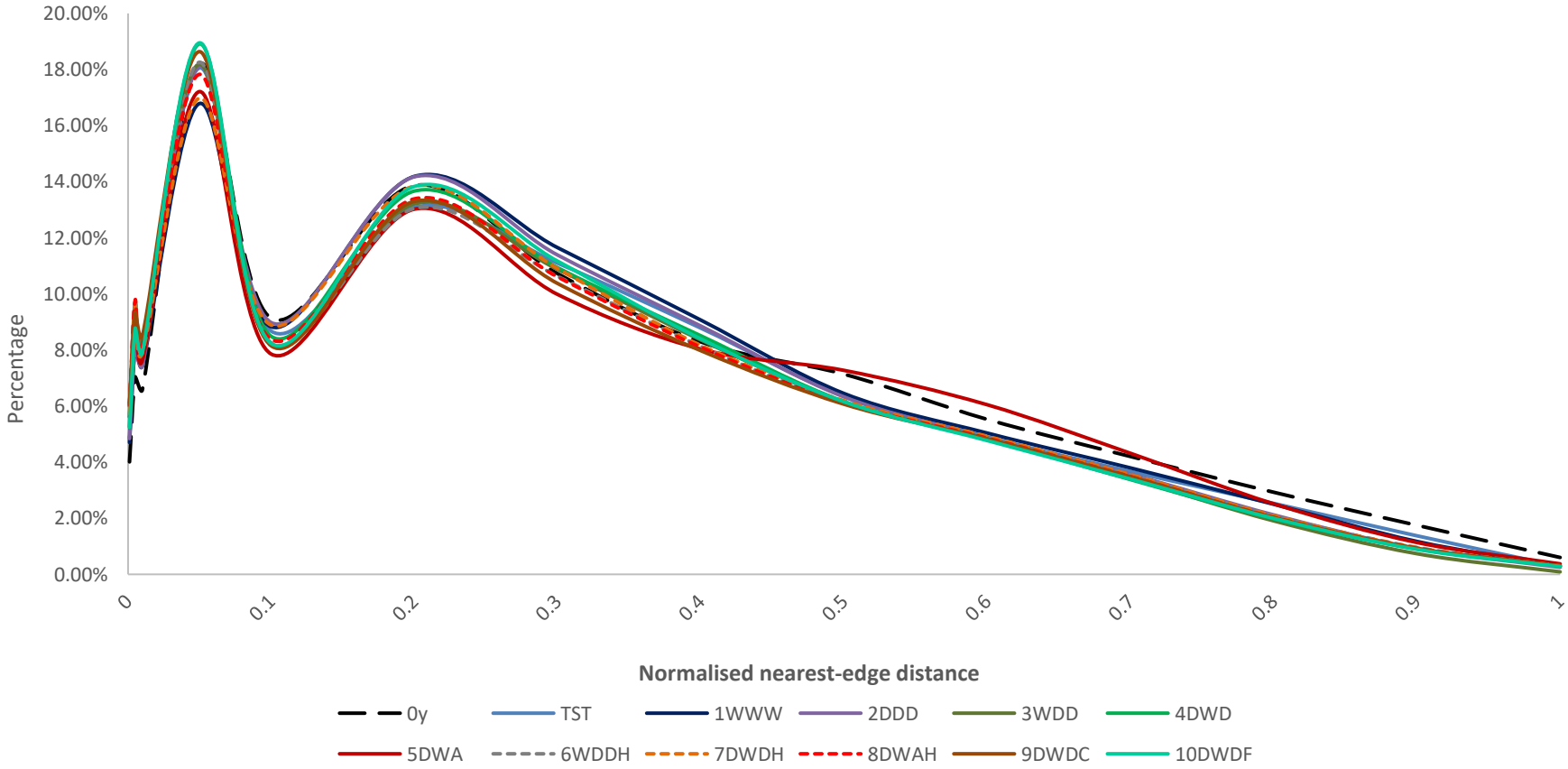

Figure 6.22 Normalised nearest-edge distance (NED) at 30 years, Devi catchment.

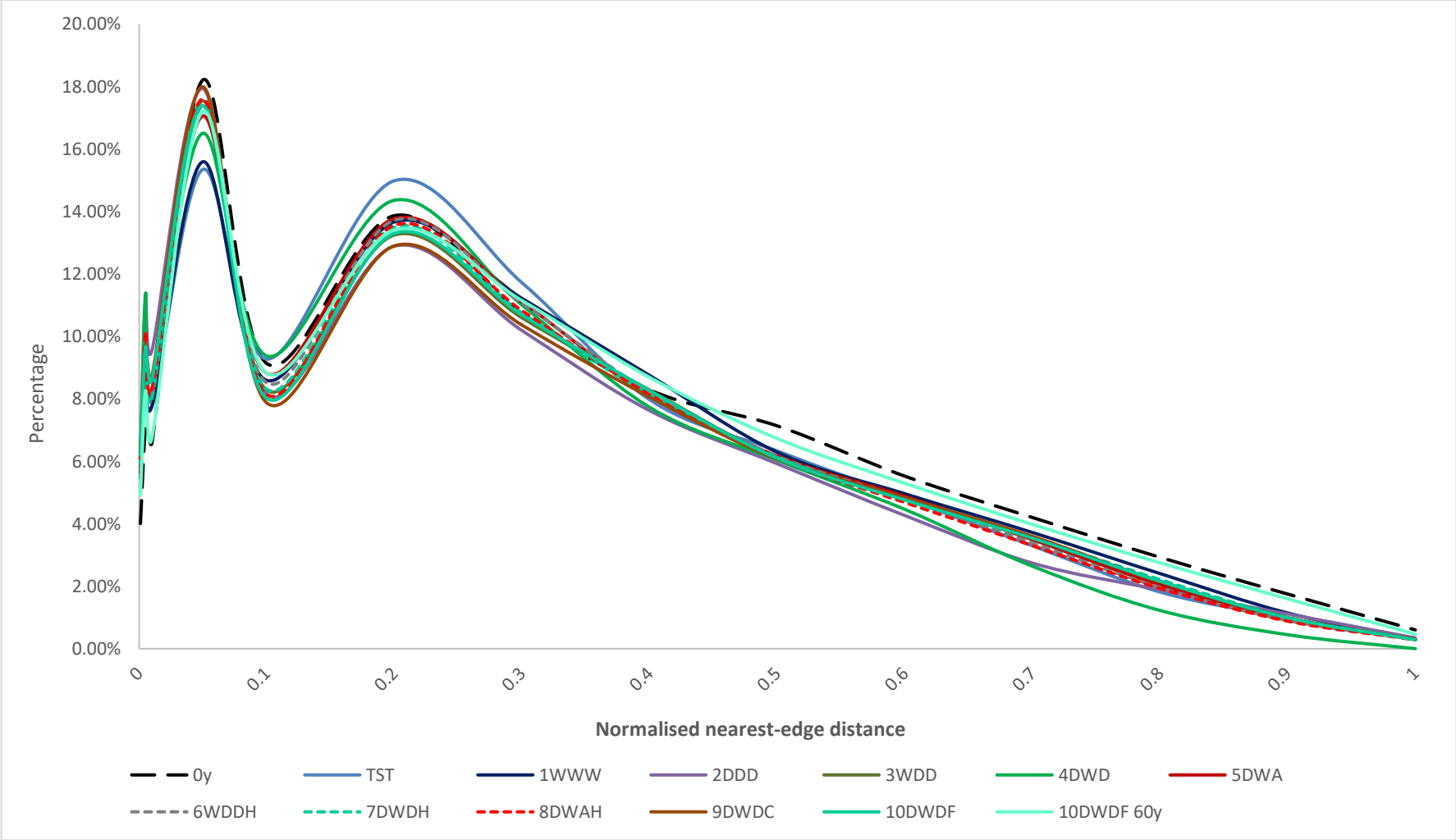

Figure 6.23 Normalised nearest-edge distance (NED) at 50 years, Devi catchment. NED at 60 years is also shown for scenario 10DWDF.

6.1.2 Mahanadi Catchment

6.1.2.1 Sediment loss and elevation change

Figures 6.24 and 6.25 show the net sediment loss and elevation change at 30 years and 50 years, respectively, under scenario TST. Figure 6.26 shows elevation change between 30 and 50 years for scenario TST. The same maps for scenario 4DWD can be found in Appendix C (figures C.33 – C.35). Figure 6.27 does however show net sediment loss for scenario 4DWD for comparison. Table 6.4 shows the total net sediment change under both scenarios at 30 and 50 years.

The spatial pattern of elevation change and net sediment loss between the baseline (TST) and most likely meteorological pathway (4DWD) scenario is remarkably similar at 30 years into the simulation period. As was the case in the Devi catchment under both of these scenarios, areas of net sediment loss and gain are spread relatively evenly across the catchment from apex to mouth; although there is a more pronounced gain both in the upper and lower reaches for the Mahanadi catchment. Levee development is more substantial in the upper reaches, as opposed to the middle reaches for the Devi. Levee development does however occur after a bifurcation of the main channel in both catchments. As in the Devi under these scenarios, overall there is a net gain of sediment within the catchment (table 6.4). Net gain in the Mahanadi catchment at 30 years under scenario TST is 6.24E+07 m^3 (compared to 9.03E+06 m^3 in the Devi catchment). Under scenario 4DWD the net gain is 5.85E+07 m^3 (compared to 9.86E+06 m^3 in the Devi catchment). Maximum accretion is much lower than in the Devi catchment, at 14 m for both scenarios (compared to 23 m at 30 years in the Devi). Maximum erosion at 30 years is 8 m under scenario TST and 7 m under scenario 4DWD.

At 50 years into the simulation period there is a substantial net gain of sediment across the catchment under both scenarios, providing a stark contrast with the results seen for the Devi catchment. Net gain in the Mahanadi catchment at 50 years under both scenarios is 3.01E+08 m^3; compared to losses of 6.60E+07 m^3 and 6.50E+07 m^3 under scenarios TST and 4DWD, respectively, in the Devi catchment). Whilst maximum accretion equals that of the Devi catchment at 23 m, the primary difference is seen across the floodplain channels; whereby significant

accretion is seen along a majority of ephemeral channels. The only noteworthy area of erosion seen in the Mahanadi under scenario TST, occurs where the channel has widened in the lower reaches of the catchment. A new channel system has also developed that connects two bifurcations of the main channel.

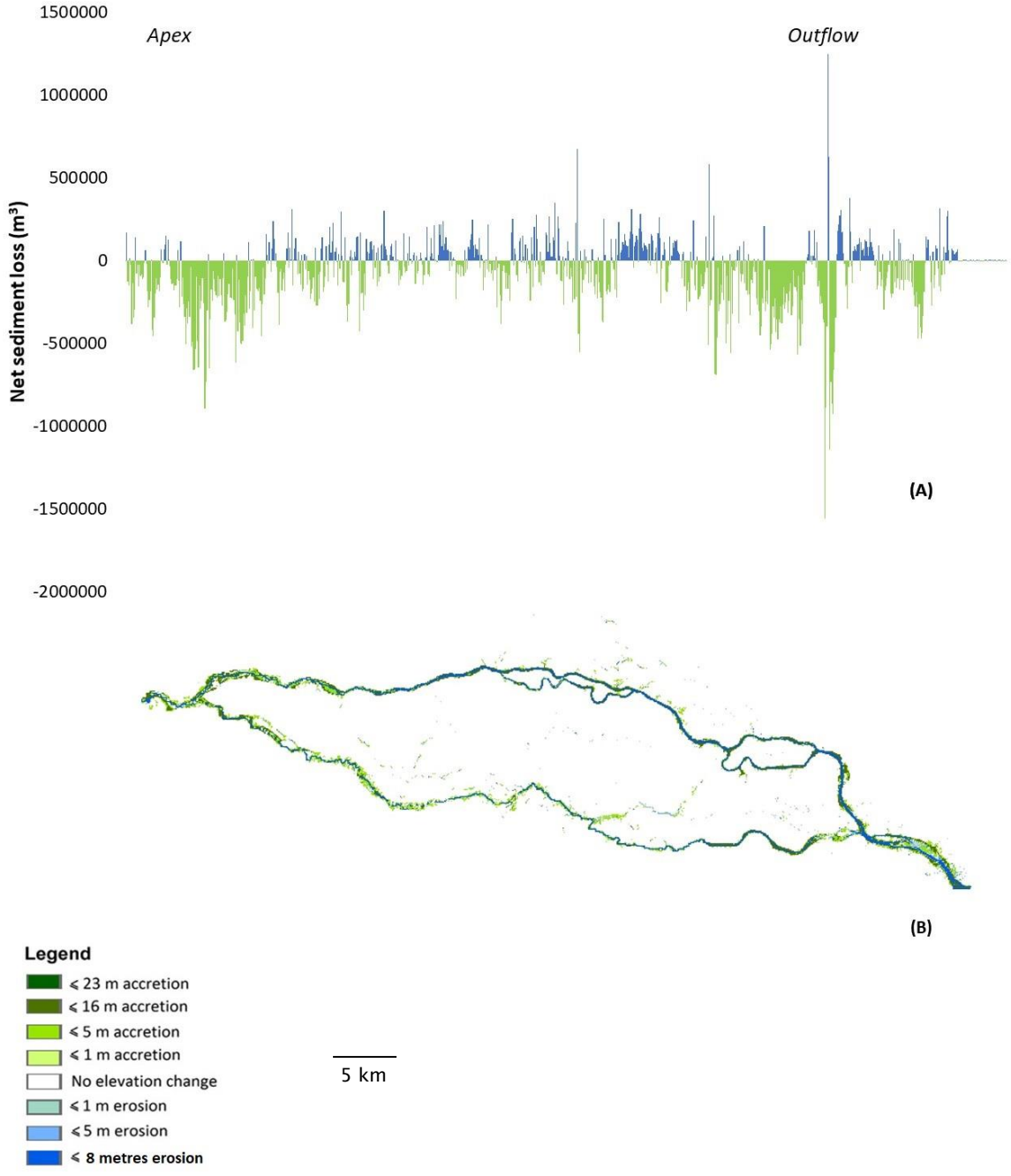

Figure 6.24 (A) Net sediment loss and (B) Elevation change at 30 years under scenario TST, Mahanadi catchment.

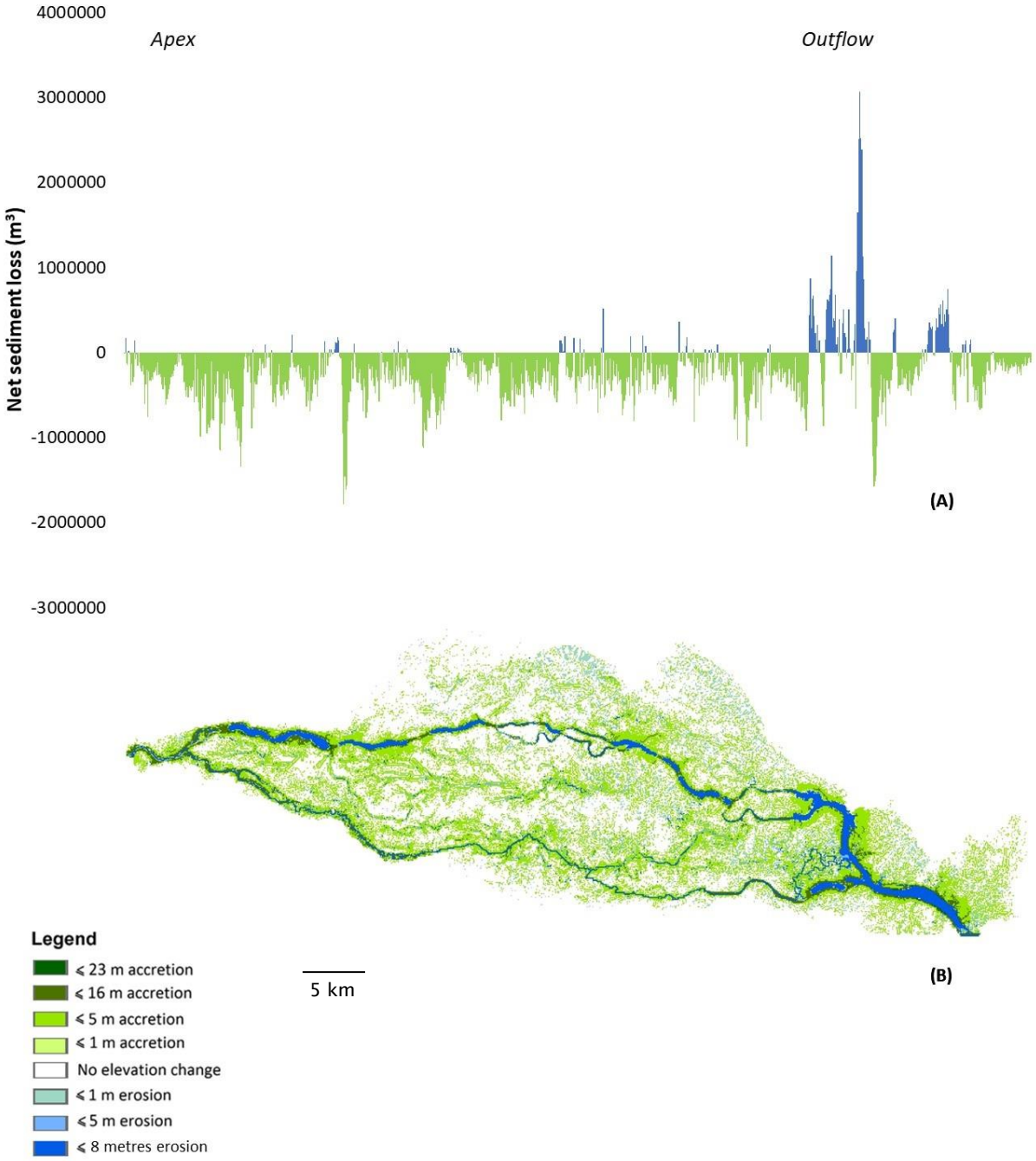

Figure 6.25 (A) Net sediment loss and (B) Elevation change at 50 years under scenario TST, Mahanadi catchment.

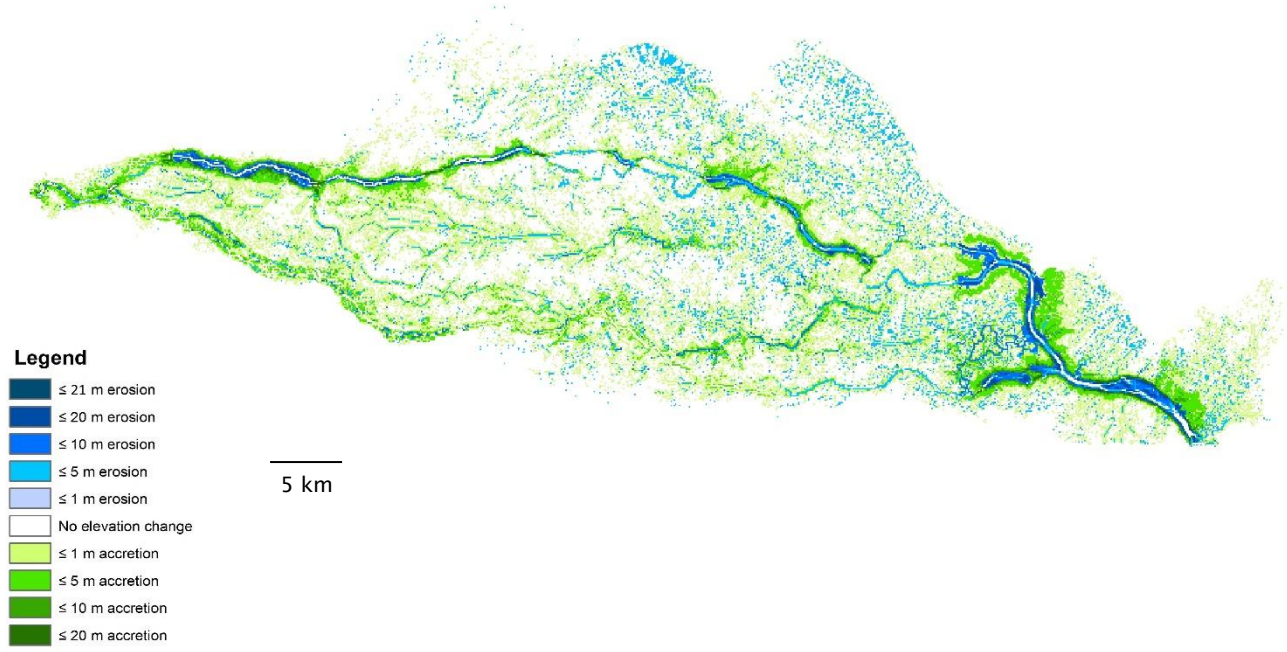

Figure 6.26 Elevation change between 30 and 50 years under scenario TST, Mahanadi catchment

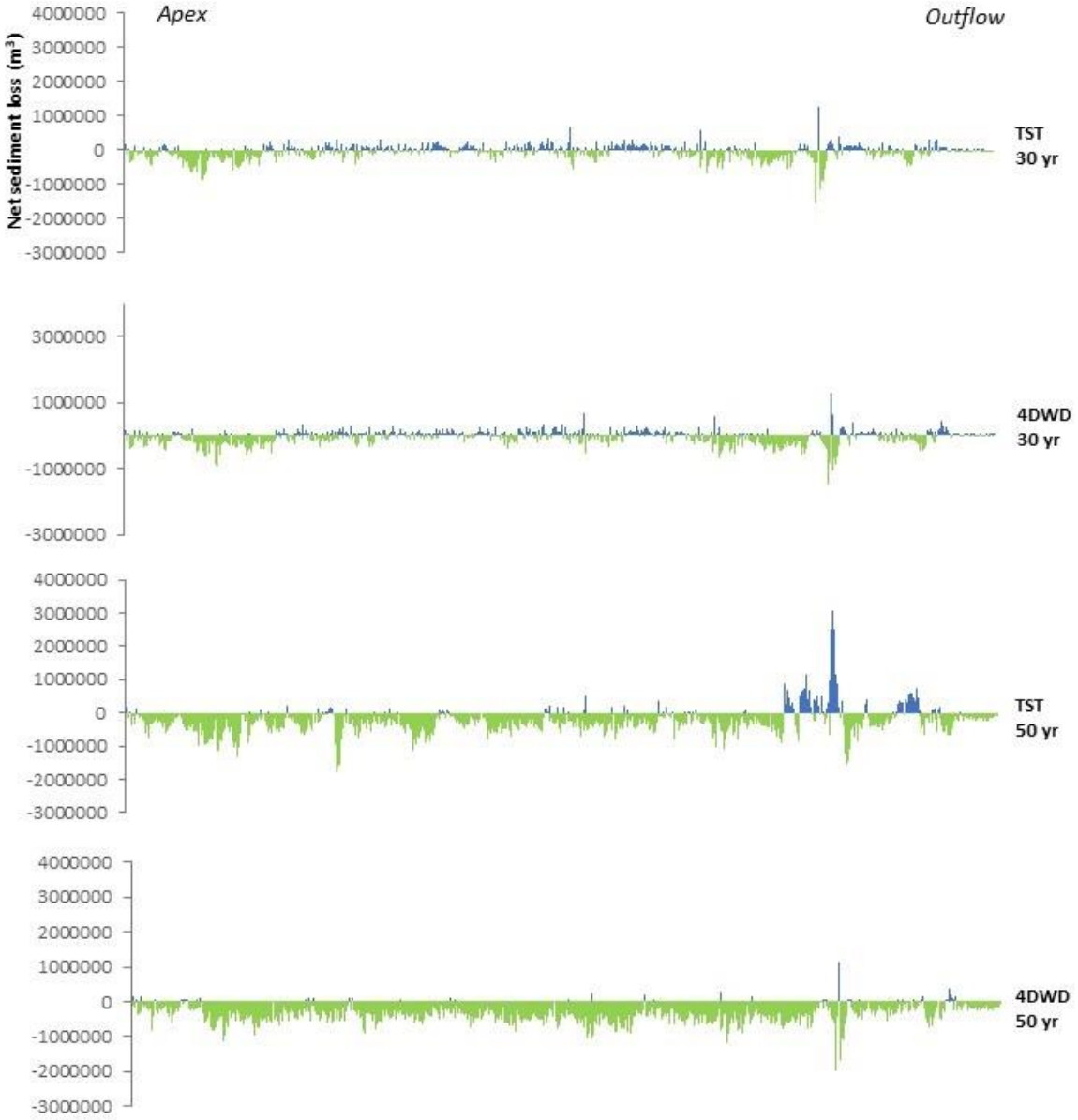

Figure 6.27 Net sediment loss for scenarios TST and 4DWD; Mahanadi catchment. Blue indicates net sediment loss and green indicates net sediment gain.

Table 6.4 Net sediment change, Mahanadi catchment (Blue indicates increase; red decrease)

Scenario	Net sediment change (m^3)	
	30 years	50 years
TST	6.24E+07	3.01E+08
4DWD	5.85E+07	3.01E+08

6.1.2.2 Morphological Response Units (MRUs)

The floodplain MRUs identified in figure 6.28 show the close morphological resemblance between scenarios TST and 4DWD. The primary contrast between the Devi and Mahanadi catchments under these scenarios is that the extent of floodplain channels at 30 years into the simulation is much greater in the Devi. As discussed in the previous section however, these channels primarily act as a sediment sink across the delta plain in the Mahanadi, compared to the significant scouring seen in ephemeral channels in the Devi catchment.

Two crevasse splay formations develop ~40 km downstream of the apex under both scenarios by 30 years, and remain at 50 years. A large crevasse splay forms under scenario TST at 50 years at the point where the two major bifurcations of the river meet 10 km upstream of the mouth. Channels have developed within this splay, acting to connect these two bifurcations further upstream.

Widespread levee formation occurs along a majority of the main channel and its bifurcations. This contrasts with the same two scenarios in the Devi catchment where at 50 years into the simulation period levee development is inhibited in the lower catchment due to significant lateral erosion. Figure 6.29 shows an example area of levee formation for scenario TST, where extensive lateral erosion and an increase in levee height can be seen. At 30 years 58.0% of levees measure between 1 and 5 m in height; decreasing to 56.7% at 50 years. The proportion of levees measuring between 10 and 14 m, however, increases over this period; from 42.0% to 43.3%. The Mahanadi catchment therefore has a much greater proportion of higher levees than the Devi catchment under the baseline scenario TST, where just 4.4% of levees measured between 10 and 15 m in height at 50 years into the simulation. Far more linear levee formation is also observed in the Mahanadi catchment.

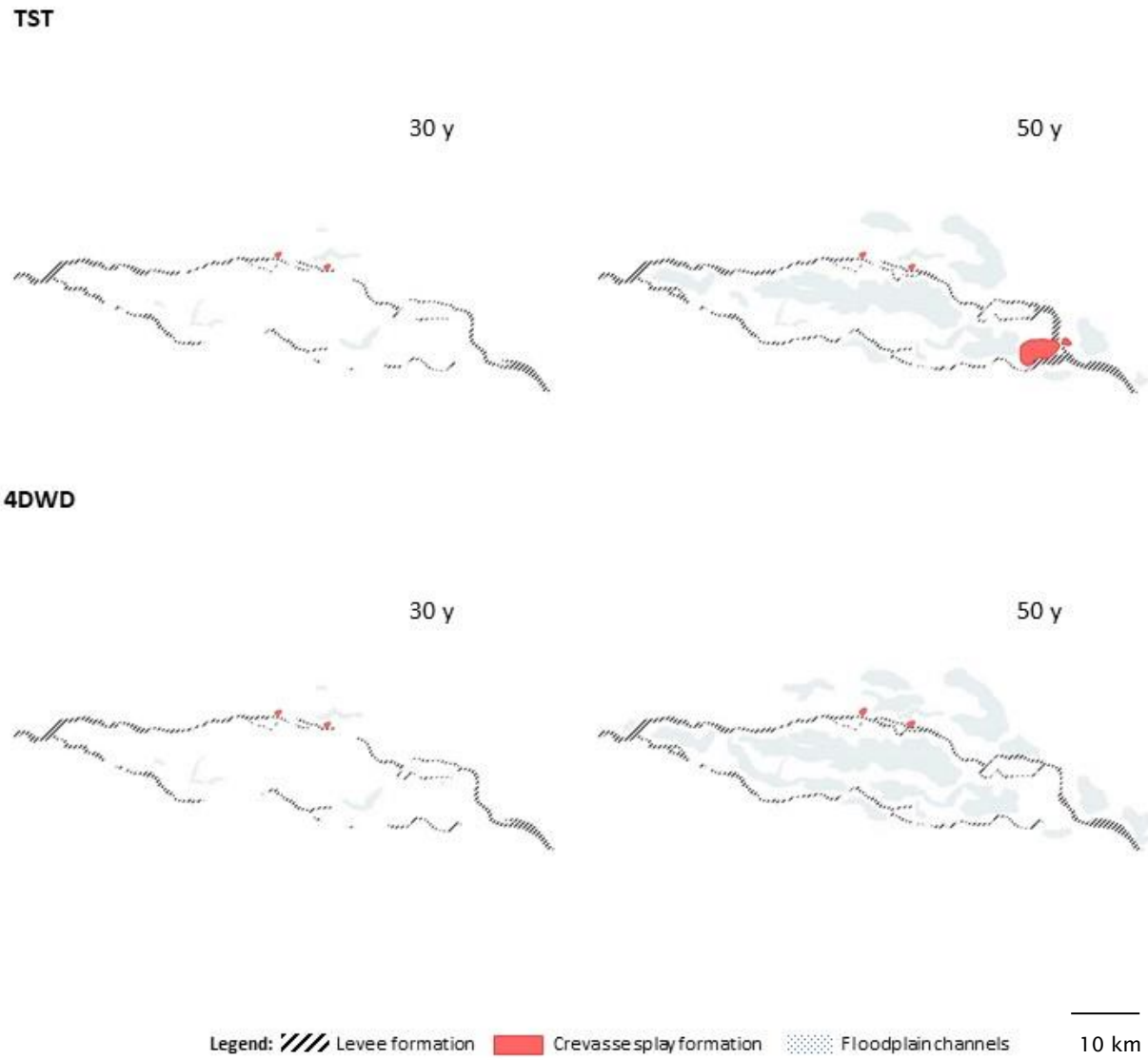

Figure 6.28 Floodplain morphological responses units (MRUs) for scenarios TST and 4DWD; Mahanadi catchment.

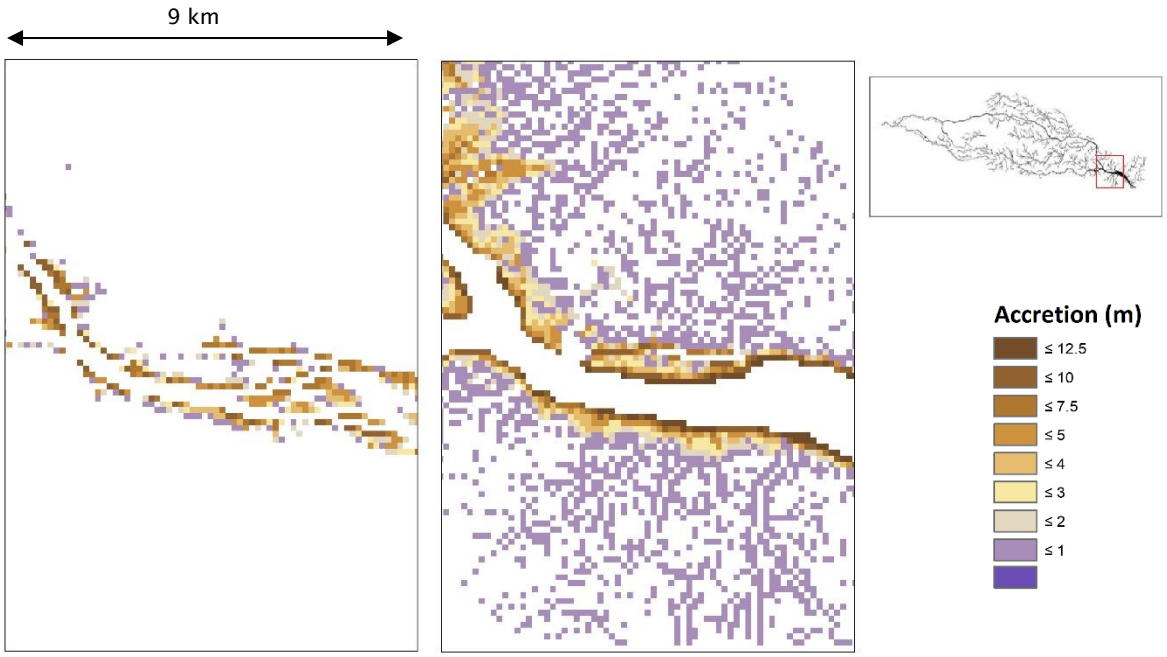

Figure 6.29 Levee formation under scenarios TST; Mahanadi catchment.

Figure 6.30 shows channel MRUs for the Mahanadi catchment; whereby each grid represents an area of 6 x 6 grid cells in the model (where each grid cell is 90 m^2).The reason for this slightly larger MRU size in the Mahanadi catchment is to account for the fact that the main Mahanadi River channel is generally wider than the Devi River. Lateral erosion does occur in the lower reaches of the catchment under both scenarios at 50 years, particularly from the point at which the two major bifurcations of the main channel re-merge. There is also extensive lateral erosion in the northern bifurcation of the main channel under scenario TST. As can be seen in figure 6.30, this widening of the channel occurs predominantly before areas of significant mid-channel bar formation. However, upon viewing the DEM for the Mahanadi catchment at 50 years (figure 6.31), it is clear that these mid-channel bars have actually formed dams across the main channel. This unusual morphological change is not however seen under scenario 4DWD; or indeed under any scenario in the Devi catchment. At 50 years into the simulation there is a decrease of 80.7% in the area affected by lateral erosion between scenarios TST and 4DWD in the Mahanadi catchment; compared to just 3.9% in the Devi catchment. Channel incision is evident throughout much of the main channel for both scenarios at 30 and 50 years.

The number of mid-channel bar MRUs under scenario TST was 44 at 30 years, increasing to 47 at 50 years. Under scenario 4DWD at 30 years mid-channel bar

frequency is 9.09% higher at 48, before falling to 46 at 50 years. However as seen in figure 6.31, some of these mid-channel bar MRUs are actually not true islands but rather have acted to dam the channel. A similar pattern is seen for point bar formation under scenario TST: at 30 years the count is 23, increasing to 27 at 50 years. Under scenario 4DWD however the number of point bars is 33 at 30 years; 43.5% higher than in scenario TST. By 50 years this value has reduced to 28. As in the Devi catchment, the spatial distribution of mid-channel bar and point bar MRUs remains fairly consistent between the two scenarios.

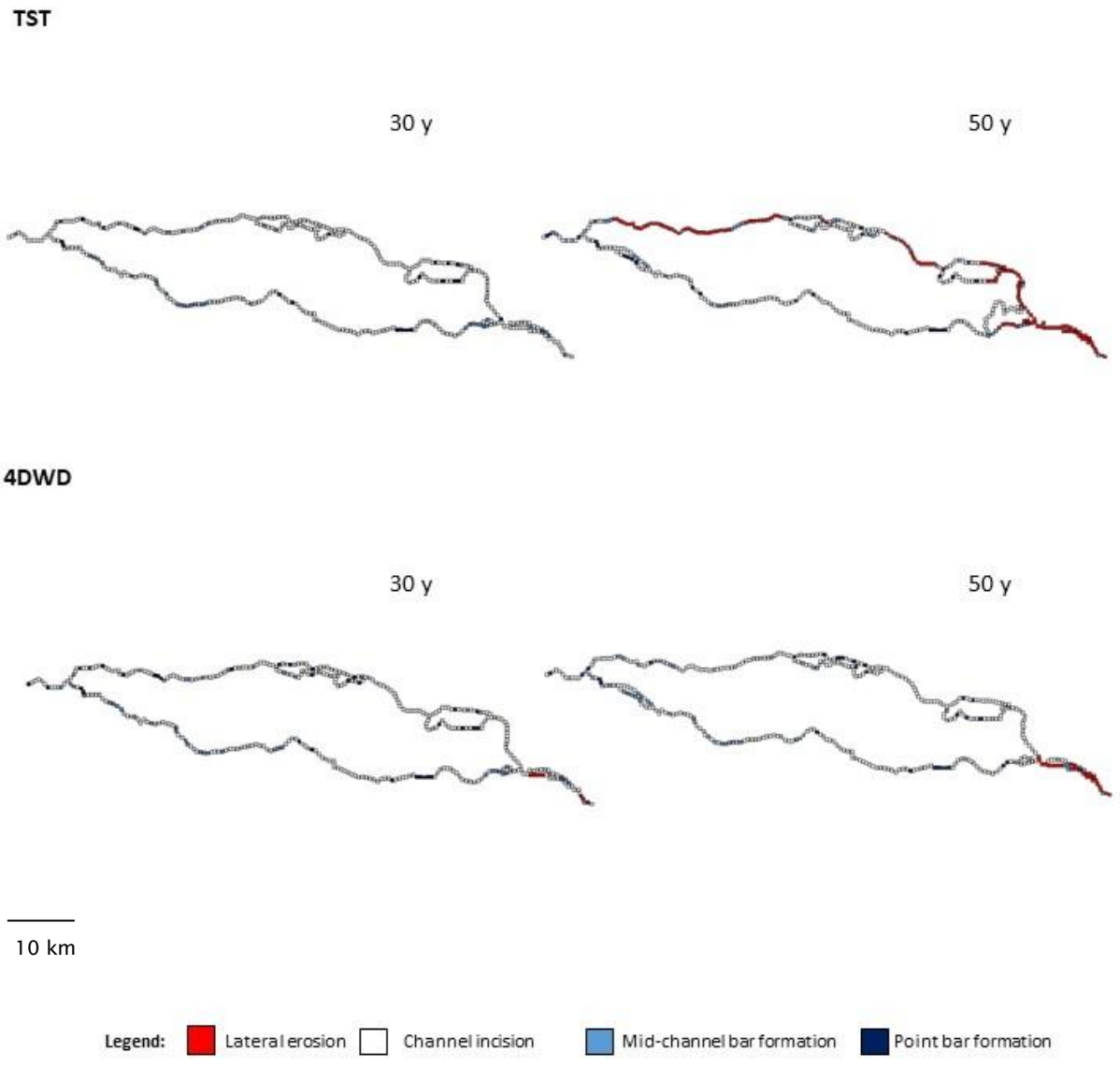

Figure 6.30 Channel morphological responses units (MRUs) for scenarios TST and 4DWD; Mahanadi catchment

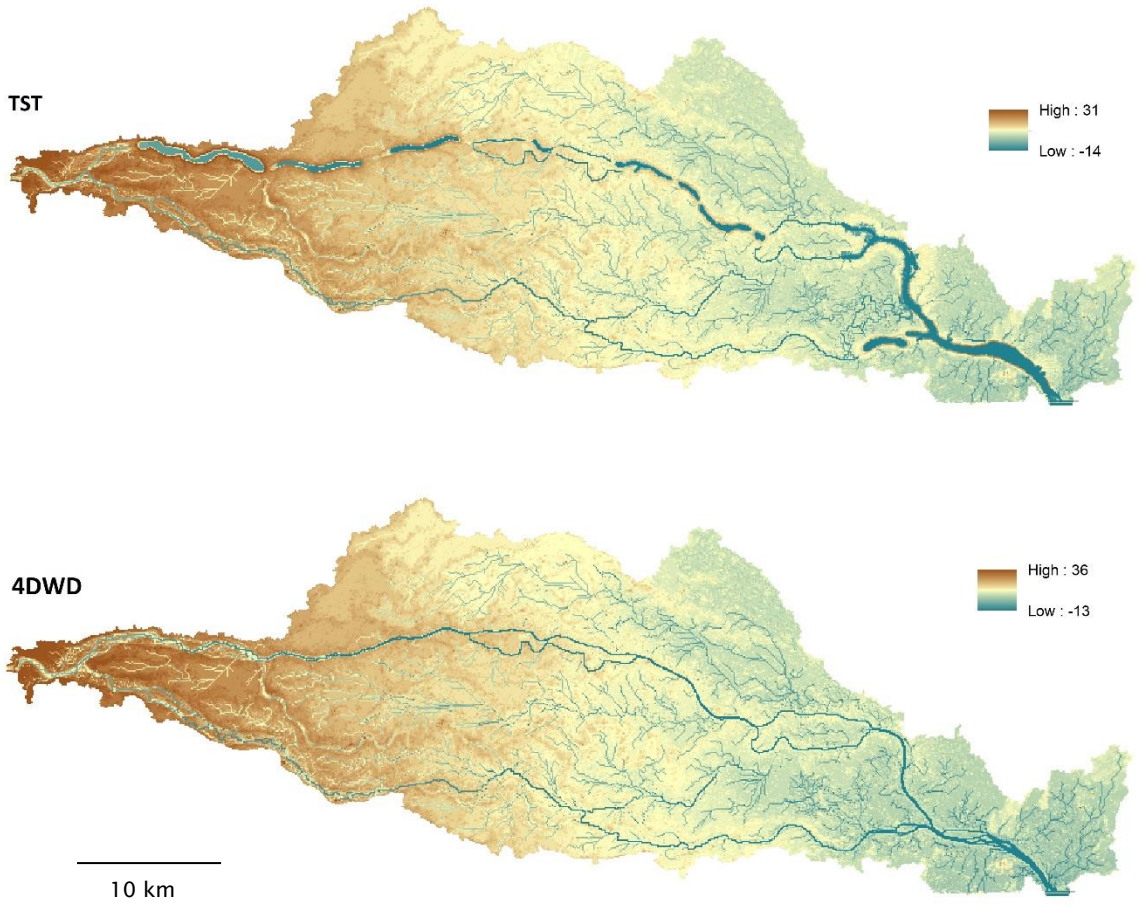

Figure 6.31 DEMs at 50 years for scenarios TST and 4DWD; Mahanadi catchment.

6.1.2.3 Fractal dimension

The fractal box-counting dimension value (D) decreased by 0.04 at 30 years into the simulation period under scenario TST; in contrast to the Devi catchment where D increased by 0.05 (table 6.5). At 50 years D increased considerably by 0.11 to a value of 1.55. Under scenario 4DWD however there was no change in channel density by 30 years, and even at 50 years D only increased slightly by 0.01. This again provides a contrast to the Devi catchment where an increase of 0.07 was observed over this period.

Table 6.5 Box-counting dimension (D), Mahanadi catchment (Blue indicates increase; red indicates decrease)

Scenario	Box-counting dimension (D)		
	0 years	30 years	50 years
TST	1.48	1.44 (-0.04)	1.55 (+0.11)
4DWD		1.48	1.49 (+0.01)

6.1.2.4 Distribution of island sizes

Figure 6.32 shows island size distribution for scenarios TST and 4DWD in the Mahanadi catchment. As in the Devi catchment, the results demonstrate a clear dominance of smaller island sizes under both scenarios. At 30 years, 51.1% and 54.2% of islands measured ≤1 km^2 under TST and 4DWD, respectively. By 50 years into the simulation period these figures reduce slightly to 47.4% and 53.4%. By this time, 84.2% (TST) and 82.2% (4DWD) of islands measured ≤5 km^2. Large islands measuring ≤100 km^2 account for 8.8% (TST) and 11.0% (4DWD). There is therefore a slightly higher proportion of larger islands in the Mahanadi catchment compared to the Devi.

Table 6.6 outlines the total number of islands for each scenario as well as modal, minimum and maximum island size. Both scenarios show an increase in the total number of islands forming within the catchment from the 0 year count of 20. Under scenario 4DWD the number of islands increases to 73. This provides a contrast to the number of mid-channel bar MRUs, which decreased in frequency over this period. This would suggest that island formation is most active outside of the main channel.

Modal island size was 0.54 km^2 at 30 years into the simulation under both scenarios. Minimum island size also remained equal at 0.36 km^2. Maximum island size reduced under both scenarios. Modal, minimum and maximum island size does however decrease under scenario TST at 50 years; whereas these values remain unchanged and/or increase under scenario 4DWD.

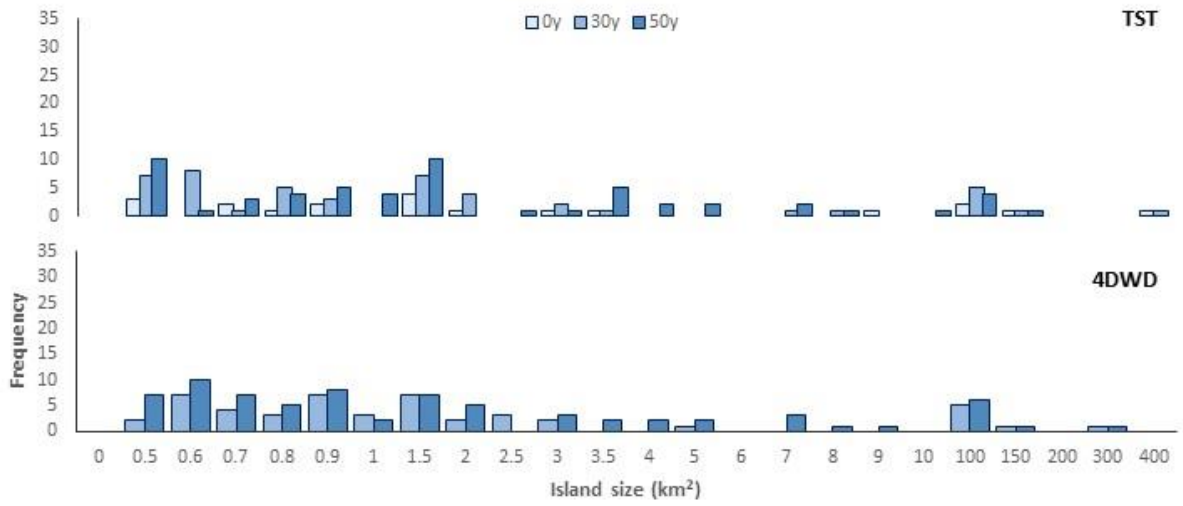

Figure 6.32 Island size distribution for scenarios TST and 4DWD; Mahanadi catchment.

Table 6.6 Total number and size of islands, Mahanadi catchment (Blue indicates increase; red indicates decrease)

Scenario	Total number of islands			Modal island size (km²)			Minimum island size (km²)			Maximum island size (km²)		
	0 yr	30 yr	50 yr	0 yr	30 yr	50 yr	0 yr	30 yr	50 yr	0 yr	30 yr	50 yr
TST	20	47	57	0.36	0.54	0.36	0.36	0.36	0.27	331.92	327.42	118.08
4DWD		48	73		0.54	0.54		0.36	0.36		273.42	276.21

6.1.2.5 Nearest-edge distance

Figures 6.33 and 6.34 show normalised nearest-edge distance (NED) at 30 years and 50 years, respectively. A similar distribution of NED values is evident for the Mahanadi catchment as compared to those in the Devi; with two peaks in the distribution at values of ~0.05 and ~ 0.2, and very little change observed between 30 and 50 years into the simulation period. As in the Devi catchment, the modal class for both scenarios is 0.01 ≤ NED 0.05; representing 17.4% (TST) and 20.7% (4DWD) of values at 30 years, and 21.0% (TST) and 21.0% (4DWD) of values at 50 years.

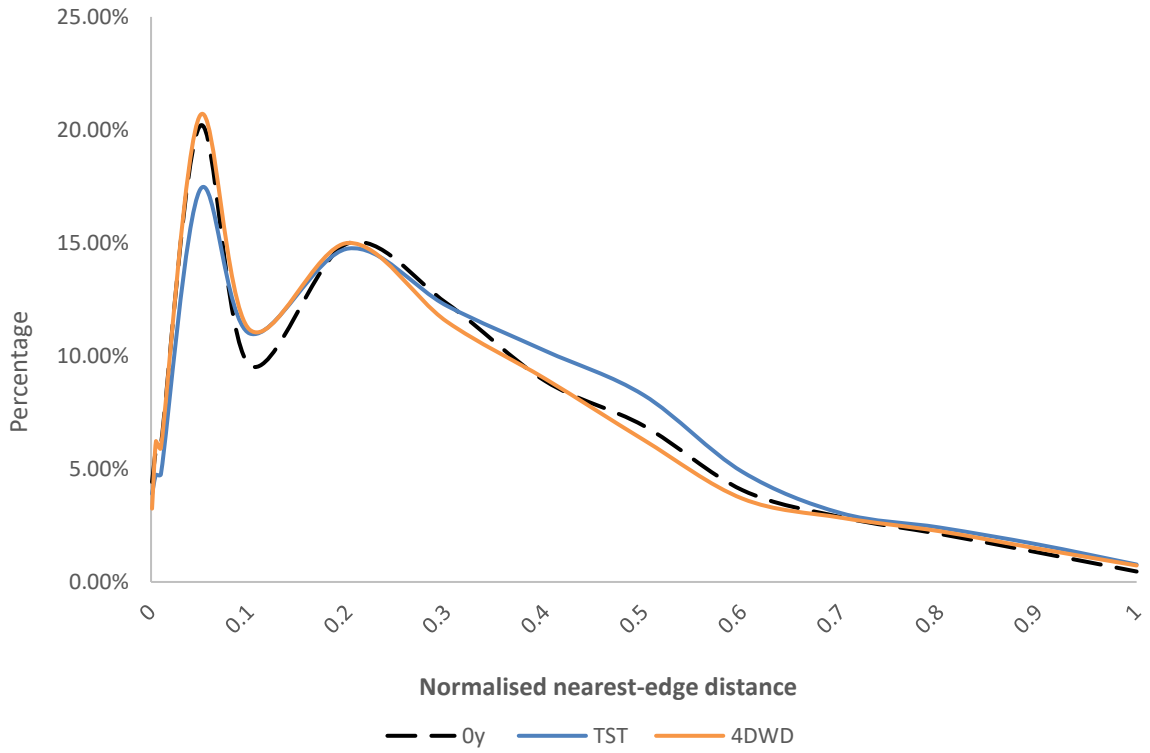

Figure 6.33 Normalised nearest-edge distance (NED) at 30 years, Mahanadi catchment.

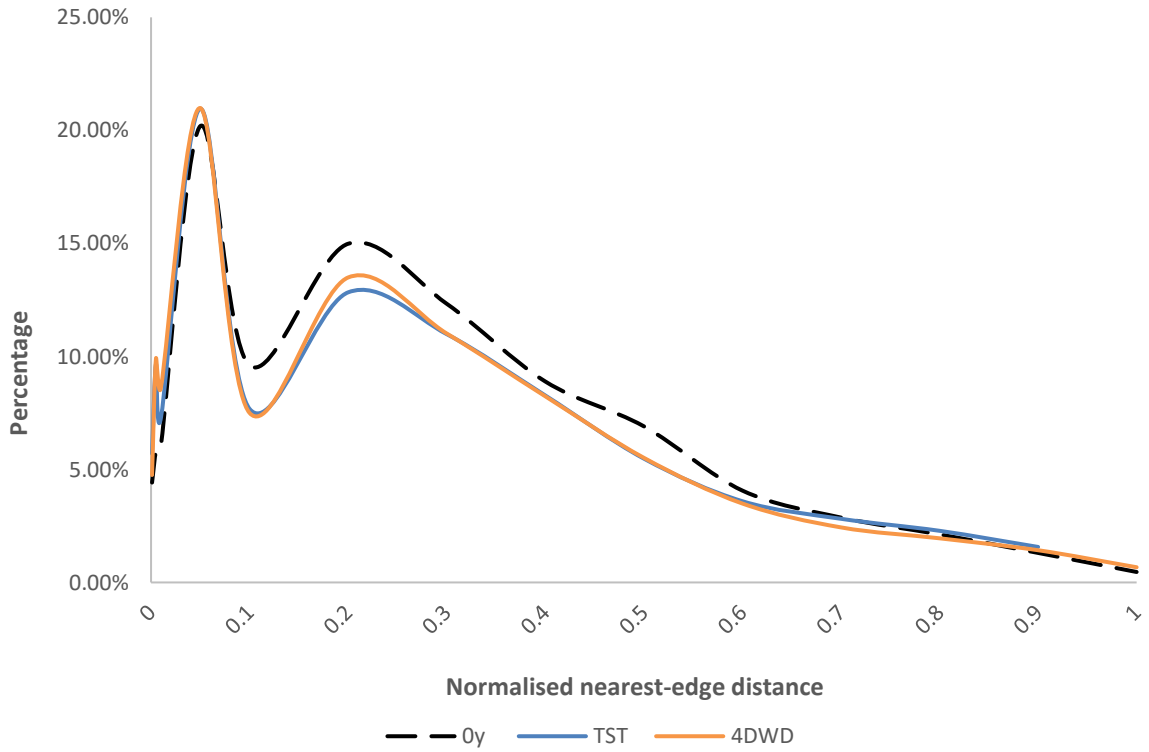

Figure 6.34 Normalised nearest-edge distance (NED) at 50 years, Mahanadi catchment.

6.2 Discussion of Results

The results above provide a useful indication of what areas of the Devi and Mahanadi catchments may experience significant morphological change under a range of climatic and environmental change scenarios. They identify which areas are likely to aggrade to safer elevations with respect to flooding, and which areas are likely to erode; as well as providing relative trajectories of the rate and magnitude of this change over the next 50 to 60 years. As will be discussed fully at the end of this section, it has become apparent during the critical analysis of these results that the magnitude of certain changes observed in the model outputs lie outside the expected range for the Mahanadi Delta system. As such it is recommended that until further validation of the model setup is able to be undertaken, the results of this study are not viewed as projections of absolute morphological change. This should also be taken into account during the discussion in this chapter. Rather, the results serve to demonstrate the relative morphological trajectories that may be experienced in the Mahanadi region under various climatic scenarios. Most importantly, the need to further validate the setup of the model does not in any way detract from the success of achieving the primary aim of this study: to develop an innovative and transferable framework for analysis of multidecadal change in deltaic environments. As such the outputs of this study still provide valuable information for stakeholders in the Mahanadi region, and, particularly when combined with the further analysis in chapter 7, could contribute towards the development of climate-resilient adaption strategies. The purpose of this research, however, is not purely to use C-L to identify regions of potential vulnerability in the Mahanadi Delta; but rather as a tool to enhance our understanding of how emergent processes influence the multidecadal evolution of deltaic environments more generally. A deeper analysis of what the above results may indicate about system behaviour under increasing conditions of climatic stress is therefore required. Despite some reservations regarding the absolute values of the projections, the nature of the observed changes has produced some insightful and fascinating areas of discussion, as is presented below.

An interesting pattern to emerge from the morphological results is that there appears to be two distinct trajectories of evolution within the Devi catchment; particularly in terms of where elevation change occurs and the total net sediment change across the system (figure 6.35). To analyse this further, we extend the analysis to include the 5 year recording intervals between the simulation periods. For the purpose of this discussion, these shall be referred to as group A and group B scenarios: Group A describes those scenarios that follow a similar morphological trajectory to that of the baseline scenario, TST. This group includes scenarios 1WWW; 2DDD; 4DWD; and 10DWDF. At 30 years into the simulation all group A scenarios have resulted in a net gain of sediment across the Devi catchment, with the greatest gain observed under scenario 1WWW (1.36E+07 m^3). Areas of erosion and accretion are spread relatively evenly across the catchment from apex to mouth; although there is a more pronounced net gain in the upper reaches and more pronounced net loss in the lower reaches. In the years preceding this point the system oscillates between periods of relatively minor net sediment gain and net sediment loss. This oscillation occurs over approximately 10 year intervals. Between 30 and 40 years, as climatic and environmental stressors on the system are amplified, these 4 scenarios split on to two different trajectories: scenarios TST, 1WWW and 2DDD start to experience net sediment loss at a fairly consistent rate. Conversely, scenarios 4DWD and 10DWDF result in a substantial net gain of sediment within the catchment at 40 years; nearly seven times greater than the gain experienced at 30 years into the simulation. By 50 years however there is a considerable net loss of sediment across the catchment that is of similar magnitude for all group A scenarios (with the exception of 10DWDF; discussed later in this section). Areas of net sediment gain are concentrated to the floodplain west of the main river channel and in areas of significant levee development in the mid catchment. Sediment loss and channel widening is concentrated in the lower reaches.

Group B describes those scenarios that follow a very different trajectory to those in group A, particularly in the initial 30 year simulation period. This includes scenarios 3WDD; 5DWA; 6WDDH; 7DWDH; 8DWAH and 9DWDC. These scenarios experience a much greater net sediment gain by 10 years into the simulation. In contrast to group A scenarios, this increase continues at a rapid rate over the next decade. By 30 years into the simulation period however net sediment loss is

observed throughout the catchment. The greatest loss is experienced under scenario 6WDDH, at 1.13E+08 m^3. Interestingly a spatial pattern of elevation change emerges that is more alike that observed at 50 years for group A, with substantial erosion occurring in the lower reaches of the catchment. All group B scenarios experience a sharp increase in net sediment deposition towards 40 years into the simulation period; although only scenarios 5DWA and 8DWAH maintain sufficient quantities to cause a net gain within the catchment. At 50 years into the simulation period, all group B scenarios experience large net losses of sediment, ranging between 2.20E+08 m^3 and 2.75E+08 m^3. Sediment loss and channel widening remains concentrated to the lower reaches. As in the scenarios in group A, the range between the different scenarios decreases.

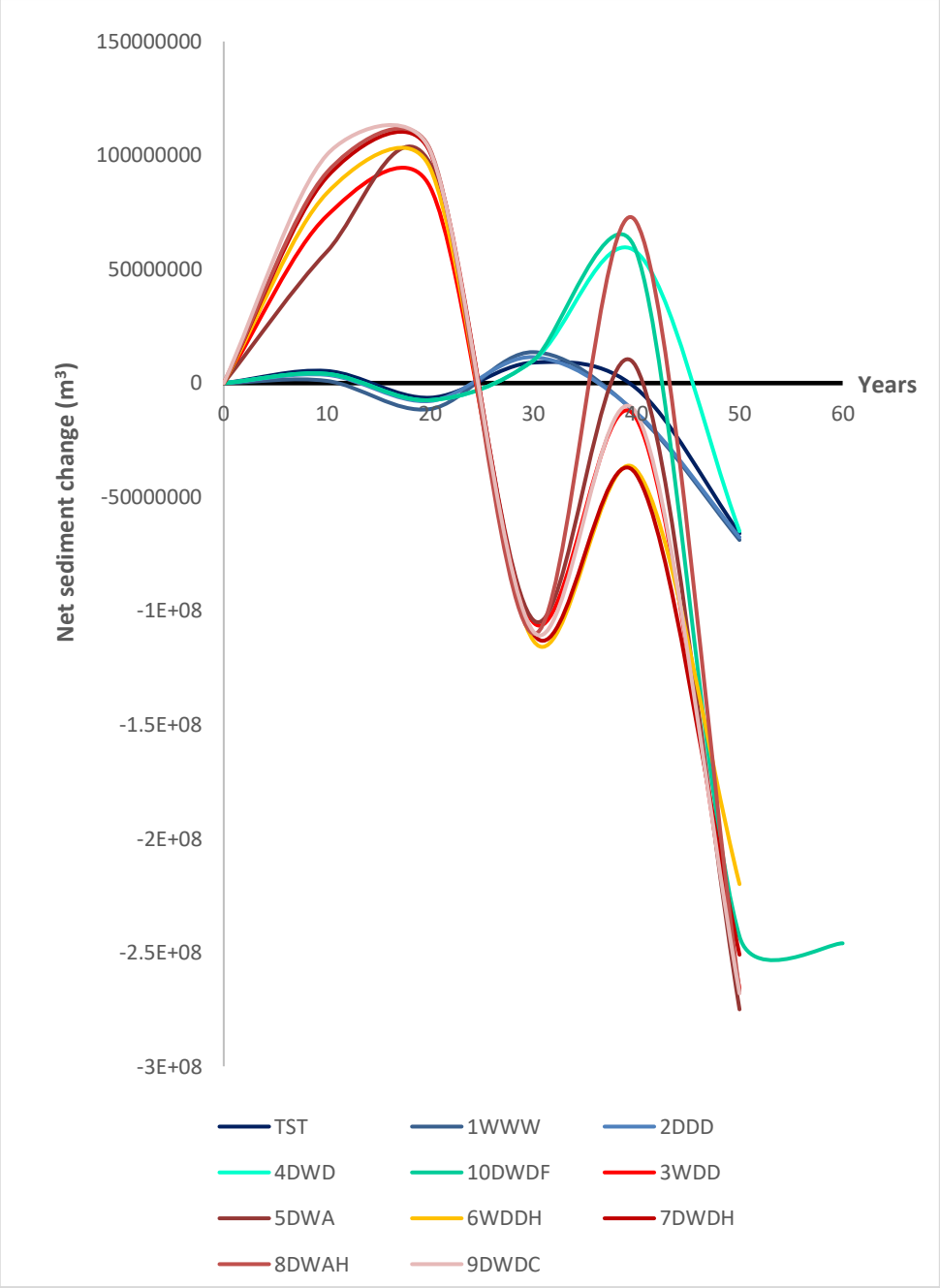

Figure 6.35 Net sediment change across all scenarios; Devi catchment. Two distinctive morphological pathways emerge from the results, referred to as group A (shown in shades of blue) and group B scenarios (shown in shades of red).

An obvious first step when presented with such data is to attempt to identify which mechanistic driver (the rate of sea-level rise, monsoon precipitation totals,

etc.) may be causing this categorical split. However following this investigation there is no obvious singular factor resulting in this emergent behaviour: Group B does include all scenarios where sea-levels increase at the higher rate of 1 cm per year (6WDDH, 7DWDH and 8DWAH). It was also evident that in the initial morphological analysis that higher sea-levels appear to be linked to increased rates of sediment loss at 30 years into the investigation. This is due to enhanced erosion rates in the lower reaches, as a result of a gradual rise in the plane of activity at which tidal forces operate. Understanding these impacts is important as the effects of coastal erosion, as a result of rising sea-levels in the vicinity of inlets, are often considerably underestimated (Ranasinghe *et al.*, 2013). However scenarios 3WDD, 5DWA and 9DWDC also follow similar trajectories despite sea-level rising at a slower rate of just 0.6 cm per year. Furthermore, with the exception of higher rates of sea-level rise all drivers for scenarios 6WDDH and 8DWAH are set to the same values as for scenarios 3WDD and 5DWA, respectively. One may therefore expect that these runs could indeed follow a similar morphological pathway given that tidal influences are restricted to only the lower regions of the catchment. However, if this was a universal rule then scenarios 4DWD and 7DWDH would not be split between the different groups.

Equally there is no simple relationship to be found between an increase or decrease in seasonal precipitation totals and what trajectory the Devi system follows. Scenarios 1WWW and 2DDD, for example, should theoretically provide a stark contrast to each other; where precipitation totals (and therefore river flows) become progressively wetter or drier, respectively, throughout the year. Despite these increasingly dissimilar climatic conditions, both scenarios fit within group A and follow analogous trajectories. Whilst there are indeed small differences in the volume of sediment gained and lost within the catchment system, the spatial distribution and timing of these changes is remarkably similar. Under increasingly wet climatic conditions one would expect enhanced rates of lateral erosion in response to increased flood frequency, with less time for recovery by contraction (Erskine *et al.*, 1998). However in the Mahanadi Delta, the extensive system of levees that exists across the delta plain restricts a majority of morphological activity in response to floods within the channel itself (Kale, 2003). During the largest floods there is a significant decrease in the width-depth ratio, resulting in an increase in stream energy per unit area and in boundary shear stress. As a result

significant quantities of coarse bed material can be transported during flood events (Kale *et al.* 1994). This could contribute to the apparently similar morphological response experienced under the contrasting scenarios 1WWW and 2DDD. In reality of course the wider impacts on biophysical vulnerability under these two trajectories would be significant. More frequent extreme flood and drought events would likely have devastating impacts in a region such as the Mahanadi that is highly dependent upon agriculture, with significant shifts to crop production and food security (Islam, 2017). This issue will be explored in greater detail in chapter 7.

It is also an interesting point of discussion that scenario 4DWD, deemed the most likely meteorological pathway (see chapter 5), follows a very similar trajectory to that of the baseline run, TST. The same is true of scenario 10DWDF; which follows the same pathway as 4DWD until approximately 40 years into the simulation, as monsoon precipitation totals become increasingly divergent. This might be expected given that these climatic changes – an increasingly drier and more variable monsoon, wetter post-monsoon period and drier dry season - are already being observed in the Mahanadi region and therefore there is less deviation from the historical data upon which the baseline run is generated (Singh *et al.,* 2014; Dash *et al.,* 2007; Asokan and Dutta, 2008), particularly during the initial 30 year simulation period. Alternatively, one could argue that the scenarios in group A are not driving the observed morphological changes, but rather are not acting in such a way, or over long-enough timescales, so as to tip the system onto a new morphological trajectory. In other words, do group A scenarios simply project a future state that the Mahanadi system has already been 'locked' into? Could it be that linear changes in the precipitation regime – as experienced in scenarios 1WWW and 2DDD – or gradual changes to the existing precipitation regime – as experienced in scenarios 4DWD and the initial ~40 years of 10DWDF – do not cause a significant enough perturbation within the morphological system to result in the transition to those patterns observed under group B scenarios? It is well documented that many deltaic biophysical systems are able to adapt when system drivers change in such a way that is progressive, linear or slow (Renaud *et al.,* 2013; Anderson *et al.,* 2004). However, even under constant forcing or linear conditions of external change, deltaic processes are complex and difficult to predict due to the autogenic variability coming from the self-organization of channel processes (Liang *et al.,* 2016; Hajek and Wolinsky, 2012). Increasing variability to any particular

driver, or indeed combination of drivers, is however more likely to push the morphological system towards a new evolutionary pathway. As was presented in detail in the literature review in chapter 3, thresholds are a defining driver of non-linear change in CSES, and it is therefore critical that a morphological model is able to successfully capture such behaviour. Such threshold-dependent changes may cause the system to move relatively smoothly from one state to another; or might result in a critical transition whereby there is an abrupt and potentially irreversible change to system functioning (Scheffer *et al.,* 2009). Whilst there may be no singular mechanism causing group B scenarios to push the system towards this new state, something that all of these scenarios *do* have in common is that at least one driver follows a pathway that presents a significant stress on the system and some level of increasing variability. These stressors include a wetter and more variable monsoon; accelerated dry season drought conditions; high rates of sea-level rise; and an increased frequency of severe storms. All of these stressors diverge more considerably from the historical conditions experienced in the Mahanadi Delta; and do so in such a way that these deviations do not amplify in a linear way. Although some of these external drivers only deviate significantly from baseline conditions over relatively short timescales, Medeiros *et al.* (2017) demonstrate how critical transitions can occur within limit cycles – an oscillation in response to a seasonal forcing, such as the monsoon. Furthermore, even if the system is undergoing a linear response to a change in one particular condition, the system may be less resilient during this adaption phase and could reach a tipping point under even a low intensity or short-term external stressor (Renaud *et al.,* 2013).

To investigate these patterns further, it is necessary to look not only at the raw outputs of the model, but also towards the two analytical concepts utilised by this study to aid in understanding the morphological evolution of the catchment system. The floodplain MRUs presented in section 6.1.1.2 largely reinforce the patterns observed in the analysis of sediment loss and elevation change. Once again there is a distinctive resemblance in the spatial distribution of features at 30 years for group A scenarios; and similarly for group B scenarios. Floodplain channels cover approximately a third more of the catchment area under the group B scenarios; which would support the hypothesis that the enhanced rates of net sediment loss seen under these scenarios is likely due to the relatively minor, but widespread, erosion across the floodplain. This is a significant result, as such a

large change in the areal density of floodplain channels will have significant implications for the routing of water and sediment across the distributary system. As will be discussed in chapter 7, such changes can have important impacts on factors effecting habitability such as flood risk and habitat cover. As in prior net sediment analysis, by 50 years into the simulation the number of floodplain channels in group A and group B scenarios converge. Scenarios in which the rate of sea-level rise is higher however tend to have a greater extent of active floodplain channels. This is likely due in part to backwater effects favouring avulsion (Chatanantavet *et al.,* 2012). Furthermore, the greater extent of inundation in the tidal reaches of the catchment results in a larger proportion of ephemeral channels registering a water depth ≤ 1 m (as required in this study to be defined as a 'channel'). Many of these floodplain channels are formed within existing paleo channel belts.

Crevasse splay formation occurs between 5 and 20 km downstream of the apex under all 11 scenarios. However, there is far greater variability in both their distribution and frequency for group A scenarios. Scenarios with higher total seasonal flows tend to produce higher numbers of crevasse splay formations: Scenario 1WWW and 2DDD for example, for the first time show more significant morphological differences; the former resulting in 8 splays and the latter just 2. This is unsurprising given that crevasse splay features form following flood events (Pondrelli *et al.,* 2008). Many channel avulsions on deltaic plains begin with crevasse splay formation (Stouthamer, 2001); thus these features play a significant role in determining the multidecadal and indeed centennial evolution of these environments. Such avulsions can often take decades to be completed, due to the significant volume of sediment that is required to be removed from the floodplain in order to carve out a new channel (Syvitski *et al.,* 2012). The avulsion itself is therefore unlikely to be captured over the timescales analysed in this study, however we can use crevasse splays as a potential early warning signal of where such changes could take place. There is far less variation observed between the group B scenarios, with all resulting in 4 or 5 crevasse splay formations by 30 years into the simulation period. A large crevasse splay forms approximately 55 km downstream under all group B scenarios at 30 years. By the end of the simulation, a splay is also formed at the same location under scenarios 2DDD, 4DWD and 10DWDF. This might suggest that this is a particularly vulnerable breaching point in

the levee system; which is likely given that levee height at this location only reaches a maximum of 3 m.

Widespread levee formation along the main channel is observed in the upper and middle reaches of the catchment across all scenarios at 30 years; as would be expected in a system that experiences regular seasonal flood events. There is however no straightforward relationship to be identified between annual river discharge and levee formation: whilst regular flooding provides the mechanism of overbank deposition required to build up the levees, large floods can also act to damage levee structures (Rakhecha, 2002). Furthermore the extent to which a levee gains height is limited, in that each time a higher flood is required in order to overtop the banks and thus supply the sediment. Significant levee development in the lower catchment is only observed under the group A scenarios; with only fragmented areas of accretion seen under the group B scenarios. This is likely due to the fact there is a net deficit of sediment within the catchment at this point in the simulation period for all group B scenarios. This, combined with extensive lateral erosion in the lower catchment, inhibits the formation of levees in the lower reaches of the floodplain. It should of course be noted that artificial or stabilised levees along the Devi channel will in reality respond differently to environmental stress than areas of natural levee deposition (Syvitski and Saito, 2007). Auerbach *et al.* (2015), for example, find that islands in the GBM delta that are enclosed by artificial embankments have lost between 1.0 – 1.5 m of elevation over the last half a century; compared to the neighbouring Sundarban mangrove forest which has remained relatively stable. In C-L however both artificial and natural levees are simply treated as grid cells of higher elevation and, furthermore, will exist in the same locations under all eleven scenarios.

As one might expect given prior analysis, by 50 years into the simulation there is a notable spatial resemblance between the identified channel MRUs under all 11 scenarios. At 30 years however more distinct patterns emerge. Most notably, lateral erosion is far more extensive under the scenarios where the rate of sea-level rise is high. The occurrence count of lateral erosion MRUs is 81.3 units for those scenarios where the rate of sea-level rise is high, compared to just 24.5 units for those where it is moderate or low. This difference predominantly arises in the lower reaches of the catchment where tidal and storm surge influence is greatest. Extensive lateral

erosion is also observed at 30 years for scenario 9DWDC; whereby there is a 1420% increase in the affected area compared to scenario 4DWD. This is likely not due to gradual changes in eustatic sea-level, but rather due to a higher frequency of short-term extreme events as a result of increased cyclone frequency. Large synoptic systems ranging in force from tropical lows to cyclones are the main cause of unusually large floods on the Indian Peninsular Rivers (Ramaswamy, 1987). By 50 years into the simulation however there is once again convergence between the group A and group B scenarios, with the effects of sea-level appearing to have a negligible effect. As discussed previously, scenarios 1WWW and 2DDD show remarkably similar results in terms of net sediment change and elevation change results; despite the stark contrast between the climatic drivers experienced in the two runs. Here however, as was also the case with the crevasse splay analysis, more distinct differences in the morphological response begin to emerge: At 30 years into the simulation the number of grid cells impacted by lateral erosion is 83.3% less in scenario 2DDD compared to the baseline TST; compared to 66.7% for scenario 1WWW. This is because lateral erosion is inhibited during periods of drought or more variable flow activity. Lateral erosion, also referred to in the literature as 'sweeping', has been found to be the primary control of channel migration in deltaic environments (Hudson and Kesel, 2000). It is therefore important that this process is able to be reliably simulated in C-L. As discussed in detail in chapter 3, the lateral erosion algorithm has been significantly improved in this most recent version of C-L by allowing the distribution of the eroded sediment across the channel, and thus preventing unnatural channel narrowing as a result of positive feedback (see Coulthard *et al.* 2013). The model also allows for differential rates of lateral erosion dependent on sediment cohesiveness and vegetation cover adjacent to the channel. Nonetheless it is important to consider that due to the relatively large grid size utilised in this study (90 m^2), only decadal trends in lateral erosion may be analysed here. Annual rates of bank erosion (commonly < 10 m per year) are not able to be captured unless this rate of erosion is sustained at a given location. The rate of lateral erosion is greatest on the outside of meander bends or where the highest flows are concentrated. High rates of lateral erosion are therefore also associated with an increased frequency of point bar formations and increased localised sinuosity (Black, 2018).

As discussed previously the extensive system of levees that exists across the delta plain, combined with the highly seasonal nature of flooding in the Mahanadi basin, restricts a majority of morphological activity in response to moderate floods within the channel itself (Kale, 2003). Subsequently there are more quantifiable differences in the distribution and frequency of channel MRUs between the different scenarios than there are for floodplain MRUs. The frequency of occurrence of mid-channel and point bar MRUs do not appear to show any notable split between the group A and group B scenarios. Instead, there appears to be a closer resemblance between those scenarios for which precipitation follows the 'DWD' trajectory; with scenarios TST, 4DWD, 7DWDH, 9DWDC and 10DWDF all experiencing a reduction in mid-channel bar formation between 30 and 50 years. This would imply that the development of mid-channel and point bar MRUs is more sensitive to shifts in seasonal precipitation variability – and therefore to seasonal river flows – than to other mechanistic drivers such as sea-level rise and cyclone frequency. This is reinforced by the fact that once again a more distinct difference appears between the contrasting scenarios 1WWW and 2DDD: the former seeing an increase in mid-channel bar formation of 3.9% and 12.5% at 30 and 50 years, respectively, when compared to baseline run TST. For scenario 2DDD, these values are considerably higher at 15.4% and 45.8%. A stark contrast remains between these scenarios during point-bar MRU analysis: under scenario 1WWW a decrease in point-bar formation of 6.3% and 14.3% is experienced at 30 and 50 years, respectively, when compared to baseline run TST. For scenario 2DDD, this reduction is much higher at 25.0% and 71.4%. This reduction experienced under scenario 2DDD is likely due to the fact that the rate of bed incision and lateral erosion is reduced under sustained low flow conditions, and thus the amount of sediment available to be deposited on the inside of meanders is also reduced. The rate of sea-level rise has very little impact on the occurrence of mid-channel and point bar MRUs. The only exception to this are scenarios 5DWA and 8DWAH; whereby a higher rate of sea-level rise occurs with a 700% increase in the number of point bar MRUs by 50 years into the simulation period. There is no clear answer as to why this might occur; however it could be suggested that the effects of a higher rate of sea-level rise, and therefore a greater tidal influence upon system dynamics, are likely to be amplified in a catchment where the fluvial influence has been significantly reduced by increasingly severe drought conditions (note that under these scenarios dry season precipitation

totals decrease at a linear rate, reaching -25% by the year 2075; see chapter 5 for full details). The spatial distribution of mid-channel bar MRUs remains fairly consistent across all scenarios, with the most significant development often occurring in the middle reaches at the point where the main channel bifurcates. The spatial distribution of point bar MRUs however is far more variable.

Next, the results of the metrics as utilised by Edmonds *et al.* (2011) are considered further. Channel density increased by 30 years into the simulation for all scenarios; with no clear distinction made between group A and group B, or indeed any other mechanistic driver. This is somewhat surprising given that previous studies have found an association between higher rates of relative sea-level rise and an increase in channel network fractality (Liang *et al.,* 2016). As has been apparent in previous analysis, it would seem that the greater variability observed over the initial 30 year period converges as the simulation reaches 50 years; with 9 of the eleven scenarios, including the baseline run TST, observing a value of D = 1.53. A similar distribution of NED values is also found across all scenarios in the Devi catchment throughout the simulation period; and indeed to those found by Edmonds *et al.* (2011). As discussed in chapter 5, this is likely related to an internal feedback mechanism which results in the channel network organising itself in such a way so as to maintain a spatially consistent average NED. Edmonds *et al.* propose that this is driven by an internal feedback mechanism, whereby areas with high NED receive less sediment over time, thus becoming topographic depressions. Depressions in the floodplain tend to attract channels, thereby reducing the NED. Areas with low NED will distribute water and sediment most efficiently, via a complex network of channels that tend to have a high frequency of small islands (Passalacqua *et al.* 2013). Numerous studies suggest that this self-organisation propagates across the entire delta system, so as to increase the number of sediment transport pathways to the shoreline (Tejedor *et al.,* 2017). In the Devi system, the middle reaches of the catchment demonstrate the lowest NED values across all scenarios. What is particularly interesting is that NED remains spatially consistent even for those scenarios in which sediment supply becomes increasingly variable. It is unclear as to whether this suggests that this an internal dynamic that is intrinsic to system functioning; or whether at this temporal scale of analysis (multidecadal) this magnitude of variability does not apply any significant stress upon the functioning of this feedback mechanism.

There is a clear dominance of smaller island sizes across all scenarios, with over half of islands in all model runs measuring ≤1 km^2 at 30 years into the simulation period. At 50 years into the simulation, between 87.8% and 96.5% of islands measured ≤5 km^2. This unimodal distribution is similar to that found by Edmonds *et al.* (2011), which would be expected in a morphologically active catchment such as the Devi where bifurcation is a dominant driver of change (Passalacqua *et al.* 2013). The development of an extensive network of floodplain channels under all scenarios is also responsible for this high frequency, as interdistributary islands are formed between the new channels that cut across the floodplain. At 30 years into the simulation group A scenarios produce fewer islands on average than group B (45.8 compared to 57.2, respectively). There is no singular forcing factor that appears to be driving this pattern. Once again by the end of the simulation period this contrast between the two groups has decreased; with group A scenarios actually producing a slightly higher number of islands on average than group B (59.2, compared to 55.7). This is likely due to the extensive lateral erosion experienced under many of the group B scenarios; as erosion rather than deposition dominates throughout much of the main channel. With the exception of scenario 6WDDH, those scenarios where total monsoon precipitation has remained at a baseline value or has increased demonstrate a higher island frequency than for those where it has declined. Traditionally deltaic islands have been thought of as somewhat of a secondary feature of the landscape, with the distributary channels themselves dominating the defined hydrological network and research base. Increasingly these features are being recognised as critical and active components of the delta CSES. Hiatt and Passalacqua (2015) argue that the quantification of environmental fluxes to, within and out of interdistributary islands is of significant importance to the understanding of the processes that shape the evolution of delta systems. In their study of interdistributary islands in the Wax Lake Delta, USA, the authors find that islands can slow the flux of water by as much as 300% compared to channels where islands are not present; with 23-54% of the water flux actually entering the island itself. They also highlight how interdistributary islands that receive little flux of water and sediment from major channels, tidal forces and even the wind can exert significant effects on flow dynamics of surface water and minor channels across the island surface. Mid-channel islands (or bars) are amongst the most mobile features of the deltaic landscape. As will be discussed further in

chapter 7, the succession of vegetation on new island areas is an important factor effecting the stability of these island areas. Equally changes in land-use and vegetation cover within the catchment can have a significant impact on island formation. Godoy and Lacerda (2014), for example, found that a large increase in the area of land converted to plantations in the Jaguaribe River basin, Brazil, resulted in an additional 282,322 $t.yr^{-1}$ of sediment reaching the estuary. As discussed in chapter 2, this resulted in an increase of 24.15 ha in the area of islands in the channel between 1988 and 2010, and a subsequent increase in the area of mangrove vegetation colonising these depositional landforms.

Next we compare the morphological response of the Devi catchment with that of the Mahanadi, under the baseline scenario, TST; and the most likely meteorological scenario, 4DWD. As discussed in section 4.2, a catchment-based approach presents several methodological advantages, as well as logistical benefits from a governance perspective, over undertaking a study at the delta system level. One of these advantages is that such an approach permits the comparison between regions of the same delta that are dominated by differing morphological processes. Both catchments in this study receive the same sediment and water supply at their apex, and also experience identical climatic conditions at the multidecadal scale. The Mahanadi catchment however is approximately 58% larger than the Devi, and has also become increasingly morphologically inactive over recent decades compared to the Devi River channel. The Mahanadi catchment is also more greatly affected by coastal processes; with significant erosion at the mouth near to the town of Paradip (see chapter 4).

Figure 6.36 shows net sediment change under the two scenarios in both catchments. During the first 10 years of the simulation the catchments follow divergent trajectories under both scenarios, with the Mahanadi experiencing a substantial loss of sediment. By 30 years into the simulation period a net gain in sediment is observed under both scenarios for both catchments. This gain is greater in the Mahanadi however: at 6.24E+07 m^3 (compared to 9.03E+06 m^3 in the Devi catchment) under scenario TST; and 5.85E+07 m^3 (compared to 9.86E+06 m^3 in the Devi catchment) under scenario 4DWD. This is likely due to the larger size of the Mahanadi catchment and in particular the more extensive floodplain which acts as a sink for sediment. It is at 40 years that the greatest range is observed between

the different responses within the individual catchment. By 50 years into the simulation period these responses once again converge between scenarios TST and 4DWD.

The contrast between the catchments at this stage however is significant: There is a rapid net gain of sediment across the Mahanadi catchment under both scenarios, providing a contrast with the results seen for the Devi for all eleven scenarios. Spatial analysis of elevation data combined with the identification of MRUs within the Mahanadi catchment shows that the primary reason for the substantial difference is due to widespread accretion, or rather infilling, across a majority of ephemeral channels on the floodplain. This point in the simulation therefore appears to capture a critical stage in the evolution of the Mahanadi catchment: where sediment supply is still sufficient that this widespread accretion can take place, although not sufficient enough to increase the height of the floodplain itself. As these channels become shallower and increasingly disconnected from the main channel of the Mahanadi River, fluvial input (and therefore sediment flux) to the floodplain will be gradually reduced. Eventually this can lead to a total elimination of sediment to this region of the distributary network, causing an abandonment of the delta lobe (Roberts, 1997). It is difficult to project an exact point in time at which this abandonment could take place, given that the process can occur over decadal to millennial timescales, and furthermore is significantly influenced by human intervention (Milliman *et al.,* 2008). In coastal regions of the floodplain, marine processes will play an increasingly dominant role in reworking the abandoned lobe once this fluvial input is reduced. Neinhuis *et al.* (2013) discuss how shoreline geometry and wave climate at the point of abandonment can be a good predictor of the 'abandonment mode'. They identify four distinct modes of marine working of abandoned deltaic lobes providing a quantitative framework with which to analyse this process. Currently it would not be possible to fully simulate these processes in C-L given that waves are not able to be included as a driver; however this would make a fascinating avenue for further study.

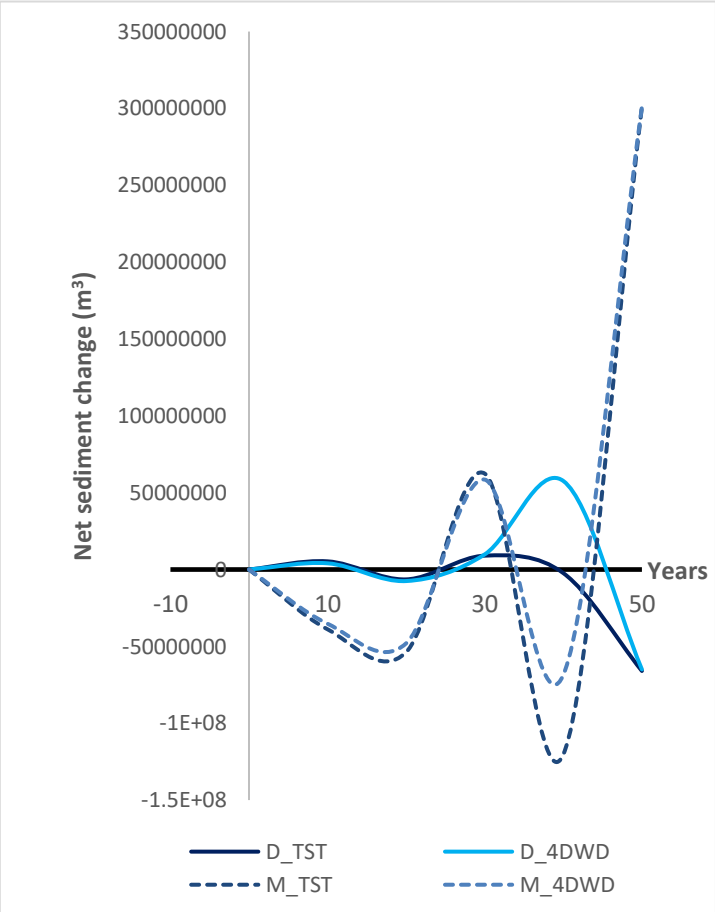

Figure 6.36 Net sediment change under scenarios TST and 4DWD; Devi and Mahanadi catchments. The dotted lines represent the morphological response of the Mahanadi catchment.

Whilst the widespread infilling of ephemeral channels across the floodplain may suggest that the Mahanadi catchment is indeed becoming increasingly disconnected from the primary river channels, there are still significant changes taking place within the main channel itself. Under scenario TST, for example, a large crevasse splay is formed approximately 10 km upstream of the mouth, at the point where two major bifurcations of the Mahanadi River remerge. Between 30 and 50 years into the simulation period a channel system develops and extends across this splay feature, eventually connecting these two bifurcations at a new location (figure 6.37). Widespread levee formation occurs along a majority of the Mahanadi channel and its bifurcations. This contrasts with the same two scenarios in the Devi

catchment, where at 50 years into the simulation period levee development is inhibited in the lower catchment due to extensive lateral erosion. This could be due to the fact that as a greater proportion of floodplain channels become shallower or disconnected in the Mahanadi catchment, peak flows are less able to be distributed evenly across the catchment. Subsequently the flow becomes more restricted to the primary river channels, meaning flood levels in these channels will be higher, therefore enabling the overbank deposition to take place in order to increase the height of the levee network.

One of the greatest contrasts between scenarios TST and 4DWD in the Mahanadi catchment is the distribution and frequency of lateral erosion and mid-channel bar MRUs. By 50 years into the simulation under scenario TST there is extensive lateral erosion in the lower reaches of the catchment, and in the northern bifurcation of the main Mahanadi channel. In some areas up to 180 m of floodplain has been eroded; thus implying an average rate of lateral erosion of 3.6 m per year in these locations. From the perspective of policy makers, it would be useful to confirm a more reliable annual rate of erosion by re-running the simulation in these potentially vulnerable locations utilising a higher resolution DEM model. As was observed in figure 6.30, this widening of the channel occurs predominantly before areas of significant mid-channel bar formation. This could suggest that the material eroded from the banks is being redeposited as island features further downstream. What is unusual about these mid-channel bars is that in several locations these areas of deposition have spread across the entire width of the channel; thus acting to dam the river. This is likely the cause of the net deficit of sediment observed under this scenario in the lower reaches of the Mahanadi catchment. Such a response is not observed under any scenario in the Devi catchment; perhaps again supporting the fact that the Mahanadi catchment is potentially moving towards a trajectory whereby fluvial forces play an increasingly less dominant role in determining the morphological evolution of the catchment. It is also interesting that this unusual response occurs under the baseline scenario TST, rather than under increasing conditions of climatic stress. It would be useful to explore further the impacts of the remaining nine scenarios in the Mahanadi catchment, in order to better understand the possible trajectories that this system may follow over forthcoming decades.

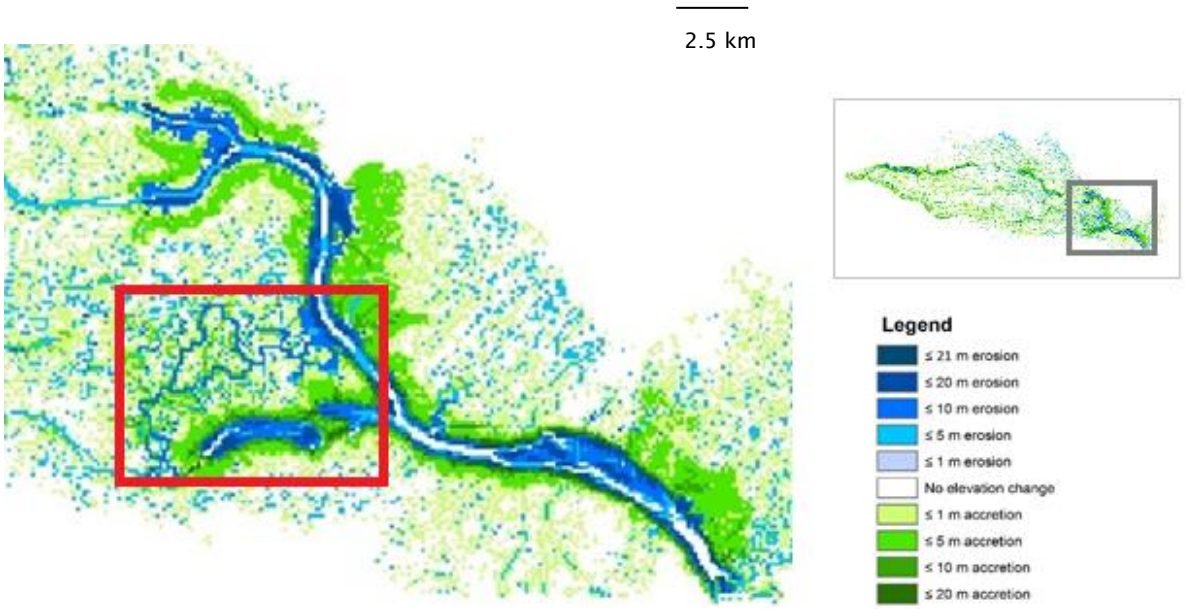

Figure 6.37 A new channel system develops between 30 and 50 years under scenario TST, thereby connecting two bifurcations of the main Mahanadi channel (highlighted in red).

The fractal box-counting dimension value (D) decreased by 0.04 at 30 years into the simulation period under scenario TST in the Mahanadi catchment; providing a contrast to the Devi where D increased by 0.05. As suggested by Edmonds *et al.* (2011) this is indicative of the rate of channel bifurcation decreasing in the Mahanadi catchment, as would be expected in an older or less active system. By 50 years into the simulation D then increases by 0.11 to a value of 1.55. However, this value is likely reflective of the widespread accretion occurring in the ephemeral floodplain, as opposed to a true increase in channel density. Under scenario 4DWD in the Mahanadi catchment channel density only increased by 0.01 over the entire simulation period, compared to an increase of 0.07 in the Devi catchment. Given that the most significant changes in elevation change and MRU distribution occurred under the baseline scenario TST in the Mahanadi catchment, it is not surprising that the same can also be said for this metric. Both catchments share a similar unimodal distribution of island sizes; though there is a slightly higher proportion of larger islands in the Mahanadi catchment compared to the Devi. This is due to larger areas of land located between bifurcations of the main channel, as opposed to a significant difference in the size of mid-channel bar formations. We

also find a similar distribution of NED values in the Mahanadi catchment to those observed in the Devi; with two peaks at values of ~0.05 and ~ 0.2, and very little change observed over the entire simulation period. This reinforces further the theory of Edmonds *et al.* (2011) that this factor is controlled by an internal feedback mechanism within the wider delta system.

Whilst this discussion reveals a lot about the multidecadal behaviour of the morphological system, several questions are also raised: Firstly, are these catchment systems limited to a set number of morphological trajectories (within the timeframes applied in this study)? Whilst there are of course significant differences in the localised morphological response for all scenarios, why is it that eleven sets of such contrasting climatic and environmental conditions result in just two broad categories of evolutionary pathway in the Devi catchment? After all, in such a complex system one might expect an equally complex set of responses. However it is important to remember that morphological change is not purely driven by the external forcings explored in this study. As discussed in detail in chapter 2, external drivers that are not able to be fully integrated into the C-L model - such as waves; spatially variable subsidence; and land cover changes – all have a significant impact upon the system. Similarly, it is difficult to fully quantify the complex internal dynamics and autogenic variability that leads to the development of the emergent features and processes explored in this research (Liang *et al.,* 2016).

Secondly, if there is indeed a limited number of multidecadal evolutionary pathways operating in the Mahanadi system, how do these trajectories continue to develop over the remainder of the 21st century? In the Devi catchment the various metrics analysed in group A and group B scenarios appear to converge by the end of the simulation period. Likewise in the Mahanadi catchment, the contrasting scenarios TST and 4DWD also follow similar trajectories in terms of net sediment fluxes. Would this convergence continue over the forthcoming decades as the system moves towards a new state altogether; or would an increasing contrast develop between the differing scenarios? In truth these questions cannot be addressed from this study alone, as further extended modelling would be required. The only scenario to undergo an extended simulation was 10DWDF; whereby monsoon precipitation becomes increasingly variable and reduced, until it eventually fails between 50 and 60 years. Results from this extended run

demonstrate very little change in terms of the spatial patterns of sediment loss and elevation change experienced in this final decade. However as shown in figure C.30, there is no further scouring or lateral erosion across much of the main river channel due to the significant reduction in annual water inflow. As seen in figure 6.35, net sediment change in the Devi catchment actually starts to increase under this scenario in the final 10 year period; although as was the case in the Mahanadi catchment, this could be indicative of infilling of ephemeral channels as opposed to progradation of the floodplain area. It is difficult to say, however, whether this would also be the case for the other scenarios, given the short time period over which this change occurs. Whilst the C-L model is entirely capable of operating over much longer timescales than those applied in this study (Coulthard *et al*., 2012), it also must be considered, in moving toward centennial-scale modelling in an attempt to address these issues, that there is far greater uncertainty in terms of the range of climatic stressors we could potentially observe in the Mahanadi region. The relevance of these outputs to stakeholders in the Mahanadi region therefore, may be significantly reduced.

Another area requiring further exploration is to better understand what might be driving the observed convergence of the quantified metrics at the end of the simulation period; particularly given that at this point the differences in the climatic and environmental conditions experienced under each scenario are at their greatest possible range. This result be indicative of equifinality within the CSES, where an end state can be reached by two or more different means. Beven and Freer (2001) discuss how equifinality may be endemic to mechanistic modelling of CSES in that there are many different model structures and parameter sets that may reproduce the same observed behaviour within the system. What is difficult to segregate is whether this equifinality is the result of the way in which these parameters are represented in morphological models, or whether the differences in the set-up of the chosen climatic and environmental drivers do actually have relatively little impact on the functioning of the system over the chosen temporal and spatial scales.

Finally, in order to carry out the additional morphological modelling required to explore the questions above, further validation of the setup of the model in both catchments would be necessary. As presented in section 5.3, 30 years of historical

data (1974-2004) was utilised to validate the setup of the C-L model prior to scenario testing. LANDSAT images from the years 1973 and 2003 showed that the pattern of accretion and erosion, and the rate of change in a 2D plain, lied within the expected range for the Mahanadi system: Channel width varied by a maximum of 0.09 km over the validation period in both catchments and C-L successfully reproduced the correct locations of channel narrowing in the model domain. Most islands remained stationary over the 30 year period, but fluctuated in width and length. This was also reflective of the patterns observed in LANDSAT images. Changes in the fractal dimension, the distribution of island sizes and nearest-edge distance over the 30 year period were also compared with the results of Edmonds *et al.* (2011), who demonstrated the application of these metrics to a broad range of both real and theoretical deltas. The distributions found in validation also matched satisfactorily with their results. However, the results presented in this chapter would suggest that the overall magnitude of adjustment experienced over the simulation period is larger than what might be considered the expected range for the Mahanadi Delta system. Therefore, some attempt of validation of the rate of morphological change in the 3D domain is recommended; although there is limited data available with which to permit this avenue of study.

One output that could have been utilised further in model validation is the total sediment delivered to the catchment outlet. Whilst the sediment discharge values used as inputs were based upon historical data (mean calculated annual Q_s = 13.95 MT, see section 5.2) the amount of sediment delivered at the outlet across all scenarios is consistently high when compared to observed historical values: A mean sediment discharge of 39.81 MT per year is recorded at the outlet of the Devi catchment over the 50 year simulation of scenario TST; whilst the maximum discharge observed for any given year across all scenarios is 62.28 MT. Observed long-term average annual sediment discharge values for the Mahanadi Delta system include: 30.1 MT (Chakrapani and Subramanian, 1990); 60 MT (Milliman and Syvitski, 1992 in Dunn *et al.,* 2018); 15.74 MT (Chakrapani and Subramanian, 1993); 15.1 MT (Gupta *et al.,* 2012); 12±5 MT (Bastia and Equeenuddin, 2016). There is also a consensus that the sediment discharge of the Mahanadi River system has decreased significantly since the late 20th Century as a result of human intervention across the basin (Syvtiski *et al.* 2009; Bastia and Equeenuddin, 2016; see discussion in section 4.3). Whilst there is considerable variation amongst the

sediment discharge values cited in the literature (partially as a product of contrasting definitions of the boundaries of the delta and differing study periods) it is clear that the consistently high sediment yields observed in this study require revalidation. This is particularly notable given that the discharge in this study is of course measured at the outlet of a single catchment, whereas the observations cited above consider the outputs of the four major watersheds that span the Mahanadi Delta system. Upon reflection, decreasing the daily input data obtained from Tikarapara gauging station may have been required to account for this. An alternative approach to explore could also be to generate idealised flow scenarios based upon total seasonal sediment delivery, as opposed to directly utilising the observed daily values. This would still permit the user to run scenarios in which daily precipitation variability decreases or increases as desired, but would smooth out the most extreme fluctuations registered upstream of the catchment apex, that in reality would have been spread out across all four watersheds.

Correspondingly the total net sediment excavation values as shown in tables 6.1 and 6.4, are also considerably higher than what might be expected. In the Devi catchment at 50 years into the simulation the observed net sediment excavation values lie between 6.50E+07 m^3 (scenario 4DWD) and 2.75E+08 m^3 (scenario 5DWA); equivalent to a loss of 0.0023 MT per km^2 per year and 0.0097 MT per km^2 per year, respectively. Conversely, in the Mahanadi catchment a net accretion of 0.0068 MT per year per km^2 is observed under both scenarios TST and 4DWD after 50 years. Bastia and Equeenuddin (2016), however, calculate the mean erosional rate of the Mahanadi River to be 0.00027±0.00013 MT per km^2 per year between 1980 and 2010. Given the similarity between their study period and the baseline period utilised in this research (1974-2004), these results would again suggest that the current setup of the C-L model may be causing an overestimation of the rate of morphological change across all scenarios. Soil erosion rates may also provide an additional means of validation in a delta with limited data availability. Mishra and Das (2017) estimate the soil erosion rate in coastal regions of the southern Mahanadi Delta to be 0.0039 MT per km^2 per year; and thus of a more similar magnitude to the sediment excavation rates found in this study. In fact the authors find the soil erosion rate across the southern deltaic plain as a whole (including the Devi catchment) to be 0.0835 MT per km^2 per year; notably higher than any result found here. This latter estimate however also includes the hills of the Eastern Ghats

for which slope is considerably higher and thus the erosion rate will also increase. These results were calculated utilising the Universal Soil Loss Equation (USLE) (Wischmeier and Smith, 1978) and therefore cannot be utilised as a direct comparison given that erosion from fluvial processes is not considered. However, given that the factors incorporated in the USLE do include precipitation, slope and soil type, there are some crossovers with the data utilised to generate the inputs for this study, and thus it is useful to consider.

Incision was evident throughout the main channel across all scenarios; with a majority of the channel in both catchments scouring to a depth of 9 m by 30 years, and 10 m by 50 years. The rate of incision was therefore significantly higher in the early stages of the simulation, whereas in the latter stages lateral erosion becomes a far more dominant process. This initial rapid incision has been observed in other large delta systems where the natural sediment load has been decreased due to human intervention: Lu *et al.* (2007), for example, report a maximum incision rate of > 1 m per year in the lower Pearl River Delta in China following significant sediment depletion in the 1990s. It has also been noted by Hancock *et al.* (2017) that C-L has produced 'aggressive' denudation rates in the early stages of their simulations, investigating the morphological impacts of precipitation variability on a post-mining landscape. Nonetheless given that the incision rate follows a similar pattern across all scenarios regardless of sediment input, the rather sudden transition from vertical to lateral erosion as the depth of incision approaches 10 m would strongly suggest that the bedrock parameter file is the dominant driver resulting in this new morphological regime. In turn this will also have a significant impact upon the development of both channel and floodplain MRUs in the latter stages of the simulation, and indeed the total net sediment loss overall. In C-L bedrock is a layer below which erosion and slope processes cannot occur. As described in Appendix A, in the Mahanadi Delta the depth of the bedrock varies from 1 m to 20 m, but due to a lack of spatial data a homogenous value of 10 m was applied across both catchments. This issue was initially not detected during validation due to the fact that bedrock depth did not become a limiting factor until after the end of the initial 30 year test period. Despite a lack of data from the Mahanadi region, it would be beneficial to explore the morphological impacts of spatially variable bedrock depths, perhaps utilising data from another delta of similar geology.

Sedimentation rates also provide a means of verifying the observed magnitudes of morphological change in the studied catchments. Chakrapani and Subramanian (1993) find sedimentation rates of 5.08-20.39 mm per year in the Mahanadi Delta; over a 50 year period as simulated in this study this would be equivalent to between 0.61 and 1.02 m of accretion. In the Devi catchment under scenario TST, 30.34% of grid cells that underwent elevation change gained ≤ 1 m of sediment; accounting for 47.55% of accreting cells or 2.58% the catchment area. In the Mahanadi catchment under the same scenario, 55.24% of grid cells that underwent elevation change gained ≤ 1 m of sediment; accounting for or 74.47% of accreting cells or 25.45% of the catchment area. Given the likely overestimation of total net sediment excavation discussed above, it would appear that the rate of accretion across a majority of the floodplain is generally more in line with observed values; but once again there is very limited data available to assess this with high certainty. Across all scenarios, localised extreme elevation gains of up to 23 m were observed in both catchments. As discussed earlier in this chapter, this occurs across a very small number of cells (< 0.01% of catchment area) at locations where a new levee has been deposited into a cell that was once part of the active channel.

It is worth noting of course that whilst sense checking the outputs of this study is an integral part of critical analysis there is an element of circularity here; given that the available datasets with which to compare these results are in themselves subject to large uncertainties and are fairly limited. Nonetheless the issues discussed here highlight some of the challenges of setting up a flow routing model in a deltaic environment. The complex nature of flows in low-lying distributary channels, backwater effects, and the interaction of fluvial and marine processes, all contribute to this. As discussed by Liang *et al.* (2015), whilst C-L has demonstrated good performance in low-gradient environments, the authors suggest that certain parameters would likely need to be modified to account for flow characteristics of deltaic systems; particularly those with a dominant marine influence. Whilst it is clear that some further validation of the setup of the model would be necessary in order to better assess the magnitude of the physical processes observed in this study, the results nevertheless provide a valuable insight into the relative trajectories of the nature of morphological change under various climatic scenarios. Most importantly to the aims of this research, the results also provide a suite of metrics that can be utilised by stakeholders not just in the

Mahanadi system, but indeed in other deltaic environments. As presented in chapter 3, C-L is an ideal tool with which to tackle the broader spatial and temporal challenges associated with modelling CSESs; and this has proven to be the case given the successful development of this methodological framework. Despite this accomplishment, further validation of the model to increase the reliability of the morphological projections is something that would render the framework an even more useful tool.

The outputs discussed in this chapter provide the foundation for the remaining part of the methodological framework. This latter component of the research aims to explore what the morphological behaviour within the delta system can help us to understand about biophysical vulnerability in the Mahanadi region. It is evident, for example, how the Mahanadi catchment may respond very differently to the Devi catchment under the same climatic conditions. However what has not been explored is whether this makes one catchment any more vulnerable to environmental stress: does a slower rate of morphological change in a less active region 'buy more time'; or rather does it indicate a decline in the health of the morphological system which will become less resilient to climatic pressures? Tejedor *et al.* (2015) suggest that metrics such as those explored in this study can be utilised to explore biophysical vulnerability; in that optimal configurations (i.e. a high diversity of sediment transport pathways across the plain to the shoreline) enhance the dampening of perturbations to the CSES. In the next chapter, I attempt to address these issues in further detail focusing on the most likely climate pathway scenario, 4DWD.

Chapter 7 **Linking Morphology and Habitability**

7.1 Introduction

In the final stage of this study three additional short investigations are undertaken to explore how the analysis of morphological behaviour can help better understand how biophysical vulnerability in the delta may change under increasing conditions of climatic stress. As discussed in detail in section 3.1.4, given that the term vulnerability can encompass such a wide variety of factors it is important to define how it will be quantified in this study: Here the capacity of the catchment system to meet the needs of those living in the region is assessed. Vulnerability in any given area is deemed to increase as the rate and magnitude of biophysical change increases in such a way as to reduce the capacity for basic habitable needs to be met. Specifically the aim is to provide categorical measures of vulnerability for two key biophysical stressors under scenario 4DWD; designed to represent the most likely climatic pathway (see chapter 5). As will be seen in sections 7.2 and 7.3, these categorical measures are applied over gridded areas of 5 km^2 for each catchment. This relatively coarse resolution was selected as it was felt it provided an efficient means of comparison between the different stressors and catchments. Furthermore this is an appropriate scale for policy makers given that it ensures most minor-moderate size settlements are able to be included in one cell. Firstly, the extent to which morphological change influences inundation of the catchment to an extreme flood event is investigated. Next, I explore the possible impacts to habitat cover under this scenario. In addition, I also demonstrate the use of the C-L model to explore potential engineering strategies that could be applied in the region in order to reduce these impacts.

These three exploratory investigations are not meant to be a substitute to a more detailed, more accurate risk assessment for a specific site. This is particularly pertinent given the need for further validation of the model in terms of the magnitude of morphological change experienced, as discussed in detail at the end of section 6.2. As such, the results presented in this chapter should be interpreted as relative as opposed to absolute values. Rather, the aim is to explore what the morphological metrics analysed in the previous chapter can tell us about areas that

may be at greater risk under scenario 4DWD, and which are more resilient. More crucially, this section therefore provides a worked example of how these morphological outputs could be utilised to develop a vulnerability index. Together with the metrics applied in chapter 6, this provides a novel framework of tools that could directly contribute towards the development of climate adaption strategies in the Mahanadi region. This therefore also addresses the final research objective of this study: to provide outputs that are directly useful to stakeholders. However, the design of these tools is such that they could easily be adapted for application in other deltaic regions.

7.2 Flood hazard following a severe cyclone event

The Mahanadi Delta has regularly been highlighted in recent research as being at increased risk from flooding due to shifts in seasonal precipitation variability and anthropogenic interventions; both within its distributary network and also across the wider Mahanadi basin (Syvitski *et al.,* 2009; Jena *et al.,* 2014; Gosain *et al.,* 2006). As discussed in chapter 4, the average discharge of the Mahanadi River is 2,119 $m^3.s^{-1}$, with flooding typically occurring when discharge at the mouth exceeds 17,150 $m^3.s^{-1}$ (Mohanti and Swain, 2011). In developed areas protected by flood embankments, flooding typically occurs when the discharge exceeds 26,900 $m^3.s^{-1}$ (Khatua and Mahakul, 1999). Many argue, however, that whilst such embankments offer short-term protection against a majority of moderate floods, the restriction such levee features impose on natural morphological processes can actually act to reduce resilience to flooding over the long-term (Chhortray and Few, 2012; D'Souza, 2002). Furthermore, as discharge at the delta apex can exceed 45,000 $m^3.s^{-1}$ during the most extreme floods, these artificial levee structures are often breached; acting to concentrate flows onto relatively small areas of the floodplain. As discussed in chapter 4, both the magnitude and frequency of flood events have increased in the Mahanadi Delta, particularly during the peak monsoon season (June – September). Flooding has occurred more times in the last decade than in any other on record, with a reduced return period between extreme events (Pearce, 2014). Five of these floods have been caused by extreme rainfall events not within the delta itself, but rather concentrated in the middle reaches of the Mahanadi basin upstream (Jena *et al*., 2014). Distributary channels in coastal areas are less easily-flooded during high flows due to the opposing non-linear interactions between river discharge and the tide (Hoitink *et al.,* 2017). However, coastal regions of the delta do generally experience the most regular flood events due to the combined impacts of fluvial and marine stressors (Panda *et al.,* 2013; Beura, 2015). During a tropical cyclone or severe storm there are often two waves of flooding in coastal areas: the first associated with the storm surge that occurs during the event; and the second often occurring several days later when peak fluvial flows reach these lowest reaches of the basin. Thus whilst the height of flood waters in coastal regions may not always be as significant as in the upper and middle reaches of the delta plain, the extent of

the inundation in these low-lying areas, combined with increased salinisation and the staggered effect of secondary flooding, means that coastal regions often suffer the worst impacts of flood events.

Here I investigate the relationship between morphology and habitability within the context of an extreme flood event under the scenario 4DWD. Two additional 1 year model runs are undertaken in both the Devi and Mahanadi catchments: firstly utilising the original baseline DEM for the catchment (i.e. 0 years into the simulation); and secondly using the DEM generated after a full run of scenario 4DWD (50 years into the simulation). During this time the hydrological and tidal parameters representing those experienced between 15 November 1998 and 14 November 1999 are input into C-L; thus including the 1999 Odisha cyclone at the end of the simulation period. As discussed in chapter 4, On 29 October 1999 Cyclone 05B made landfall in the Mahanadi Delta with peak wind speeds exceeding 260 $km.hr^{-1}$; the most powerful storm recorded in the northern Indian Ocean (Panigrahi, 2003). As a result of the storm, coastal districts were submerged by a 7 metre storm surge that extended up to 20 km inland (Khatua and Dash, 2013).The decision was made to include the year before the event in order to capture more accurately the preceding hydrological conditions. Water depth outputs were then extracted at daily intervals; allowing the comparison of inundation extent if the same event were to happen in the present day delta, or in the simulated delta at 50 years under scenario 4DWD. Figure 7.1 shows water depth at the end of the 1 year extended simulation period using the 0 year and 50 year DEM for the Devi catchment. Figure 7.2 shows the same results for the Mahanadi catchment. Figures 7.3 and 7.4 show floodplain inundation depths for the Devi and Mahanadi catchments, respectively (where water in channels is removed). As discussed earlier in this chapter, the following results should be interpreted in terms of relative vulnerability as opposed to absolute risk.

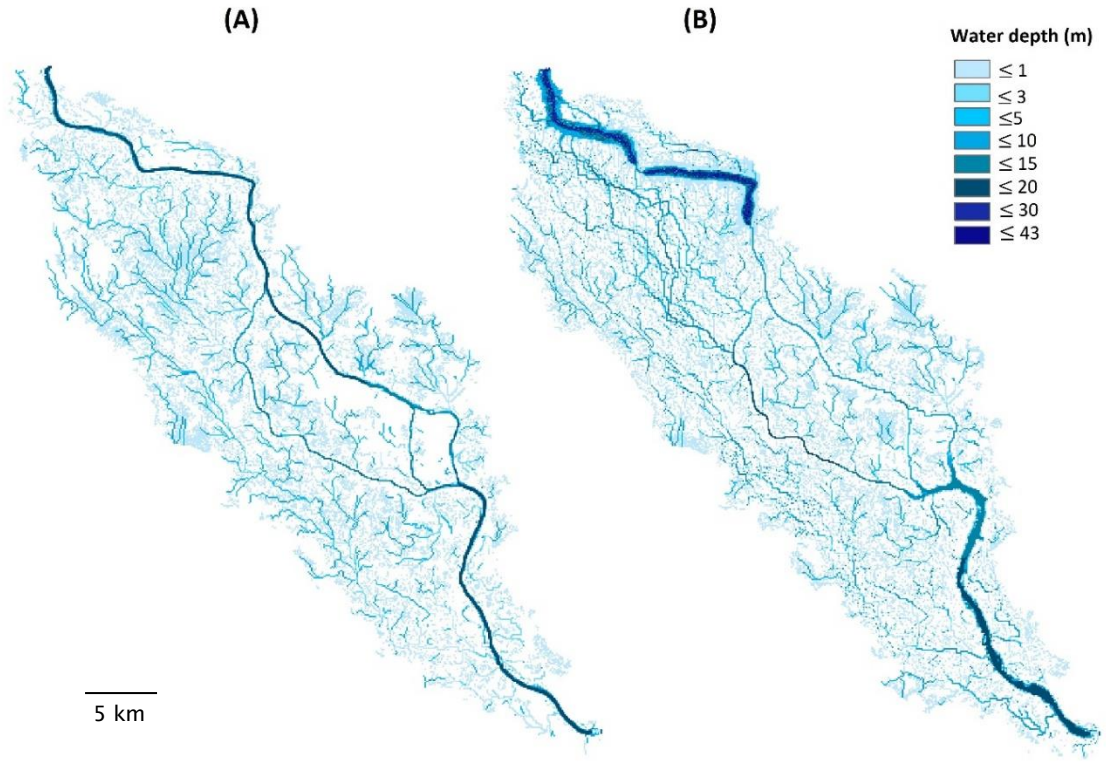

Figure 7.1Water depth following the extended flood simulation run utilising the (A) baseline (0 year) DEM and (B) the 4DWD 50 year DEM; Devi catchment.

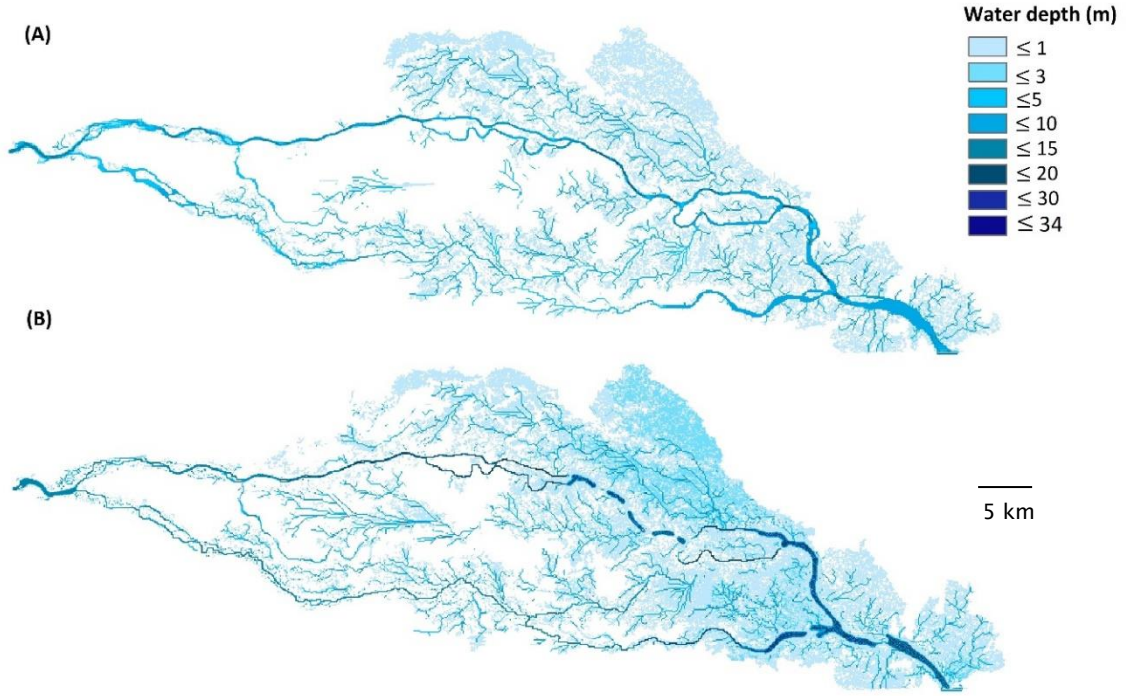

Figure 7.2 Water depth following the extended flood simulation run utilising the (A) baseline (0 year) DEM and (B) the 4DWD 50 year DEM; Mahanadi catchment.

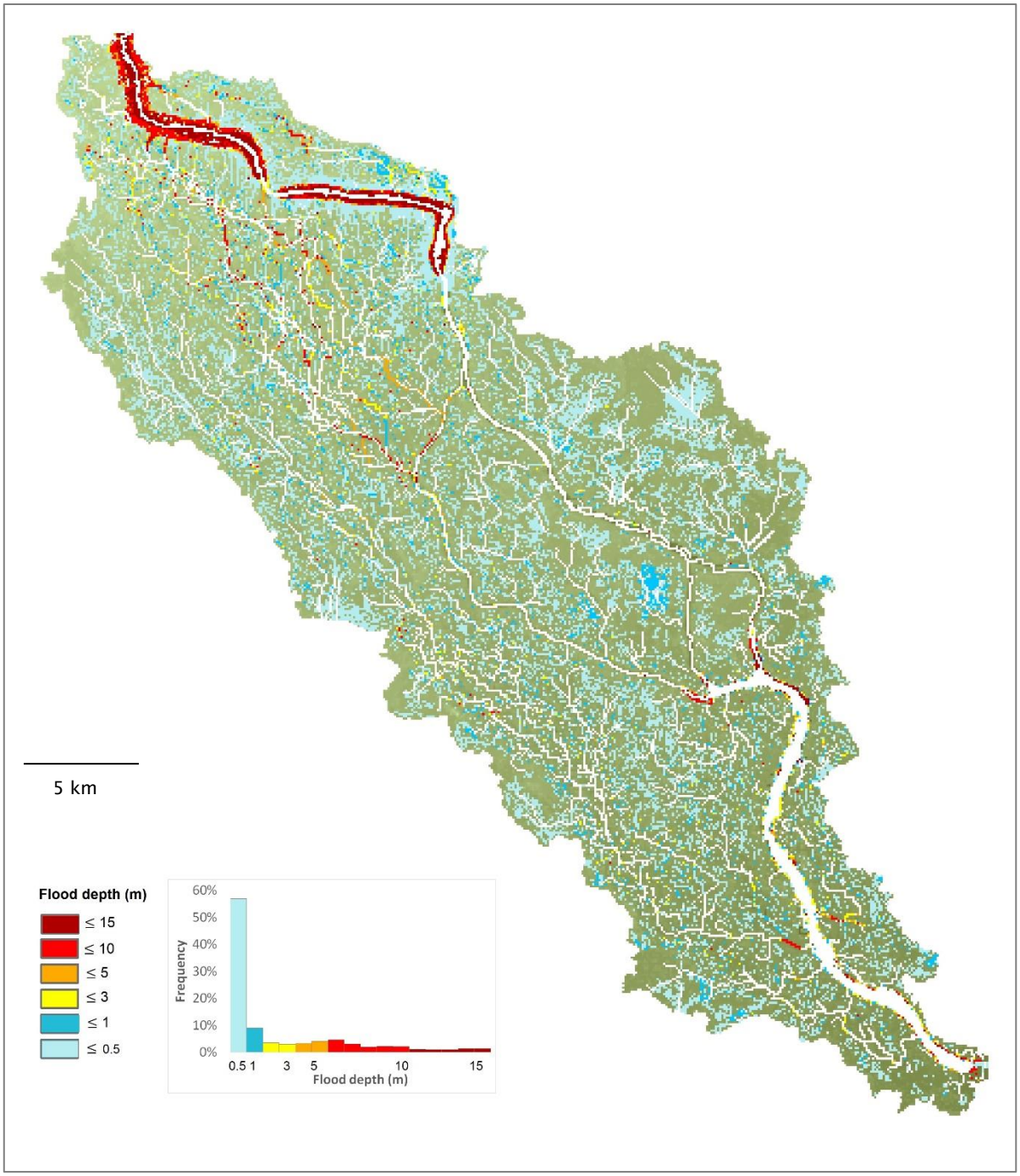

Figure 7.3 Floodplain inundation depth at the end of the one year extended simulation period (utilising the 4DWD 50 year DEM); Devi catchment. The inset graph shows the frequency distribution of flood depth values

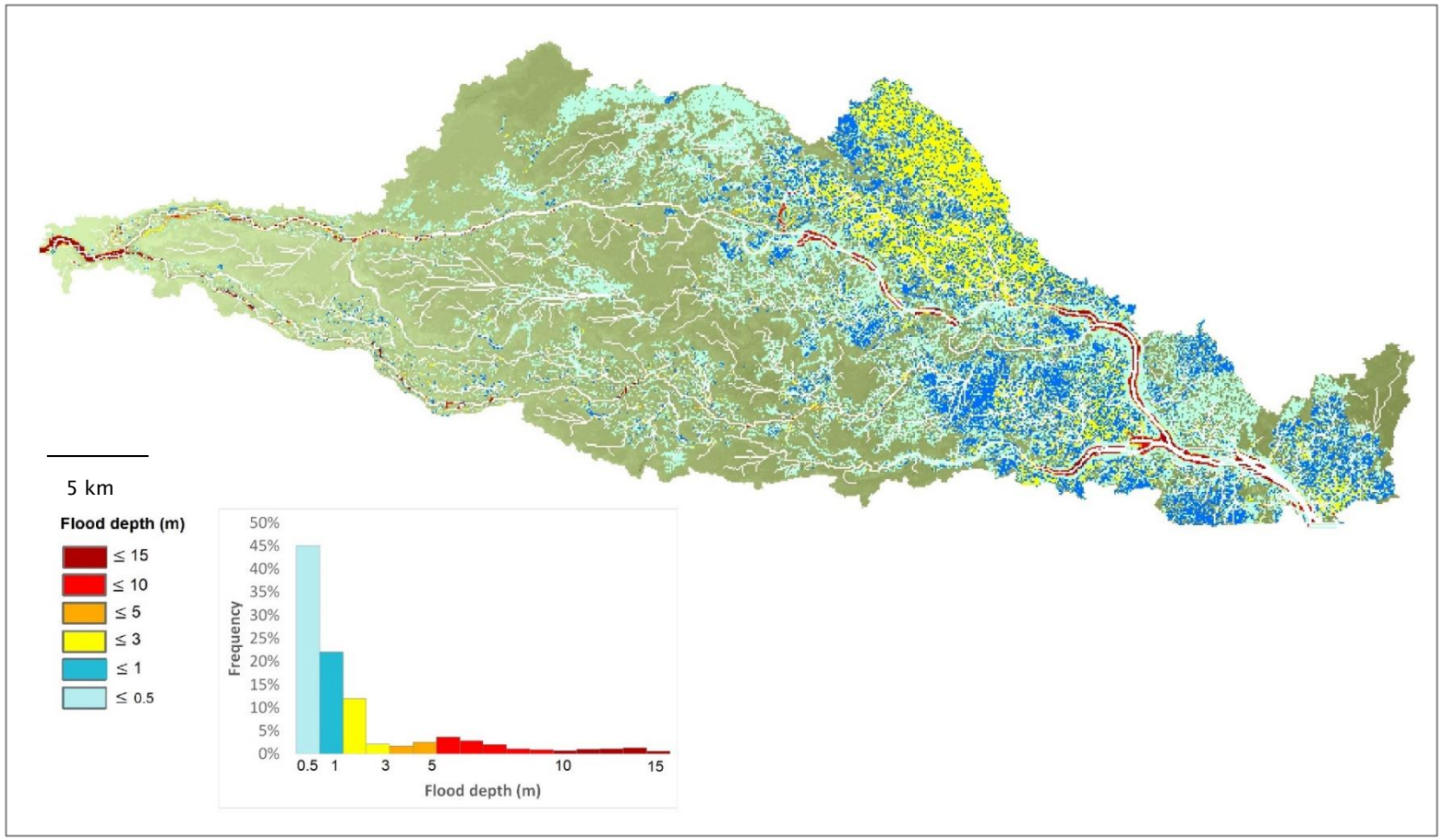

Figure 7.4 Floodplain inundation depth at the end of the one year extended simulation period (utilising the 4DWD 50 year DEM); Mahanadi catchment. The inset graph shows the frequency distribution of flood depth values.

An increase in the area flooded following the cyclone event is observed in both catchments as a result of the morphological changes simulated under scenario 4DWD. In the Devi catchment, the area flooded utilising the 50 year 4DWD DEM increases by 8.1% when compared to the present-day delta. This increase is concentrated in the upper reaches of the catchment, particularly adjacent to the main Devi River channel where the highest flood levels are observed. As highlighted in figure 7.5, these extreme levels (10 ≤ 15 m) occur in areas where much of the existing levee network has been eroded; thus resulting in a local increase in channel width. Figure 7.5 also shows that these extreme flood levels are drastically reduced at the point where levee accretion begins, approximately 30 km downstream of the apex; as also shown in MRU analysis in section 6.1.

In the Mahanadi catchment a larger increase in the flooded area is observed, at 19.6%. Much of this increase is spread more evenly throughout the middle and lower reaches of the catchment; this is where prior morphological analysis showed accretion across a majority of ephemeral channels on the floodplain (as discussed in section 6.2). Channel depth in many of these floodplain channels decreased by between 1 and 5 m, thus significantly reducing the overall capacity of the distributary network during high flow events. Coastal regions in particular are more significantly inundated in the Mahanadi catchment. This is to be expected given that the outflow of the simulated Mahanadi catchment terminates at the open coast; whereas the outflow of the Devi catchment terminates into an estuary located approximately 15 km upstream of the shoreline. The Mahanadi catchment is therefore more vulnerable to tidal flooding during cyclonic events. Extreme flood levels of up to 15 m are also observed in the initial 10 km of the main Mahanadi channel (figure 7.4). Conversely to the Devi catchment, this area is dominated by the widespread development of levees, with levee height increasing by between 1 and 5 m over the 50 year simulation period. One factor that must therefore be considered is whether these extreme flood levels in the uppermost reaches of the catchment could be partly caused by a parameter effect. As described in chapter 5 the inflow of water into the catchment is divided over two grid cells as opposed to one in order to prevent excessive scouring in the upper reaches. Prior analysis suggests that this set-up is effective at reducing this effect, however the pulse of water entering the catchment during such a large flood event is still significant. It

should also be considered that whilst the relatively large grid cell size (90 m^2) utilised in these projections may be suitable for analysing multidecadal change at the catchment scale, a smaller grid cell size would likely be more appropriate at projecting flood risk over annual or event scales.

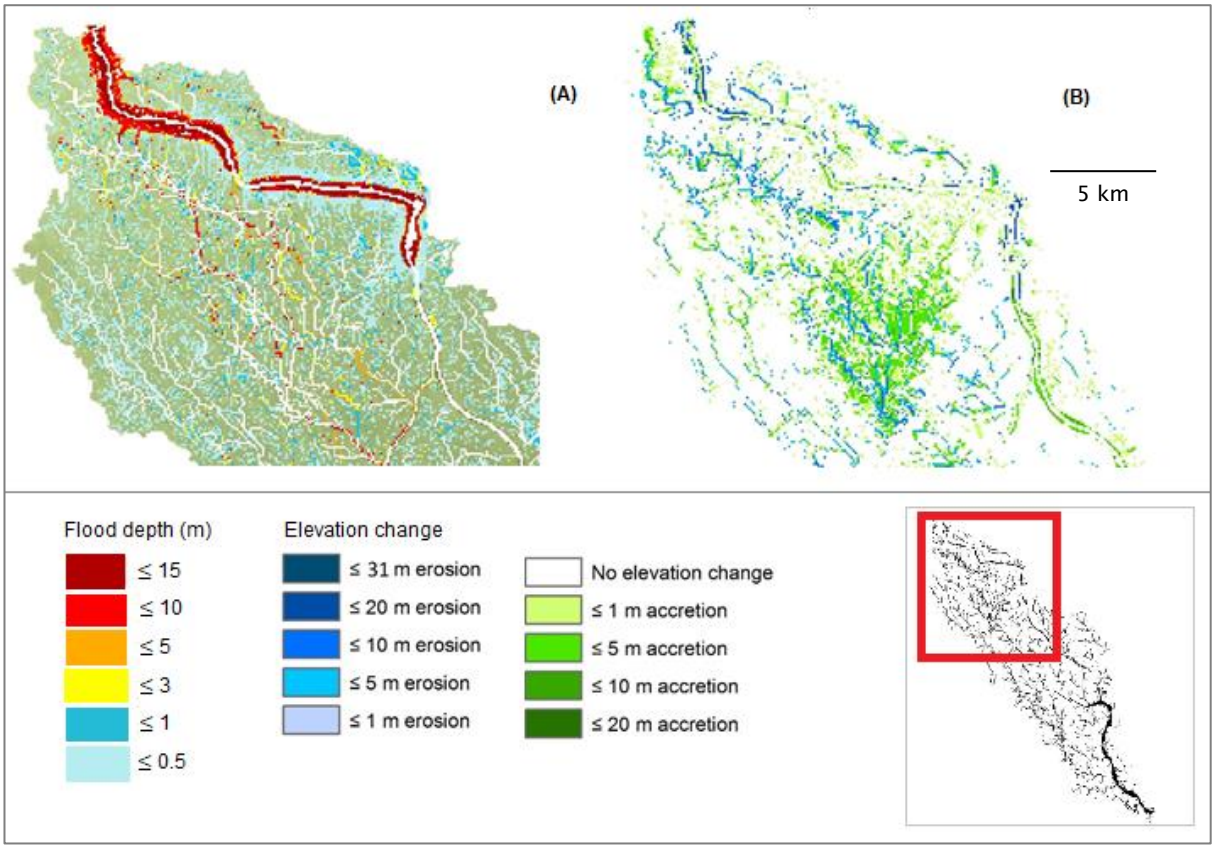

Figure 7.5 (A) Floodplain inundation depth at the end of the one year extended simulation period (utilising the 4DWD 50 year DEM) and (B) Elevation change between 30 and 50 years under scenario 4DWD, highlighting areas of levee erosion and levee development; Devi catchment

Whilst the spatial distribution of flood levels varies considerably between the catchments, the frequency distribution of flood depth magnitude is fairly similar (inset in figures 7.3 and 7.4): Both catchments exhibit a unimodal distribution, with depths of up to 0.5 m observed in 57% and 45% of inundated cells in the Devi and Mahanadi catchments, respectively. Moderate flood depths of up to 5 m are observed over a greater area in the Mahanadi catchment; covering 85% of inundated cells compared to 79% in the Devi catchment. The Devi catchment however exhibits a slightly higher proportion of extreme flood levels; with 6% of inundated cells measuring water depths of 15 m < $d \leq 20$ m; compared to a value of 4% in the Mahanadi catchment. Whilst flood depth data

from the present-day Mahanadi Delta is fairly limited, a study by Patro *et al.* (2009) describes observed flood levels between 0.5 and 5 m during the 2001 monsoon season. The maximum depths observed after the extended flood run of scenario 4DWD clearly exceed these levels and could indicate an overestimation in the model; which would be in line with the analysis in section 6.2. However, as described above this is also in part due to the significant erosion of levee structures over the simulation period.

As shown in figures 7.6 and 7.7, categorical measures of vulnerability to an extreme flood event have been generated for the Devi and Mahanadi catchments, respectively, under scenario 4DWD. As described in section 7.1, vulnerability is measured over a series of grid cells measuring 5 km^2. Four categories are applied whereby ≥50% of the cell area meets the following criteria: (1) High vulnerability: those areas where flood levels measuring 5 m ≤ d ≤15 m are experienced; (2) Moderate vulnerability: those areas where flood levels measuring 3 m ≤ d < 5 m are experienced and/or ≤ 80% of the area is inundated; (3) Low vulnerability: those areas where flood levels measuring < 3 m are experienced; (4) Very low: those areas where < 50% of the area suffers inundation and maximum flood levels < 3m. This resolution of analysis shows that almost the entirety of the Devi catchment is vulnerable to flooding following such an extreme event, with the upper reaches experiencing the highest inundation levels. Conversely many regions of the Mahanadi catchment have only a very low vulnerability to flooding. However a greater proportion of the catchment is subject to high or moderate levels, particularly in coastal areas.

It is important to note that this analysis does not necessarily correlate directly with flood risk, but rather provides a measure of the severity of inundation following a cyclone event that could be easily compared between different climatic and environmental scenarios. An important next step from this study would be to carry out the same investigation for the remaining synergistic scenarios in the Devi and Mahanadi catchments. Specifically for the Devi, it would be interesting to see whether there continues to be a quantifiable split between the 'group A' and 'group B' scenarios that were described in detail in chapter 6: Floodplain channels cover approximately a third more of the catchment area under group B scenarios (3WDD, 5DWA, 6WDDH, 7DWDH, 8DWAH, 9DWDC). Such a large change in the areal density of floodplain channels would be expected to have significant implications for the routing of water across the floodplain and

therefore the level of inundation experienced. Another future area of investigation would be to analyse the temporal variation in flood vulnerability: In this initial exploration inundation levels are analysed at the end of the 50 year simulation period; however this does not necessarily reflect which areas may be most vulnerable during extreme flood events over shorter timescales. This has significant implications as a key element in determining how vulnerable or resilient an area may be overall depends not only on the magnitude of the stressor (inundation) but also on the frequency (reoccurrence and subsequent recovery time) of such events. Before further analysis is carried out however, it would be wise to calibrate this particular set-up of the C-L model specifically with inundation levels (as water depth was not measured as part of the validation process discussed in chapter 5), in addition to the revalidation recommendations discussed in section 6.2.

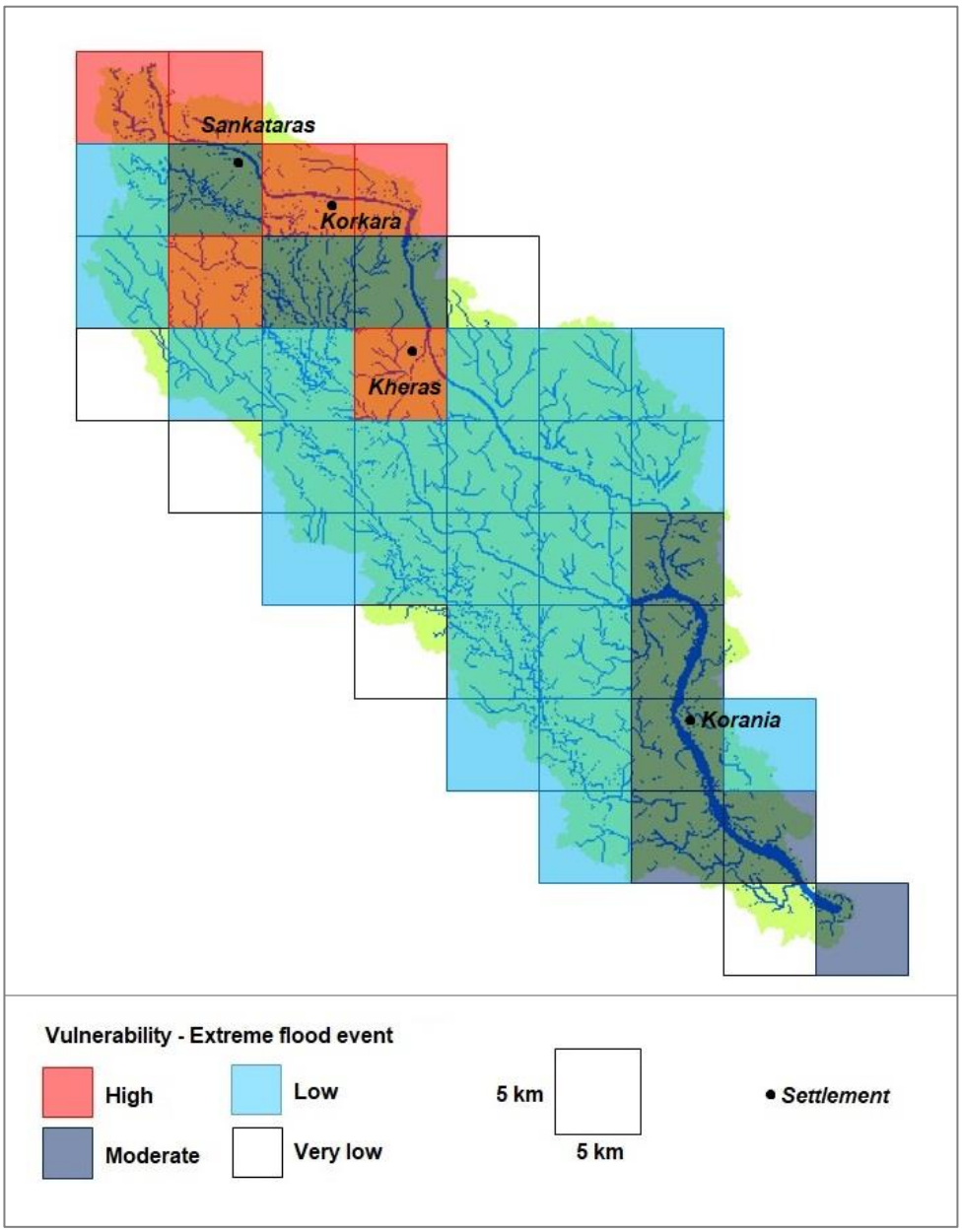

Figure 7.6 Categorical measure of vulnerability to an extreme flooding event, scenario 4DWD; Devi catchment. Large settlements at high or moderate risk are shown for reference.

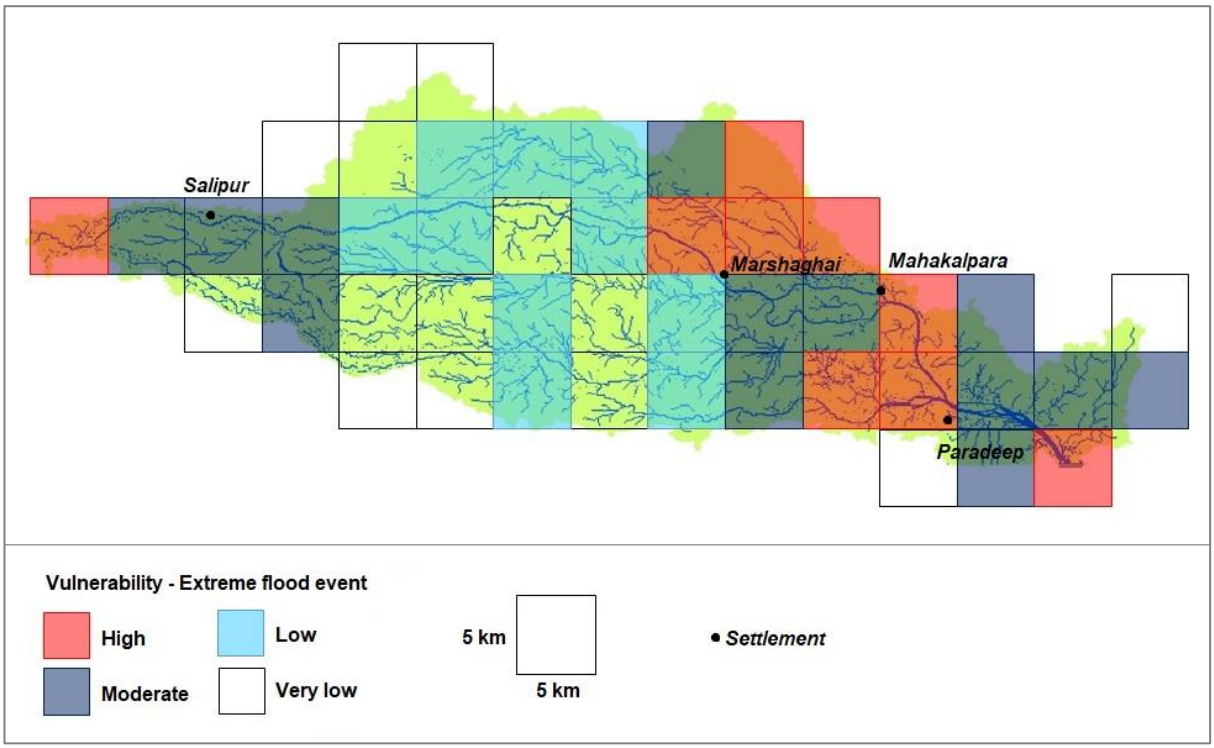

Figure 7.7 Categorical measure of vulnerability to an extreme flooding event, scenario 4DWD; Mahanadi catchment. Large settlements at high or moderate risk are shown for reference.

7.3 Changes in habitat cover

As discussed in chapter 2, shifts in habitat cover can have a significant influence on the capacity to maintain ecosystem services within the deltaic system (Leh *et al.*, 2011). Habitat cover therefore has a direct impact on how vulnerable or resilient a given area may be to increasing conditions of climatic stress. As 60% of the land in the Mahanadi Delta is utilised for agricultural purposes (Jena *et al.,* 2014), it is even more important to understand how changes in the morphological regime of both the Devi and Mahanadi catchments might impact the high proportion of the population that are dependent on rural livelihoods.

Changes in vegetation type or density can have a large effect on the distribution of sediment and water fluxes across the distributary network. An increase in the area of land used for grazing, for example, has been shown to significantly increase the total sediment load entering the distributary system (Godoy and Lacerda, 2014; Walling, 1999). The subsequent effects of such a change are complex and potentially long-lasting; influencing both the morphological processes that occur across the wider floodplain, as well as within the channels themselves. Often changes in habitat cover are driven by anthropogenic controls such as shifts in agricultural practices or urbanisation. However climatic factors such as changes in precipitation patterns, and environmental stressors such as locally enhanced subsidence rates, also play a critical role. Indeed, deltaic evolution itself is driven by a complex web of biogeomorphological interactions operating across multiple temporal and spatial scales; whereby factors such as salinity and elevation can have huge consequences in terms of controlling the distribution of floral and faunal assemblages (Pasternack and Brush, 2002).

Despite the importance of habitat cover in both determining and being determined by morphological processes in deltaic CSES, at present many studies neglect the role of such interactions (Wolanski *et al.*, 2009). This is largely because representing these complex feedback mechanisms accurately in numerical models is extremely challenging. As was discussed in detail in chapter 3, even in the recent version of C-L utilised in this study vegetation simply exists to allow a protective mat of grass to develop over flood deposits (Coulthard, 2000). If a cell remains dry for 10 years full vegetation cover is assumed to develop. Alternatively if the layer is eroded, material is removed from the

vegetation fraction of the active layer and treated as if it were washed out of the catchment. The user can define how quickly vegetation reaches maturity and to what extent it limits lateral erosion, however this can only be applied homogenously across the catchment; thus limiting the ability to explore the interactions between the morphological system and different land cover types.

Whilst it is not currently possible to integrate habitat cover types directly into the scenarios explored in this study, it is possible to infer the potential impacts to broad habitat classifications under these differential climatic conditions: Here I develop a novel framework that explores how the morphological outputs extracted in prior analysis may be utilised to identify which areas of the catchment system may be vulnerable to changes in habitat cover following a 50 year run of scenario 4DWD. As the predominant linkages between the physical and ecological environment depend heavily on access to water and sediment supply, I focus on outputs that aid in understanding how these factors in particular may be altered by morphological change. These outputs include: vulnerability to an extreme flood event (as described in section 7.2); hypsometry; net elevation change; floodplain morphological response units (MRUs); and channel MRUs. Originally the distribution of nearest-edge distance (NED) values was also going to be utilised given that it provides a useful metric with which to infer the distribution of floral species: Areas with high average NED values, for example, are likely to be preferentially colonized with species that need less access to water; and vice versa (Edmonds *et al.*, 2011). However, given that there was shown to be little alteration to the spatial distribution of NED values in both the Devi and Mahanadi catchments (see sections 6.1.1.5 and 6.1.2.5, respectively); and indeed very little variability between the different scenarios, this measure would not help to identify areas that are potentially vulnerable to habitat change.

In order to maintain consistency with the categorical measures discussed previously in this chapter, each catchment was divided into a series of grid cells measuring 5 km^2. The dominant habitat cover for each cell (covering ≥ 50% of cell area) is applied utilising the land-use map generated by Wetlands International (2014a; refer to figure 4.3). As shown in figures 7.8 and 7.9, both the Devi and Mahanadi catchments are dominated by land utilised for single and double crop agriculture (approximately 79% and 67% of catchment area, respectively). The Mahanadi catchment however has a greater variety of habitats, including

intertidal wetlands and mangrove forests, owing primarily to its lower elevation. The proportion of different habitat cover types in the Mahanadi catchment is more representative of that found across the Mahanadi Delta as a whole (Jena *et al.,* 2014). Similarly the dominant value or category for each of the outputs described above was prescribed for each cell. The figures for each of these variables can be found in Appendix D (figures D.1 – D.10). Rather than attempt to predict what trajectory of habitat change these numerous interacting factors may cause (which would require a model capable of accurately simulating multiple biogeomorphological interactions) the focus of this novel exploratory investigation is to provide categorical measures of vulnerability which indicate the likelihood of habitat cover changing as a result of the drivers simulated in scenario 4DWD. As discussed in section 3.2, this post-processing approach can therefore be viewed as GIS-based suitability analysis (Malczewski, 2004); whereby the capacity of the system to meet the needs of a stakeholder is assessed. This methodology does not attempt to quantitatively assess whether this change is detrimental or beneficial to those living in the effected regions; although this may be qualitatively inferred for high risk areas. It is assumed however that any significant risk of habitat change over such a relatively short time period (50 years) is likely to be detrimental to those whose livelihoods are intrinsically linked to the provision of ecosystem services as they are at present.

As shown in table 7.1, a score is applied for each cell for each of the outputs, dependent on how likely that metric is to effect the current habitat classification. These scores are then added together in order to give an overall value between 0 and 25. This framework is then used to provide a categorical measure of vulnerability to changes in habitat cover for each cell: whereby a 'Very high' score lies between 15 and 25; 'High' between 10 and 14; 'Moderate' between 5 and 9; 'Low' between 3 and 4; and 'Very low' between 0 and 2. As before, given the issues discussed in section 6.2 the focus of the interpretation of these results should be on the relative values between cells and the development of a unique biophysical vulnerability index, as opposed to absolute values.

Areas with a higher vulnerability to an extreme flood event score more highly due to the increased risk of fluvial and/or tidal inundation. Most habitat types located across the delta plain, and particularly agricultural areas, benefit from a moderate flood regime in that flood waters are a key source of nutrient-rich sediment (Le *et al.,* 2007). Furthermore, flooding of agricultural lands

ensures that the acidic waters found in many deltaic soils are washed out at the beginning of the monsoon season, thus improving productivity (Pho and Tuan, 2005 in Le *et al.*, 2007). Extreme flood events however, and particularly those caused by storm surges, do not carry the same environmental benefits. Larger or more regular floods are likely to lead to habitat degradation, particularly across agricultural lands and riparian forests and marshes. Areas at high risk of flooding also face habitat loss due to enhanced rates of bank erosion, and higher levels of disease related to freshwater contamination (Pearce, 2014). Whilst a worsening flood risk will have similarly detrimental impacts in wetland and mangrove habitats, these areas are more resilient to flooding and indeed act as an efficient buffer against storm surges and high flows (Das, 2009). Consequently the scores have been reduced for these habitat classifications in order to reflect this. The same scoring has been applied for hypsometry: areas at lower elevations score more highly as these regions will be more sensitive to changes in relative sea-level. Sea-level rise not only extends the area that is inundated during the monsoon season, but also prolongs the time that vegetation is submerged. This can have devastating impacts for certain crops, and particularly for rice production (Syvitski *et al.,* 2009). Salinisation can also have devastating impacts on agricultural productivity and freshwater supplies (Johnson, 2014). Mangroves and wetland areas will still be detrimentally impacted by rising sea-levels, but are less likely to experience habitat change as rapidly as the other classifications. Thus the scores have once again been adjusted to reflect this.

For the remaining outputs the scores as shown in table 7.1 are kept homogenous across all habitat classifications. Net elevation change is weighted not by the magnitude of the erosion or accretion taking place (as this is reflected in hypsometry and MRU analysis), but rather by the spatial extent of the change. Cells where elevation change is restricted purely to distributary channels (via scouring, for example) score lower than those where the elevation change extends out of the channels and across on to the floodplain. This is because the latter represents more significant changes to the distributary network, and therefore upon the distribution of sediment and water fluxes to adjacent habitats. Dominant floodplain MRUs are identified where they occur in over 50% of the cell area. Despite the fact that the development of floodplain channels would have significant impacts on water and sediment distribution across the landscape, this MRU actually scores lower due to the fact that a vast majority of these ephemeral

channels already existed at the start of the simulation period. The morphological changes that take place therefore are restricted to within the channels themselves, and are thus unlikely to have significant impacts on habitat cover over relatively short timescales. Features that alter sediment distribution across a larger area of the floodplain (such as crevasse splays), or those that result in significant localised accretion (such as levees) score more highly; as do areas where multiple MRUs interact. Levees are particularly important features in terms of controlling the natural sedimentation of habitats across the deltaic plain, depriving the floodplain of vital nutrients often with detrimental effects to ecosystem productivity (Day *et al.,* 1999). Dominant channel MRUs are identified where they occur in over 50% of the main Devi and Mahanadi channel areas within any given cell. Areas that experience lateral erosion score more highly in terms of vulnerability to habitat change. This is because lateral erosion acts to both decrease the area of habitats adjacent to channel, as well as increasing sediment supply within the distributary channels themselves. Point bars and channel bars both provide new opportunities for colonisation by pioneer vegetation species, provided these features are stable enough to ensure the correct conditions are met in terms of both elevation and the frequency and duration of flooding (Boniface, 1985). Given the relatively coarse spatial resolution of the grid size utilised in the C-L model ($90m^2$) it is assumed that these features are well established within the landscape and thus are likely to fulfil these requirements.

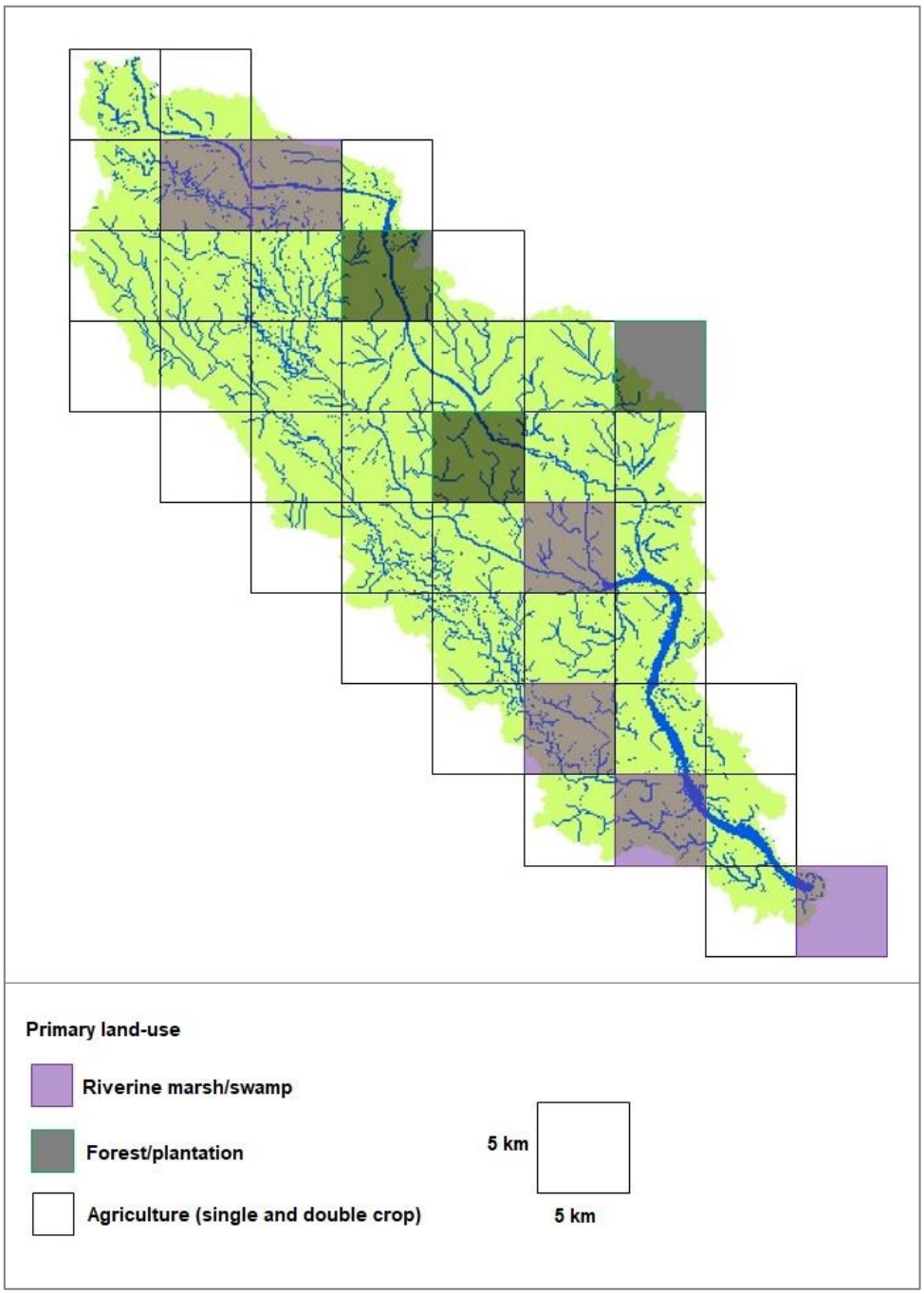

Figure 7.8 Dominant habitat classifications in the Devi catchment; extracted utilising land-use data from Wetlands International (2014a). Agricultural land covers approximately 79% of the catchment area.

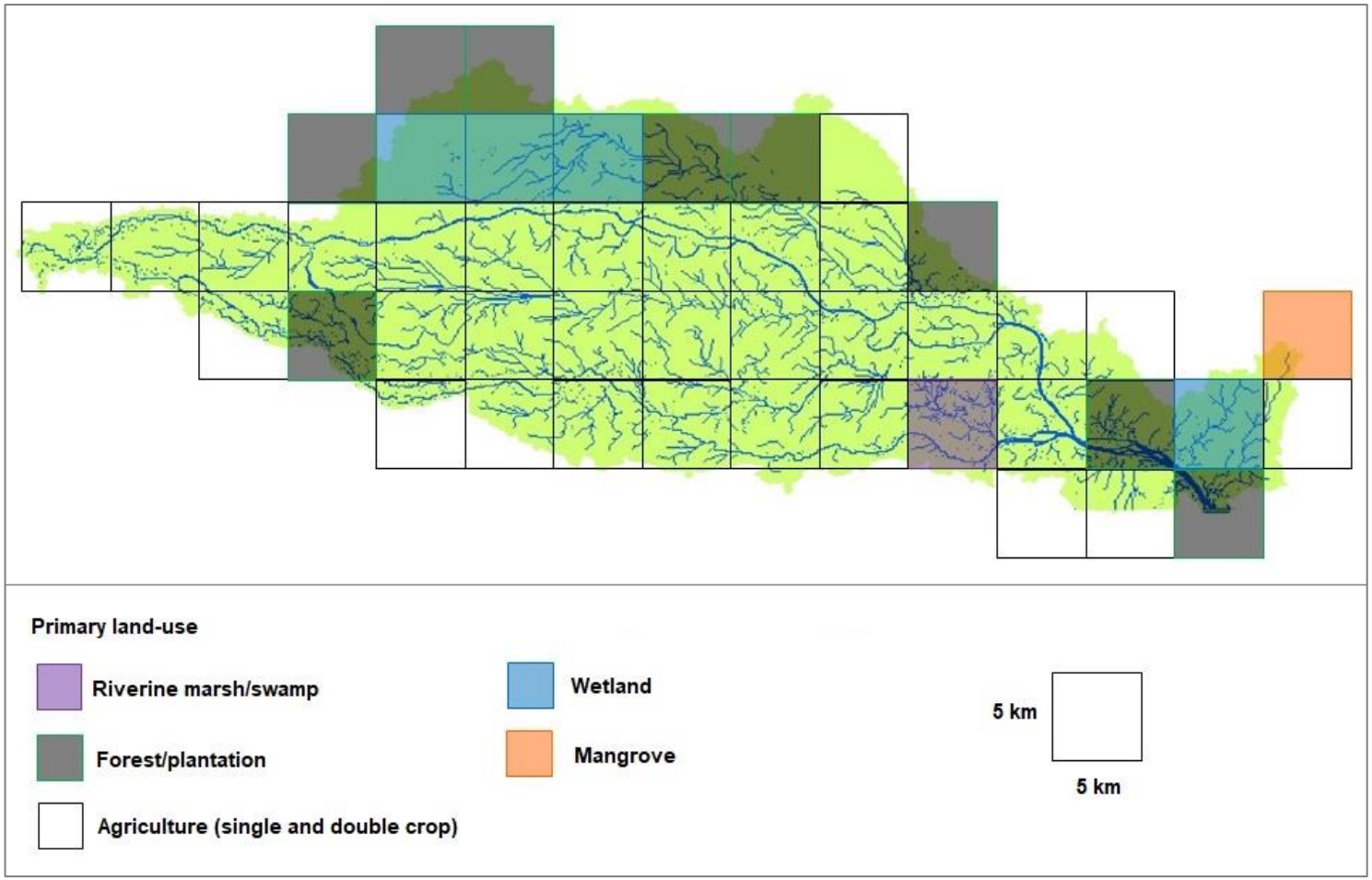

Figure 7.9 Dominant habitat classifications in the Mahanadi catchment; extracted utilising land-use data from Wetlands International (2014a). Agricultural land covers approximately 67% of the catchment area; whilst forests and plantations cover 20%.

Table 7.1 Scoring utilised to define categorical measures of vulnerability to habitat cover change. A score for each output is assigned dependent on the dominant habitat cover. These are then summed to produce an overall score.

Output	Prescribed category (where change occurs across ≤50 % cell area)	Vulnerability score for primary habitat cover classification				
		Agricultural	Forest/ plantation	Riverine marsh/swamp	Wetland	Mangrove
Vulnerability to an extreme flood event	High	5	5	5	3	3
	Medium	3	3	3	1	1
	Low	1	1	1	0	0
	Very low	0	0	0	0	0
Hypsometry	≤ 5 m	5	5	5	1	1
	≤ 10 m	3	3	3	0	0
	≤ 15 m	0	0	0	0	0
Net elevation change	Occurs across floodplain	5	5	5	0	0
	Occurs adjacent to channels	3	3	3	3	3
	Occurs only within channels	1	1	1	1	1
	None	0	0	0	0	0
Dominant floodplain MRU	Floodplain channels and levee formation	5	5	5	5	5
	Levee formation	3	3	3	3	3
	Crevasse splay formation	3	3	3	3	3
	Floodplain channels	1	1	1	1	1
Dominant channel MRU (*main Devi and Mahanadi channels only*)	Lateral erosion	5	5	5	5	5
	Channel/point bar formation	1	1	1	1	1
	Channel incision	0	0	0	0	0

Total Score	*Very High*	*15 - 25*
	High	*10 – 14*
	Moderate	*5 - 9*
	Low	*3 - 4*
	Very Low	*0 - 2*

Figures 7.10 and 7.11 show categorical measures of vulnerability to habitat cover change for the Devi and Mahanadi catchments, respectively, under scenario 4DWD. In the Devi catchment the areas deemed to be at the highest risk of habitat cover change are located adjacent to the main channel of the Devi River itself. This is to be expected given that the Devi River is recognised as being the most morphologically active in the distributary network. The widespread development of levees in some locations and extensive lateral erosion in others, combined with a high vulnerability to fluvial flooding along much of the main channel, all contribute to significant shifts in both fluvial and sediment supply to the delta plain, as well as the frequency and extent of inundation. Just 7% of the total area is identified as being of 'very high' vulnerability. All of these cells are designated as agricultural habitat cover and are subject to localised lateral erosion, thus directly reducing the area of land available for crops. Approximately one third of the catchment area is found to be highly vulnerable, whilst another third is found to be moderate. Areas designated as being of 'low' or 'very low' vulnerability are all located on the eastern and western fringes of the catchment away from where the main channel has a significant morphological influence.

In the Mahanadi catchment however a substantial proportion of the total area is found to be highly vulnerable to potential habitat cover change: 46% of the area is identified as being of 'very high' vulnerability whilst a further 41% is classified as 'high'. This notable difference between the catchments is likely due to two dominating factors: firstly, the elevation of the Mahanadi catchment is considerably lower than that of the Devi: 30% of the Mahanadi catchment is located ≤ 5 m above sea-level, compared to just 3% in the Devi catchment. Subsequently the Mahanadi catchment scores much higher in terms of vulnerability due to hypsometry, with habitats here subject to more regular tidal inundation and increasing salinisation. Secondly, as discussed in detail in sections 6.1.2 and 6.2, the significant accretion observed across a majority of ephemeral channels on the floodplain results in a higher score across a majority of cells in terms of MRU analysis. As these minor channels become shallower and increasingly disconnected from the main distributary system, fluvial input (and therefore sediment flux) to the floodplain will be gradually reduced. Without more detailed investigation it is difficult to predict what impacts this will have on the different habitat classifications located in these regions. Eventually however this process is likely to result in the abandonment of

the delta lobe, and an increasingly dominant role of marine processes (Roberts, 1997). The most vulnerable locations in the Mahanadi catchment are identified near to the river mouth, where high rates of lateral erosion and low hypsometry values result in an increased risk of habitat cover change.

Interestingly the only cell dominated by mangrove cover also has the lowest vulnerability score. This is somewhat surprising given that one of the most significant changes in land cover over recent decades in the Mahanadi Delta has been a rapid reduction in mangrove area (Pattanaik and Prasad, 2011). However, whilst some of this decline has occurred due to enhanced erosion, a majority of this loss is attributable to the growth of the aquaculture industry. Such agent-based parameters are not accounted for in this methodology; perhaps highlighting a limitation of utilising this format of vulnerability assessment. As was discussed in detail in chapter 2, anthropogenic factors such as widespread channel modification and land-use changes have resulted in significant alterations to the morphological regime of many deltas worldwide (Syvtiksi *et al.* 2009), including the Mahanadi. This can have both a direct effect on the distribution of habitat classifications within the delta, and also indirect impacts due to shifts in sediment and water dynamics across the distributary network. Whilst the methodology described here will capture the indirect effects of such anthropogenic factors at the very start of the simulation period in C-L, the overall measures of vulnerability to habitat cover change are based on outputs that assume no further human modifications take place over the 50 year simulation. Clearly in reality this would not be the case. This is why a system as complex as the Mahanadi Delta may benefit from an integrated assessment tool (IAT) approach in order more accurately capture a true picture of biophysical vulnerability, where such agent-based decisions can be built in to the outcomes of different scenarios (see section 3.1.3 for further discussion).

Nonetheless the approach described above still provides a useful baseline study to complement an IAT-based assessment by highlighting which areas of the catchment are intrinsically vulnerable to potential habitat cover change under increasing conditions of climatic stress. As with assessing vulnerability to an extreme flood event, an important next step for future investigations would be to expand this analysis across all other synergistic scenarios. Furthermore, being able to integrate differential types of vegetation directly into the morphological model

would provide a significant step forward, in that certain biogeomorphological interactions would then be explicitly incorporated into the set-up of different scenarios. At present this can be only be partially represented in C-L; either by utilising a spatially variable Manning's value, or through the modification of the hydrological inputs (Coulthard, 2016). The inclusion of such feedbacks however would enable a more comprehensive assessment of potential habitat change: identifying not only *where* might be vulnerable to significant change but also *how* different habitats may respond under different climatic and environmental scenarios.

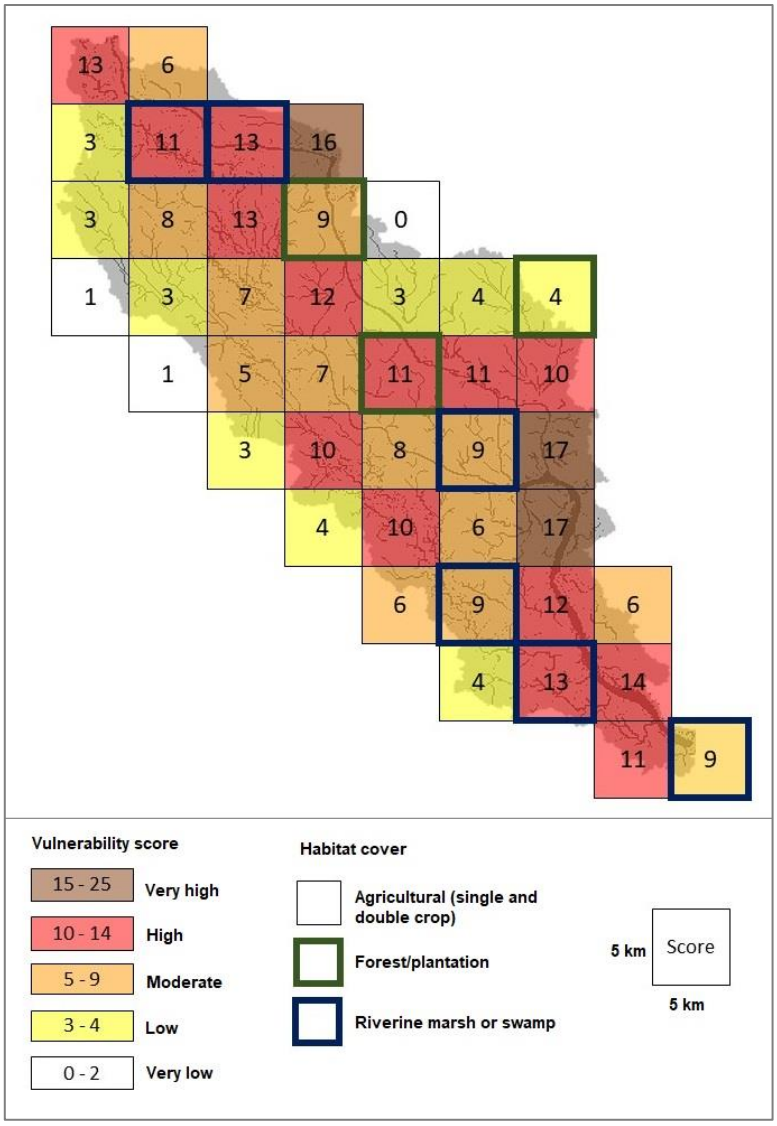

Figure 7.10 categorical measures of vulnerability to habitat cover change under scenario 4DWD; Devi catchment. The scores correlate to those described in table 7.1.

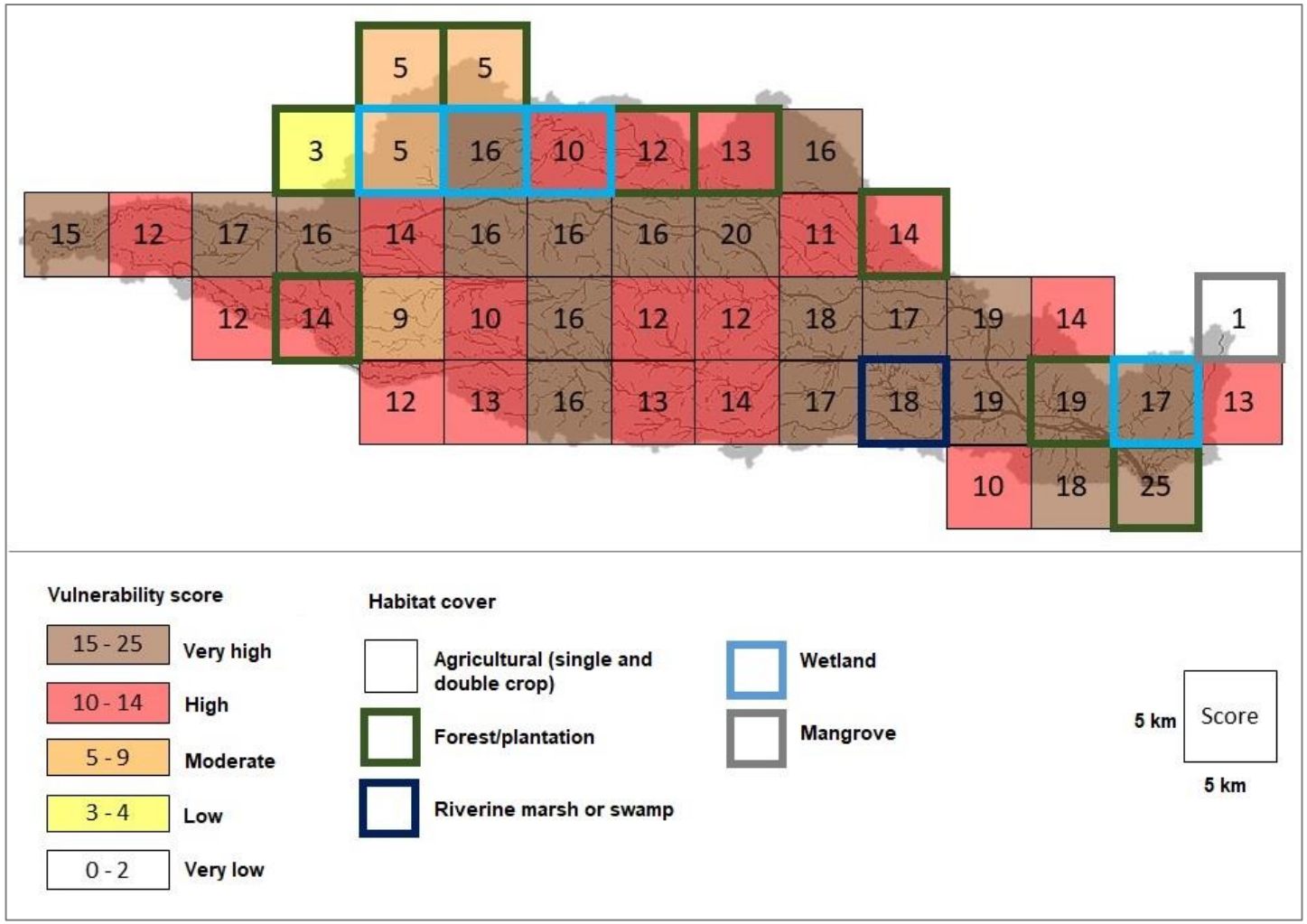

Figure 7.11 Categorical measures of vulnerability to habitat cover change under scenario 4DWD; Mahanadi catchment. The scores correlate to those described in table 7.1

7.4 Engineering strategies

In this final exploratory investigation, I demonstrate the use of the C-L model to simulate engineering strategies that could be applied in the Mahanadi region to reduce the impacts of detrimental morphological change. This is an important step in maximising the potential of the vulnerability indices developed in this chapter as a tool for policy makers. Restorative approaches that promote natural deltaic processes that have been inhibited, or re-establishing lost habitats such as mangrove forests, have become a central focus of deltaic management projects over recent years (Giosan *et al*., 2013; Das *et al.,* 1997). This concept, known as 'de-engineering', is increasingly being viewed as being favourable over more traditional – and often more expensive – methods of hard engineering (Giosan *et al*. 2014).

Here two such methods of delta restoration (refer to figure 2.6) are explored: Firstly the deliberate breaching of levees is simulated in order to increase sediment supply to the delta plain, and furthermore to reduce the likelihood of a catastrophic breach during high flow events (Pinter *et al.,* 2016). The impacts of this strategy are demonstrated in an agricultural region of the Devi catchment that was identified in prior analysis as being of 'high' vulnerability to potential changes in habitat cover, and furthermore is located adjacent to a particularly morphologically active section of the main Devi River channel. This is achieved by modifying the elevation of 15 cells in the 0 year (baseline) DEM utilising the RasterEdit software. The elevation of 0.54 km of levees is reduced to match that of the channel, essentially removing the levees from the landscape (figure 7.12). Secondly, an artificial internal subdelta is constructed with the aim of increasing sedimentation across the flood plain. Such an approach is already being implemented in lagoons of the Atchafalaya Basin, USA (Giosan *et al.,* 2014). This second investigation is focused on an area of riverine marsh located near to the mouth of the Devi catchment that was identified in prior analysis as being vulnerable to both sea-level rise and enhanced rates of lateral erosion. Once again the RasterEdit software is utilised to modify the elevation of 28 cells in the baseline DEM, so as to create a small distributary network comprising of three new channels (figure 7.13).

The initial 30 year period of scenario 4DWD is re-run utilising the modified DEMs for each restoration scenario. The results of this are then compared with elevation change under the same scenario utilising the original baseline DEM for the Devi catchment. Figures 7.14 and 7.15 show these results for the levee break scenario and subdelta scenario, respectively.

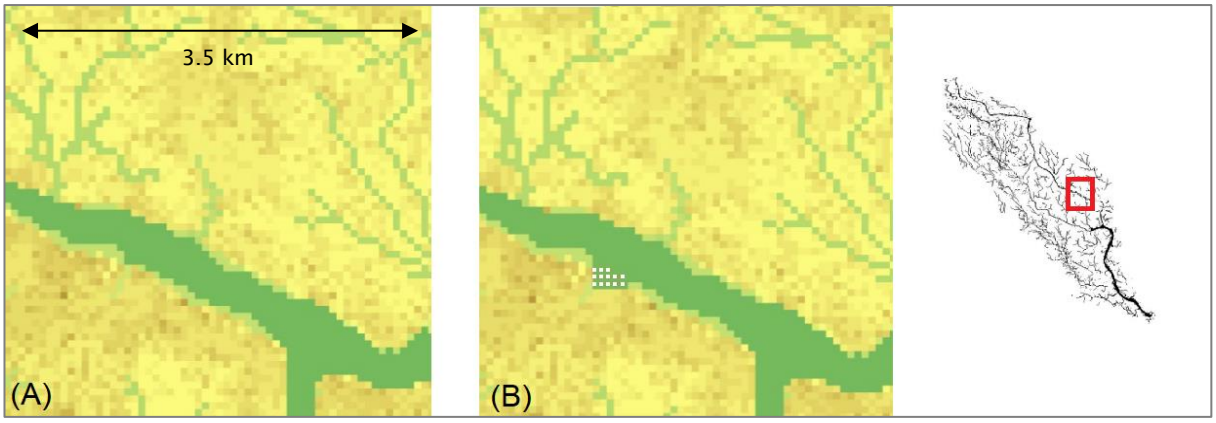

Figure 7.12 Creation of an artificial levee breach in the RasterEdit software by taking the baseline 0 year DEM for the Devi catchment (A) and modifying the elevation of cells to remove the levee structure (B). Modified cells are highlighted with white dots.

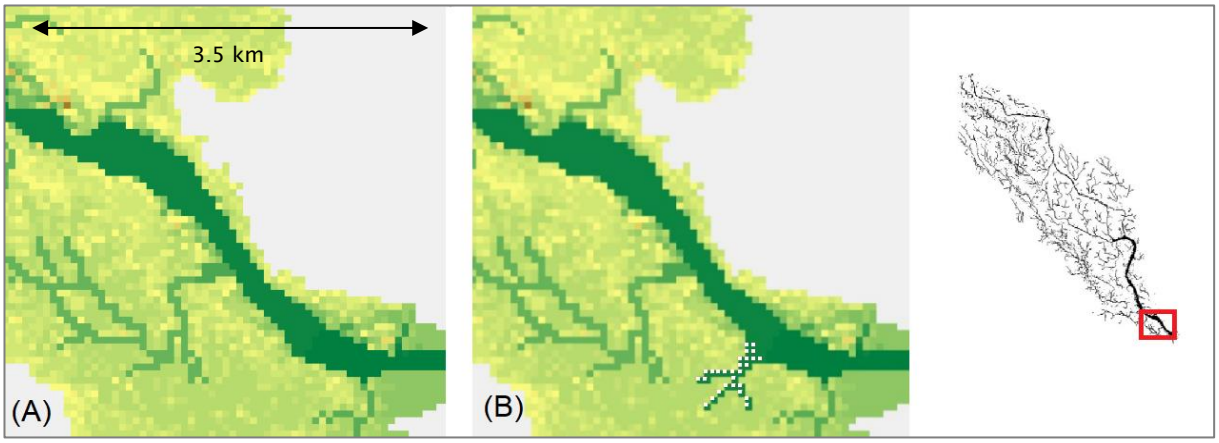

Figure 7.13 Creation of an artificial subdelta in the RasterEdit software by taking the baseline 0 year DEM for the Devi catchment (A) and modifying the elevation of cells to create a new distributary network (B). Modified cells are highlighted with white dots.

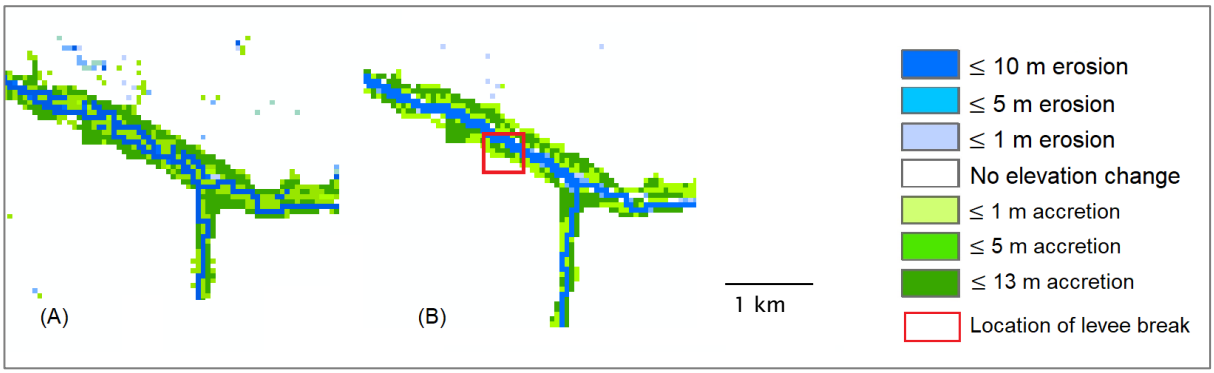

Figure 7.14 (A) Localised elevation change for a chosen section of the Devi catchment at 30 years under scenario 4DWD, where no modifications have been made to the initial baseline DEM (B) Localised elevation change for the same section after the simulated levee break has been applied. The location of the break (as shown in figure 7.12) is outlined by the red box.

As shown in figure 7.14, by 30 years into the simulation period the location of the levee break has been infilled by new sediment. Whilst the width of this feature remains the same as under scenario 4DWD, the height of the new levee is up to 3 m lower as sediment is reworked to fill in the break. Perhaps the most notable difference is that following the installation of the levee break the development of islands within this section of the channel has been completely inhibited. This is likely because any sediment that was being deposited in the channel has been redistributed to reform the levee. As a result of this, localised flows travel at a higher velocity under this scenario, thus the channel itself has become straighter and wider. Whilst the impacts of this management strategy provides an intriguing result morphologically (although, once again, these results should be considered carefully given the issues discussed in section 6.2), it is unclear whether it has been successful from a management perspective: As shown in figure 7.14B there is no clear evidence of restorative value on the floodplain adjacent to the levee break. Analysis of interim data (collected every 5 years during the simulation period) also shows no changes to the elevation of the floodplain. Questions arising from this exploratory investigation are therefore: is C-L capable of accurately simulating such an engineering intervention? And, furthermore, how quickly during the initial 5 year interim period does this reformation of the levee structure take place? It could be the case that if sediment is reworked before any major flood event, this would prevent increased sedimentation to the floodplain during moderate high flows. What is likely

however given these results is that flood risk has been reduced locally due to the increased capacity of the main channel. It is important to recognise however that the increased velocity of flows at this location could act to increase flood risk downstream.

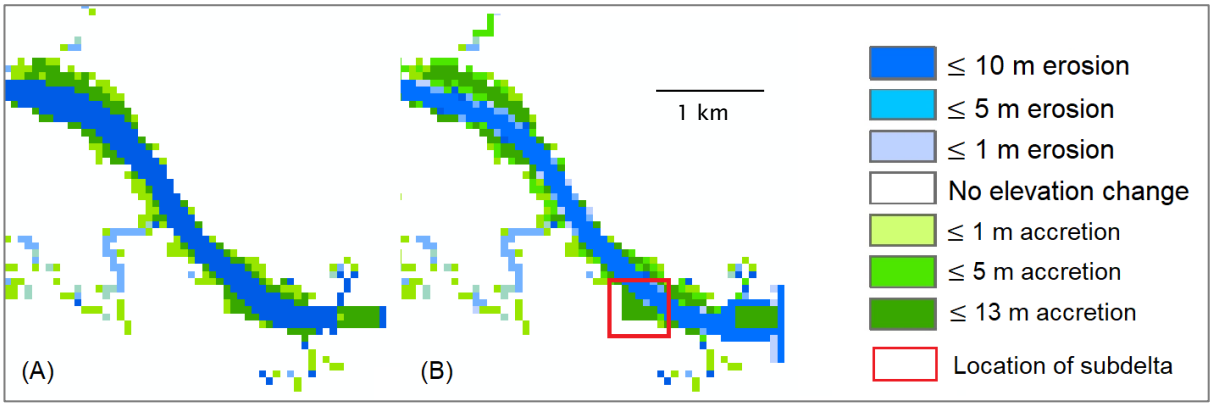

Figure 7.15 (A) Localised elevation change for a chosen section of the Devi catchment at 30 years under scenario 4DWD, where no modifications have been made to the initial baseline DEM (B) Localised elevation change for the same section after the simulated subdelta has been created. The location of the subdelta (as shown in figure 7.13) is outlined by the red box.

As shown in figure 7.15, the installation of an artificial subdelta in the lower reaches of the Devi catchment has a less notable effect on elevation changes over the 30 year simulation period when compared to scenario 4DWD. Overall there is very little difference in the location and height of levee structures adjacent to the main channel; and indeed in the floodplain channels. There is however an increase in localised accretion at the site of installation: The triangular feature outlined in red in figure 7.15B shows an increase in elevation of 9 m adjacent to channel and 7 m where it meets the delta plain; representing where the primary artificial distributary channel has been infilled. This significant area of accretion effectively cuts off the remainder of the channels that were artificially cut into the landscape to create the subdelta. These are not visible in figure 7.15 as there is no change in the depth of these channels (4 m) beyond the initial area of deposition. However, without direct access to the main Devi River these channels are not able to contribute to the broader sedimentation of the floodplain at this location. Indeed, it is likely that if the simulation were to be extended then these ephemeral features would become increasingly abandoned

and subject to reworking via marine processes (Roberts, 1997). Likewise the depth and width of the main Devi River channel shows negligible variability over the simulation period; with the exception of the area located at the mouth of the catchment. Whilst the bar feature formed under both scenarios remains unchanged in spatial area (0.15 km^2), there are notable differences in the structure of the deposit: As shown in figure 7.16, under the subdelta scenario the mouth bar is more conical in shape with a peak elevation gain of 9 m. Furthermore, the channel has scoured up to 10 m surrounding the deposit, and along the eastern extent of the model domain. Under scenario 4DWD however the mouth bar deposit extends across the width of the channel, and is more graded in terms of its elevation gain. It is unclear exactly what is driving this change in water and sediment distribution; indeed it is somewhat surprising that the most notable different in channel structure occurs not at the site of subdelta construction, but rather downstream of this intervention. What is clear however is that if these results do reflect the likely morphological impacts of implementing this management strategy, then the restorative success in terms of increasing sedimentation to the floodplain is uncertain.

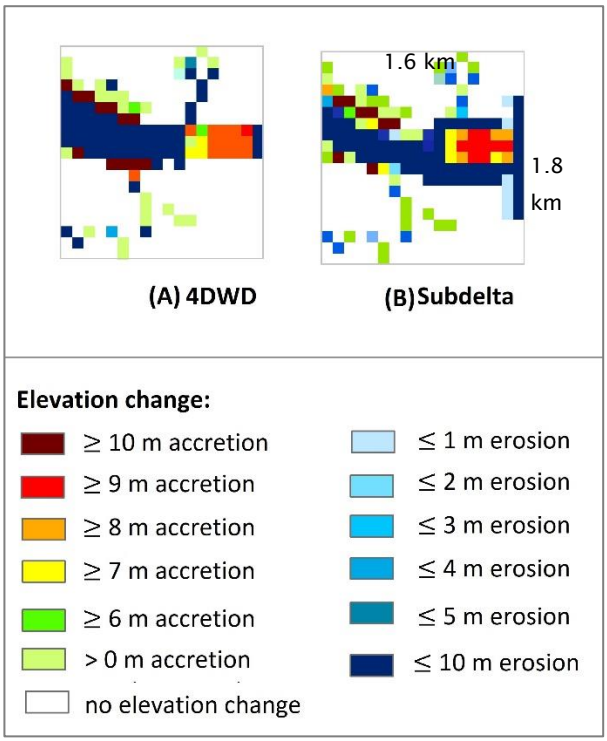

Figure 7.16 (A) Localised elevation change at the mouth of the Devi catchment at 30 years under scenario 4DWD, where no modifications have been made to the initial baseline DEM; and (B) Localised elevation change for the same section after the simulated subdelta has been created. The colour scale has been modified to highlight changes in the structure of the mouth bar.

The scenarios above both demonstrate that C-L can indeed be a useful platform to investigate the morphological impacts of restorative management strategies. However, as was also highlighted in the analysis of potential habitat cover change in section 7.3, one of the greatest challenges when interpreting the value of these results is that they exclude the ongoing impact of agent-based decisions. After the initial anthropogenic intervention has been implemented at the start of the simulation, it is not possible to continue maintenance of the artificial structure at regular intervals as would be required in the real-world delta. Significant accretion such as that observed at the apex of the new subdelta, for example, would likely be unblocked before it reached the point of abandonment. It might therefore be more appropriate to run these management simulations over shorter temporal scales so that such intervention could be implemented at the required intervals; thus running a 'stop-start' simulation as opposed to continuous. Before making such adjustments it would be highly beneficial to

calibrate this adapted set-up of C-L utilising a real-world example of an implemented management strategy. A more robust validation process would also mean that the other outputs generated for all other synergistic scenarios could be interpreted with increased confidence.

Chapter 8 **Conclusions**

8.1 Introduction

Deltas are major ecological and social centres that are widely recognised as being highly vulnerable to the combined impacts of climate change and human activity. Anthropogenic interventions that drive sediment starvation and accelerated subsidence, and climatic stressors such as increasing precipitation variability and eustatic sea-level rise, act synergistically to put increasing pressure on these naturally dynamic environments. Edmonds *et al.* (2017) estimate that of the 300 million people currently living on deltas, approximately 69% occupy the low elevation coastal zone (< 10 m above sea-level) that is particularly vulnerable to coastal flooding. Furthermore, Edmonds *et al.* find that the population of deltas is growing at 1.59% per year, which outpaces the world growth rate of 1.11%. In order for these growing populations to thrive under increasing conditions of environmental stress, it is critical that we have a better understanding of how these multiple stressors might impact the biophysical evolution of these vulnerable systems. This study aimed to contribute towards this by developing a management relevant set of tools that explore the nature of multidecadal morphological change in delta catchment systems under a range of climatic and environmental change scenarios. Utilising the Mahanadi Delta in India as a case study, this thesis sought to explore three distinct objectives in order to achieve this:

8.2 Objective 1: The influence of emergent processes

The first objective of this study was to enhance our understanding of how emergent processes influence the multidecadal evolution of deltaic environments. Specifically, this objective addressed the need to simultaneously model the synergistic impacts of both long-term, slow morphological processes and extreme, short-term, events. As discussed in detail in chapter 2, modern controls on delta morphology are diverse, interactive and operative over a variety of spatiotemporal scales. To create reliable projections of how these systems might respond to these complex interactions, it is important to develop methodologies and frameworks that are based on the mathematical concepts of complexity theory. Such approaches enable us to gain a better understanding of the

morphological responses that could lead to unpredictable system change. To ensure this was fulfilled in this study I designed a methodological framework building upon the key themes of complex social-ecological systems (CSESs) theory as identified by Glasser *et al.* (2008) (non-linear interactions; emergent behaviour; vulnerability; resilience; and adaptive capacity). Emergent behaviour is absolutely central to this approach, whereby the cumulative effects of small-scale phenomena influence large-scale system properties. As critical transitions can occur at any given scale, the effects of crossing multiple thresholds at smaller scales can accumulate to trigger events of significant concern (Lenton, 2013). Despite this, as explored in chapter 3, compared to terrestrial catchments there are very few studies that aim to simulate emergent phenomena in river deltas. In addition, far fewer studies attempt to use quantitative metrics to describe emergent features in distributary channel networks when compared to tributary systems (Fagherazzi *et al.,* 1999). I addressed this knowledge gap by building on the methodological framework of Edmonds *et al.* (2011), and applying such metrics in two contrasting catchments in the Mahanadi Delta under a range of climatic and environmental change scenarios. Furthermore, I explored how such metrics can be utilised along with morphological outputs to improve understanding of the complex interactions between the emergent morphological system and habitability. It is hoped that by doing so this study makes a significant and novel contribution towards filling these knowledge gaps identified in deltaic regions, and inspires further research utilising such approaches.

Furthermore, the successful implementation of the CAESAR-Lisflood (C-L) model in a deltaic setting provides an example of how a cellular-automata (CA) model can provide a large range of valuable outputs, and indeed reveal a great deal about complex morphological behaviour. Such tools have multiple advantages over arguably more sophisticated numerical models: Whilst the representation of fluvial and hillslope processes in CA models tends to be relatively simple, their combined and repeatedly iterated effect is such that they successfully simulate complex non-linear behaviour. CA models are therefore highly effective at representing the feedback dynamics associated with emergent system processes (Van De Wiel *et al.,* 2007). Of course, as presented in chapters 3, 6 and 7 there are limitations associated with utilising such tools: Liang *et al.* (2015) highlight some of the challenges of setting up a flow routing model such as C-L in a deltaic environment; including the complex nature of flows in low-lying

distributary channels, backwater effects, and the interaction of fluvial and marine processes. As discussed in section 6.2, it became apparent during analysis of the morphological results that the setup of C-L utilised in this study may not have been optimal for the Devi and Mahanadi catchments. The reworking of coastal sediments via wave action also is not accounted for in the current version of C-L and this is a very important point to consider when assessing the transferability of the proposed framework. Whilst this has a relatively limited effect on the results for the catchments analysed in this study, this would have potentially very significant implications for deltas dominated by marine processes. Furthermore, spatial variability amongst certain parameters that are important controls of morphological change in deltaic environments, such as vegetation cover and subsidence, are not able to be integrated into C-L at present. Consequentially, such factors have to be incorporated during the post-processing stage; and thus do not play a direct role in driving the observed morphological changes. Finally, whilst sediment and water fluxes can be varied over time in order to simulate shifts in anthropogenic and/or climatic stressors, the effects of certain interventions are not able to be incorporated into the scenario design. Localised changes in land-use, for example, or the installation of artificial channels or levees, are both important controls of delta morphology that would be very useful to be able to integrate directly into the simulations. Despite these limitations, the application of C-L in this study provides a transferable, innovative and accessible methodological framework that could be utilised to produce multidecadal projections of morphological change in a broad range of deltaic settings.

For the reasons outlined above, the results produced by this study contribute from a methodological perspective towards an exciting and progressive field of complex system science. However they also provide valuable information about potential relative trajectories of morphological change in the Mahanadi region under increasing conditions of climatic stress. In particular, the impacts of a wide range of scenarios are explored in the Devi River catchment; including shifts in seasonal precipitation variability, differential rates of sea-level rise and increased cyclone frequency. Of course these results can be utilised within a localised context - They identify which areas are likely to aggrade to safer elevations with respect to flooding, and which areas are likely to erode; as well as providing projections of the nature of this change over the next 50 to 60 years. As discussed in section 6.2, it is likely that the projected rates and overall

magnitude of change experienced in the simulations may be excessive when compared to real-world observations. Nonetheless the nature of many of these projected changes support well-established theories in the literature: Scenarios in which the rate of sea-level rise is higher, for example, tend to have a greater extent of active floodplain channels due in part to backwater effects favouring channel avulsion (Chatanantavet *et al.,* 2012). Furthermore, a similar distribution of nearest-edge distance (NED) values is found across all scenarios; supporting the theory proposed by Edmonds *et al.* (2011), that this is driven by an internal feedback mechanism.

This research also reveals some interesting results that challenge the way in which we interpret the multidecadal behaviour of the morphological system. As presented in section 6.2, one of the dominating patterns to emerge in the Devi catchment is that there appears to be two distinct trajectories of evolution; particularly in terms of where elevation change occurs and the total net sediment change across the system (see figure 6.35). These were referred to as 'group A' and 'group B' scenarios: under the former group, total net sediment change oscillates only slightly around the baseline value over the initial 30 year simulation period, before sharply declining by 50 years. Under the latter group, the system undergoes more severe fluxes between periods of net sediment gain and loss throughout the run, experiencing a considerably greater loss by the end of the simulation. No specific mechanistic driver could be identified that caused this distinctive split. Indeed, scenarios within these groups present very different climatic trajectories that one would assume would result in equally contrasting morphological responses. Rather, it is hypothesised that the underlying cause of this split is dependent upon the magnitude and frequency of the applied system stressors. It would appear that linear or gradual changes in the precipitation regime do not cause a significant enough perturbation within the catchment system to result in the severe fluxes observed under group B scenarios. Increasing variability to any particular driver, or extreme shifts in these drivers, does however appear to tip the morphological system towards this unstable pathway. A wetter and more variable monsoon, accelerated dry season drought conditions, high rates of sea-level rise, and an increased frequency of severe storms; all of these stressors appear to amplify the non-linear response of the Devi catchment. As explored in section 6.2, during this adaption phase the

system may be less resilient to even short-term or low intensity external stressors (Renaud *et al.*, 2013).

Some of the outputs analysed did, however, show direct correlations with specific drivers. Scenarios with higher total seasonal flows, for example, tend to produce higher numbers of crevasse splay formations. As many channel avulsions on deltaic plains arise from splay formations (Stouthamer, 2001), these features could be utilised as potential early warning signals indicating where such significant changes could take place later in the 21st century. This is also beneficial given that such features are readily identifiable from freely available satellite imagery. Furthermore, we find that lateral erosion is more extensive where the rate of sea-level rise is high, or where the highest flows are concentrated. Mid-channel and point bar formation on the other hand is found to be more sensitive to shifts in seasonal precipitation variability.

8.3 Objective 2: Linking morphology and habitability

The second objective of this study aimed to explore how the changes observed in the morphological system may influence the habitability of the delta. This was partly inferred directly from the analysis of morphological results: Floodplain channels, for example, cover approximately a third more of the Devi catchment area under 'group B' scenarios. Such a significant change in the density of floodplain channels is likely to have major implications in determining flood risk and habitat cover. Slater (2016), for example, finds that a 10% increase (decrease) in channel capacity results in a decrease (increase) in the flood frequency of approximately 1.5 days per year across 41 rivers in the UK. Under the scenarios also run in the Mahanadi catchment however, significant accretion was observed across a majority of ephemeral channels across the floodplain. It is believed that this captures a critical stage in the morphological evolution of the Mahanadi catchment: whereby sediment supply is still sufficient that such extensive accretion can take place, however not sufficient enough to increase the elevation of the floodplain itself. As these channels become increasingly disconnected from the Mahanadi River, this could eventually lead to an

abandonment of the delta lobe. As a consequence of this, marine processes are likely to play an increasingly dominant role across these floodplains, having significant implications for the populations occupying this region of the delta. The 67% of the Mahanadi catchment that currently supports single and double-crop agriculture is likely to be most significantly affected.

A crucial component of this part of the research however was the development of a transferable vulnerability index that, together with the metrics presented in chapter 6, provides a unique set of management relevant tools. In chapter 7 I presented three exploratory investigations that aimed to demonstrate an alternative framework for linking what has been learnt about the emergent morphological system to certain aspects of biophysical vulnerability. This novel aspect of this research assessed the capacity of the catchment system to meet the needs of those living in the region under scenario 4DWD; the scenario representing the most likely climatic pathway based on the present literature. Specifically two categorical measures of vulnerability in the Devi and Mahanadi catchments were provided: Firstly, potential inundation following an extreme flood event was assessed. This is a particularly important avenue for future investigation, given that the Mahanadi Delta has been highlighted as being one of the most vulnerable deltas to increased flood risk due to climate change (Jena *et al.,* 2014). It was found that almost the entirety of the Devi catchment is vulnerable to inundation levels of up to 3 m following the simulated severe cyclone event. Upper reaches of the catchment in particular were deemed very vulnerable to more extreme levels of inundation. In the lower-lying Mahanadi catchment, a greater proportion of the area is subject to high or moderate levels of vulnerability to an extreme flood event, particularly in coastal regions as a result of tidal inundation.

Next, I utilised the morphological metrics to assess which areas of the catchments may be vulnerable to habitat cover change. Changes in vegetation type and extent can have a significant effect on the distribution of sediment and water fluxes in deltaic environments. Likewise, a complex web of biogeomorphological interactions operating across multiple temporal and spatial scales can have significant consequences in terms of controlling the distribution of habitats. Despite this, at present the role of such interactions is often excluded in many morphological investigations, primarily due to the fact that representing these complex mechanisms accurately in numerical models is extremely

challenging (Wolanski *et al*., 2009; Reyes, 2009) Whilst it was not possible in this study to integrate habitat cover types directly into C-L, this issue was addressed by providing a framework to enable users to infer the potential impacts to broad habitat classifications under differential climatic conditions. As many of the linkages in the biogeomorphological environment depend on the frequency of access to water and sediment supply, morphological outputs were used to understand how these relationships might be effected under differential climatic conditions. It was found that in the Devi catchment the areas deemed to be at greatest risk of habitat cover change are located adjacent to the main channel of the Devi River itself. In the Mahanadi catchment, 87% of the area was identified as being of 'very high' or 'high; vulnerability; primarily due to the combined threats of sea-level rise and widespread infilling of ephemeral floodplain channels. It must be stressed however that such inferences are indeed just that – whilst the innovative framework developed by this study helps in addressing the gap that biogeomorphological linkages are simply ignored, it is recognised that this cannot replace a more accurate risk assessment that is able to directly incorporate such feedbacks during the simulation itself. As presented in chapter 3, system-based models such as the Barataria–Terrebone Ecological Landscape Spatial Simulation (BTELSS) model (Reyes *et al.,* 2000) and the Mississippi Delta Model (Martin, 2000) are continually being developed in what is a very progressive field of study. Improving on this even further would be to develop a methodology that enables agent-based decisions such as land-use changes and shifts in agricultural practices to be applied in such a way so that they are able to vary through time and space. This would better represent the complex reality of interactions between humans and the biophysical system in these highly productive ecological environments.

8.4 Objective 3: To provide outputs that are useful to stakeholders

The third and final objective of this study was to provide outputs that would be directly useful to stakeholders in the Mahanadi Delta**.** The morphological metrics and model outputs described in chapter 6, combined with the categorical measures of vulnerability presented in chapter 7, come together to create a novel set of tools that could be of great use to stakeholders. The Mahanadi system has regularly been highlighted in recent research as being at

significant risk from the pressures of climate change, and yet to date, to the author's knowledge, there have been no prior attempts to model potential morphological changes over the 21st century. This need in part drove the decision to carry out this study at the catchment scale – not only because it is the most appropriate scale at which to simulate multidecadal emergent processes, but also because it is arguably the most relevant scale to be utilised by policy makers. In the Devi catchment in particular, the broad range of scenarios assessed has provided insight into two potential morphological trajectories over forthcoming decades (referring to group A and group B scenarios). Whilst identifying which areas are likely to aggrade and which areas are likely to erode provides useful information to stakeholders with respect to issues such as flood management, improving our understanding of the forces driving the behaviour of the emergent morphological system is perhaps even more valuable. Such analysis of the underlying system dynamics is crucial in order to understand how increasing conditions of climatic stress may result in critical transitions within the morphological component of the delta system. As discussed in chapter 4, it is hoped that the multiple time series and maps produced as a result of this study could contribute significantly towards the biophysical element of the Integrated Assessment Tool (IAT) being developed by the DECCMA Project. The IAT aims to combine social, economic and biophysical knowledge to explore the implications of various adaptation strategies in the Mahanadi region, with a focus on planned migration (DECCMA 2015b). Through being integrated with socio-economic data in this way the impact of this research can be maximised.

In addition, I also demonstrated the use of the C-L model to explore potential engineering strategies that could be applied in the Mahanadi region in order to reduce the negative impacts of environmental change. As with the other exploratory investigations presented in chapter 7, this aspect of the research highlights the versatility of the C-L model to address a number of different aspects effecting vulnerability and resilience. This supports a particular strength of this research study in that the methodological framework presented here is easily transferable to many other deltaic environments. The scenarios analysed by this study not only encapsulate stressors that are representative of modern pressures experienced in the Mahanadi region, but also those that are common to a broad range of deltas worldwide (Syvitksi *et al.,* 2009). Furthermore, through focusing on variability in the South-West Monsoon in the scenario design, this has

also increased the relevance of these results to many global megadeltas in which the morphological behaviour is predominantly driven by a wet/dry season precipitation regime.

8.5 Recommendations for further research

Moving forward from this study, several aspects warranting further investigation can be identified:

- Firstly, after addressing the issues regarding model setup as outlined in section 6.2, it would be beneficial to explore further the impacts of the full set of synergistic scenarios in the Mahanadi catchment. This would help improve our understanding of the possible trajectories that this system may follow over forthcoming decades, as well as providing additional information for policy makers in the Mahanadi region. In doing so it may also help to address the query raised in section 6.2, in that it is important to identify whether these catchment systems are limited to a set number of morphological trajectories within the timeframes applied in this study. The implications of this are significant as, if this were to be the case, it is likely that similar patterns might be observed in other deltaic systems experiencing similar conditions of environmental stress.

- Furthermore, expanding the analysis in the Mahanadi catchment would help to increase the transferability of this research by improving understanding of how emergent morphological processes may operate in a region that is likely to become increasingly dominated by marine processes over forthcoming decades. It could be however that C-L is not the most appropriate tool to utilise for this investigation at present, given that wave action is not able to be incorporated into the model and that this would become an increasingly important driver of change.

- What C-L would enable us to do very efficiently however is to expand the temporal scale of analysis over the remainder of the 21st century. In particular, it would be interesting to investigate further how the apparent convergence of many of the morphological outputs towards the end of the

current simulation period would continue to develop over a subsequent 50 year period (or longer). Additionally, this might help address what factors, if any, are driving this convergence.

- Finally, with continual developments in the abilities of the C-L model, and indeed in similar CA applications, it is likely that in the very near future both spatially variable vegetation cover and subsidence could be included explicitly in the set-up of the scenarios, as opposed to during the post-processing stage. This would significantly improve our understanding of the internal factors driving change within the biophysical system.

It is hoped that this research project inspires others working in this progressive field at the interface of environmental and social science, to continue to develop approaches utilising the CSES framework in order to improve our understanding of delta morphodynamics. It is to be hoped that this work provokes discussion and further investigation concerning the importance of emergent behaviour in controlling the trajectory of these sensitive environments. Furthermore, continual developments in both the reliability and versatility of CA models will enable projections such as those made in this study to be made in other vulnerable deltas worldwide; including those where data resources are more limited.

Appendix

A. Parameter setup – baseline scenario (TST)

The setup for each of the parameters as shown in table 5.5 are described below for the TST scenario. Many values are based on the recommendations as in the C-L manual provided by Coulthard (2016).

Mode

C-L can be run in catchment mode (utilising rainfall to generate runoff); reach mode (inputting river discharge); tidal mode (inputting tidal data at the outflow of the model domain); or a combination of these. In this study the model is being run in reach and tidal mode simultaneously.

DEM file

This is an ASCII format .txt file comprised of 6 lines of header and then rows and columns of the elevations of each cell. C-L automatically reads in the number of rows and columns and the grid cell size. DEMs for the Devi and Mahanadi catchments have been prepared in ArcGIS 10.3.

Grain data file

This is an optional file that contains the bed and subsurface grain size information. This is not required in this study.

Bedrock data file

This file describes the location of the bedrock for the DEM. It must be the same size and format as the DEM for each catchment. In C-L, bedrock is a layer below which erosion and slope processes cannot occur. The depth of the bedrock varies from 1 m to 20 m throughout the Mahanadi Delta. As there is very limited spatial data available however, a value of 10 m was chosen for the TST run.

Save file every (minute)

If selected, C-L will save outputs at the specified time step under a unique file name. If not selected, only the final output data is saved. For TST a file is saved every 2628000 minutes.

Generate time series output

If selected all of the sediment and water that exits the domain will be recorded. At the specified time step C-L will generate a text file with 14 columns of data containing: time, Q_w actual, Q_w expected, blank, total sediment output (m^3), the volumes of sediment for each of the nine separate grain size fractions (m^3). For TST this value is set to 525600 minutes.

Minimum time step

C-L will automatically find an appropriate minimum time step. However, this parameter may be changed in order to improve the computational speed of runs that have timescales of decades or centuries. This parameter must be set to at least 1 in order to prevent numerical instabilities building up between the flow model and erosion/deposition. As the runs in this study are multidecadal, a minimum time step of 60 seconds was selected.

Maximum time step

In order to prevent C-L running too fast and skipping important peak flow events, it is recommended to set this value to 3600 seconds. C-L will automatically match the input time step.

Run time start

The time at which simulation begins. This should be set to 0 unless otherwise required.

Maximum run duration

This parameter describes how long the model run will last before it stops. This should correspond to the length of the input data; however can be shortened (i.e. if one only wants to observe the first decade of a 60 year simulation). Initially for model validation this was set to a 30 year run (262980 hours). For a 60 year run this is set to 525960 hours.

Memory limit

This parameter is purely computational that determines the size of the array that holds the grain size values. When it is set to the default value of 1 it means that there are as many places in the grain size array as there are grid cells.

Run with all grain sizes

Up to nine grain sizes can be run in C-L, but if these are not all required then un-checking this box increases running speed. Only three grain sizes are required in this study.

Grain sizes 1-9

For each grain size utilised in the model, the size should be provided in metres, and the initial proportion given as a fraction of 1. In this study the three grain sizes run in C-L are 0.00005, 0.000075 and 0.0002 m^3. The proportions are 0.95, 0.027 and 0.023, respectively.

Suspended sediment fall velocity

Selecting this parameter will treat the designated grain size as suspended sediment. The fall velocity of 0.024 ($m.s^{-1}$) was calculated utilising the instructions provided in the C-L manual. This controls how rapidly sediment drops out of the water/sediment mix.

Sediment transport law

In C-L fluvial erosion and deposition can be calculated utilising either the Einstein-Brown (1950) or Wilcock and Crowe (2003) formulation. The latter was selected in this study as it is recommended for braided or meandering channels.

Maximum velocity used to calculate Tau

This function is rarely used to calculate sediment transport but is sometimes required where slope gradient is very high. This has been left at the default value of 5 $m.s^{-1}$ for this study.

Maximum erode limit

This parameter specifies the maximum volume of material that can be eroded or deposited within a cell, in order to prevent numerical instability. It also controls the time step, which is limited to allow this value to be moved from one cell to another. The default value of 0.02m^3 has been utilised.

Active layer thickness

This specifies the thickness of a single active layer in C-L. The value should lie between 0.1 and 0.2 m, and must be at least 4 times the maximum erode limit. The default value of 0.1 m has been utilised in order to correspond with the default maximum erode limit value.

Proportion of sediment to be re-circulated

When C-L is operating in reach mode, this parameter describes the proportion of sediment that exits the model domain that is fed back to the reach inputs. This is not required by this study.

In-channel lateral erosion rate

This parameter defines how the cohesiveness of sediment influences channel geometry. Unconsolidated sediment (represented by a larger value) is more readily eroded and thus laterally transported within the channel, resulting in a shallow, wide channel. If the sediment is more cohesive (smaller value), lateral erosion is more limited resulting in a narrower, deeper channel. For a given cell a and receiving cell b, it can be represented by the following formula (Equation 16):

$$dZ_b = \frac{E_b L(Z_a - Z_b)}{dx} \quad [16]$$

Where dZ_b is the change in elevation of the receiving cell (m), E is the volume of sediment eroded during that iteration (m^3), L is the in-channel erosion rate parameter, Z is cell elevation (m), and dx is the grid cell size (m). Values between 10 and 20 are recommended for smaller and larger rivers respectively. This parameter was left at the default value of 20 in this study.

Lateral erosion

Selecting this parameter permits bank erosion; which is clearly required in this study. This differs from the above parameter which is concerned with lateral erosion within the channel itself.

Lateral erosion rate

The rate of lateral erosion (if selected as above), is calculated via the edge counting method as described in Coulthard and Van de Wiel (2007). A value of

0.0001 $m.s^{-1}$ is recommended by Coulthard (2016) for meandering channels. This parameter is independent of grid cell size.

Number of passes for edge smoothing filter

This value describes how well smoothed the calculated curvature of the channel is. It is recommended that the value should be set to an integer that represents either the frequency of meanders within a grid cell for coarse DEMs, or the number of grid cells between 2 meanders in high resolution DEMs. A value of 10 was found to be appropriate in both the Devi and Mahanadi catchments.

Number of cells to shift lateral erosion downstream

This parameter allows meander bends and/or bars to migrate downstream. Coulthard (2016) suggests the value is approximately 10% of the value used for the number of passes for edge smoothing filter, with values between 1 and 5 working best. A value of 1 was therefore utilised in this study.

Maximum difference allowed in cross channel smoothing of edge values

Once the radius of curvature for the outside edge of a bend has been calculated, C-L then needs to interpolate this value across the channel to allow sediment to be transported laterally. This parameter will smooth the values until the difference between smoothing iterations is less than the value entered; in this instance the recommended default of 0.0001 is utilised. If the value is set too high, there may be additional deposition in the centre of large channels.

Description

This allows the user to enter text about the simulation that is then stored in the configuration file. For this scenario it is simply 'TST'.

Override header

This option allows the user to override the information in the header file of the DEM. This is not required in this study.

Inflow coordinates

These are the coordinates (x,y) of the inflow point(s) for water and sediment discharge when operating in reach mode. These are (42,2) , (40, 2) for the Devi catchment; and (9, 136) , (9, 138) for the Mahanadi.

Inflow header file

This is a text file that describes the volume of water and sediment (for each grain size fraction) input to the model at each given time step. The format is as shown previously in table 5.4. For TST hydrological and sediment inflows are created from two cycles of historical data from 1974-2004.

Divide inputs by

This option allows the user to divide the total input by a given value in order to prevent incision at just one point. For both the Mahanadi and Devi the input is spread over 2 cells.

Input data time step

The time step of the inflow data in minutes. This value is set to 1440 for all scenario runs.

'M' value

This variable controls the peak and duration of the hydrograph generated by a rainfall event. It is only required when running in catchment mode and thus not by this study.

Rainfall data file

This is the text file for rainfall input. It is only required when running in catchment mode and thus not by this study.

Rainfall data file time step

This is the time step of rainfall data in minutes. It is only required when running in catchment mode and thus not by this study.

Spatially variable rainfall

This permits spatially variable rainfall across the DEM. It is only required when running in catchment mode and thus not by this study.

Stage/Tidal input

This is a text file containing the stage/tidal data. It is a singular column showing the elevation of the water surface (in metres) at a given time step. As described previously, for scenario TST a month of tidal data was continued over a 30 and then 60 year period. For each year sea-level was increased in correspondence to the moderate scenario as provided by the Met Office. Extreme sea-level events as a result of a severe cyclone occur every 50 years.

Stage/Tidal coordinates

These four boxes contain the x_{min}, x_{max}, y_{min} and y_{max} coordinates delineating an area within which tidal data will be added. For all cells within this area the elevation of the water surface is adjusted to this value. These are (443, 440, 483, 481) for the Devi catchment; and (830, 847, 316, 318) for the Mahanadi.

Input data time step

This parameter describes the time step (in minutes) for which each line of the tidal/stage text file represents. As there are two high and two low tides a day in the Mahanadi Delta, this value is set to 360.

Grass maturity growth rate

This value describes the speed at which vegetation reaches full maturity (in years). A value of 1 was selected for the Mahanadi Delta.

Vegetation critical shear

Above this value vegetation will be removed by fluvial erosion. Thus the lower it is set, the more easily vegetation is swept away; the higher it is set, the more resistant. 180 is a recommended value.

Proportion of erosion that can occur when vegetation is grown

This parameter determines how vegetation maturity influences both the in-channel lateral erosion rate, and the lateral (bank) erosion rate. If set to 0 then when vegetation is fully matured, there can be no erosion via these two methods. If set to 1, then vegetation will have no effect whatsoever. If set to 0.5, 50% of normal erosion will be allowed. The proportion of erosion permitted by vegetation is also influenced by the grass maturity growth rate. A value of 0.5 was selected for the Mahanadi and Devi catchments.

Creep rate

A value of 0.0025 is recommended for this parameter that describes the soil creep rate on slopes. It is given by a simple diffusive soil creep function (Equation 17):

$$\frac{Slope.Creep\ rate.T}{dx} \quad [17]$$

Where T is time (s) and dx is the slope gradient (degrees).

Slope failure threshold

This is the angle in degrees above which landslides can occur. The recommended value is 45.

Soil erosion rate

This value represents the rate of soil erosion as a function of the slope length, slope gradient, and a series of coefficients. The recommended value is 0.

Soil erosion varies according to j_mean

This is an experimental function that relates the soil erosion rate as above to the saturation of the soil. It is as yet untested and therefore has not been utilised in this study.

SIBERIA sub model

This allows the SIBERIA sub model to be run instead of C-L, or alongside it. This is not required in this study.

Dune model

The dune functions on C-L are still being developed and are not required by this study. The parameters allow the user to integrate Aeolian processes into the hydrological model.

Input/output difference allowed

This parameter (in cumecs) is useful to speed up model operation. When the discharge exiting the DEM is equal to that being added, then one can assume the flow model is running in a steady state. If so, the time step of the flow model can be detached from that of the erosion/deposition model and allow the time steps to extend to that being determined by erosion/deposition. This therefore increases the time step of the model during low flow periods or static flows when less morphological work is occurring. There is no set value for this parameter, but it is recommended that it should be set close to a low flow value and/or mean annual flow for that river system. A value of 350 has been utilised in both the Devi and Mahanadi catchments as this is the modal annual flow.

Minimum Q for depth calculation

This parameter describes a threshold above which C-L will calculate a flow depth, in order to avoid wasting computational time calculating flow depths of fractions of a millimetre that will not cause any erosion or deposition. This recommended value for this variable is 0.01 per metre cell size; therefore for a resolution of 90 m a value of 0.9 has been chosen.

Maximum Q for depth calculation

This describes the maximum value for depth calculation. Reducing this value will force water to be added more in the headwaters rather than progressively throughout the catchment. It should be left at a default value of 1000.

Water depth thresholds over which erosion will happen (m)

This is the flow depth at which point C-L begins to calculate erosion (in metres). It is recommended to utilise the default value of 0.01.

Slope for edge cells

The gradient of the exit cells is an important parameter that controls the erosion and deposition that occurs at the outflow of the DEM. If set too low this can result in extreme deposition; if set too high then this can cause scouring to occur upstream. After multiple trial runs at different values, a value of 0.002 was found to be optimal for both catchments.

Evaporation rate

This is the mean evaporation rate for the catchment (in metres per day). This was found to be 0.00446 by Rao *et al.* (2012).

Courant number

The courant number is a value that controls the numerical stability and speed of the flow model in C-L. It should only range between 0.3 and 0.7; with 0.7 recommended for DEMs with a resolution of 50 metres of more.

hFlow threshold

This parameter is found in the Lisflood-FP component of the C-L model, where hflow is the water surface elevation between two cells. A threshold value is

required to prevent the flow model from moving water when there are very small gradients between cells. A recommended value is 0.00001 metres.

Frounde number flow limit

This parameter allows C-L to prevent flows exceeding this value passing between cells. It is recommended to utilise the default value of 0.8 unless modelling deep flows and/or lakes at fine grid cell resolutions.

Mannings n

This is the roughness coefficient utilised in C-L. A spatially homogenous value of 0.03 was selected, using the reference guide suggested in the C-L user manual (Forest Science Labs, 2015).

Spatially variable Mannings n

This is a text file that is the same format and size as the DEM, in which a different n value can be applied to each cell as required. This option is not being utilised by this study.

Soil development

The soil development components of C-L allow sediment and soil within the model to weather down over time to smaller grain size fractions. This is at present experimental and therefore not utilised in this study.

B. Setup of remaining synergistic scenarios

For the remaining 10 synergistic scenarios, the inflow header file, stage/tidal input file and description tab are modified as below. All other model parameters are set as in table 5.5 and remain at the baseline value.

1WWW (Wet monsoon, Wet post-monsoon, Wet dry season, moderate temperature increase)

This scenario explores the impact of increased precipitation throughout all seasons.

Inflow header file: Seasonal precipitation totals increase at a linear rate, reaching +15% by the year 2075. Daily variability and extreme rainfall events are unchanged. Average annual air temperature increases at a linear rate, reaching +1.1˚C by 2100.

Stage/tidal input: Local mean sea-level increases at a linear rate, reaching +0.36 metres by the year 2075.

2DDD (Dry monsoon, Dry post-monsoon, Dry dry season, moderate temperature increase)

This scenario investigates the impact of decreased precipitation throughout all seasons.

Inflow header file: Seasonal precipitation totals decrease at a linear rate, reaching -25% by the year 2075. Daily variability and extreme rainfall events are unchanged. Average annual air temperature increases at a linear rate, reaching +1.1˚C by 2100.

Stage/tidal input: Local mean sea-level increases at a linear rate, reaching +0.36 metres by the year 2075.

3WDD (Wet monsoon, Dry post-monsoon, Dry dry season, moderate temperature increase)

This scenario explores the impact of the monsoon becoming increasingly wetter and more variable, whilst decreased precipitation is experienced during other seasons.

Inflow header file: Monsoon precipitation totals increase at a linear rate, reaching +15% by the year 2075. Daily variability of monsoon precipitation fluctuates at a linear rate by up to +30%/-15% by the year 2075. Post-monsoon and dry season precipitation totals decrease at a linear rate, reaching -25% by the year 2075. Daily variability during these seasons is unchanged. Average annual air temperature increases at a linear rate, reaching +1.1˚ C by 2100.

Stage/tidal input: Local mean sea-level increases at a linear rate, reaching +0.36 metres by the year 2075.

4DWD (Drier, more variable monsoon, Wet post-monsoon, Dry dry season, variable sediment supply, moderate temperature increase)

This scenario describes the 'most likely pathway' for the Mahanadi region based on the current literature.

Inflow header file: Monsoon precipitation totals decrease at a linear rate, reaching -25% by the year 2075. Daily variability of monsoon precipitation fluctuates at a linear rate by up to 50%/-25% by the year 2075. Post-monsoon precipitation totals increase at a linear rate, reaching -+15% by the year 2075. Dry season precipitation totals decrease at a linear rate, reaching -25% by the year 2075. Daily variability during these seasons is unchanged. Daily sediment totals fluctuate by up to +/-30% by the year 2065 although the total available to the system each year remains the same. Average annual air temperature increases at a linear rate, reaching +1.1˚ C by 2100.

Stage/tidal input: Local mean sea-level increases at a linear rate, reaching +0.36 metres by the year 2075.

5DWA (Drier, more variable monsoon, Wet post-monsoon, Accelerated drought in dry season, moderate temperature increase, variable sediment supply)

This scenario investigates the impacts of extreme drought during the dry season.

Inflow header file: As in 4DWD but with modified dry season precipitation. Dry season precipitation totals decrease at an enhanced rate, reaching -25% by the year 2075. Daily variability during these seasons is unchanged. Average

annual air temperature increases at a linear rate, reaching +1.1˚ C by 2100. Daily sediment totals fluctuate by up to +/-30% by the year 2065.

Stage/tidal input: Local mean sea-level increases at a linear rate, reaching +0.36 metres by the year 2075.

6WDDH (Wet monsoon, Dry post-monsoon, Dry dry season, High sea-level rise, high temperature increase)

This scenario investigates the impact of high sea-level rise and seasonal precipitation variability.

Inflow header file: As in 3WDD, however average annual air temperature increases at a linear rate, reaching +2.3˚ C by 2100.

Stage/tidal input: Local mean sea-level increases at a higher linear rate, reaching +0.6 metres by the year 2075.

7DWDH (Drier, more variable monsoon, Wet post-monsoon, Dry dry season, High sea-level rise, high temperature increase, variable sediment supply)

This scenario investigates the impact of high sea-level rise and seasonal precipitation variability.

Inflow header file: As in 4DWD, however average annual air temperature increases at a linear rate, reaching +2.3˚ C by 2100.

Stage/tidal input: Local mean sea-level increases at a higher linear rate, reaching +0.6 metres by the year 2075.

8DWAH (Drier, more variable monsoon, Wet post-monsoon, Accelerated drought in dry season, High sea-level rise, high temperature increase, variable sediment supply)

This scenario investigates multiple stressors including the impact of high sea-level rise, sediment flux variability and extreme drought.

Inflow header file: As in 5DWA, however average annual air temperature increases at a linear rate, reaching +2.3˚ C by 2100.

Stage/tidal input: Local mean sea-level increases at a higher linear rate, reaching +0.6 metres by the year 2075.

9DWDC (Drier, more variable monsoon, Wet post-monsoon, Dry dry season, increase severe Cyclone frequency, moderate temperature increase, variable sediment supply)

This scenario explores the impacts of increased severe cyclone frequency.

Inflow header file: As in 4DWD, with a 1 in 10 year severe cyclone frequency.

Stage/tidal input: Local mean sea-level increases at a linear rate, reaching +0.36 metres by the year 2075.

10DWDF (Drier, more variable monsoon, Wet post-monsoon, Dry dry season, Failure of monsoon rains from 2065, moderate temperature increase, variable sediment supply)

This extreme scenario investigates the impact of the monsoon rains failing from the year 2065.

Inflow header file: As in 4DWD until 2065. From 2065-2075 the monsoon rains fail and instead dry season precipitation totals persist into the summer months.

Stage/tidal input: Local mean sea-level increases at a linear rate, reaching +0.36 metres by the year 2075.

C. Morphological modelling results

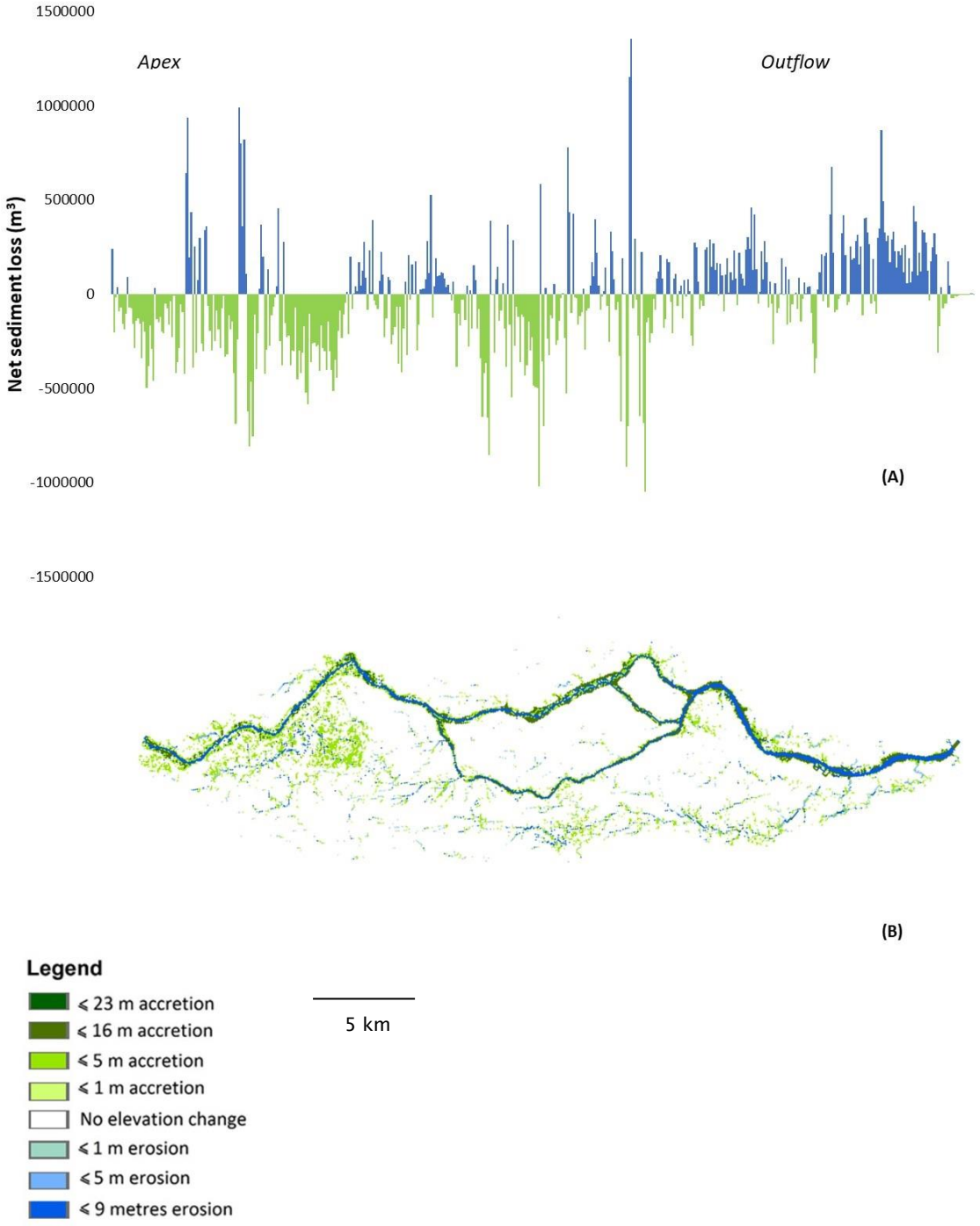

Figure C.1 **(A)** Net sediment loss and (B) Elevation change at 30 years under scenario 1WWW, Devi catchment. The x-axis in figure A corresponds to distance from the catchment apex (left) to the catchment outflow (right).

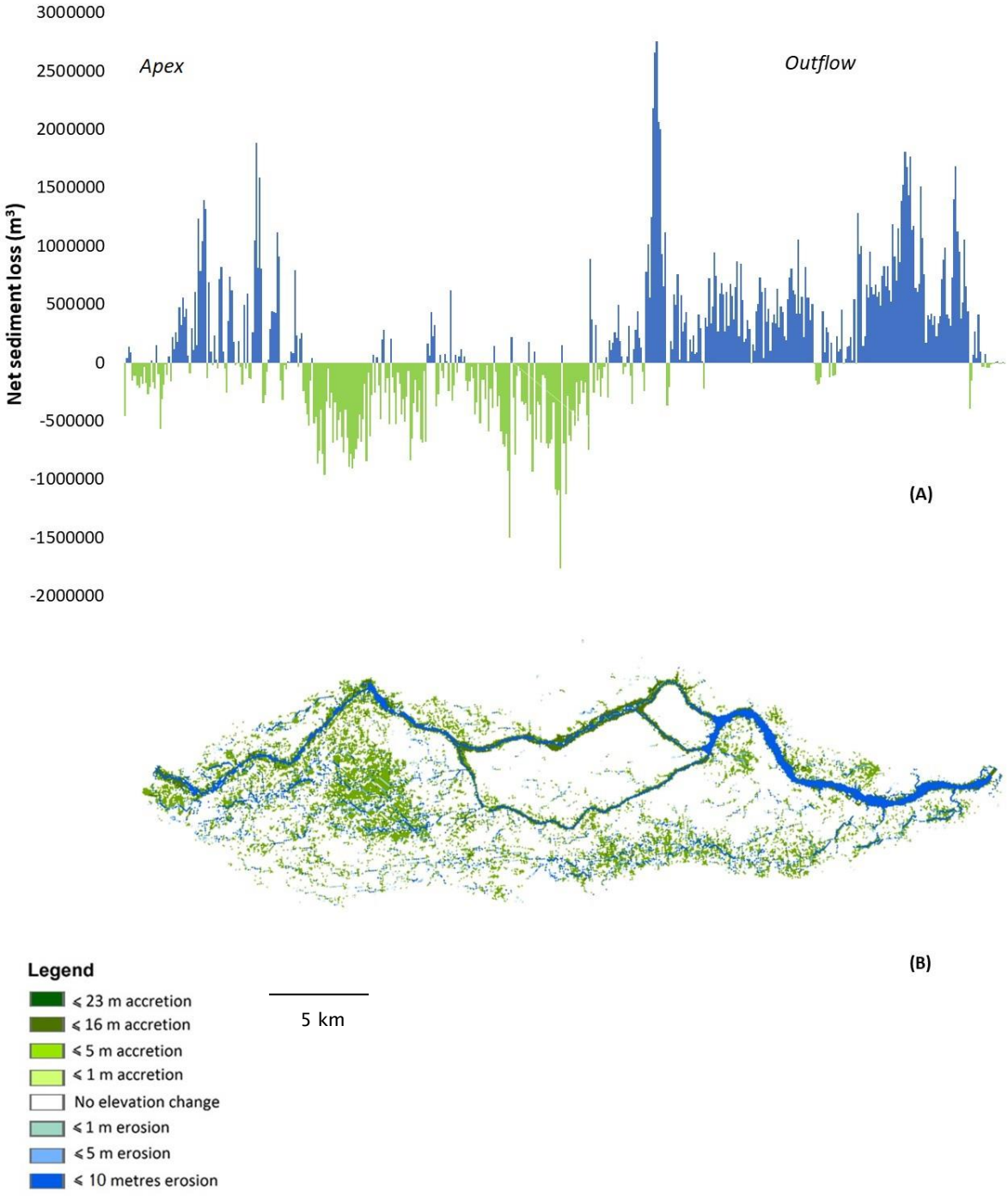

Figure C.2 (A) Net sediment loss and (B) Elevation change at 50 years under scenario 1WWW, Devi catchment. The x-axis in figure A corresponds to distance from the catchment apex (left) to the catchment outflow (right).

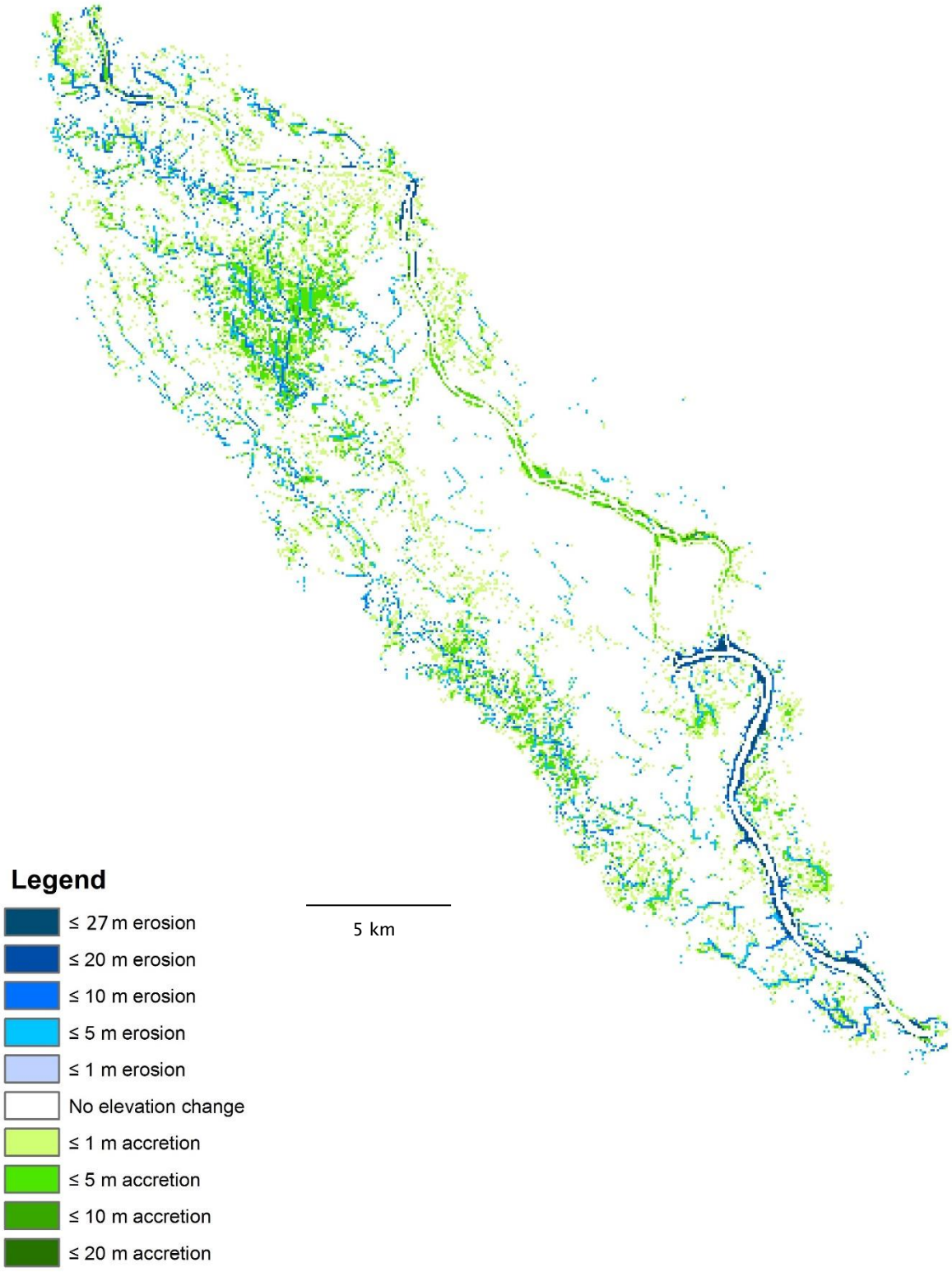

Figure C.3 Elevation change between 30 and 50 years under scenario 1WWW, Devi catchment.

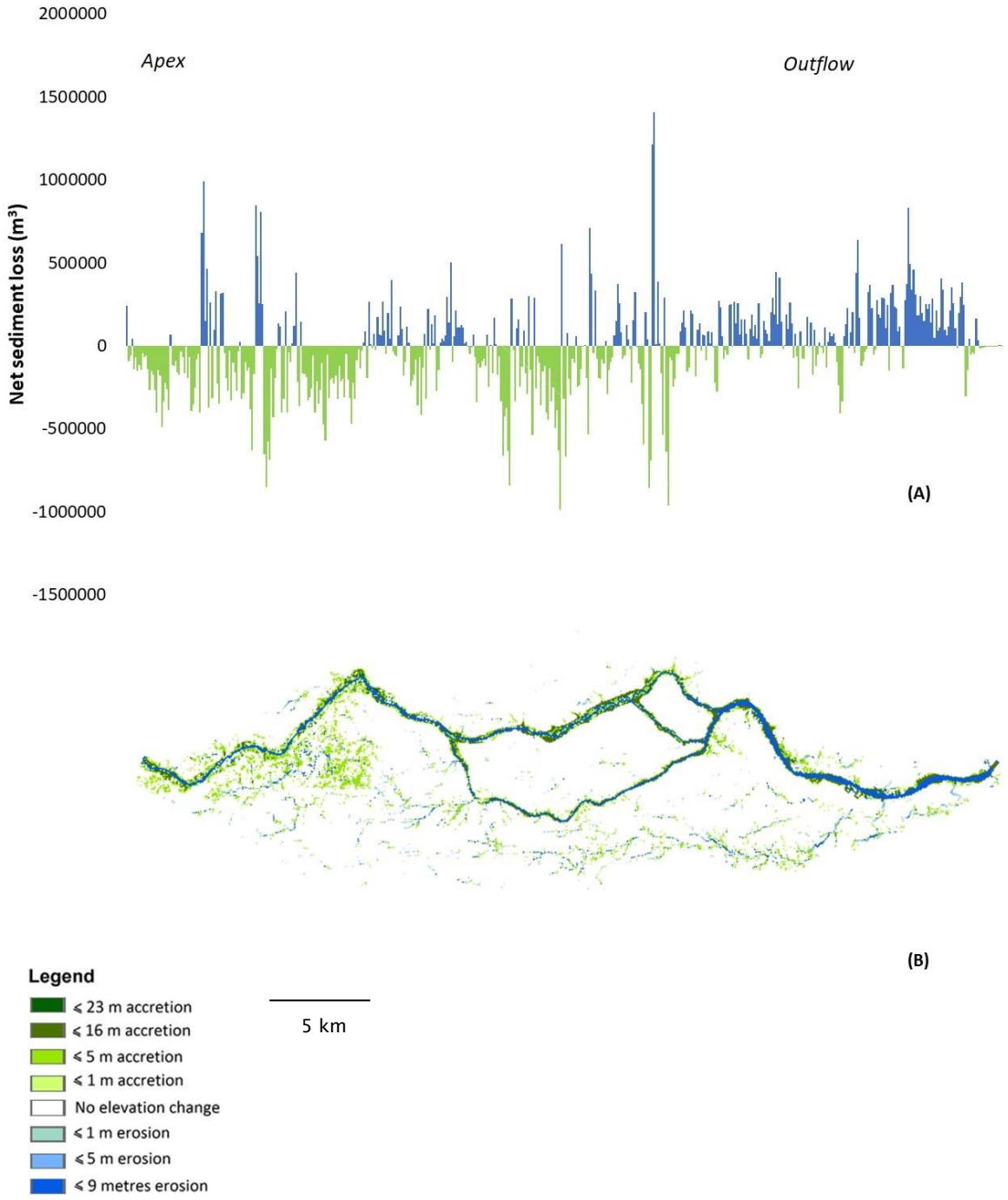

Figure C.4 (A) Net sediment loss and (B) Elevation change at 30 years under scenario 2DDD, Devi catchment. The x-axis in figure A corresponds to distance from the catchment apex (left) to the catchment outflow (right).

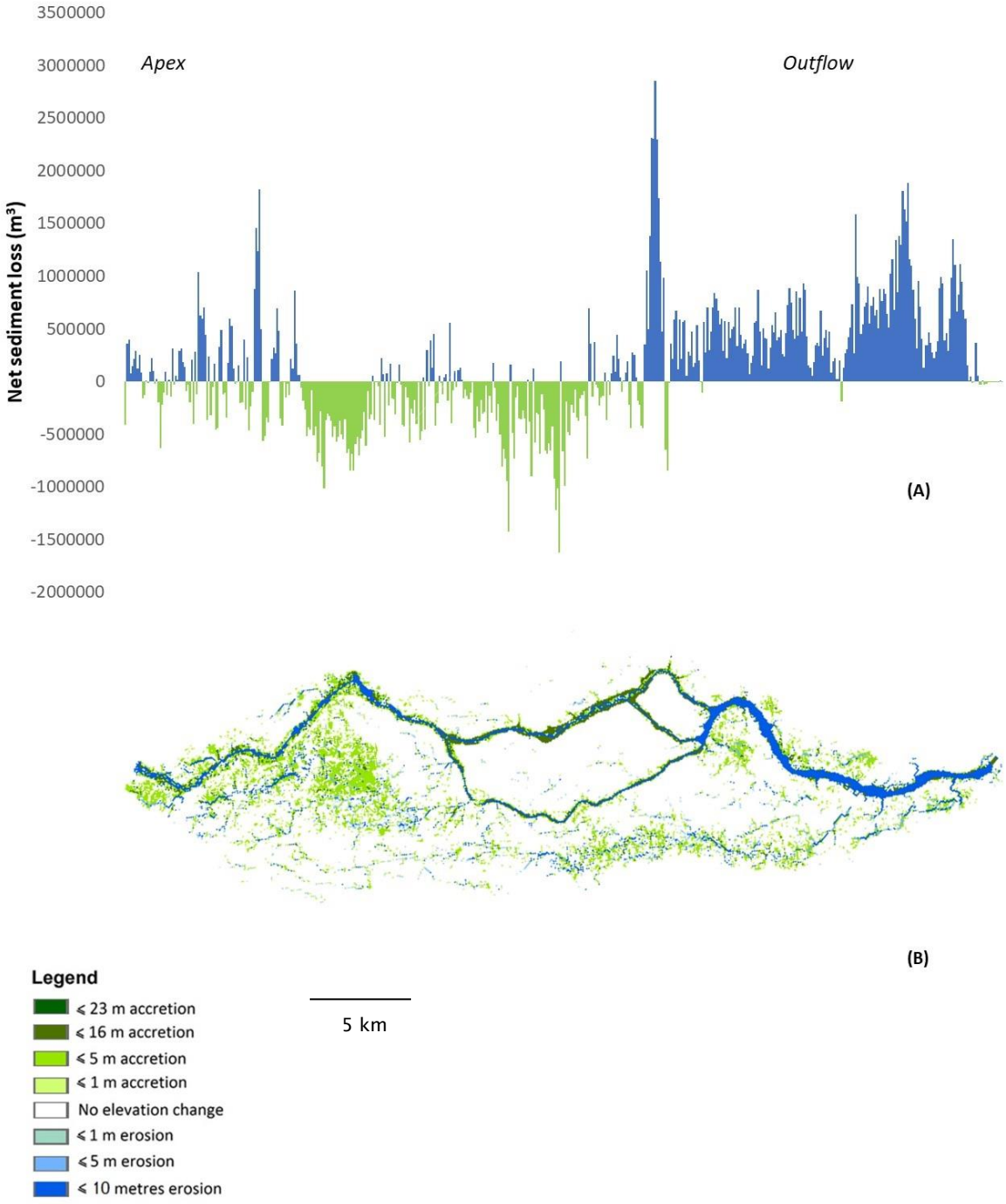

Figure C.5 (A) Net sediment loss and (B) Elevation change at 50 years under scenario 2DDD, Devi catchment. The x-axis in figure A corresponds to distance from the catchment apex (left) to the catchment outflow (right).

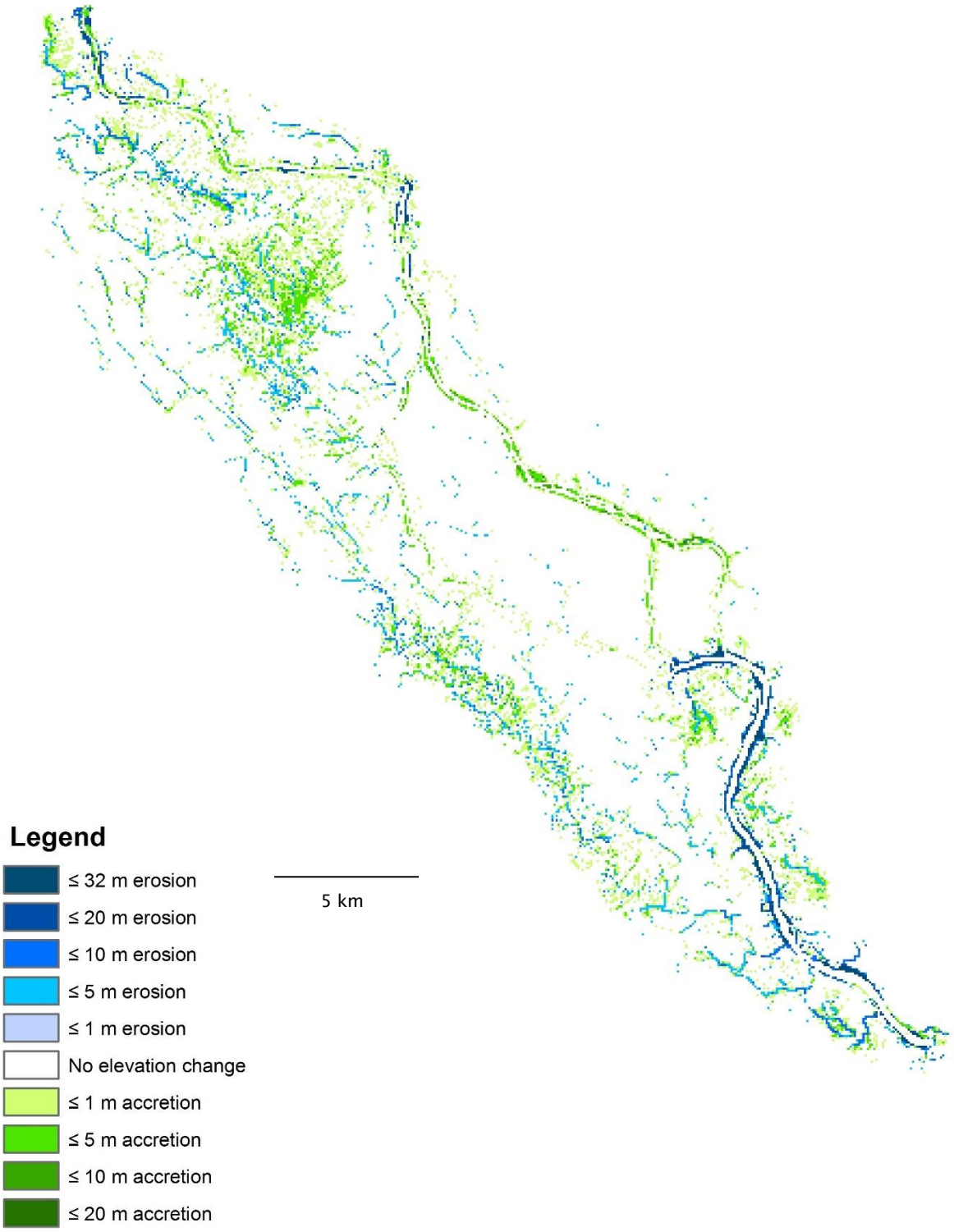

Figure C.6 Elevation change between 30 and 50 years under scenario 2DDD, Devi catchment.

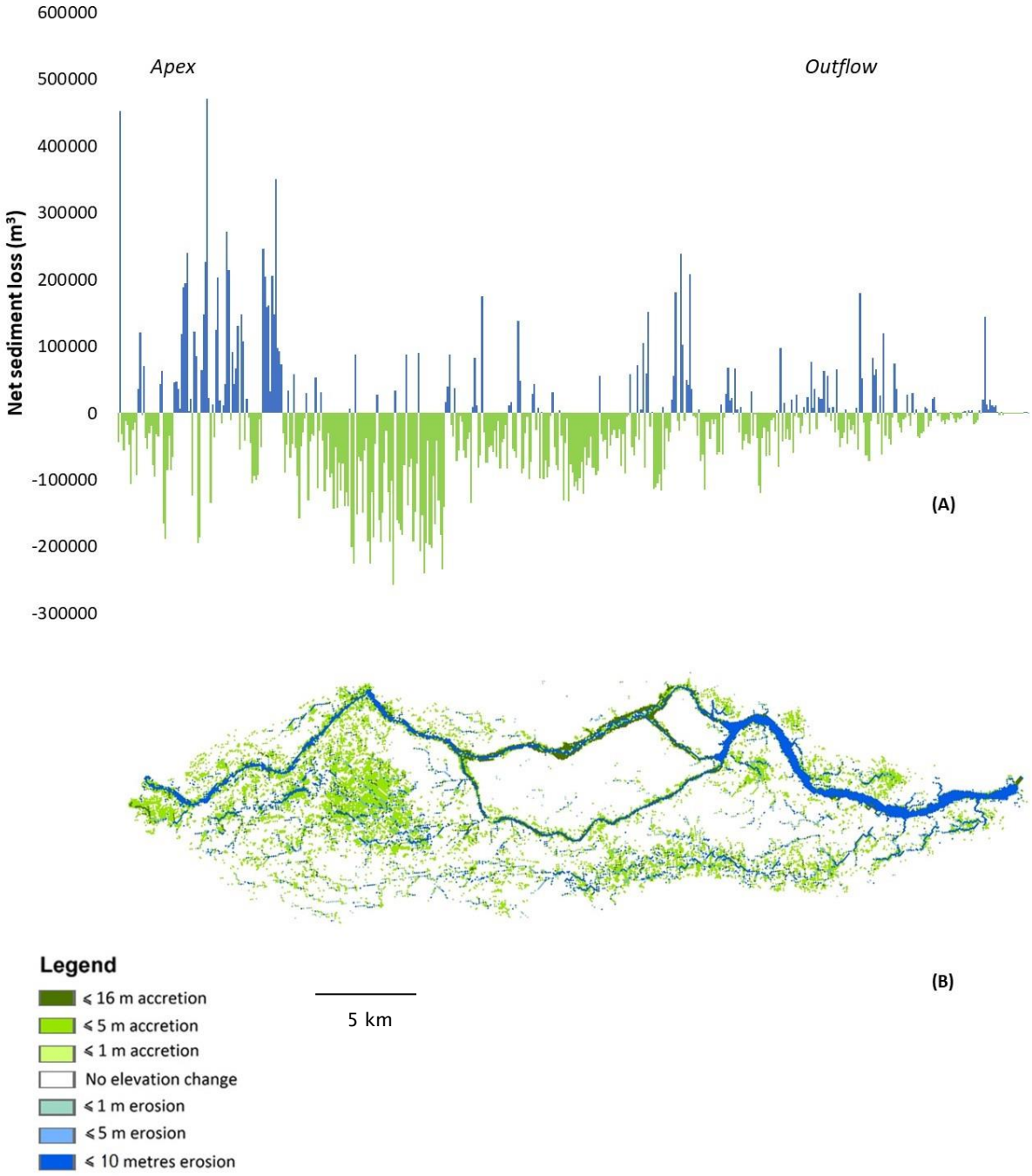

Figure C.7 (A) Net sediment loss and (B) Elevation change at 30 years under scenario 3WDD, Devi catchment. The x-axis in figure A corresponds to distance from the catchment apex (left) to the catchment outflow (right).

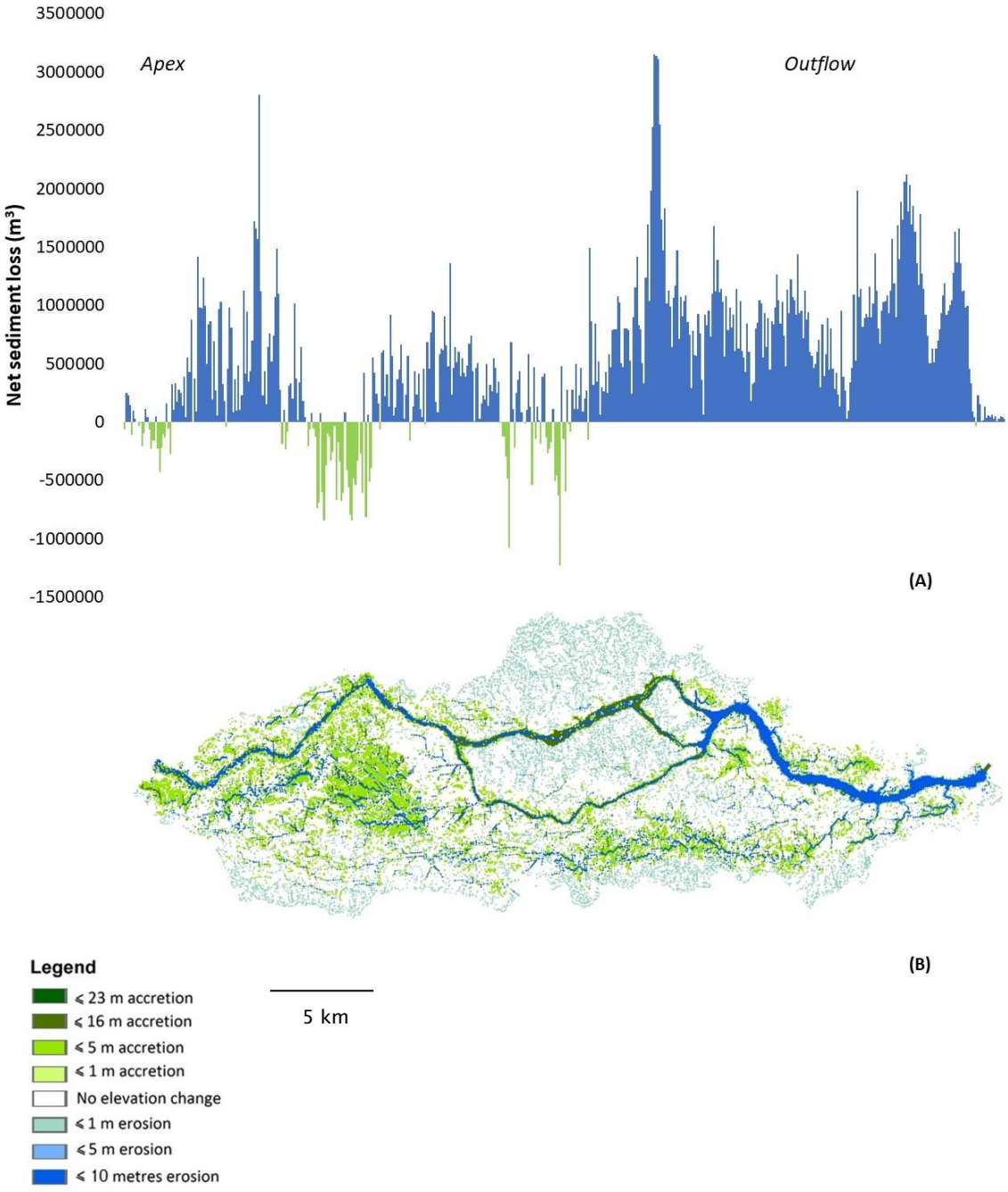

Figure C.8 (A) Net sediment loss and (B) Elevation change at 50 years under scenario 3WDD, Devi catchment. The x-axis in figure A corresponds to distance from the catchment apex (left) to the catchment outflow (right).

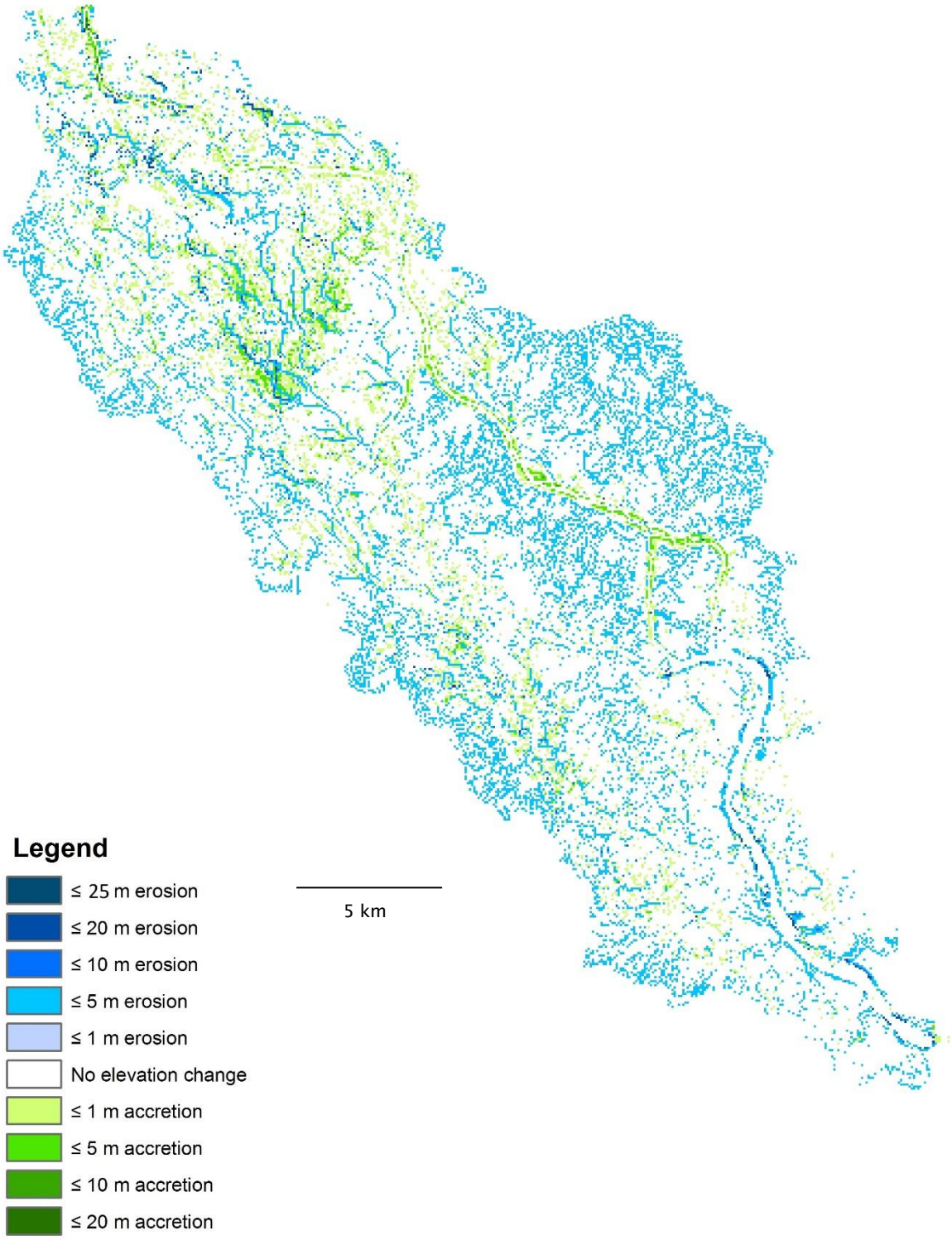

Figure C.9 Elevation change between 30 and 50 years under scenario 3WDD, Devi catchment.

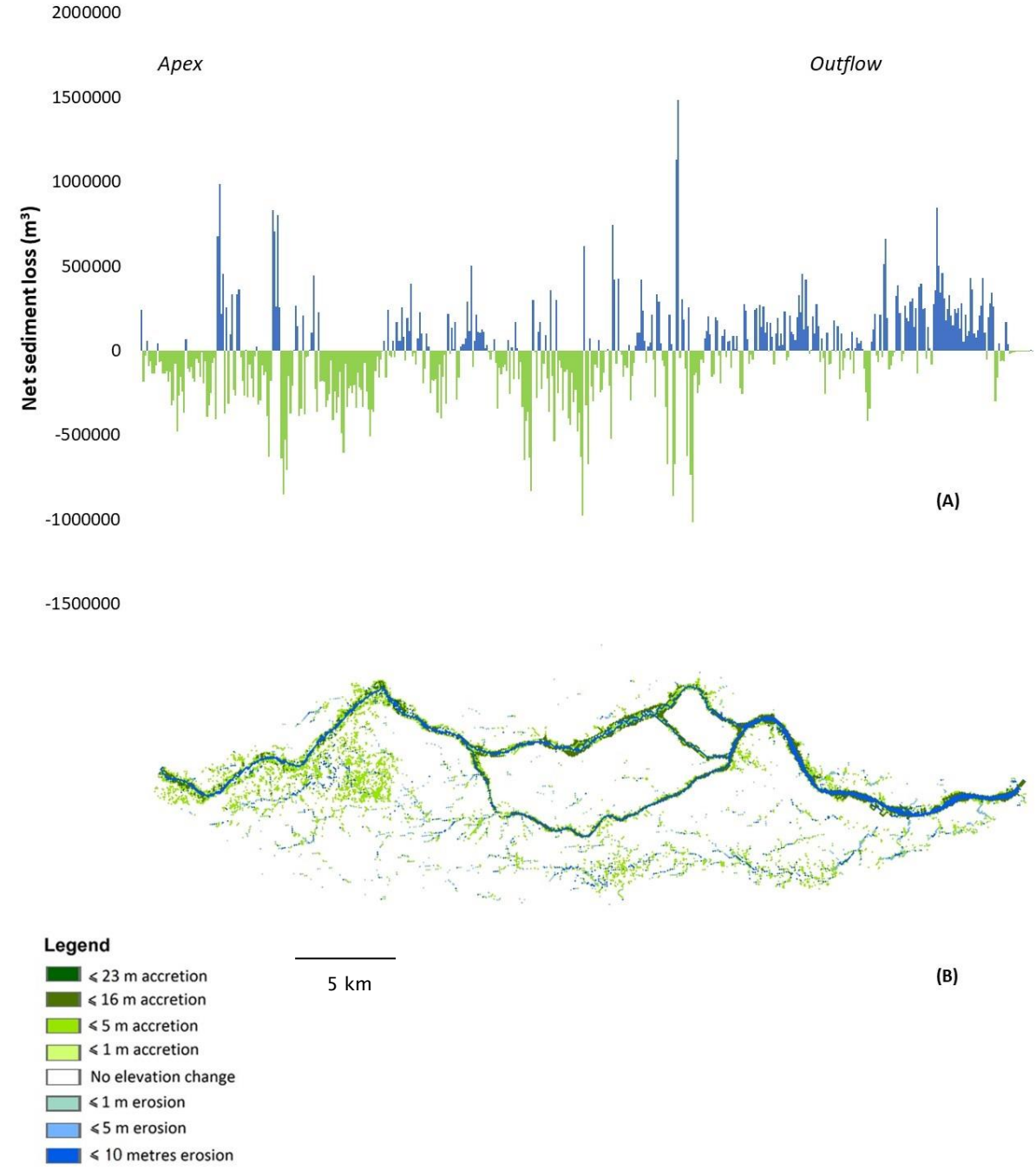

Figure C.10 (A) Net sediment loss and (B) Elevation change at 30 years under scenario 4DWD, Devi catchment. The x-axis in figure A corresponds to distance from the catchment apex (left) to the catchment outflow (right).

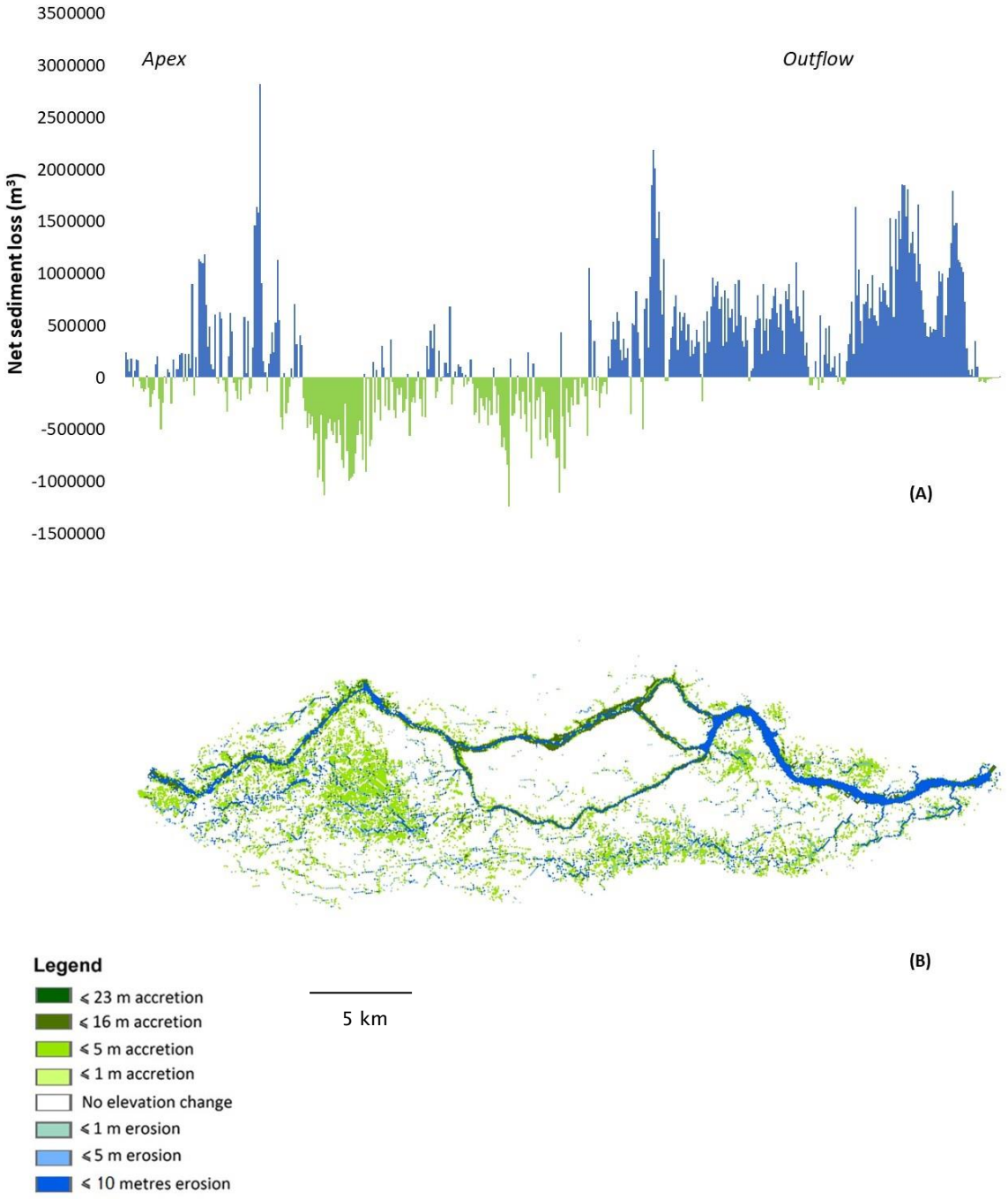

Figure C.11 (A) Net sediment loss and (B) Elevation change at 50 years under scenario 4DWD, Devi catchment. The x-axis in figure A corresponds to distance from the catchment apex (left) to the catchment outflow (right).

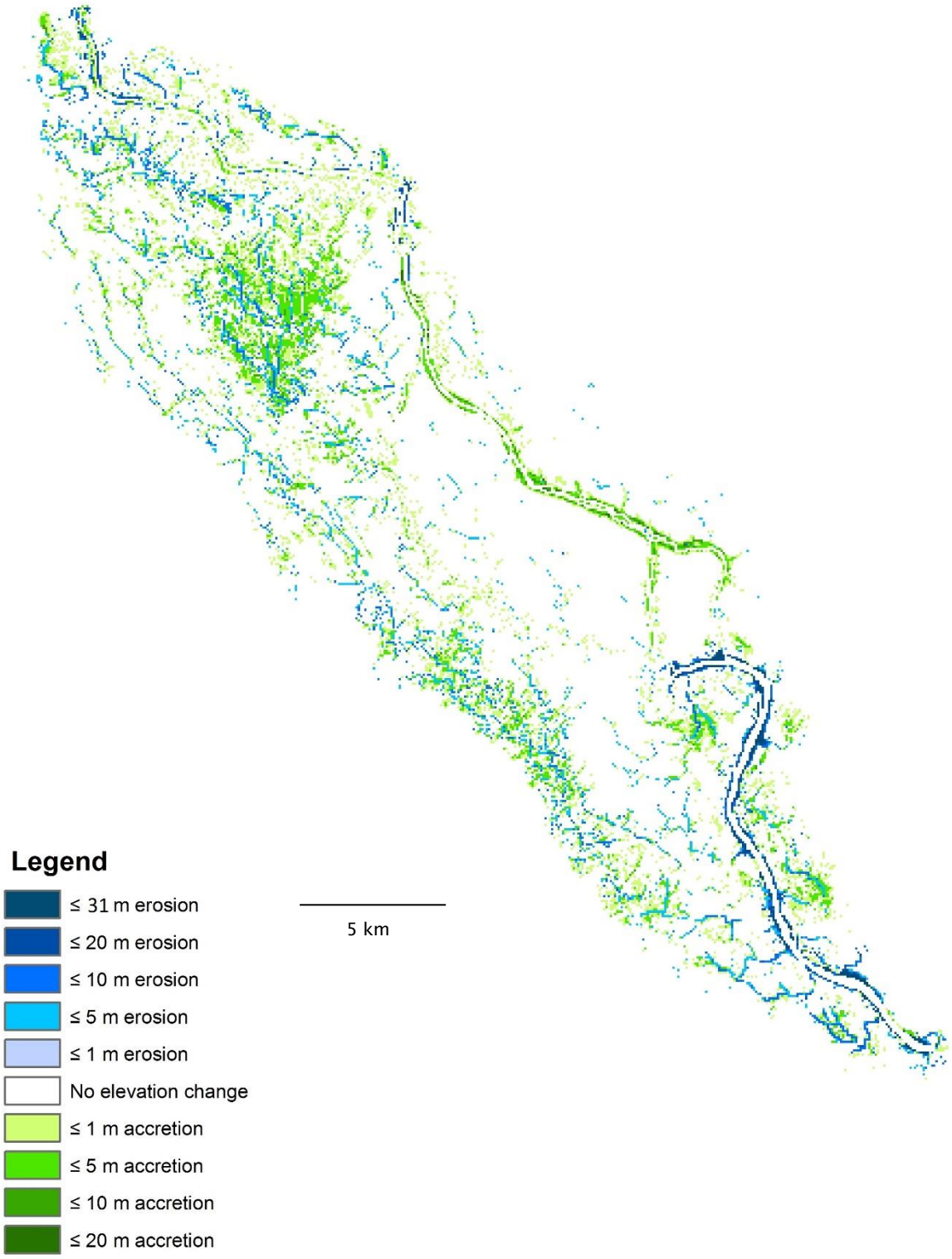

Figure C.12 Elevation change between 30 and 50 years under scenario 4DWD, Devi catchment.

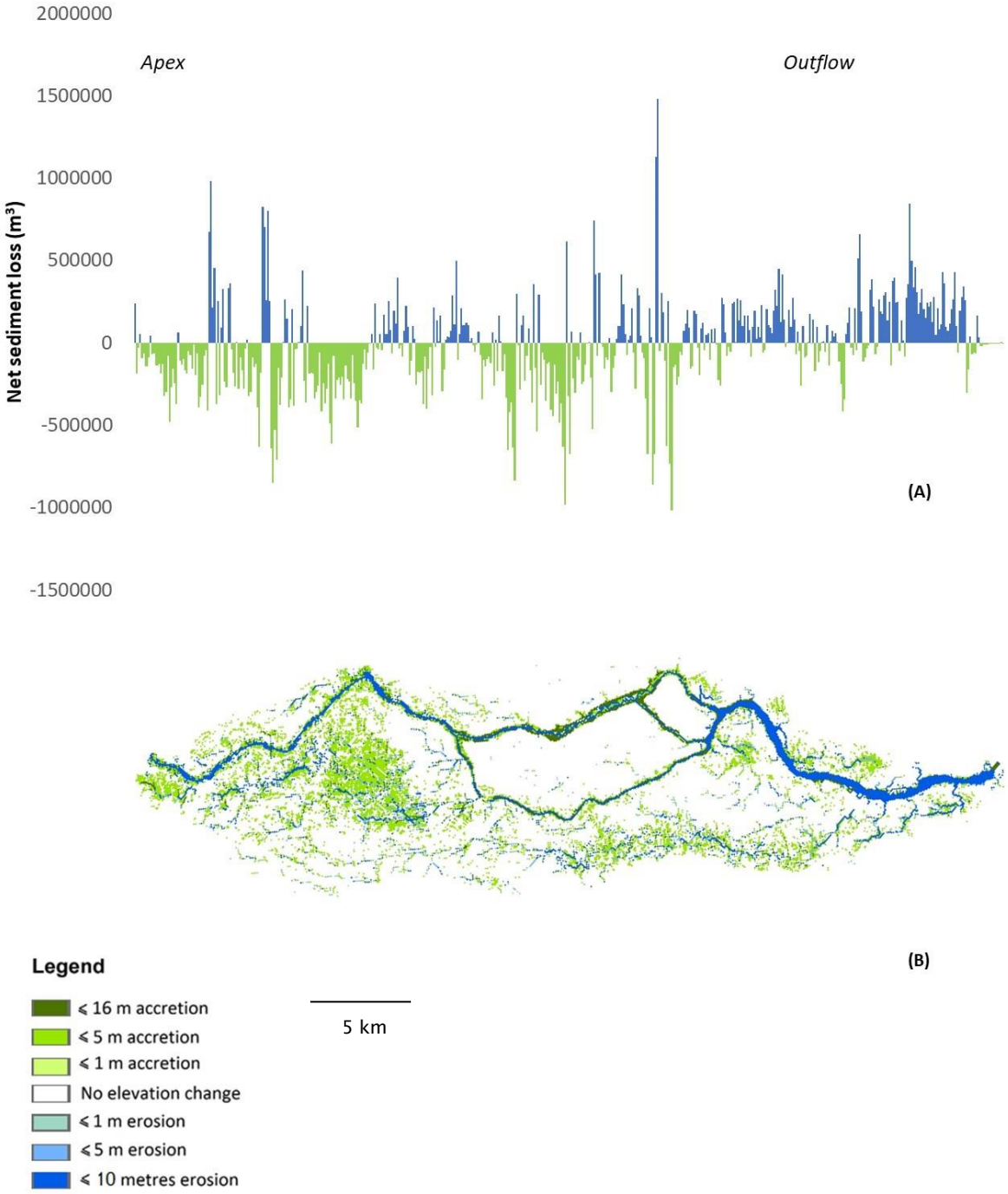

Figure C.13 (A) Net sediment loss and (B) Elevation change at 30 years under scenario 5DWA, Devi catchment. The x-axis in figure A corresponds to distance from the catchment apex (left) to the catchment outflow (right).

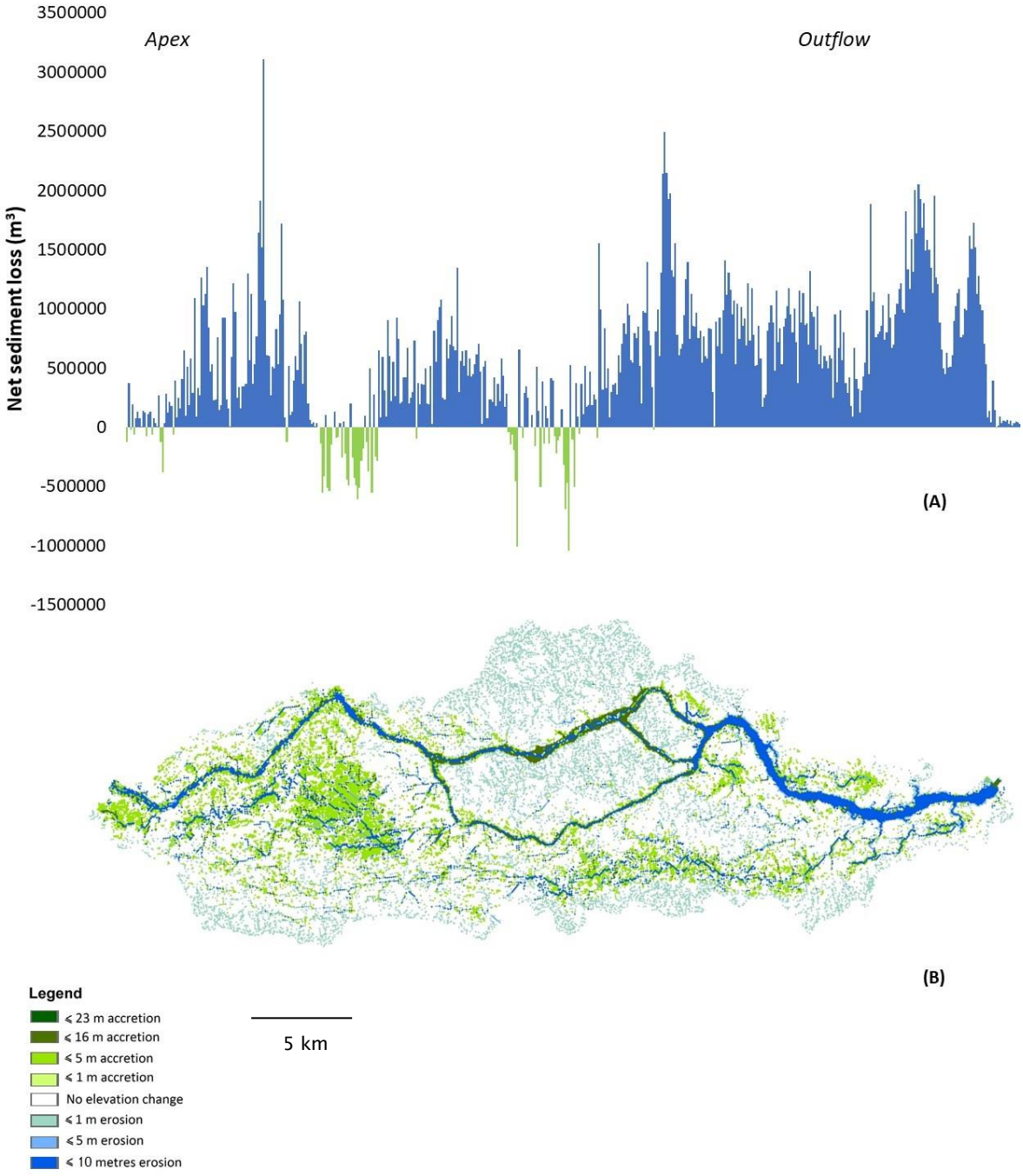

Figure C.14 (A) Net sediment loss and (B) Elevation change at 50 years under scenario 5DWA, Devi catchment. The x-axis in figure A corresponds to distance from the catchment apex (left) to the catchment outflow (right).

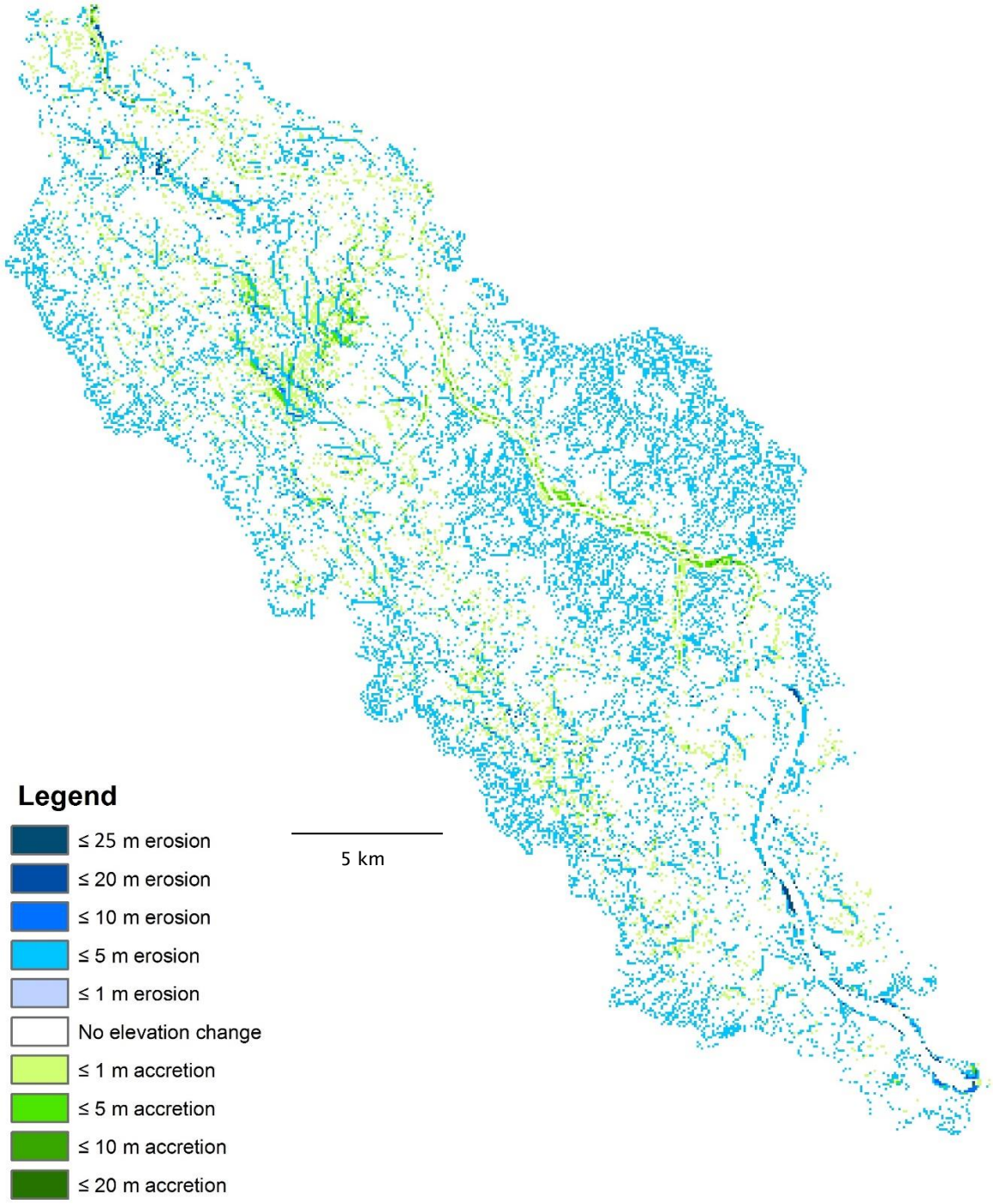

Figure C.15 Elevation change between 30 and 50 years under scenario 5DWA, Devi catchment.

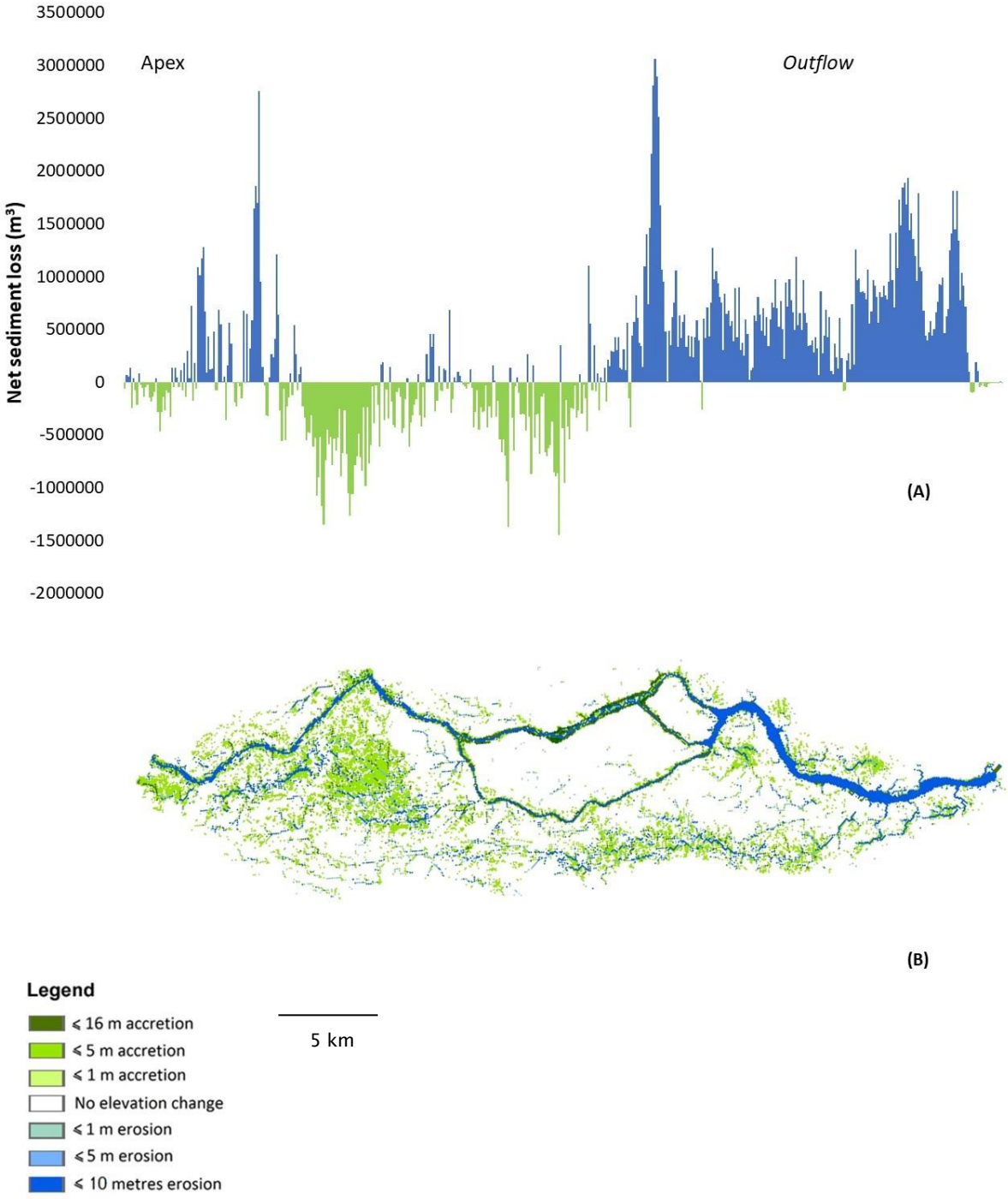

Figure C.16 (A) Net sediment loss and (B) Elevation change at 30 years under scenario 6WDDH, Devi catchment. The x-axis in figure A corresponds to distance from the catchment apex (left) to the catchment outflow (right).

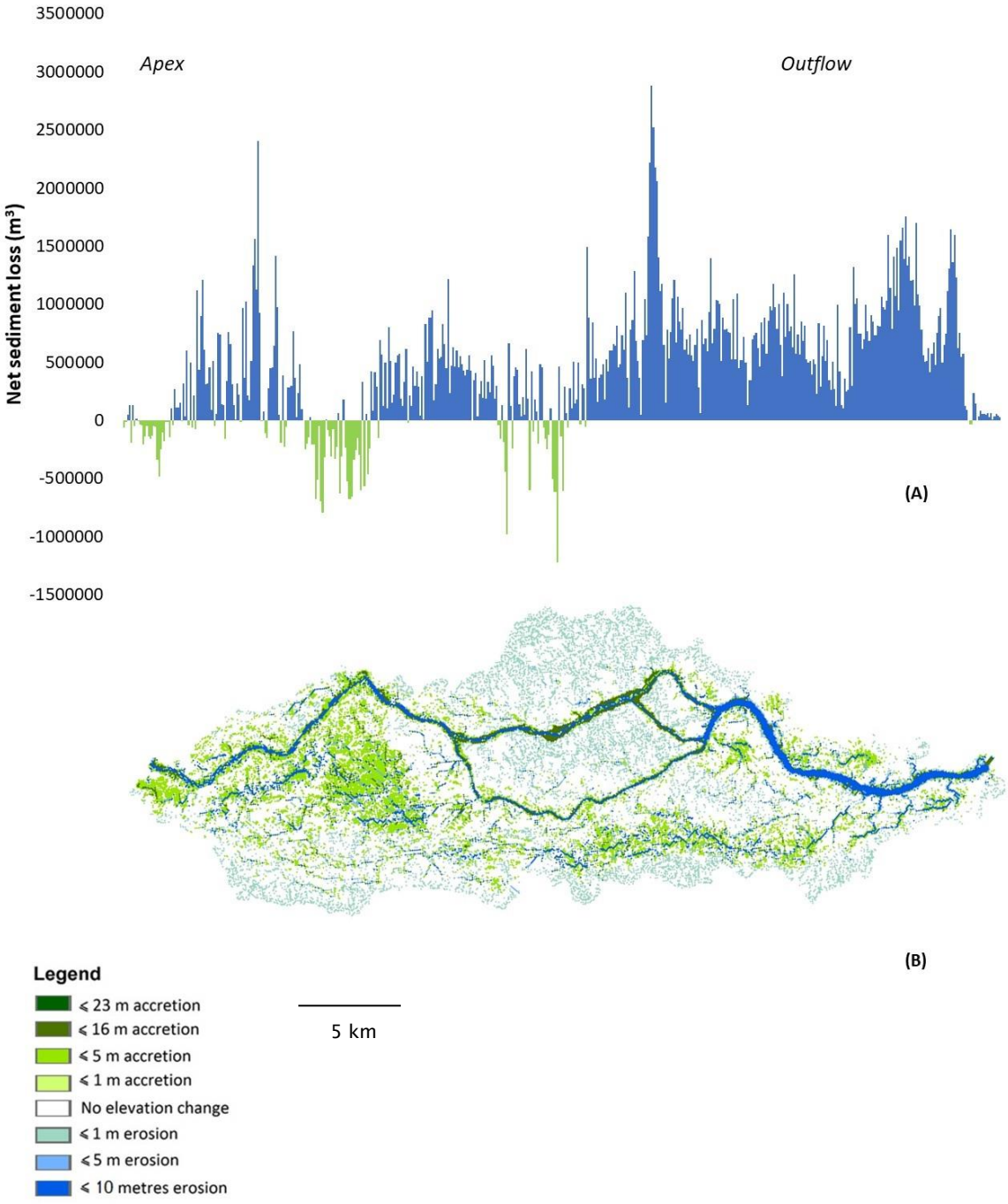

Figure C.17 (A) Net sediment loss and (B) Elevation change at 50 years under scenario 6WDDH, Devi catchment. The x-axis in figure A corresponds to distance from the catchment apex (left) to the catchment outflow (right).

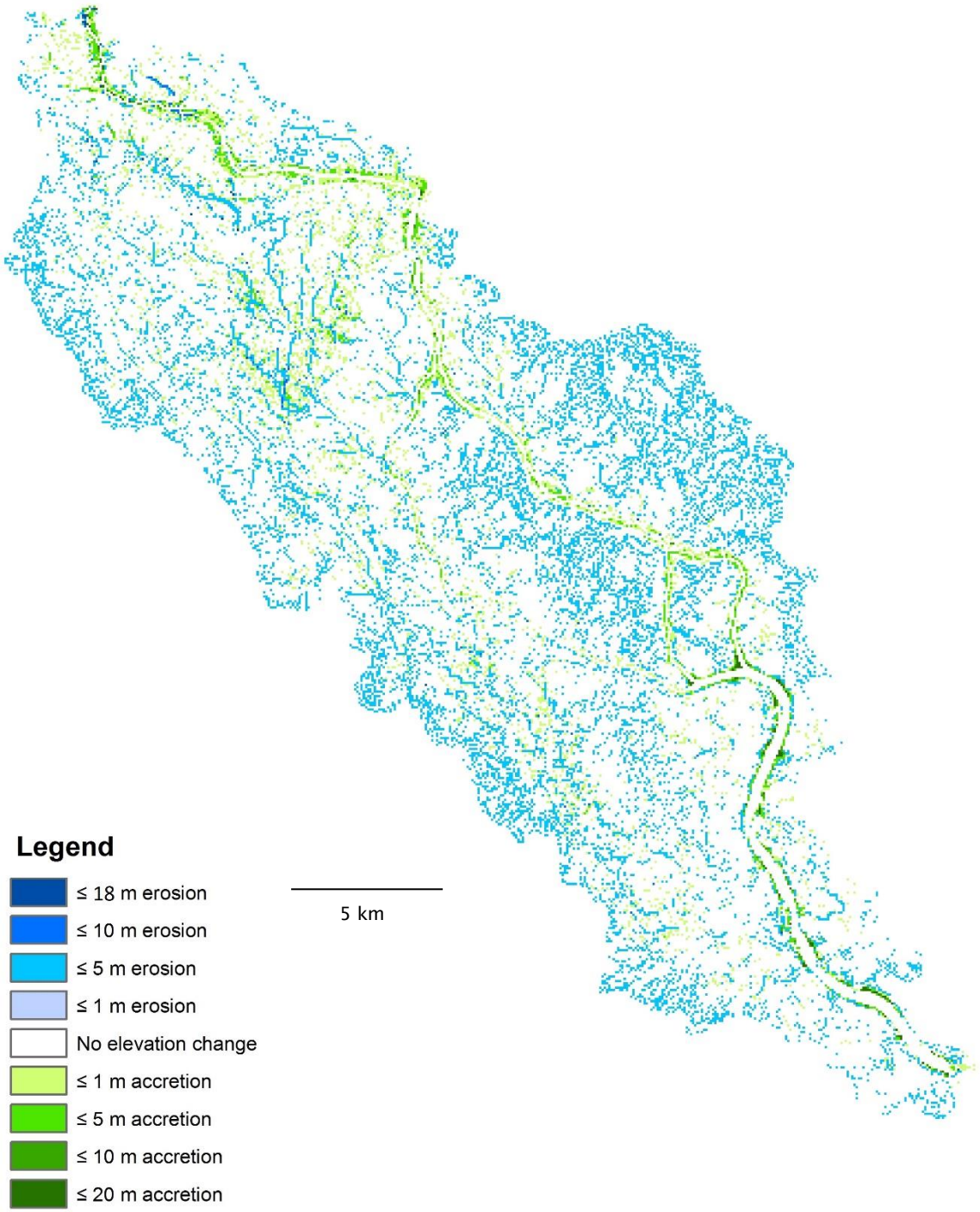

Figure C.18 Elevation change between 30 and 50 years under scenario 6WDDH, Devi catchment.

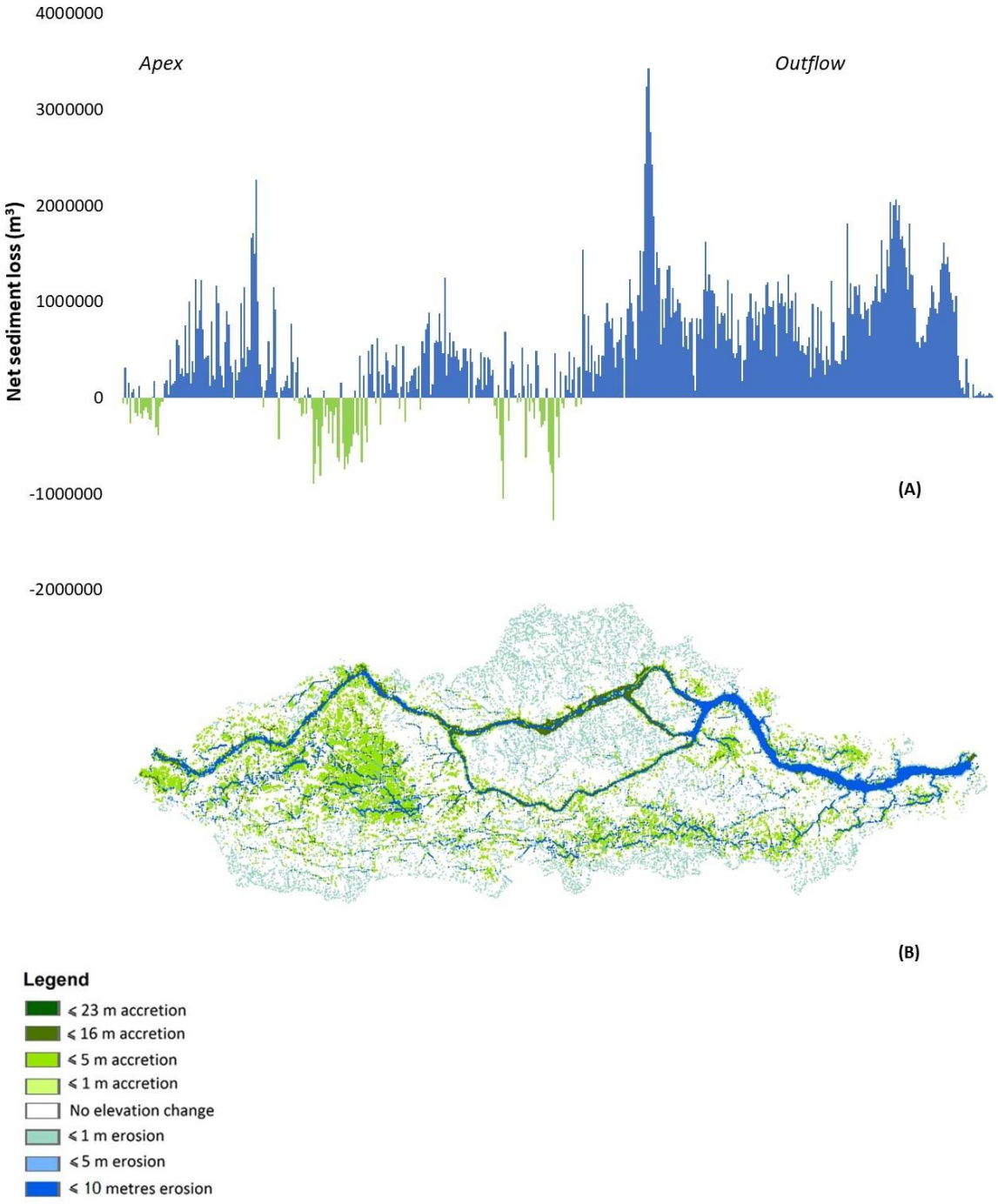

Figure C.19 (A) Net sediment loss and (B) Elevation change at 30 years under scenario 7DWDH, Devi catchment. The x-axis in figure A corresponds to distance from the catchment apex (left) to the catchment outflow (right).

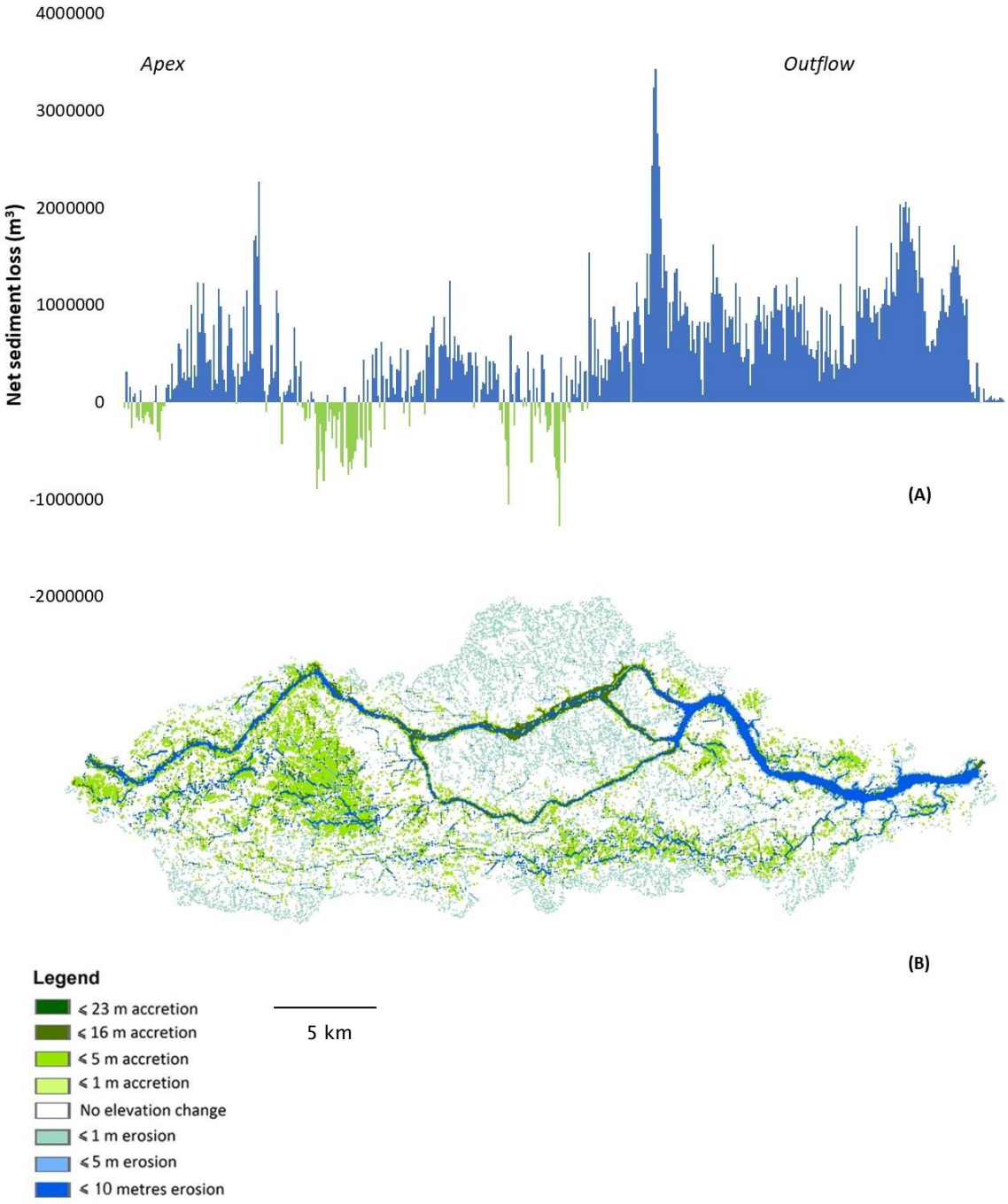

Figure C.20 (A) Net sediment loss and (B) Elevation change at 50 years under scenario 7DWDH, Devi catchment. The x-axis in figure A corresponds to distance from the catchment apex (left) to the catchment outflow (right).

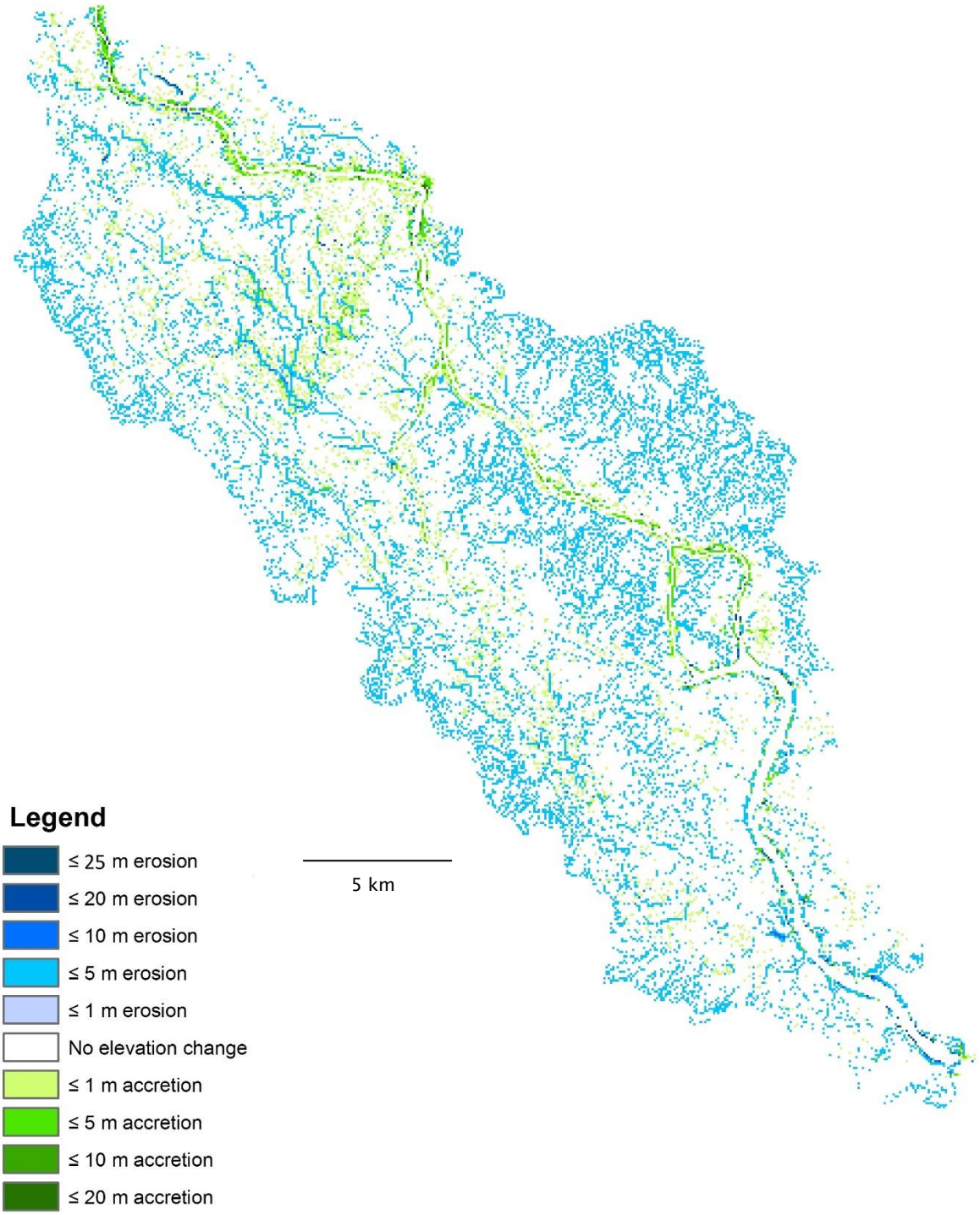

Figure C.21 Elevation change between 30 and 50 years under scenario 7DWDH, Devi catchment.

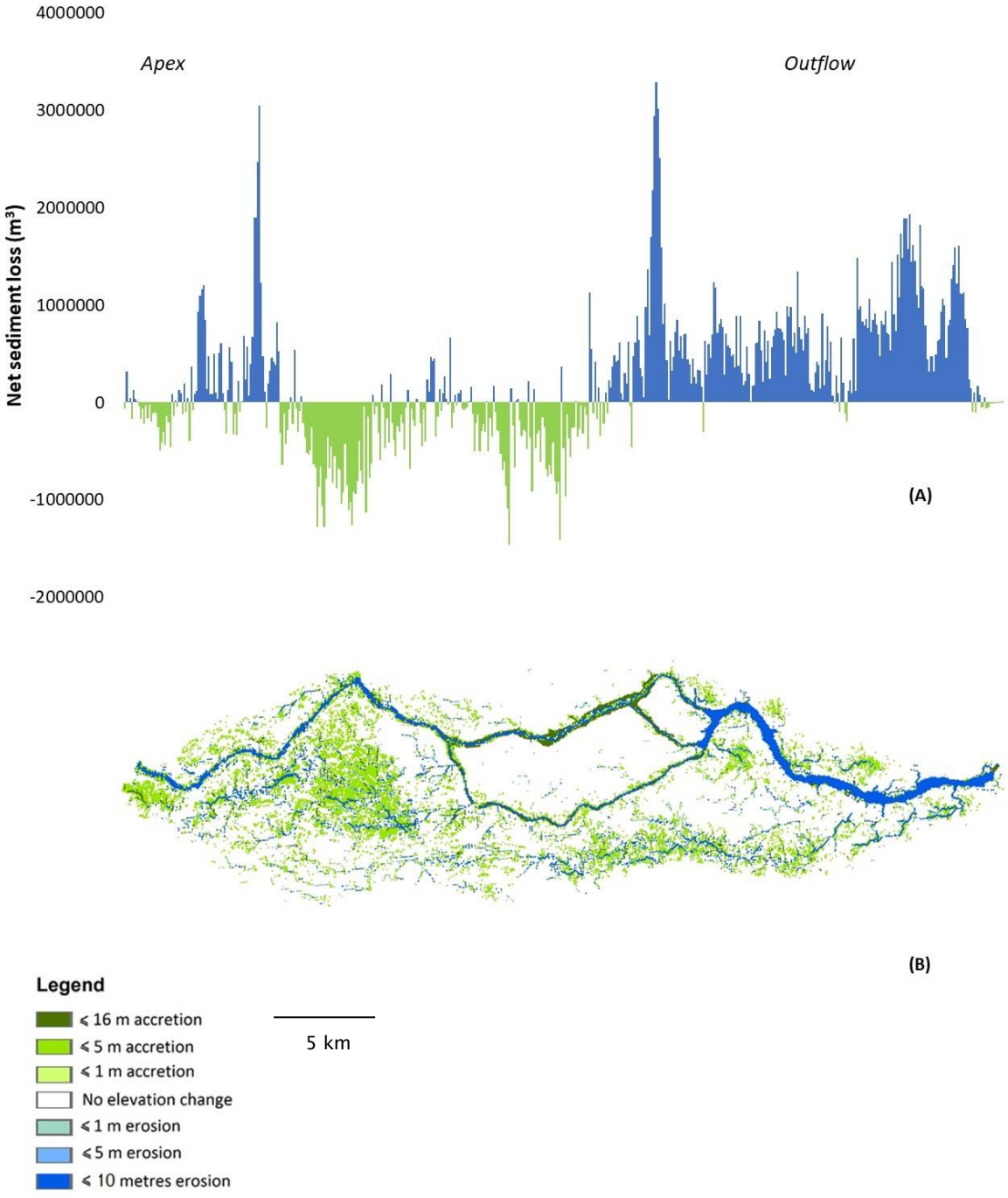

Figure C.22 (A) Net sediment loss and (B) Elevation change at 30 years under scenario 8DWAH, Devi catchment. The x-axis in figure A corresponds to distance from the catchment apex (left) to the catchment outflow (right).

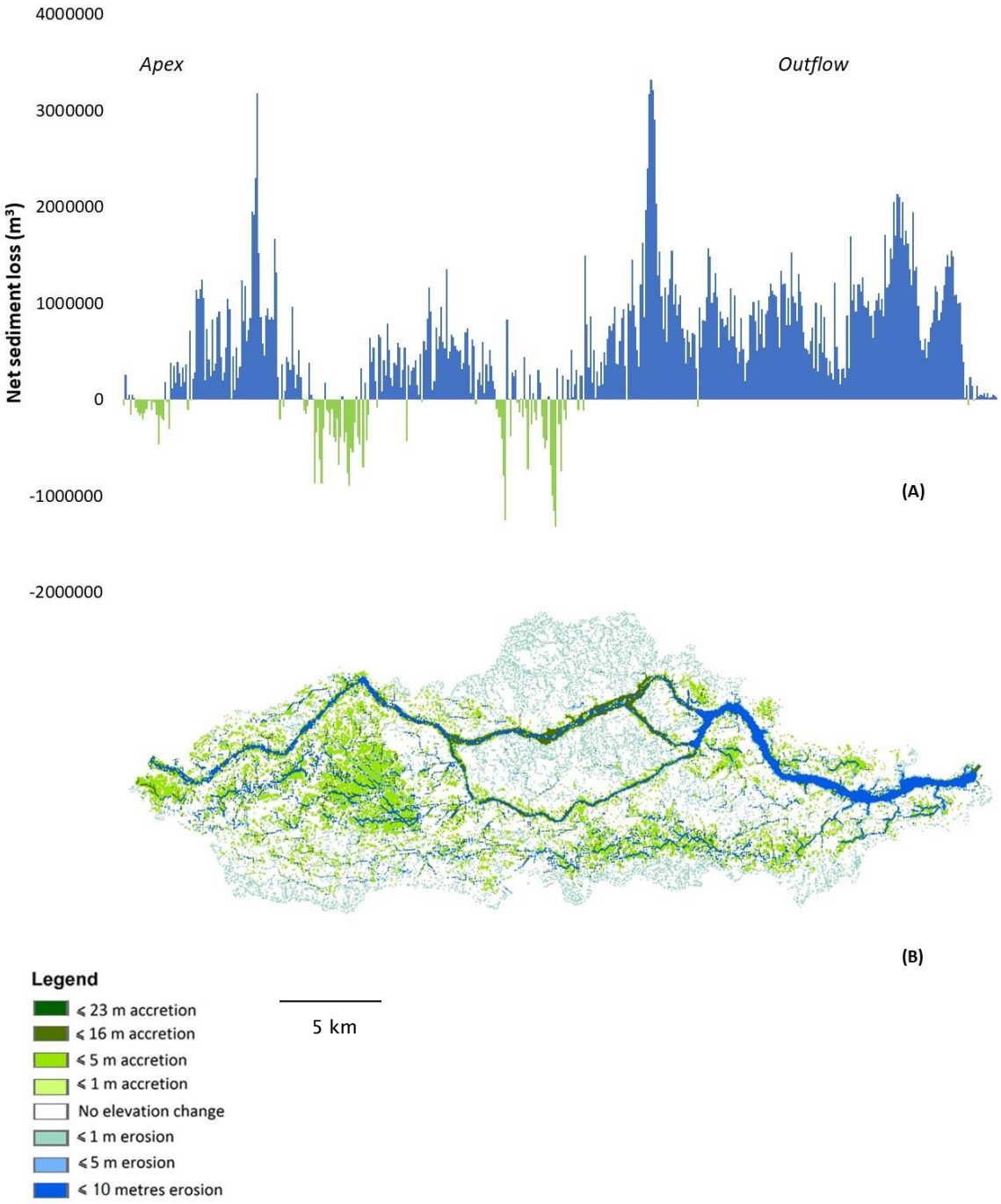

Figure C.23 (A) Net sediment loss and (B) Elevation change at 50 years under scenario 8DWAH, Devi catchment. The x-axis in figure A corresponds to distance from the catchment apex (left) to the catchment outflow (right).

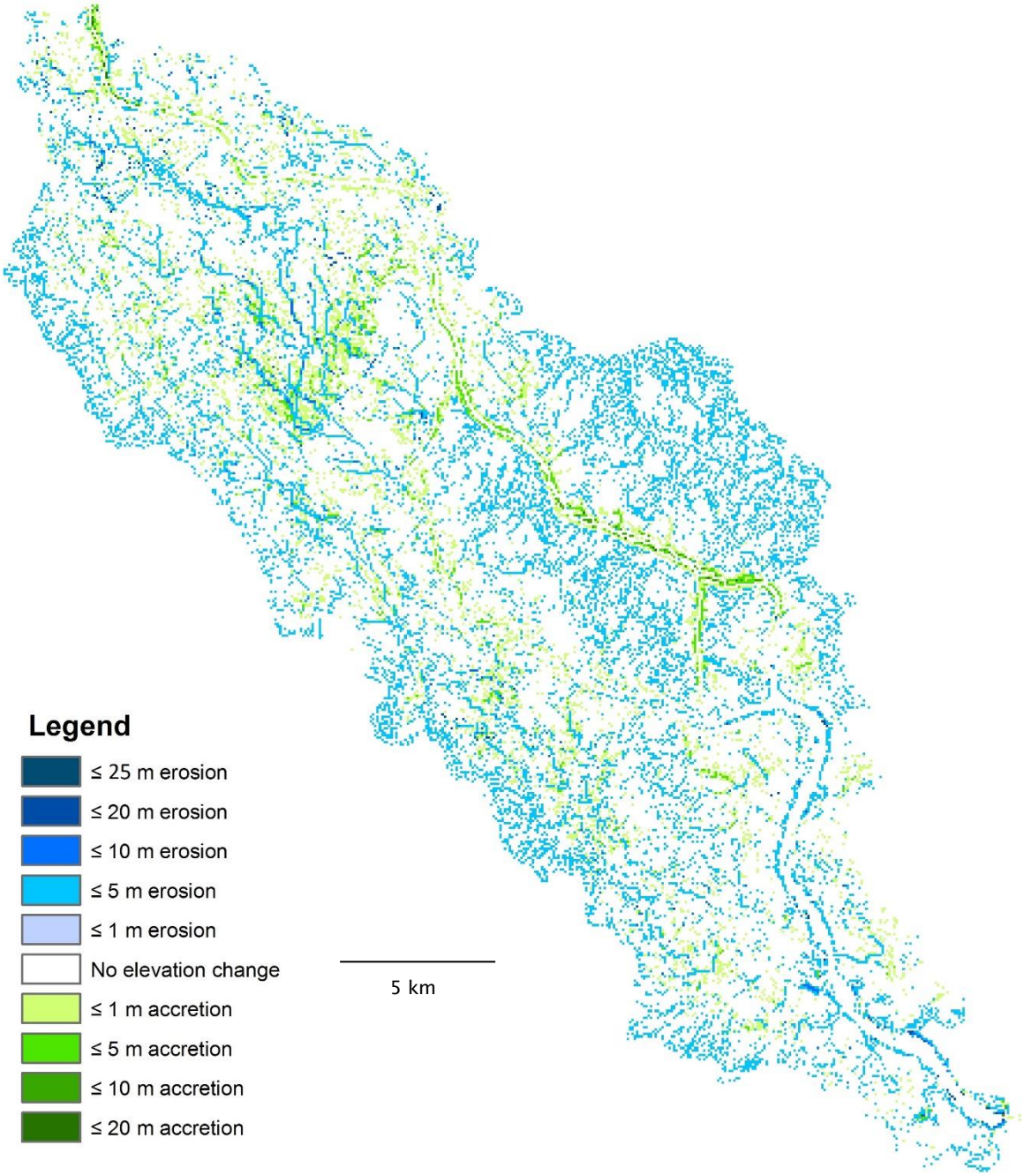

Figure C.24 Elevation change between 30 and 50 years under scenario 8DWAH, Devi catchment.

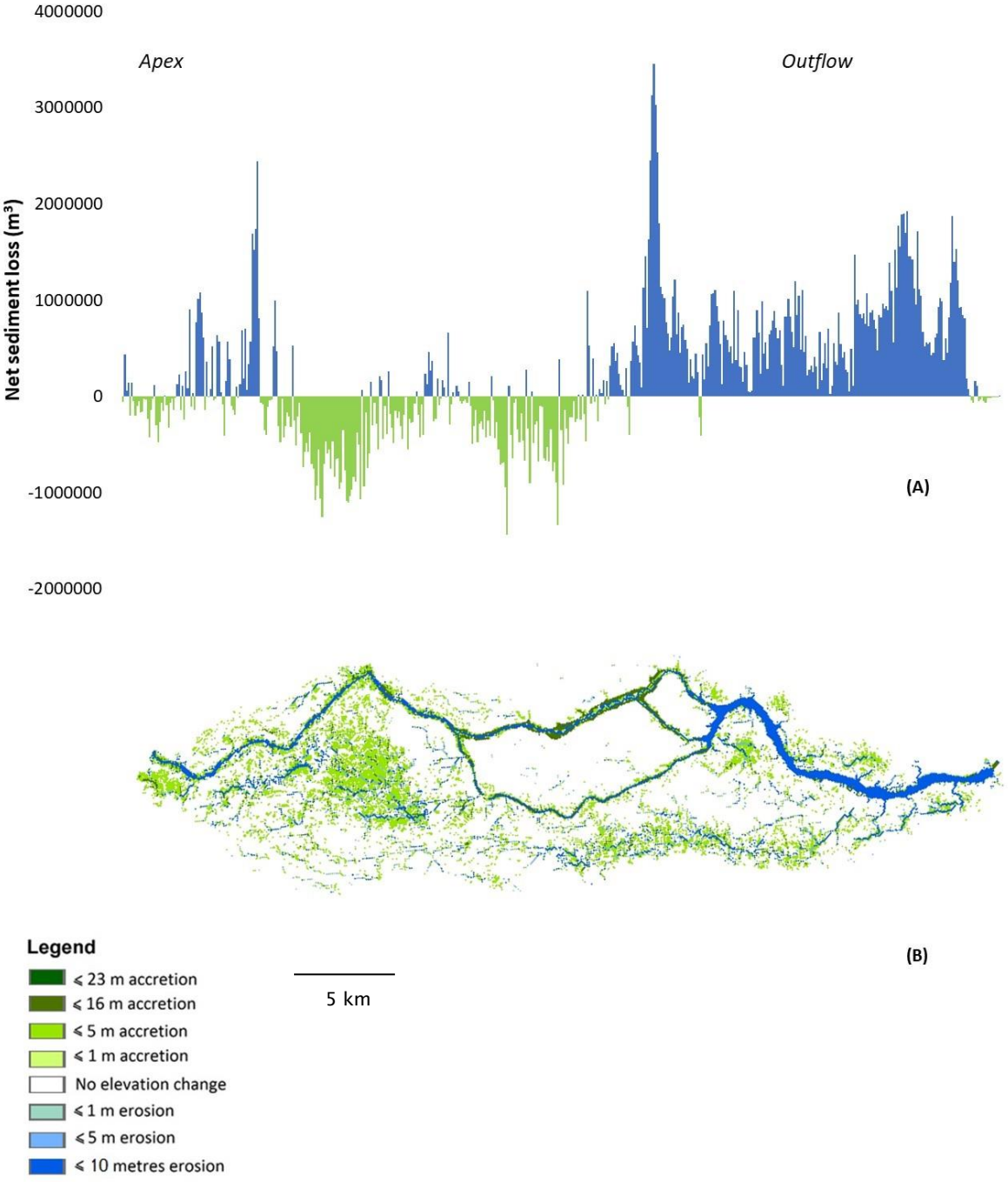

Figure C.25 A) Net sediment loss and (B) Elevation change at 30 years under scenario 9DWDC, Devi catchment. The x-axis in figure A corresponds to distance from the catchment apex (left) to the catchment outflow (right).

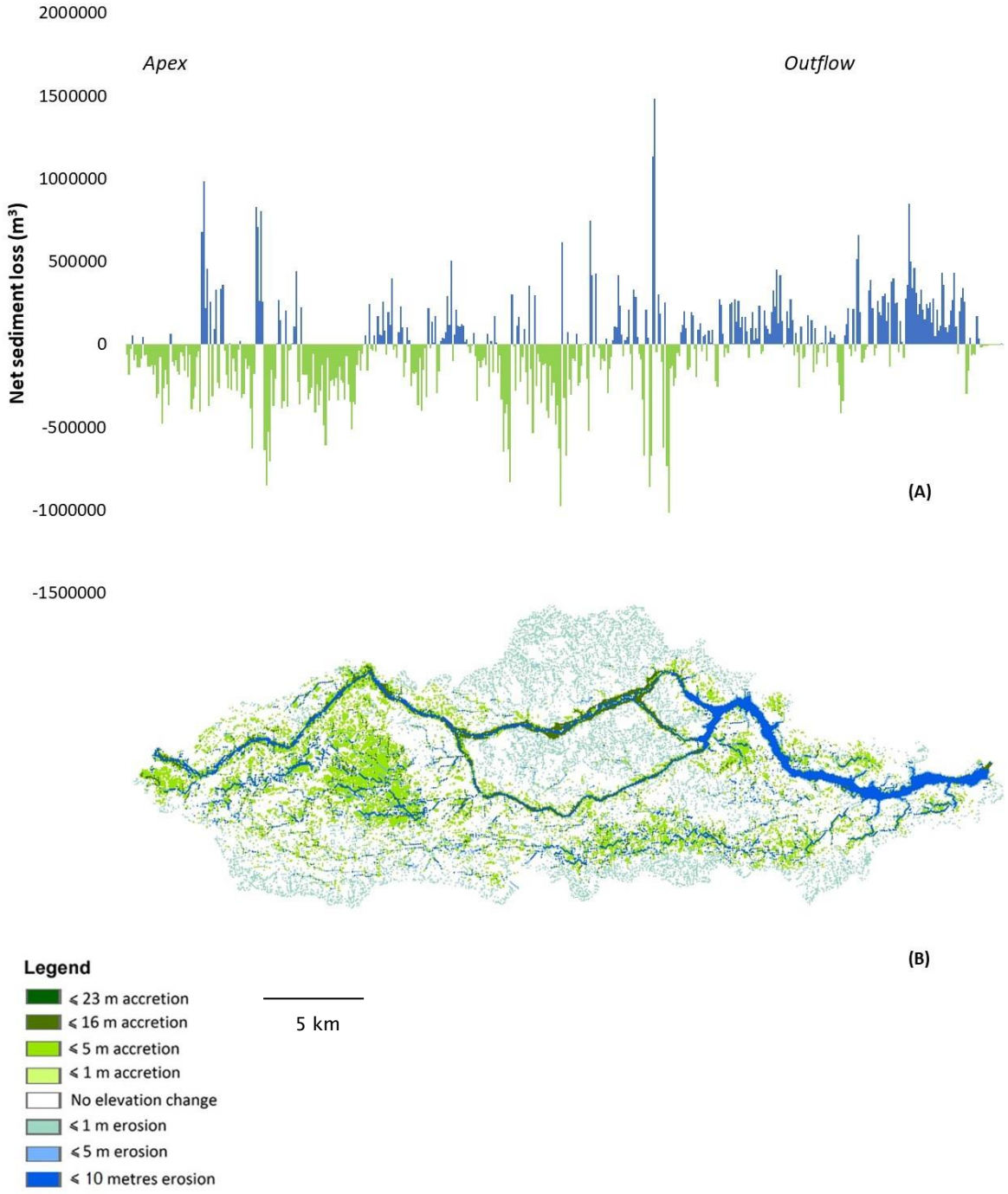

Figure C.26 (A) Net sediment loss and (B) Elevation change at 50 years under scenario 9DWDC, Devi catchment. The x-axis in figure A corresponds to distance from the catchment apex (left) to the catchment outflow (right).

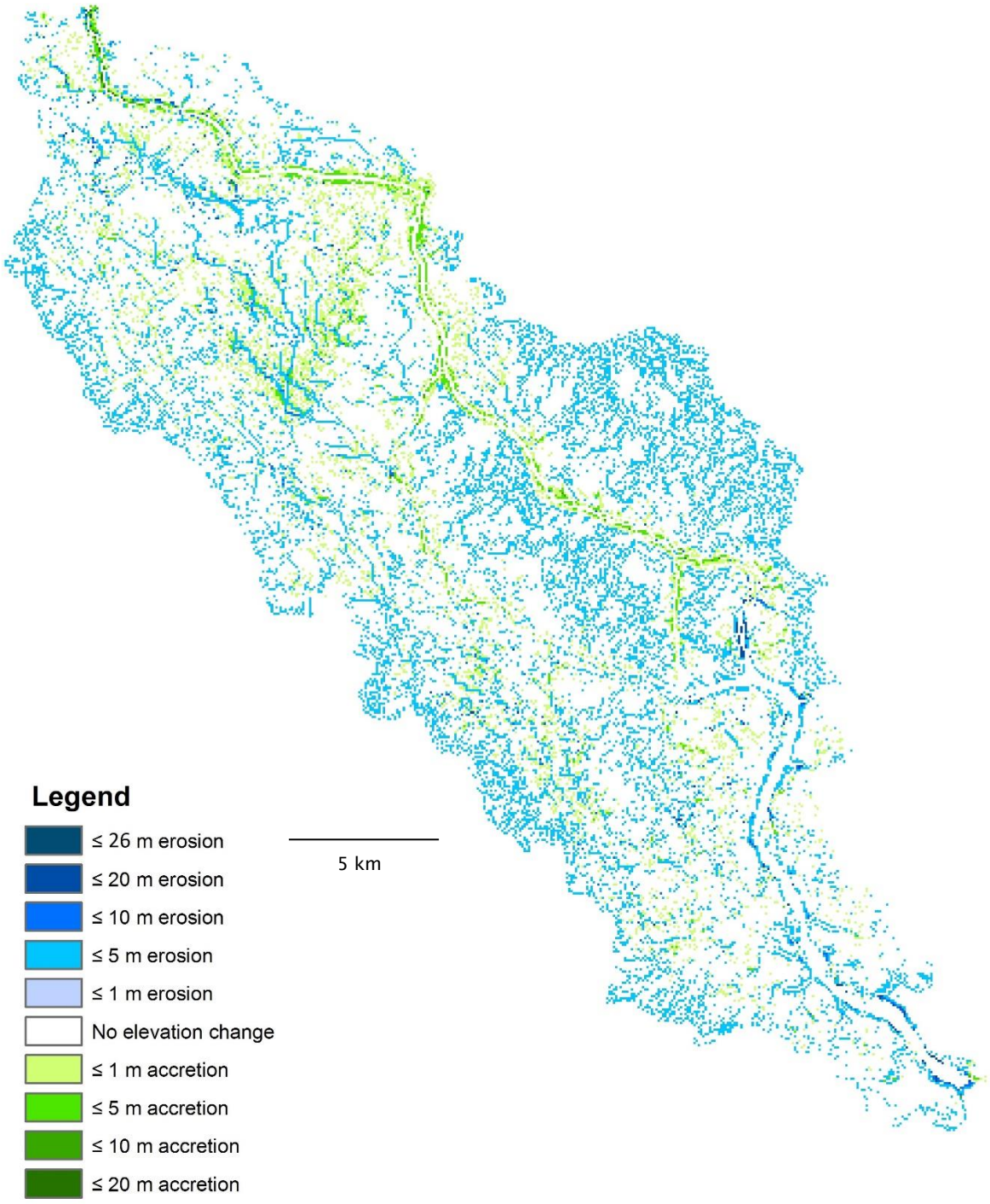

Figure C.27 Elevation change between 30 and 50 years under scenario 9DWDC, Devi catchment.

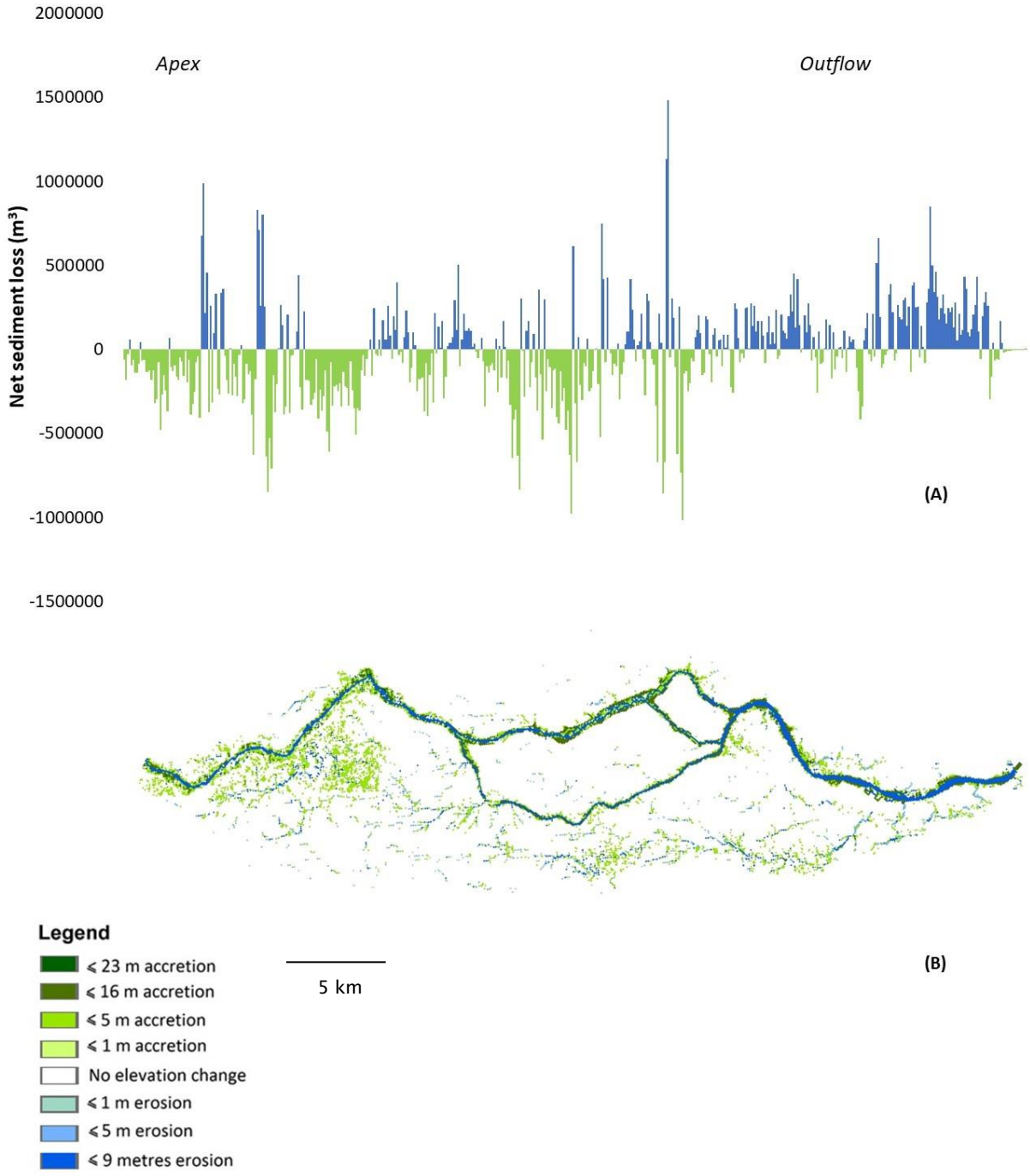

Figure C.28 (A) Net sediment loss and (B) Elevation change at 30 years under scenario 10DWDF, Devi catchment. The x-axis in figure A corresponds to distance from the catchment apex (left) to the catchment outflow (right).

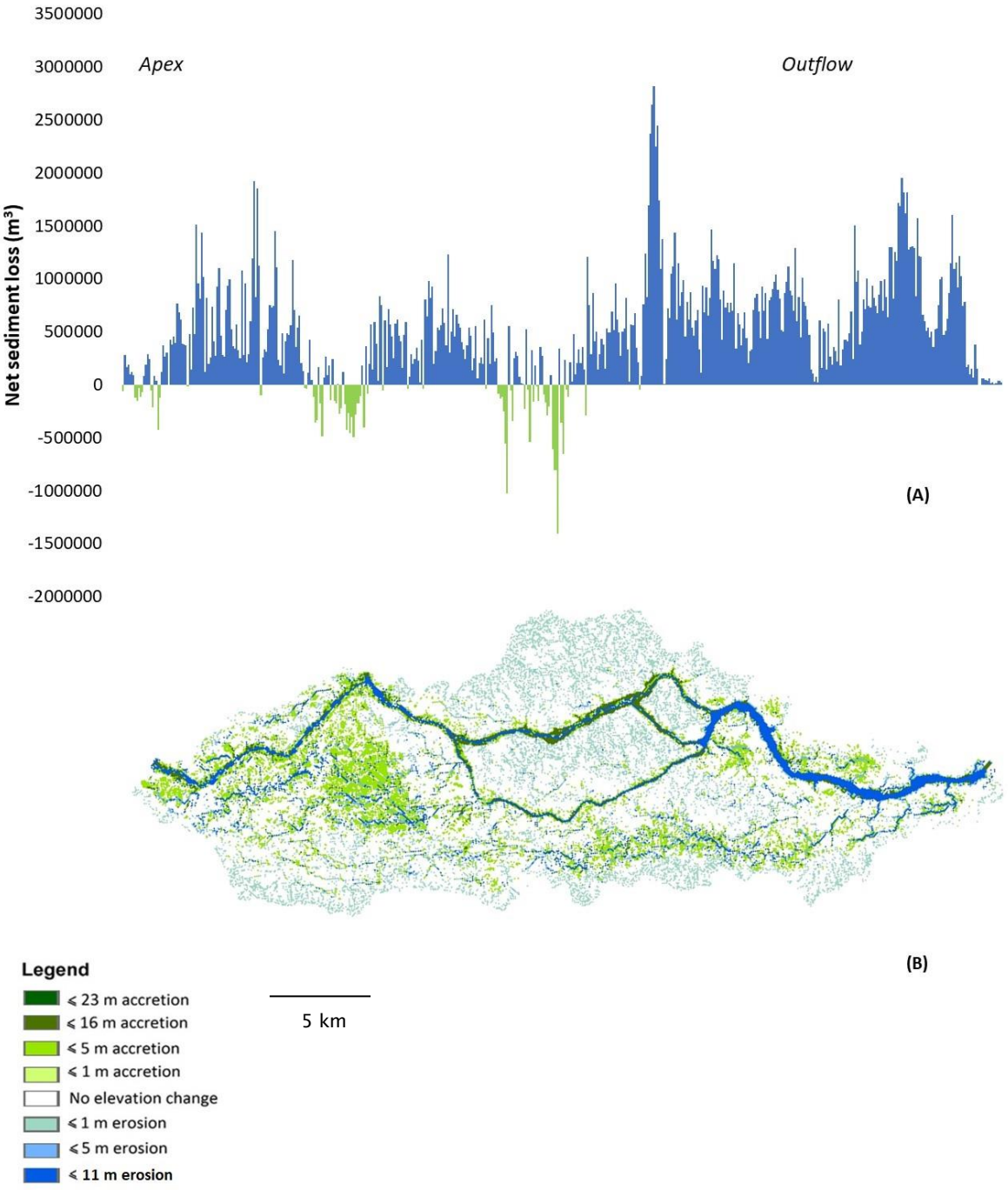

Figure C.29 (A) Net sediment loss and (B) Elevation change at 50 years under scenario 10DWDF, Devi catchment. The x-axis in figure A corresponds to distance from the catchment apex (left) to the catchment outflow (right).

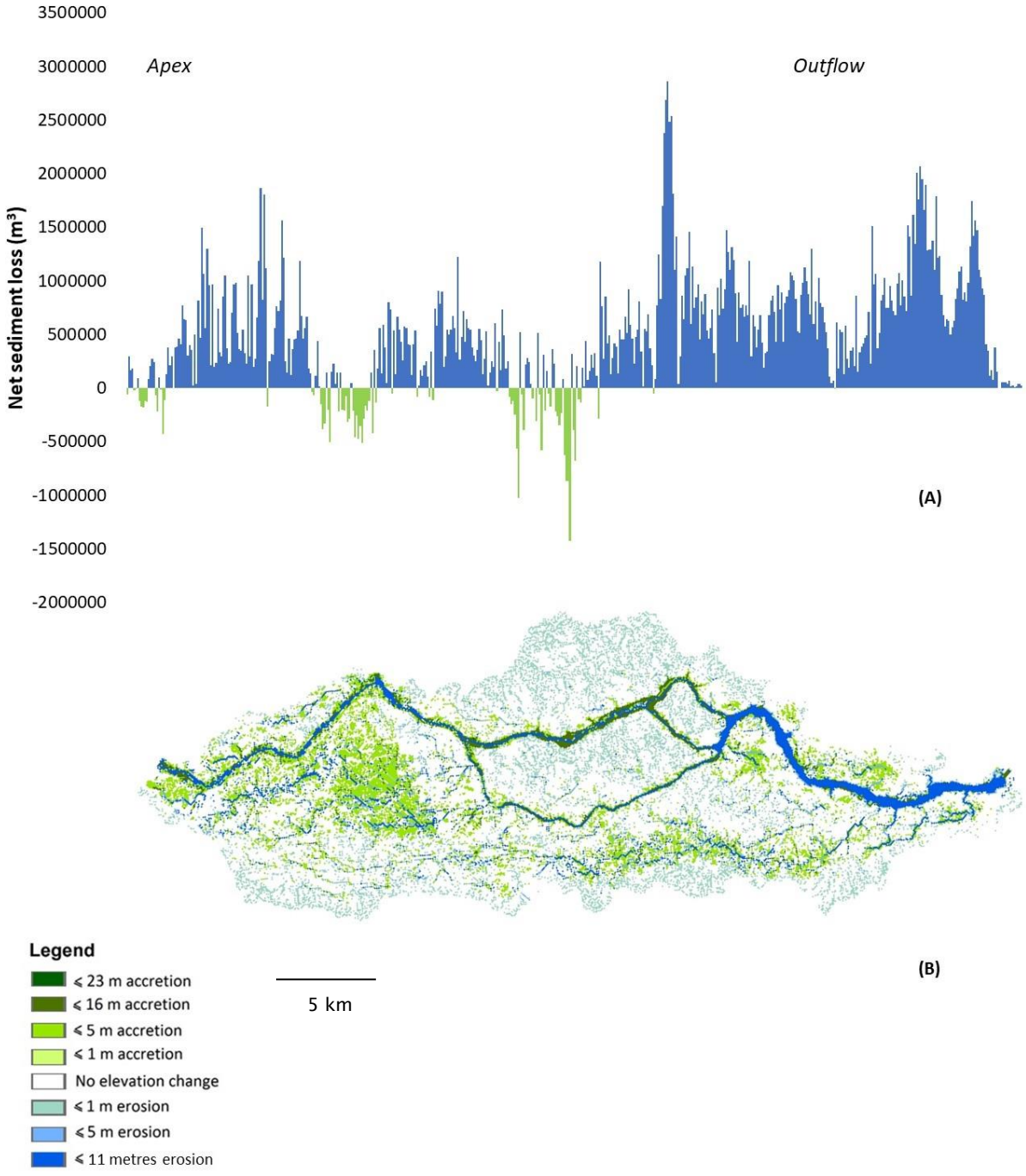

Figure C.30 (A) Net sediment loss and (B) Elevation change at 60 years under scenario 10DWDF, Devi catchment. The x-axis in figure A corresponds to distance from the catchment apex (left) to the catchment outflow (right).

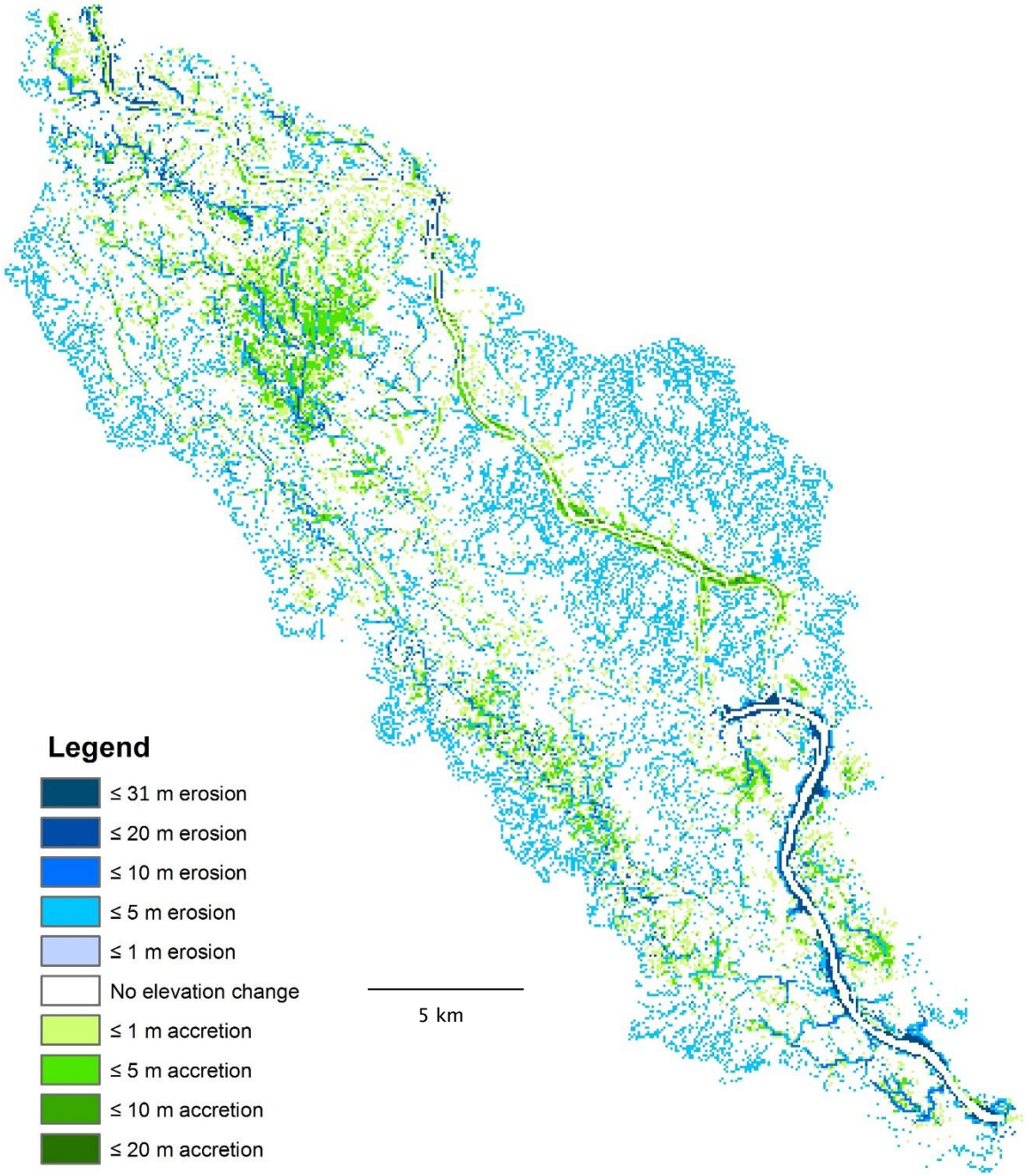

Figure C.31 Elevation change between 30 and 50 years under scenario 10DWDF, Devi catchment.

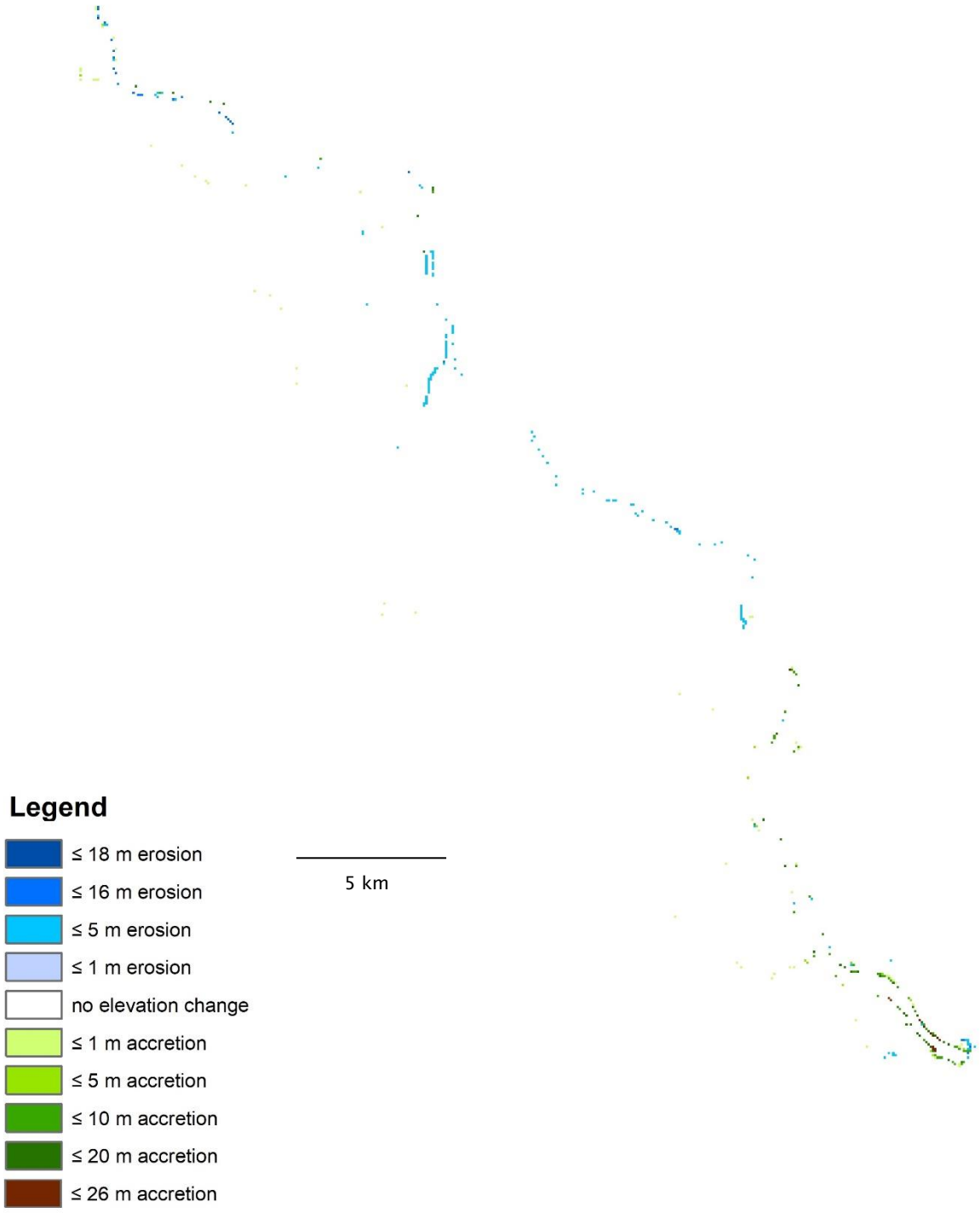

Figure C.32 Elevation change between 50 and 60 years under scenario 10DWDF, Devi catchment.

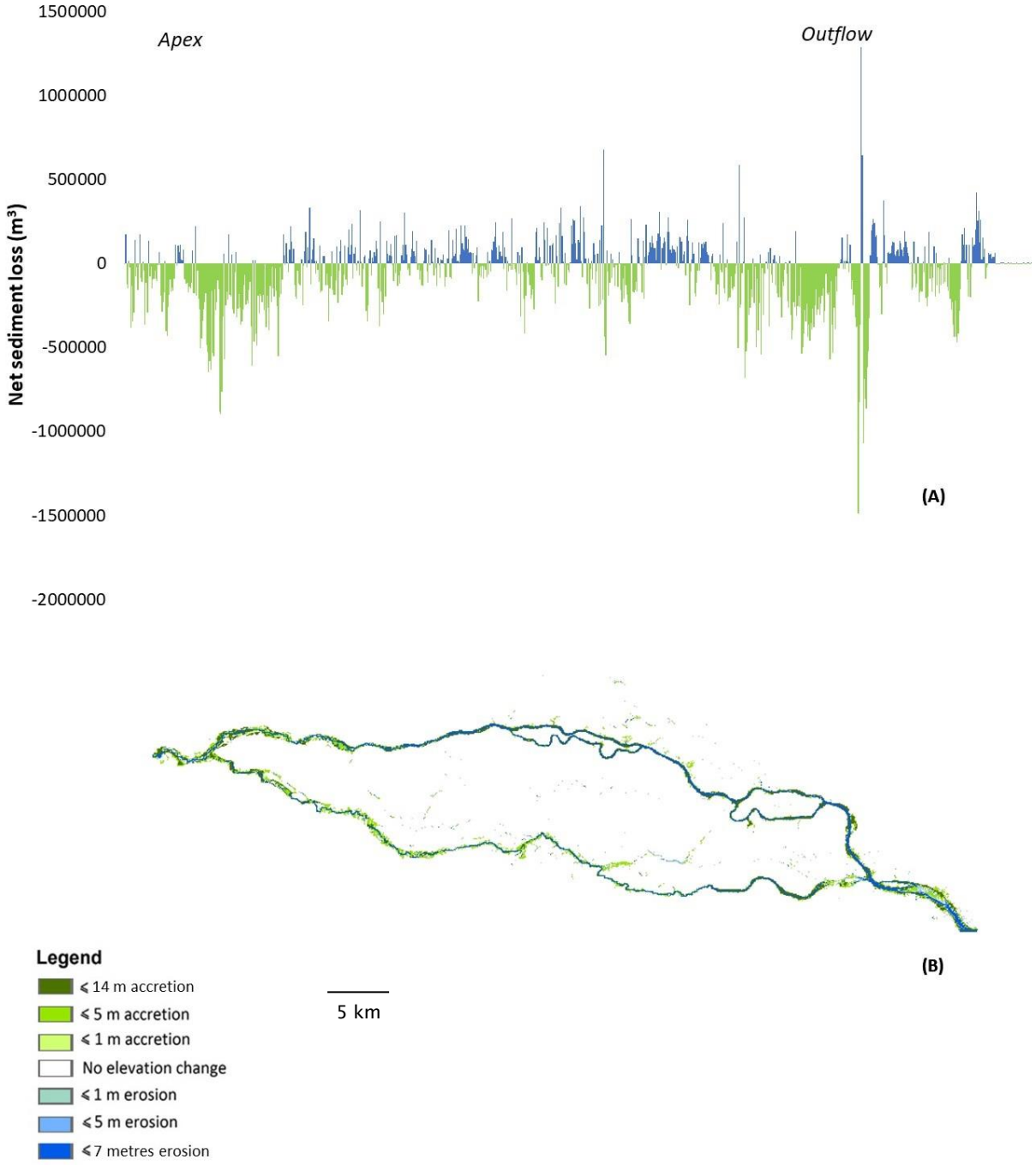

Figure C.33 (A) Net sediment loss and (B) Elevation change at 30 years under scenario 4DWD, Mahanadi catchment. The x-axis in figure A corresponds to distance from the catchment apex (left) to the catchment outflow (right).

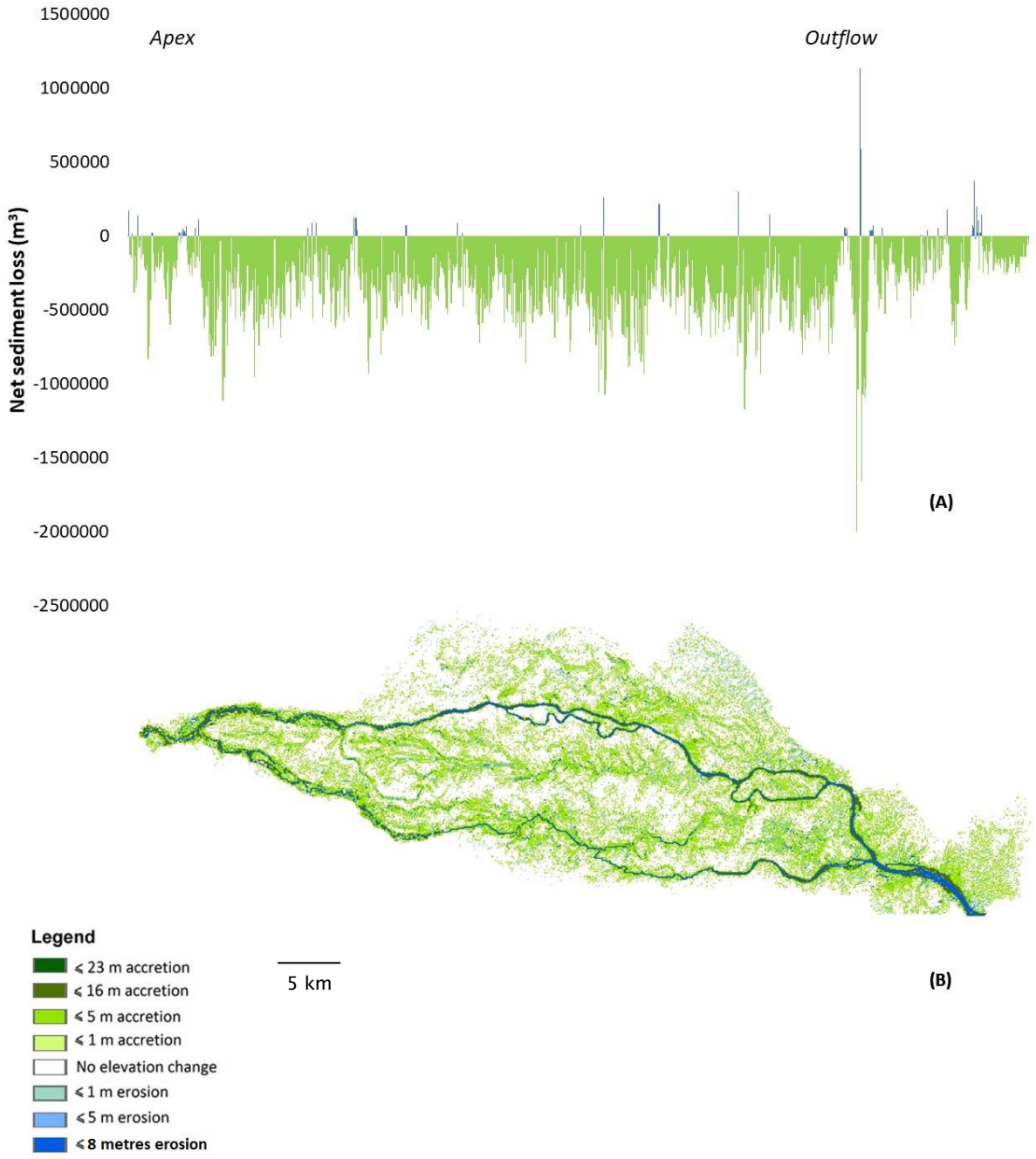

Figure C.34 (A) Net sediment loss and (B) Elevation change at 50 years under scenario 4DWD, Mahanadi catchment. The x-axis in figure A corresponds to distance from the catchment apex (left) to the catchment outflow (right).

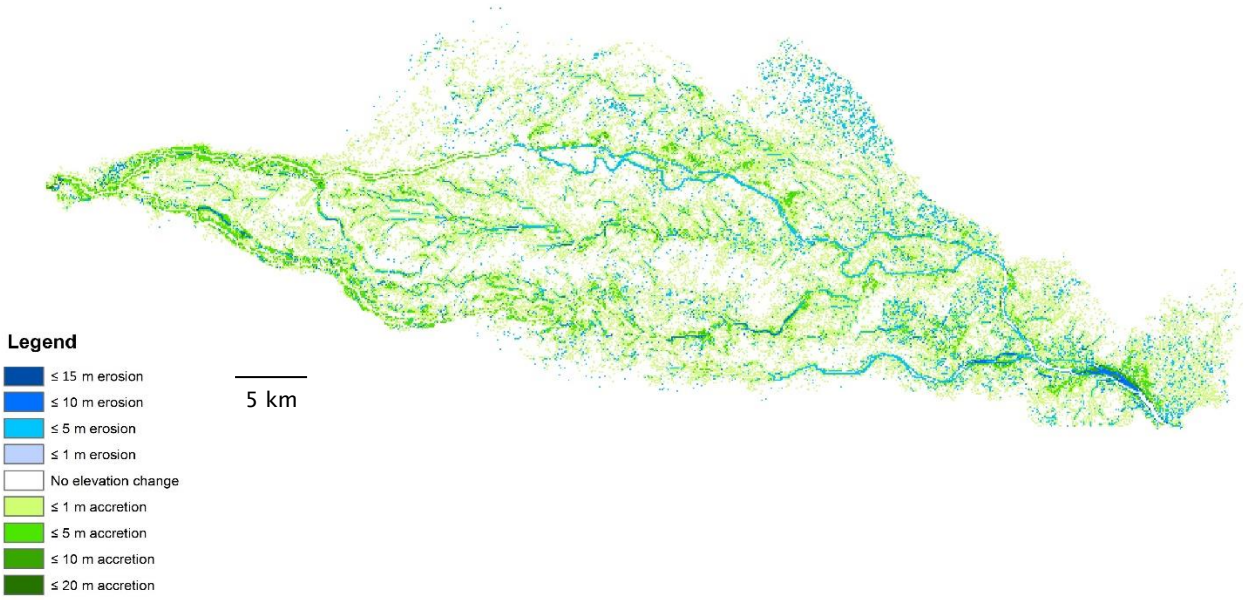

Figure C.35 Elevation change between 30 and 50 years under scenario 4DWD, Mahanadi catchment.

D. Outputs utilised to explore potential changes in habitat cover

Each catchment was divided into a series of grid cells measuring 5 km^2. The dominant habitat cover for each cell (covering ≥ 50% of cell area) is applied utilising the land-use map generated by Wetlands International (2014a) (figures 7.8 and 7.9). Similarly the dominant value or category for each of the following outputs was prescribed for each cell: Figures D.1 and D.2 show vulnerability to an extreme flood event for the Devi and Mahanadi catchments, respectively. The production of these values is explained in full in section 7.2. Figures D.3 and D.4 show hypsometry for the Devi and Mahanadi catchments, respectively. The value for each cell is based upon the elevation covering ≥ 50% of the cell area. Figures D.5 and D.6 show net elevation change for the Devi and Mahanadi catchments, respectively. As described in section 7.3, cells where elevation change is restricted purely to distributary channels (via scouring, for example) are deemed less vulnerable than those where the elevation change extends out of the channels and across on to the floodplain. Figures D.7 and D.8 show dominant floodplain morphological response units (MRUs) for the Devi and Mahanadi catchments, respectively. Dominant floodplain MRUs are identified where they occur in over 50% of the cell area. Finally, figures D.9 and D.10 show dominant channel MRUs for the Devi and Mahanadi catchments, respectively. Dominant channel MRUs are identified where they occur in over 50% of the main Devi and Mahanadi channel areas within any given cell.

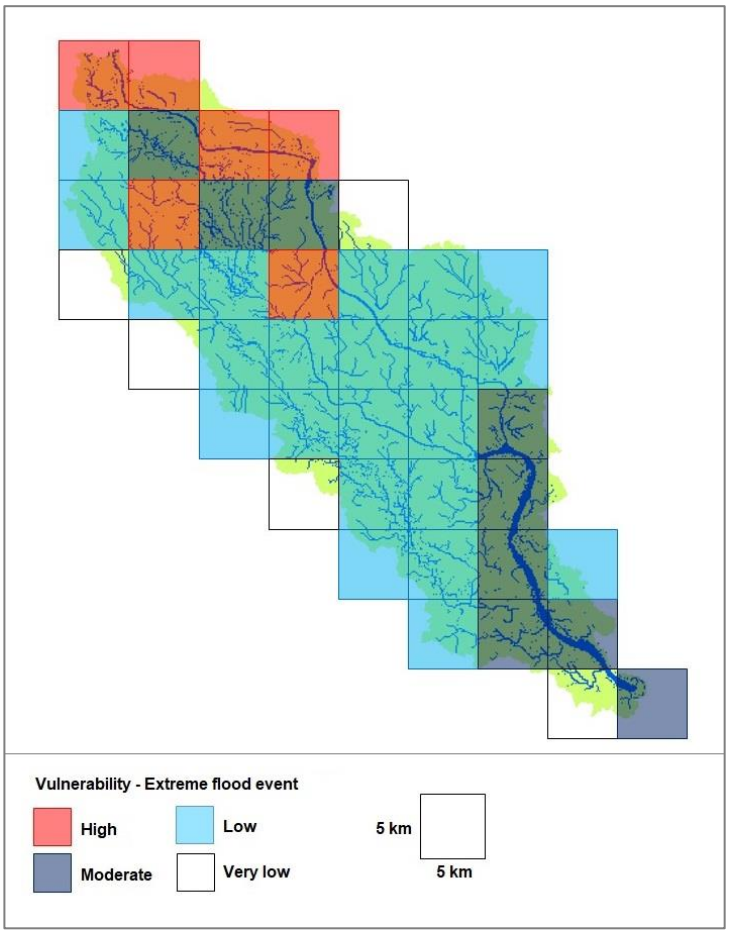

Figure D.1 Categorical measure of vulnerability to an extreme flooding event, scenario 4DWD; Devi catchment.

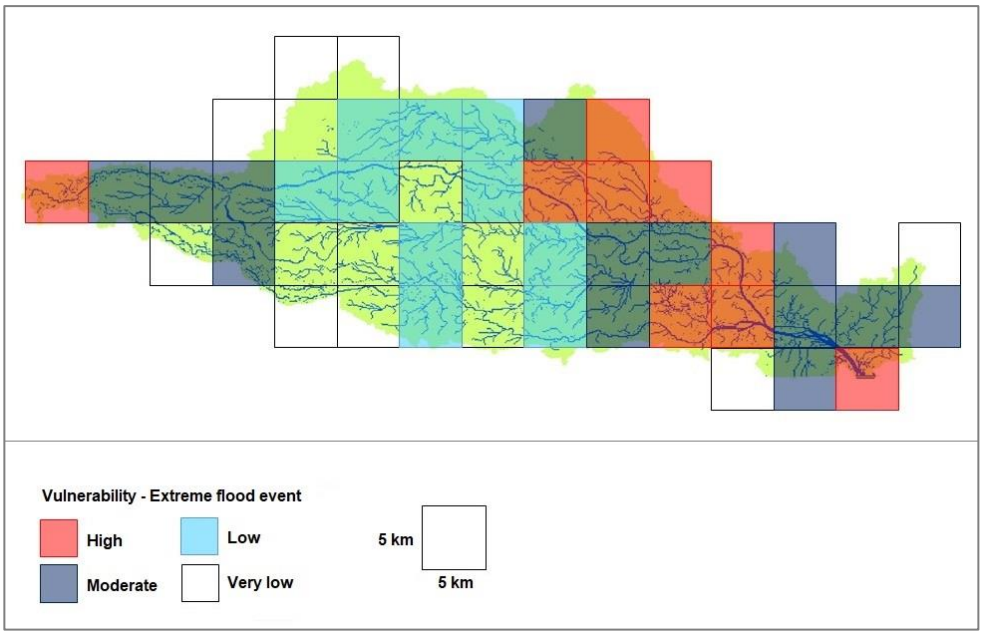

Figure D.2 Categorical measure of vulnerability to an extreme flooding event, scenario 4DWD; Mahanadi catchment.

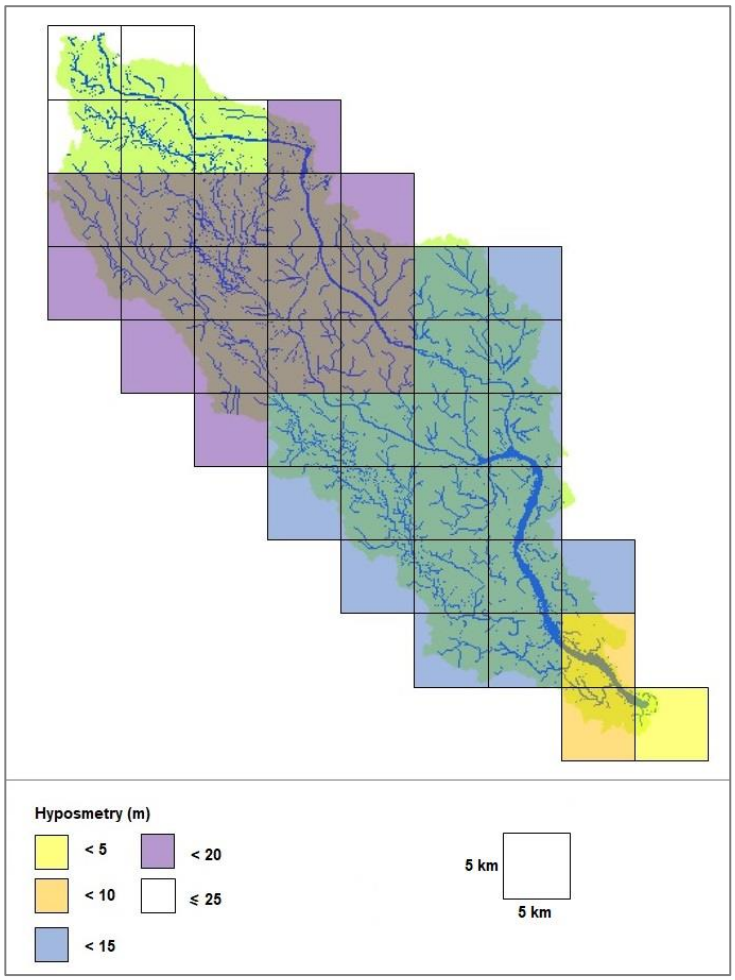

Figure D.3 Modal hypsometry values under scenario 4DWD; Devi catchment.

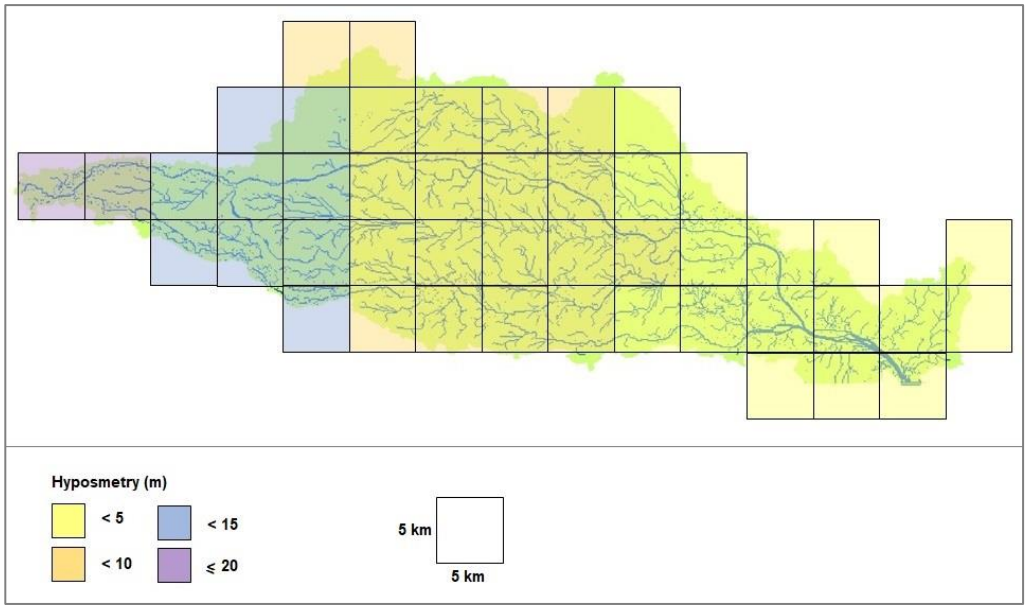

Figure D.4 Modal hypsometry values under scenario 4DWD; Mahanadi catchment.

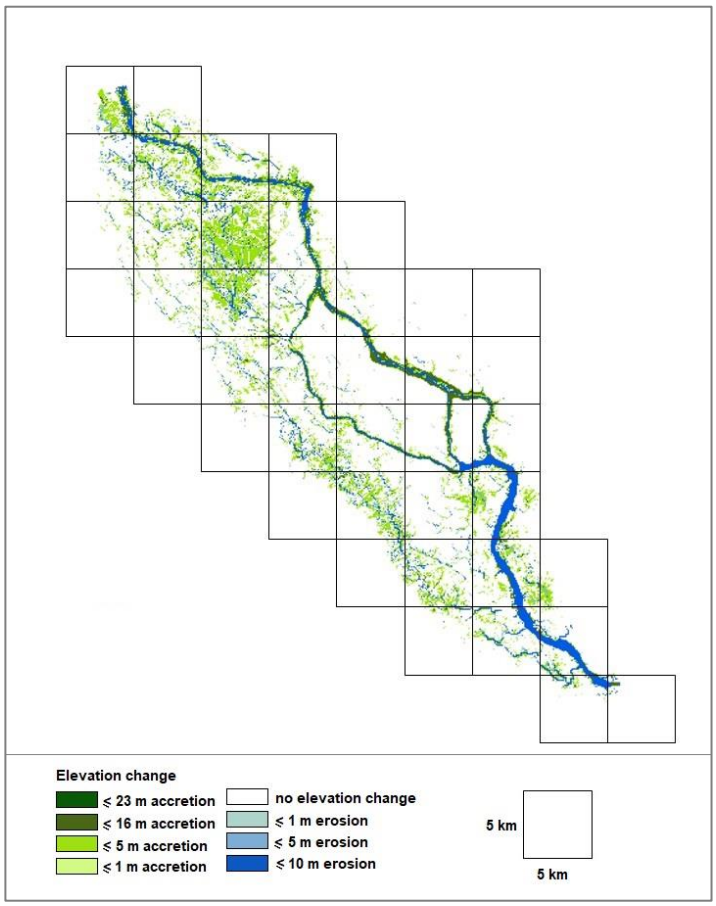

Figure D.5 Net elevation change under scenario 4DWD; Devi catchment.

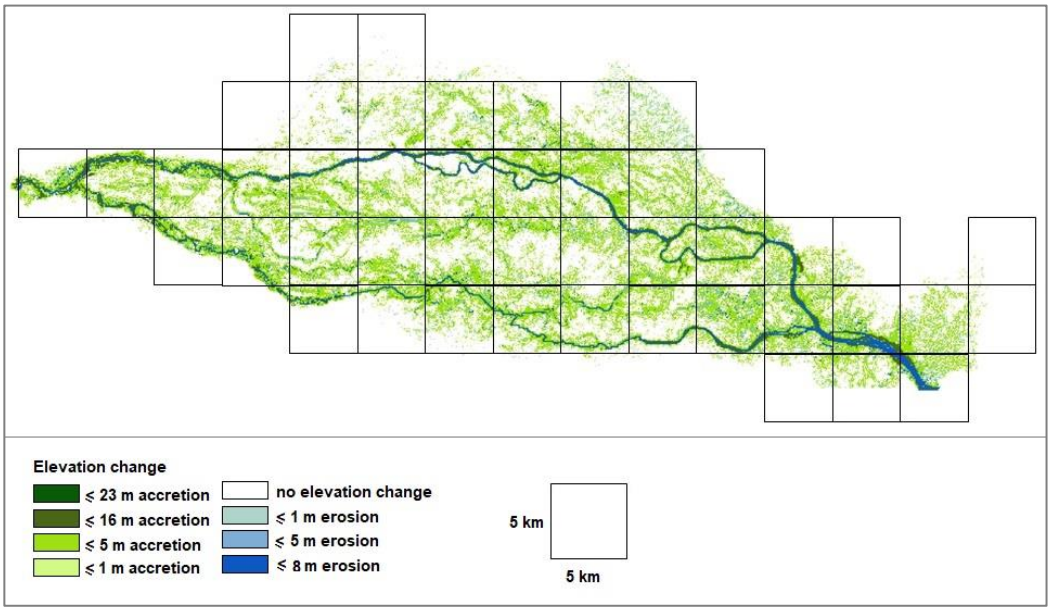

Figure D.6 Net elevation change under scenario 4DWD; Mahanadi catchment.

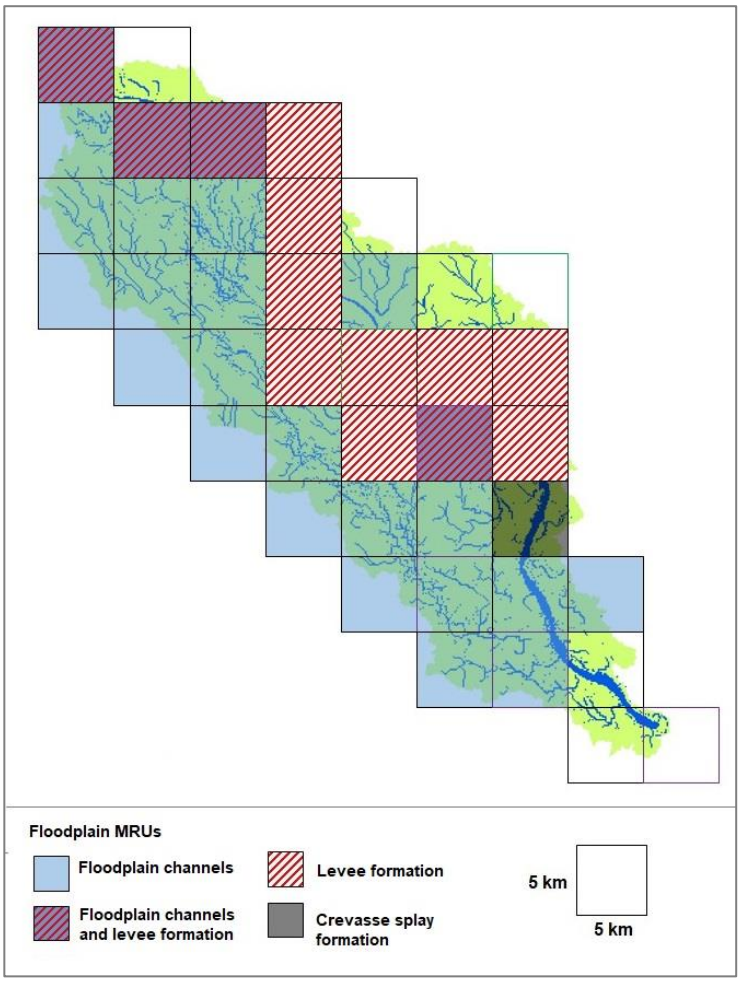

Figure D.7 Dominant floodplain morphological response units (MRUs) under scenario 4DWD; Devi catchment.

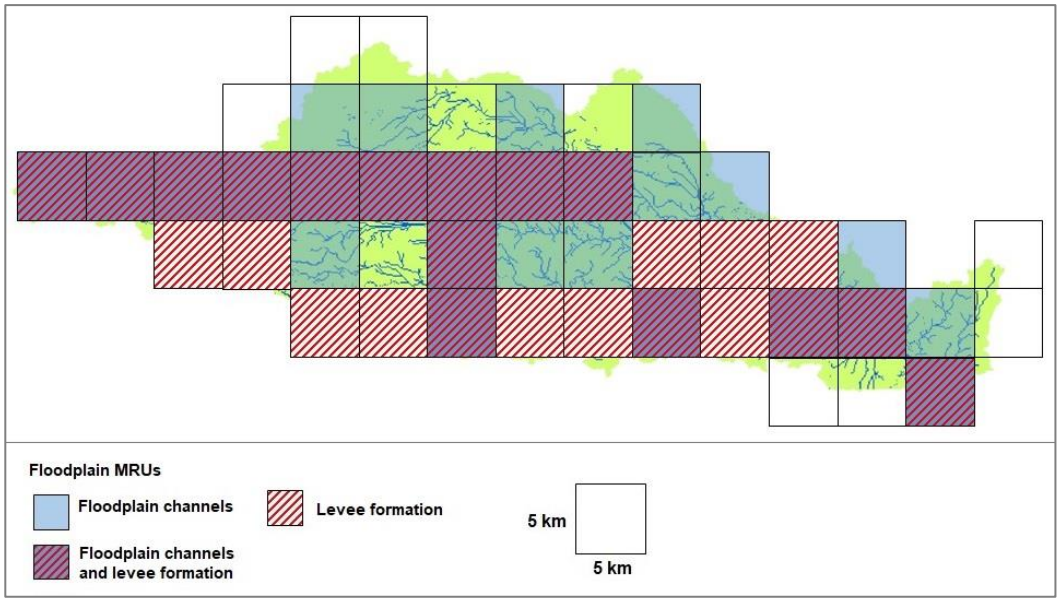

Figure D.8 Dominant floodplain morphological response units (MRUs) under scenario 4DWD; Mahanadi catchment.

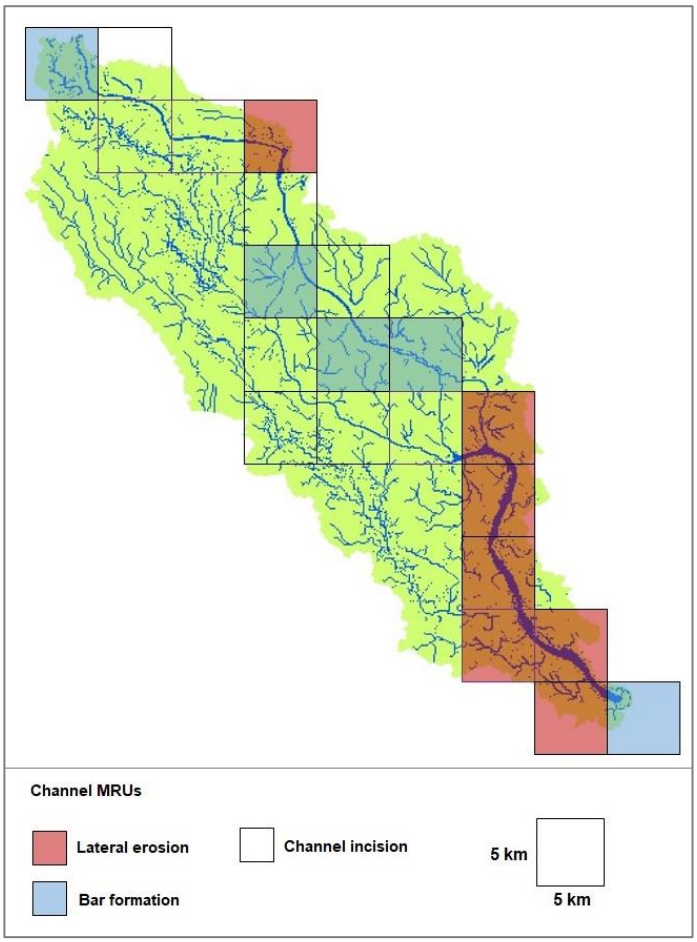

Figure D.9 Dominant channel morphological response units (MRUs) under scenario 4DWD; Devi catchment.

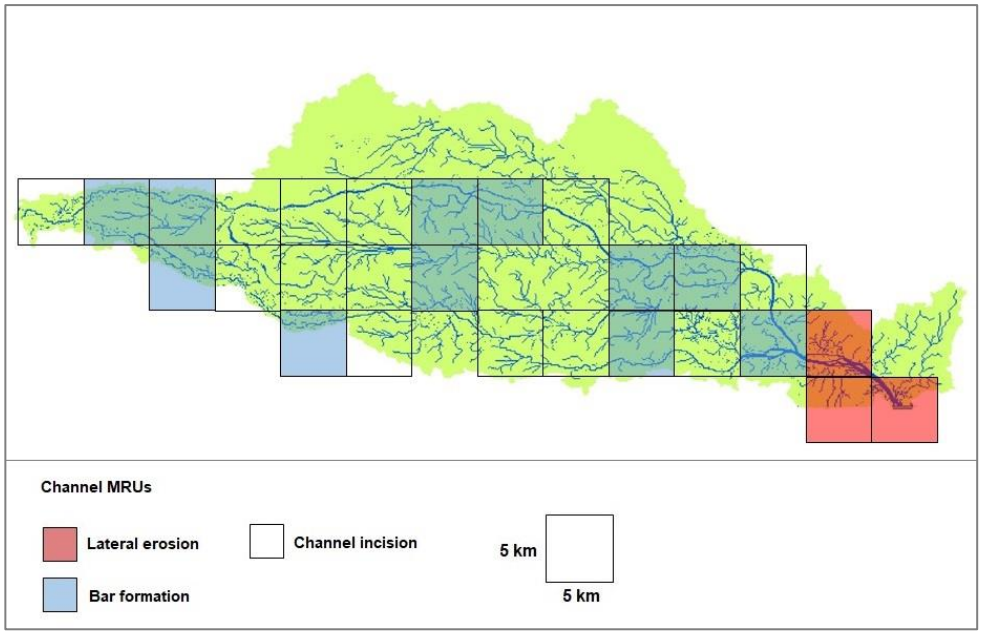

Figure D.10 Dominant channel morphological response units (MRUs) under scenario 4DWD; Mahanadi catchment.

List of References

Adams, P. N., Slingerland, R.L. and Smith, N.D. (2004), Variations in natural levee morphology in anastomosed channel flood plain complexes, *Geomorphology*, 61(1-2), 127-142.

Alley R.B, Marotzke J, Nordhaus WD, Overpeck JT, Peteet DM, Pielke RA, Pierrehumbert RT, Rhines PB, *et al*., Abrupt climate change, *Science*, 299:2005-2010

Ali, A.M.S. (2011) Rice to shrimp: Land use/land cover changes and soil degradation in Southwestern Bangladesh, *Land Use Policy*, 23(4):421-435.

Allison, M.A. (1998) Geological framework and environmental status of the Ganges-B. Delta, *Journal of Coastal Research*, 14(3):826-836.

Alongi, D. M. (2002) Present state and future of the world's mangrove forests, *Environmental Conservation*, 29(3):331-349.

Alongi, D.M. (2009) *The Energetics of Mangrove Forests*, Springer Science and Business Media.

Anderson P.W. (1972) More is different. Broken symmetry and the nature of the hierarchical structure of science, *Science*, 177, 404(7): 393-396.

Anderson, P.E., Jensen, H.J., Oliveria, .LP. and Sibani, P. (2004) Evolution in complex systems, *Wiley Periodicals Inc.,* 10(1):49-56.

Anthony, E.J. and Blivi, A.B. (1999) Morphosedimentary evolution of a delta-sourced, drift-aligned sand barrier-lagoon complex, western Bight of Benin, *Marine Geology*, 158:161-176

Ashfaq, M., Shi, Y., Tung, W.W., Trapp, R.J., Gao, X., Pal, J.S., and Diffenbaugh, N.S. (2009), Suppression of south Asian summer monsoon precipitation in the 21st century, *Geophysical. Research. Letters*, 36: L01704.

Ashton, A. D., and A. B. Murray (2006), High-angle wave instability and emergent shoreline shapes: Wave climate analysis and comparisons to nature, *Journal of Geophysical Research,* 111.

Asokan, S. M., and Dutta, D. (2008), Analysis of water resources in the Mahanadi River Basin, India under projected climate conditions, *Hydrological. Processes*, 22: 3589-3603.

Auerbach, L. W., Goodbred, S. L., Mondal, D. R., Wilson, C. A., Ahmed, K. R., Roy, K., and Ackerly, B. A. (2015) Flood risk of natural and embanked landscapes on the Ganges-Brahmaputra tidal delta plain, *Nature Climate Change*, 5(2), 153-157.

Balbi, S., Perez, P. and Giupponi, C. (2010) A spatial agent-based model to explore scenarios of adaptation to climate change in an alpine tourism destination, in Ernst, A. and Kuhn, S. (Eds.) *3rd World Congress of Social Simulation.*

Baran, E. and Hambrey, J. (1998) Mangrove conservation and coastal management in Southeast Asia: What impact on fishery resources? *Marine Pollution Bulletin*, 37 (8-12): 431-440.

Bastia, F. and Equeenuddin, Sk. Md. (2016) Spatio-temporal variation of water flow and sediment discharge in the Mahanadi River, India, *Global and Planetary Change,* 144: 51-66.

List of References

Bates, P.D. *et al*. (2010) A simple inertial formulation of the shallow water equations for efficient two-dimensional flood inundation modelling, *Journal of Hydrology,* 388: 33-45.

Becker, E. (2010) *Socio-ecological systems as epistemic objects*, viewed 23rd November 2014, <http://www.isoe.de/ftp/publikationen/eb_socecsystem2010.pdf>,

Benini, L., Bandini, V., Marazza, D. and Contin, A. (2010) Assessment of land use changes through an indicator based approach: A case study from the Lamone river basin in Northern Italy, *Ecological Indicator*s, 10:4-14.

Beura, D. (2015) Floods in Mahanadi River, Odisha, India: Its Causes and Management, *International Journal of Engineering and Applied Science,* 2(2): 51 55.

Beven (2007) Towards integrated environmental models of everywhere: uncertainty, data and modelling as a learning process*, Hydrology and Earth System Science*, 11(1):460-467.

Beven, K. and Freer, J. (2001) Equifinality, data assimilation, and uncertainty estimation in mechanistic modelling of complex environmental systems using the GLUE methodology, *Journal of Hydrology*, 249(1–4): 11-29.

Bhat, G. S. (2006) The Indian drought of 2002—a sub-seasonal phenomenon?. *Q.J.R. Meteorol. Soc*., 132: 2583-2602.

Bhawan (2014) Central Ground Water Board (CGWB) *Ministry of Water Resources, River Development and Ganga Rejuvenation*, viewed 30 April 2017, <http://cgwb.gov.in/NEW/WQ/Costal%20Report.pdf>,

Black, A. (2018) Rivers and their Catchments: Flooding, Bank Erosion and Channel Change, *Information and Advisory Notes*, no. 21, viewed 15 April 2018, <http://www.snh.org.uk/publications/on-line/advisorynotes/21/21.htm>

Blum, M.D. and Roberts, H.H. (2009) Drowning of the Mississippi Delta due to insufficient sediment supply and global sea-level rise, *Nature Geoscience*, Letters (2):488-491.

Bollasina, M., Ming, Y. and Ramaswamy, V. (2011), Anthropogenic aerosols and the weakening of the South Asian summer monsoon, *Science,* 28: 502-505.

Bonabeau, E. (2002) Agent-based modeling: Methods and techniques for simulating human systems, *PNAS,* 99(3): 7280-7287.

Boniface, C. (1985) *Vegetation succession on mid-channel bars of the Fraser River, British Columbia,* MSc Geography Thesis, Simon Fraser University, viewed 6 April 2018, < http://summit.sfu.ca/item/6417>

Breemen M.T.J. van (2008) *Salt intrusion in the Selangor: model study with Delft3D estuary in Malaysia*, Civil Engineering and Management MSc Thesis, University of Twente, viewed 11 August 2016, <http://essay.utwente.nl/58269/>

Bruckner, T., Petschel-Held, G., Toth, F.L., Fussel, H.M., Helm, C., Leimbach, M. and Schellnhuber, H.J. (1999) Climate change decision support and the tolerable windows approach, *Environmental Modelling and Assessment*, 4: 217-234.

Caldwell, R.L. and Edmonds, D.A. (2014) The effects of sediment properties on deltaic processes and morphologies: A numerical modelling study, *Journal of Geophysical Research: Earth Surface*: 961-982.

Carr, M.K. *et al.* (2016) Identifying links between Fluvial Geomorphic Response Units (FGRUs) and fish species in the Assiniboine River, Manitoba, *Ecohydrology,* 9: 1154-1165.

Chakrapani, G. and Subramanian, V. (1990) Factors controlling sediment discharge in the Mahanadi River Basin, India*, Journal of Hydrology*, 117: 169-185.

Chakrapani, G.J. and Subramanian, V. (1993) Rates of erosion and sedimentation in the Mahanadi river basin, India, *Journal of Hydrology*, 149: 39-48.

Chapman, A. and Darby, S. (2016) Evaluating sustainable adaptation strategies for vulnerable mega-deltas using system dynamics modelling: Rice agriculture in the Mekong Delta's An Giang Province, Vietnam, *Science of the Total Environment,* 559:326-388.

Chatanantavet, P., Lamb, M.P. and Nitrrouer, J.A. (2012) Backwater controls of avulsion location on deltas, *Geophysical Research Letters,* 39.

Chhotray, V. and Few, R. (2012) Post-disaster recovery and 'ongoing' vulnerability: Ten years after the super cyclone of 1999 in Orissa, India in *Global Environmental Change* 22.pp. 695-702.

Chiew, F.H.S. and McMahon, T.A. (2009) Global ENSO-Streamflow teleconnection, streamflow forecasting, and interannual variability, *Hydrological Sciences Journal*, 47(3): 505-522.

Chua, T.E. (1992) Coastal aquaculture development and the environment: The role of coastal area management, *Marine Pollution Bulletin*, 25(1-4):98-103.

Church, J.A. *et al* (2013) Sea-level Change, *Fifth Assessment Report of the Intergovernmental Panel on Climate Change*, Cambridge University Press, Cambridge, UK, 1137-1216.

Cilliers, P. (1998) *Complexity and Postmodernism: Understanding complex systems*, Routledge, London.

Clough J.S. and Park R.A. (2007) *Technical Documentation for SLAMM 5.0*., Warren Pinnacle Consulting, Inc.

Coleman, J.M.and Huh, O.K. (2004) *Major World Deltas, a perspective from space,* Louisiana State University, Baton Rouge.

Constanza R.and Ruth, M. (1998) Using Dynamic Modeling to Scope Environmental Problems and Build Consensus, Environmental Management, 22(2):183-195.

Constanza, R., Sklar, F.H. and White. M.K. (1990) Modeling coastal landscape dynamics. *BioScience,* 40:91–107.

Coulthard, T.J. (1999) *Modelling upland catchment response to Holocene environmental change,* PhD Thesis, University of Leeds.

Coulthard, T.J. (2014) *What is CAESAR-Lisflood? Background and Development,* viewed 1 February 2016, <https://sourceforge.net/p/caesar-lisflood/wiki/Background/>

Coulthard, T.J. (2016) *CAESAR-Lisflood Landscape Evolution Model*, online manual, viewed 1 March 2016, < https://sourceforge.net/p/caesar-lisflood/wiki/Instructions/>

Coulthard, T.J. and Van De Wiel, M.J. (2006) A cellular model of river meandering, *Earth Surface Processes and Landforms,* 31(1): 123-132.

Coulthard, T.J. and Van De Wiel, M.J. (2012) Modelling river history and evolution, *Phil. Trans. R. Soc*. A 370 (1966): 2123-2142.

Coulthard, T.J. Hicks, D.M., Van De Wiel, M.J. (2007) Cellular modelling of river catchments and reaches: Advantages, limitations and prospects, *Geomorphology* 90(3-4): 192-207.

Coulthard, T.J., Kirkby, M.J. and Macklin, M.G. (2000) Modelling geomorphic response to environmental change in an upland catchment, *Hydrological Processes*, 14(11-12): 2031-2045.

Coulthard, T.J., Macklin, M.G. and Kirby, M.J. (2002) Simulating upland river catchment and alluvial fan evolution *Earth Surface Process and Landforms,* 27: 269-288

Coulthard, T.J., Neal, J.C., Bates, P.D., Ramirez, J., Almeida, G.A.M. and Hancock, G.R. (2013) Integrating the LISFLOOD-FP 2D hydrodynamic model with the CAESAR model: implications for modelling landscape evolution, E*arth Surface Processes and Landforms* 38(15): 1897-1906.

Coulthard, T.J., Ramirez, J., Fowler, H.J., Glenis, V. (2012) Using the UKCP09 probabilistic scenarios to model the amplified impact of climate change on drainage basin sediment yield, *Hydrology and Earth System Sciences*, 16 (11): 4401-4416

Crosato A, Desta F.B, Cornelisse J., Schuurman F., Uijttewaal W.S.J. (2012) Experimental and numerical findings on the long-term evolution of migrating alternate bars in alluvial channels, *Water Resources Research*, 48.

Dail, M.B., Corbett, D.R. and Walsh, J.P. (2007) Assessing the importance of tropical cyclones on continental margin sedimentation in the Mississippi delta regions, *Continental Shelf Research*, 27:1857-1874.

Dammers, E., Bregt, A.K., Edelenbos, J., Meyer, H. and Pel, B. (2014) Urbanized deltas as complex adaptive systems: implications for planning and design, *Built Environment*, 40.

Das, P., Basak, U.C. and Das, A.B. (1997) Restoration of the mangrove vegetation in the Mahanadi Delta, Orissa, India, *Mangroves and Salt Marshes*, 1(3):155-161.

Das, S. (2009) *Addressing coastal vulnerability at the village level: the role of socio-economic and physical factors*, Working Paper Series No. E/295/2009, Institute of Economic Growth, New Delhi.

Dash, S.K. *et al. (*2007) Some evidence of climate change in twentieth-century India, *Climatic Change,* 85(3–4):299–321.

Day Jr., J. W. *et al.* (2007) Restoration of the Mississippi Delta: Lessons from hurricanes Katrina and Rita, *Science,* 315: 1679–1684.

Day Jr., J.W., Rybczyk, J., Scarton, F., Rismondo, A., Are, D. and Cecconi, G. (1999) Soil accretionary dynamics, sea level rise and the survival of wetlands in Venice Lagoon: a field and modelling approach, *Estuarine, Coastal and Shelf Science*, 49:607-628.

Dearing, J. A. (2007) Human–environment interactions. Learning from the past. In, Costanza, Robert, Graumlich, Lisa and Steffen, Will(eds.) *Sustainability or Collapse? An Integrated History and Future of People on Earth.* The MIT Press, pp. 19-38.

Dearing, J.A. *et al*. (2014) Safe and just operating spaces for regional socio-ecological systems, *Global Environmental Change*, 28: 227-238.

Dearing, J.A., Plater, A., Richmond, N. Prandle D. and Wolf, J. (2005) *Towards a high resolution cellular model for coastal simulation (CEMCOS)*, Tyndall Centre Technical Report No. 26, Tyndall Centre for Climate Change Research.

Dearing, J.A., Richmond, N., Platter, A.J., Wolf, J., Prandle, D. and Coulthard, T.J. (2006) Modelling approaches for coastal simulation based on cellular automata: the need and potential, *Philosophical Transactions of the Royal Society,* 364: (1841).

Debsarma, S.K. (2007) Numerical simulations of storm surges in the Bay of Bengal, *Marine Geosdesy,* 32(2).

DECCMA (2015a) *Project Overview*, viewed 1 May 2015, <http://www.geodata.soton.ac.uk/deccma/overview/>.

DECCMA (2015b) *Work Package 2*, viewed 1st May 2015, <http://www.geodata.soton.ac.uk/deccma/work_packages/WP2/>.

DEFRA (2013) *Catchment Based Approach: Improving the quality of our water environment,* viewed 12 January 2019, <https://assets.publishing.service.gov.uk/government/uploads/system/uploads/attachment_data/file/204231/pb13934-water-environment-catchment-based-approach.pdf>

Deltares (2014) *Delft3D-WAVE Simulation of short-crested waves with SWAN*, *User Manual, version: 3.05.34160*, Deltares, The Netherlands.

Déqué M., Rowell D., Lüthi D., Giorgi F., *et al.* (2007) An intercomparison of regional climate simulations for Europe: assessing uncertainties in model projections, *Climate Change*, 81(S1):53–70.

Ditlevsen, P. D., and Johnsen, S.J. (2010) Tipping points: Early warning and wishful thinking, *Geophysical Research Lett*ers, 37.

Dixit, P.R. *et al*., (2013) Seasonal Variation of the Physicochemical Properties of Water Samples in Mahanadi Estuary, East Coast of India, *Journal of Environmental Protection,* 4: 843-848.

Druckenmiller, D., Acar, W. and Troutt, M, (2004) Agent Based Modeling and Simulation of Causal Maps*, AMCIS 2004 Proceedings*, Paper 217.

D'Souza, R (2002) Colonialism, capitalism and nature: debating the origins of Mahanadi Delta's hydraulic crisis (1803–1928), *Economic and Political Weekly*, 30:1261–1272.

Dunn, F.E., Nicholls, R.J., Darby, S.E., Cohen, S., Zarfl, C. and Fekete, B.M. (2018) Projections of historical and 21st century fluvial sediment delivery to the Ganges-Brahmaputra-Meghna, Mahanadi, and Volta deltas, *Science of the Total Environment,* DOI:10.1016/j.scitotenv.2018.06.006.

Edmonds, D. A. and Slingerland, R.L. (2007) Mechanics of river mouth bar formation: Implications for the morphodynamics of delta distributary networks, *Journal of Geophysical Research*, 112: F02034.

Edmonds, D. A. and Slingerland, R.L. (2010) Significant effect of sediment cohesion on delta morphology, *Nature Geoscience,* 3:105-109.

Edmonds, D. A., Slingerland, R. L., Best, J., Parsons, D. and Smith, N. (2010) Response of river-dominated delta channel networks to permanent changes in river discharge, *Geophysical Research Letters*, 37:1-5.

Edmonds, D. A., Paola, C., Hoyal, D. C. J. D. and Sheets, B.A. (2011), Quantitative metrics that describe river deltas and their channel networks, *Journal of Geophysical Research*, 116: F04022.

Edmonds, D.A. *et al.* (2009) Predicting delta avulsions: implications for coastal wetland restoration, *Geology*, 37:759-762.

Edmonds, D.A. *et al.* (2017) *A global analysis of human habitation on river deltas,* 19th EGU General Assembly, EGU2017, proceedings from the conference held 23-28 April 2017 in Vienna, Austria, p.10832.

Einstein, H.A. and Brown, C.B. (1950) Bedload function for sediment transportation, In: Rouse Hunter (ed.) *Engineering Hydraulics*, John Wiley and Sons, New York.

El-Moattassem, M. *et al.* (2015) *Modelling of sedimentation process in Aswan High Dam reservoir*, Nile Research Institute (NRI), National Water Research Center (NWRC),

Ericson J.P., Vörösmarty C.J., Dingman S.L., Ward L.G., and Meybeck, M. (2006) Effective sea-level rise and deltas: causes of change and human dimension implications, *Glob Planetary Change*, 50:63–82.

Erskine, W. and Warner, R. (1988) Geomorphic Effects of Alternating Flood- and Drought-Dominated Regimes on NSW Coastal Rivers, *Fluvial geomorphology of Australia*, 223-244.

ESPA (2015) *Assessing Health, Livelihoods, Ecosystem Services and Poverty Alleviation In Populous Deltas,* viewed 17 January 2015, <http://www.espadelta.net>

European Environment Agency (2014) *Digest of EEA Indicators*, EEA Technical Report, No. 8/2014, Luxembourg.

Fagherazzi S., Bortoluzzi, A., Dietrich, W.E., Adami, A., Lanzoni, S., Marani, M. and Rinaldo, A. (1999) Tidal networks: 1. Automatic network extraction and preliminary scaling features from digital terrain maps, *Water Resources Research*, 35(12): 3891–3904.

Faisal, I.M. and Parveen, S. (2004) Food security in the face of climate change, population growth, and resource constraints: implications for Bangladesh, *Environmental management*, 34(4): 487-98.

Falk, G.C. (2000) *Delta growth despite a rise in sea-level – has Bangladesh got the all clear?,* viewed 20 November 2014, <http://geoapps.ph-freiburg.de/bangladesh/documents/Terrasse%20English%20Version.pdf>.

Fanos, A.M. (1995) Impact of Human Activities on the Erosion and Accretion of the Nile Delta Coast, *Journal of Coastal Research*, 11(3):821-833.

Feng, L., Bin, C., Tasawar, H., Ahmend, A. and Bashir, A. (2015) Modelling the influence of thermal discharge under wind on algae, *Physics and Chemistry of the Earth,* 79: 108-114.

FeoJi, E., Vuerich, L.G. and Zerihun, W. (2002) Evaluation of environmental degradation in northern Ethiopia using GIS to integrate vegetation, geomorphological, erosion and socioeconomic factors, *Agriculture, Ecosystems and Environment*, 91(1-3): 313-325.

Fernandez, G.F. *et al.* (2015) Land Cover Change in the Andes of Southern Ecuador—Patterns and Drivers, *Remote Sensing* 7(3):2509-2542.

Folke, C. (2006) Resilience: the emergence of a perspective for social–ecological systems analyses, *Global Environmental Change*, 16:253-267.

Fox, W. T. and Davis Jr., R.A. (1978) Seasonal variation in beach erosion and sedimentation on the Oregon coast, *Geological Society of America Bulletin*, 89 (10):1541-1549.

French, J.R. (2015) *Seminar: Modelling Coastal Systems*, University of Southampton, delivered November 2015.

Frihy, O.E. (1988) Nile Delta Shoreline Changes: Aerial Photographic Study of a 28-Year period, *Journal of Coastal Research*, 4(4):597-606.

Frihy, O.E. *et al.* (1998) Natural and Human Impact on the North-eastern Nile Delta Coast of Egypt, *Journal of Coastal Research*, 14(3):1109-1118.

Frissell, C., Liss, W.J., Warren, C.E., and Hurley, M.D. (1986) A hierarchical framework for stream habitat classification: Viewing streams in a watershed context, *Environmental Management*, 10: 199-214.

Fritz, H.M., Blount, C.D., Thwin, S., Thu, M.K. and Chan, N. (2009) Cyclone Nargis storm surge in Myanmar, *Nature Geoscience*, 2, 448 - 449

Furukawa, K. and Wolanski, E. (1996) Sedimentation in Mangrove Forests*, Mangroves and Salt Marshes*, 1(1):3-10.

Galloway, W.E. (1975) Process framework for describing the morphologic and stratigraphic evolution of deltaic depositional systems, In Broussard, M.L. (ed.) *Deltas, Models for Exploration*, pp. 87–98, Houston Geological Society, Houston, TX.

Geleynse, N., Voller, V.R., Paola, C. and Ganti, V. (2012), Characterization of river delta shorelines, *Geophysical Research Letters*, 39: L17402.

Gelfenblum, G., Stevens, A., Elias, E. and Warrick, J. (2009) Modeling sediment transport and delta morphology on the dammed Elwha River, Washington State, USA, *Coastal Dynamics*, 109: 1-15.

Ghose, D.K. and Swain, P.C. (2011) erosion and sediment characteristics of peninsular river India, a case study*, International Journal of Engineering Science and Technology*, 3(5):3716-3725.

Giambastiani, B. *et al*. (2007) Saltwater intrusion in the unconfined coastal aquifer of Ravenna (Italy): A numerical model, *Journal of Hydrology*, 340(1-2):91-104.

Giosan, L., Constantinescu, S., Clift, P.D., Tabrez, A.R., Danish, M. and Inam, A. (2006) Recent morphodynamics of the Indus delta shore and shelf, *Continental Shelf Research*, 26(14):1668-1684.

Giosan, L., Constantinescu, S., Filip, F. and Deng, B. (2013) Maintenance of large deltas through channelization: Nature vs. humans in the Danube delta, *Anthropocene*, 11:1-11.

Giosan, L., Syvitski, J., Constantinescu, S. and Day, J. (2014) Protect the World's Deltas, *Nature Comment*, 516: 31-33.

Giupponi, C. (2007) Decision Support Systems for implementing the European Water Framework Directive: The MULINO approach, *Environmental Modelling and Software*, 22(2): 248-58.

Glasser, M., Krause, G., Ratter, B. and Welp, M. (2008) Human-Nature Interaction in the Anthropocene – Potential of Social-Ecological Systems, *GAIA*, 1(8): 77-80.

Godoy, M.D.P. and de Lacerda, L.D. (2014) River-island morphological response to basin land-use change within the Jaguaribe River estuary, NE Brazil, *Journal of Coastal Research*, 30(2): 399-410.

Goodbred, S.L. Jr. (2003) Response of the Ganges dispersal system to climate change: a source-to-sink view since the last interstade, *Sedimentary Geology,* 162(1): 83-104.

Gornitz, V. (1991) Global coastal hazards from future sea level rise, *Palaeogeography, Palaeoclimatology, Palaeoecology*, 89: 379-398.

Gosain, A. K. *et al*. (2006) Climate Change Impact Assessment on Hydrology of Indian River Basins, *Current Science*, 90(3): 346–353.

Goswami, B. N. and Mohan, R.S.A. (2001) Intraseasonal oscillations and interannual variability of the Indian summer monsoon, *Journal of Climate*, 14: 1180–1198.

Grattan, S.R. *et al*. (2002) Rice is more sensitive to salinity than previously thought, *California Agriculture*, 56(6):189-198.

Gupta, H., Kao, S.J. and Dai, M. (2012) The role of mega dams in reducing sediment fluxes: a case study of large Asian rivers, *Journal of Hydrology,* 464-465: 447-458.

Guo, L., van der Wegen, M., Roelvink, D. and He, Q. (2015) Exploration of the impact of seasonal river discharge variations on long-term estuarine morphodynamic behaviour, *Coastal Engineering,* 95: 105-116.

Gutiérrez, F. and Dracup, J.A. (2001) An analysis of the feasibility of long-range streamflow forecasting for Colombia using El Niño- Southern Oscillation indicators, *Journal of Hydrology*, 246:181-196.

Haasnoot, M. *et al*. (2014) Fit for purpose? Building and evaluating a fast, integrated model for exploring water policy pathways, *Environmental Modelling and Software*, 60: 99-120.

Habets, F., LeMoigne, P. and Noilhan, J. (2004) On the utility of operation precipitation forecasts to served as input for streamflow forecasting, *Journal of Hydrology*, 293: 270-288.

Hajek, E. A. and Wolinsky, M.A. (2012), Simplified process modeling of river avulsion and alluvial architecture: Connecting models and field data, *Sedimentary Geology*, 257–260.

Hancock, G.R., Verdon-Kidd, D. and Lowry, J.B.C. (2017) Soil erosion predictions from a landscape evolution model – An assessment of a post-mining landform using spatial climate change analogues, *Science of the Total Environment,* 601-602: 109-121.

Hansen, J., Sato, M. and Ruedy, R. (2012) Perception of climate change, *PNAS*, 109: 14726-14727.

Hanson, S. *et al*. (2007) *Capturing coastal morphological change within regional integrated assessment: an outcome-driven fuzzy logic approach*, Tyndall Centre for Climate Change Research, WP 113.

Haq, B.U. (1994) *Sea Level Rise and Coastal Subsidence*, Land, Water and Natural Habitats Division, Environment Department, The World Bank, 34 pp.

Haq, M., Mia, M.A.T., Rabbi, M.F. and Ali, M.A. (2011) Incidence and Severity of Rice Diseases and Insect Pests in Relation to Climate Change, In: Lal, R., Sivakumar, M., Faiz, S., Mustafizur Rahman, A. and Islam, K. (eds) *Climate Change and Food Security in South Asia*, Springer, Dordrecht.

Harrison, S. (2001) On reductionism and emergence in geomorphology, *Transactions of the Institute of British Geographers*, 26: 327–339.

Hartmann, D.L., Klein Tank, A.M.J., Rusticucci, M., Alexander, L.V., Brönnimann, S., Charabi, Y., Dentener, F.J., Dlugokencky, E.J., Easterling, D.R., Kaplan, A., Soden, B.J., Thorne, P.W., Wild, M. and Zhai, P.M. (2013) Observations: Atmosphere and Surface, In Stocker, T.F., Qin, D., Plattner, G.K., Tignor, M., Allen, S.K., Boschung, J., Nauels, A., Xia, Y., Bex, V. and Midgley, P.M. (eds.) *Climate Change 2013: The Physical Science Basis*, Contribution of Working Group I to the Fifth Assessment Report of the Intergovernmental Panel on Climate Change Cambridge University Press, Cambridge, United Kingdom and New York, NY, USA.

Henderson-Sellers, A., Zhang, H., Berz, G., Emanuel, K., Gray, W., Landsea, C., Holland, G., Lighthill, J., Shieh, S.L., Webster, P. and McGuffie, K. (1998) Tropical cyclones and global climate change: A post-IPCC assessment, *Bulletin of the American Meteorological Society* 79: 19–38.

Hensel,P.F., Day, Jr., J.W. and Pont, D. (1999) Wetland Vertical Accretion and Soil Elevation Change in the Rhone River Delta, France: The Importance of Riverine Flooding, *Journal of Coastal Research*, 15(3).

Hereher, M.E. (2011) Mapping coastal erosion at the Nile Delta western promontory using Landsat imagery, *Environmental Earth Science,* 64(1117).

Hiatt, M. and Passalacqua, P. (2015) Hydrological connectivity in river deltas: The first-order importance of channel-island exchange, *Water Resources Research*, 51(4).

Hoitink, A.J.F. *et al.* (2017) Tidal controls on river delta morphology, *Nature Geoscience,* 10: 637-645.

Hu, K., Chen, Q. and Wang, H. (2015) A numerical study of vegetation impact on reducing storm surge by wetlands in a semi-enclosed estuary, *Coastal Engineering*, 95: 66-76.

Hubbard, B. and Glasser. N. (2005) *Field techniques in glaciology and glacial geomorphology*, 400 pp, J. Wiley & Son, Chichester.

Huddart, D. and Stott, T. (2010) *Earth Environments, Past, Present and Future*, Wiley Blackwell. Oxford.

Hudson, P.F. and Kesel, R.H. (2000) Channel migration and meander-bend curvature in the lower Mississippi River prior to major human modification, *Geology*, 28(6): 531-534.

Ingebritsen, S.E., Ikehara, M.E., Galloway, D.L. and Jones, D.R. (2000) *Delta subsidence in California; the sinking heart of the state,* USGS, Fact Sheet 005-00.

Intergovernmental Panel on Climate Change (IPCC) (2007) Climate Change 2007: The Physical Science Basis, Cambridge University Press, Cambridge, United Kingdom.

Islam, S. (2017) Assessment of the Impact and Management of Flood, Drought and River Bank Erosion: A Case Study of Char Land Peoples of Gangachara Upazila, Rangpur District, Bangladesh, *Imperial Journal of Interdisciplinary Research*, 3(4): 96-111.

Jena, P.P., Chatterjee, C., Pradhan, G. and Mishra, A. (2014) Are recent floods in Mahanadi Basin in Eastern India due to an increase in extreme rainfalls? *Journal of Hydrology,* 517:847-862.

Jerolmack, D. J. and Swenson, J. (2007), Scaling relationships and evolution of distributary networks on wave-influenced deltas, *Geophysical Research Letters*, 34(23): L23402.

Jerolmack, D.J. (2009) Conceptual framework for assessing the response of delta channel networks to Holocene sea level rise, *Quaternary Science Reviews*, 28:1786-1800.

Johnson, C. (2014) *As waters rise, Mekong rice farmers switch to shrimp*, viewed 20 March 2015, <http://www.marketplace.org/topics/world/waters-rise-mekong-rice-farmers-switch-shrimp>.

Kale, V. S., Ely, L. L., Enzel, Y. and Baker, V. R. (1994) Geomorphic and hydrologic aspects of monsoon floods on the Narmada and Tapi Rivers in central India, *Geomorphology*, 10: 157–168.

Kale, V. S., Hire, P., and Baker, V. R. (1997) Flood hydrology and geomorphology of monsoon dominated rivers: The Indian Peninsula, *Water International,* 22: 259–265.

Kale, V.S. (2003) Geomorphic Effects of Monsoon Floods on Indian Rivers. In: Mirza, M.M.Q., Dixit, A., Nishat, A. (eds.) *Flood Problem and Management in South Asia*, Springer, Dordrecht.

Kar, M. (2014) Violent sea leaves Satabhaya on edge, *Telegraph India,* viewed 24 August 2015, <http://www.telegraphindia.com/1141115/jsp/odisha/story_19031667.jsp#.VdcNtJdMIs>

Khadka, N.S. (2016) India Ganges floods 'break previous records', *BBC News*, viewed 1 April 2018, <http://www.bbc.co.uk/news/world-asia-india-37217679>.

Khatua, K. and Mahakul, B. (1999) Flood in Mahanadi Delta stage ii area, *Proceedings of the National Seminar on Disaster Management,* UCE Burla, Orissa, 12-13 November 1999.

Khatua, S.K.K. and Dash, D.R.N. (2013) *Management of super cyclone and flood in Orissa*, India Environmental Portal, Report, viewed 10 August 2016, < http://www.indiaenvironmentportal.org.in/files/file/management%20of%20super%20cylone%20in%20Orissa_0.pdf>.

Kim, W. S., Mohrig, D., Twilley, R. R., Paola, C. and Parker, G. (2009) Is it feasible to build new land in the Mississippi River delta, *Eos Transactions of the American Geophysical Union*, 90(42): 373–374.

Kondolf, G. M. *et al*. (2014), Sustainable sediment management in reservoirs and regulated rivers: Experiences from five continents*, Earth's Future*, 2: 256–280.

Kumar, A. and Pattnaik, D.R. (2010) Prediction of summer monsoon rainfall over India using the NCEP climate forecast system, *Climate Dynamics*, 34: 557–572.

Kumar, R. and Pattnaik, A.K. (eds) (2010) *CHILIKA Newsletter*, Volume 5, Wetlands International, New Delhi, India.

Lambin, E.F., Geist, H.J. and Lepers, E. (2003) Dynamics of land-use and land-cover change in tropical regions, *Annual Review of Environment and Resources*, 28:205-41.

Lata, S. and Nunn, P. (2012) Misperceptions of climate-change risk as barriers to climate-change adaptation: a case study from the Rewa Delta, Fiji, *Climatic Change*, 110(1-2):169-186.

Le, T.V.H. *et al.* (2007) The combined impact on the flooding in Vietnam's Mekong River delta of local man-made structures, sea level rise, and dams upstream in the river catchment, *Estuarine, Coastal and Shelf Science*, 71: 110-116.

Leemans, R. *et al.* (2003) Drivers of change in ecosystems and their services, In: Mooney, H., Cropper, A. and Reid, W., *Ecosystems and Human wellbeing: A framework for assessment,* Island Press, Washington D.C.

Leh, M., Bajwa, S. and Chaubey, J. (2011) Impact of land use change on erosion risk: an integrated remote sensing, geographic information system and modeling methodology, *Land Degradation and Development*, doi: 10.1002/ldr.1137

Lenton, T. M. (2012), Arctic climate tipping points, *AMBIO*, 41:10-22.

Lenton, T.M. (2013) Environmental tipping points, *Annual Review of Environment and Resour*ces, 38: 1-29.

Lenton, T.M. *et al*. (2008) Tipping elements in the Earth's climate system, *PNAS*, 105(6):1786-1793.

Lesser, G.R., Roelvink, J.A., van Kester, J.A.T.M. and Stelling, G.S. (2004) Development and validation of a three-dimensional morphological model, *Coastal Engineering,* 51: 883–915.

Levin, S.A. (1998) Ecosystems and the Biosphere as Complex Adaptive Systems, *Ecosystems*, 1(5):431-36.

Lewis, M. *et al.* (2013) A storm surge inundation model of the northern Bay of Bengal using publicly available data, *Quarterly Journal of the Royal Meteorological Society,* 139(671):358-69.

Liang, M., Voller, V. R., and Paola, C. (2015) A reduced-complexity model for river delta formation – Part 1: Modeling deltas with channel dynamics, Earth Surface Dynamics, 3: 67–86.

Liang, M., Van Dyk, C. and Passalacqua, P. (2016) Quantifying the patterns and dynamics of river deltas under conditions of steady forcing and relative sea level rise, *Journal of Geophysical Research*: *Earth Surface,* 121(2): 465-496.

Ligon, F.K. *et al*. (1995) Downstream Ecological Effects of Dams, *Ecology of Large Rivers*, 45(3):183-192.

Lindenschmidt, K. and Long, J. (2012) A GIS approach to define the hydro-geomorphological regime for instream flow requirements using geomorphic response units (GRU), *River Systems,* 20(3-4):261-275.

Little Jr., C.D. and Biedenharn, D.S. (2014) *Mississippi River Hydrodynamic and Delta Management Study – Geomorphic Assessment*, US Army Corps of Engineers, viewed 30 September 2016, < http://acwc.sdp.sirsi.net/client/en_US/default/search/detailnonmodal/ent:$002f$002fSD_ASSET$002f0$002f1035581/ada/?qu=Old+River+Control+Complex+%28La.%29>.

Lu, X.X. *et al.* (2007) Rapid channel incision of the lower Pearl River (China) since the 1990s as a consequence of sediment depletion, *Hydrology and Earth System Sciences*, 11:1897-1906.

Ly, C.K. (1980) The role of the Akosombo dam on the Volta River in causing coastal erosion in central and eastern Ghana (WA), *Marine Geology*, 37:323-332.

Lytle, D.A. and Poff, N.L. (2004) Adaption to natural flow regimes, *Trends in Ecology & Evolution*, 19(2):94-100.

Magic Seaweed (2016) *Puri Surf Report*, viewed 1 October 2016, http://magicseaweed.com/Puri-Beach-Surf-Report/840/>.

Mahalik, N.K., Das, C.D. and Maejima, W. (1996) Geomorphology and evolution of the Mahanadi Delta, *Journal of Geosciences*, 39(6): 111-122.

Mahata, K.R. (2010) Improving rice productivity in the coastal soils of the Mahanadi Delta of India through integrated nutrient management, in Hoanh, C.T., Szuster, B.W., Suan-Pheng, K., Ismail, A.M. and Noble, A.D., *Tropical Deltas and Coastal Zones, Food Production, Communities and Environment at the Land–Water Interface*, Ch.18, pp.239-248, CABI.

Malczewski, J. (2004) GIS-based land-use suitability analysis: a critical overview, *Progress in Planning*, 62:3-65.

Maren, D.S., van Kessel, T., Cronin, K. and Sittoni, L. (2015) The impact of channel deepening and dredging on estuarine sediment concentration, *Continental Shelf research*, 95: 1-14.

Maritan, A., Rinaldo, A., Rigon, R., Giacometti, A., and RodriguezIturbe, R. (1996) Scaling laws for river networks, *Phys. Rev. E*, 53:1510–1515.

Martin, J. F., Reyes, E., Kemp, G. P., Mashriqui, H. and Day Jr., J. W. (2002) Landscape modelling of the Mississippi Delta, *BioScience*, 52:357-365.

Martin, J.F. (2000) *Manipulations of natural system functions within the Mississippi Delta: A simulation-modelling study*, PhD thesis, Louisiana State University, Baton Rouge.

Martin, J.F., White, M.L., Reyes, E., Kemp, G.P., Mashriqui, H. and Day Jr., J.W. (2000) Evaluation of coastal management plans with a spatial model: Mississippi Delta, Louisiana, USA, *Environmental Management*, 26: 117-129.

Martin, M. *et al*. (2013) *Climate change, migration and human cognition in an Asian Mega-delta*, Working paper, Refugee and Migratory Movements Research Unit, Gobeshona.

Maunder, M.N. and Punt, A.E. (2013) A review of integrated analysis in fisheries stock assessment, *Fisheries Research*, 142:61-74.

Mayhew, S. (2009) Dictionary of Geography (4th ed.), Oxford University Press.

Mazzoti, S., Lambert, A., Van der Kooij, M. and Mainville, A. (2009) Impact of anthropogenic subsidence on relative sea-level rise in the Fraser River delta, *Geology*, 37(9): 771-774.

Mcleod, E., Poulter, B., Hinkel, J., Reyes, E. and Salm, R. (2010) Sea-level rise impact models and environmental conservation: A review of models and their applications, *Ocean and Coastal Management*, 53:507-517.

McManus, J. (2002) Deltaic responses to changes in river regimes, *Marine Chemistry*, 79:155–170.

Meckel, T.A., Ten Brink, U.S. and Williams, S.J. (2007) Sediment compaction rates and subsidence in deltaic plains: numerical constraints and stratigraphic influences, *Basin Research*, 19:19–31.

Medeiros, E.S., Caldas, I.L, Baptista, M.S. and Feudel, U. (2017) Trapping phenomenon attenuates the consequences of tipping points for limit cycles, *Nature,* Scientific Reports, 7: number 42351.

Mehta, N. *et al.* (2013) *Cyclone Phailin: Recovery challenge looms in Odisha, Andhra Pradesh*, viewed 4 April 2015, <http://www.livemint.com/Politics/zqBu8p6YrcpRXHIkWuWtQI/Cyclone Phailin-hits-Odisha-rescue-workers-start-to-assess.html>.

Met Office (2014) *Ensemble forecasting*, viewed 12 February 2015, <http://www.metoffice.gov.uk/research/areas/data-assimilation-and-ensembles/ensemble-forecasting>.

Michels, K.H., Kudrass, H.R., Hubscher, C., Suckow, A. and Wiedicke, M. (1998) The submarine delta of the G-B: cyclone-dominated sedimentation patterns, *Marine Geology*, 149:133-154.

Millennium Ecosystem Assessment (2005) *Ecosystems and human well-being: synthesis*, Washington, DC: Island Press.

Milliman, J. D., Farnsworth, K.L., Jones, P.D., Xu, K.H. and Smith, L.C. (2008), Climatic and anthropogenic factors affecting river discharge to the global ocean, 1951–2000, *Global Planetary Change*, 62(3-4): 187–194.

Moffatt and Nichol Engineers (2000) *Barataria Basin existing data and numerical model review and analysis: Final report to Louisiana Department of Natural Resources*, Baton Rouge: Moffatt and Nichol Engineers.

Mohanti, M. (1993) Coastal processes and management of the Mahanadi River deltaic complex, East Coast of India. *Proceedings Coastal Zone*, 93: 75 – 90.

Mohanti, M. (2000) Unprecedented Super Cyclone on the Orissa Coast of the Bay of Bengal, India, *Cogeoenvironment*, Newsletter 16:11-13.

Mohanti, M. and Swain, M.R. (2011) Mahanadi River Delta, East Coast of India: An Overview On Evolution And Dynamic Processes, viewed 12 August 2015, <http://www.indiawaterportal.org/sites/indiawaterportal.org/files/mahanadi.pdf>.

Morton, R.A. and Bernier, J.C. (2010) Recent Subsidence-Rate Reductions in the Mississippi Delta and Their Geological Implications, *Journal of Coastal Research*, 26(3): 555-561.

Murray, A.B. and Paola, C. (1994) A cellular model of braided rivers, *Nature*, 371:54–57.

Murray, A.B. and Paola, C. (1997) Properties of a cellular braided stream model, *Earth Surface Processes and Landforms*, 22: 1001–1025.

Natesan, U. *et al*. (2013) Estimation of wave heights during cyclonic conditions using wave propagation model, *Natural Hazards*, 69(3):1751-1766.

Nayak, B.K. *et al*. (2004) Variation of water quality in Chilika Lake, Orissa, Indian *Journal of Marine Sciences*, 33(2):164-169.

Neunhuis, J. (2011*) Modeling deltaic response to changes in fluvial sediment delivery*, University of Twente, viewed 1 March 2016, < https://www.researchgate.net/publication/279483390_Modeling_deltaic_response_to_changes_in_fluvial_sediment_delivery>.

New Indian Express (2015) *New Colony for Satabhaya Villagers yet to Come Up*, published online 20 April 2015, viewed 26 August 2015, <http://www.newindianexpress.com/states/odisha/New-Colony-for-Satabhaya-Villagers-Yet-to-Come-up/2015/04/20/article2773333.ece>.

Nicholas, A.P. (2005) Cellular modelling in fluvial geomorphology, *Earth Surface Processes and Landforms,* 30(5): 645-649.

Nicholls, R.J. and Goodbred Jr., S.L. (2004) *Towards Integrated Assessment of the Ganges-Brahmaputra Delta*, Paper for Proceedings of the 5th International Conference on Asian Marine Geology.

Nicholls, R.J., Wong, P.P., Burkett, V.R., Codignotto, J.O. Hay, J.E., McLean, R.F., Ragoonaden, S. and Woodroffe, C.D. (2007) *Coastal systems and low-lying areas. Climate Change 2007: Impacts, Adaptation and Vulnerability*, Contribution of Working Group II to the Fourth Assessment Report of the Intergovernmental Panel on Climate Change M.L. Parry, O.F. Canziani, J.P. Palutikof, P.J. van der Linden and C.E. Hanson, Eds., Cambridge University Press, Cambridge, UK: 315-356.

Nicolis, G. and Nicolis, C. (2012) *Foundations of Complex Systems*, World Scientific.

Nienhuis, J.H., Ashton, A.D., Roos, P.C., Hulscher, S.J.M.H. and Giosan, L. (2013) Wave reworking of abandoned deltas, *Geophysical Research Letters*, 40: 5899 – 5903.

Norgaard, R.B. *et al*. (2009) Collectively engaging complex socio-ecological systems: re-envisioning science, governance and the California Delta, *Environmental Science and Policy*, 12:644-652.

Odisha Channel Bureau (2015) *Rehabilitation of sea erosion hit villagers begins in Odisha*, viewed 26 August 2015, <http://odishachannel.com/index.php/4735/rehabilitation-of-sea-erosion-hit-villagers-begins-in-odisha/>.

Ogundtunde, P.G. *et al*. (2006) Hydroclimatology of the Volta River Basin in West Africa, *Physics and Chemistry of the Earth*, 31:1180-1188.

Olesen, K.W., Ammentorp, H.C. and Hvam Petersen, N. (2011) Mega Deltas and the Climate Change Challenges, *International Network on Erosion and Sedimentation*, Beijing.

Olsson, P. and Folke, C. (2008) *Focus on coastal zones saves coral reefs*, viewed 17 December 2014, <http://sustainability.formas.se/en/Issues/Issue-3/Content/Articles/Storms-and-flooding-damage-the-coast/>.

Pagano, T. and Garen,D. (2005) A Recent Increase in Western U.S. Streamflow Variability and Persistence, *American Meteorological Society.*

Panda, D.K. *et al*. (2013) Streamflow trends in the Mahanadi River basin: Linkages to tropical climate variability*, Journal of Hydrology*, 495:135-149.

Panda, U.C. *et al.* (2006) Application of factor and cluster analysis for characterization of river and estuarine water systems – A case study: Mahanadi River (India), *Journal of Hydrology,* 331(3-4):434-445.

Panigrahi, N. (2003) Disaster management and the need for convergence of services of welfare agencies-A case study of the Super Cyclone of Orissa, *Social Change*, 33(1): 1-25.

Paola, C. *et al*. (2011) Natural Processes in Delta Restoration: Application to the Mississippi Delta, *Annual Review of Marine Science*, 3:67-91.

Passalacqua, P., *et al.* (2013) The signature of delta forming processes, vegetation and anthropogenic disturbance in the Ganges-Brahmaputra delta, in Coco, G., Blanco, B, Olabarreita, M. and Tinoco, R. (eds.) *The 8th Symposium on River, Coastal and Estuarine Morphodynamics*, Book of abstracts, Santander, Spain.

Passalacqua, P., S. Lanzoni, C. Paola, and A. Rinaldo (2013), Geomorphic signatures of deltaic processes and vegetation: The Ganges-Brahmaputra-Jamuna case study, *Journal of Geophysical Research: Earth Surface,* 118: 1838–1849.

Pasternack, G. B. and Brush, G. S. (2002) Biogeomorphic controls on sedimentation and substrate on a vegetated tidal freshwater delta in upper Chesapeake Bay, *Geomorphology,* 43:293-311.

Patterson, J. and Billington, K. (2013) Where are we heading in catchment management?. Water, *Journal of the Australian Water Association*, 40:76-80.

Pati, B.K. (2009) *River bank erosion in Orissa: the bitter truth*, viewed 21 August 2015, <http://www.orissadiary.com/ShowOriyaColumn.asp?id=13776>.

Patro, S., Chatterjee, C., Singh, R. and Raghuwanshi, N. (2009) Hydrodynamic modelling of a large flood-prone river system in India with limited data, *Hydrological Processes*, 23: 2774 - 2791.

Pattanaik, C. and Prasad, S.N. (2011) Assessment of aquaculture impact on mangroves of Mahanadi Delta (Orissa), East coast of India using remote sensing and GIS, *Ocean and Coastal Management*, 54(11): 789-95.

Pearce, F. (2014*) Living with floods in the Mahanadi Delta*, viewed 25 March 2015, <http://www.wetlands.org/News/tabid/66/ID/4097/STORY-Living-with-floods-in-the-Mahanadi-Delta India.aspx>.

Piechota, T. C., Chiew, F.H.S, Dracup, J.A. and McMahon, T.A. (1998) Seasonal streamflow forecasting in eastern Australia and the El Niño–Southern Oscillation, *Water Resources Research*, 34(11):3035–3044.

Pielke Jr., R. A., Landsea, C., Mayfield, M., Laver, J. and Pasch, R. (2005) Hurricanes and Global Warming, *Bulletin of the American Meteorological Soc*iety, 86: 1571–1575.

Pinter, N., Huthoff, F., Dierauer, J., Remo, J.W.F. and Damptz, A. (2016) Modeling residual flood risk behind levees, Upper Mississippi River, USA, *Environmental Science and Policy*, 58.

Pisaric, M.F.J. *et al.* (2011) Impacts of a recent storm surge on an Arctic delta ecosystem examined in the context of the last millennium, *PNAS,* 108(22).

Pondrelli, M., Pio Rossi, A., Marinangeli, L., Hauber, E., Gwinner, K., Baliva, A. and Di Lorenzo, S. (2008) Evolution and depositional environments of the Eberswalde fan delta, *Mars. Icarus*, 197:429–451.

Popescu, I. *et al.* (2015) Use of hydrodynamic models for the management of the Danube Delta wetlands: The case study of Sontea-Fortuna ecosystem, Environmental Science and Policy, 46:48-56.

Radhakrishna, I. (2001) Saline fresh water interface structure in Mahanadi Delta region, Orissa, India, *Envrionmental Geology,* 40(3):369-380.

Rakhecha, P.R. (2002) Highest floods in India, in Snorrason, A., Finnsdotir, H. and Moss, M.E., *The Extremes of the Extremes: Extraordinary Floods*, International Association of Hydrological Sciences, Wallingford.

Ramaswamy, C. (1987) *Meteorological Aspects of Severe Floods in India 1923–1979*, MMH No. 10, India Meteorological Department, New Delhi.

Ranasinghe, R., Duong, T.M., Uhlenbrook, S., Roelvink, D. and Stive, M. (2013) Climate-change impact assessment for inlet-interrupted coastlines, *Nature Climate Change,* 3:83-87.

Rao, B.B., *et al*. (2012) *Potential Evapotranspiration estimation for Indian conditions: Improving accuracy through calibration coefficients*, Technical Bulletin No 1. National Initiative on Climate Resilient Agriculture.

Rao, P.G. (1993) Climatic changes and trends over a major river basin in India, *Climate Research*, 2:215-223.

Rao, P.G. (1995) Effect of Climate Change on Streamflows in the Mahanadi River Basin, India, *Water International*, 20(4): 205-212.

Raworth, K. (2012) *A Safe and Just Space for Humanity: Can we live within the doughnut*?, Oxfam International.

Reidsma, P., *et al*. (2011) Methods and tools for integrated assessment of land use policies on sustainable development in developing countries, *Land Use Policy*, 28:604-617.

Renaud, F.G., *et al*. (2013) Tipping from the Holocene to the Anthropocene: How threatened are major world deltas?, *Current Opinion in Environmental Sustainability*, 5(6): 644-654.

Renaud, F.G., *et al*. (2014) Tipping points for delta social-ecological systems, *Inprint*(1): 5-13.

Reyes, E. (2009) Wetland landscape spatial models, in: Perillo, G.M.E., Wolanski, E., Cahoon, D.R., Brinson, M.M.(eds.), *Coastal Wetlands: An integrated Ecosystem Approach*, Elsevier Science, Amsterdam.

Reyes, E., White, M.L., Martin, J.F., Kemp, G.P., Day Jr., J.W. and Aravamuthan, A. (2000) Landscape modelling of coastal habitat change in the Mississippi Delta, *Ecology,* 81: 2331–2349.

Roberts, H. H. (1997) Dynamic changes of the Holocene Mississippi River delta plain: The delta cycle, *Journal of Coastal Research,* 13(3): 605–627.

Robinson, J. (2003) Future subjective: backcasting as social learning. *Futures* (2003): 839-856.

Rockström, J., *et al*. (2009a) A safe operating space for humanity, *Nature*, 461:472-475.

Rockström, J., *et al.* (2009b) Planetary boundaries: exploring the safe operating space for humanity, *Ecology and Society*, 14.

Rodriguez-Iturbe, I. and Rinaldo, A. (1997), *Fractal River Basins: Chance and Self-Organization*, Cambridge University Press, Cambridge, U. K.

Rotmans, J. and Loorbach, D. (2009), Complexity and Transition Management, *Journal of Industrial Ecology*, 13: 184–196.

Rotmans, J., *et al.* (1994) *Global change and sustainable development. A modelling perspective for the next decade*, The National Institute for Public Health and the Environment, Copenhagen, Denmark.

Saito, Y., Chaimanee, N., Jarupongsakul, T. and Syvitski, J.P.M. (2007) Shrinking megadeltas in Asia: Sea-level rise and sediment reduction impacts from case study of the Chao Phraya Delta, *Inprint Newsletter: Land Ocean Interaction in the Coastal Zone*, 2007/2, 3–9.

Sambasiva, R., *et al.* (1978) *Morphology and Evolution of Mahanadi and, Brahmani Baitarani deltas, Symposium on Morphology and Evolution of Landforms*, Department of Geology, University of Delhi, New Delhi.

Sanchez-Archilla, A., Jimenez, J. A., and Valdemoro, H. I. (1998) The Ebro Delta: Morphodynamics and Vulnerability, *Journal of Coastal Research*, 14: 754-772.

Scheffer, M. *et al.* (2009) Early-warning signals for critical transitions, *Nature,* 461(3):53-59.

Schewe, J. and Levermann, A. (2012) A statistically predictive model for future monsoon failure in India, *Environmental Research Letters,* 7(4).

Schott, T., Landsea, C., Hafele, G., Lorens, J., Taylor, A., Thurm, H., Ward, B., Willis, M. and Zaleski, W. (2012) *The Saffir-Simpson Hurricane Wind Scale*, National Weather Services, National Hurricane Centre, National Oceanic and Atmospheric Administration (NOAA) factsheet, viewed 23 August 2016, <http://www.nhc.noaa.gov/pdf/sshws.pdf>.

Schumm, S.A. and Lichty, R. W. (1965) Time, space and causality in geomorphology *American Journal of Scienc*e, 263:110–119.

Scottish Environment Protection Agency (SEPA) (2009) *Flood Risk Management (Scotland) Act 2009: The National Flood Risk Assessment Methodology*, SEPA, Stirling.

Scrase, J. I. and Sheate, W. R. (2002) Integration and integrated approaches to assessment: what do they mean for the environment?, *Environmental Policy and Planning*, 4: 275–294.

Selvam, V. (2003) Environmental classification of mangrove wetlands of India, *Current Science,* 84(6):757-765.

Seto K.C. (2011) Exploring the dynamics of migration to mega-delta cities in Asia and Africa: Contemporary drivers and future scenarios, *Global Environmental Change*, 21(S1):S94-S107.

Seybold, H., Andrade, J.S. and Herrmann, H.J. (2007), Modeling river delta formation, *PNAS,* 104(43): 16,804–16,809.

Shaban, M., Urban, B., El Saadi, A. and Faisal, M. (2010) Detection and mapping of water pollution variation in the Nile Delta using multivariate clustering and GIS techniques, *Journal of Environmental Management,* 91(8):1785-1793.Sharma, M. and Norton, B.G. (2005) A policy decision tool for integrated environmental assessment, *Environmental Science and Policy*, 8:356-66.

Shukla, P.R., *et al*. (eds.) (2003) *Climate Change and India: Vulnerability Assessment and Adaptation*, Universities Press, India.

Simeoni, U., Fontolan, G., Tessari, U. and Corbau, C. (2007) Domains of spit evolution in the Goro area, Po Delta, Italy, *Geomorphology*, 86: 332-348.

Singh, D., *et al.* (2014) Observed changes in extreme wet and dry spells during the South Asian summer monsoon season, *Nature Climate Change,* 4: 456–461.

Slater, L. J. (2016) To what extent have changes in channel capacity contributed to flood hazard trends in England and Wales?, *Earth Surface Processes and Landforms*, 41: 1115–1128.

Slingerland, R. and Smith, N.D. (1998) Necessary conditions for a meandering-river avulsion, *Geology* 26 (5): 435–438.

Somanna, K., *et al*. (2013) Geomorphology and Evolution of the Modern Mahanadi Delta Using Remote Sensing, *International Journal of Science and Research,* Paper ID: NOV161394.

Soria, J.L.A., Siringan, F.P. and Rodolfo, K.S. (2005) Compaction rates and paleo- sea levels along the delta complex north of Manila Bay, Luzon Island, Phillippines, *Science Diliman*, 17(2):39-45.

Sorte, C.J.B. Williams, S.L. and Zerebecki, R.A. (2010) Ocean warming increases threat of invasive species in a marine fouling community, *Ecology*, 91:2198–2204.

Stanley, D.J. and Warne, A. G. (1998) Nile Delta in its destructive phase, *Journal of Coastal Research*, 14:794–825.

Stanley, D.J. and Warne, A.G. (1993) Nile Delta: Recent Geological Evolution and Human Impact, *Science*, 260(5108): 628-634.

Stanley, D.J. and Warne, A.G. (1994) Worldwide Initiation of Holocene Marine Deltas by Deceleration of Sea-Level Rise, *Science*, 265(5169): 228-231.

Stive, M. J. F., Wang, Z.B., Capobianco, M., Ruol, P. and Buijsman, M.C. (1998) Morphodynamics of a tidal lagoon and the adjacent coast, In Dronkers, and Scheffers (eds.) *Physics of Estuaries and Coastal Seas*, Balkerma, Rotterdam.

Stonich, S., Bort, J. and Ovares, L. (1997) Globalization of shrimp aquaculture: The impact on social justice and environmental quality in Central America, *Society and Natural Resources*, 10 (2): 161-179.

Stouthamer, E. (2001) Sedimentary products of avulsions in the Holocene Rhine–Meuse Delta, The Netherlands, *Sediment Geology*, 145(1–2): 73–92.

Susnik, J., *et al.* (2014) Interdisciplinary assessment of sea-level rise and climate change impacts on the lower Nile Delta, Egypt, *Science of the Total Environment*, 503-504:279-288.

Syvitski, J. P. M. and Saito, Y. (2007) Morphodynamics of deltas under the influence of humans, *Global Planetary Change*, 57:261–282.

Syvitski, J.P.M and Milliman, J.D. (2007) Geology, Geography, and Humans Battle for Dominance over the Delivery of Fluvial Sediment to the Coastal Ocean, *Journal of Geology*, 115(1): 1-19.

Syvitski, J.P.M, Overeem, I., Brankenridge, G.R. and Hannon, M. (2012) Floods, floodplains, delta plains — A satellite imaging approach, Sedimentary Geology, 267-268: 1-14.

Syvitski, J.P.M. (2008) Deltas at risk, *Sustainability Science*, 3(1): 23-32.

Syvitski, J.P.M., *et al*. (2009) Sinking deltas due to human activities, *Nature Geoscience*, 2: 681-686.

Syvitski, J.P.M., Vörösmarty, C.J., Kettener, A.J. and Green, P. (2005) Impacts of humans on the flux of terrestrial sediment to the global coastal ocean, *Science*, 308: 376-380.

Szuster, B.W. (2003) Shrimp farming in Thailand's Chao Phraya River Delta, viewed 29 November 2014, <http://www1a.biotec.or.th/Shrinfo/documents/szuster.pdf>.

Tamura, T., *et al*. (2012) Luminescence dating of beach ridges for characterising multi-decadal to centennial deltaic shoreline changes in the Mekong, *Marine Geology*, 326-328: 140-153.

Teatini, P., Tosi, L. and Strozzi, T. (2011) Quantitative evidence that compaction of Holocene sediments drives the present land subsidence of the Po Delta, Italy, *Journal of Geophysical Research*, 116(B8).

Tejedor, A., Longjas, A., Edmonds, D.A., Zaliapin, I., Georgiou, T.T., Rinaldo, A. and Foufoula-Georgiou, E. (2017) Entropy and optimality in river deltas, *PNAS,* 114(44): 11651-11656.

Tejedor, A., Longjas, A., Zaliapin, I. and Foufoula-Georgiou, E. (2015) Delta channel networks: 1. A graph-theoretic approach for studying connectivity and steady state transport on deltaic surfaces, *Water Resources Research,* 51:3998–4018.

Thorp, J.H., Thoms M.C. and Delong, M.D. (2008) *The Riverine Ecosystem Synthesis: Toward Conceptual Cohesiveness in River Science,* Elsevier.

Thorp, J.H., Thoms, M.C. and Delong, M.D.(2006) The riverine ecosystem synthesis: biocomplexity in rver networks across space and time, *River Research and Applications,* 22: 123-147.

Torbjörn, E.*et al*., (2008) Mississippi Delta subsidence primarily caused by compaction of Holocene strata, *Nature Geoscience*, 1:173 – 176.

Turner, A.G. and Annamalai, H. (2012) Climate Change and the South Asian Monsoon, *Nature Climate Change,* 2: 587-595.

Turner, M.G., O'Neill, R.V., Gardner, R.H. and Milne, B.T. (1989) Effects of changing spatial scale on the analysis of landscape pattern, *Landscape Ecology,* 3: 153-162.

Turner, R.E., Baustian, J.J., Swenson, E.M. and Spicer, J.S. (2006) Wetland sedimentation from hurricanes Katrina and Rita, *Science,* 314: 449–452.

Tweel, A.W. and Turner, R.E. (2014) Contribution of tropical cyclones to the sediment budget for coastal wetlands in Louisiana, USA, *Landscape Ecology,* 29(6):1083-1094.

Uthes, S., *et al*. (2010) Policy relevance of three integrated assessment tools – A comparison with specific reference to agricultural policies, *Ecological Modelling*, 221:2136-2152.

Van Asselt, M.B.A. (2000) Perspectives on uncertainty and risk, *The PRIMA Approach to Decision Support,* Springer, Netherlands.

Van de Wiel, M.J., Coulthard T.J., Macklin, M. and Lewin, J. (2007) Embedding reach-scale fluvial dynamics within the CAESAR cellular automaton landscape evolution model, *Geomorphology*, 90: 283–301.

Vaz, N., Dias, J. and Chambel, L. (2009) Three-dimensional modelling of a tidal channel: the Espinheiro Channel (Portugal), *Continental Shelf Research,* 29.

Vörösmarty, C., Syvitski, J. P. M., Day, J., Paola, C. and Serebin, A. (2009) Battling to save the world's river deltas, *Bulletin of the Atomic Scientists*, 65: 31–43.

Walling, D.E. (1999) Linking land use, erosion and sediment yields in river basins, *Hydrolbiologia,* 418: 223-240.

Walling, D.E. and Webb, B.W. (1996) Erosion and sediment yield: a global overview, *Proceedings of the Exeter Symposium, July 1996,* IAHS Publication No. 236.

Wang, Y. (2013) *Simulating complex hydro-geomorphic changes in lake-catchment systems*, PhD Thesis, University of Southampton.

Wei, C., *et al*. (2014) Constructing an assessment indices system to analyse integrated regional carrying capacity in the coastal zones – A case in Nantong, *Ocean and Coastal Management*, 93:51-59.

Weng, Q. (2006) Land use change analysis in the Zhujiang Delta of China using satellite remote sensing, GIS and stochastic modelling, *Journal of Environmental Management*, 64: 273-284.

Werner, B.T. (2003) Modeling Landforms as Self-Organized, Hierarchical Dynamical Systems, in Prediction, In: *Geomorphology* (eds P. R. Wilcock and R. M. Iverson), American Geophysical Union, Washington, D. C.

Wetlands International (2014a) *About the Mahanadi Delta*, viewed 10 February 2015, <http://www.wetlands.org/Whatarewetlands/Riversanddeltas/AbouttheMahanadiDelta,India/tabid 2314/Default.aspx>.

Wetlands International (2014b) *Managing water with communities in the Mahanadi Delta, India*, viewed 19 August 2015, <http://www.wetlands.org/Whatwedo/Ouractions/tabid/2661/mod/601/articleType/ArticleView/ar cleId/2452/Default.aspx>.

Wetlands International (2014c) *Wetlands and Water Management*, viewed 12 February 2015, <http://south-asia.wetlands.org/WhatWeDo/WetlandsandWaterManagement/tabid/643/Default.aspx>.

Wichelns, D. (2010) Policy Recommendations to Maintain and Enhance Agricultural Productivity in the Nile River Delta, *International Journal of Water Resources Development*, 16(4).

Wilcock, P. R., and Crowe, J.C. (2003) Surface-based transport model for mixed-size sediment, *Journal of Hydraulic Engineering,* 129:120 – 128.

Williams, H.F.L. (2012) Magnitude of Hurricane Ike storm surge sedimentation: implications for coastal marsh aggradation, *Earth Surface Processes and Landforms*, 37:901–906.

Willson, M.F. and Halupka, K.C. (1995) Anadromous fish as keystones species in vertebrate communities, *Conservation Biology*, 9(3):489-497.

Wischmeier, W.H. and D.D. Smith (1978) *Predicting Rainfall Erosion Losses: A Guide to Conservation Planning*, Agriculture Handbook No. 537, USDA/Science and Education Administration, US. Govt. Printing Office, Washington, DC.

Wolanski, E. (2009) Coastal Wetlands: A synthesis, In: Perillo, G.M.E., Wolanski, E., Cahoon, D.R., Brinson, M.M. (eds.), *Coastal Wetlands: An integrated Ecosystem Approach*, Elsevier Science, Amsterdam.

Wolfram, S. (1984) Cellular automata as models of complexity, *Nature,* 311:419-424.

Wolinsky, M.A., Edmonds, D.A., Martin, J. and Paolo, C. (2010) Delta allometry: Growth laws for river deltas, *Geophysical Research Letters*, 37:1-6.

Wong, P.P., Losada, I.J., Gattuso, J.P., Hinkel, J., Khattabi, A., McInnes, K.L., Saito, Y. and Sallenger, A. (2014) Coastal systems and low-lying areas, In: Field, C.B., *et al. (eds.) Climate Change 2014: Impacts, Adaptation, and Vulnerability. Part A: Global and Sectoral Aspects*, Contribution of Working Group II to the Fifth Assessment Report of the Intergovernmental Panel on Climate Change, Cambridge University Press, Cambridge, United Kingdom and New York, NY, USA, pp. 361-409.

Woodroffe, C. D. and Saito, Y. (2011) River-Dominated Coasts, In: Wolanski, E. and McLusky, D. (eds.) *Treatise on Estuarine and Coastal Science: Volume 3 Estuarine and Coastal Geology and Geomorphology*, Elsevier.

Woodroffe, C.D. (1992) Mangrove Sediments and Geomorphology, in Robertson, A.I. and Alongi, D.M. (eds.) *Tropical Mangrove Ecosystem, Coastal and Estuarine Studies*, Volume 41: pp 7-41.

Woodroffe, C.D. (2002) *Coasts: Form, Process and Evolution*, Cambridge University Press, Cambridge, UK.

Woodroffe, C.D. (2010) Assessing the vulnerability of Asian mega deltas to climate change using GIS, in Green (eds.) *Coastal and Marine Geospatial Technologies*, London, Springer.

Wynn, G. (2014) 'Indian monsoon becoming more erratic – study', *Climate Change News,* 30 April, viewed November 2016, <https://www.climatechangenews.com/2014/04/30/indian-monsoon-becoming-more-erratic-study/>

Xenarios, S., Polatidis, H., Sekhar, N.U., Biswas, J.C., Maniruzzaman, M. and Sarker, G.W. (2013) *Alleviating climate change impacts in rural Bangladesh through efficient agricultural interventions*, RICE CLIMA Project, Dhaka, Bangladesh.

Yadav R.K., Yoo, J.H., Kucharski, F., Abid, M.A. (2010a) Why is ENSO influencing northwest India winter precipitation in recent decades?, *Journal of Climate* 23: 1979–1993.

Yadav, R.K., Kumar, K.R. and Rajeevan, M. (2010b) Climate change scenarios for Northwest India winter season, *Quaternary International,* 213(1): 12-19.

Yang, S.L., Milliman, J.D., Li, P. and Xu, K. (2010) 50,000 dams later: erosion of the Yangtze River and its delta, *Global and Planetary Change*, 75:14-20.

Zhang, X., and J. A. Church (2012) Sea level trends, interannual and decadal variability in the Pacific Ocean, *Geophysical Research Letters*, 39(21): L21701.

Zhao, M., Held, I.M., Lin, S. and Vecchi, G.A. (2009) Simulations of Global Hurricane Climatology, Interannual Variability, and Response to Global Warming Using a 50-km Resolution GCM, *Journal of Climate*, 22: 6653-78.

Zong, Y., Huang, G., Switzer, A.D., Yu, F. and Yim, W.W. (2009) An evolutionary model for the Holocene formation of the Pearl River delta, China, *The Holocene*, 19(1): 129-142.

Supplementary materials

DOI: 10.5258/SOTON/D0944

‘Devi River and Mahanadi River catchments modelled elevation change’.

The supplementary material for this thesis can be found online at: https://doi.org/10.5258/SOTON/D0944